Appendix B

Experiments on materials on DVD

B.1 Introduction

This report presents the experimental work performed in order to obtain the material properties required for the hybrid sandwich beam experiments. A typical cross section of the investigated beams is illustrated in Figure B.1. The beams consist of three different layers: a self-compacting normal weight concrete (NC) and a glass fiber- reinforced polymer (GFRP) profile used as face sheet materials, while the core material consisted of two different lightweight concrete (LC) compositions exhibiting different material brittleness: sand lightweight concrete (SLWAC) and all lightweight aggregate concrete (ALWAC), classified according to [Fau03] and [ACI05]. Two types of GFRP-LC interfaces were investigated: one unbonded and one adhesively bonded with an epoxy resin. The target weight for the LC core of the hybrid beam was approximately 1100 kg/m^3.

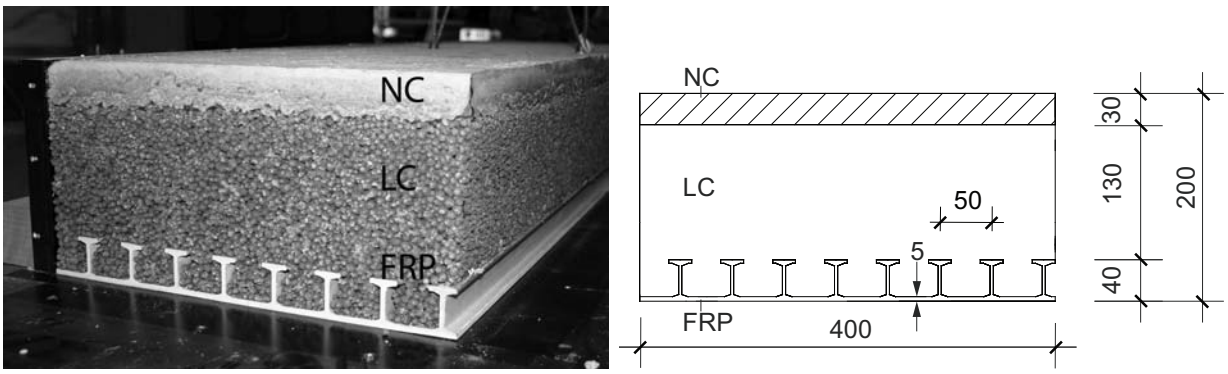

(a) Hybrid beam cross section (b) Dimension of hybrid beam cross section

Figure B.1: Hybrid beam system.

B.2 Experiments on LC core materials

The experimental program comprises two different densities of SLWAC (LC900 and LC1300), and five different ALWAC mixtures (LC1000P-1/2, LC1200P, LC1000 and LC1000A). LC900 and LC1300 were used for the S1 beam series, and the LC1000P-1/2 and LC1200P compositions were used for the preliminary research investigation of ALWAC material properties (denoted with P). As a result, the LC1000P-1/2 compositions were slightly varied for the second hybrid beam series S2, where LC mixtures LC1000 and LC1000A were used. The labeling of the LCs was chosen according to their density. An overview of the experimental investigation and experiment dates are given in Table B.1. For each LC type six cylinders were cast, three being used for determination of the Young's modulus and compressive strength, while splitting tensile tests were performed on the remaining three cylinders. In the case of the SLWAC compositions, three additional cubes were investigated under direct load transmission.

Table B.1: Experimental program.

Composition	LC type	Aggregate type	Date of experiment
LC900	SLWAC	F3 (85 Vol%), sand (15 Vol%)	06.07.2005
LC1300	SLWAC	F3 (70 Vol%), sand (30 Vol%)	19.07.2005
LC1000	ALWAC	F3 (50 Vol%), Liaver (50 Vol%)	30.06.2006
LC1000A	ALWAC	F3 (50 Vol%), Liaver (50 Vol%)	14.07.2006
LC1000P-1	ALWAC	F3 (55 Vol%), Liaver (45 Vol%)	04.11.2005
LC1000P-2	ALWAC	F2.9 (55 Vol%), Liaver (45 Vol%)	04.11.2005
LC1200P	ALWAC	F2.9 (55 Vol%), Liapor sand (45 Vol%)	04.11.2005

B.2.1 SLWAC compositions: LC900 and LC1300

Conventional sand lightweight concretes (SLWACs) with two different densities were used for the first series of hybrid beam experiments (S1) reported in Appendix C: LC900 (low density) and LC1300 (high density). Both mixtures consisted of sand, Portland cement CEM I 42.5 N, water and expanded clay lightweight aggregates F3 ($\varnothing = 4\text{-}8\,\text{mm}$, aggregate density $\rho_a = 550\text{-}650\ \text{kg/m}^3$) from Liapor, [Lia06]. Table B.2 gives the composition of LC900 and LC1300 and their macrostructure is shown in Figure B.2.

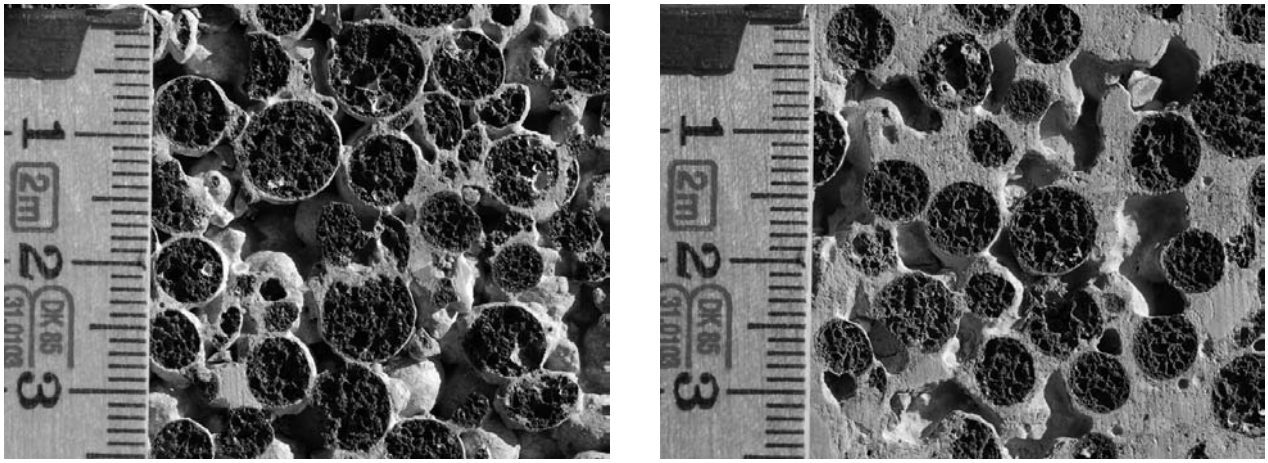

(a) LC900 (b) LC1300

Figure B.2: LC macrostructure.

Table B.2: Composition of LC900 and LC1300 in [kg/m^3].

LC type	Liapor F3	Sand	Cement	Water
LC900	400 (85 Vol%)	315 (15 Vol%)	250	95
LC1300	295 (70 Vol%)	570 (30 Vol%)	305	195

For each LC, six cylinders with a diameter of 16 cm and height of 32 cm were cast at the same time as the beams were cast. The cylinders were then stored in a climate room for 28 days at 20°C and 95% relative humidity. After the beam experiments, five cores of diameter 100 mm for each mixture were taken from the beams, mainly to investigate the degree of concrete compaction.

The rounded average densities of 900 and 1300 kg/m^3 were obtained from the cylinders and cores from each concrete mixture after the 28-day storage. The compressive strength and Young's modulus were determined according to Swisscode SIA 162/1 on three cylinders ($\varnothing = 160$ mm) of each mixture, while only the compressive strength was measured on the cores. The Young's modulus was always determined by the force-deformation response between zero and 1/3 of the compressive strength. Figure B.3-a shows the resulting stress-strain curves of all LC cylinders. Stiffness slightly but steadily decreased up to failure, which was more brittle for the lower density cylinders. Typical failed cylinders are shown in Figure B.3-b-c, indicating that failure occurred due to crushing of the lightweight aggregates. In addition, splitting tensile tests were performed on the remaining three cylinders of each mixture according to Swisscode SIA 262. The resulting material properties are summarized in Table B.3 (average values and standard deviations).

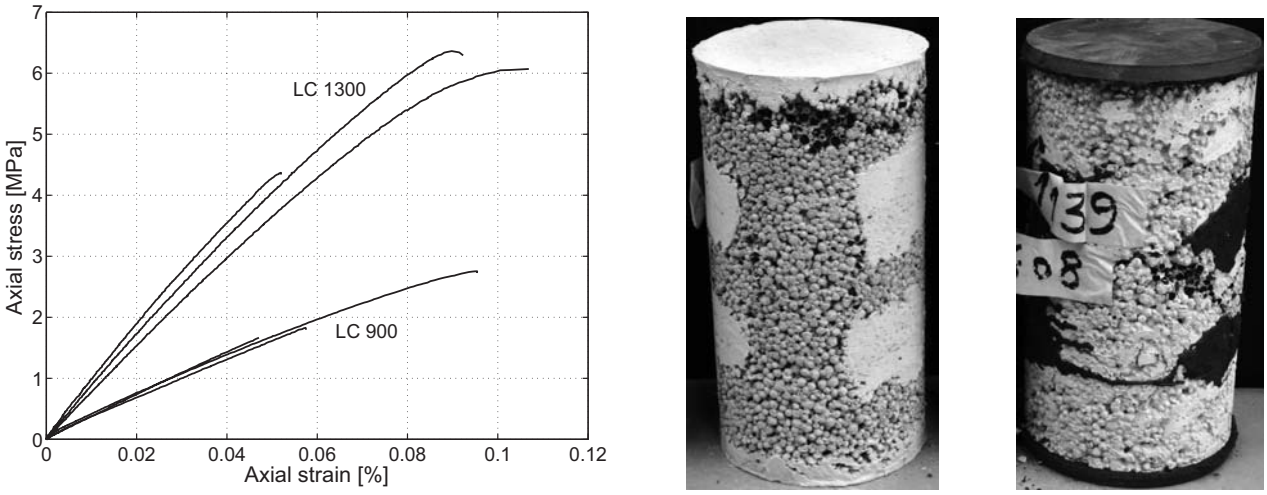

(a) (b) LC900 (c) LC1300

Figure B.3: Stress-strain curves of LC concretes and failed cylinders.

In addition to the experiments on the cylinders, direct shear experiments on three cubes of 140-mm side length for each lightweight concrete (denoted with -Q) were carried out using the Lombardi testing device, illustrated in Figure B.4-a. This testing device is actually used to determine the friction coefficient between two parts of rock, rather than to create a shear failure in concrete blocks. However, shearing experiments were performed on LC cubes

Table B.3: Material properties of LC900 and LC1300.

LC type	Density [kg/m^3]	Compressive strength [MPa]	Young's modulus [MPa]	Splitting tensile strength [MPa]
LC900	882 ± 10	2.10 ± 0.67	3463 ± 223	-
LC900-core	870 ± 19	2.00 ± 0.60	-	-
LC900-sp	943 ± 47	-	-	0.65 ± 0.07
LC1300	1294 ± 70	5.60 ± 1.20	8670 ± 1039	-
LC1300-core	1323 ± 100	6.30 ± 3.00	-	-
LC1300-sp	1297 ± 37	-	-	1.30 ± 0.17

for preliminary observations. The LC cube was embedded in a metal box with a cement, approximately 65 mm of the cube side thus being fixed in the metal box. After the cement had hardened, the whole unit was turned upside down and the remaining part of the LC cube was embedded approximately 65 mm deep in another metal box, leaving a cement-free gap of 10 mm (140 mm - 2x65 mm). After the other side had hardened, the boxes were placed in the Lombardi testing device in such a way that the gap between the metal boxes was horizontal. During the experiment, the upper metal box was pulled horizontally against the lower box at a relative displacement rate of 0.5 mm/min. The normal and tangential loads generated during shearing were recorded using a UPM60. Figure B.4-b illustrates the cracked LC cubes in the metal boxes after the experiment.

The normal load on the specimen was kept constant at approximately 0.05 MPa throughout the experiment. The tangential deformation of the specimen versus the shear stresses (calculated from the tangential loads divided by the specimen shearing surface) is illustrated in Figure B.5 and the shear strengths are summarized in Table B.4. When placing the LC1300-Q1 specimen in the testing device, a noise was heard which could indicate damaging of the cube before the experiment and explain the low ultimate value of 0.7 MPa. The great variation in the LC1300 results made the use of these values for further modeling impossible.

Table B.4: Direct shear strengths of LC900 and LC1300.

LC type	Shear strength [MPa]
LC900-Q	0.73 ± 0.04
LC1300-Q	1.27 ± 0.56

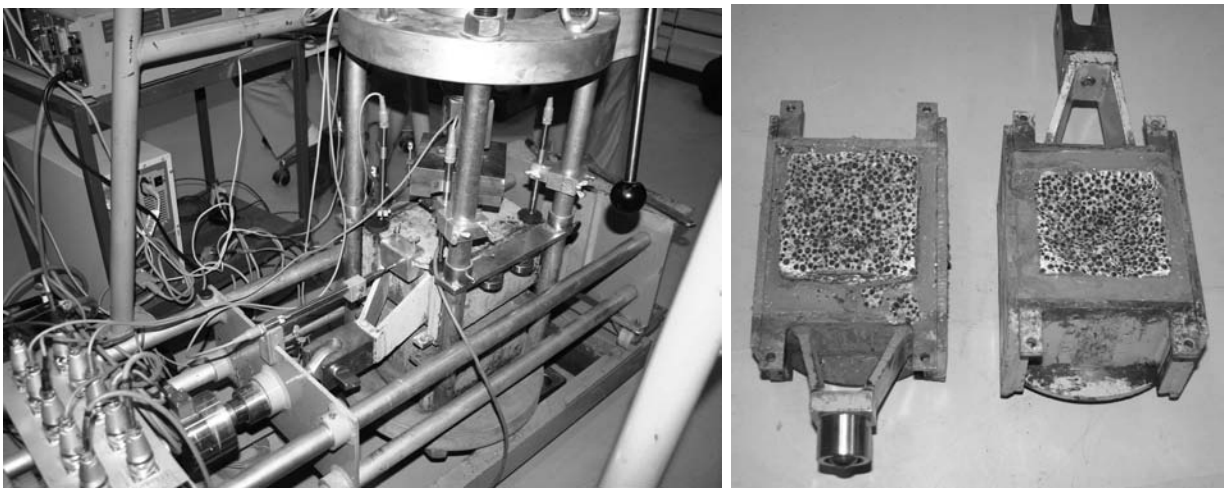

(a) Lombardi testing device

(b) LC cubes embedded in metal boxes after shear experiment

Figure B.4: Shear experiments on lightweight concrete cubes.

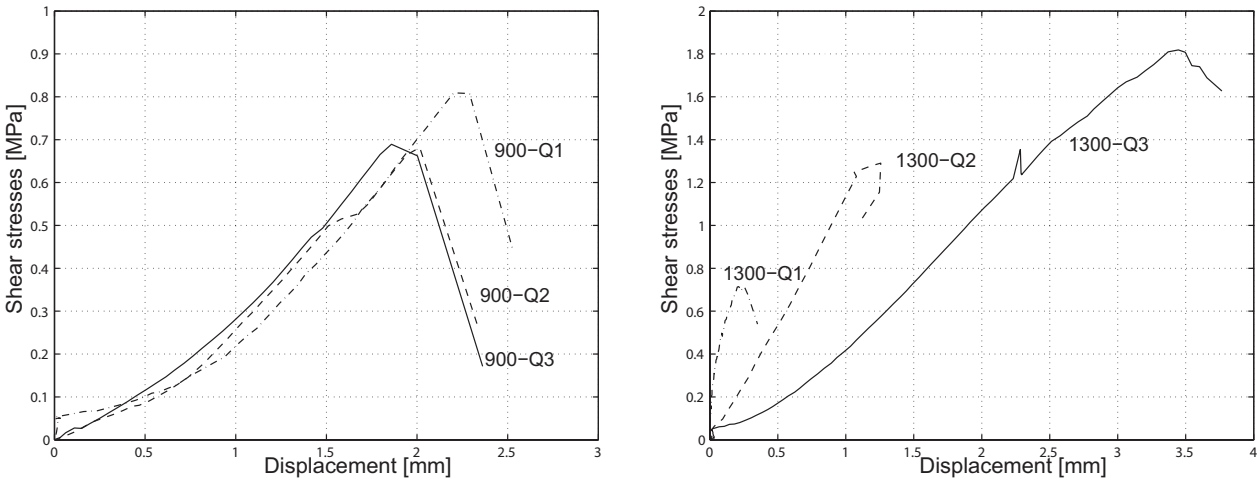

(a) 900-Q

(b) 1300-Q

Figure B.5: Shear stresses of lightweight concrete cubes.

B.2.2 ALWAC compositions: LC1000 and LC1000A

The ALWAC concrete LC1000 used for the second beam series (S2), see Appendix C, consisted of F3 expanded clay aggregates (Ø = 4-8 mm, aggregate density $\rho_a = 550\text{-}650\,\text{kg/m}^3$), Liaver expanded glass (Ø = 1-2 mm and 2-4 mm, aggregate densities $\rho_a = 350$ and $310\,\text{kg/m}^3$, respectively), both supplied by Liapor [Lia06], Portland cement CEM I 42.5, filler (ZEOTOP supplied by Hauri, Switzerland), additives (1.0% Sikament-10 plasticizer and 0.5% Sika Stabilizer-229, both supplied by Sika, Switzerland) and water. The LC macrostructure is shown in Figure B.6.

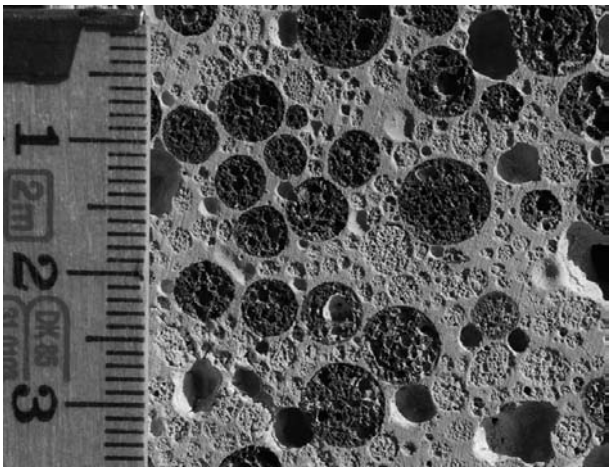

Figure B.6: LC1000 macrostructure.

Table B.5: Composition of LC1000 in [kg/m^3].

LC type	Liapor F3 (4-8 mm) 50 Vol%	Liaver (1-2 mm) 25 Vol%	Liaver (2-4 mm) 25 Vol%	Cement	Filler	Water
LC1000	261	55	49	452	50	173
LC1000A	261	56	50	452	50	173

The beams incorporating LC1000 were cast on two different dates: beams 1000 and 1000E were manufactured on 30.06.2006 using the LC1000 as the LC core, whereas beams 1000A and 1000EA with the anchor blocks were cast on 14.07.2006 using LC1000A, see Appendix C. For each LC six cylinders with a diameter of 16 cm and height of 32 cm were cast and tests to determine the compressive strength and Young's modulus were performed according to Swisscode SIA 162/1 after 28 days. Figure B.7 shows the resulting stress-strain curves of all LC cylinders. Stiffness decreased slightly but steadily up to the brittle failure. A typical failed

cylinder is shown in Figure B.8, indicating a clear failure through the cylinder due to crushing of the lightweight aggregates and the cementitious matrix. In addition, splitting tensile tests were performed on the remaining three cylindrical specimens according to Swisscode SIA 262. The resulting material properties are summarized in Table B.6 (average values and standard deviations).

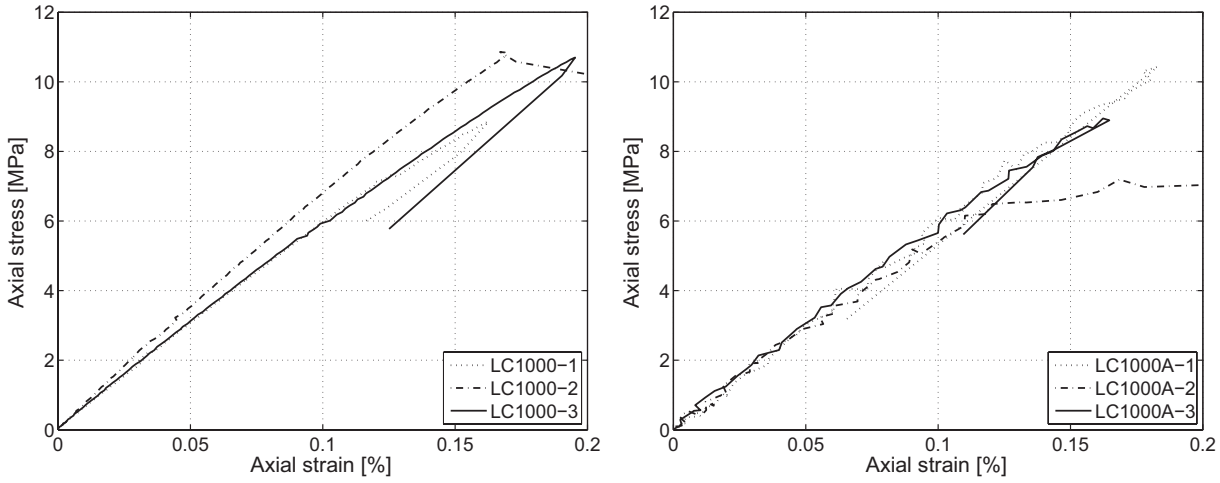

(a) LC1000 (b) LC1000A

Figure B.7: Stress-strain curves of LC concretes.

Table B.6: Material properties of LC1000 and LC1000A.

LC type	Density [kg/m^3]	Compressive strength [MPa]	Young's modulus [MPa]	Splitting tensile strength [MPa]
LC1000	1003 ± 1	10.28 ± 1.14	6586 ± 461	-
LC1000-sp	1001 ± 4	-	-	1.44 ± 0.10
LC1000A	991 ± 5	9.03 ± 1.66	6248 ± 175	-
LC1000A-sp	987 ± 6	-	-	1.24 ± 0.11

Figure B.8: Typical failed LC1000 cylinder.

B.2.3 ALWAC compositions: LC1000P-1/2

The preliminary research investigation of the ALWAC LC1000P-1 and LC1000P-2 provided the basis for the LC1000 and LC1000A compositions used in beam series S2. The mixtures consisted of both expanded clay and expanded glass, as indicated in Table B.7. While for LC1000P-1 the F2.9 aggregate from Liapor ($\varnothing = 2\text{-}8\,\text{mm}$, aggregate density $\rho_a = 500$ kg/m^3) was used, the LC1000P-2 was again composed of F3 aggregates. Both ALWACs were composed of the same Liaver expanded glass aggregates as previously described, Portland cement CEM I 42.5, fly ash, additives (1.0% Sikament-10 plasticizer and 0.5% Sika Stabilizer-229, both supplied by Sika, Switzerland) and water.

Table B.7: Composition of LC1000P-1/2 in [kg/m^3].

Type	Lightweight aggregate 55 Vol%	Liaver (1-2 mm) 22.5 Vol%	Liaver (2-4 mm) 22.5 Vol%	Cement (Filler)	Water
LC1000P-1: F2.9 (2-8 mm)	207	52	41	450 (50)	177
LC1000P-2: F3 (4-8 mm)	225	52	41	450 (50)	177

For each composition, three to four cylinders with a diameter of 16 cm and height of 32 cm were cast and tests to determine the compressive strength and Young's modulus were performed according to Swisscode SIA 162/1 after 28 days. Splitting tensile tests were performed on the remaining three cylindrical specimens according to Swisscode SIA 262. The resulting material properties are summarized in Table B.8 (average values and standard deviations) and illustrated in Figure B.9.

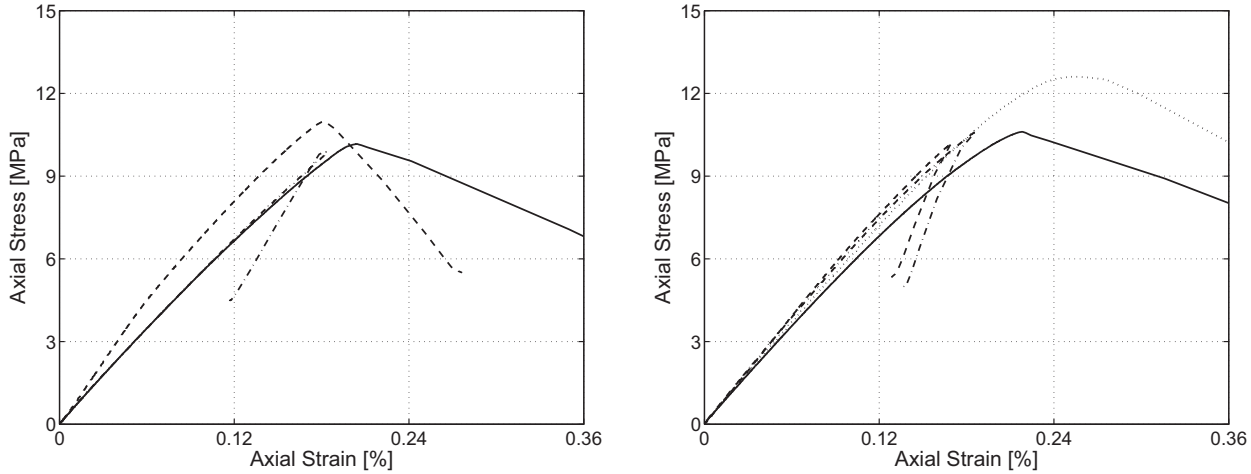

(a) LC1000P-1 (b) LC1000P-2

Figure B.9: Stress-strain curves of LC concretes.

Table B.8: Material properties of LC1000P-1/2.

LC type	Density [kg/m^3]	Compressive strength [MPa]	Young's modulus [MPa]	Splitting tensile strength [MPa]
LC1000P-1	980 ± 10	10.49 ± 0.58	6485 ± 1123	-
LC1000P-sp-1	1037 ± 21	-	-	1.56 ± 0.02
LC1000P-2	992 ± 22	11.28 ± 1.04	6361 ± 282	-
LC1000P-sp-2	1073 ± 38	-	-	1.77 ± 0.20

B.2.4 ALWAC composition: LC1200P

The LC1200P composition was similar to LC1000P-1 and LC1000P-2, but instead of Liaver expanded glass aggregates, the Liapor SL lightweight sand ($\varnothing = 0$-4 mm, aggregate density $\rho_a = 1100$-1300 kg/m^3) made of crushed Liapor aggregates was used. The resulting material properties are summarized in Table B.10 (average values and standard deviations determined on three to four cylinders) and illustrated in Figure B.10. Since the LC1200P composition attained higher densities than the previously described compositions, this mixture was not used for the beam experiments.

Table B.9: Composition of LC1200P in [kg/m^3].

LC type	Lightweight aggregate 55 Vol%	Lightweight sand (0-4 mm) 45 Vol%	Cement (Filler)	Water
LC1200P: F2.9 (2-8 mm)	229	408	400 (-)	206

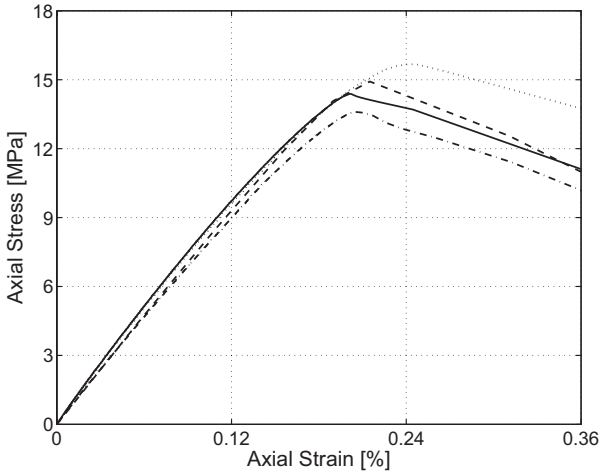

Figure B.10: Stress-strain curves of LC1200P.

Table B.10: Material properties of LC1200P.

LC type	Density [kg/m^3]	Compressive strength [MPa]	Young's modulus [MPa]	Splitting tensile strength [MPa]
LC1200P	1236 ± 13	14.34 ± 1.10	8302 ± 432	-
LC1200P-sp	1263 ± 40	-	-	2.02 ± 0.39

B.3 Face layer materials

B.3.1 Top layer: normal concrete (NC)

B.3.1.1 NC used for SLWAC beams - S1

The compression zone of the SLWAC beams (S1) consisted of a thin layer of normal performance concrete (NC) composed of gravel (4-8 mm), the Flextremo 3R cement mixture, sand and water. Flextremo 3R is a Portland cement mixture CEM II/B-M (V-LL) 32.5 R developed by Holcim, Switzerland, which consists of cement clinker, high-quality limestone, silicic acid-rich hard coal fly ash and powdered additive.

The Flextremo 3R content of the NC was 450 kg/m^3. The water/cement ratio was approximately $w/c = 0.4$. The compressive strength and Young's modulus were investigated on three cylinders with a diameter of 16 cm and height of 32 cm and are summarized in Table B.11 (average values and standard deviations).

Table B.11: Material properties of normal concrete for series S1.

NC type	Density [kg/m^3]	Compressive strength [MPa]	Young's modulus [MPa]
NC-900	2327 ± 13	46.42 ± 1.30	29896 ± 2989
NC-1300	2317 ± 17	45.06 ± 0.82	31172 ± 1292

B.3.1.2 NC used for ALWAC beams - S2

The NC layer used for the ALWAC specimens (beam series S2) consisted of Portland cement (CEM I 52.5 R), a plasticizer from Pieri, filler (ZEOTOP supplied by Hauri, Switzerland), gravel (4-16 mm), sand (0-4 mm), and water.

Table B.12: Material properties of normal concrete for series S2.

NC type	Density [kg/m^3]	Compressive strength [MPa]	Young's modulus [MPa]	Splitting tensile strength [MPa]
NC-1000	2327 ± 6	59.7 ± 1.8	30833 ± 764	-
NC-1000A	2370 ± 6	53.4 ± 0.8	27052 ± 4400	-
NC-1000A-sp	2370 ± 0	-	-	3.09 ± 0.2

The cement content was 420 kg/m^3, and filler content 80 kg/m^3. The water/cement ratio was approximately $w/c = 0.571$. The compressive strength and Young's modulus were

investigated on three cylinders with a diameter of 16 cm and height of 32 cm. Additional splitting tensile tests were performed on three cylinders from the NC-1000A. The resulting material properties are summarized in Table B.12 (average values and standard deviations).

B.3.2 Bottom layer: glass fiber-reinforced polymer (GFRP) profile

The 40HDx500 GFRP Plank profile from Fiberline with 8 T-upstands, shown in Figure B.11, was used for the hybrid beam experiments. The Plank profile consisted of E-glass fibers (approximately 45% by vol.) and a polyester resin, [Fib04], exhibiting a Young's modulus, E, of 23000 MPa in the fiber direction and a tensile strength, f_t, of approximately 240 MPa.

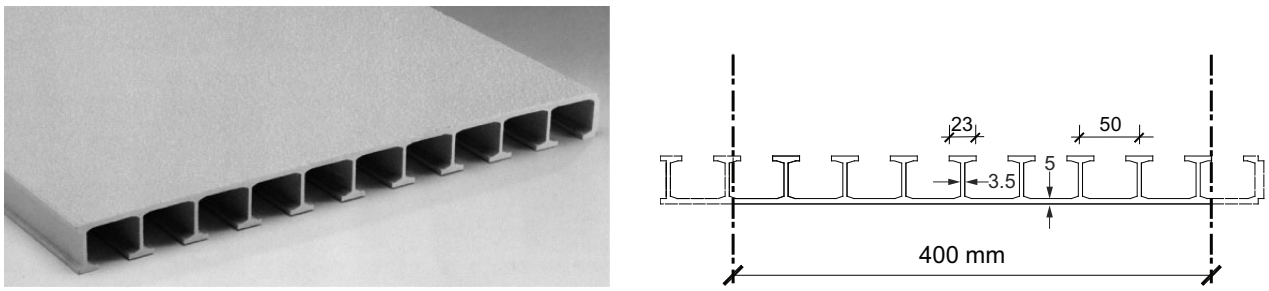

(a) 40HDx500 Plank profile (b) Profile dimensions

Figure B.11: GFRP Plank profile.

Table B.13: Geometric properties of GFRP Plank profile.

A [mm^2]	I$_y$ [mm^4]	Neutral axis y$_s$ [mm]	W$_{y,top}$ [mm^3]	W$_{y,bottom}$ [mm^3]
3615	8.51x10^5	15	56019	34315

The Plank profile weighed approximately 17 kg/m^2. The dimensions of the GFRP profiles used in the experiments was 3600 mm x 400 mm. Therefore both sides of the 40HDx500 Plank profile were cut off as shown in Figure B.11-b. The sheet thickness was 5 mm, the thickness and height of the T-upstands were 3.5 and 40 respectively, the distance between them 50 mm, and the total weight 17 kg/m^2. The geometric properties of the Plank are given in Table B.13.

B.3.3 Epoxy resin for GFRP-LC interface

For the GFRP-LC interface the SikaDur 330 cold-cured two-component epoxy resin from Sika was used. The mechanical properties were investigated at the Composite Construction Laboratory and are given in Table B.14 [KV05a].

Table B.14: Properties of SikaDur 330.

	SikaDur 330
Compressive strength [MPa]	80
Young's modulus in compression [MPa]	3000
Tensile strength [MPa]	38
Young's modulus in tension [MPa]	4550

Appendix C

Experiments on long-span beams on DVD

C.1 Introduction

The long-span beam experimental program consisted of two series: S1 and S2 using SLWAC and ALWAC compositions as core materials respectively. S1 consisted of eight and S2 of four 3600-mm-long, 400-mm-wide and 200-mm-deep beams. For details concerning material properties see explanation in Appendix B.

C.1.1 Objectives

The experimental investigation focused on the following parameters:

- the influence of the lightweight concrete (LC) type on load-bearing behavior;
- the influence of the FRP-LC interface type: either unbonded or adhesively bonded;
- the influence of anchor blocks on the supports (S2 beam series).

C.1.2 Experimental program

In the S1 series, SLWAC compositions with average densities of 900 and 1300 $\mathrm{kg/m^3}$ were used (low and high density). Two types of FRP-LC interfaces were also investigated: unbonded and adhesively bonded. The weight of the beams with lower LC density was 230 $\mathrm{kg/m^3}$ and that of those with higher density 290 $\mathrm{kg/m^3}$, thus constituting 46 and 58% respectively of the weight of a normal concrete beam of the same depth (weight 500 $\mathrm{kg/m^3}$).

In S2 an ALWAC mixture was used, for which a low density of 1000 $\mathrm{kg/m^3}$ and considerably improved compressive strength could be obtained by replacing the sand aggregates with expanded glass aggregates. Four types of LC-FRP interfaces were investigated in S2: pure mechanical interlocking between the LC and FRP T-upstands and adhesive bonding as already investigated in S1 plus two additional LC-FRP connections: the LC over the supports

was replaced by NC anchor blocks, which was predicted to prevent both the LC-FRP debonding at this location (observed for unbonded S1 beams) and crack propagation over the support (observed for bonded S1 beams). The geometry of the NC anchor blocks is shown in Figure C.1. For one experiment, the FRP-NC and FRP-LC interfaces were adhesively bonded (similarly to the bonded beams of S1) and for the second experiment, only the FRP-NC interfaces were adhesively bonded, the LC-FRP interface (between the anchor blocks) remaining unbonded (mechanical interlocking only). Table C.1 gives an overview of all investigated beam configurations and their labels. For each configuration two beams were examined in S1 (the first one fully and the second one low instrumented) and one beam in S2.

Table C.1: Experimental configurations (* rounded values).

Beam series	Beam labeling	LC type	LC density [kg/m^3]*	FRP-LC interface	NC anchor blocks	Date of experiment
S1	900-1/2	SLWAC	900	unbonded	no	16.08./26.08.2005
S1	900E-1/2	SLWAC	900	bonded	no	17.08./31.08.2005
S1	1300-1/2	SLWAC	1300	unbonded	no	22.08./05.09.2005
S1	1300E-1/2	SLWAC	1300	bonded	no	23.08./08.09.2005
S2	1000	ALWAC	1000	unbonded	no	16.08.2006
S2	1000E	ALWAC	1000	bonded	no	18.08.2006
S2	1000A	ALWAC	1000	unbonded	yes	22.08.2006
S2	1000EA	ALWAC	1000	bonded	yes	25.08.2006

C.2 Experimental specimens

C.2.1 Dimensions

Three-point bending experiments were performed on hybrid beam specimens with a length of 3.6 m, span of 3.0 m, depth of 200 mm and width of 400 mm. Hence the shear span-to-depth ratio was $a/d = 8$, where a is the distance from the load axis to the support axis, and d the effective depth. The GFRP Plank profile has a maximum depth of 40 mm, while the upper layer of normal concrete (NC) is 30 mm deep. In the case of two ALWAC beams, anchor blocks were cast using an NC over the supports. The dimensions of the different beams and their cross section are shown in Figures C.1 and C.2.

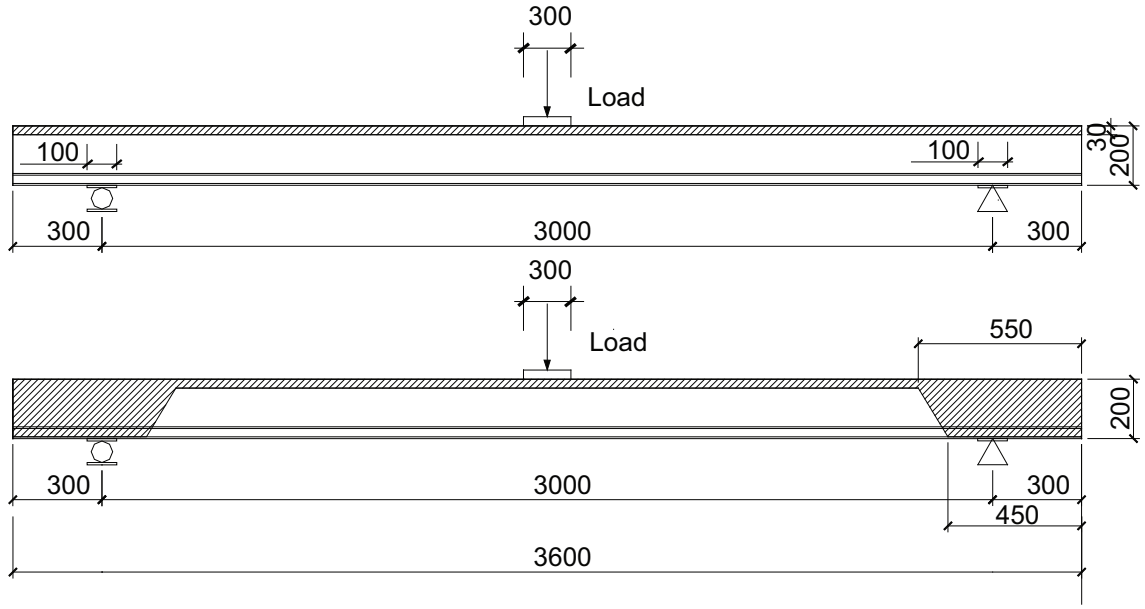

Figure C.1: Dimensions of hybrid beam specimens: above without anchor blocks, below with anchor blocks.

C.2.2 Manufacture

The SLWAC beams (S1 series) were cast at the Holcim concrete plant in Morges: the beams comprising an LC900 core were fabricated on 6.07.2005, while the beams comprising the LC1300 were cast on 19.07.05. The ALWAC beams (S2 series) were cast at the Prebeton prefabrication company in Avenches on two different days. Beams 1000 and 1000E were manufactured on 30.06.2006, while the beams with the anchor blocks, 1000A and 1000AE, were cast on 14.07.2006. The specimens were manufactured in four main steps as described below:

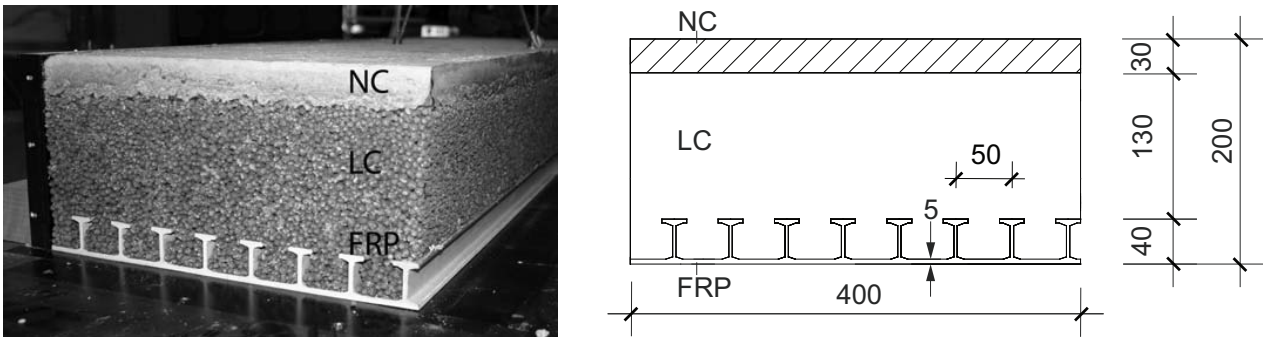

(a) Section (b) Cross section with dimensions

Figure C.2: Cross section of hybrid beam specimen.

Step 1 The manufacture of the experimental beams started with the preparation of the GFRP Plank profiles in the laboratory at EPFL. For the unbonded beams, the positions of the

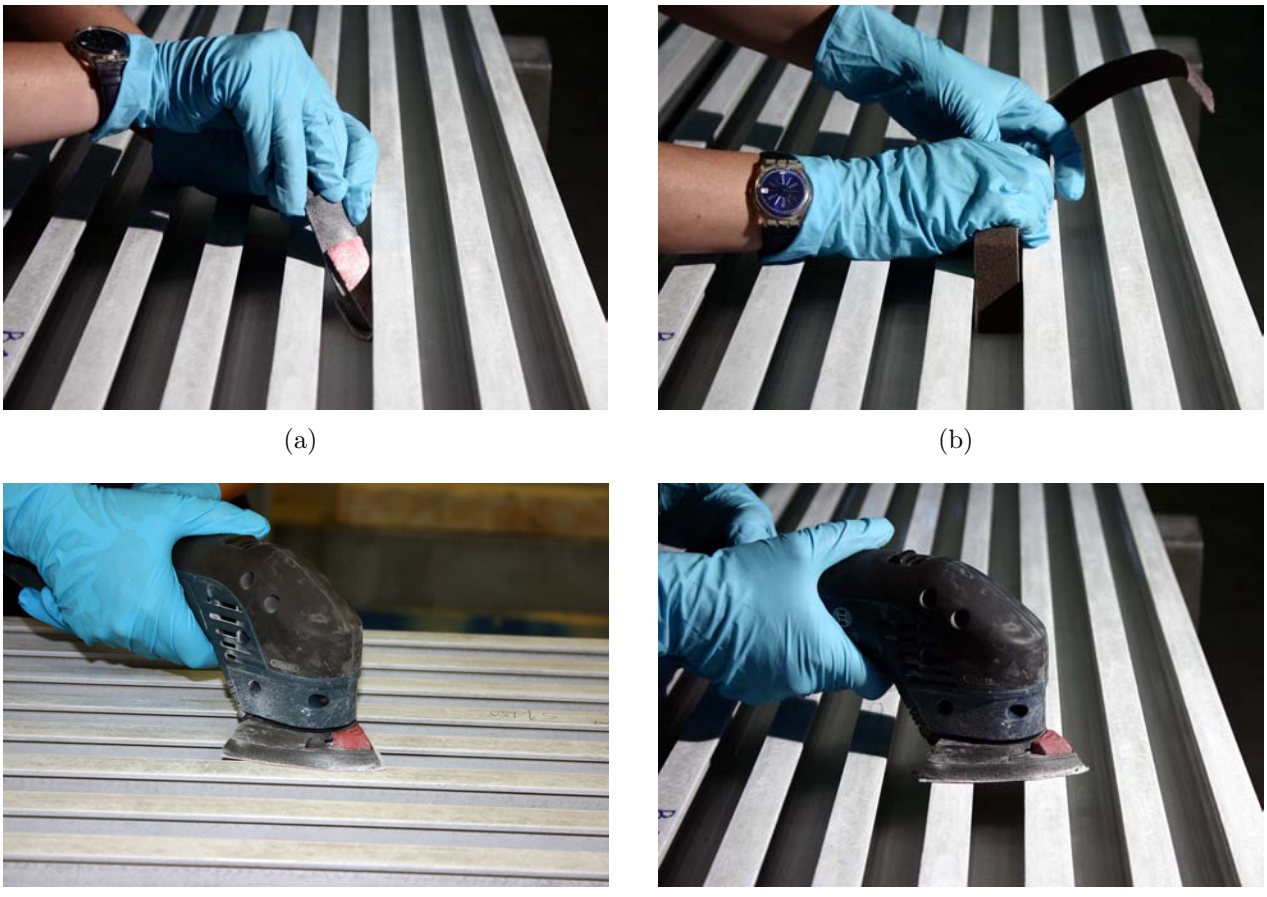

(a) (b)

(c) (d)

Figure C.3: Preparation of GFRP profiles: roughening between T-upstands (above) and of T-upstand surfaces (below).

strain gages were marked and roughened using emery paper. During the roughening process, special care was taken not to damage the rovings. In the case of the bonded beams, the GFRP surface was roughened using a grinding machine on the T-upstands and emery paper in between, as shown in Figure C.3. The marked strain gage positions were then degreased with acetone to remove deposited abrasive particles. Subsequently, the strain gages were glued, wired and protected against humidity and destructive agents using a special kit from HBM (Hottinger Baldwin Messtechnik GmbH, Germany), see Figure C.4. The GFRP profiles were then integrated into a timber formwork in the laboratory. For beams 1000A and 1000EA a special formwork - in the shape of the anchor block - was installed to protect the anchor blocks from the LC casting.

(a) Gluing of strain gages (b) Instrumented GFRP profiles

Figure C.4: Preparation of GFRP profiles, continuation.

Step 2 At a concrete plant, the epoxy adhesive was applied and the lightweight concrete was cast onto the wet epoxy for the bonded specimens, or directly onto the GFRP surface for the unbonded beams. Figure C.5 shows the application of the epoxy adhesive onto the top of the GFRP sheet and T-upstands, while for practical reasons approximately only the lower half of the webs was covered.

Step 3 After casting the LC onto the GFRP profile, the LC was compacted using a vibrator. Since the compacting proved very difficult however, particularly for the lower density LC, the LC was also compacted using a trowel. The LC surface was flattened using a specially prepared board, guaranteeing an NC depth of precisely 30 mm, as shown in Figure C.6.

Step 4 For the beams without anchor blocks, the NC layer was then applied directly onto the fresh LC. The fluid composition of the thin NC layer allowed good distribution over the beam, see Figure C.7. For beams 1000A and 1000EA the anchor formworks were removed after the LC had been compacted, the epoxy adhesive was then applied onto

(a) Applying epoxy adhesive

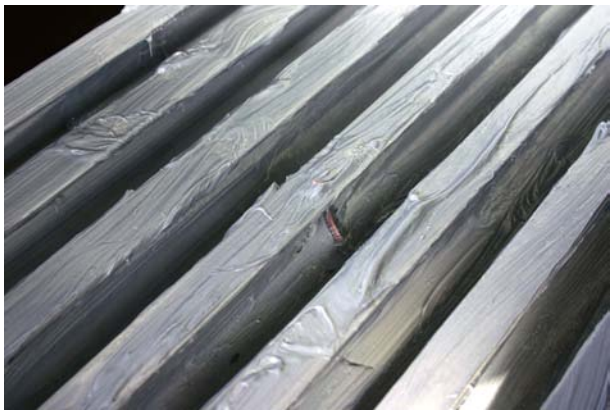

(b) Fresh epoxy on GFRP profile

Figure C.5: Applying epoxy adhesive onto GFRP profile at concrete plant.

(a) LC casting

(b) LC casting onto fresh epoxy adhesive

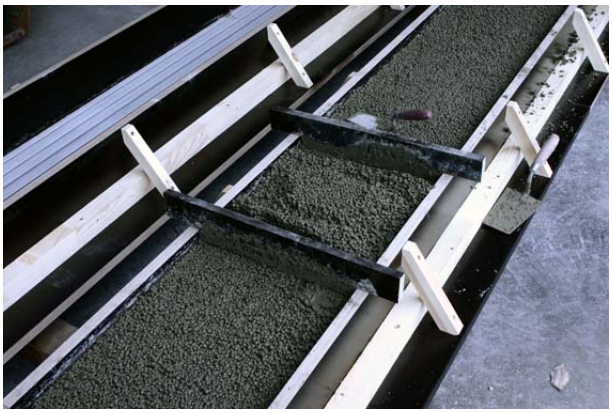

(c) LC leveling

(d) LC flattening

Figure C.6: LC casting onto GFRP profiles.

the GFRP profiles and the NC was subsequently cast at the beam ends and onto the fresh LC layer. Figure C.8 illustrates the casting of the anchor blocks.

(a) (b)

Figure C.7: NC casting onto fresh LC layer.

(a) Epoxy adhesive on GFRP profile (b) NC casting of anchor blocks and upper layer

Figure C.8: Casting specimens with anchor blocks.

C.3 Experimental procedure

C.3.1 Test setup and loading equipment

All beams were simply supported on rollers with a span length of 3.0 m and subjected to three-point bending via one hydraulic jack with a capacity of 1000 kN in static loading and a possible displacement range of up to ±125 mm. The load was applied at mid-span, 1.5 m from the support. The beam geometries and the experimental setup in the laboratory are shown in Figures C.1, C.2 and C.9. The experiments were conducted in a laboratory environment at room temperature (20°C) without any impact of temperature changes or moisture.

Figure C.9: Experimental setup.

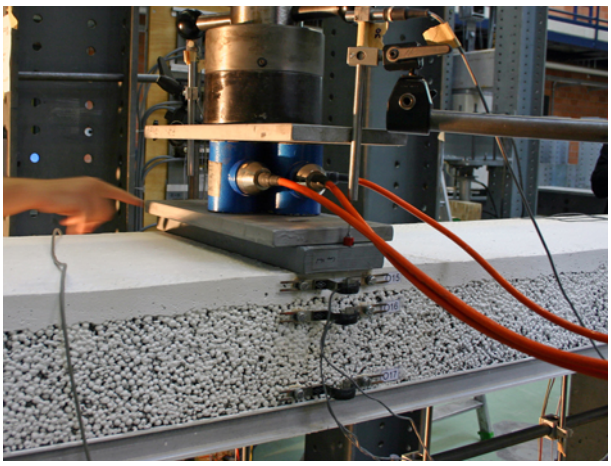

(a) Loading condition of beam 900-1

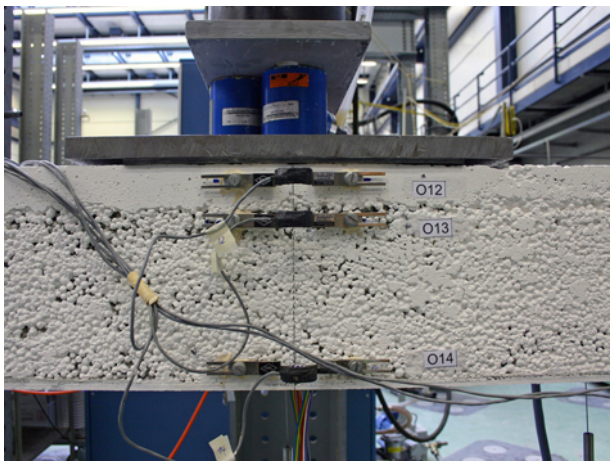

(b) Loading condition of all other beams

Figure C.10: Load distribution via a steel loading plate.

During the first experiment on beam 900-1, the load was introduced via a 15-mm-thick steel loading plate of $115 \times 400\,mm^2$, shown in Figure C.10-a). As the small loading plate was found to lead to an unfavorable load distribution, a wider loading plate was chosen for the following seven experiments. The load was then introduced via a steel loading plate of $20 \times 300 \times 400\,mm^3$ on a 10-mm-thick neoprene layer, as shown in Figure C.10-b).

The experimental beams were subjected to a constant displacement rate of 1 mm/min until failure. In order to investigate whether irreversible damage occurred during the loading process, load cycles were performed for beams 1300-2, 1300E-2, 900-1, 900E-2, 1000, 1000E and 1000A.

C.3.2 Instrumentation

All tests were performed with automated measurements taken every 9-10 s. The data acquisition unit was an HBM (Hottinger Baldwin Messtechnik GmbH, Germany) UPM 60 with 60 channels. The data acquisition was performed using the LABVIEW program, enabling the test evolution to be followed and the measurements to be displayed on different graphs throughout the experiment. The recorded data were: the load of the jack using three load cells, displacement at several sections of the beam using linear voltage displacement transducers (LVDTs), axial strains in the GFRP profile measured with strain gages, and deformation on the LC and NC surfaces using omega-shaped extensometers.

C.3.2.1 Instrumentation of S1 series

Each SLWAC beam of the S1 series was instrumented with displacement transducers, omega-shaped extensometers and strain gages. For each configuration two beams were investigated. The first SLWAC beams were always less instrumented (low) than the second SLWAC beams (full). The labeling and position of the instrumentation are shown for the low-instrumented beams in Figures C.11 and C.12, while Figures C.13 and C.14 illustrate the fully equipped specimens.

Linear voltage displacement transducers - S1

Linear voltage displacement transducers (LVDTs) from HBM of type W50 (± 50 mm with an accuracy of ± 0.10 mm) were used to measure vertical displacements within the span, vertical settling displacements on support sections and horizontal displacements at beam ends.

The D1-D5 displacement transducers were placed on the bottom centerline of the beam to measure vertical displacements at mid-span and within the span at distances of 375 mm. The DO displacement transducer was placed on the support on the top centerline of the beam, i.e. on the normal concrete layer. All beams except 900-1 were instrumented with D6, a

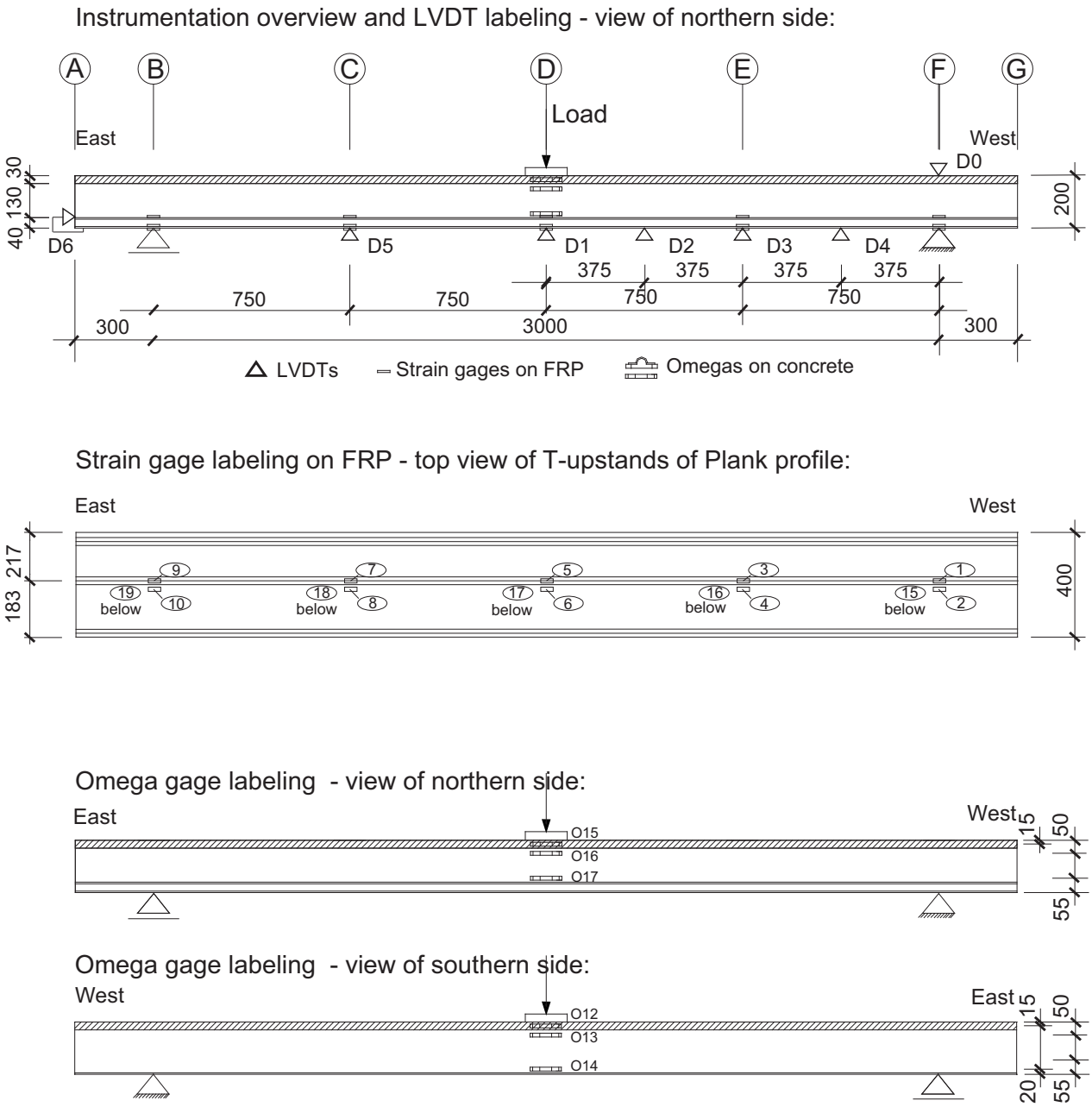

Figure C.11: S1 series: Instrumentation low-equipped.

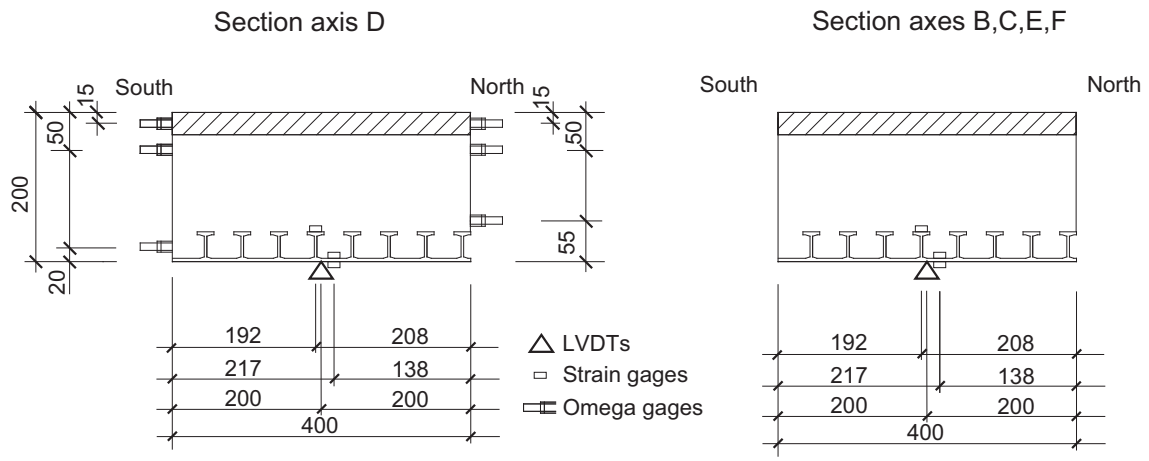

Figure C.12: S1 series: Instrumentation low equipped - section.

horizontal displacement transducer, at one end to measure whether the LC was pushed out of the GFRP profile. On the fully equipped beams an additional displacement transducer D7 was placed horizontally to measure the displacement between the normal concrete and GFRP profile.

Axial strain measurements on the GFRP profile - S1

The axial strain gages glued to the GFRP profile were of type 6/120LY11 produced by HBM. The connecting areas were roughened and degreased and gage positions precisely defined and marked before the gages were applied using an appropriate adhesive. The 6/120LY11 has a 2.8 mm x 6 mm measuring grid, 13 mm x 6 mm measuring-grid carrier and an electric resistance of 120 Ω.

Omega-shaped extensometers - S1

The omega-shaped extensometers glued onto the concrete surface were of type PI-2-100 produced by TML (Tokyo Sokki Kenkyujo Co., Ltd., Japan). The transducers were applied using an appropriate adhesive. The PI-2-100 has a capacity of ±2 mm and an electric resistance of 350 Ω (accuracy ±0.01 mm). The low-instrumented beams were equipped with 6 omega-shaped extensometers at mid-span (axis D), three on the northern side and three on the southern side of the beams. On each side the omegas were positioned to measure the axial deformations over a gage length of 100 mm on the NC surface and on the upper and lower zones of the LC, as shown in Figure C.12.

In the fully instrumented beams the concrete deformations are also measured at the fourth points and the supports (axes B, C, E, F). The upper deformation measurements were taken on

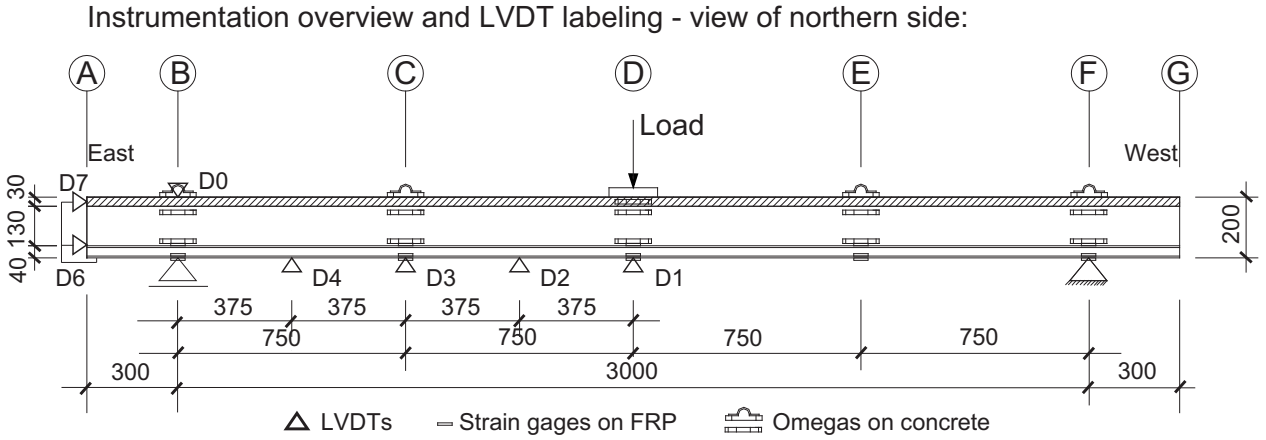

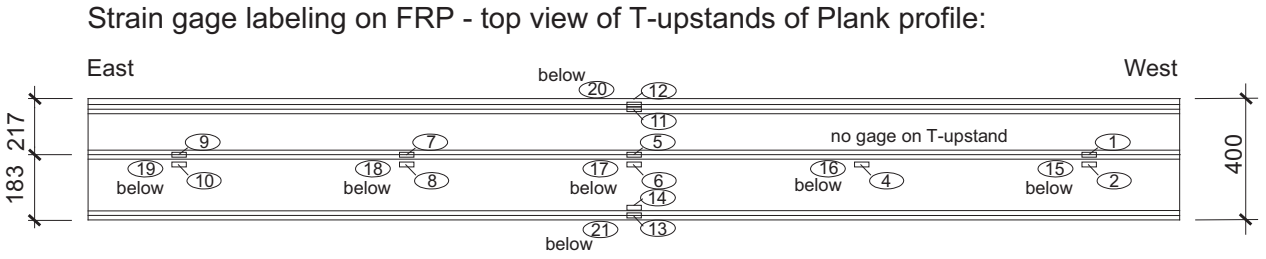

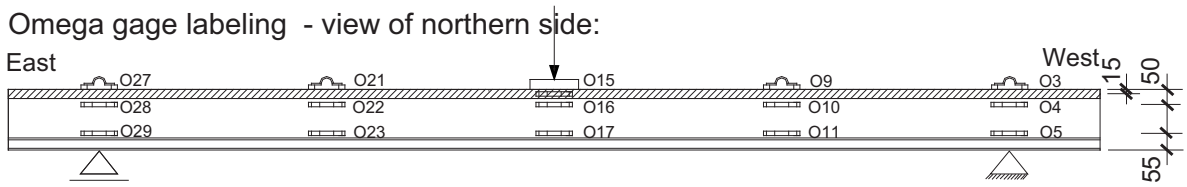

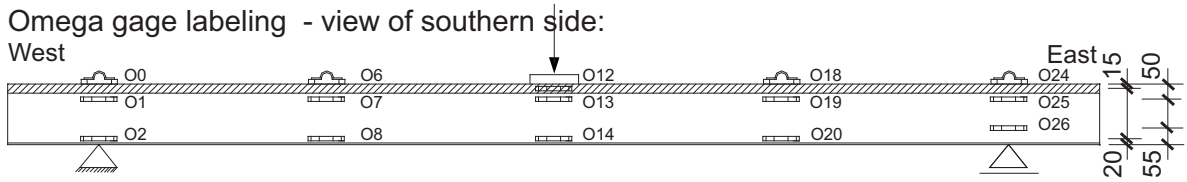

Figure C.13: S1 series: Instrumentation fully equipped.

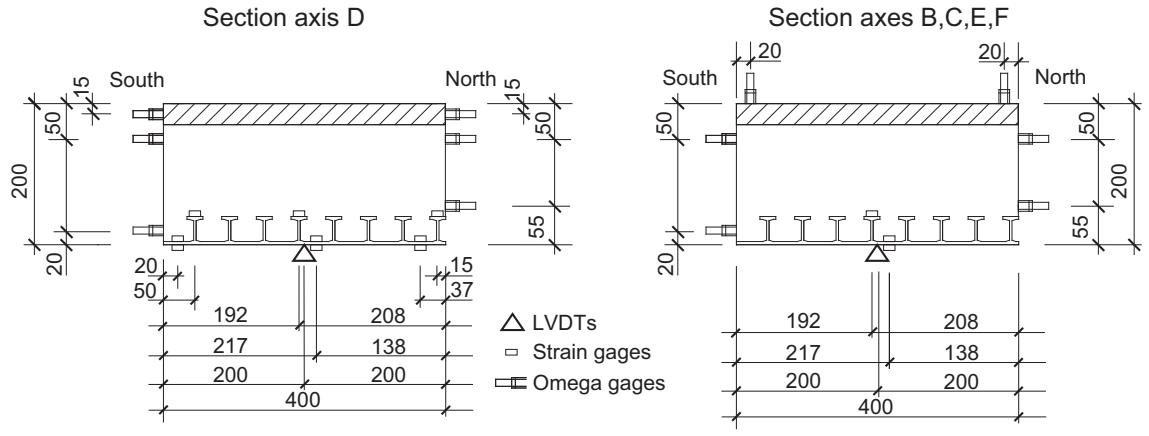

Figure C.14: S1 series: Instrumentation fully equipped - section.

the NC surface, except at mid-span. Their labeling and positions are indicated in Figures C.13 and C.14.

C.3.2.2 Instrumentation of S2 series

Each beam of the S2 series was again instrumented with displacement transducers (LVDTs), omega-shaped extensometers on the concrete and strain gages on the GFRP Plank profile. Figure C.15 shows the position and labeling of the instrumentation for the experiments, while Figure C.16 shows the cross section at mid-span and the different axes.

Linear voltage displacement transducers - S2

The same W50 displacement transducers as applied in S1 were used to measure vertical displacements in the span, vertical settling displacements on support sections and horizontal displacements at beam ends. The location of the displacement transducers is shown in Figures C.15 and C.16. The D2-D8 displacement transducers were placed on the bottom centerline of the beams to measure vertical displacements at the mid-span and every 375 mm of the beam. Displacement transducers D1 and D9 were placed over the support on the top centerline of the NC layer. All beams were instrumented with the horizontal displacement transducers D0 and D10 at the ends to measure slippage between the LC and GFRP profile.

Axial strain measurements on the GFRP profile - S2

The same axial strain gages as those applied in the S1 beam series were glued to the GFRP profile. The strain gages were stuck onto the T-upstand next to the centerline of the GFRP Plank profile and the outer bottom surface of the GFRP profile.

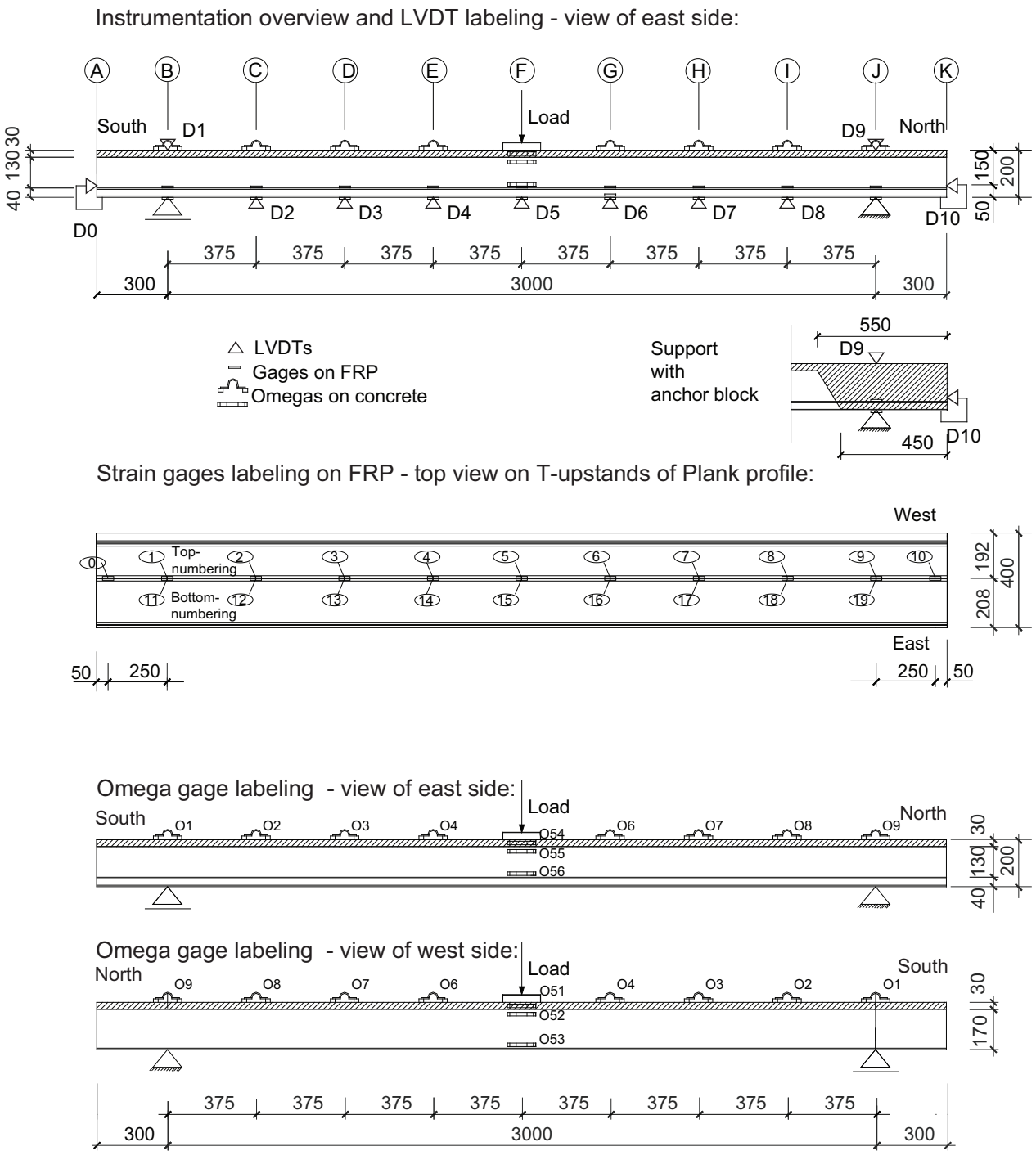

Figure C.15: S2 series: Instrumentation.

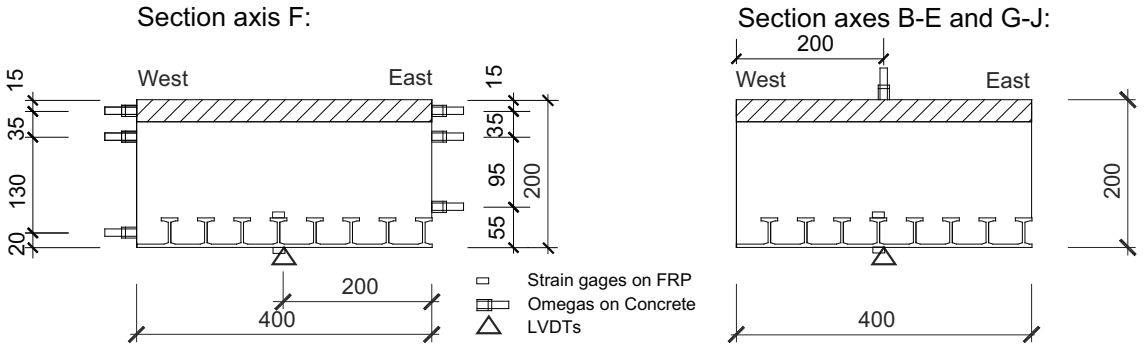

Figure C.16: S2 series: Instrumentation - section.

Omega-shaped extensometers - S2

The PI-2-100 omega-shaped extensometers (see S1 series) were glued onto the concrete surface using an appropriate adhesive. At mid-span, the beams were equipped with 6 omega-shaped extensometers, three on the northern side of the beams and three on the southern side. On each side the omega-shaped extensometers were positioned to measure the axial strains on the NC surface and on the upper and lower zones of the LC, as shown in cross section. In order to measure the strains in the NC layer, omega-shaped extensometers were placed every 375 mm on each side on the centerline of the beam.

C.4 Results of S1 series

C.4.1 Beam 900-1: Failure description and measured results (low instrumentation)

C.4.1.1 Failure description

The failure process of beam 900-1 is illustrated in Figures C.17, C.18, C.19 and C.20. This started with audible inner cracking at a load of 5.0 kN. The first obvious cracks appeared at a load of 6.8 kN at mid-span (Figure C.17-b). The ultimate load was reached at $F_u = 9.3$ kN with corresponding deflections of 11.5 mm to 17.3 mm. At this time only very small, short cracks could be observed in the tension zone at distances of up to 45 cm from the mid-span (Figure C.17-c).

Further jack displacement did not increase the load, which remained between 8.5 and 9.0 kN. The cracks started to propagate throughout the LC layer, followed by the LC debonding from the GFRP profile, and the LC being pushed out of the GFRP profile (Figure C.17-d-f). The load dropped to below 7 kN, when one of the cracks on the east side of the beam started to open significantly. It started in the tension zone in the LC at 42 cm east of the mid-span (Figure C.18-a), propagated nearly vertically towards the NC layer and horizontally along the top of the T-webs. Subsequently the crack developed horizontally through the LC core just below the LC-NC interface. Cracks also occurred on the western beam side, and LC debonding occurred progressively on both sides while the crack propagated to the supports (Figure C.18-b) and a significant pushing out of the LC could be observed (Figure C.18-c). The failed specimen is illustrated in Figures C.21 and C.22.

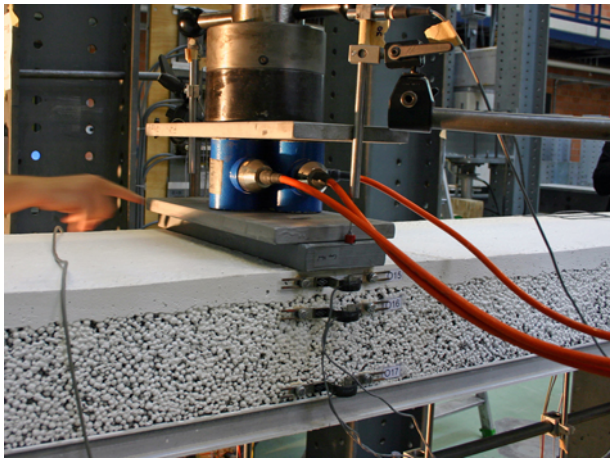

(a) Loading condition

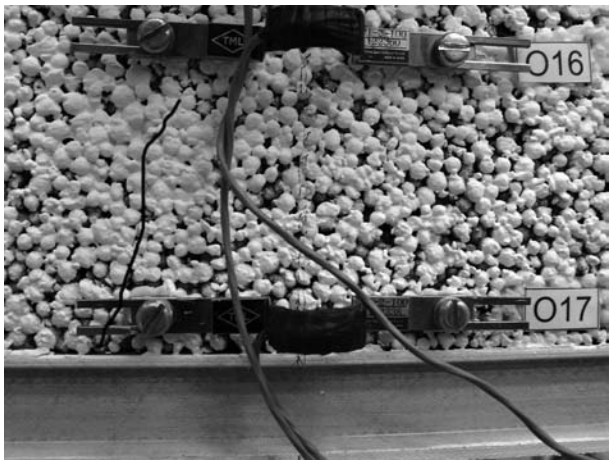

(b) First crack at 6.8 kN at mid-span - north

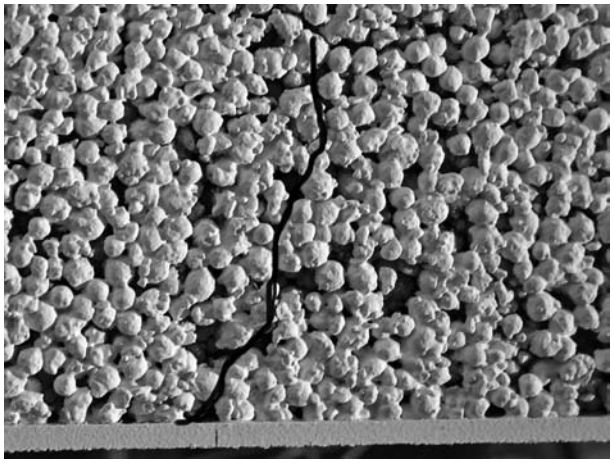

(c) Crack max load Fu = 9.3 kN at 25 cm from mid-span - south west

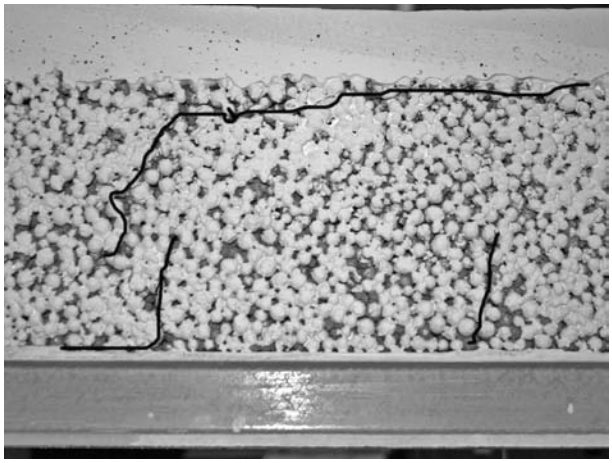

(d) First continuous vertical crack at 8.6 kN (post-peak) at 42 cm from mid-span - north east

(e) Debonding at 8.4 kN (post-peak) on north west side

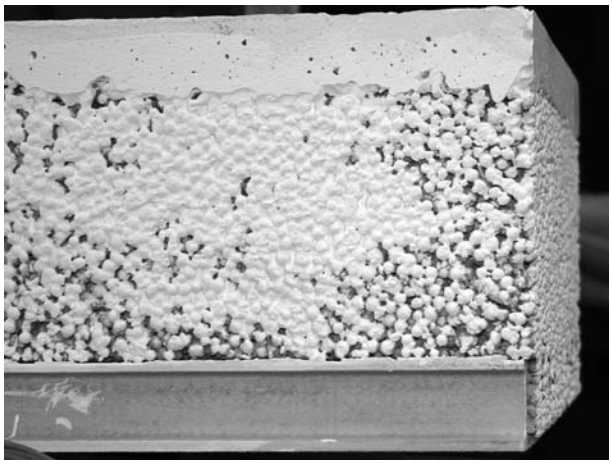

(f) LC being pushed out of GFRP profile at 8.3 kN (post-peak) at beam axis F

Figure C.17: 900-1: Failure process.

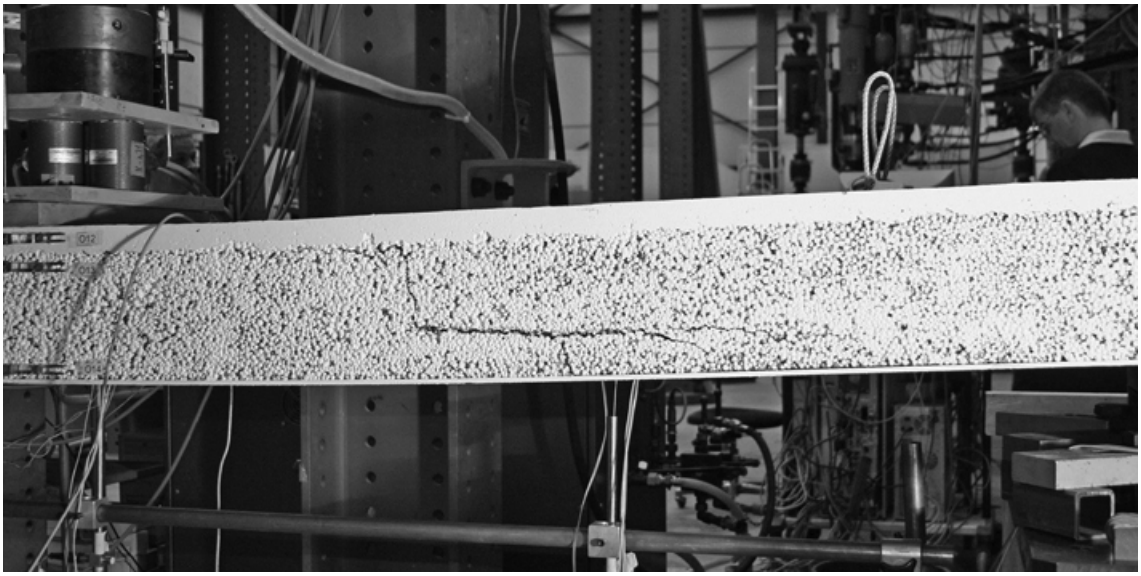

(a) Crack development on southern side at 4.0 kN (post-peak)

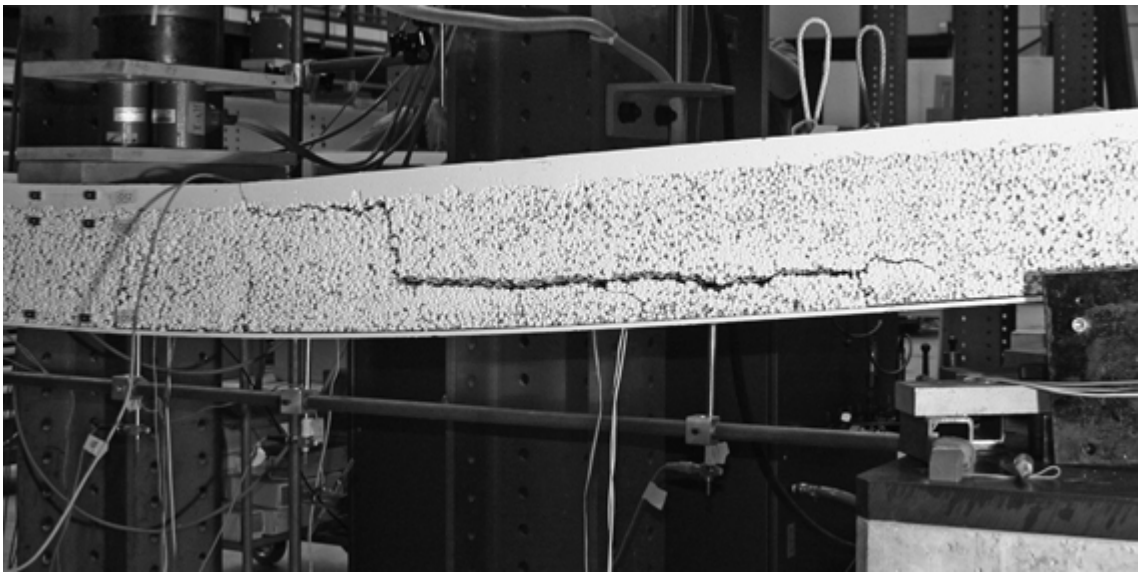

(b) Crack development on southern side at 5.0 kN (post-peak)

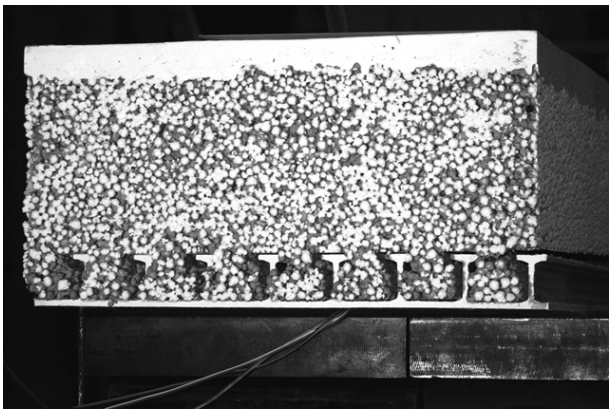

(c) View of east end of failed beam

Figure C.18: 900-1: Failure process (post-peak).

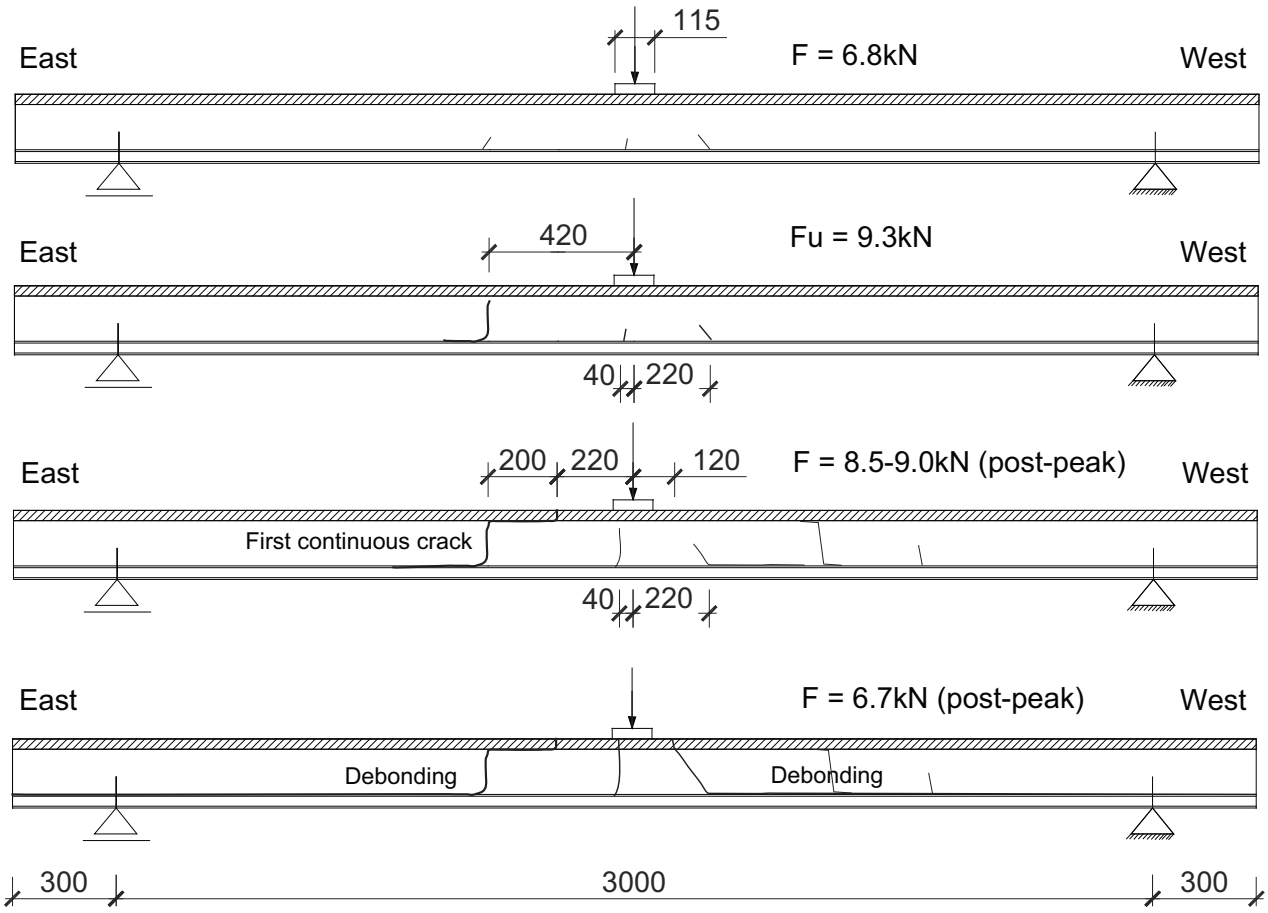

(a) View from north - failure process

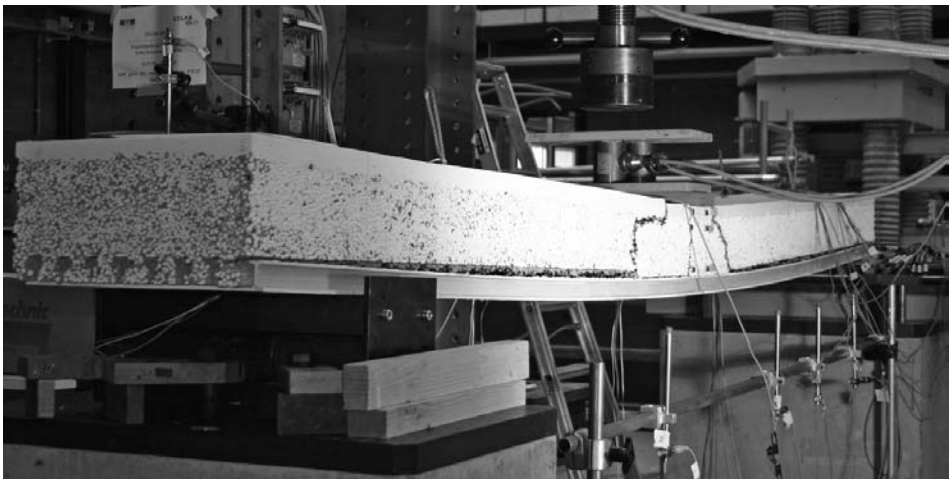

(b) View from north - unloaded failed beam after experiment

Figure C.19: 900-1: a) Failure process and b) unloaded failed beam after experiment - north.

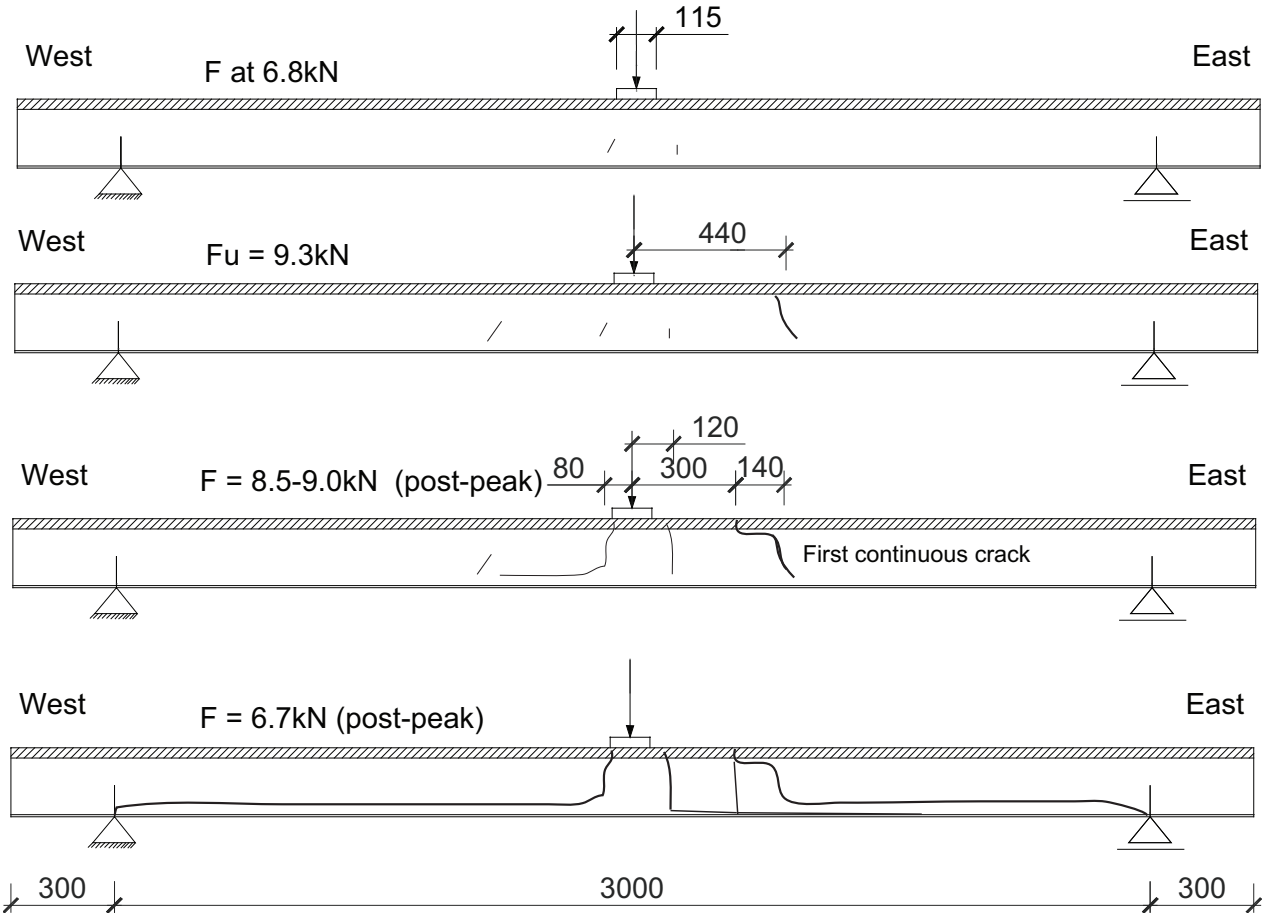

(a) View from south - failure process

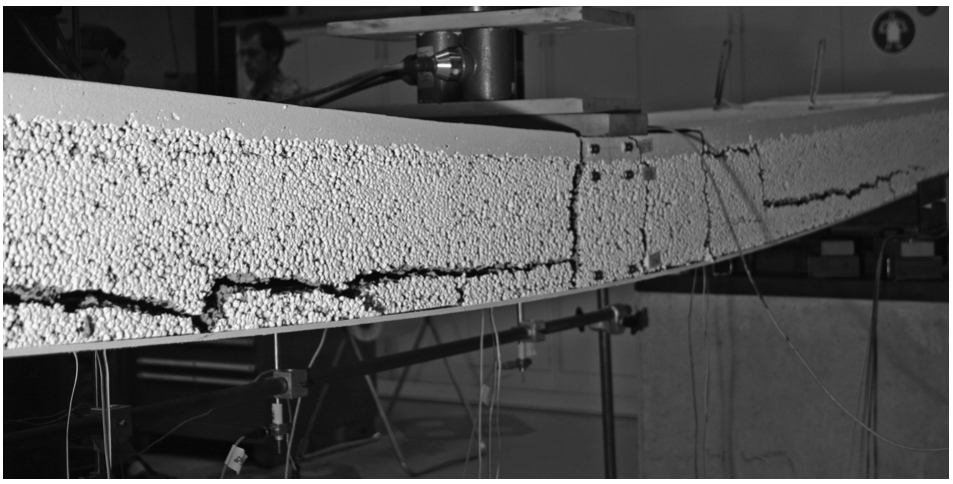

(b) View from south - unloaded failed beam after experiment

Figure C.20: 900-1: a) Failure process and b) unloaded failed beam after experiment - south.

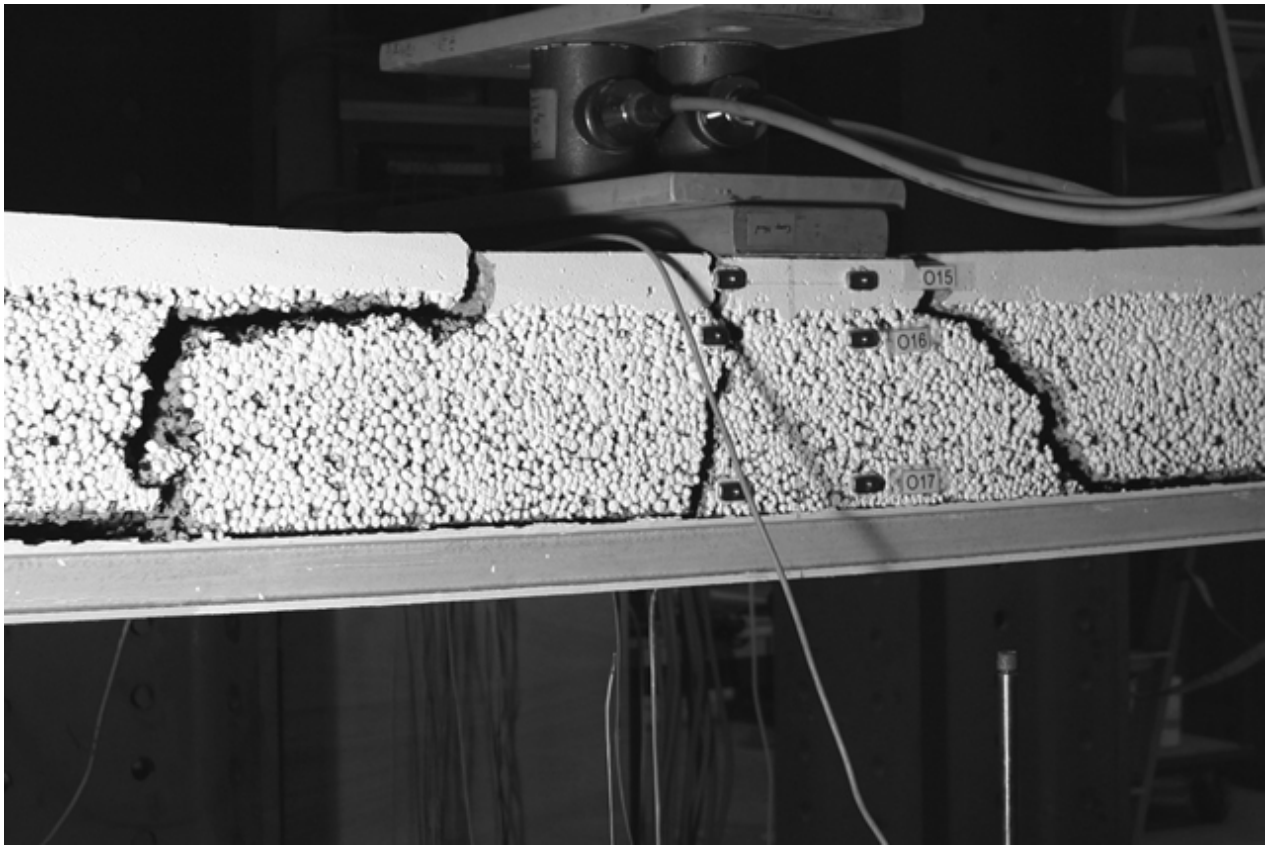

(a) View from north - mid-span

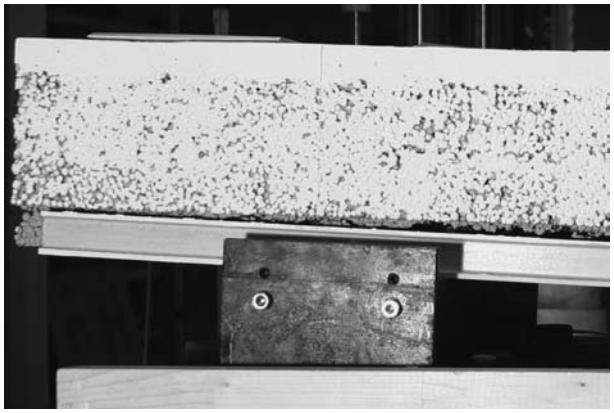

(b) View from north - axis B

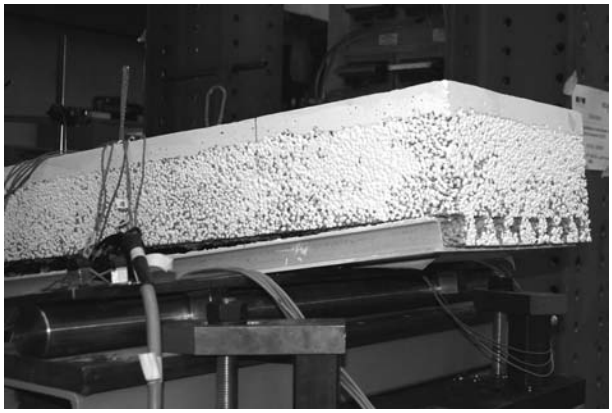

(c) View from north - axis F

Figure C.21: 900-1: Failed beam after experiment, still loaded - north.

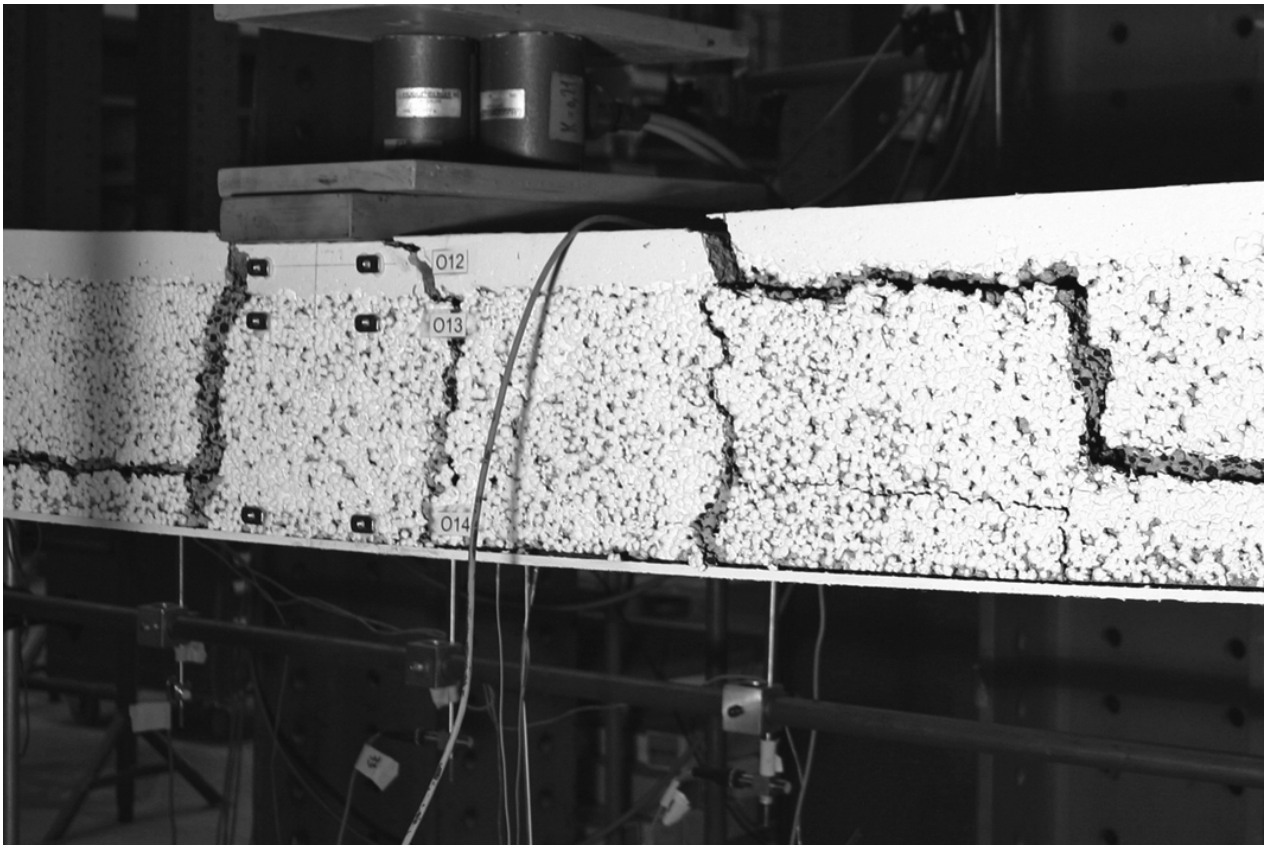

(a) View from south - mid-span

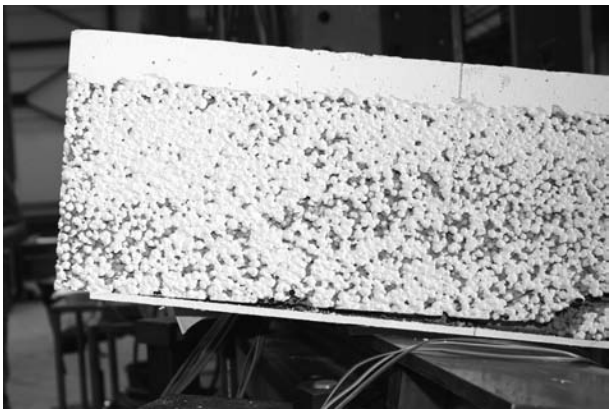

(b) View from south - axis F

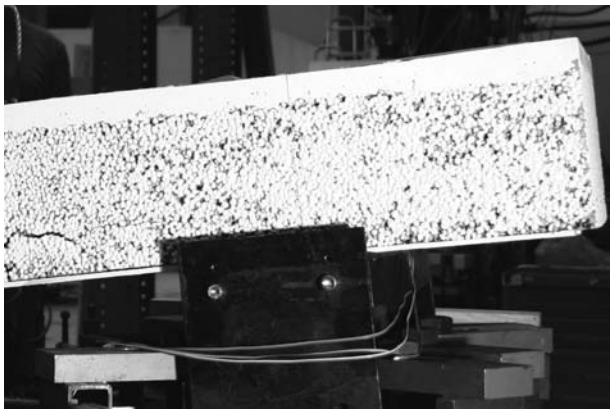

(c) View from south - axis B

Figure C.22: 900-1: Failed beam after experiment, still loaded - south.

C.4.1.2 Displacement transducers

As shown in Figures C.23 and C.24, the stiffness of the beam remained constant until the first obvious crack appeared at a load of 6.8 kN and corresponding mid-span deflection of 2.9 mm. The stiffness of the beam then decreased significantly. A load cycle was performed at 7.4 kN. It was unloaded down to a load of 1.5 kN, at which it exhibited a remaining deformation of approximately 5 mm and then reloaded. The beam exhibited almost the same stiffness as observed at the beginning of the experiment up to a value of 6.8 kN. Subsequently, the beam again lost some stiffness. However, the load could be increased until the maximum load of $F_u = 9.3$ kN with a corresponding deflection of 11.5 mm. This load could be maintained up till a deflection of 17.3 mm. The load then slightly decreased to values of between 8.5 kN to 9.0 kN. At deflections of 33 mm, the load decreased down to a value of 6.5 kN. Due to the large deformation of the beam, the instrumental equipment was removed and beam loading was continued without measurements being taken. The results from displacement transducers D0 and D6 are not illustrated since both were moved during the experiment to measure the deformation of the loading plates and thus did not offer any useful information.

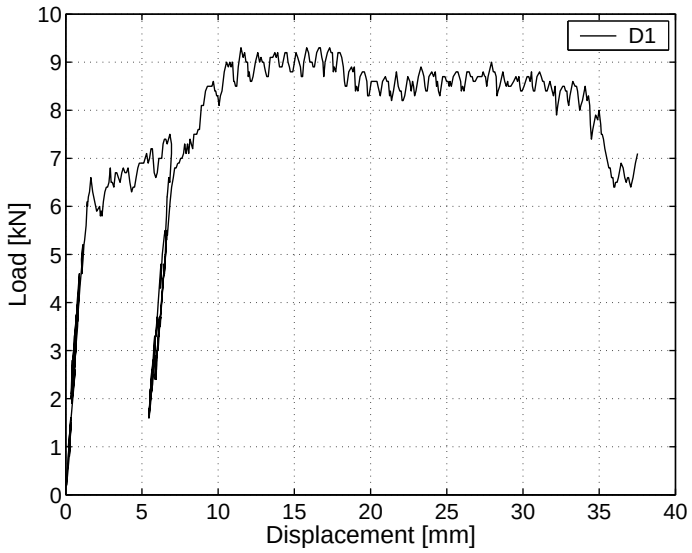

Figure C.23: 900-1: Displacement at mid-span.

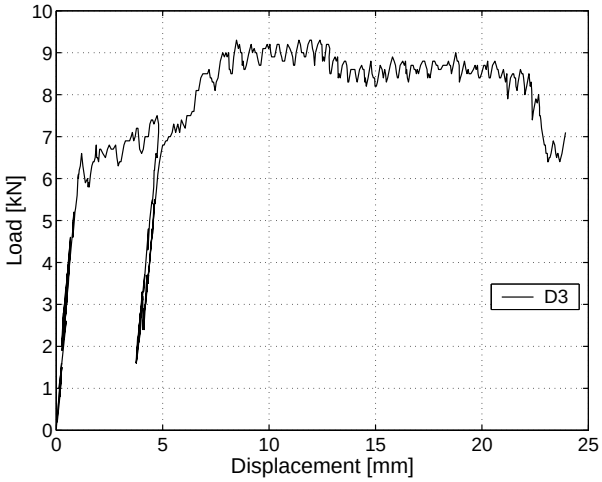

(a) Displacement - axis E

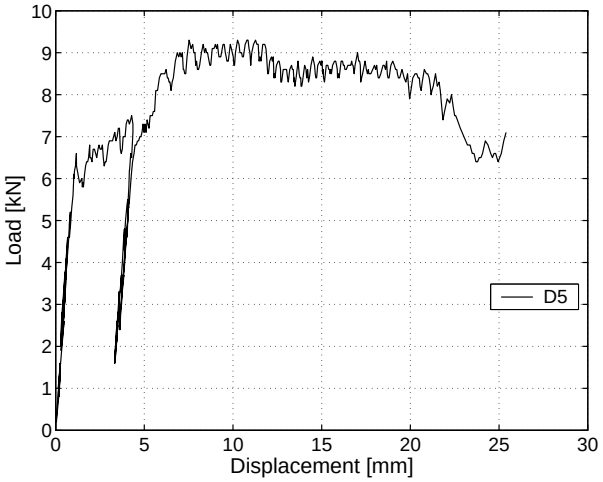

(b) Displacement - axis C

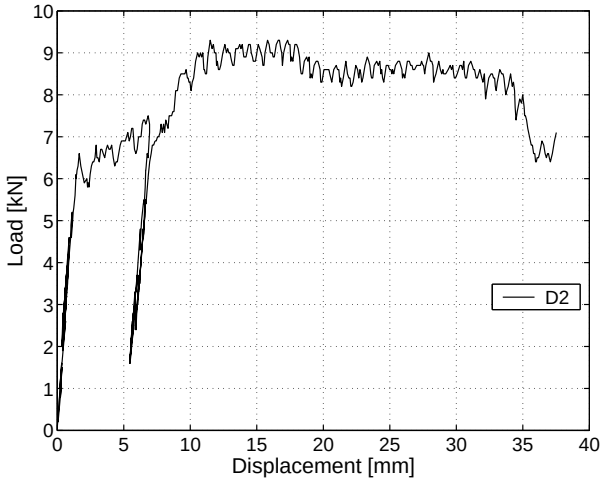

(c) Displacement - between axes D-E

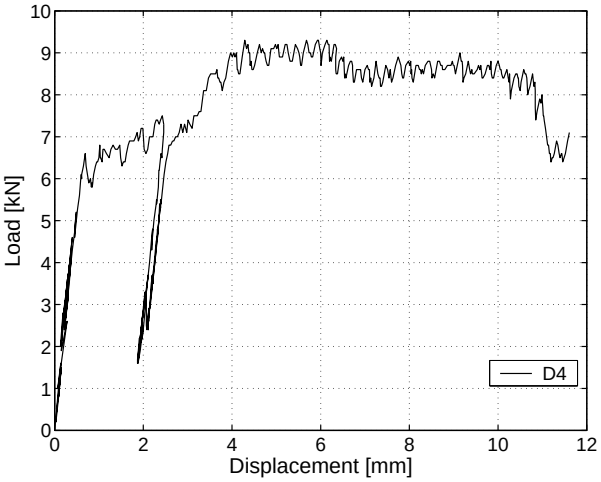

(d) Displacement - between axes E-F

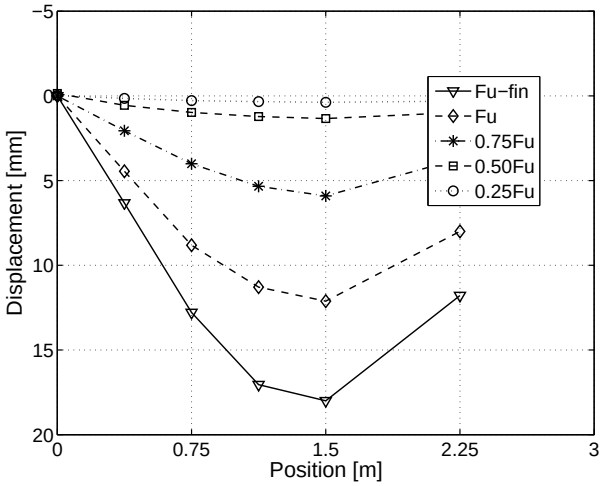

(e) Displacement along beam

Figure C.24: 900-1: Displacements at different sections and along beam ($F_u = 9.3\,\text{kN}$ with 11.5 mm and $F_{u-fin} = 9.3\,\text{kN}$ with 17.3 mm corresponding deflections).

C.4.1.3 Omega-shaped extensometers

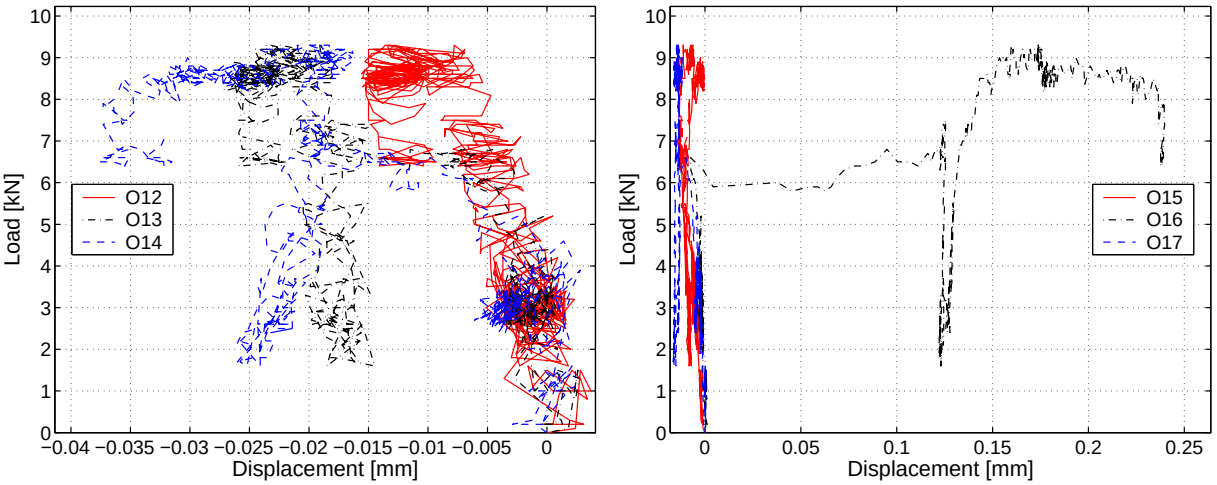

(a) Axis D (mid-span) - south

(b) Axis D (mid-span) - north

Figure C.25: 900-1: Deformations in omega-shaped extensometers at mid-span.

C.4.1.4 Strain gages on GFRP profile

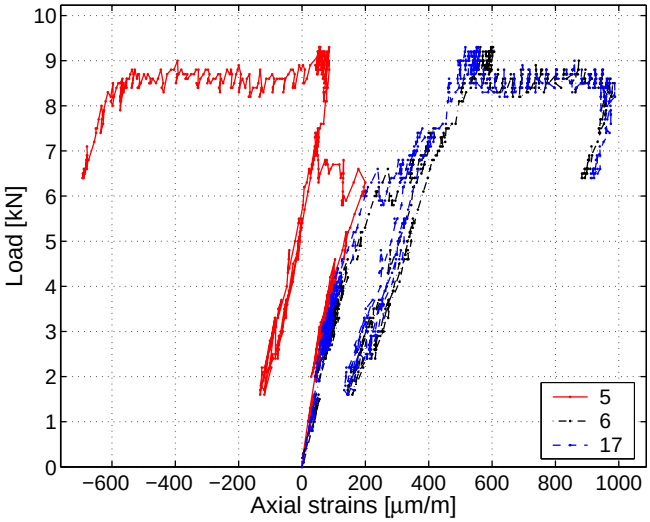

(a) Axial strains at axis D (mid-span)

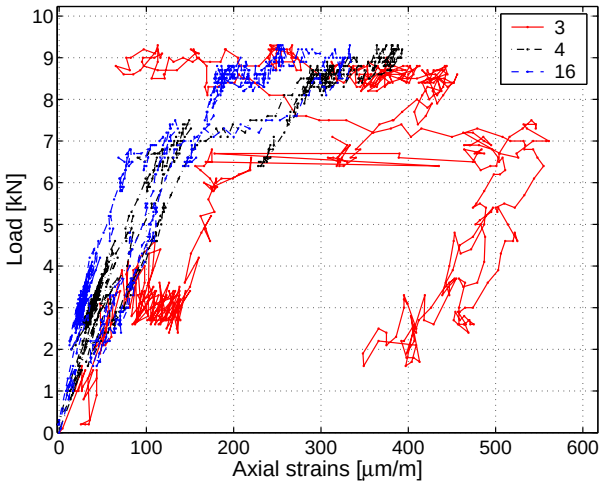

(b) Axial strains at axis E

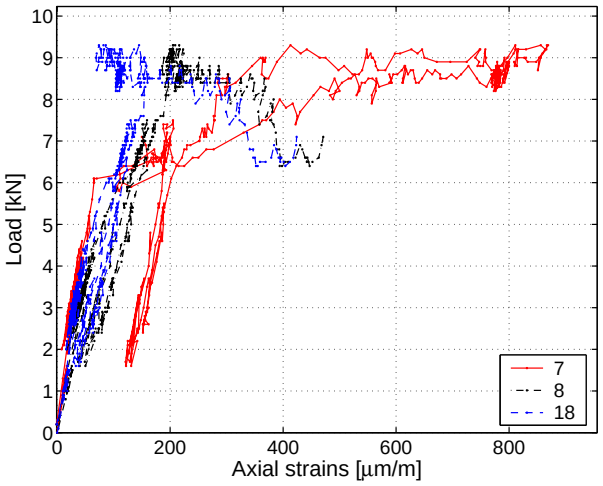

(c) Axial strains at axis C

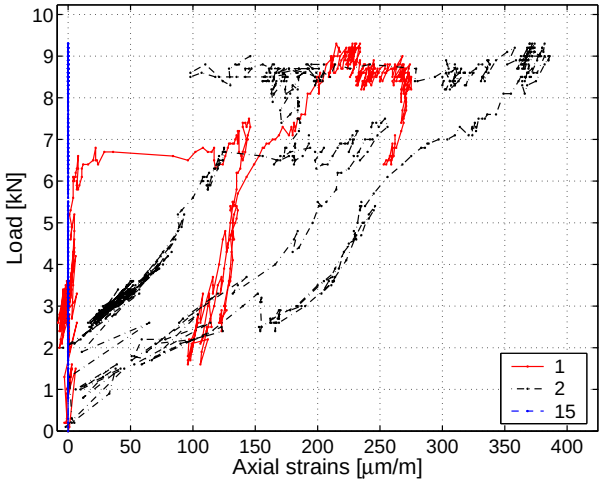

(d) Axial strains at axis F

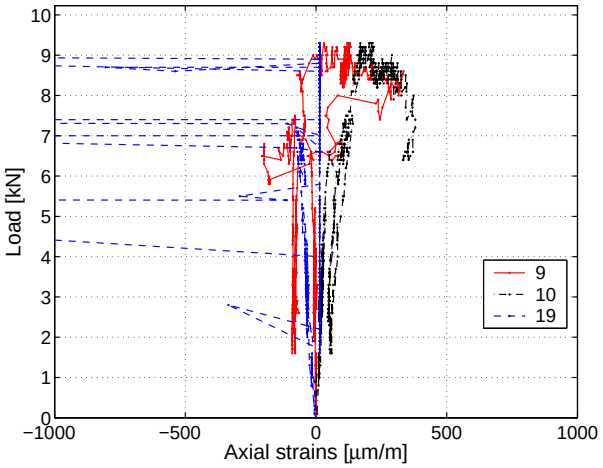

(e) Axial strains at axis B

Figure C.26: 900-1: Axial strains in GFRP profile.

C.4.1.5 Axial strains through the cross section

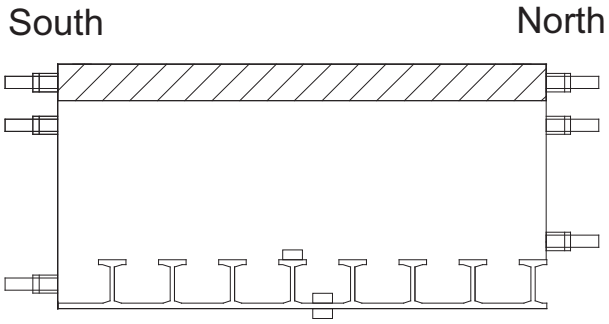

(a) Instrumentation location

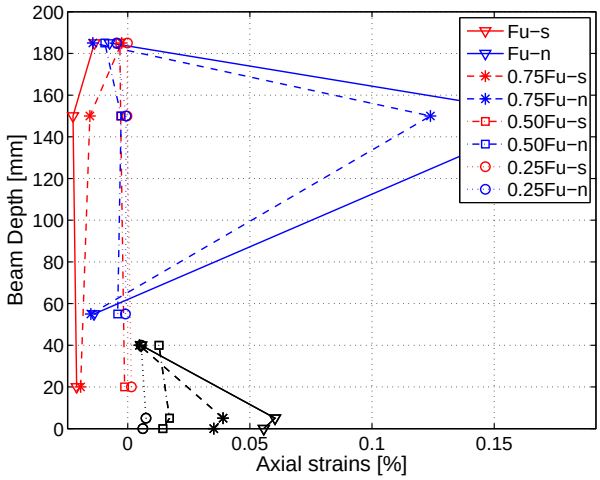

(b) Strain gages on centerline and omegas on north and south side

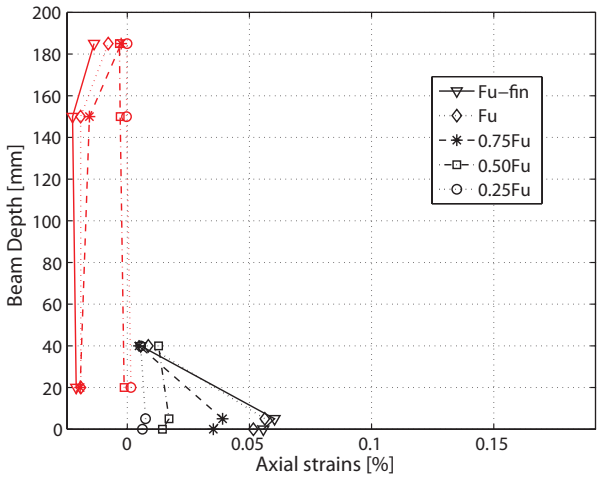

(c) South

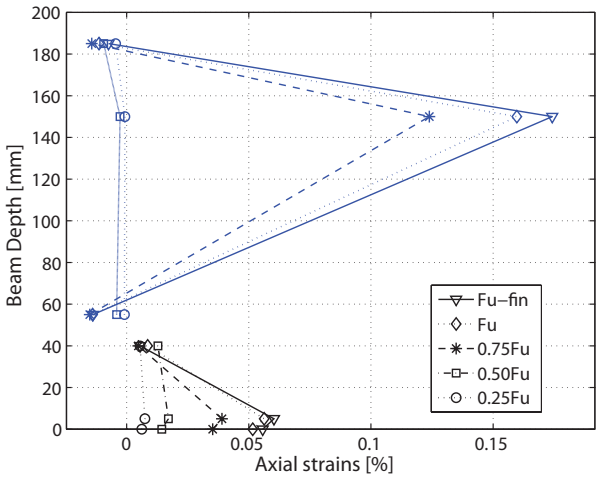

(d) North

Figure C.27: 900-1: Axial strains through cross section at mid-span at different load steps from strain gages and omega-shaped extensometers ($F_u = 9.3\,\text{kN}$ with $11.5\,\text{mm}$ and $F_{u-fin} = 9.3\,\text{kN}$ with $17.3\,\text{mm}$ corresponding deflections).

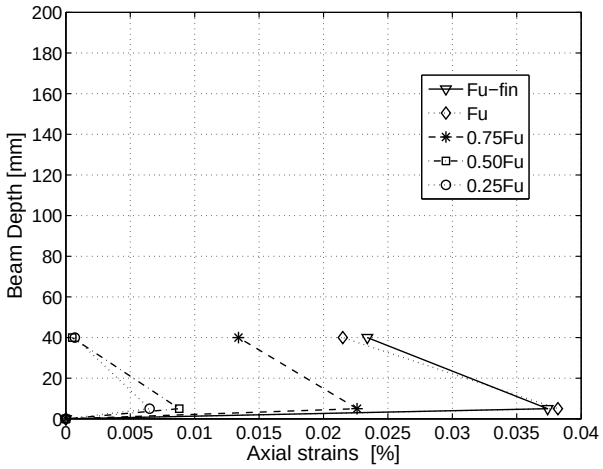

(a) Axial strains at axis F

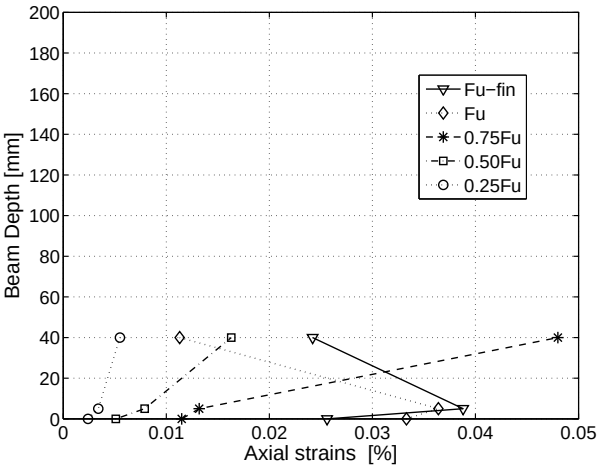

(b) Axial strains at axis E

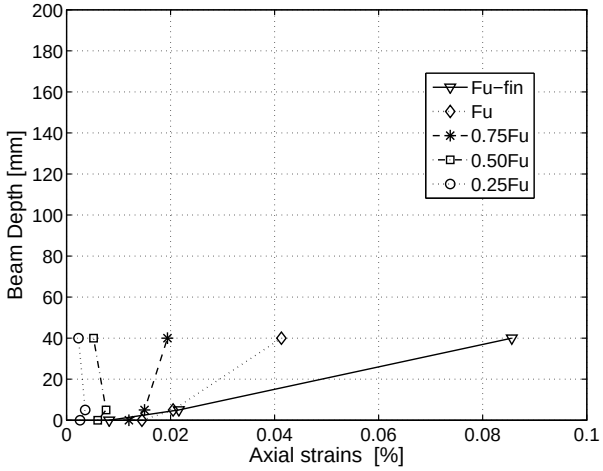

(c) Axial strains at axis C

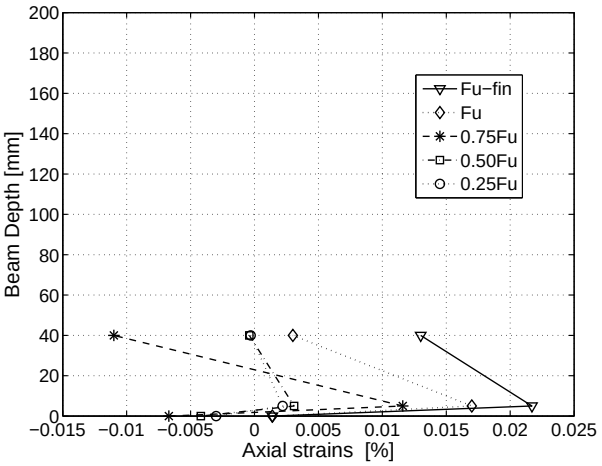

(d) Axial strains at axis B

Figure C.28: 900-1: Axial strains through GFRP cross section at different load steps ($F_u = 9.3\,\text{kN}$ with 11.5 mm and $F_{u-fin} = 9.3\,\text{kN}$ with 17.3 mm corresponding deflections).

C.4.1.6 Axial strains along the beam

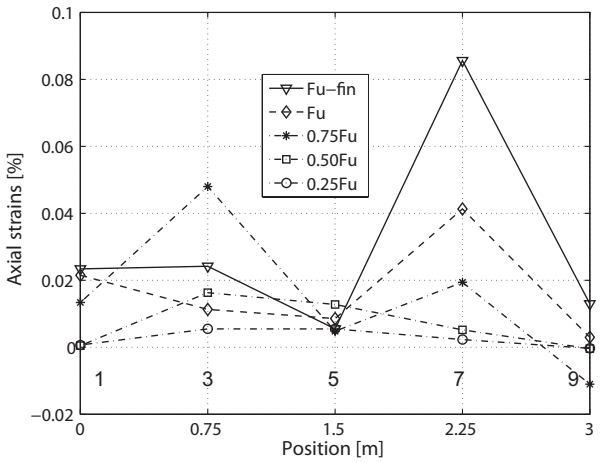

(a) Axial strains on top of T-upstands

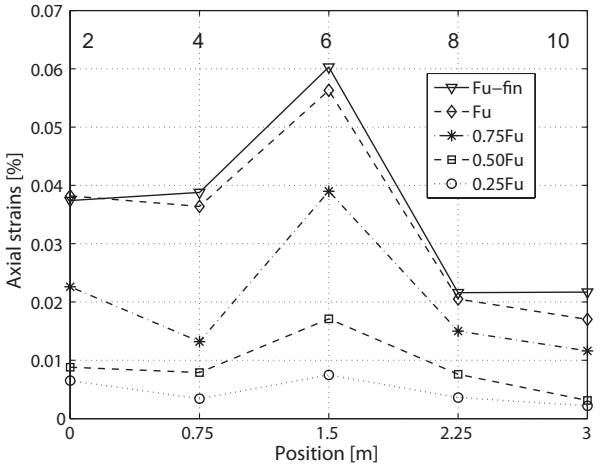

(b) Axial strains between T-upstands

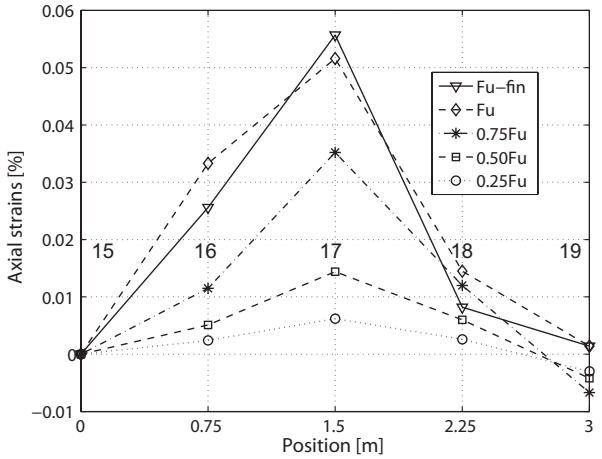

(c) Axial strains beneath GFRP sheet

Figure C.29: 900-1: Axial strains in GFRP profile along beam at different load steps ($F_u = 9.3\,\text{kN}$ with 11.5 mm and $F_{u-fin} = 9.3\,\text{kN}$ with 17.3 mm corresponding deflections).

C.4.2 Beam 900-2: Failure description and measured results (full instrumentation)

C.4.2.1 Failure description

The failure process of beam 900-2 is illustrated in Figures C.30, C.31, C.32 and C.33. The first noises were audible at a load of 4 kN and the first loud crack occurred at 9.2 kN, followed by LC debonding on the south-east side of the beam. The maximum load was reached at $F_u = 11.5$ kN with a corresponding deflection of 9.4 mm. At this load, three vertical cracks extended through the entire depth of the LC layer. A load cycle was conducted at a deflection of 10 mm. During the unloading process the cracks closed slightly and then reopened during the reloading process. The load increased up to 10.3 kN. Subsequently the load dropped to 8.6 kN and the vertical cracks started to propagate horizontally at the LC-NC and FRP-LC interfaces. The most significant vertical crack was situated approximately 55 cm west of the mid-span. At a mid-span deflection of 20 mm a third load cycle was performed. Again, after reloading a load of approximately 8.8 kN could be reached, which did not change significantly up to a mid-span deflection of 31.8 mm. The experiment was stopped after a further drop in the load to 5.6 kN. The failed specimen is illustrated in Figures C.34 and C.35.

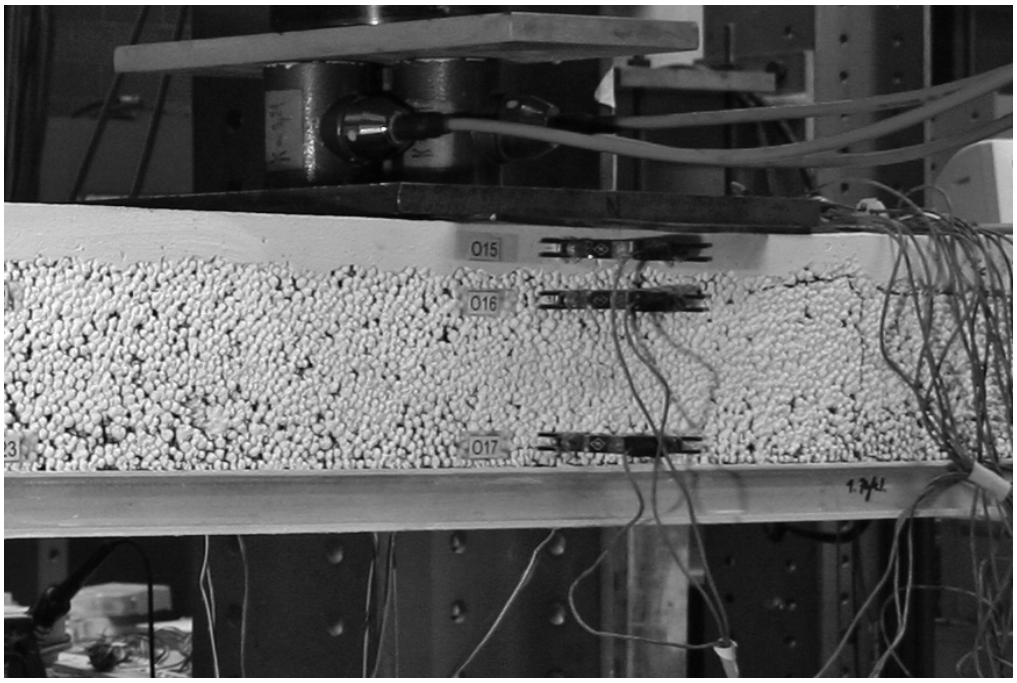

Figure C.30: 900-2: Continuous crack next to loading plate during unloading of second load cycle (post-peak).

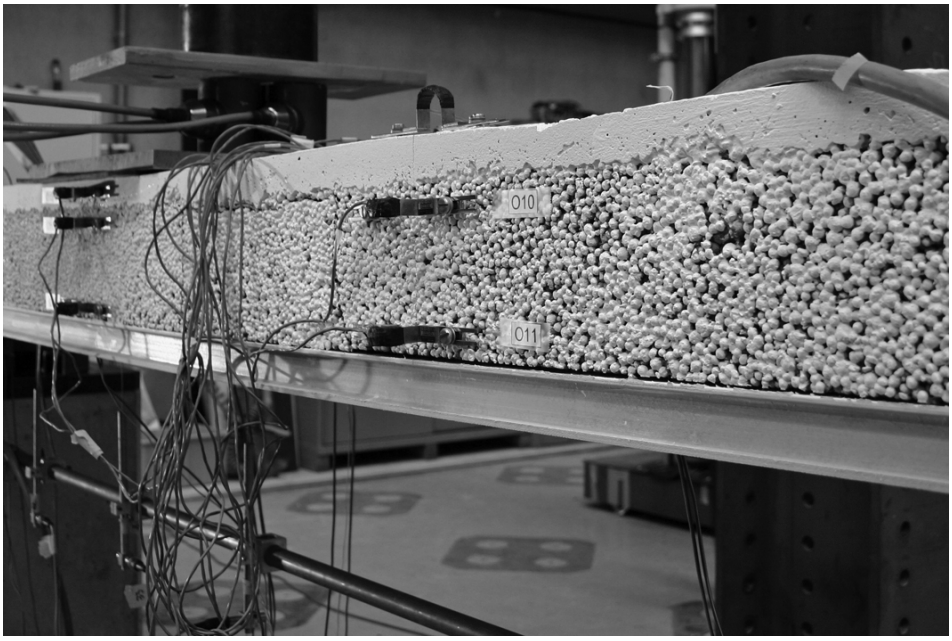

(a) Crack development after second load cycle; at $\sim 8.5\,\mathrm{kN}$

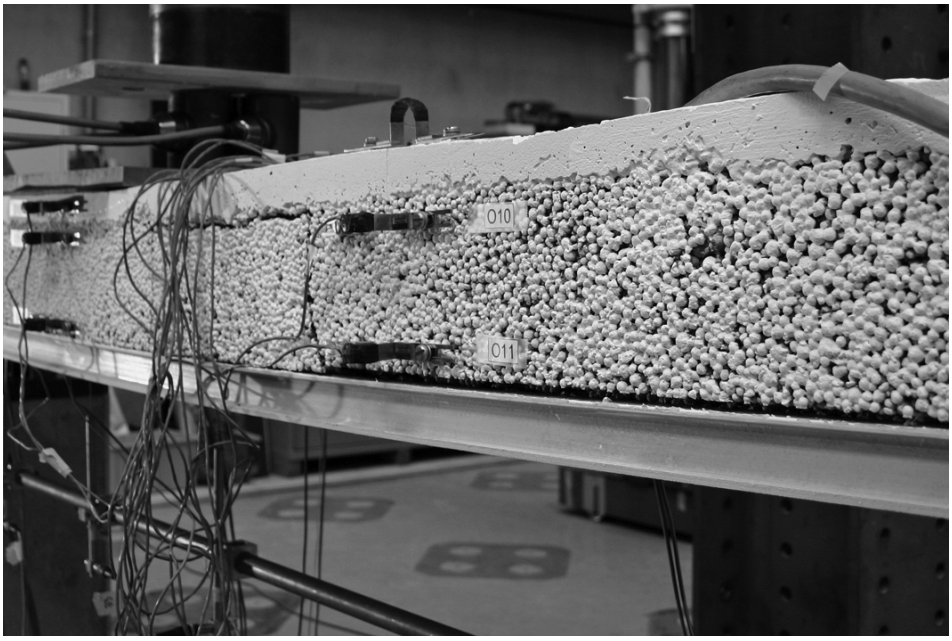

(b) Crack development after second load cycle; at $\sim 5.5\,\mathrm{kN}$

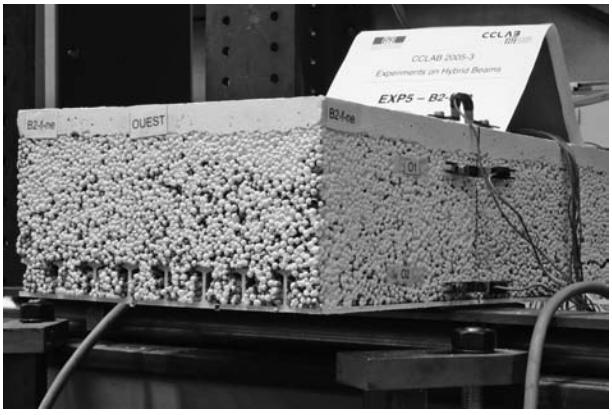

(c) LC being pushed out of GFRP profile at west end

Figure C.31: 900-2: Crack development after second load cycle (post-peak).

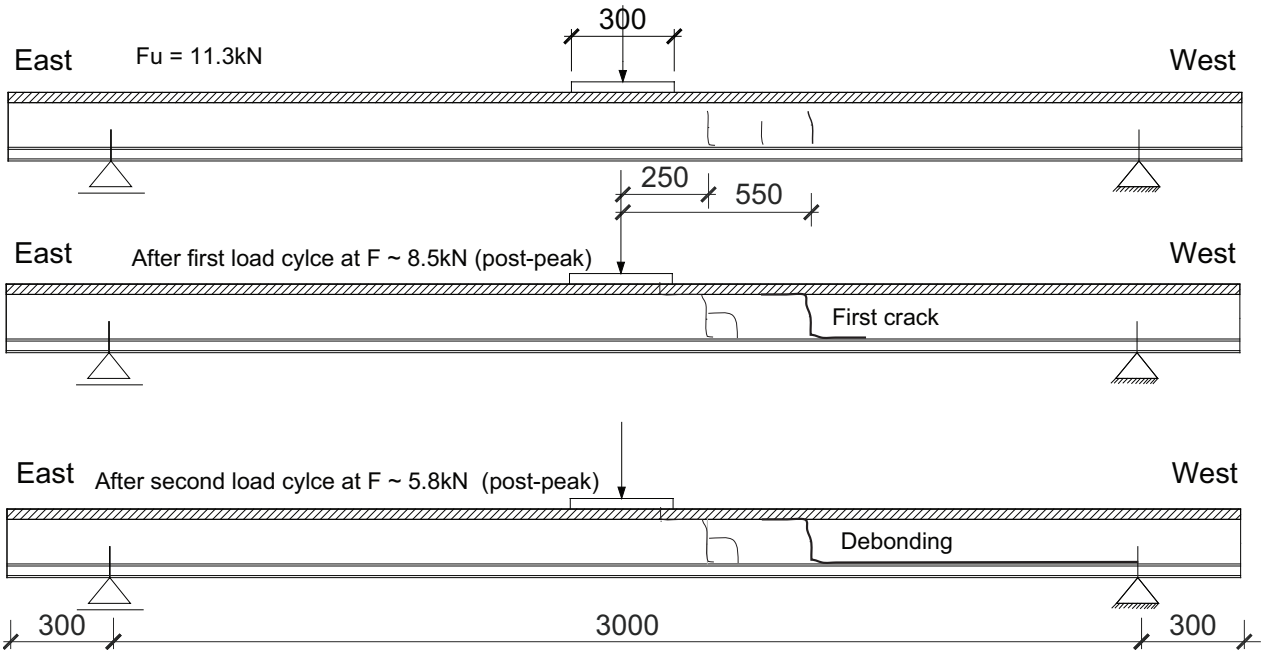

(a) View from north - failure process

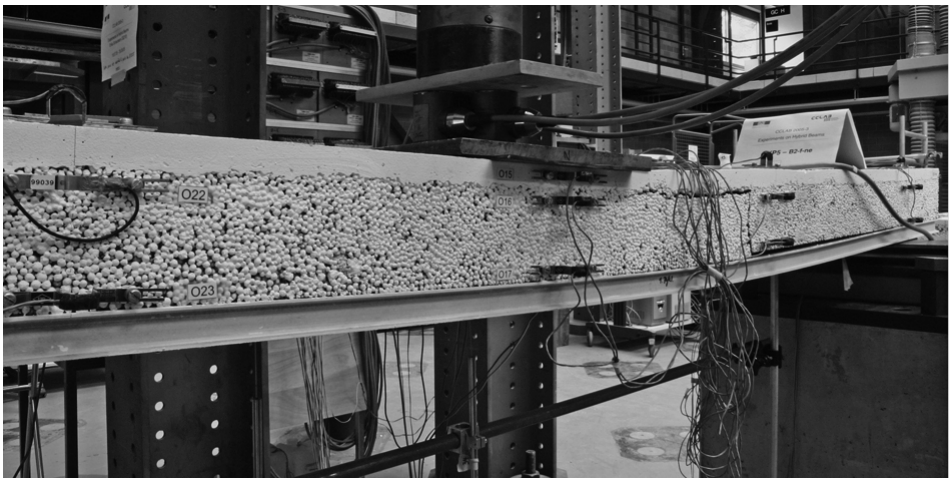

(b) View from north

Figure C.32: 900-2: a) Failure process and b) still loaded failed beam after experiment - north.

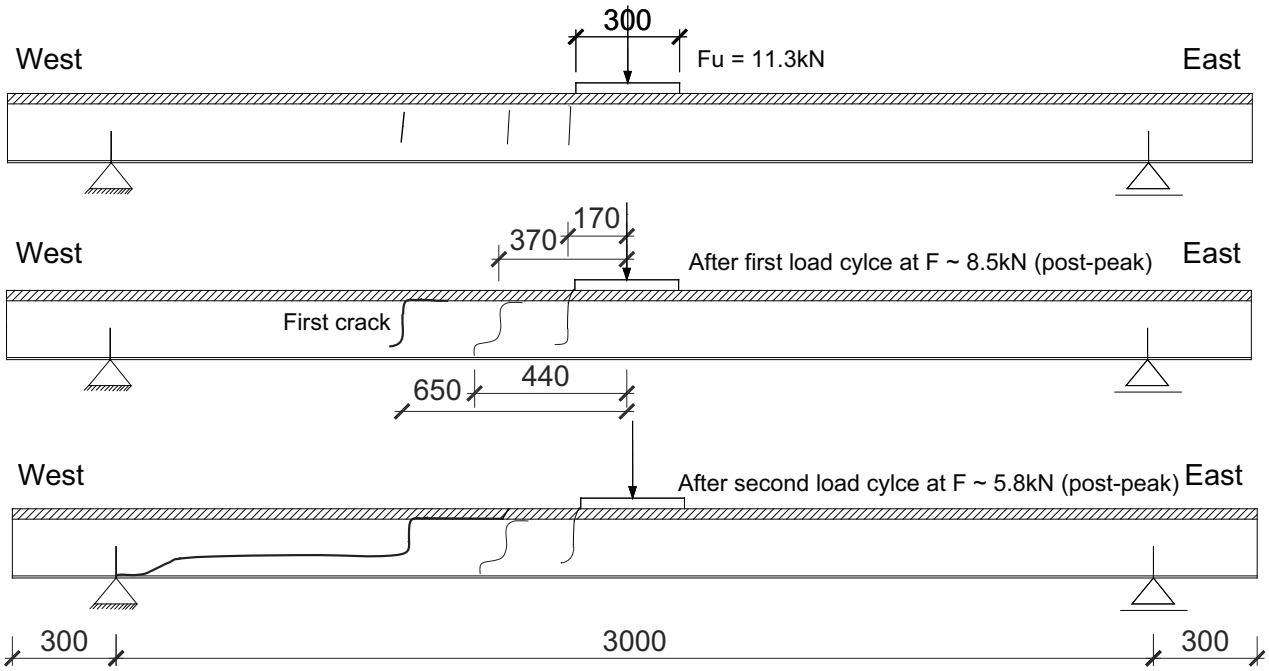

(a) View from south - failure process

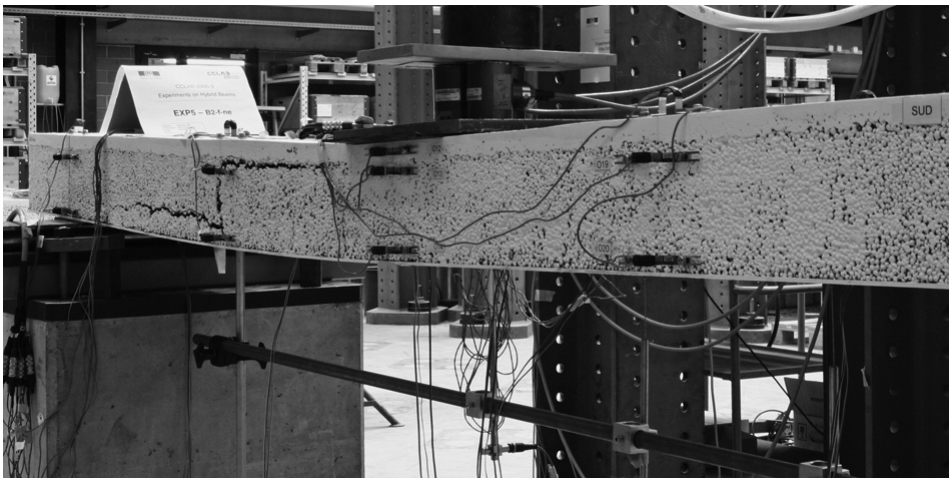

(b) View from south

Figure C.33: 900-2: a) Failure process and b) still loaded failed beam after experiment - south.

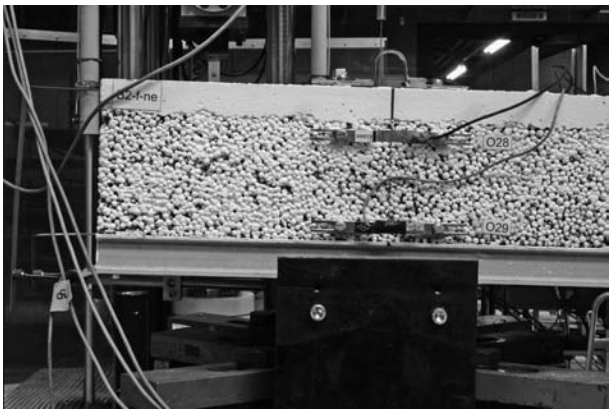

(a) View from north - axis B

(b) View from north - axis C

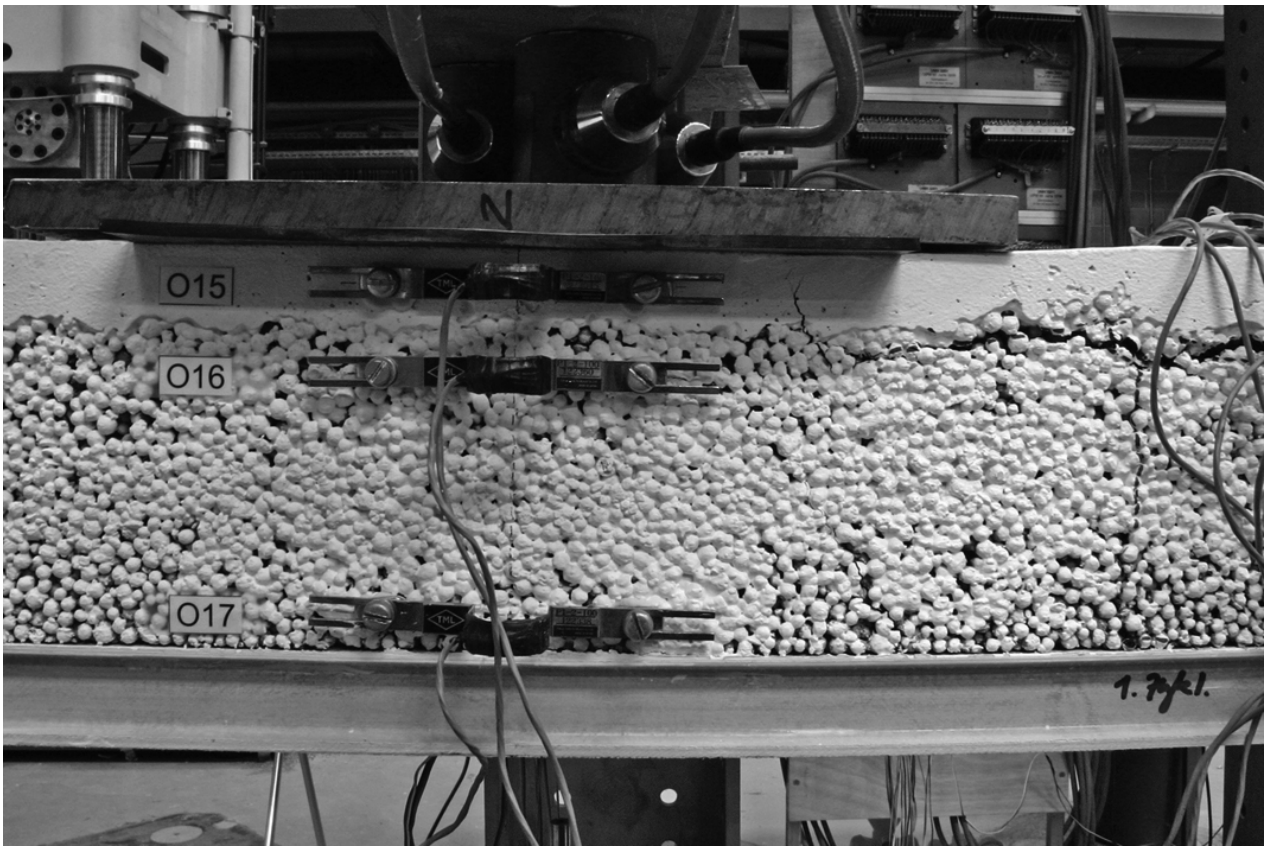

(c) View from north - mid-span

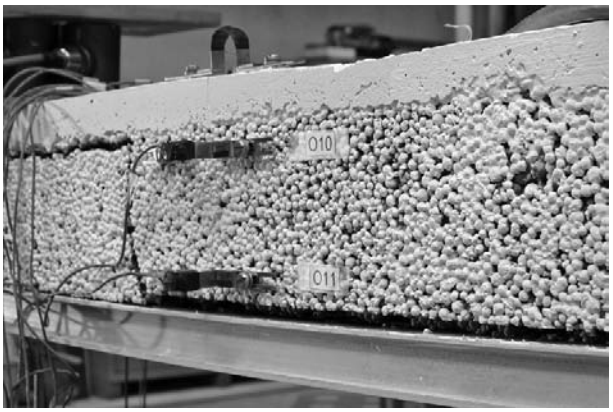

(d) View from north - axis E

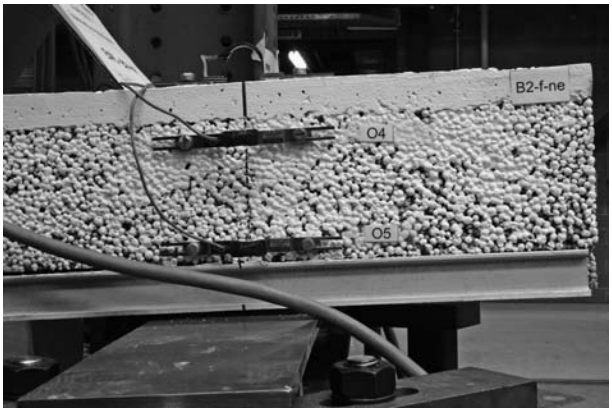

(e) View from north - axis F

Figure C.34: 900-2: Failed beam after experiment, still loaded - north.

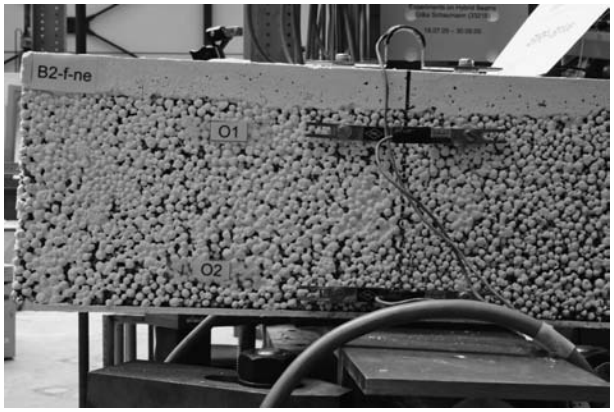

(a) View from south - axis F

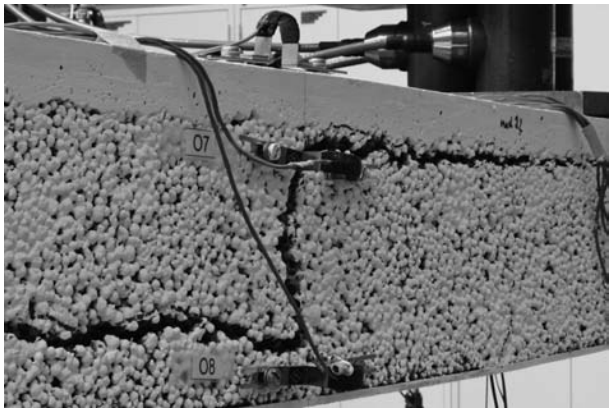

(b) View from south - axis E

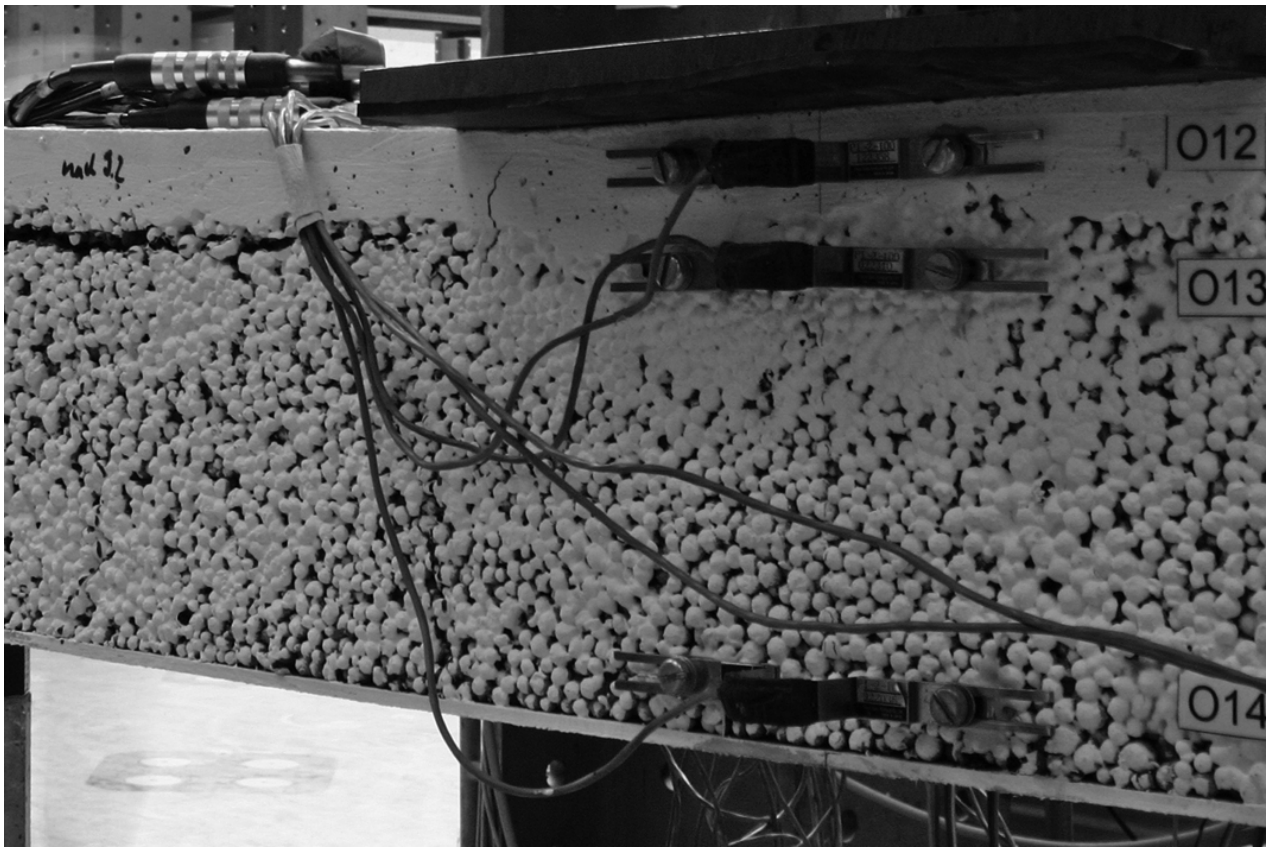

(c) View from south - mid-span

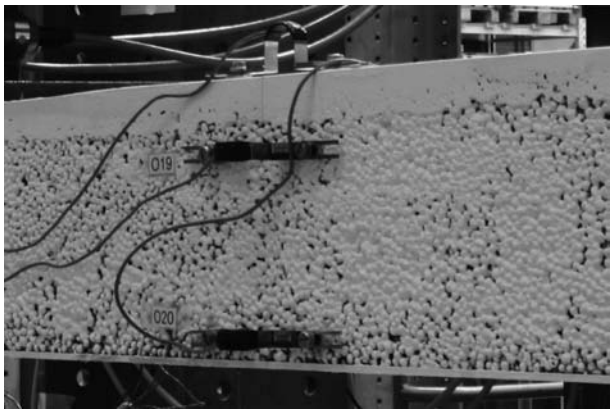

(d) View from south - axis C

(e) View from south - axis B

Figure C.35: 900-2: Failed beam after experiment, still loaded - south.

C.4.2.2 Displacement transducers

The load deflection response in Figure C.36 shows that beam stiffness remained constant up to a load of 7.5 kN. The load then dropped to 6.9 kN and increased again, but with a lower stiffness. The maximum load was reached at $F_u = 11.5$ kN with a corresponding mid-span deflection of 9.4 mm. At a 10 mm mid-span deflection, a load cycle was conducted, showing a remaining deformation of approximately 6.5 mm. Beam stiffness during the reloading process was similar to that at the beginning of the experiment. At a load of 8.8 kN, beam stiffness decreased, however the load could be increased up to 10.2 kN, where another load drop occurred. The load then remained constant at approximately 8.8 kN until the next load cycle was performed. A remaining deformation of ~ 16 mm and slight loss in beam stiffness were observed. Reloading up to the former load of 8.8 kN was possible. At the mid-span deflection of 32 mm the load dropped to a value of 5.6 kN, where the experiment was stopped. Since failure occurred at the west end of the beam, D6 and D7 did not measure any deformation and hence their results are not illustrated.

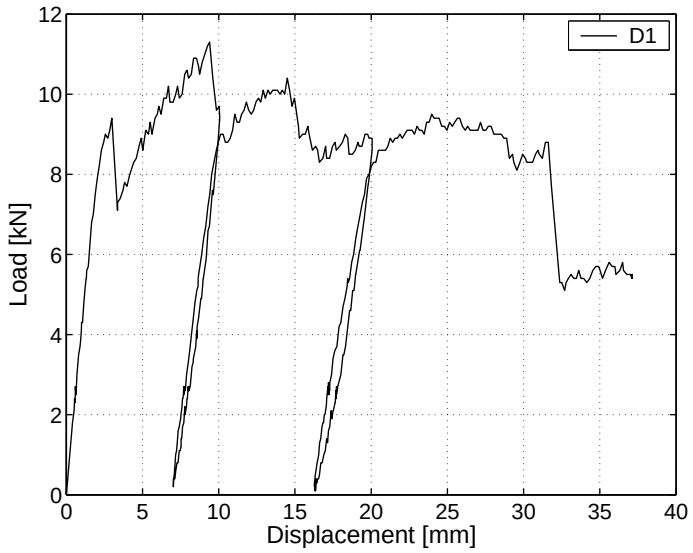

Figure C.36: 900-2: Displacement at mid-span.

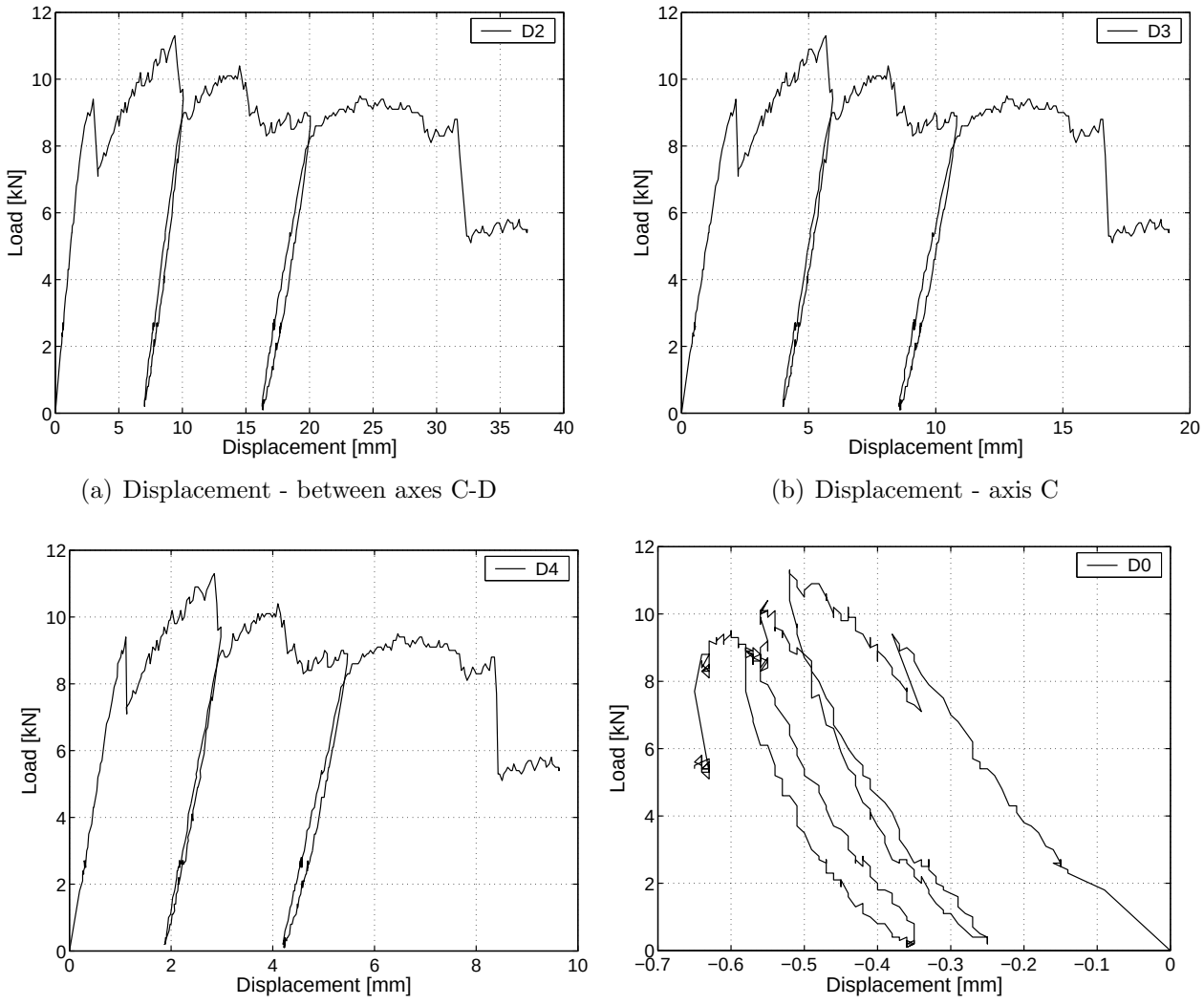

(a) Displacement - between axes C-D

(b) Displacement - axis C

(c) Displacement - between axes B-C

(d) Displacement at free support - axis F

Figure C.37: 900-2: Displacements at different sections.

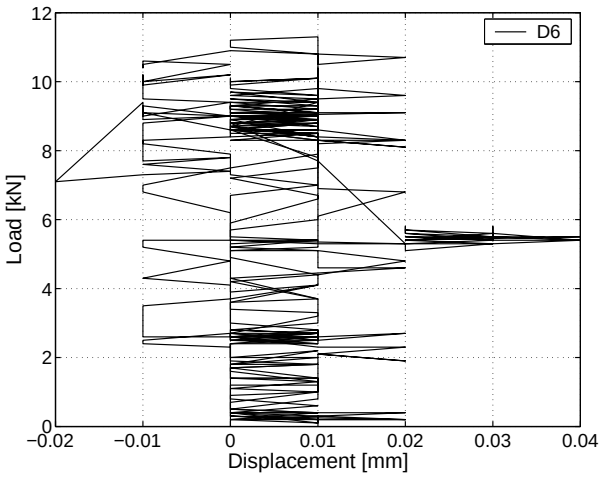

(a) Horizontal displacement of LC - axis A

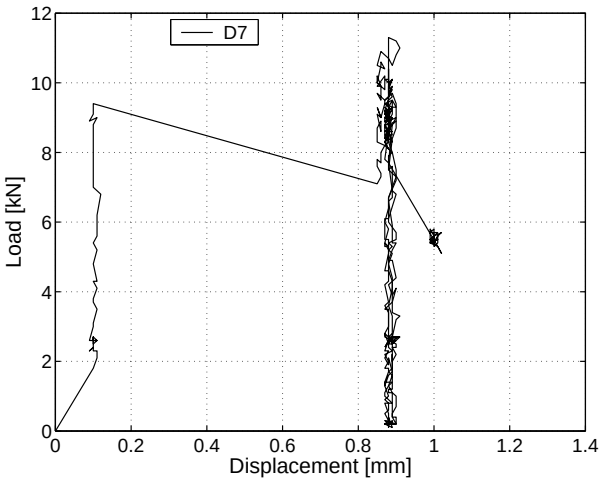

(b) Horizontal displacement of NC - axis A

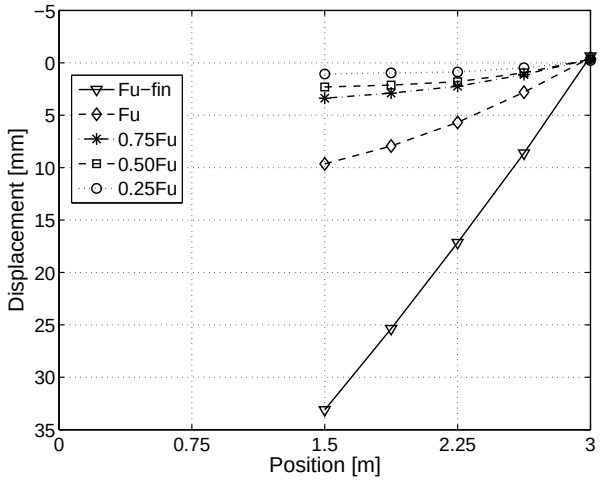

(c) Displacement along beam

Figure C.38: 900-2: Horizontal displacement and displacement along beam ($F_u = 11.5\,\text{kN}$ with 9.4 mm and $F_{u-fin} = 8.8\,\text{kN}$ with 31.8 mm corresponding deflections).

C.4.2.3 Omega-shaped extensometers

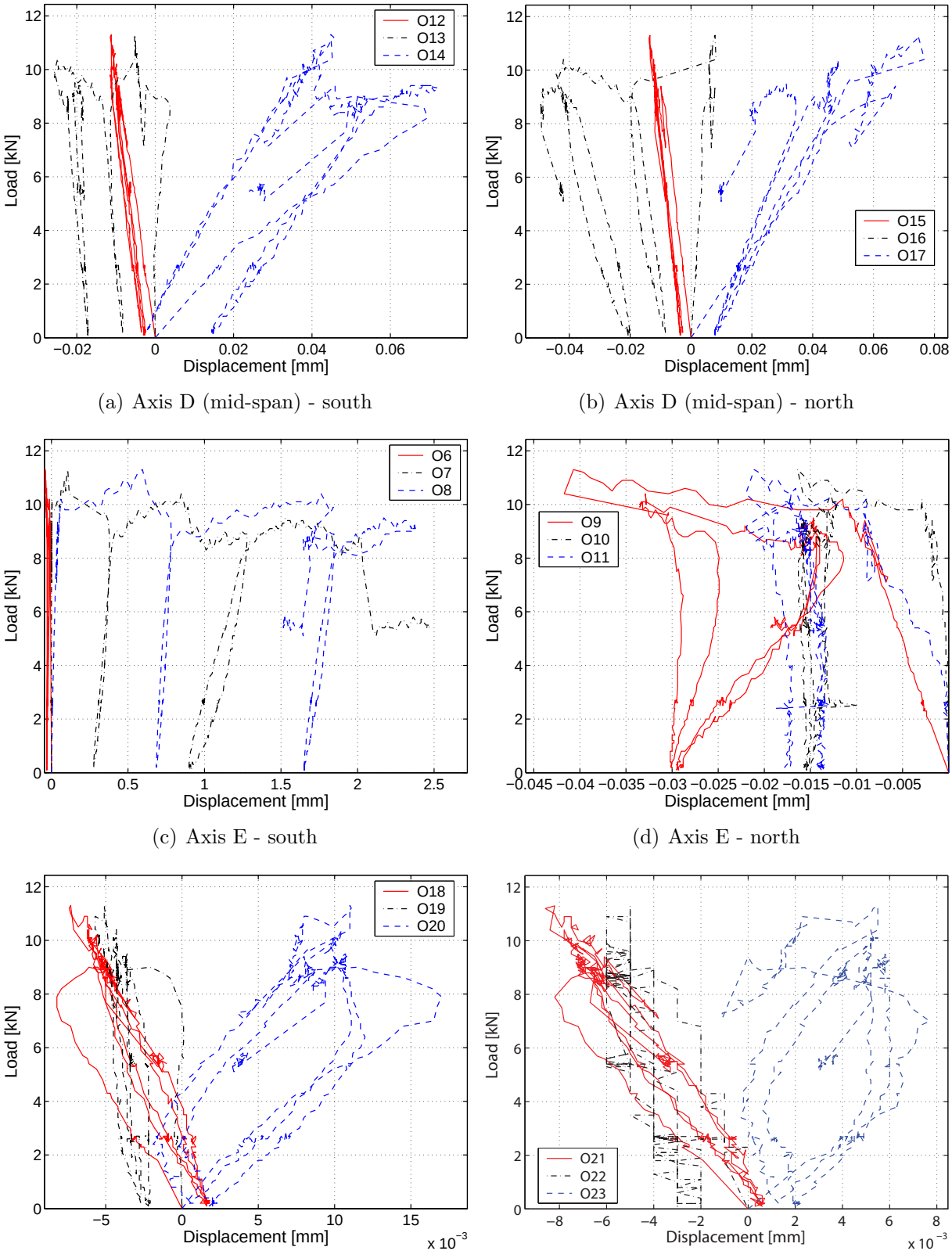

(a) Axis D (mid-span) - south

(b) Axis D (mid-span) - north

(c) Axis E - south

(d) Axis E - north

(e) Axis C - south

(f) Axis C - north

Figure C.39: 900-2: Deformations in omega-shaped extensometers at axes C-E.

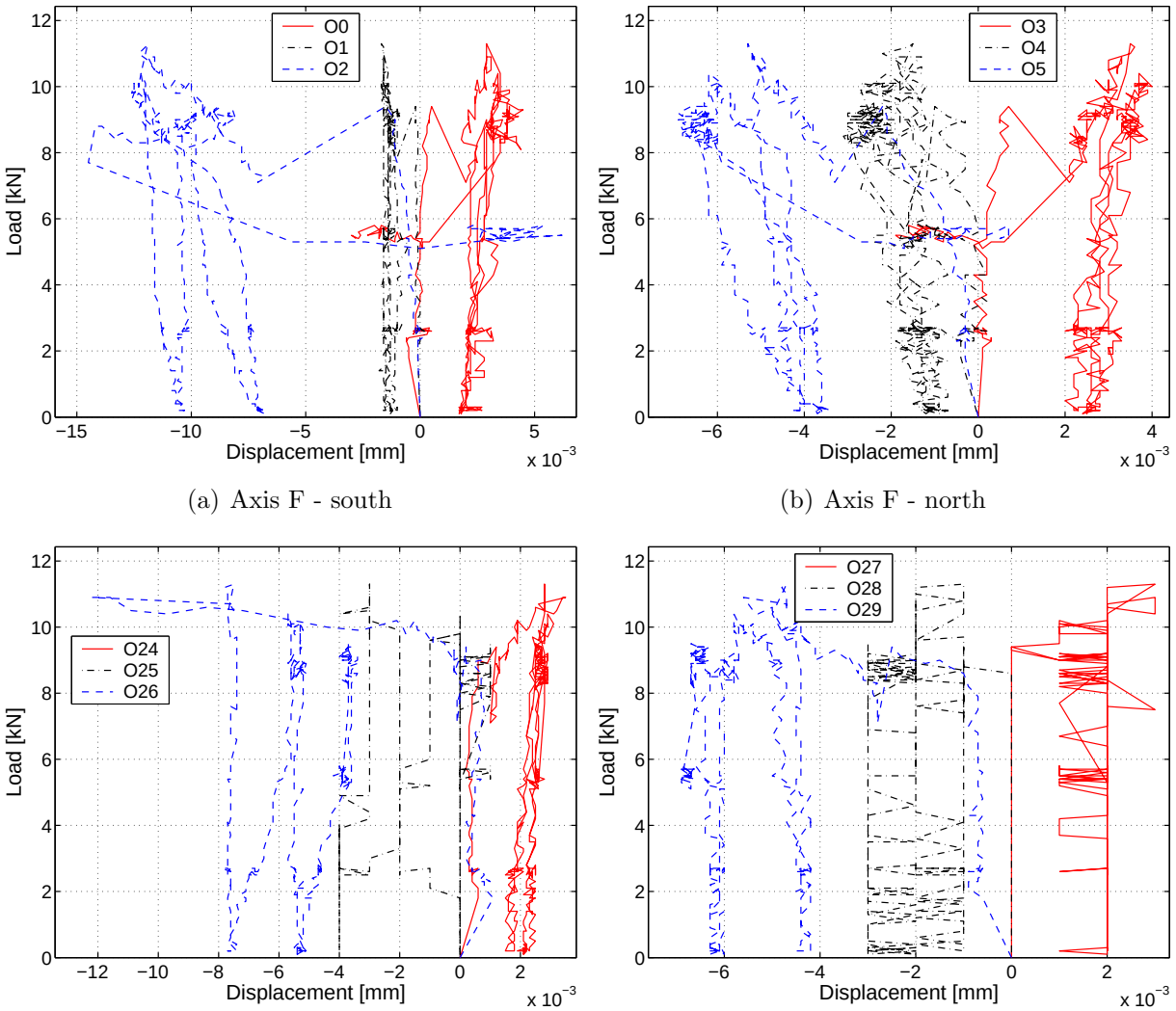

(a) Axis F - south

(b) Axis F - north

(c) Axis B - south

(d) Axis B - north

Figure C.40: 900-2: Deformations in omega-shaped extensometers over supports.

C.4.2.4 Strain gages on GFRP profile

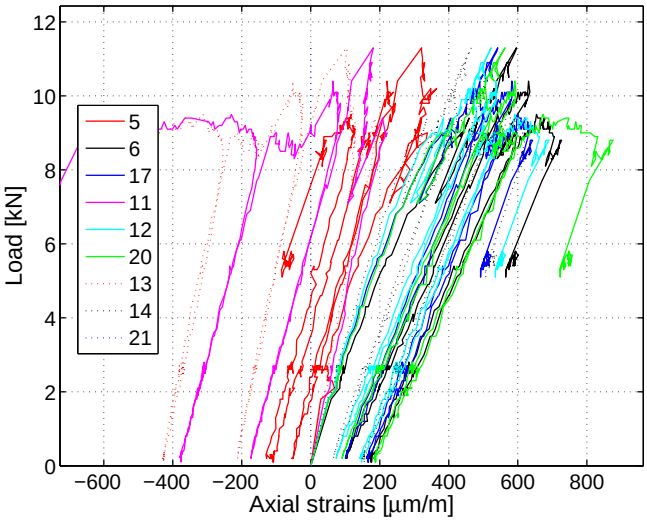

(a) Axial strains at axis D (mid-span)

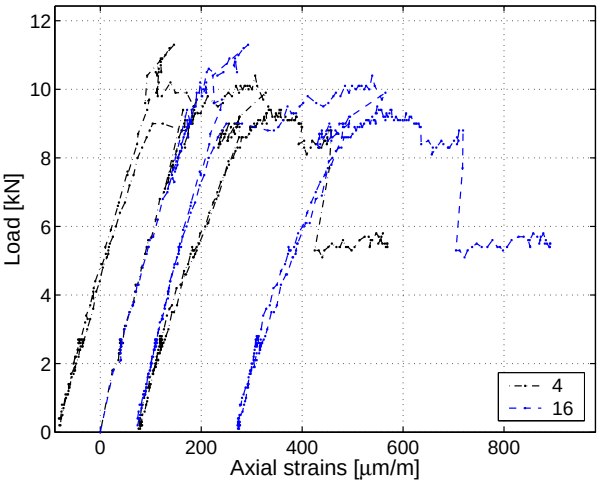

(b) Axial strains at axis E

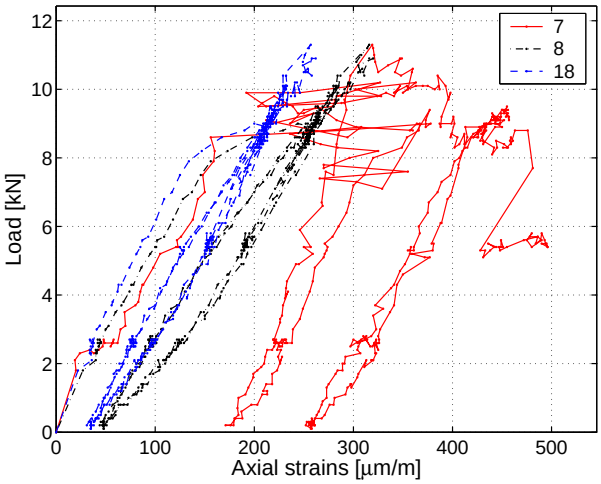

(c) Axial strains at axis C

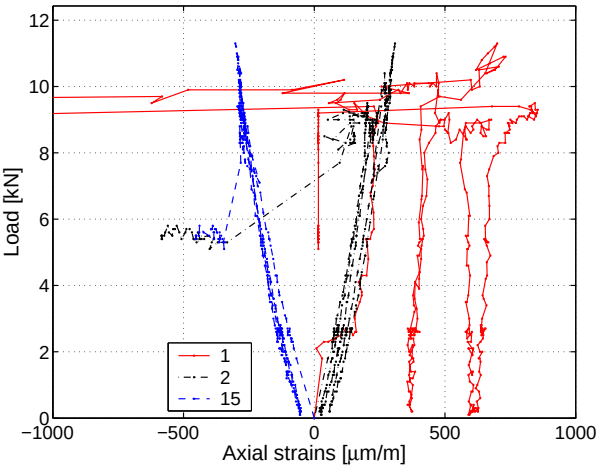

(d) Axial strains at axis F

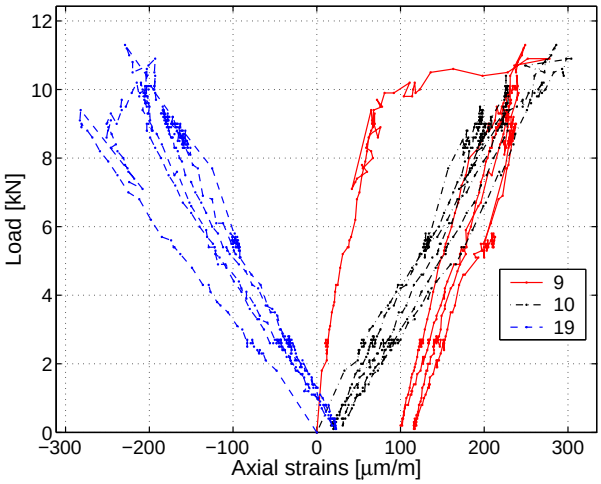

(e) Axial strains at axis B

Figure C.41: 900-2: Axial strains in GFRP profile.

C.4.2.5 Axial strains through the cross section

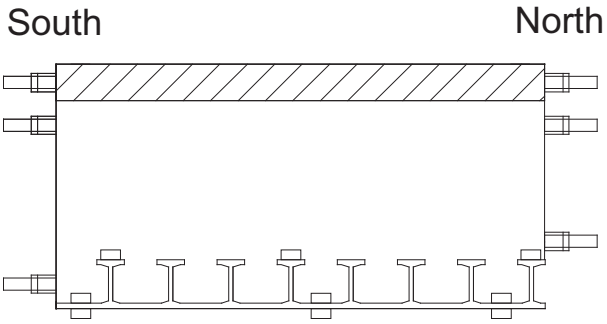

(a) Instrumentation location

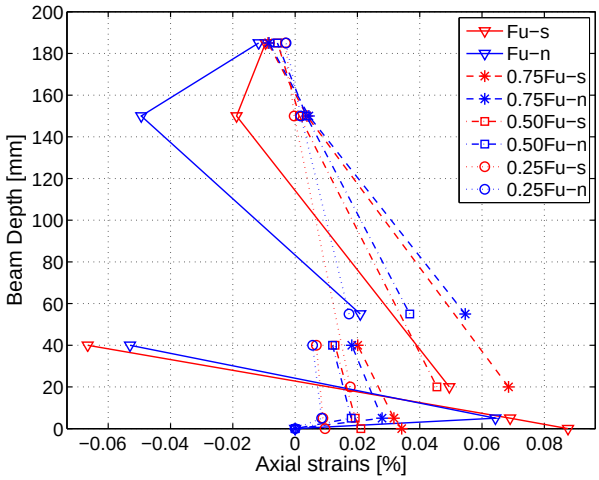

(b) Strain gages and omegas on north and south side

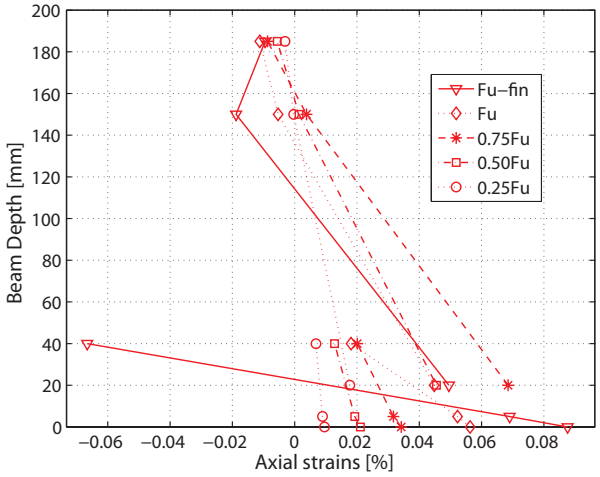

(c) South

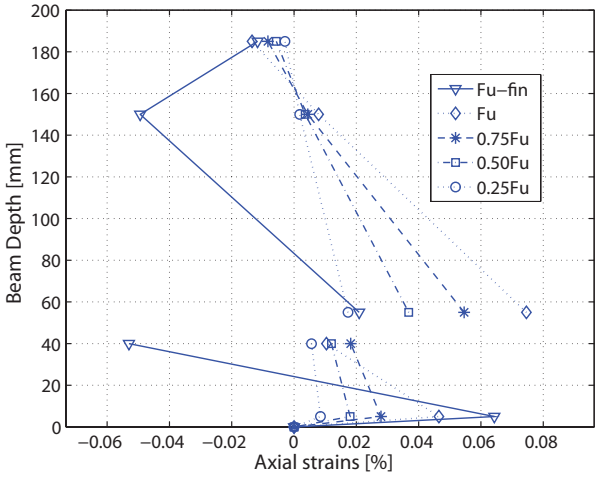

(d) North

Figure C.42: 900-2: Axial strains through cross section at mid-span at different load steps from strain gages and omega-shaped extensometers ($F_u = 11.5\,\text{kN}$ with 9.4 mm and $F_{u-fin} = 8.8\,\text{kN}$ with 31.8 mm corresponding deflections).

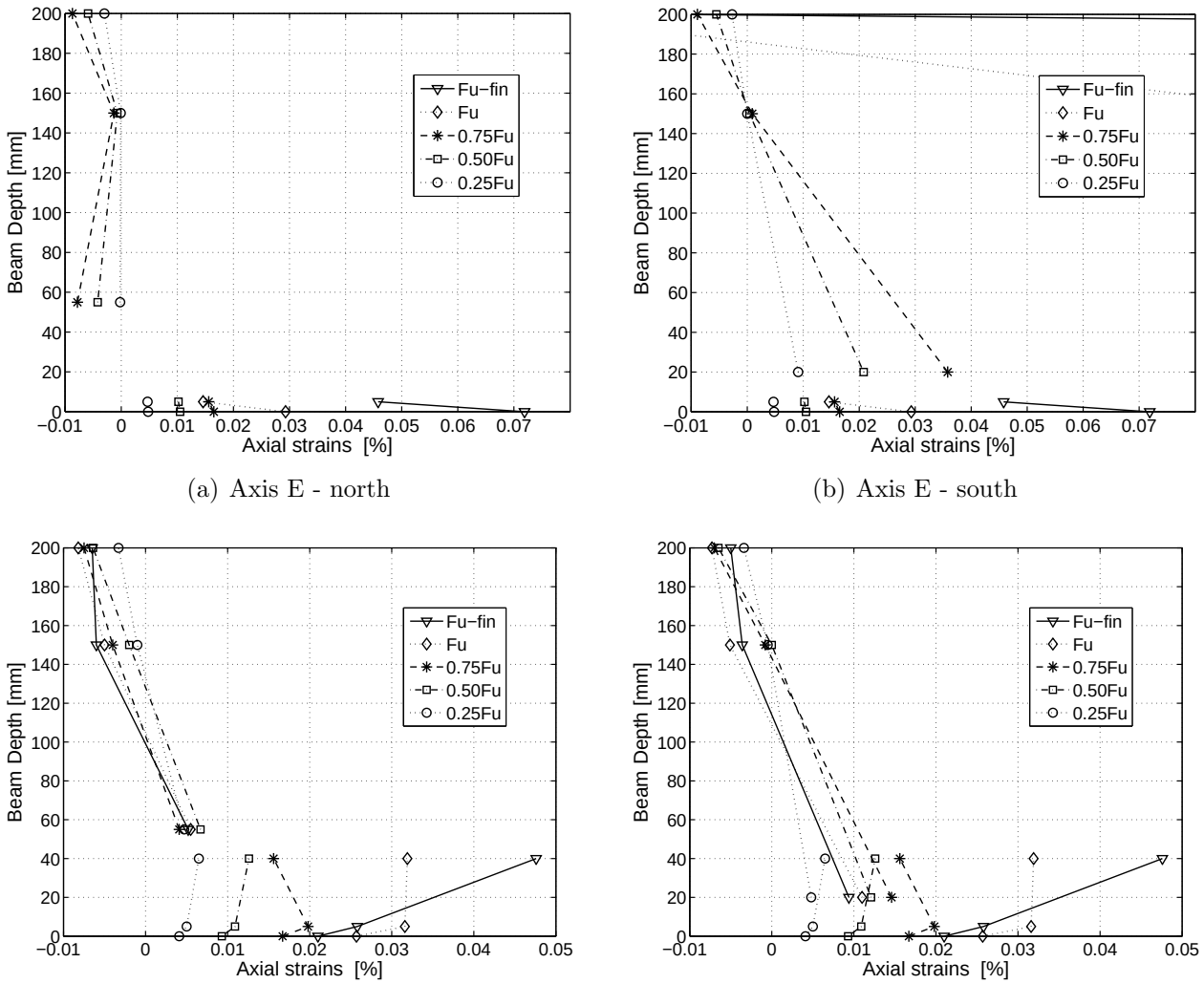

(a) Axis E - north

(b) Axis E - south

(c) Axis C - north

(d) Axis C - south

Figure C.43: 900-2: Axial strains through cross section at 0.75 m and 2.25 m at different load steps from strain gages and omega-shaped extensometers ($F_u = 11.5$ kN with 9.4 mm and $F_{u-fin} = 8.8$ kN with 31.8 mm corresponding deflections).

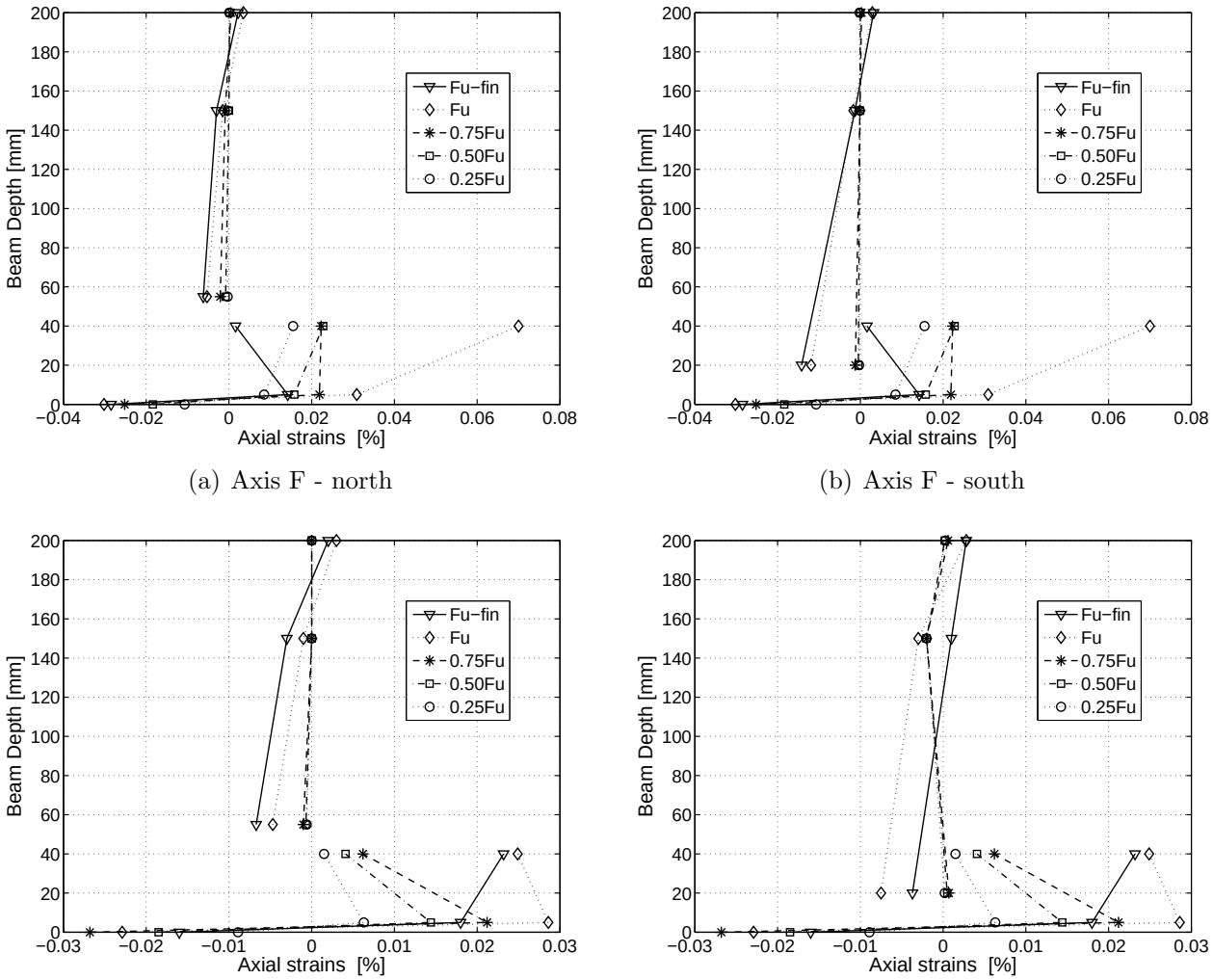

(a) Axis F - north

(b) Axis F - south

(c) Axis B - north

(d) Axis B - south

Figure C.44: 900-2: Axial strains through cross section over supports at different load steps from strain gages and omega-shaped extensometers ($F_u = 11.5\,\text{kN}$ with $9.4\,\text{mm}$ and $F_{u-fin} = 8.8\,\text{kN}$ with $31.8\,\text{mm}$ corresponding deflections).

C.4.2.6 Axial strains along the beam

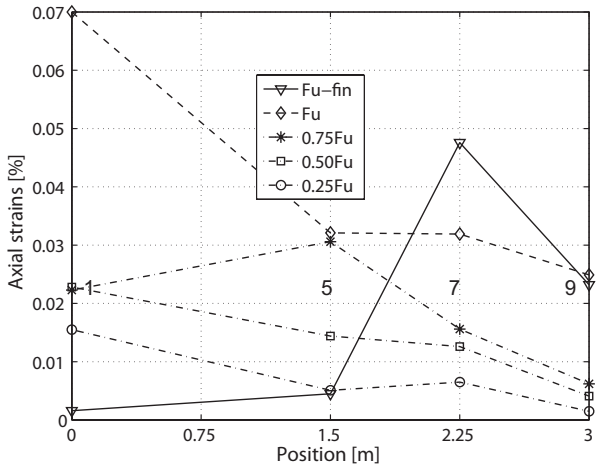

(a) Axial strains on top of T-upstands

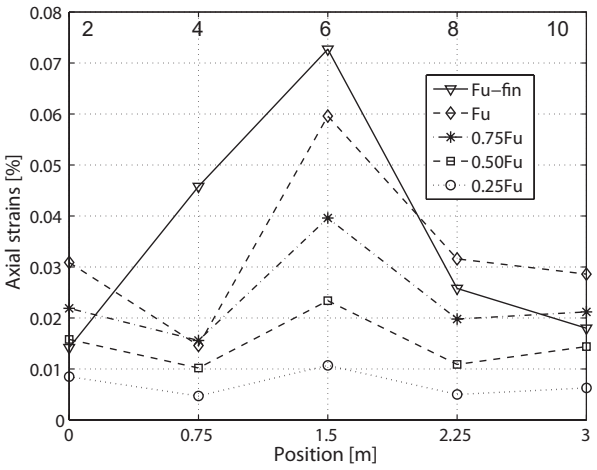

(b) Axial strains between T-upstands

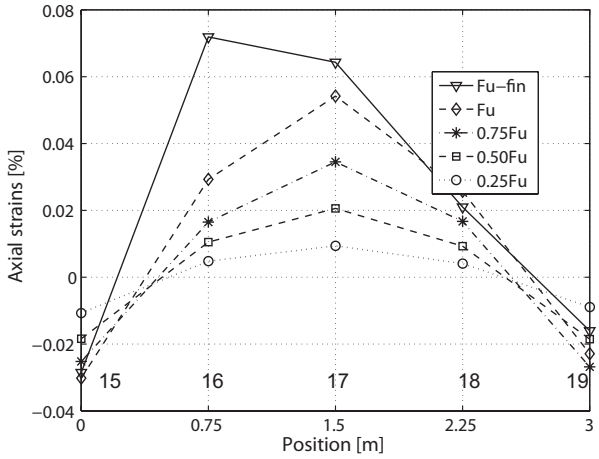

(c) Axial strains beneath GFRP sheet

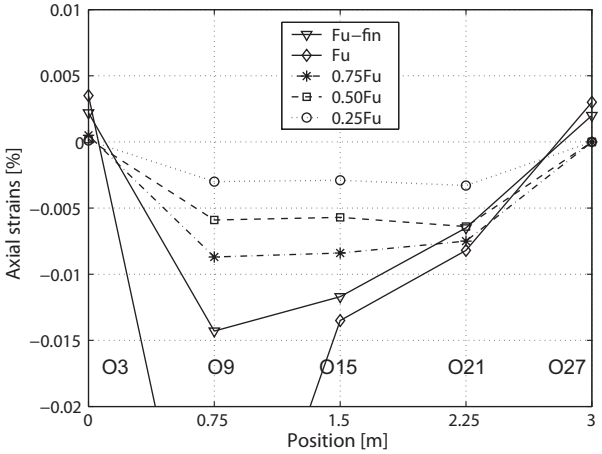

(d) Axial strains in NC layer - north

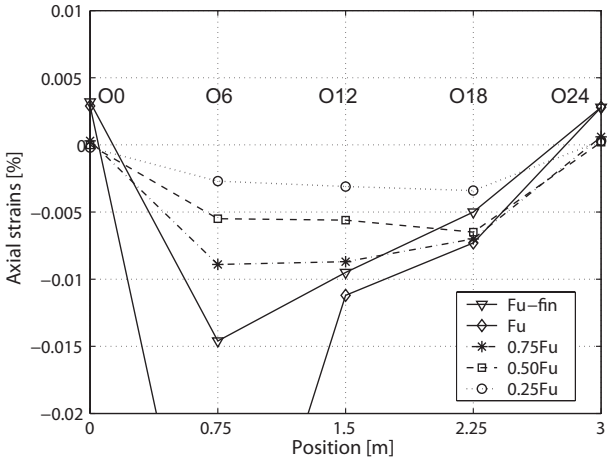

(e) Axial strains in NC layer - south

Figure C.45: 900-2: Axial strains along beam at different load steps from strain gages and omega-shaped extensometers ($F_u = 11.5\,\text{kN}$ with $9.4\,\text{mm}$ and $F_{u-fin} = 8.8\,\text{kN}$ with $31.8\,\text{mm}$ corresponding deflections).

C.4.3 Beam 900E-1: Failure description and measured results (low instrumentation)

C.4.3.1 Failure description

The failure process of beam 900E-1 is illustrated in Figures C.46, C.47 and C.48. The first noise occurred at a load of 15 kN. From 20 kN onwards, some small cracks could be observed in the tension zone of the LC layer next to the loading plate. The beam failed at the ultimate load of $F_u = 31.2$ kN and the corresponding deflection was 8.7 mm. The failure was an immediate and brittle shear failure of the lightweight concrete. The diagonal crack occurred at approximately 60 cm from the mid-span. The crack at the FRP-LC interface developed horizontally along the top of the T-webs up to the beam end (Figure C.46-a). The cracks propagated through the lightweight aggregates and the FRP-LC interface with the epoxy resin remained undamaged, (Figure C.46-b). After failure, the load decreased immediately to the final value of 3 kN, where the experiment was stopped. The failed and still loaded specimen is shown in Figures C.49 and C.50.

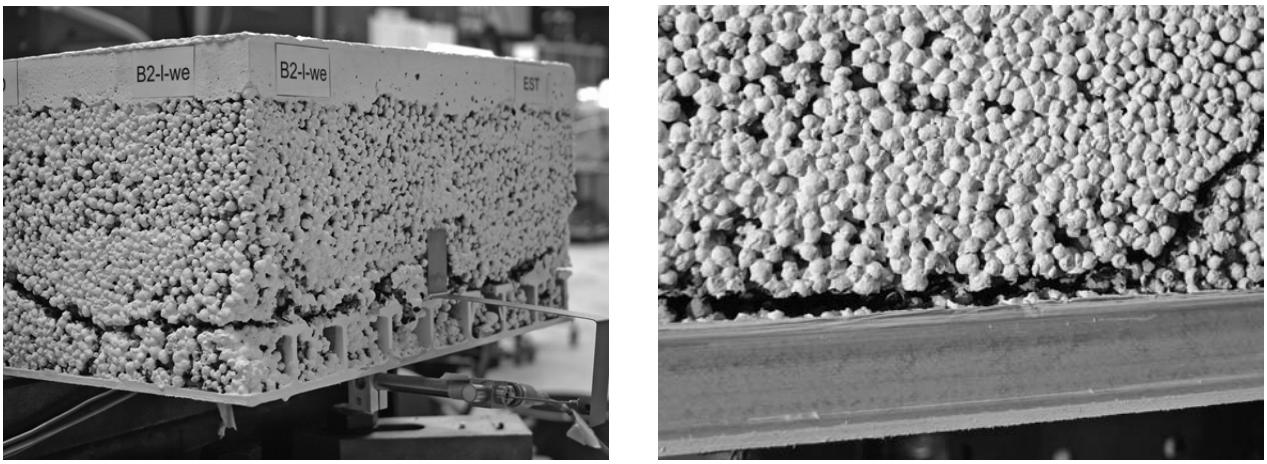

(a) Crack up to beam end (b) Shear failure through aggregate

Figure C.46: 900E-1: LC shear failure.

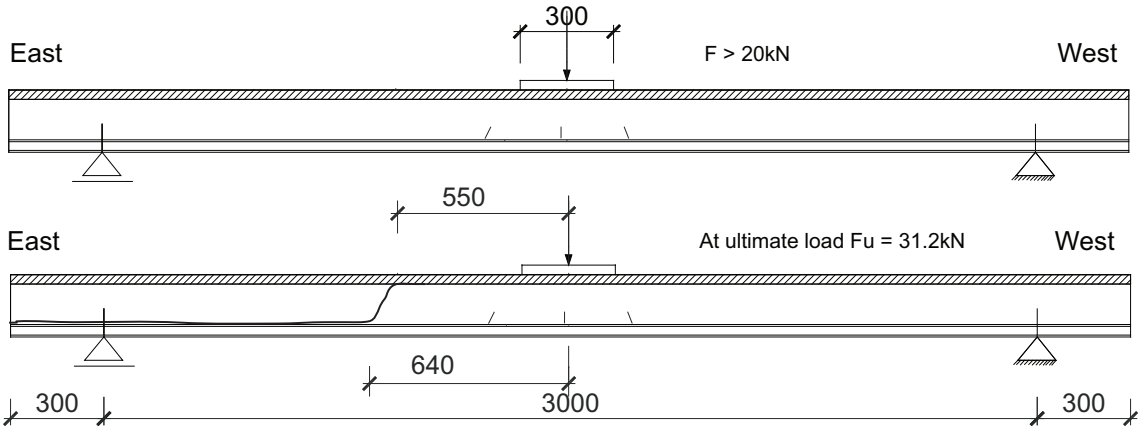

(a) View from north - failure process

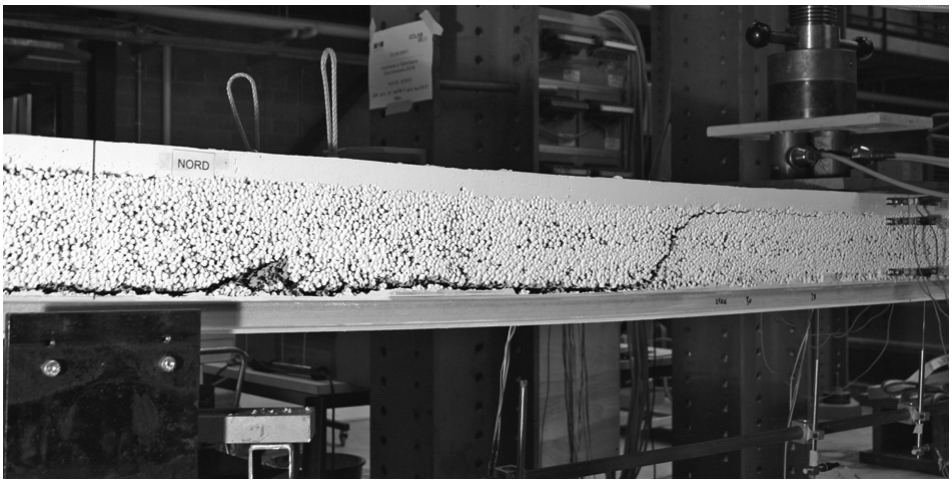

(b) View from north

Figure C.47: 900E-1: a) Failure process and b) still loaded failed beam after experiment - north.

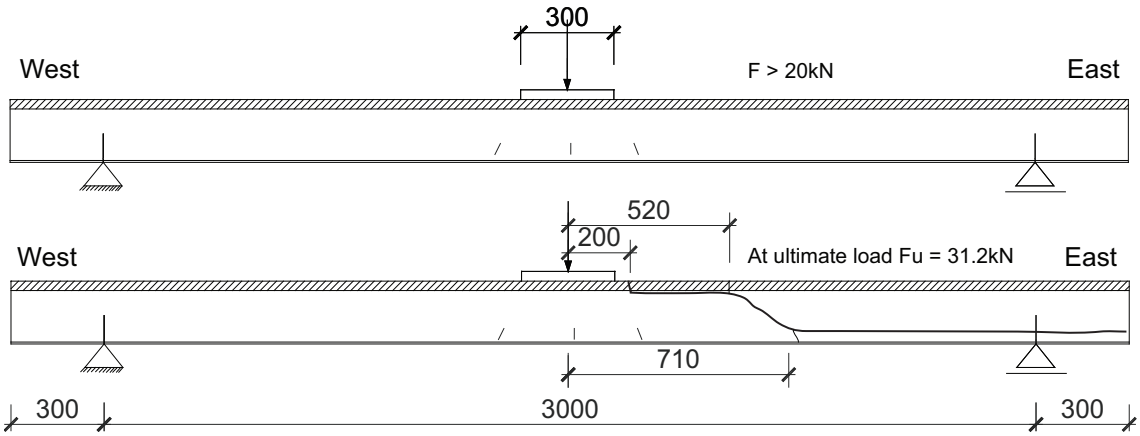

(a) View from south - failure process

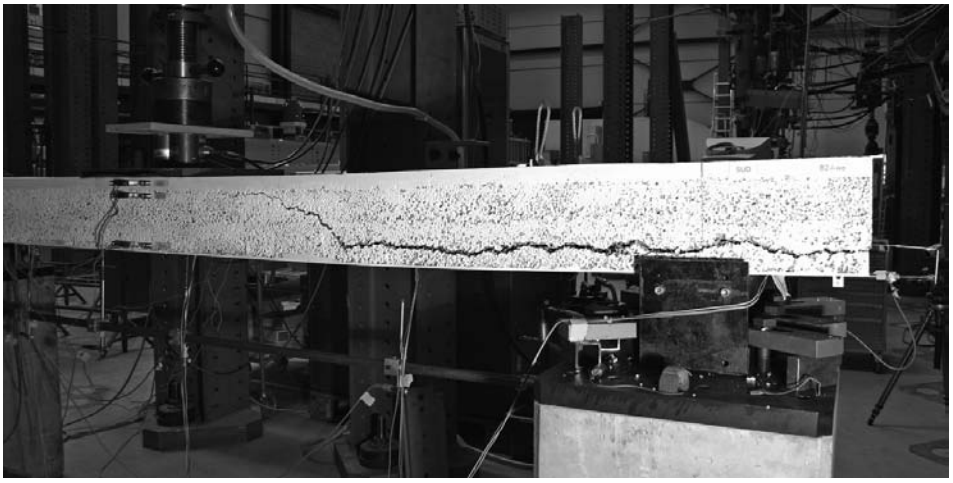

(b) View from south

Figure C.48: 900E-1: a) Failure process and b) still loaded failed beam after experiment - south.

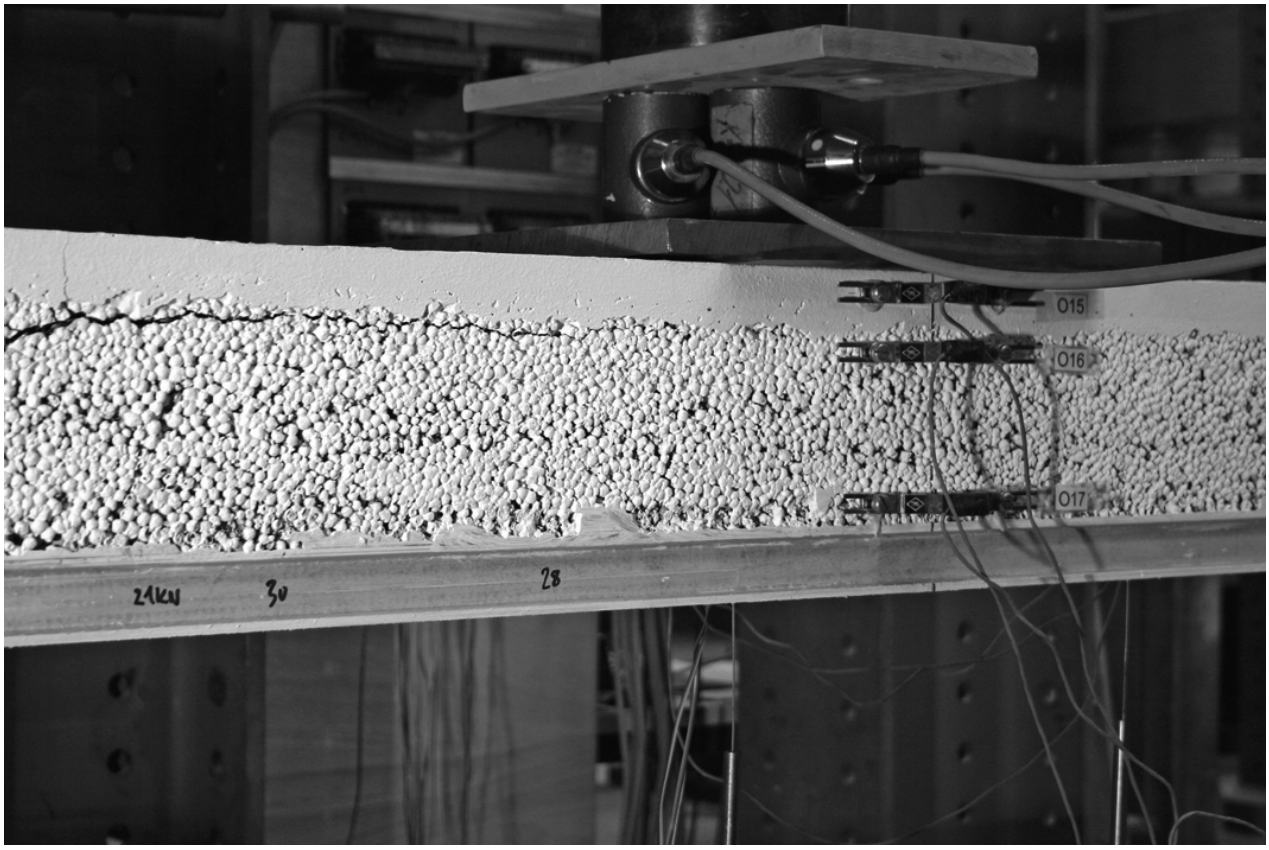

(a) View from north - mid-span

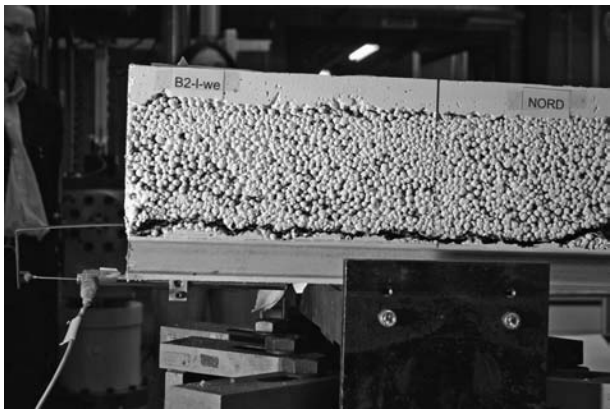

(b) Crack through eastern beam end

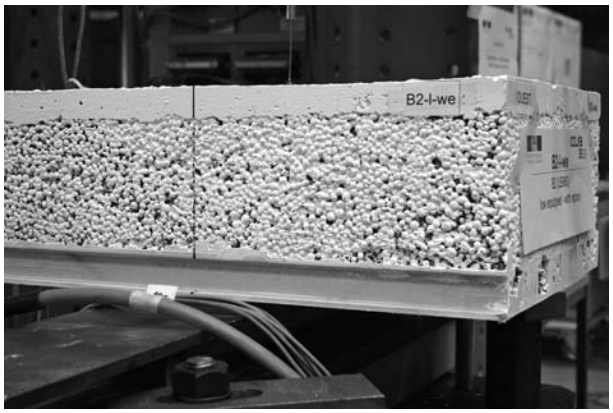

(c) Undamaged western beam end

Figure C.49: 900E-1: Failed beam after experiment, still loaded - north.

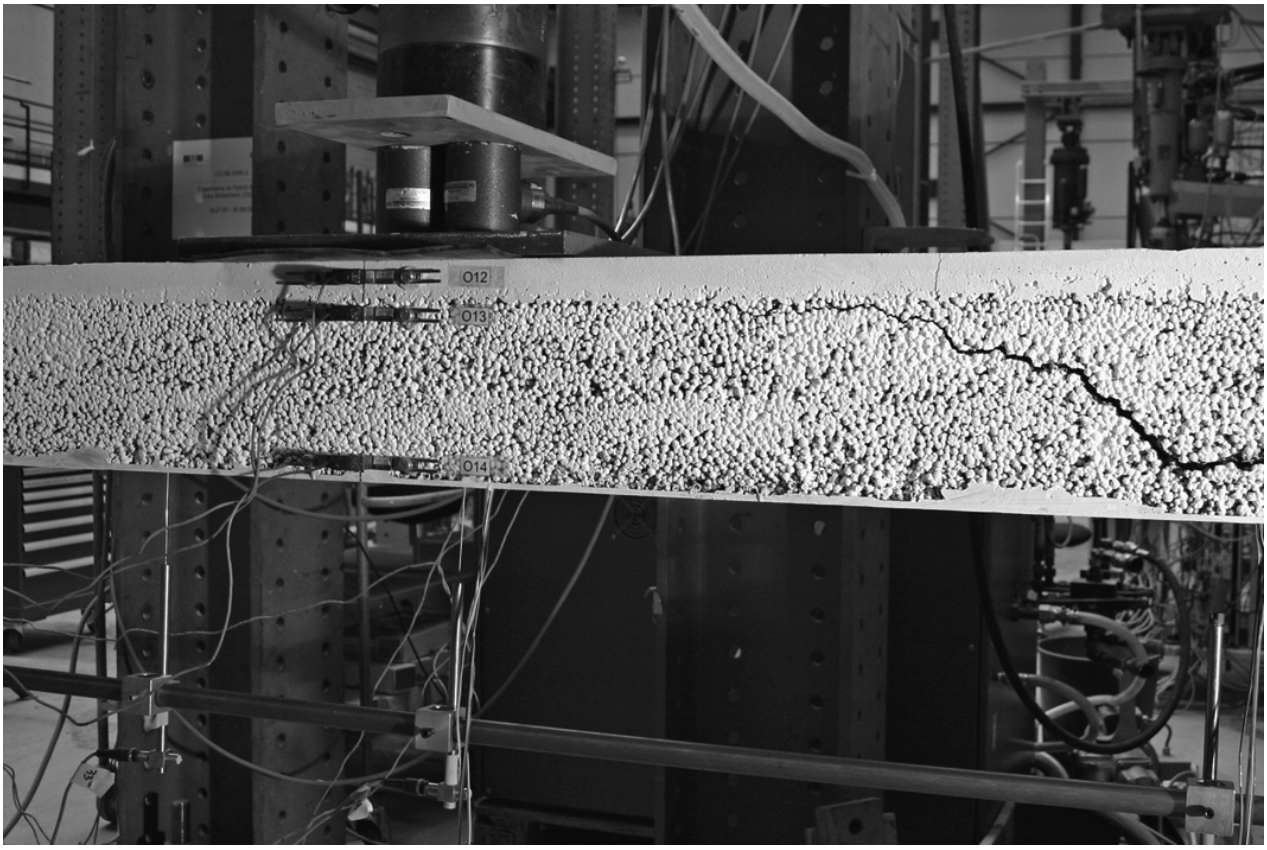

(a) View from south - mid-span

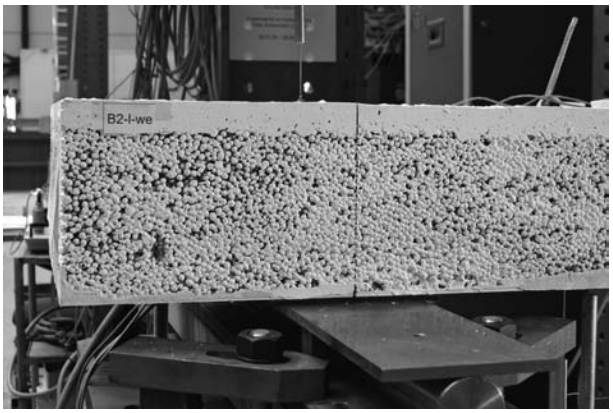

(b) Undamaged western beam end

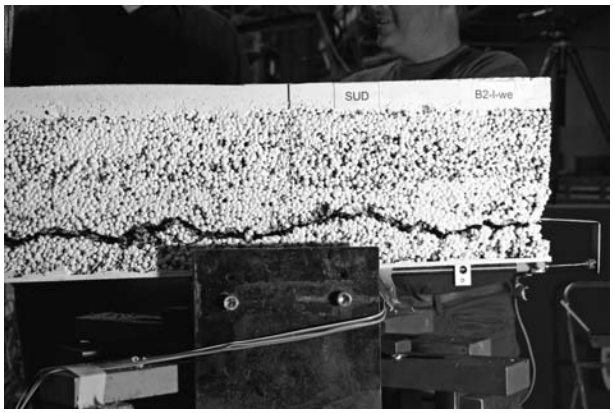

(c) Crack through eastern beam end

Figure C.50: 900E-1: Failed beam after experiment, still loaded - south.

C.4.3.2 Displacement transducers

Figure C.51 shows the load deflection response of the beam. Beam stiffness was almost constant up to the cracking load of approximately 10.5 kN, after which the beam lost its stiffness slightly. At 31.2 kN immediate failure occurred with a corresponding mid-span deflection of 8.7 mm.

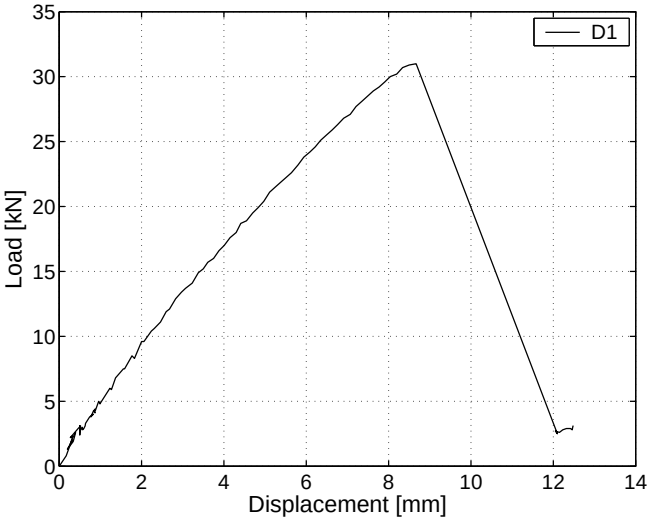

(a) Displacement at mid-span

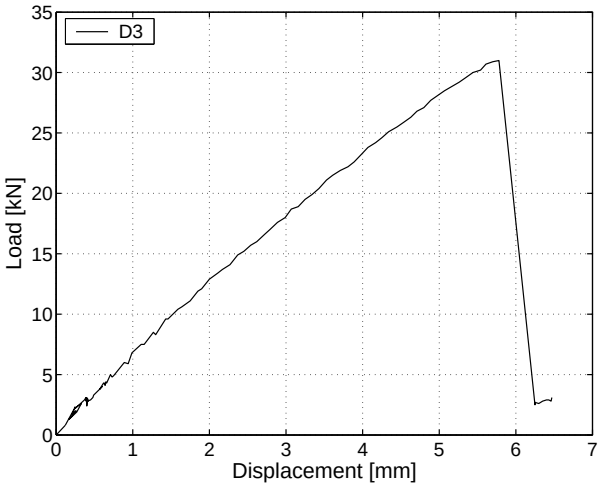

(b) Displacement - axis E

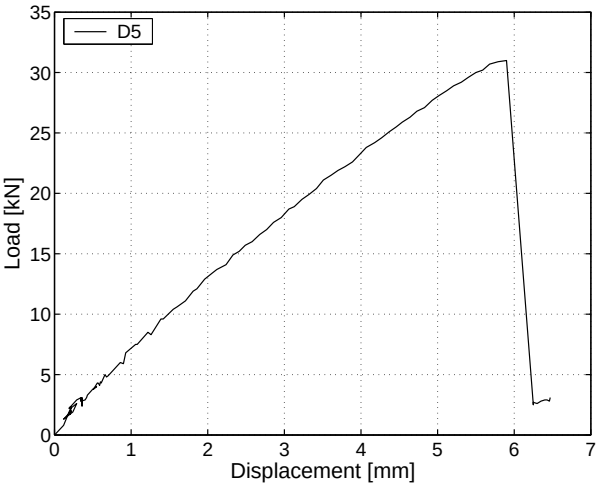

(c) Displacement - axis C

Figure C.51: 900E-1: Displacement at mid-span, at 0.75 m and 2.25 m.

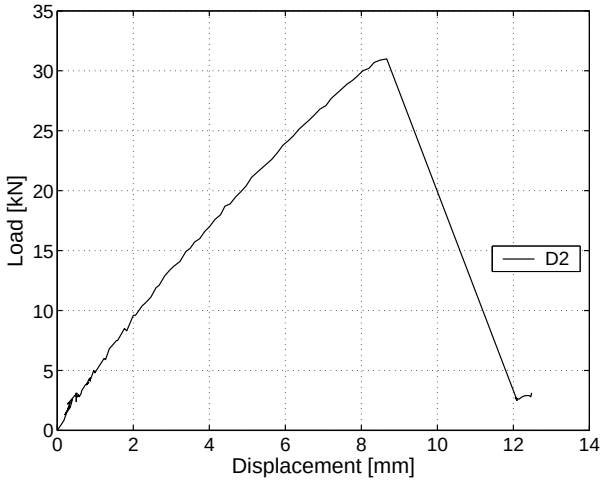

(a) Displacement - between axes D-E

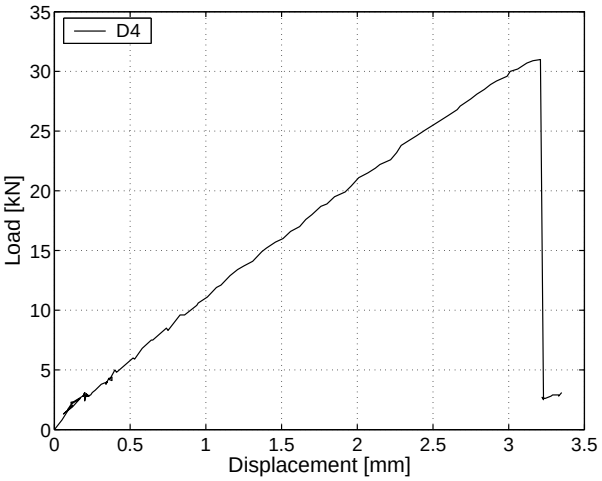

(b) Displacement - between axes E-F

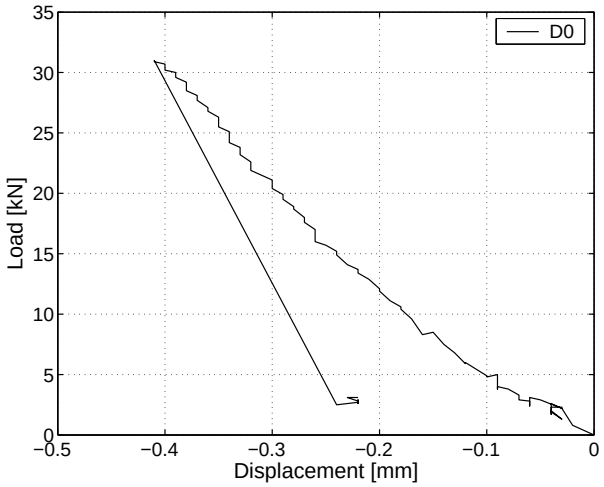

(c) Displacement at fixed support - axis F

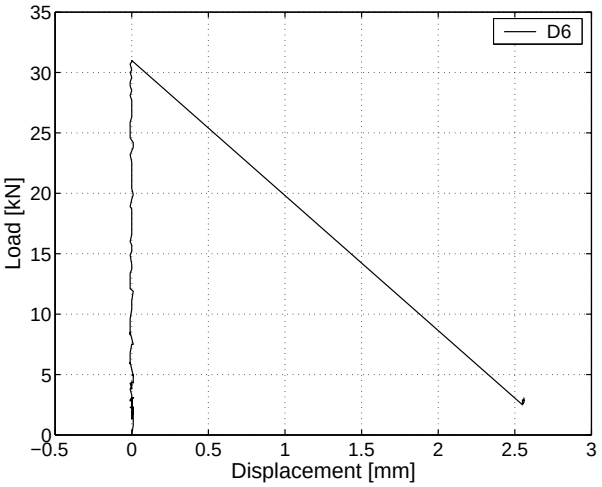

(d) Horizontal displacement of LC - axis A

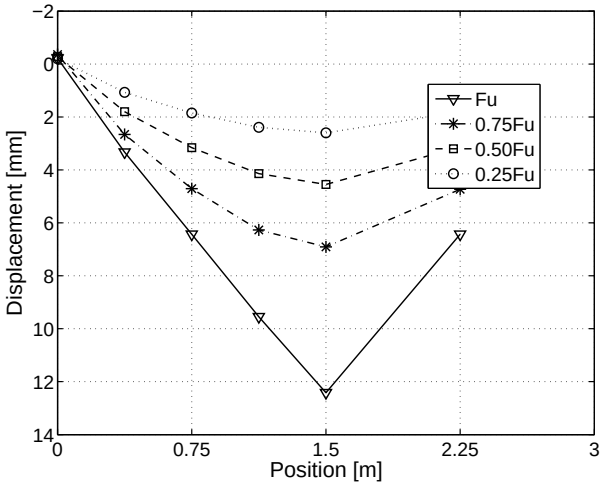

(e) Displacement along beam

Figure C.52: 900E-1: Displacements at different sections and along beam.

C.4.3.3 Omega-shaped extensometers

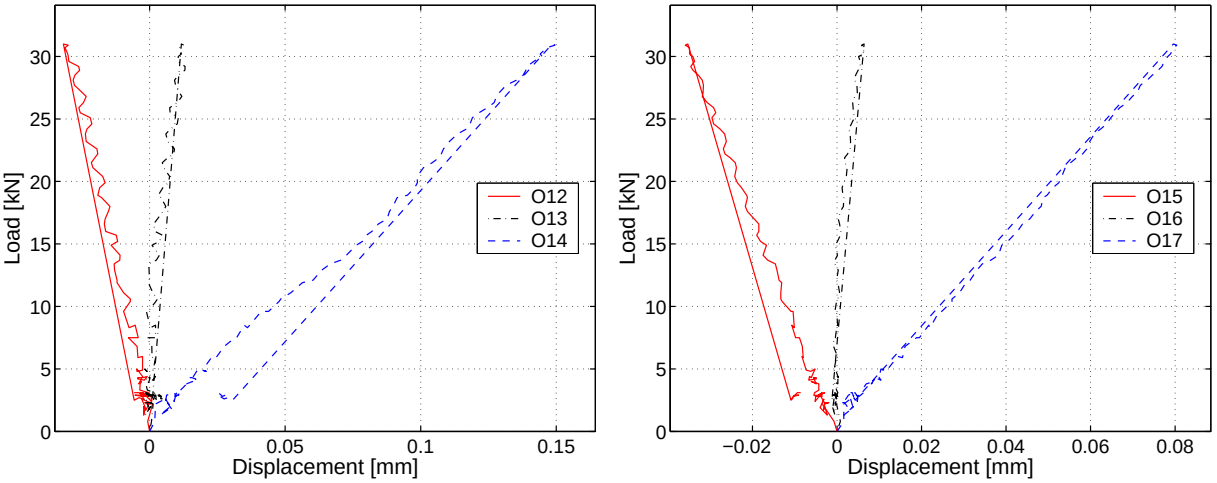

(a) Axis D (mid-span) - south

(b) Axis D (mid-span) - north

Figure C.53: 900E-1: Deformations in omega-shaped extensometers at mid-span.

C.4.3.4 Strain gages on GFRP profile

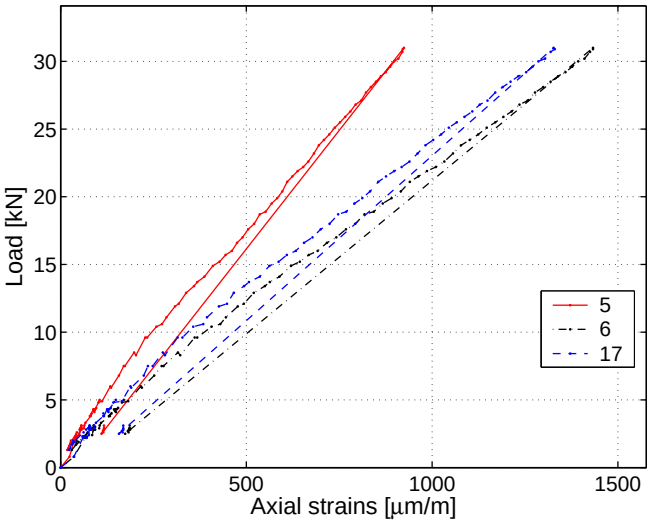

(a) Axial strains at axis D (mid-span)

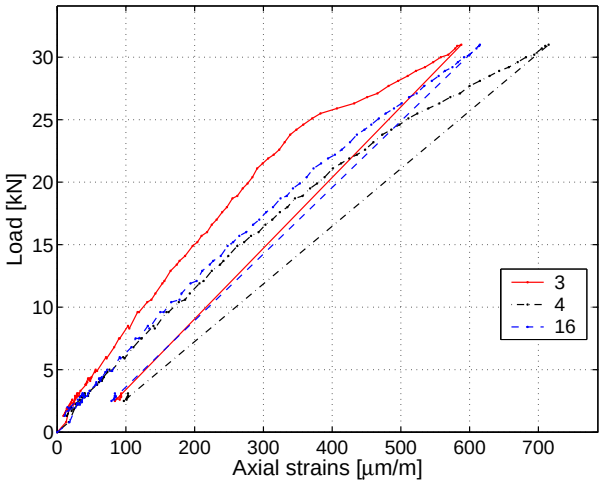

(b) Axial strains at axis E

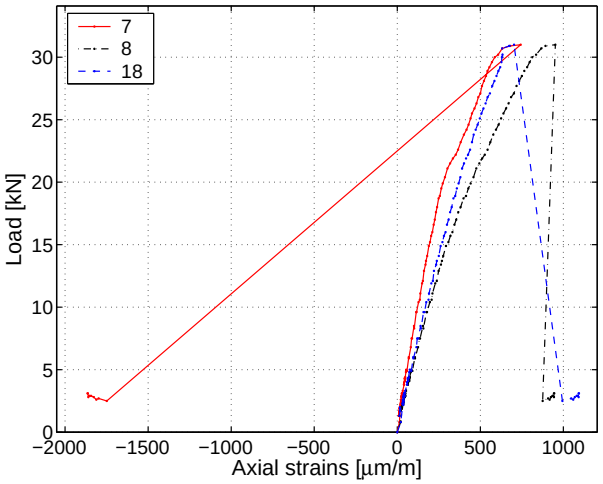

(c) Axial strains at axis C

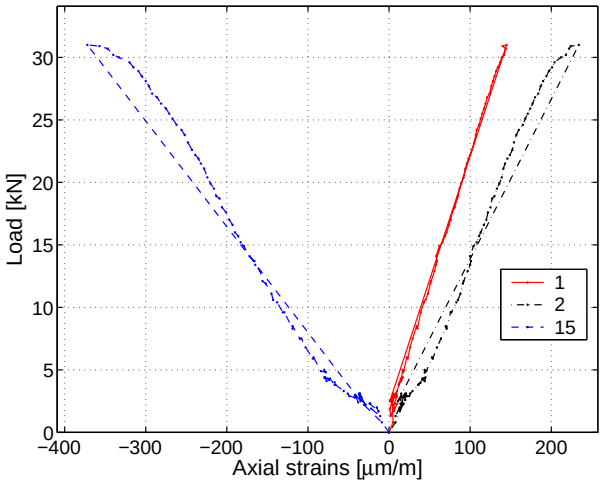

(d) Axial strains at axis F

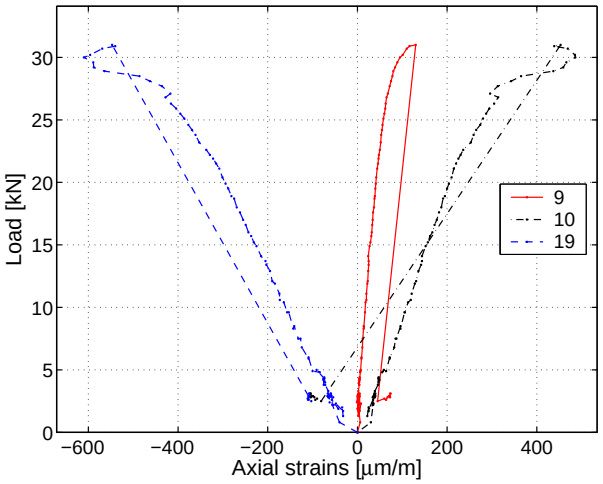

(e) Axial strains at axis B

Figure C.54: 900E-1: Axial strains in GFRP profile

C.4.3.5 Axial strains through the cross section

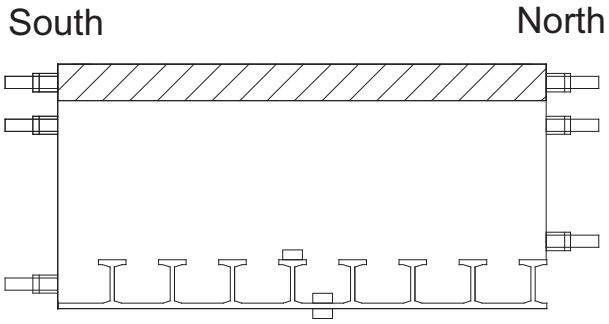

(a) Instrumentation location

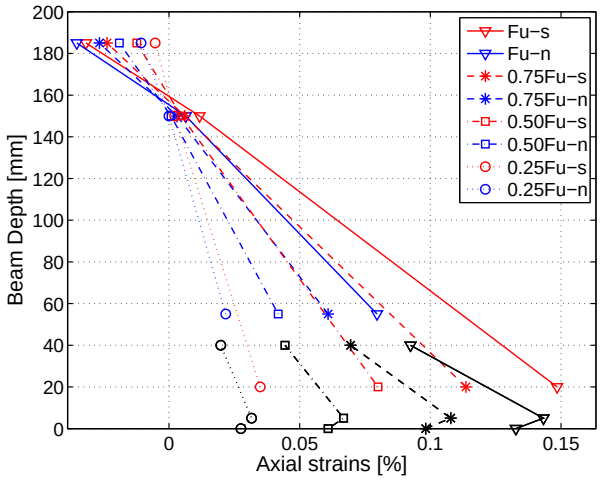

(b) Strain gages on centerline and omegas on north and south side

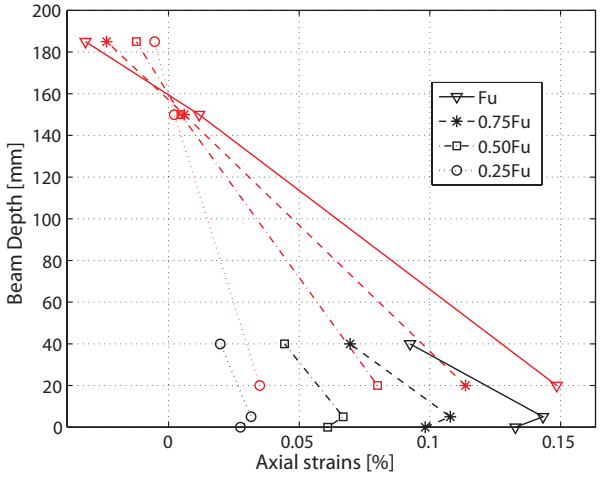

(c) South

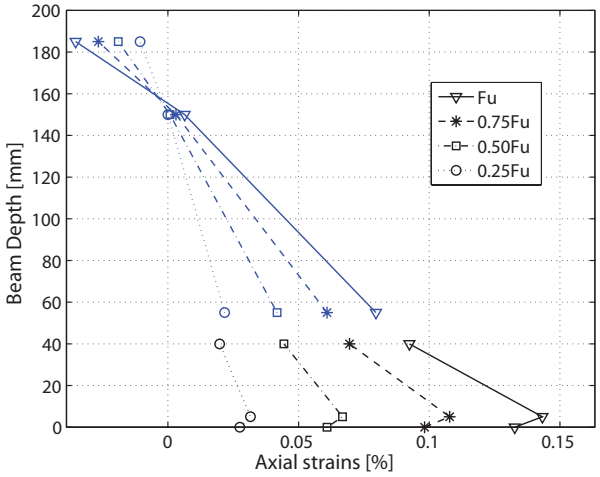

(d) North

Figure C.55: 900E-1: Axial strains through cross section at mid-span at different load steps from strain gages and omega-shaped extensometers.

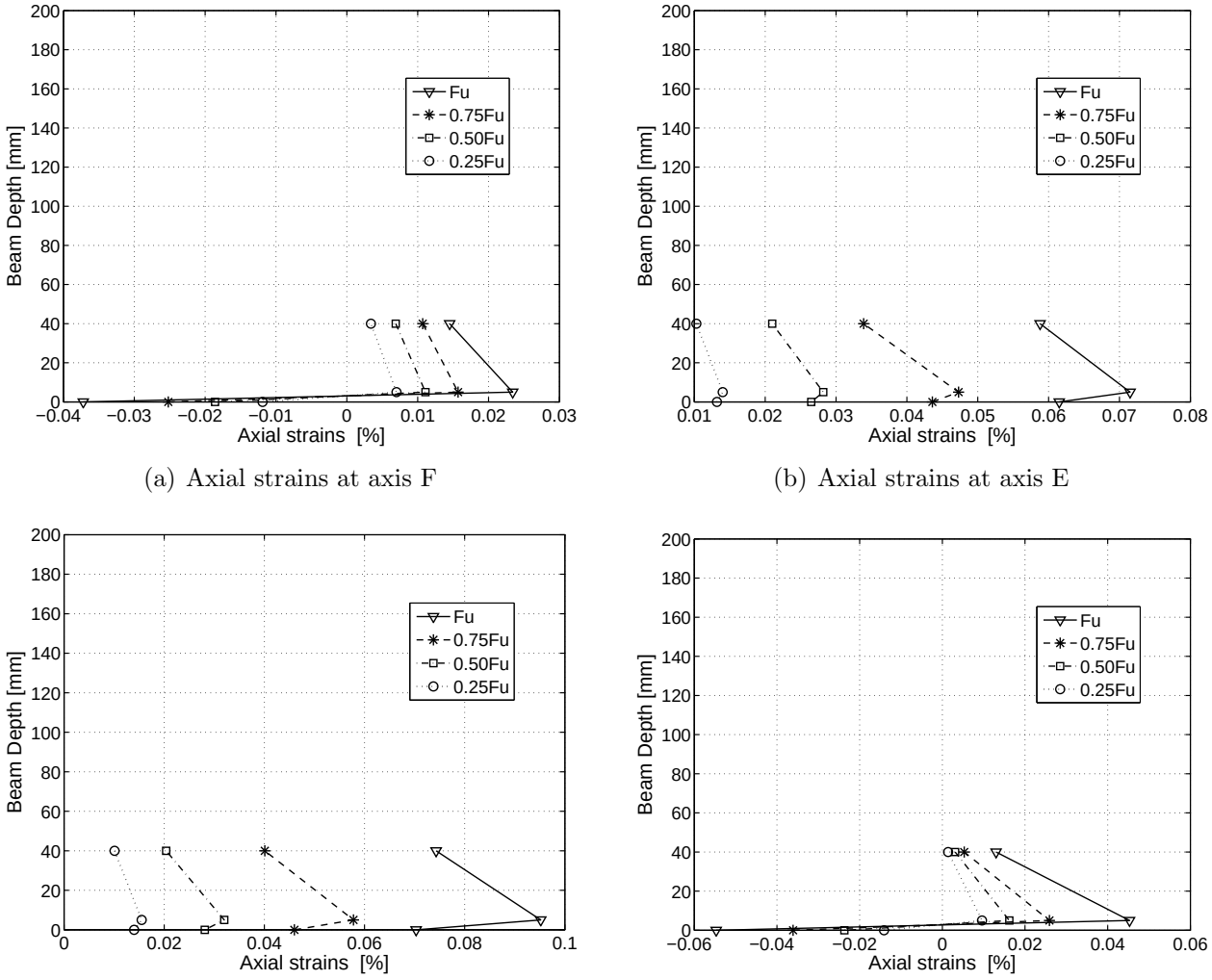

(a) Axial strains at axis F

(b) Axial strains at axis E

(c) Axial strains at axis C

(d) Axial strains at axis B

Figure C.56: 900E-1: Axial strains through GFRP cross section at different load steps.

C.4.3.6 Axial strains along the beam

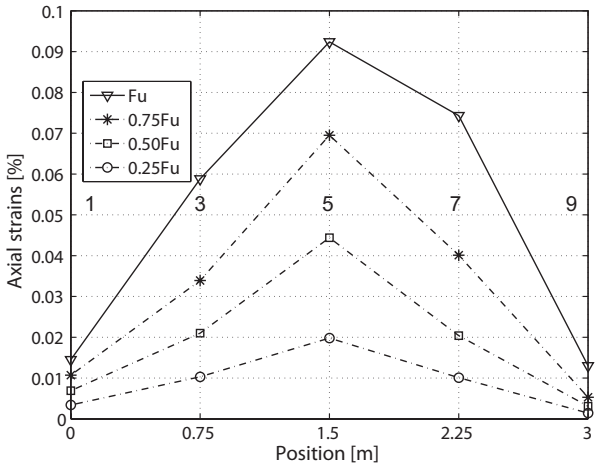

(a) Axial strains on top of T-upstands

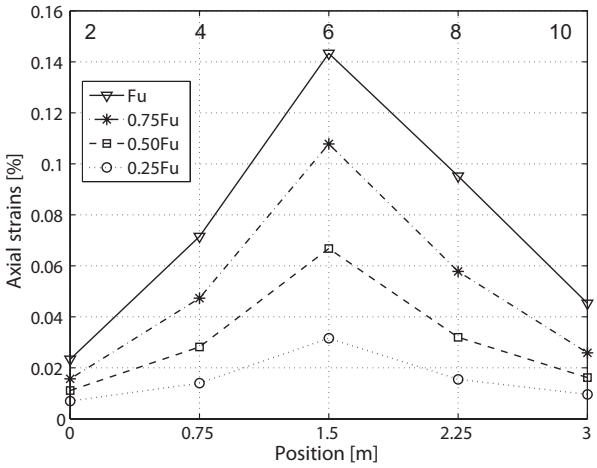

(b) Axial strains between T-upstands

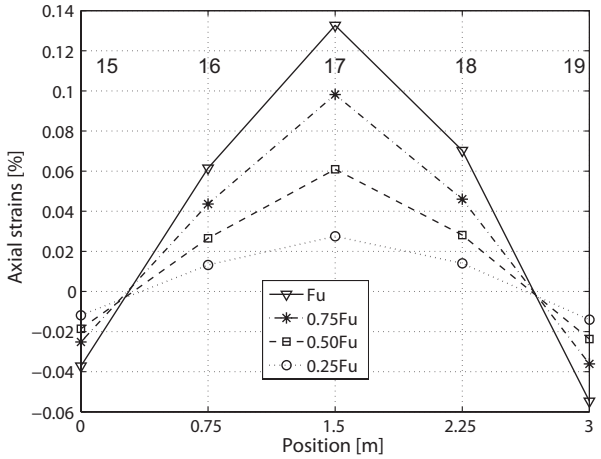

(c) Axial strains beneath GFRP sheet

Figure C.57: 900E-1: Axial strains in GFRP profile along beam at different load steps.

C.4.4 Beam 900E-2: Failure description and measured results (full instrumentation)

C.4.4.1 Failure description

The failure process of beam 900E-2 is illustrated in Figures C.58 and C.59. The first small vertical cracks occurred at a load of 26.6 kN in the tension zone of the beam and distributed along the beam length. As already observed in bonded beam 900E-1, failure was immediate and brittle. The ultimate load was $F_u = 30.4\,\text{kN}$ with a corresponding deflection of 8.1 mm. The final crack occurred diagonally through the LC layer and then immediately propagated horizontally up to the beam end. The bonded interface remained undamaged. The still loaded and failed specimen is shown in Figures C.60 and C.61.

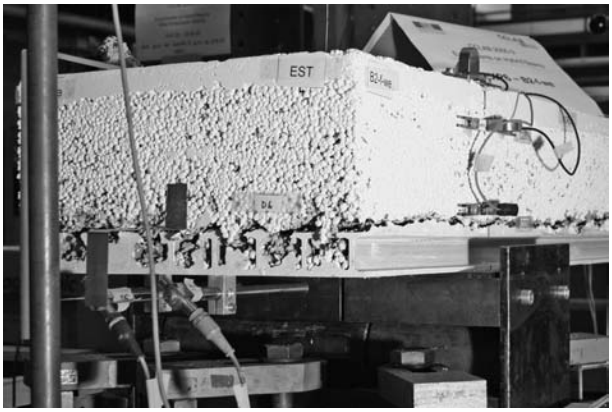

Figure C.58: 900E-2: View of beam end after experiment.

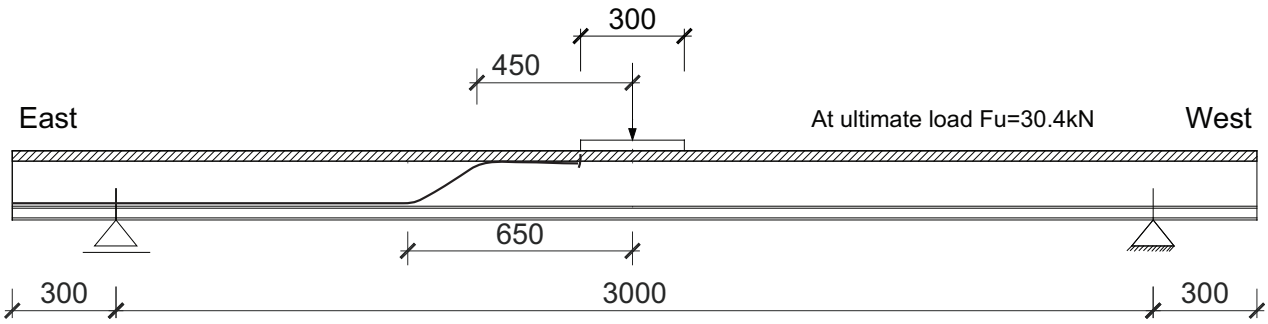

(a) View from north - cracked beam

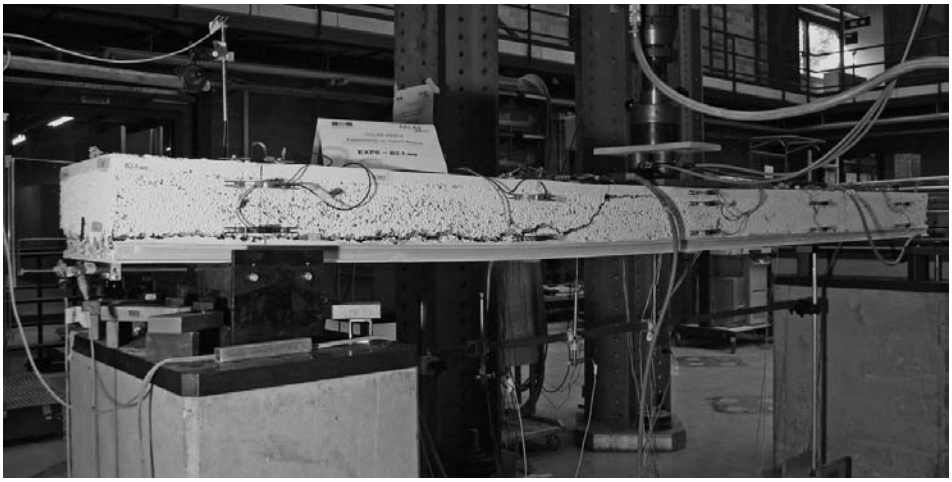

(b) View from north

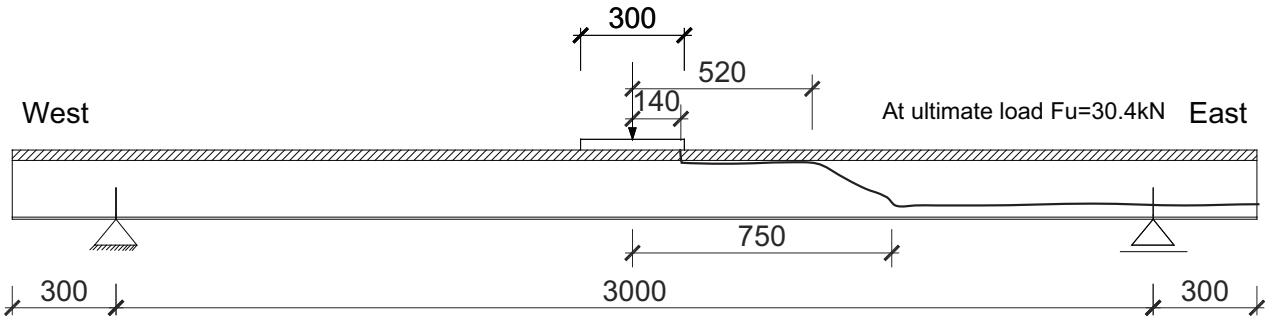

(c) View from south - cracked beam

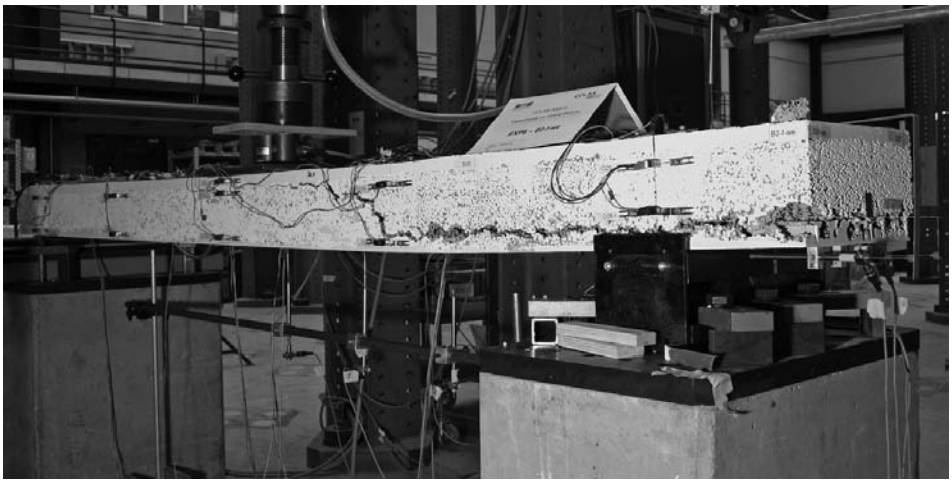

(d) View from south

Figure C.59: 900E-2: a) Failure process and b) still loaded failed beam after experiment.

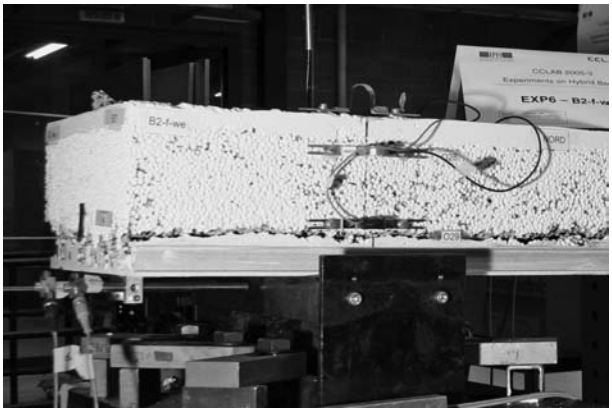

(a) View from north - axis B

(b) View from north - axis C

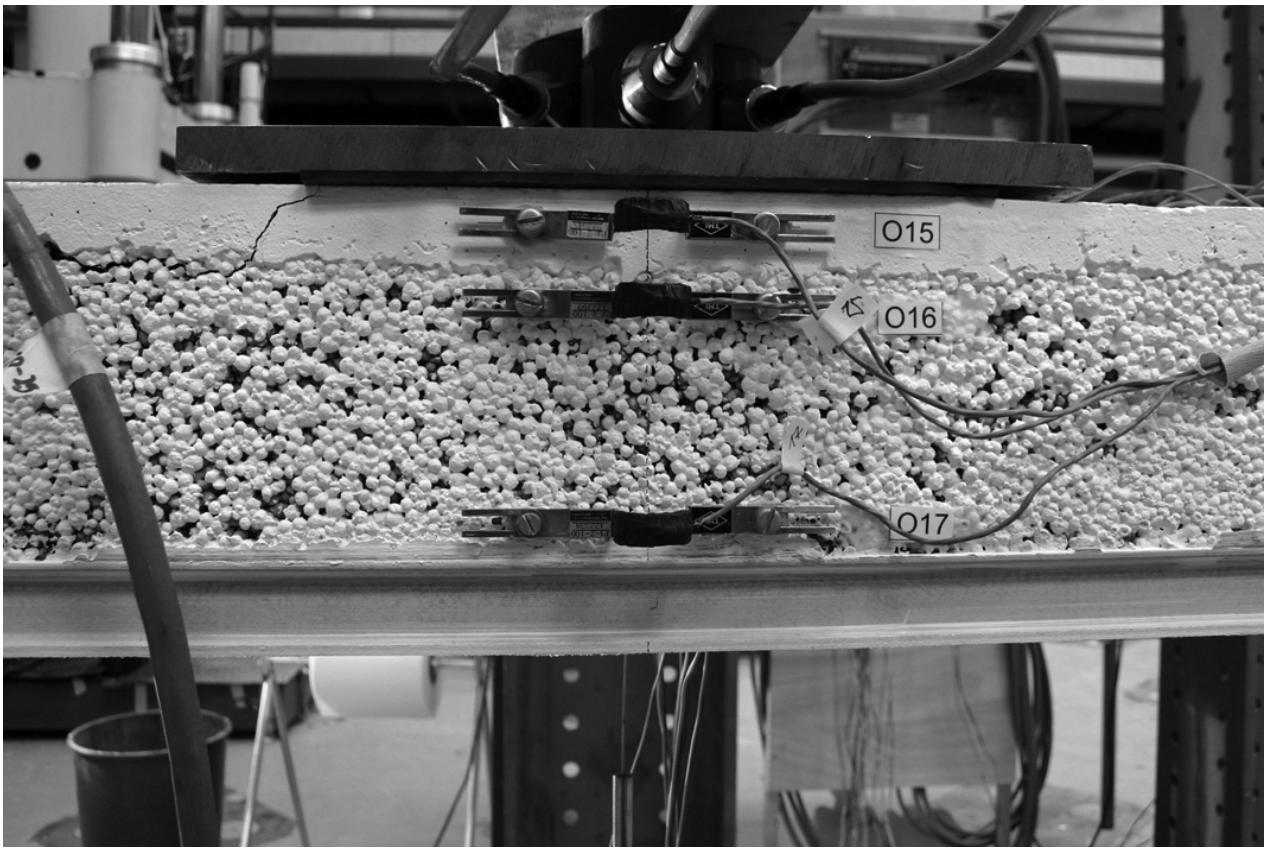

(c) View from north - mid-span

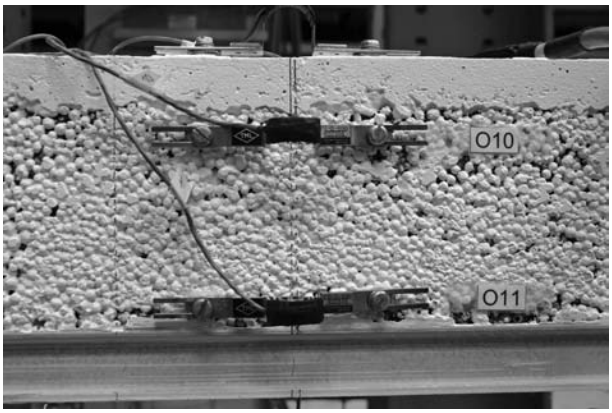

(d) View from north - axis E

(e) View from north - axis F

Figure C.60: 900E-2: Failed beam after experiment, still loaded - north.

(a) View from south - axis F

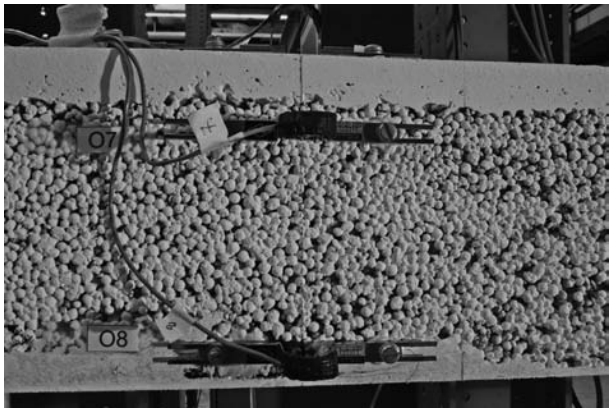

(b) View from south - axis E

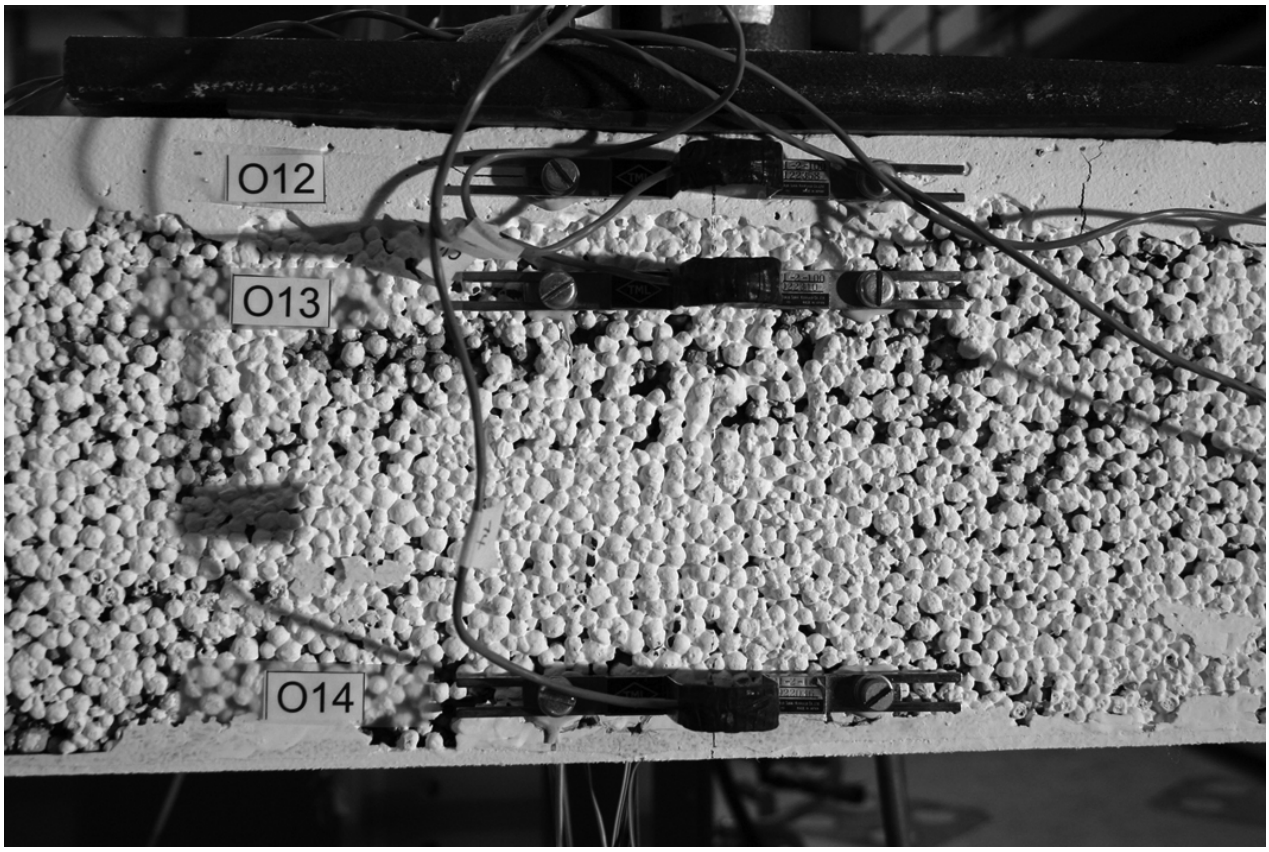

(c) View from south - mid-span

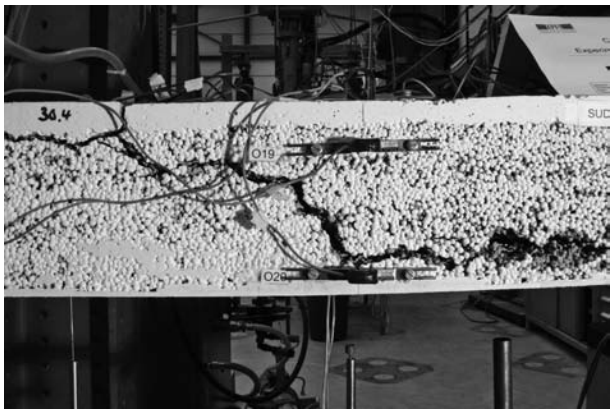

(d) View from south - axis C

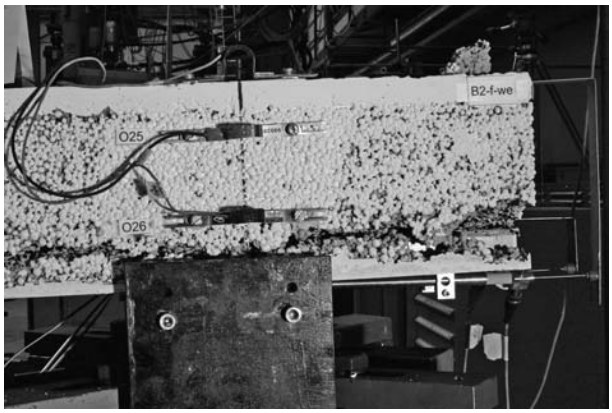

(e) View from south - axis B

Figure C.61: 900E-2: Failed beam after experiment, still loaded - south.

C.4.4.2 Displacement transducers

Figure C.62 shows the load deflection response of the beam. Beam stiffness remained almost constant up to a load of approximately 10.0 kN and then the beam lost its stiffness slightly. At 30.4 kN immediate failure occurred with a corresponding mid-span deflection of 8.1 mm.

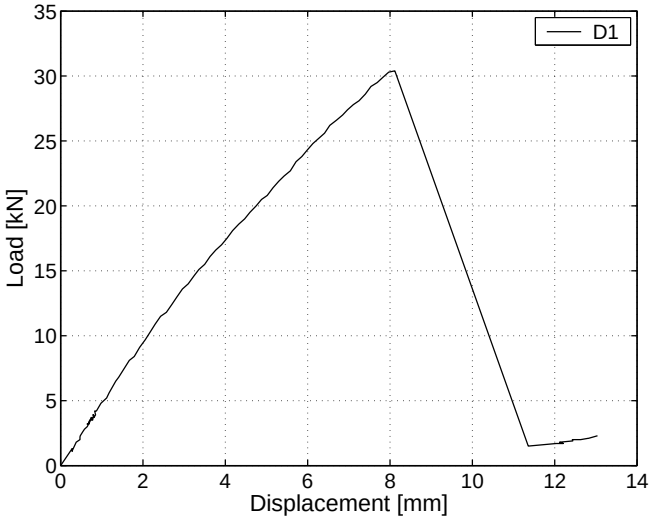

(a) Displacement at mid-span

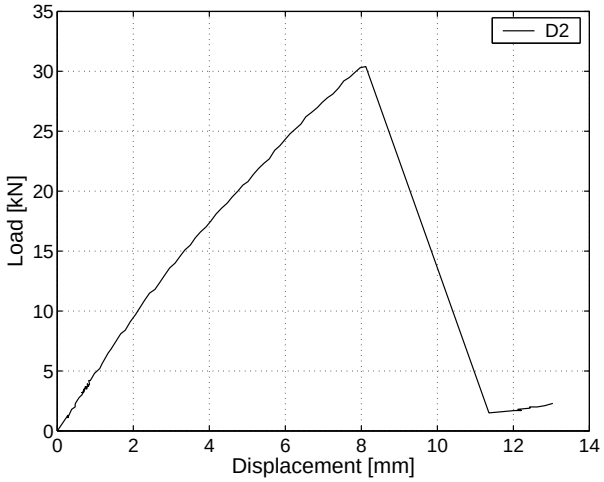

(b) Displacement - between axes C-D

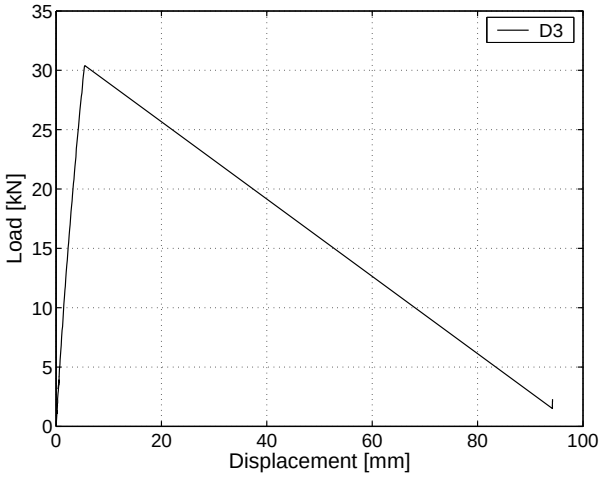

(c) Displacement - axis C

Figure C.62: 900E-2: Displacement at mid-span, at 0.75 m and 2.25 m.

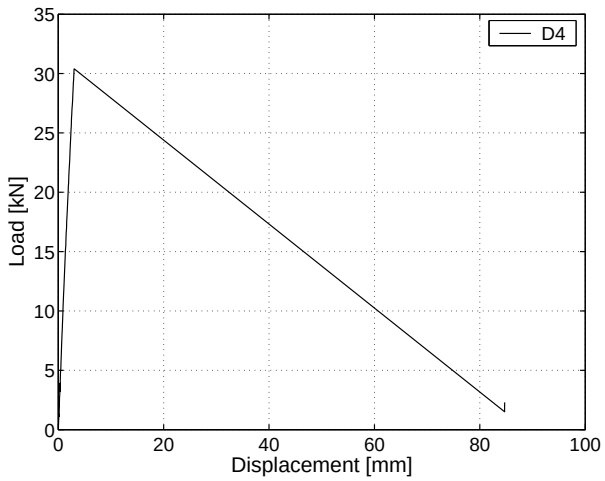

(a) Displacement - between axes B-C

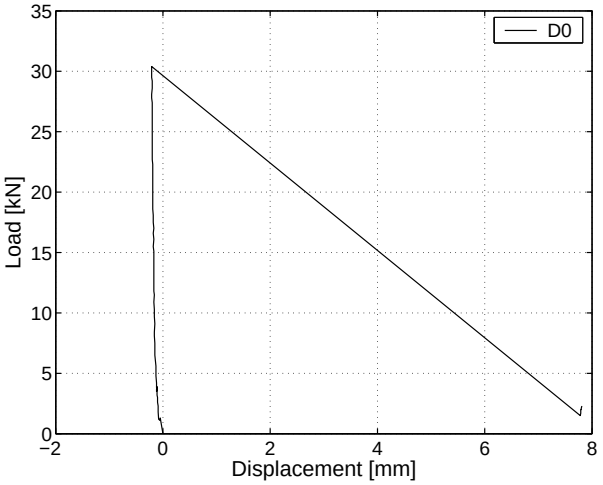

(b) Displacement at free support axis B

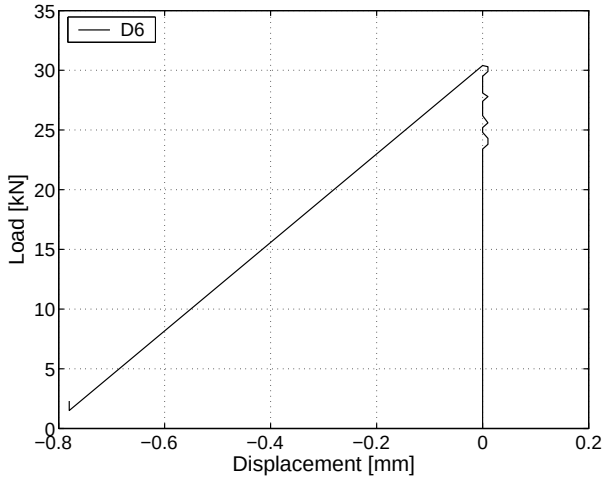

(c) Horizontal displacement of LC - axis A

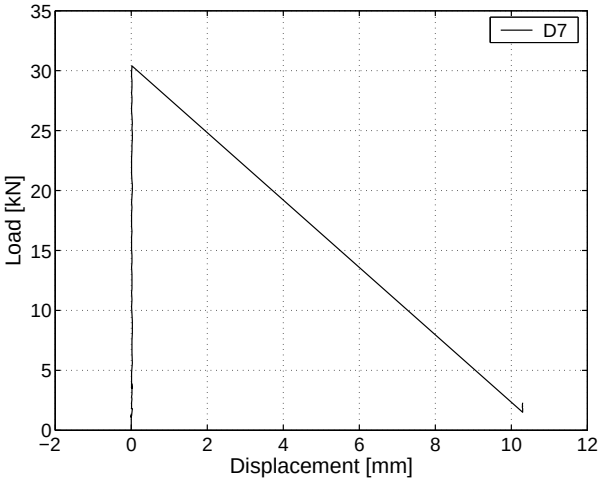

(d) Horizontal displacement of NC - axis A

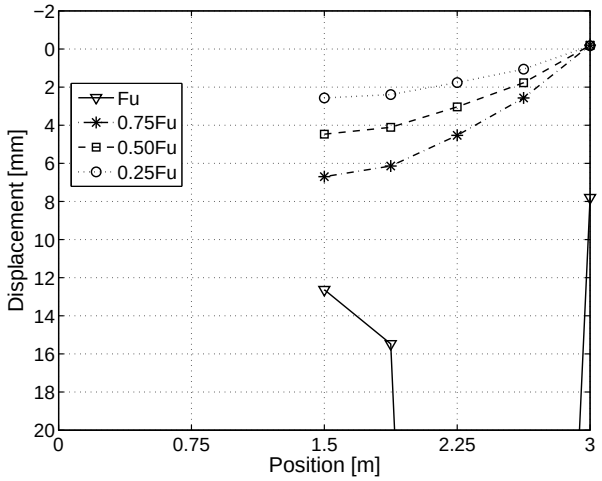

(e) Displacement along beam

Figure C.63: 900E-2: Displacements at different sections and along beam.

C.4.4.3 Omega-shaped extensometers

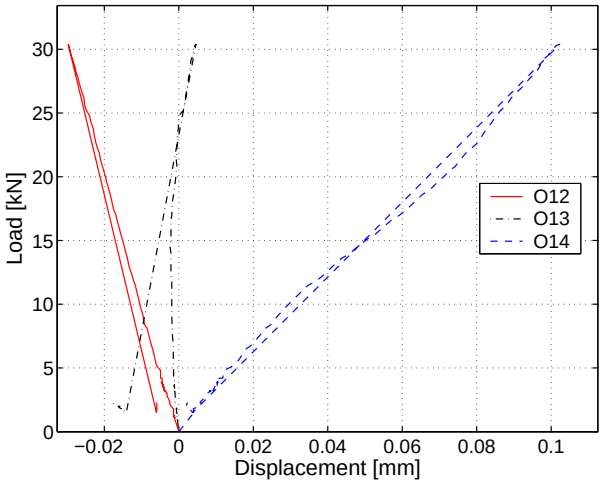

(a) Axis D (mid-span) - south

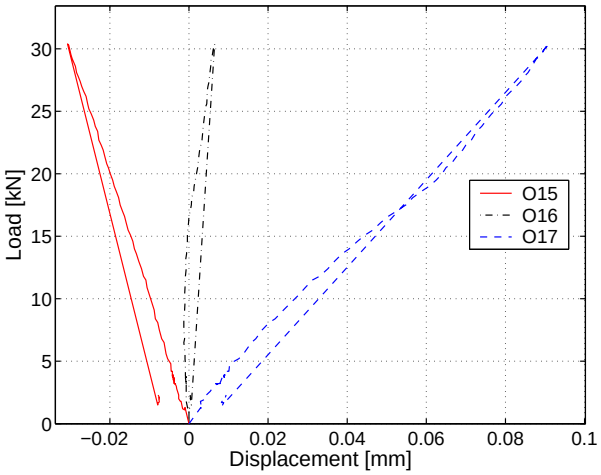

(b) Axis D (mid-span) - north

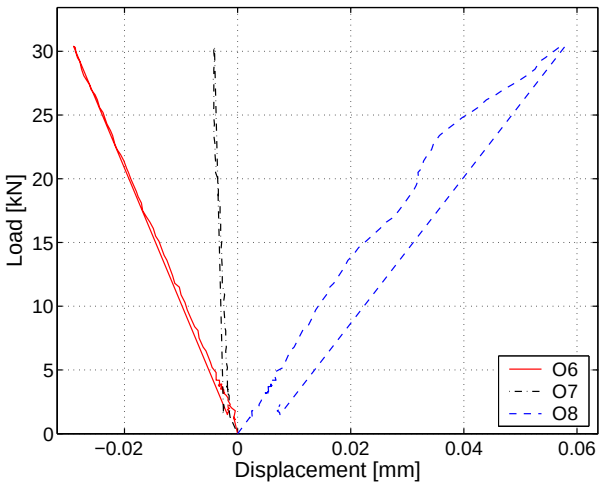

(c) Axis E - south

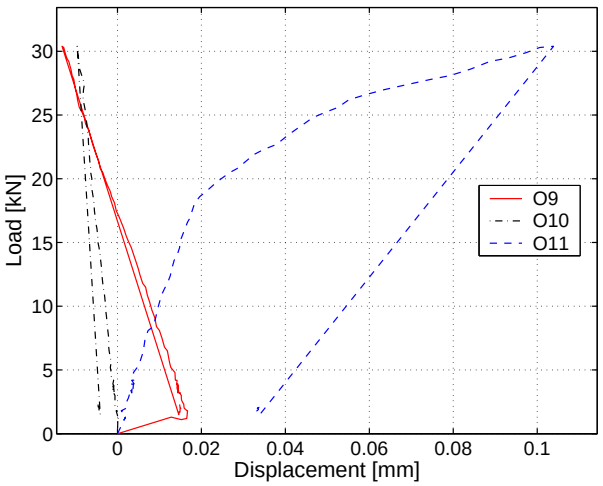

(d) Axis E - north

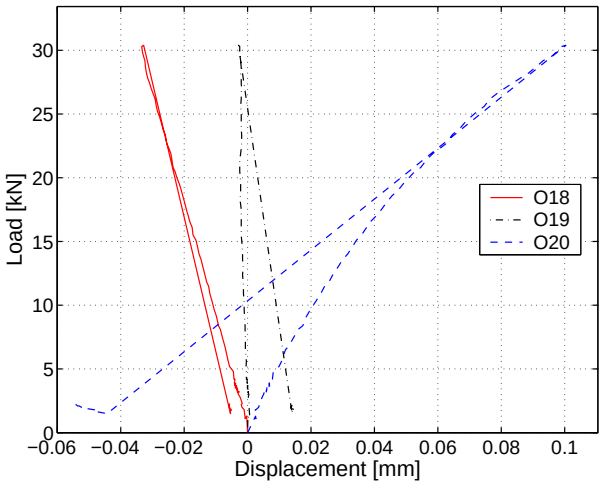

(e) Axis C - south

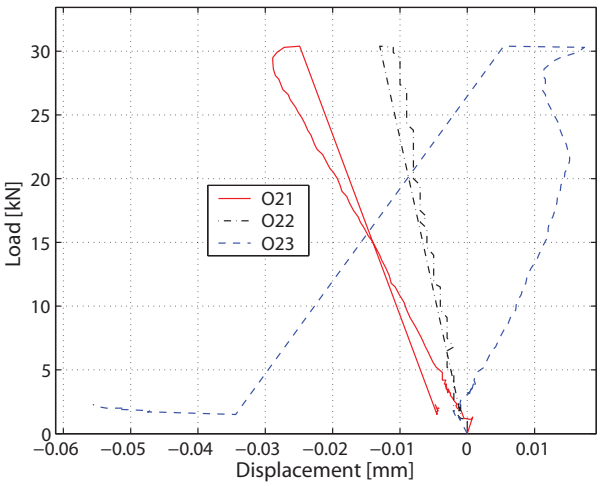

(f) Axis C - north

Figure C.64: 900E-2: Deformations in omega-shaped extensometers at axes C-E.

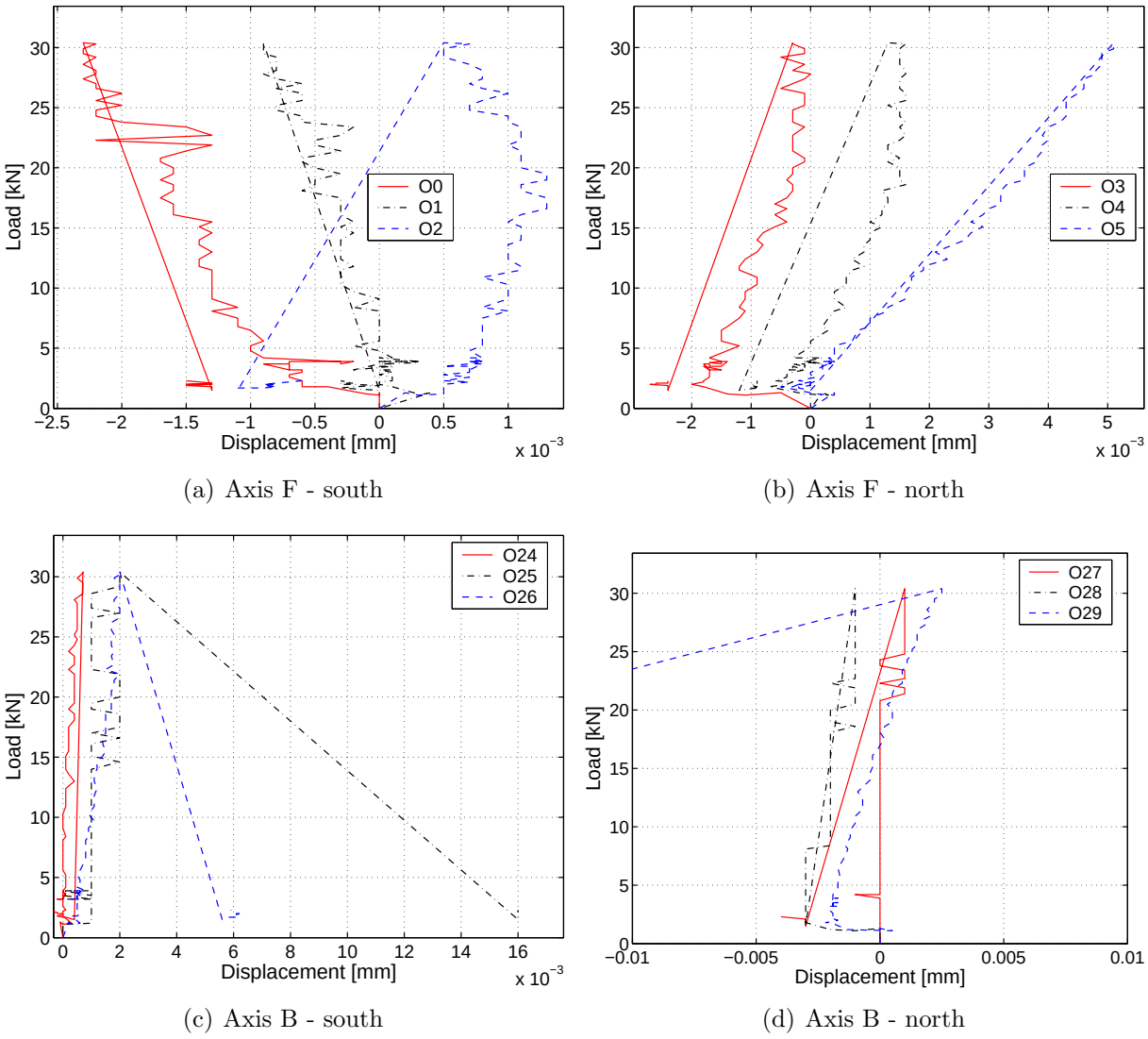

(a) Axis F - south

(b) Axis F - north

(c) Axis B - south

(d) Axis B - north

Figure C.65: 900E-2: Deformations in omega-shaped extensometers over supports.

C.4.4.4 Strain gages on GFRP profile

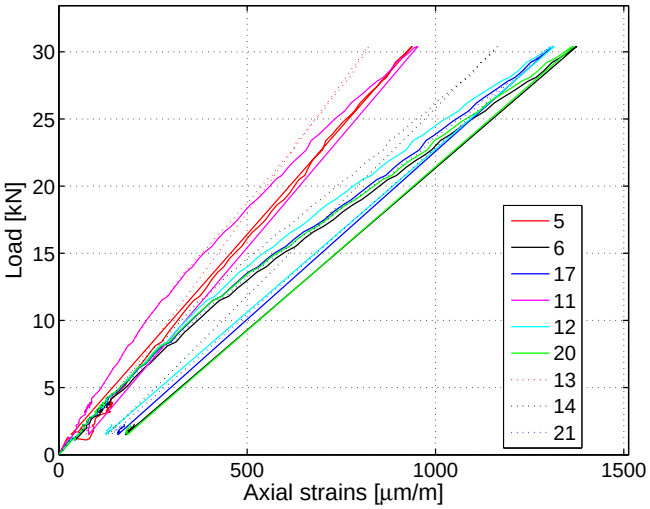

(a) Axial strains at axis D (mid-span)

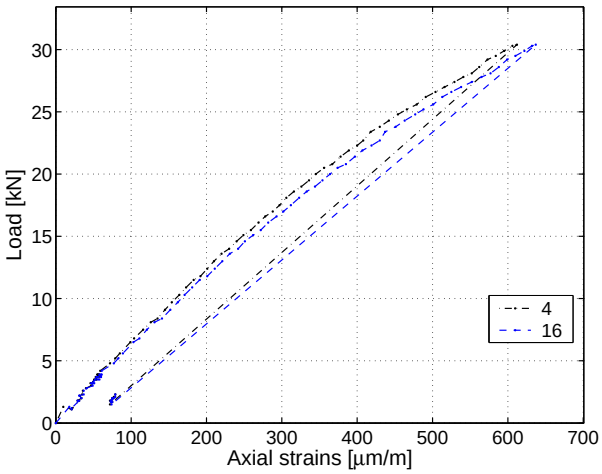

(b) Axial strains at axis E

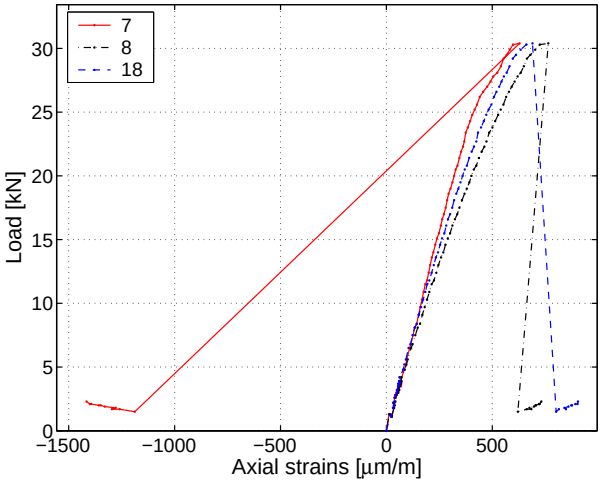

(c) Axial strains at axis C

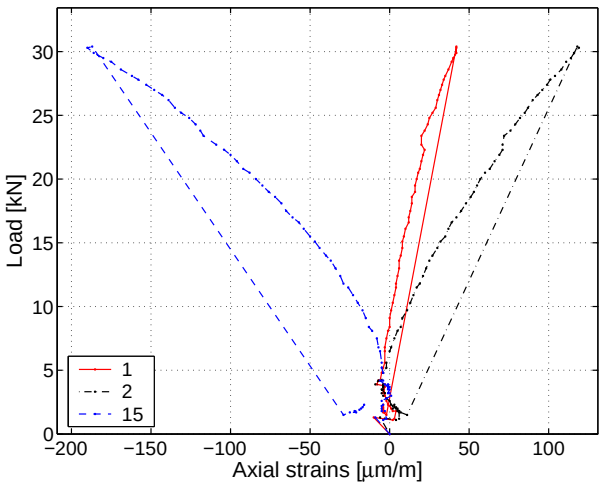

(d) Axial strains at axis F

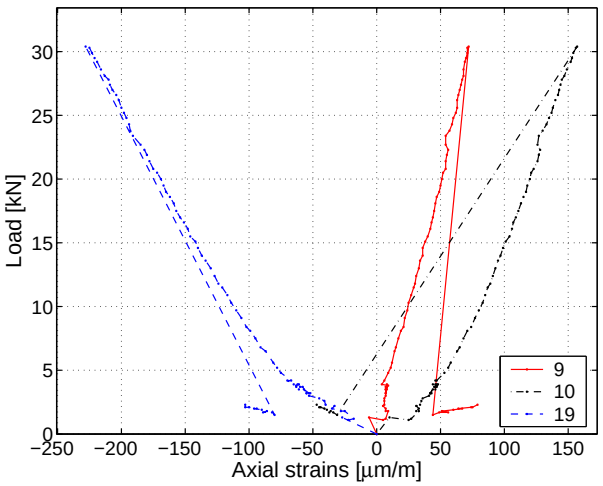

(e) Axial strains at axis B

Figure C.66: 900E-2: Axial strains in GFRP profile.

C.4.4.5 Axial strains through the cross section

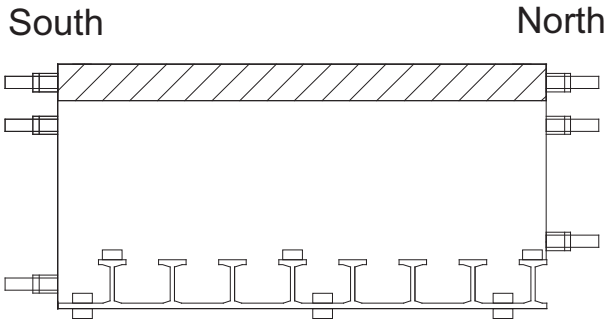

(a) Instrumentation location

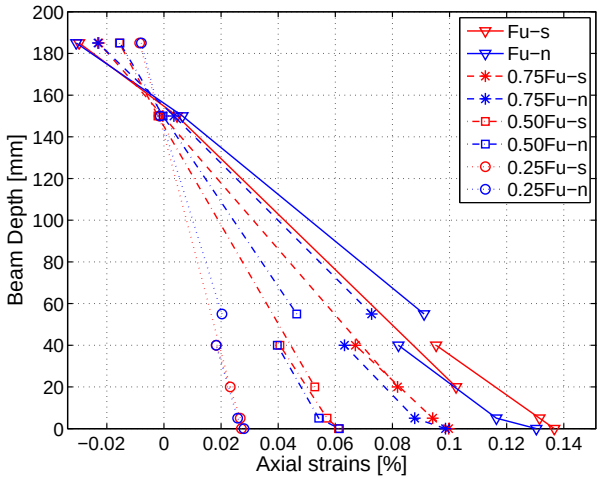

(b) Strain gages and omegas on north and south side

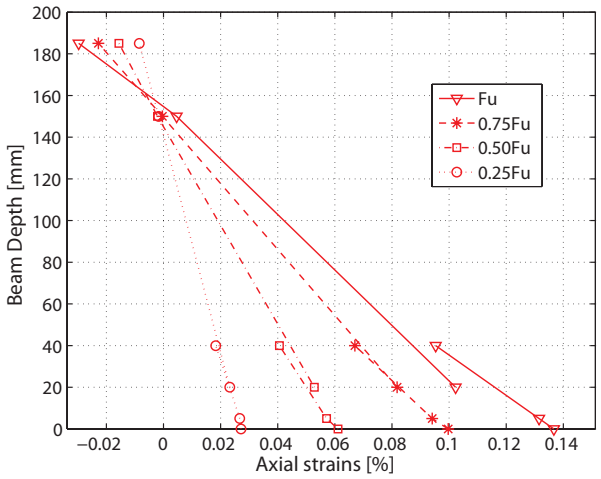

(c) South

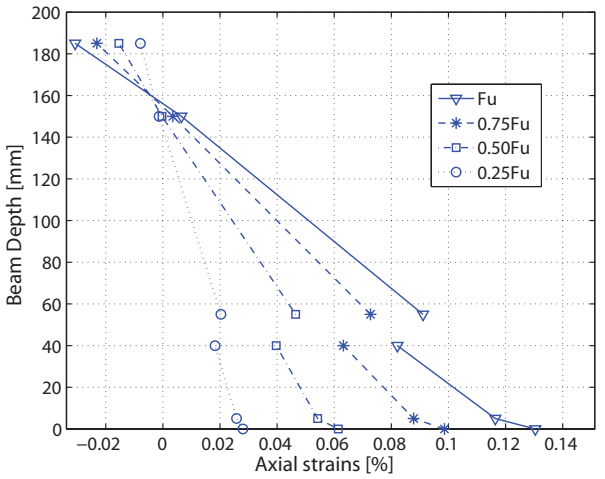

(d) North

Figure C.67: 900E-2: Axial strains through cross section at mid-span at different load steps from strain gages and omega-shaped extensometers.

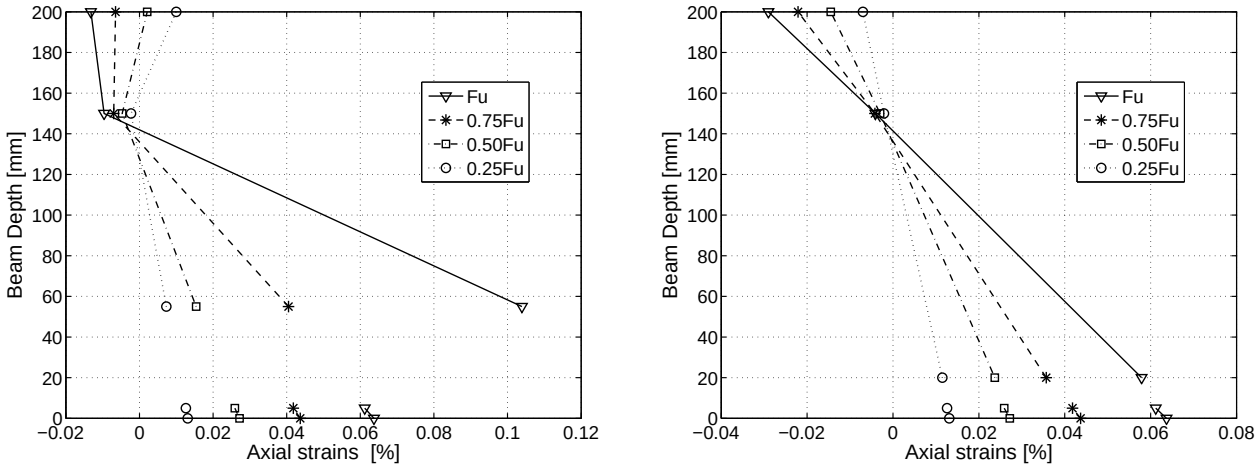

(a) Axis E - north

(b) Axis E - south

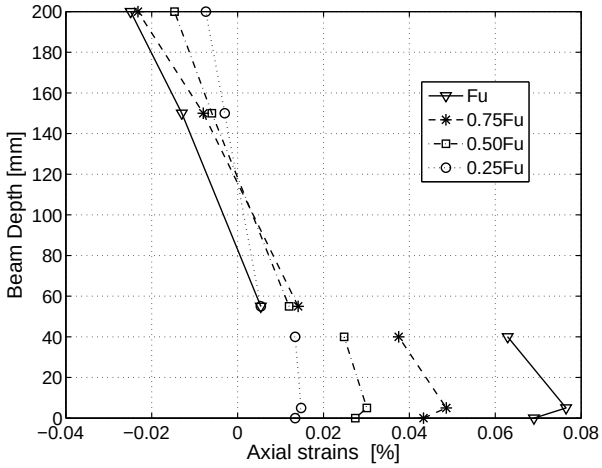

(c) Axis C - north

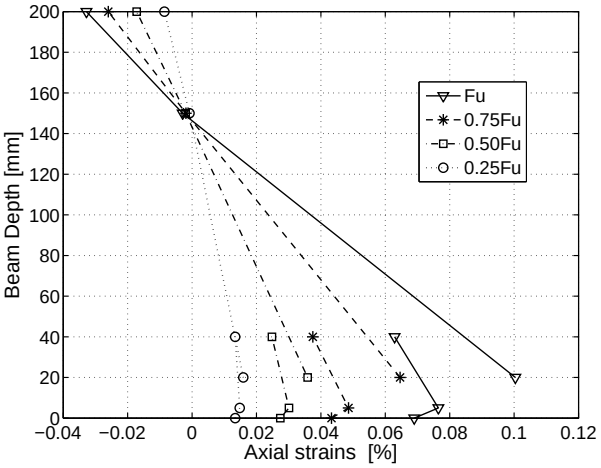

(d) Axis C - south

Figure C.68: 900E-2: Axial strains through cross section at 0.75 m and 2.25 m at different load steps from strain gages and omega-shaped extensometers.

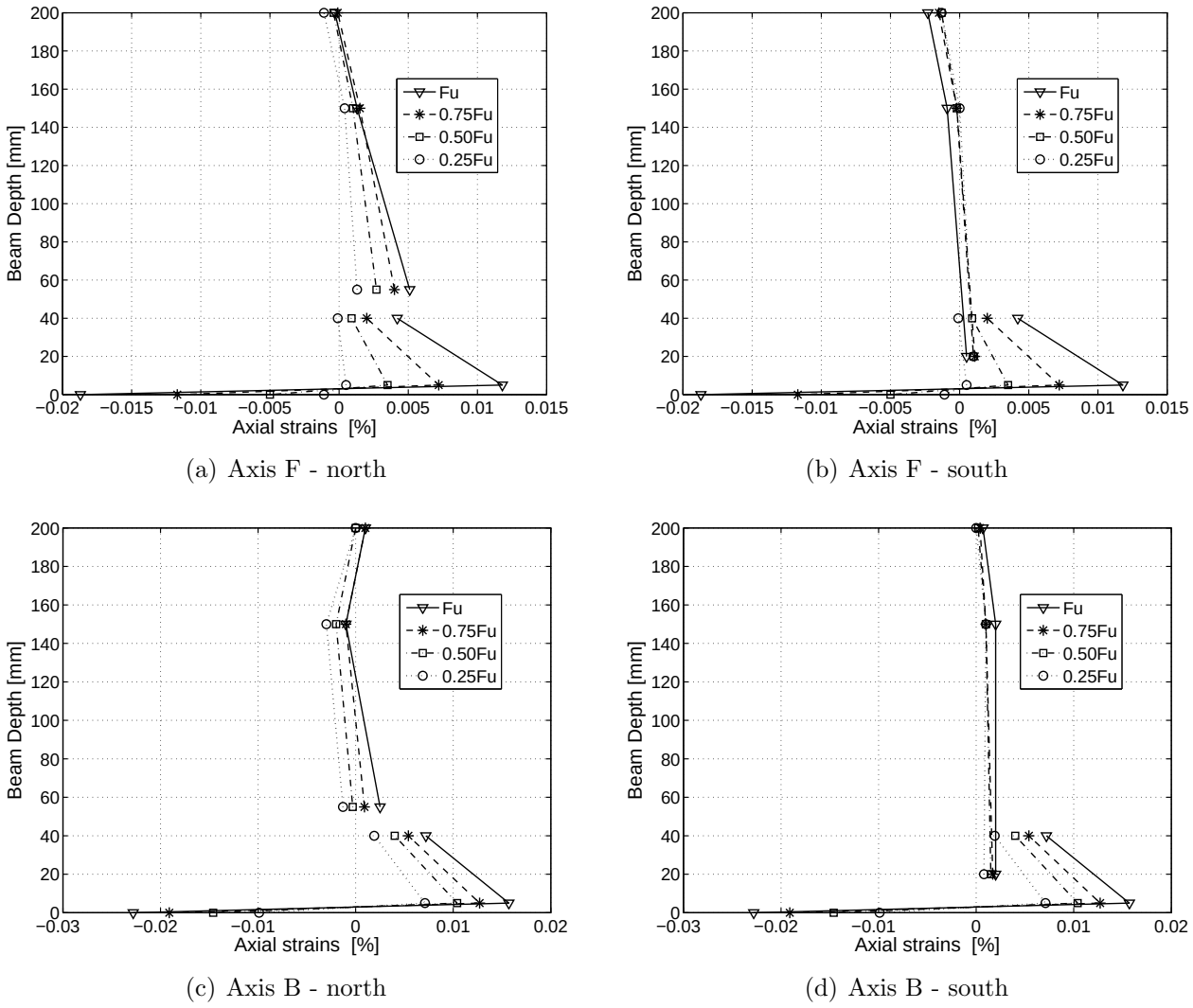

(a) Axis F - north

(b) Axis F - south

(c) Axis B - north

(d) Axis B - south

Figure C.69: 900E-2: Axial strains through cross section over supports at different load steps from strain gages and omega-shaped extensometers.

C.4.4.6 Axial strains along the beam

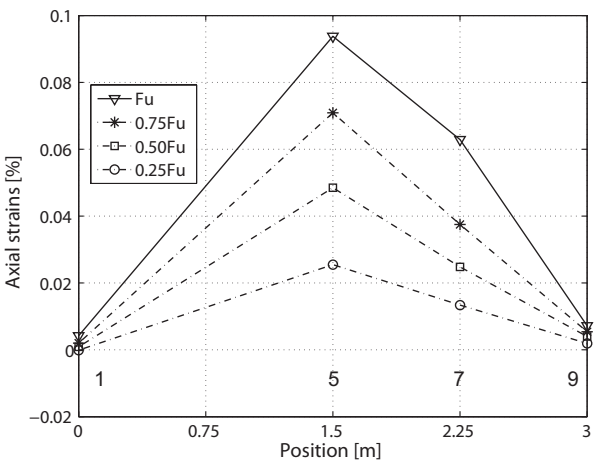

(a) Axial strains on top of T-upstands

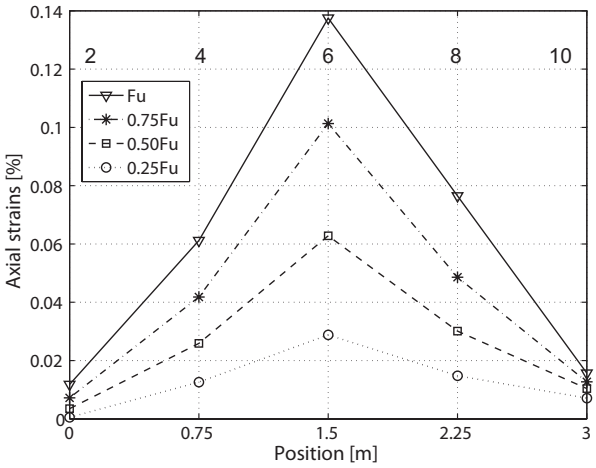

(b) Axial strains between T-upstands

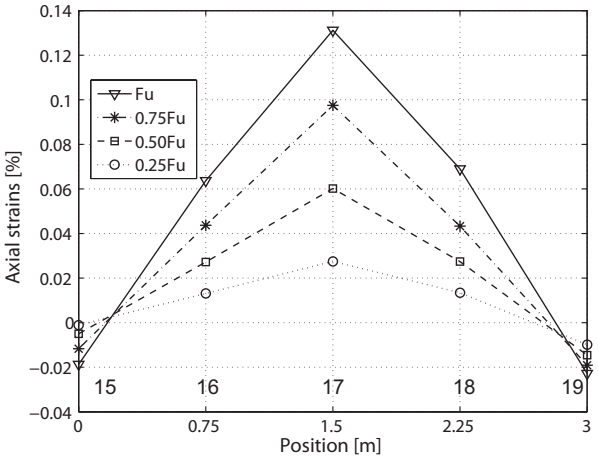

(c) Axial strains beneath GFRP sheet

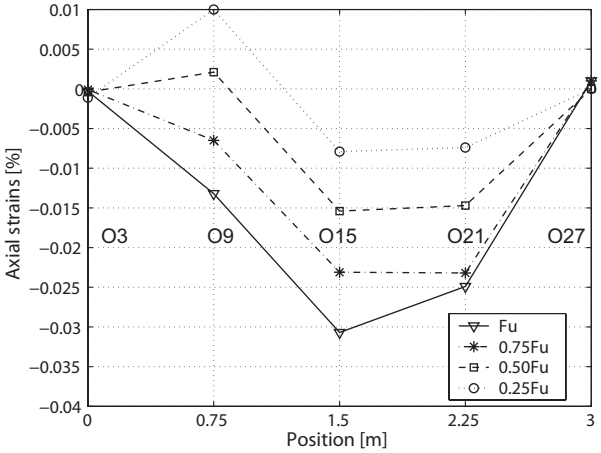

(d) Axial strains in NC layer - north

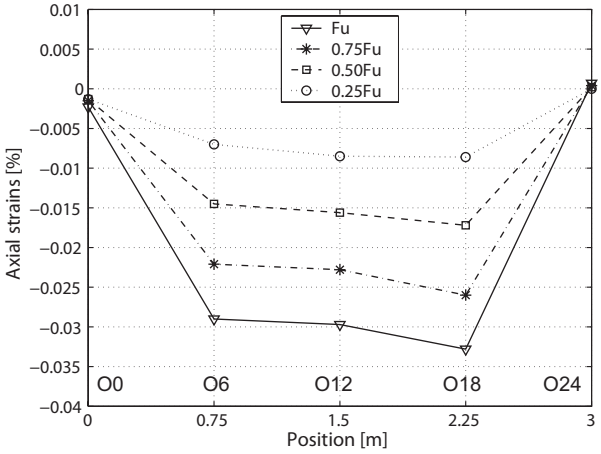

(e) Axial strains in NC layer - south

Figure C.70: 900E-2: Axial strains along beam at different load steps from strain gages and omega-shaped extensometers.

C.4.5 Beam 1300-1: Failure description and measured results (low instrumentation)

C.4.5.1 Failure description

The failure process of beam 1300-1 is illustrated in Figures C.71, C.72, C.73 and C.74. It started with noises at a load of 7.2 kN. The first small vertical cracks occurred at a load of ∼11.5 kN in the tension zone of the lightweight concrete below the loading plate. First LC debonding from the GFRP profile was observed at a load of 17 kN on the north-east side of the beam. A pushing out of the LC could be observed as from a load of 20.7 kN on the east beam end. The cracks then started to propagate vertically through the lower half of the beam depth next to the loading plate. Figure C.71 shows the cracks in the northern side of the beam at a load of approximately 30 kN. The cracks were all more or less vertically distributed and crossed the lightweight aggregates.

Figure C.71: 1300-1: Failure process before reaching ultimate load at 30.0 kN and 26.9 mm.

A first load peak could be observed at a load of 31.0 kN and 30-mm mid-span deflection. This was followed by loud noises indicating cracking within the LC. An oscillating phase occurred, during which the applied load varied seven times between 28 kN and 30 kN, each accompanied by an audible inner crack.

The beam then regained stiffness and the load could be increased again up to the ultimate load of $F_u = 32.1$ kN with a corresponding mid-span deflection of 48 mm. At this load, two vertical cracks 25-36 cm from the mid-span propagated through the LC layer and the load dropped to 16 kN, (Figure C.72-a). The continuous crack in the east side opened significantly and the contact between the GFRP and LC was lost over an extensive area (Figure C.72-b). A load decrease to 12.5 kN followed and the experiment was stopped at a mid-span deflection of 88 mm. The failed specimen is shown in Figures C.75 and C.76.

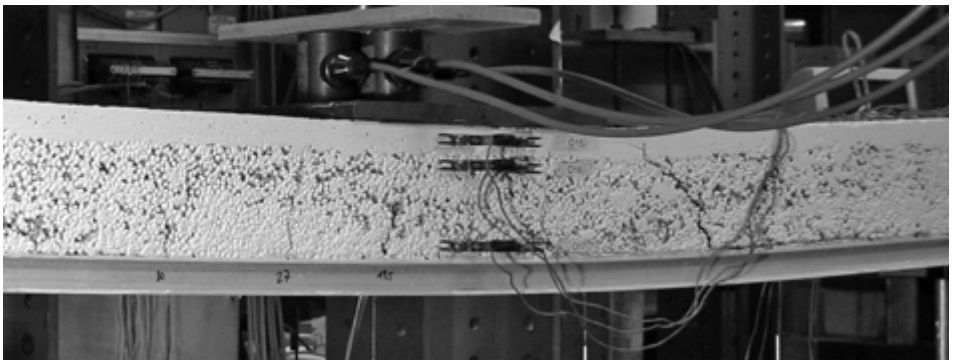

(a) Cracks propagating through LC layer at ultimate load $F_u = 32.1\,\text{kN}$ and $47.8\,\text{mm}$

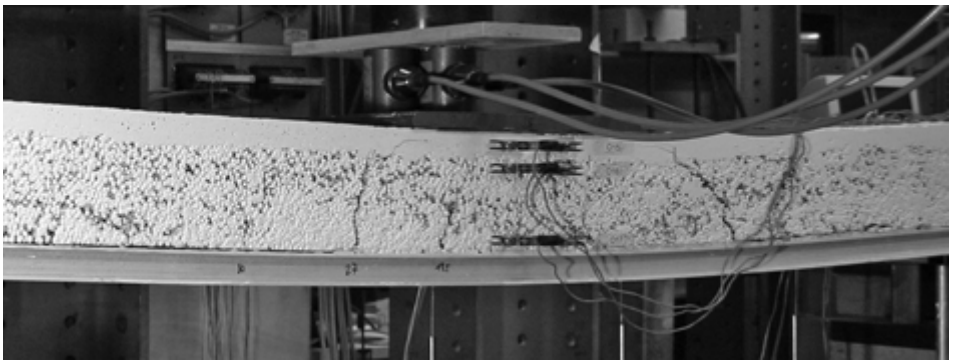

(b) Extensive LC debonding at $16.4\,\text{kN}$ (post-peak) and $55.1\,\text{mm}$

Figure C.72: 1300-1: Failure process after reaching ultimate load.

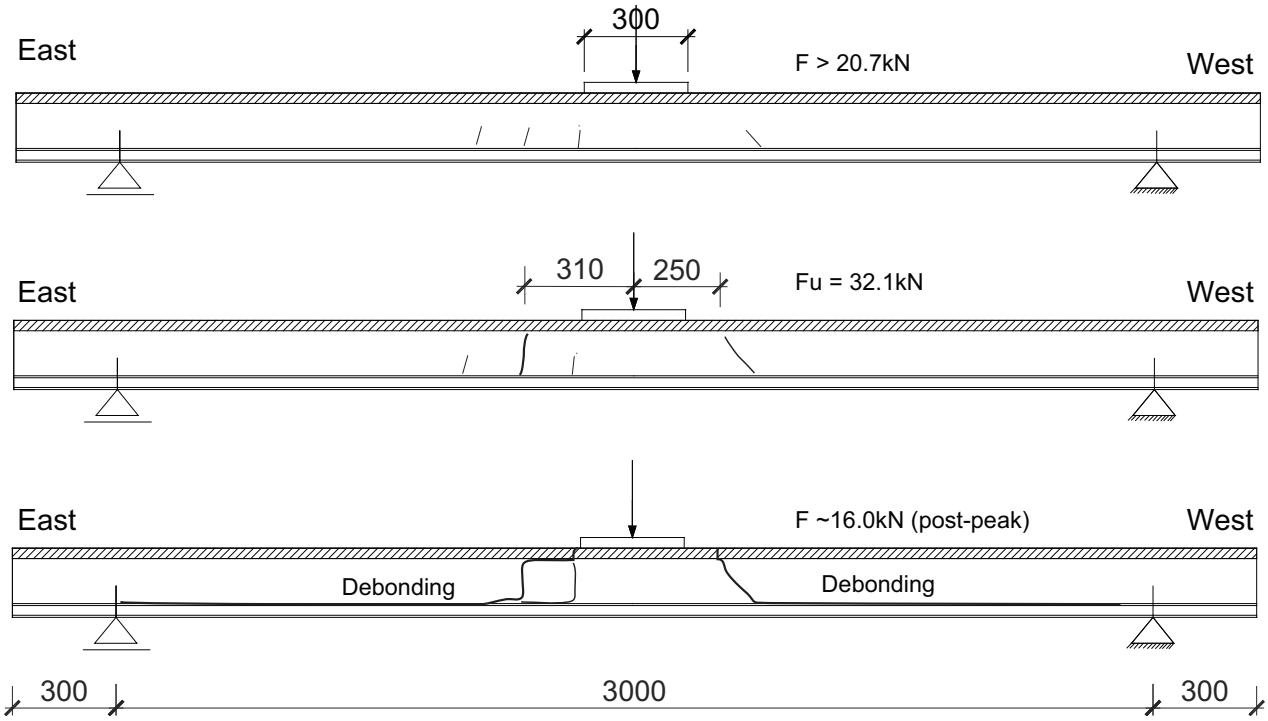

(a) View from north - failure process

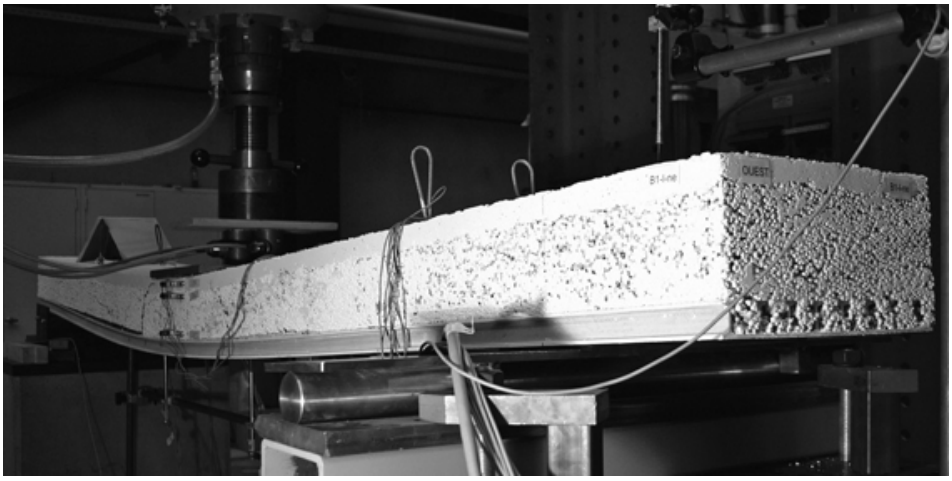

(b) View from north

Figure C.73: 1300-1: a) Failure process and b) still loaded failed beam after experiment - north.

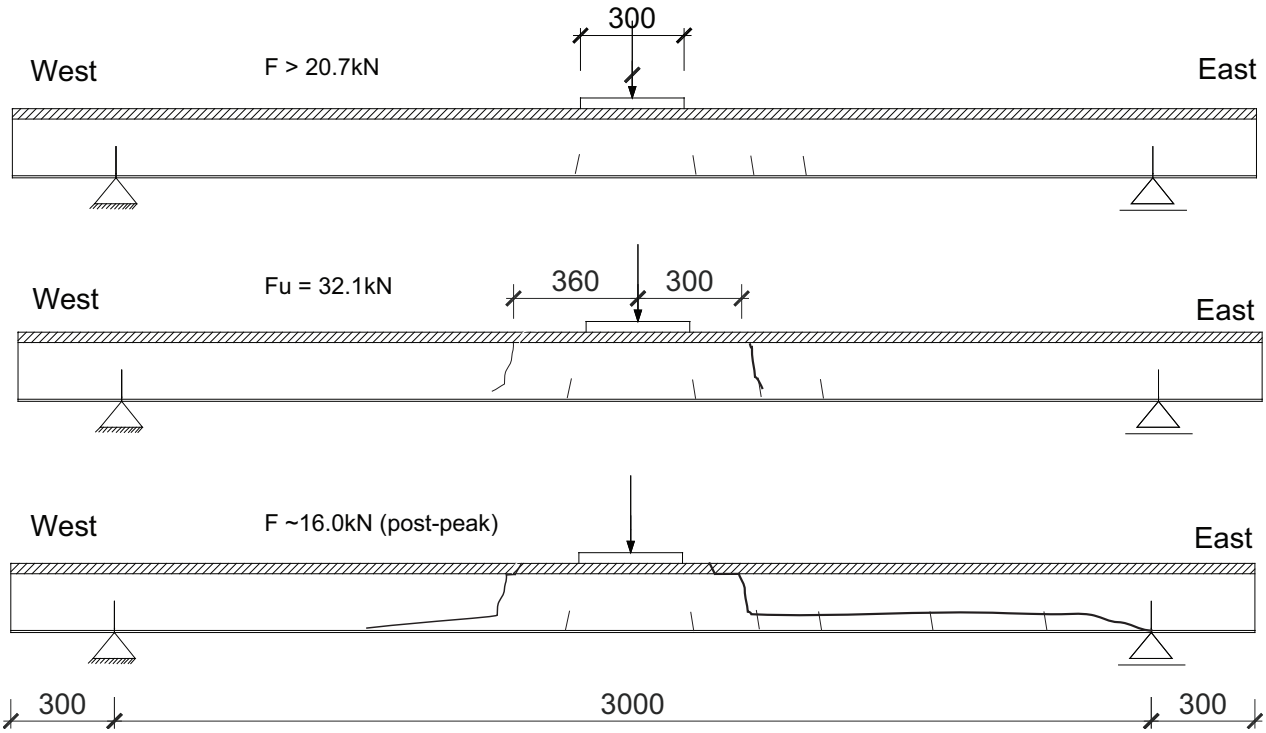

(a) View from south - failure process

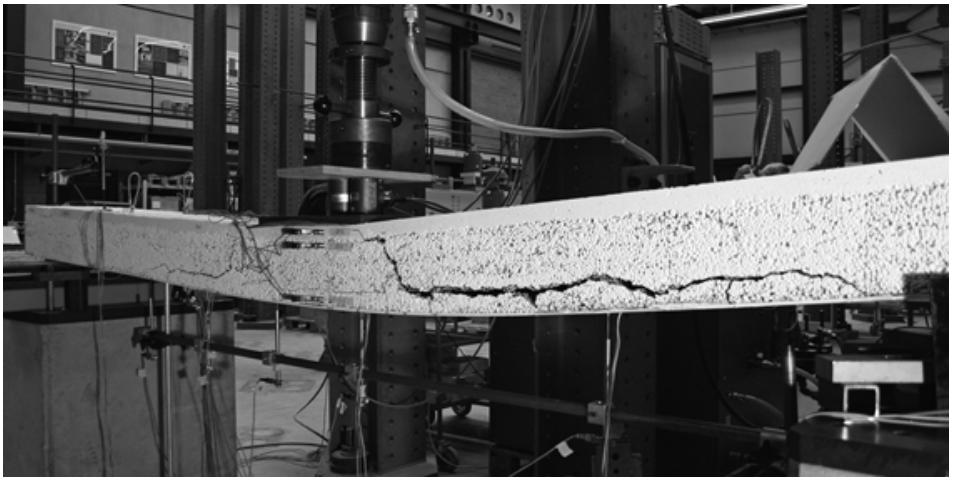

(b) View from south

Figure C.74: 1300-1: a) Failure process and b) still loaded failed beam after experiment - south.

(a) View from north - mid-span

(b) View from north - axis B

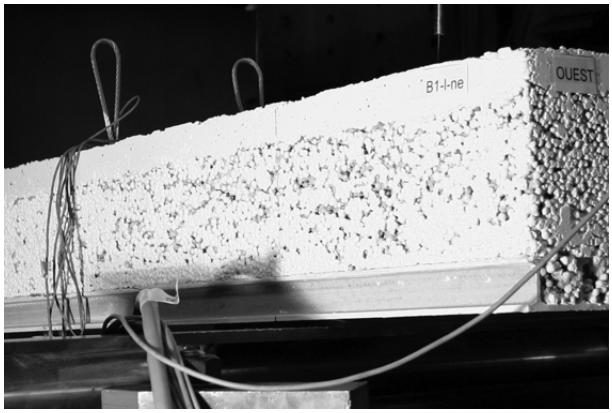

(c) View from north - axis F

Figure C.75: 1300-1: Failed beam after experiment, still loaded - north.

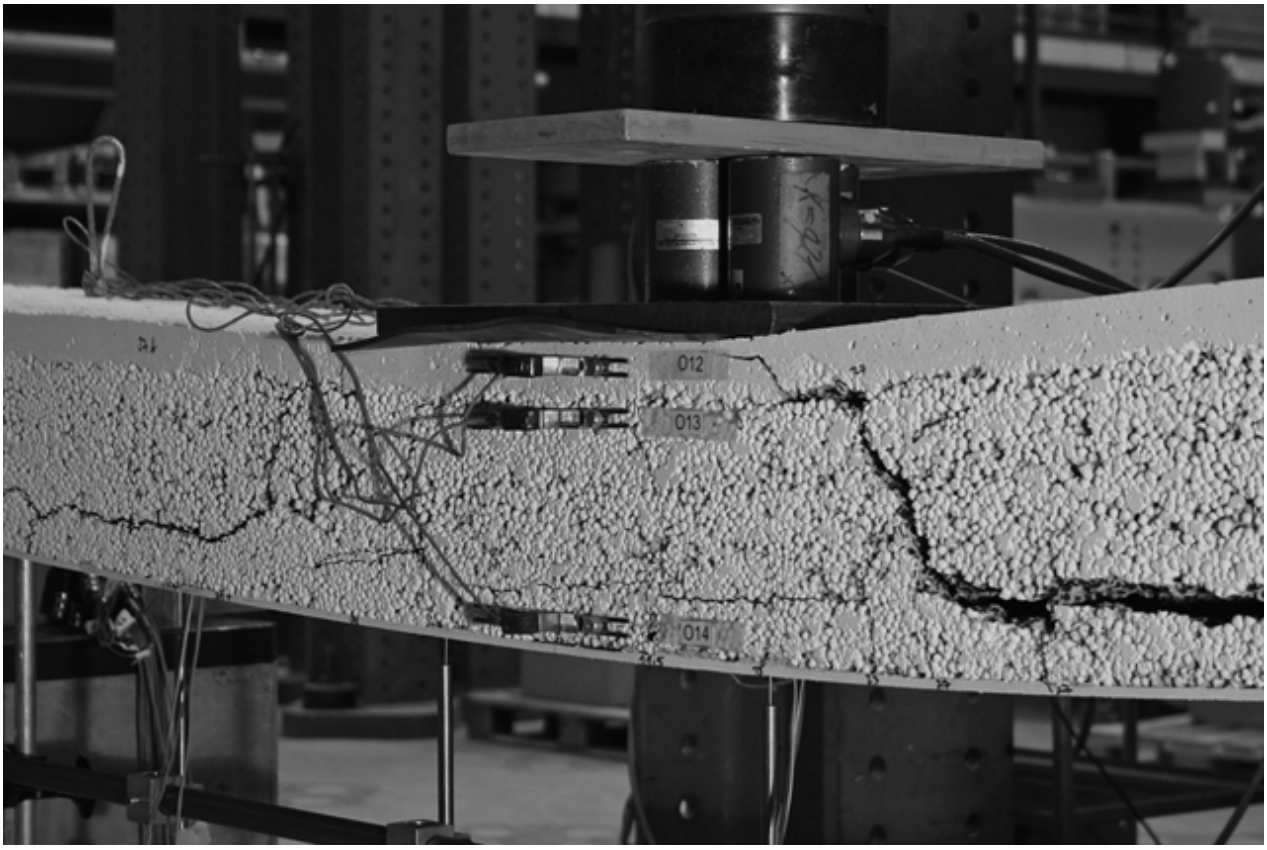

(a) View from south - mid-span

(b) View from south - axis F

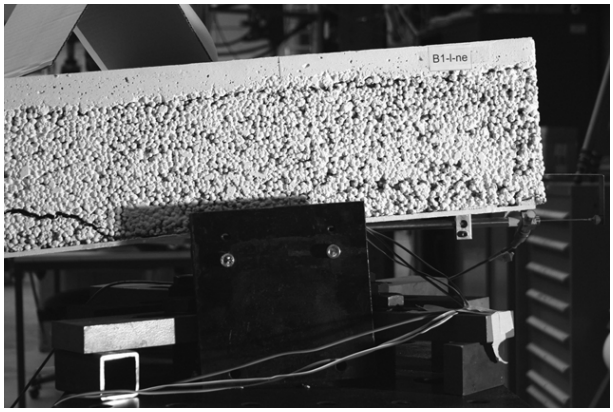

(c) View from south - axis B

Figure C.76: 1300-1: Failed beam after experiment, still loaded - south.

C.4.5.2 Displacement transducers

As shown in Figure C.77, beam stiffness was constant up to the cracking load of approximately 9.5 kN. Subsequently stiffness decreased slightly. As from 20.7 kN, slippage was measured at the east beam end, which resulted in a further stiffness drop as shown in Figures C.77 and C.78 d). The first load peak was reached at 31.0 kN and a corresponding 30-mm deflection. This was followed by an oscillating phase, during which the load varied between 28 kN and 30 kN. The beam then regained stiffness and reached the ultimate load at 32.1 kN. The corresponding deflection was 48 mm. The beam henceforth lost its stiffness and the load dropped to 16 kN where a short stabilization occurred. However, since the load could not be significantly increased, the experiment was stopped at a mid-span deflection of 88 mm.

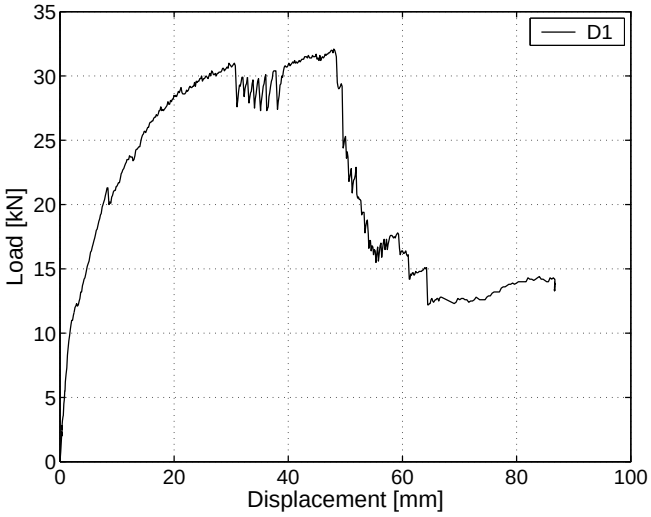

(a) Displacement at mid-span

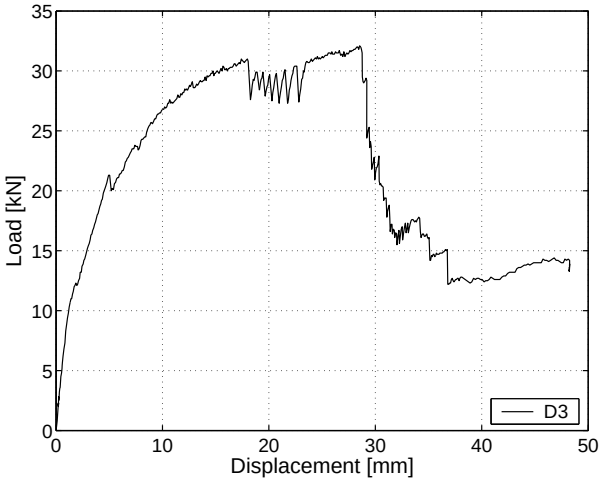

(b) Displacement - axis E

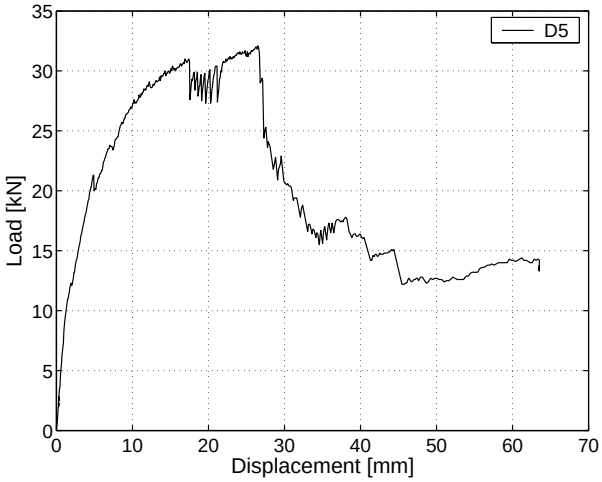

(c) Displacement - axis C

Figure C.77: 1300-1: Displacement at mid-span, at 0.75 m and 2.25 m.

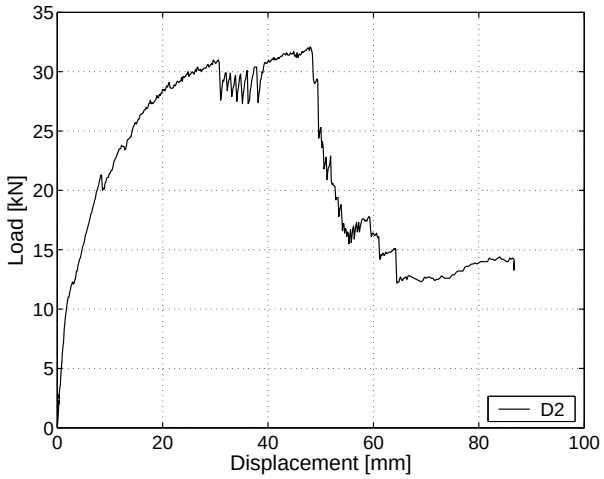

(a) Displacement - between axes D-E

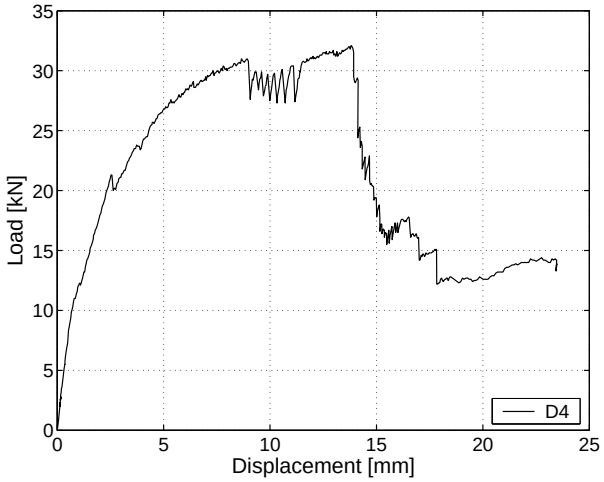

(b) Displacement - between axes E-F

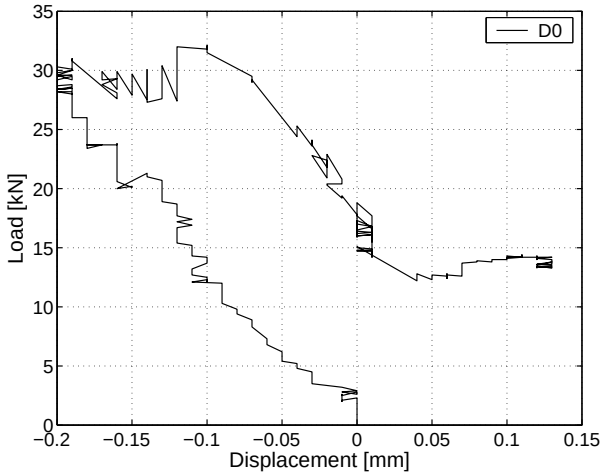

(c) Displacement at fixed support - axis F

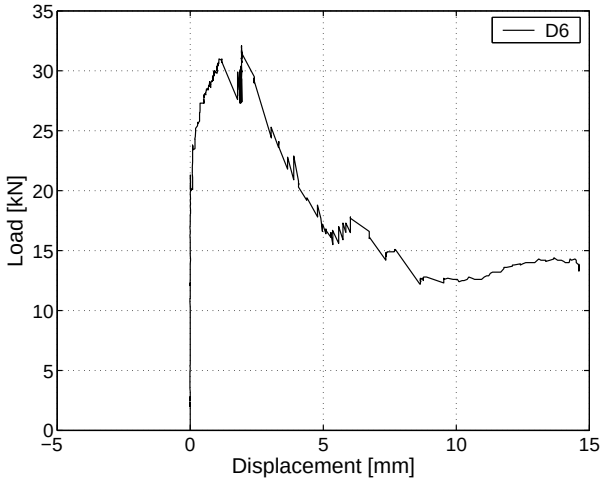

(d) Horizontal displacement of LC - axis A

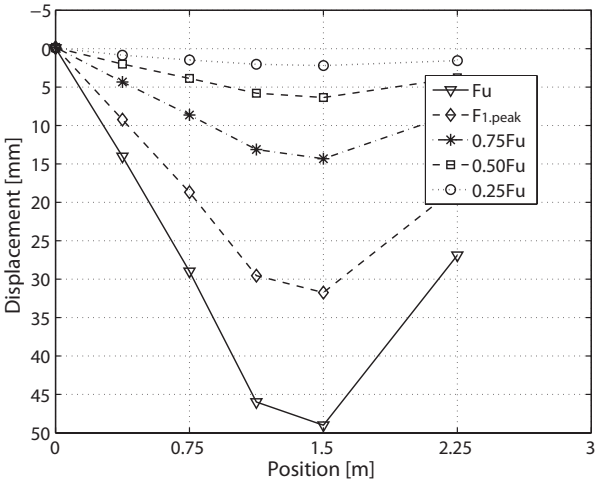

(e) Displacement along beam

Figure C.78: 1300-1: Displacements at different sections and along beam ($F_{1.peak} = 31.0\,\text{kN}$ with 30 mm and $F_u = 32.1\,\text{kN}$ with 48 mm corresponding deflections).

C.4.5.3 Omega-shaped extensometers

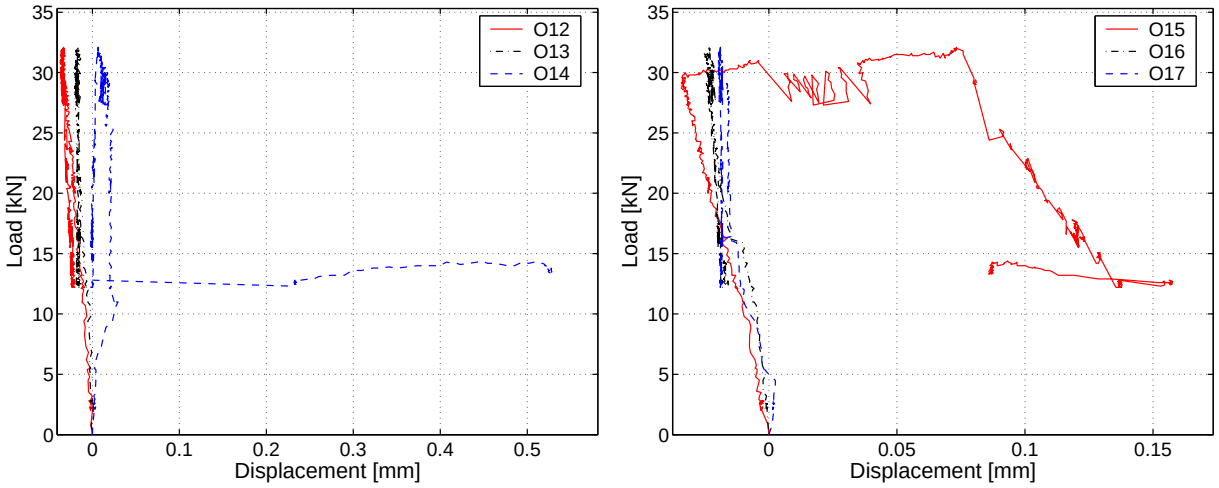

(a) Axis D - south

(b) Axis D - north

Figure C.79: 1300-1: Deformations in omega-shaped extensometers at mid-span.

C.4.5.4 Strain gages on GFRP profile

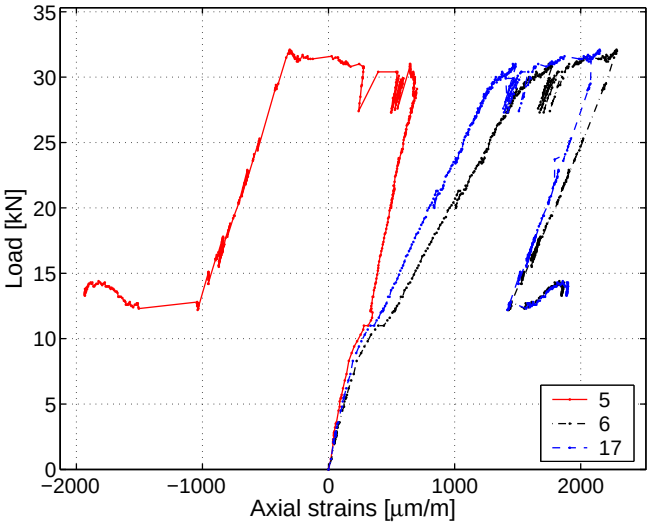

(a) Axial strains at axis D (mid-span)

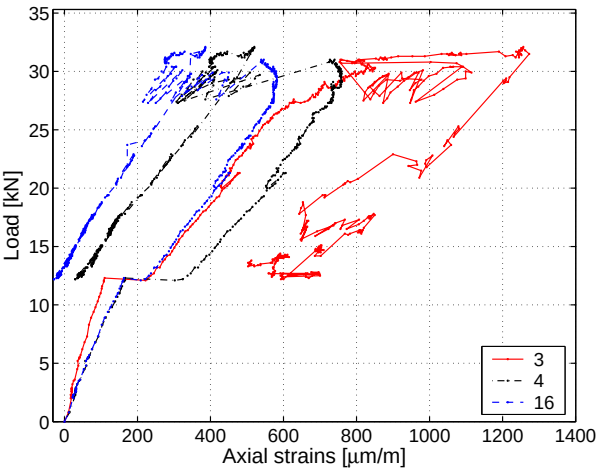

(b) Axial strains at axis E

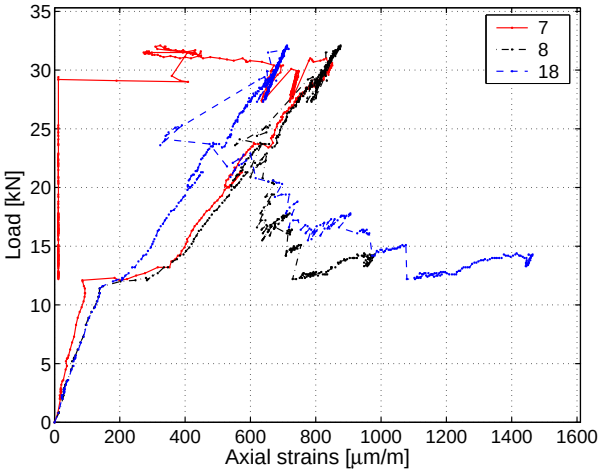

(c) Axial strains at axis C

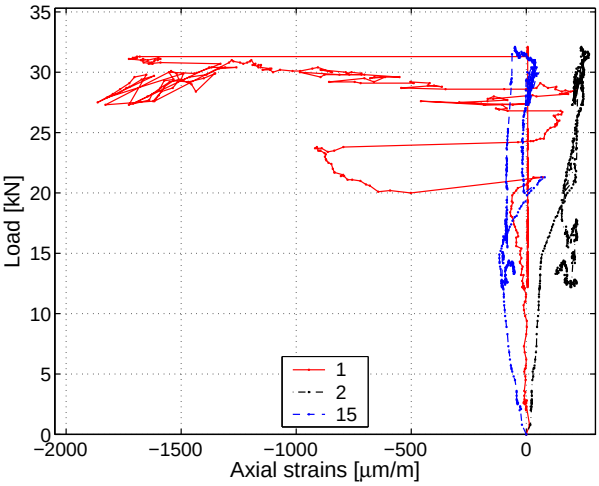

(d) Axial strains at axis F

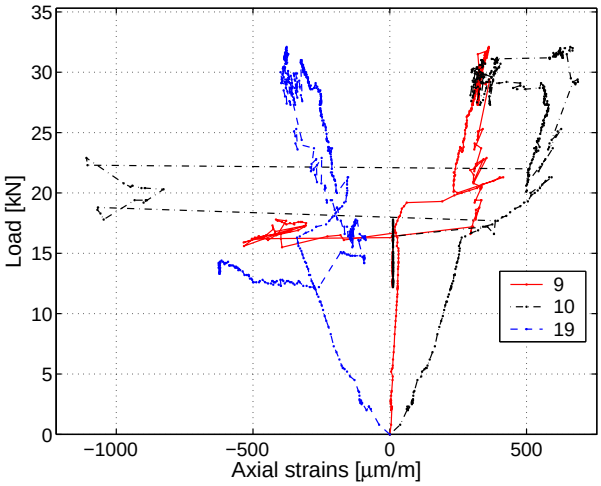

(e) Axial strains at axis B

Figure C.80: 1300-1: Axial strains in GFRP profile.

C.4.5.5 Axial strains through the cross section

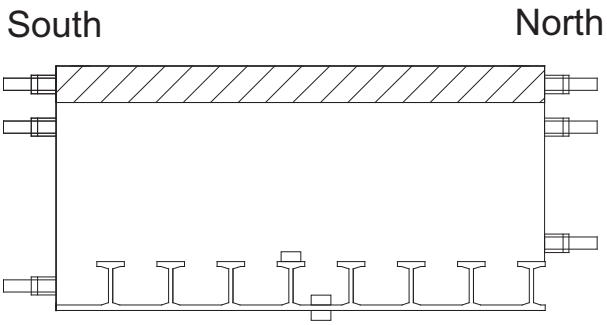

(a) Instrumentation location

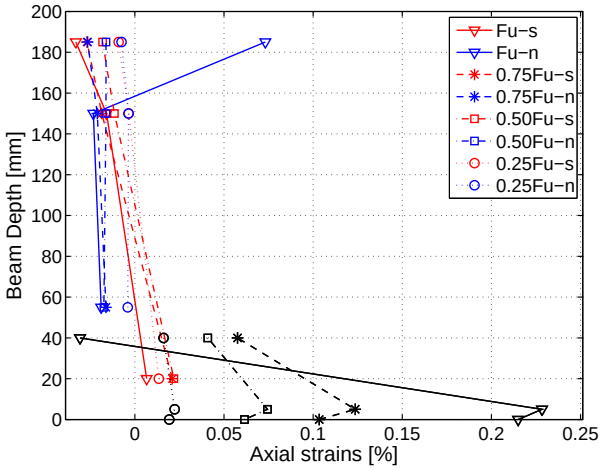

(b) Strain gages on centerline and omegas on north and south side

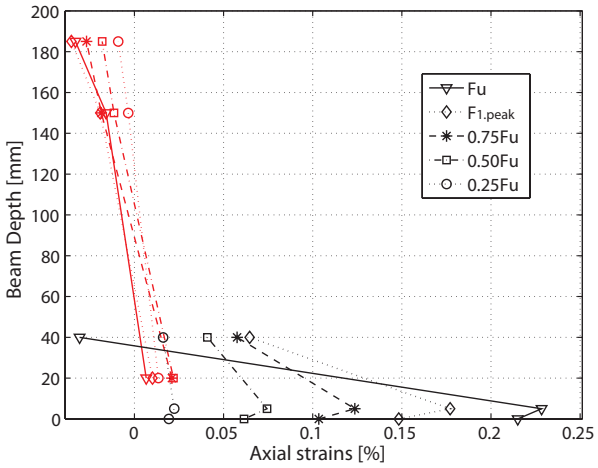

(c) South

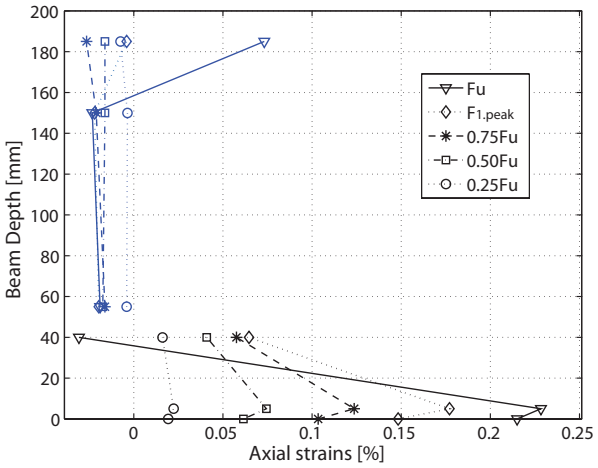

(d) North

Figure C.81: 1300-1: Axial strains through cross section at mid-span at different load steps from strain gages and omega-shaped extensometers ($F_{1.peak} = 31.0\,\text{kN}$ with $30\,\text{mm}$ and $F_u = 32.1\,\text{kN}$ with $48\,\text{mm}$ corresponding deflections)

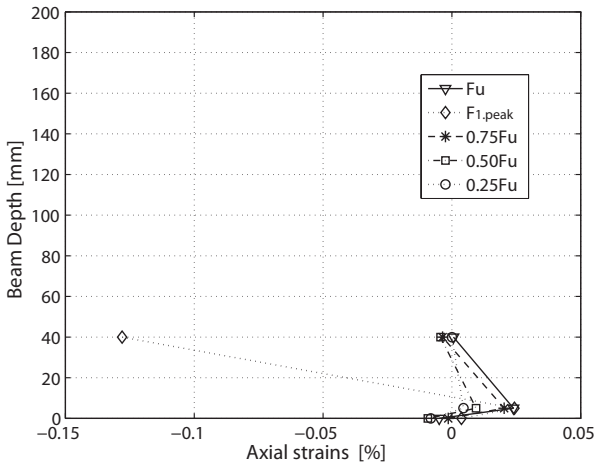

(a) Axial strains at axis F

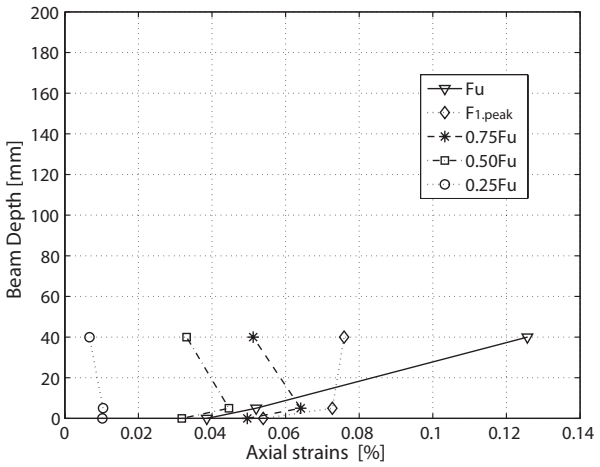

(b) Axial strains at axis E

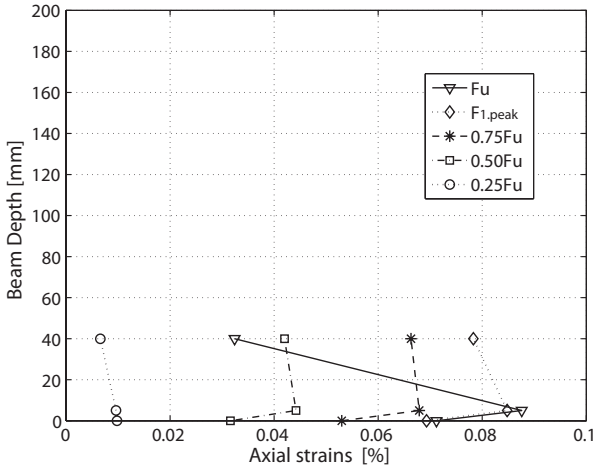

(c) Axial strains at axis C

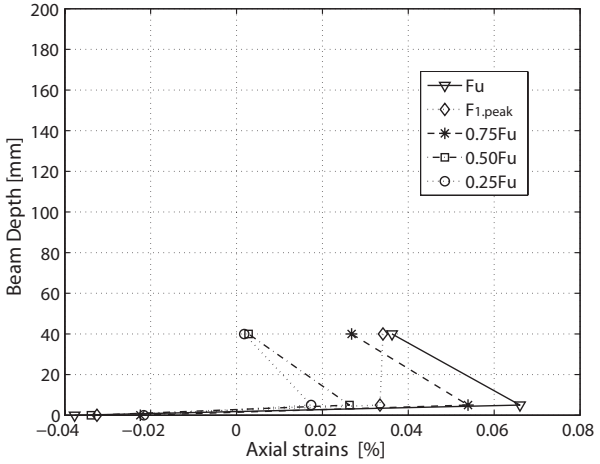

(d) Axial strains at axis B

Figure C.82: 1300-1: Axial strains through GFRP cross section at different load steps ($F_{1.peak} = 31.0\,\text{kN}$ with 30 mm and $F_u = 32.1\,\text{kN}$ with 48 mm corresponding deflections)

C.4.5.6 Axial strains along the beam

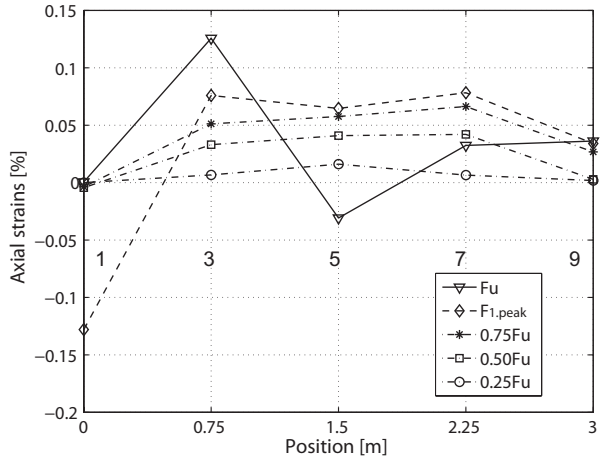

(a) Axial strains on top of T-upstands

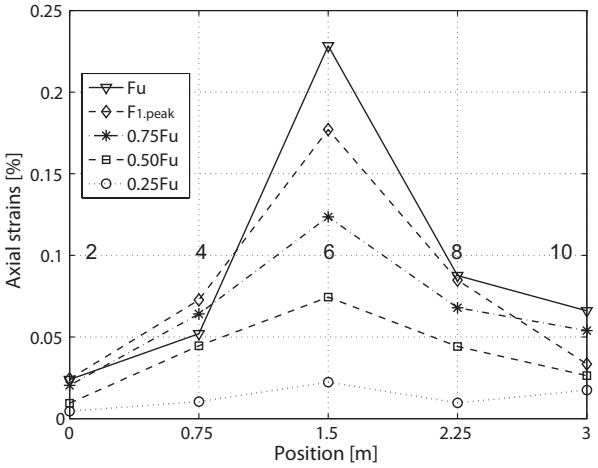

(b) Axial strains between T-upstands

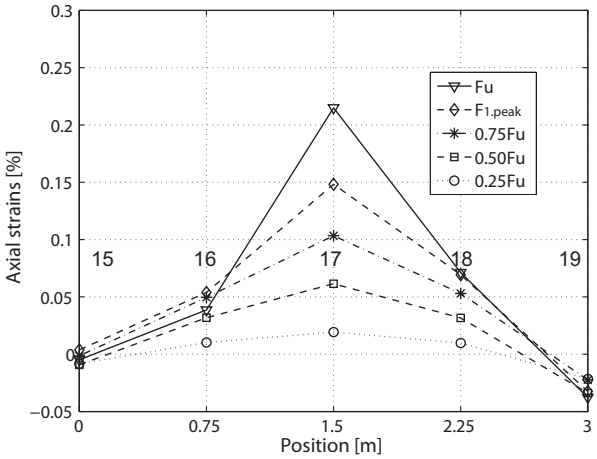

(c) Axial strains beneath GFRP sheet

Figure C.83: 1300-1: Axial strains in GFRP profile along beam at different load steps from strain gages ($F_{1.peak} = 31.0\,\text{kN}$ with 30 mm and $F_u = 32.1\,\text{kN}$ with 48 mm corresponding deflections).

C.4.6 Beam 1300-2: Failure description and measured results (full instrumentation)

C.4.6.1 Failure description

The failure process of beam 1300-2 is illustrated in Figures C.84, C.85 and C.86. The first noises were audible at a load of 8 kN, although no cracks could be observed. The first loud crack occurred at a load of 13.9 kN, followed by the development of vertical cracks spaced at a distance of 40 cm in the tension zone of the lightweight concrete next to the loading plate. Slight debonding started on the northern side at a load of 17.0 kN. The second load cycle was started after a mid-span deflection of 10 mm and corresponding load of approximately 17 kN were reached. During unloading, the vertical cracks closed but remained visible. After reloading, as from the load of 20.7 kN, audible cracks and some new vertical cracks could be observed (Figure C.84-a). At the first peak load of 23.0 kN a mid-span deflection of 18.8 mm was reached. Subsequently, an oscillating phase occurred, during which the applied load varied between 21 kN and 22.7 kN, each time accompanied by an audible inner crack (Figure C.84-b). A third load cycle was performed at the deflection of 33 mm with a corresponding load of 22.5 kN. After reloading, a slight but steady load increase was observed up to the ultimate load of $F_u = 23.3$ kN with a corresponding deflection of 40.4 mm. The cracks started to propagate horizontally and slowly up to the support (Figure C.84-c). The beam lost its stiffness and the experiment was stopped. The failed specimen is shown in Figures C.87 and C.88.

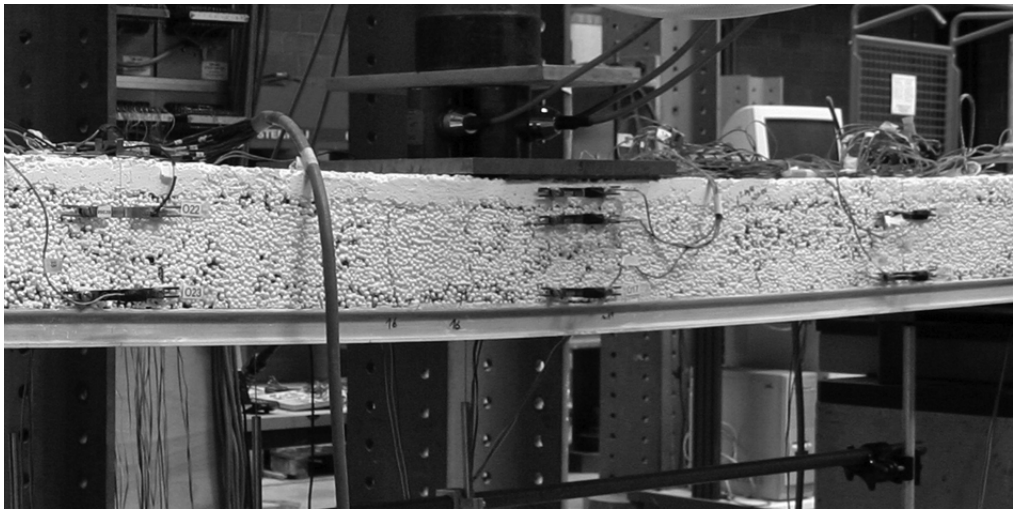

(a) Vertical cracks next to loading plate at ∼21.0 kN, second load cycle

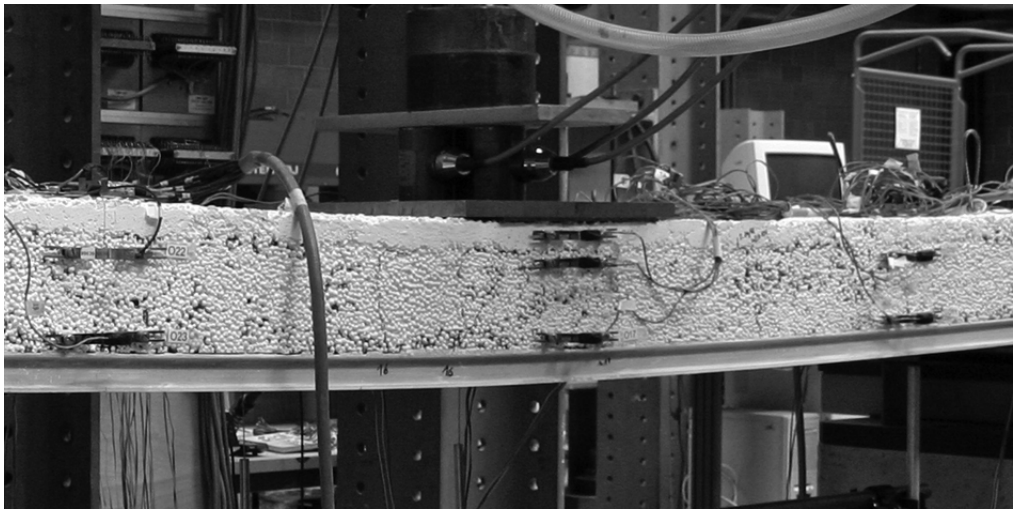

(b) Vertical cracks and debonding at ultimate load at $F_u = 23.3\,\mathrm{kN}$

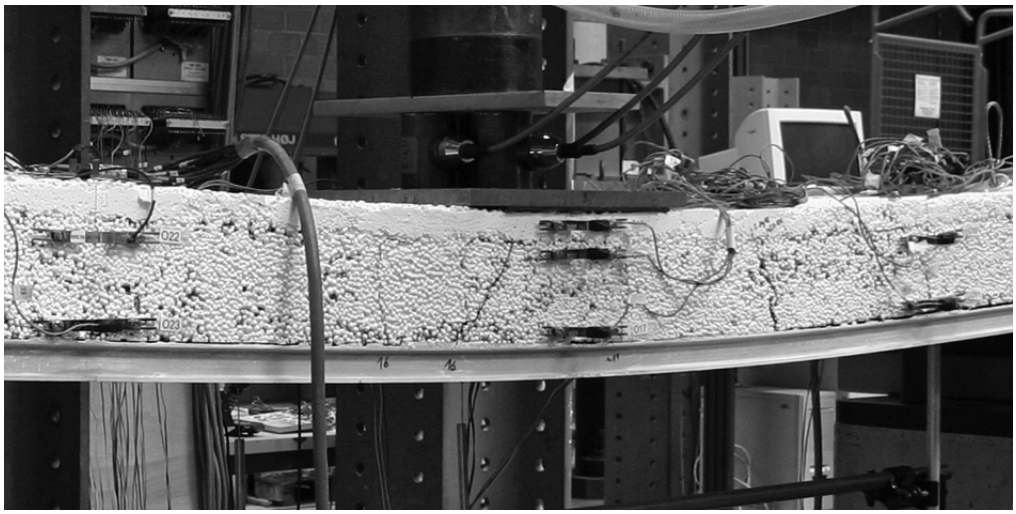

(c) Vertical cracks and debonding at ∼10 kN (post-peak)

Figure C.84: 1300-2: Failure process.

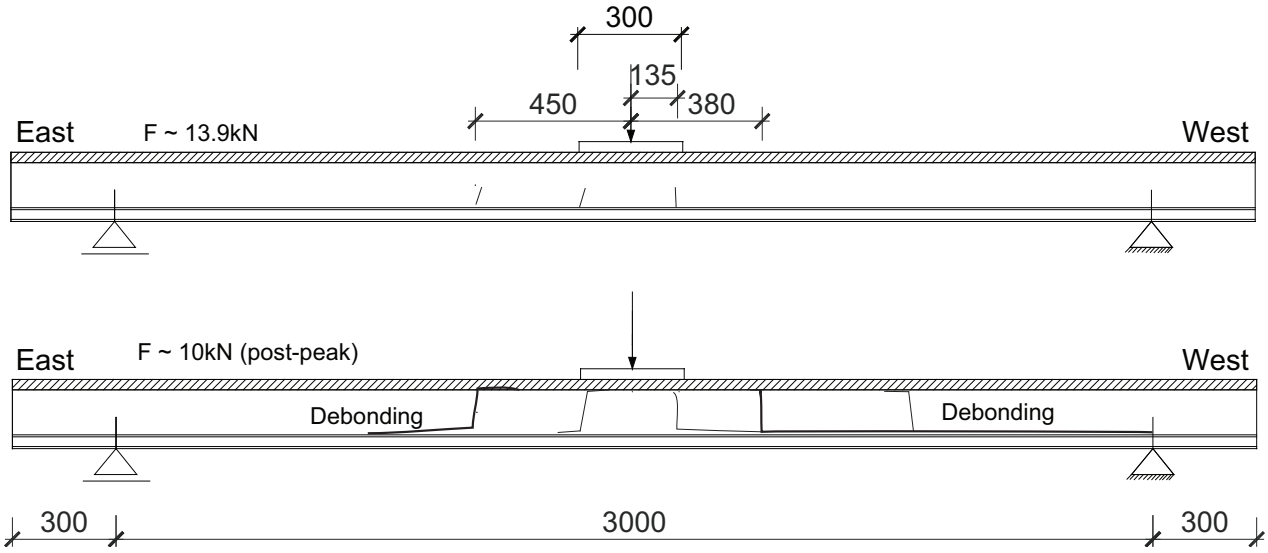

(a) View from north - cracked beam

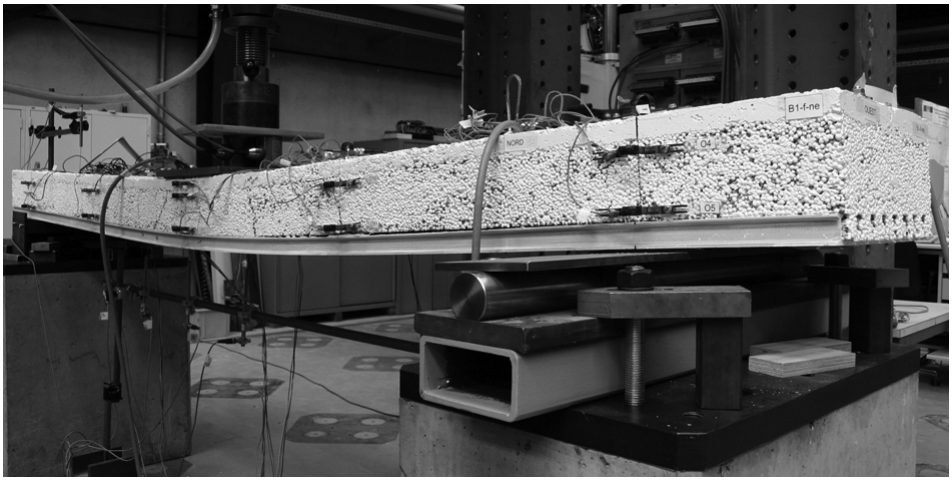

(b) View from north

Figure C.85: 1300-2: a) Failure process and b) still loaded failed beam after experiment - north.

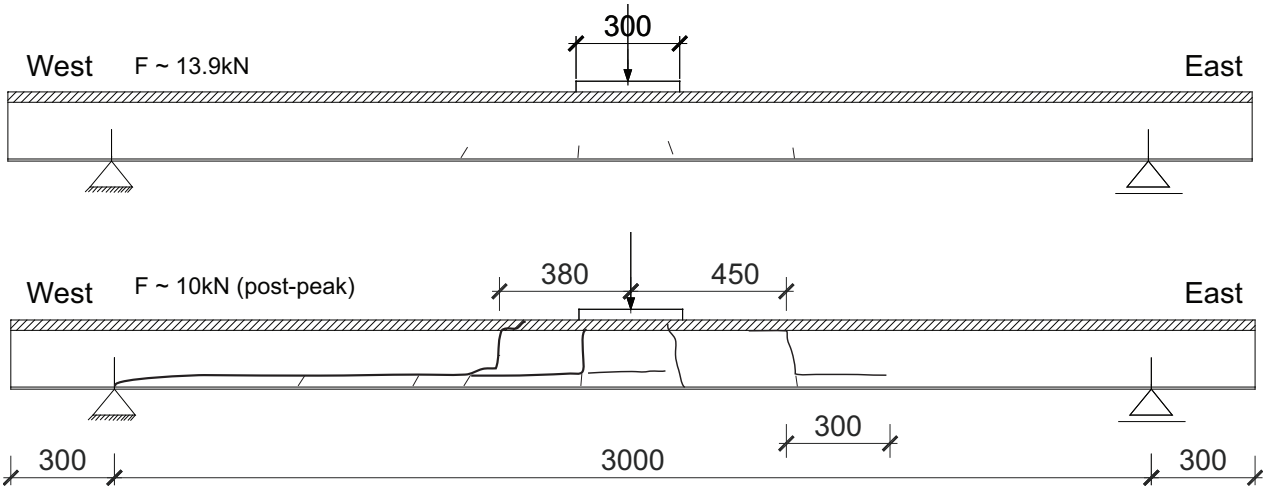

(a) View from south - cracked beam

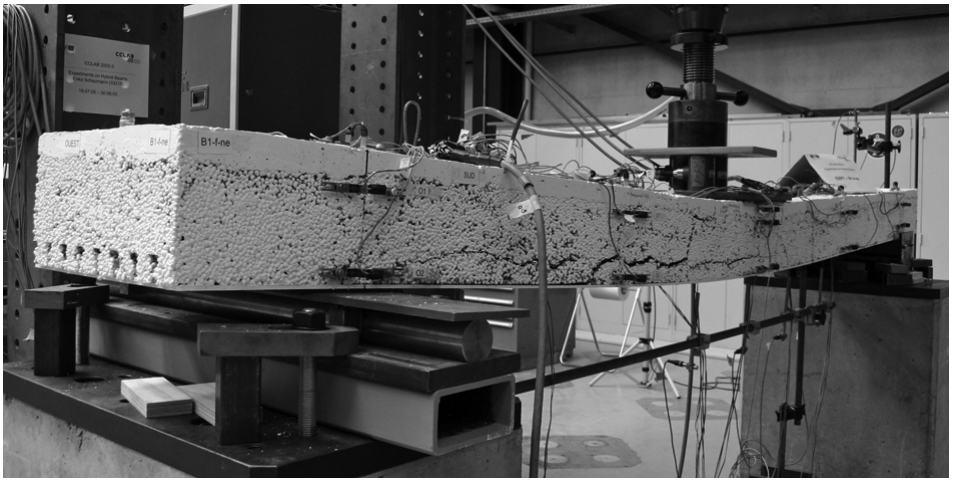

(b) View from south

Figure C.86: 1300-2: a) Failure process and b) still loaded failed beam after experiment - south.

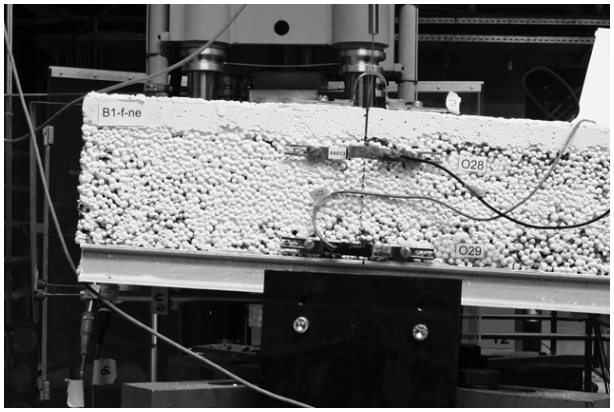

(a) View from north - axis B

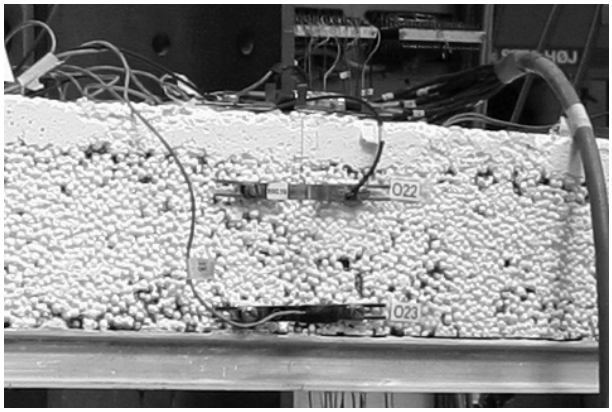

(b) View from north - axis C

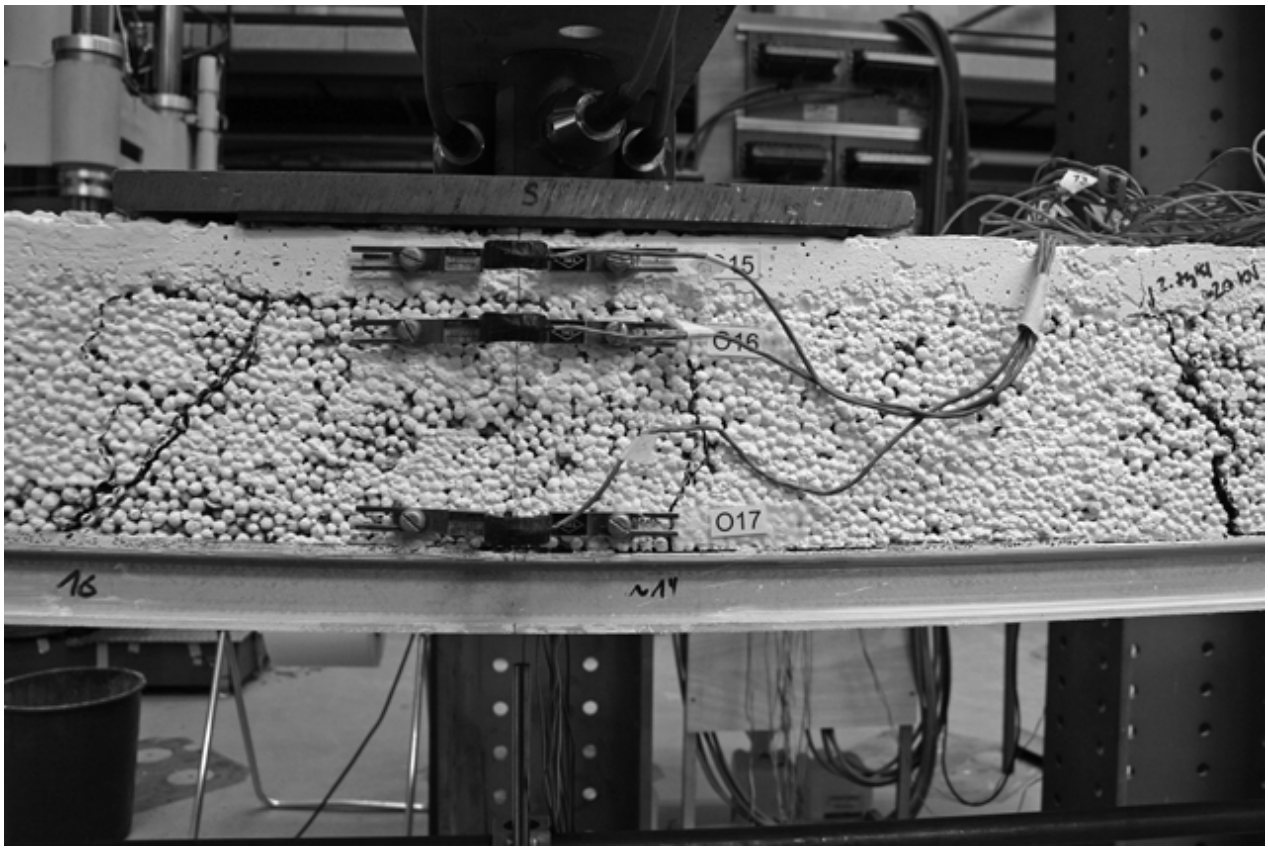

(c) View from north - mid-span

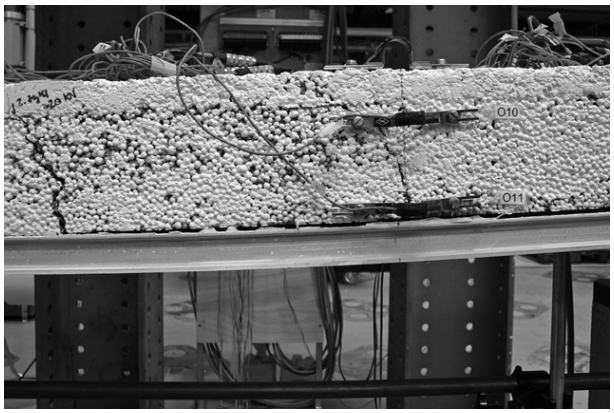

(d) View from north - axis E

(e) View from north - axis F

Figure C.87: 1300-2: Failed beam after experiment, still loaded - north.

(a) View from south - axis F

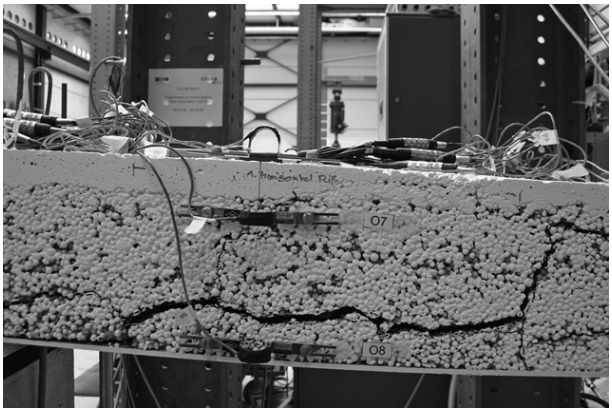

(b) View from south - axis E

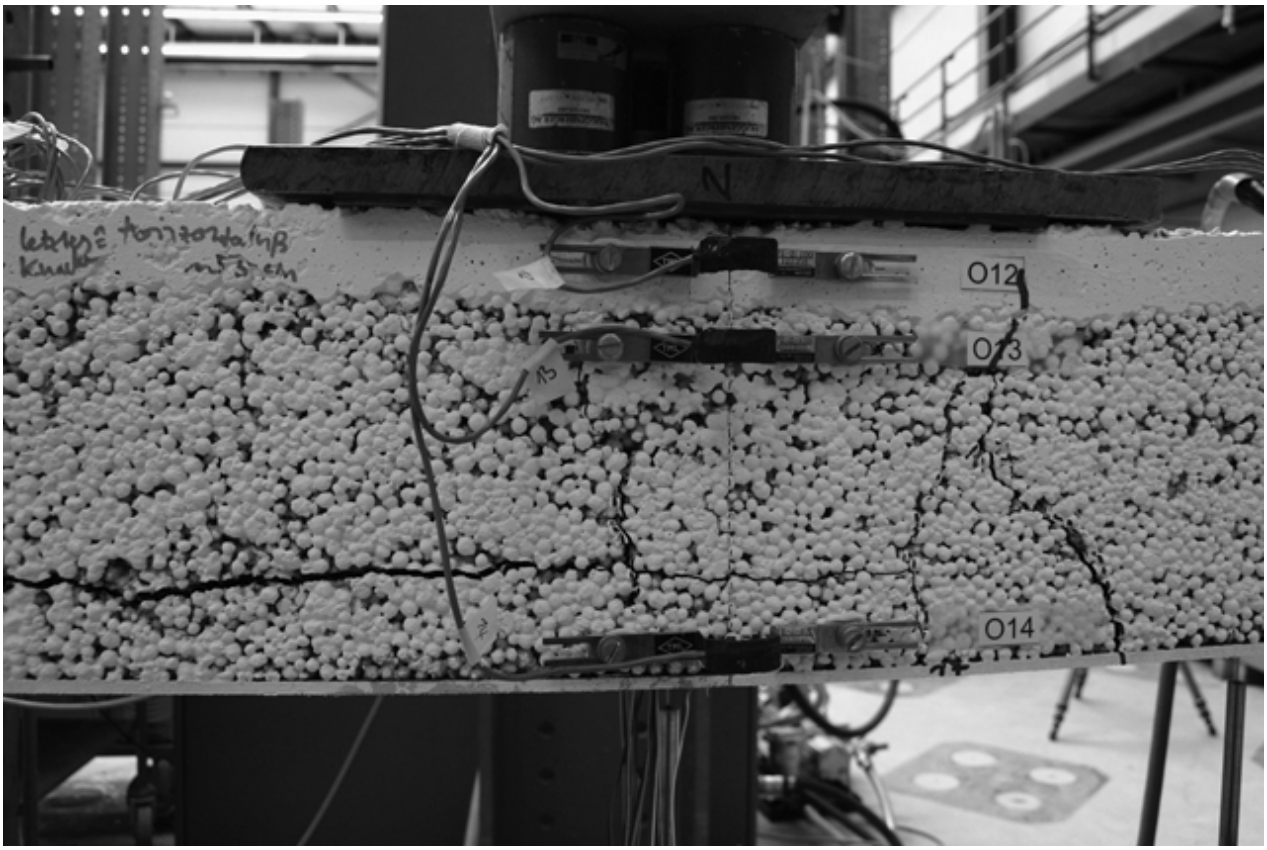

(c) View from south - mid-span

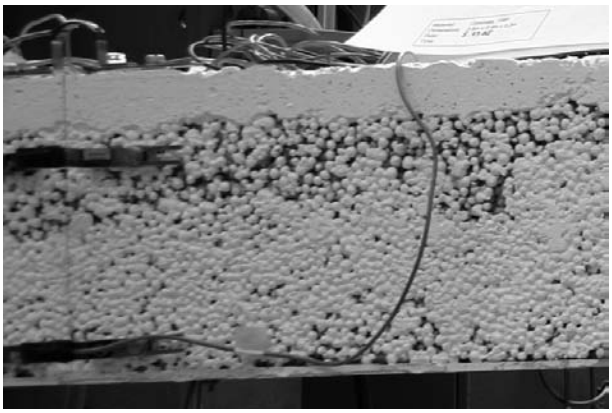

(d) View from south - axis C

(e) View from south - axis B

Figure C.88: 1300-2: Failed beam after experiment, still loaded - south.

C.4.6.2 Displacement transducers

The load deflection response in Figure C.89 indicates that beam stiffness remained constant up to the cracking load of approximately 10 kN (Figure C.90-c). Stiffness then decreased slightly and the first debonding was measured at the beam end at 17 kN. At 18.1 kN a second load cycle was performed. The beam exhibited no significant stiffness changes during unloading and reloading. Subsequently, an oscillating phase occurred at a deflection of 6 to 10 mm, during which the applied load varied between 21 kN and 22.7 kN, each time accompanied by an audible inner crack.

A third load cycle was performed at the deflection of 33 mm with a corresponding load of 22.5 kN. After reloading, a slight but steady load increase was observed up to the ultimate load of 23.3 kN with a corresponding deflection of 40.4 mm, followed by a drop in the load to 10 kN. A slight increase in stiffness could be noticed. The experiment was stopped at a deflection of 60 mm at load of 10.8 kN.

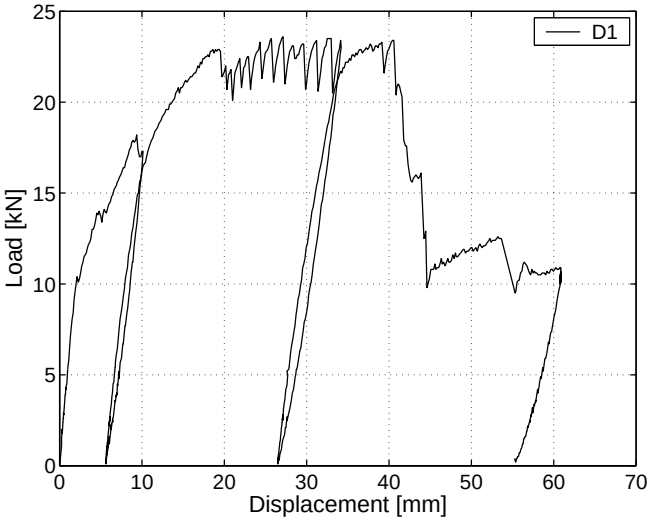

(a) Displacement at mid-span

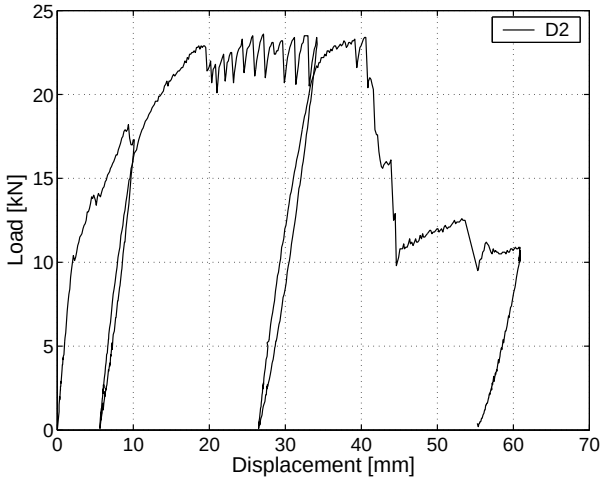

(b) Displacement - between axes C-D

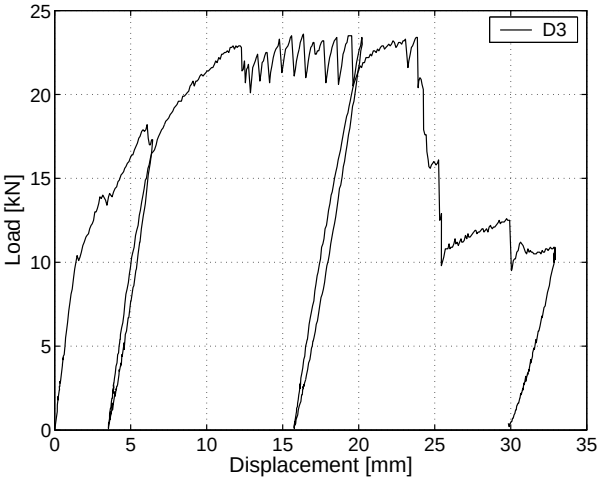

(c) Displacement - axis C

Figure C.89: 1300-2: Displacement at mid-span, at 0.75 m and 2.25 m.

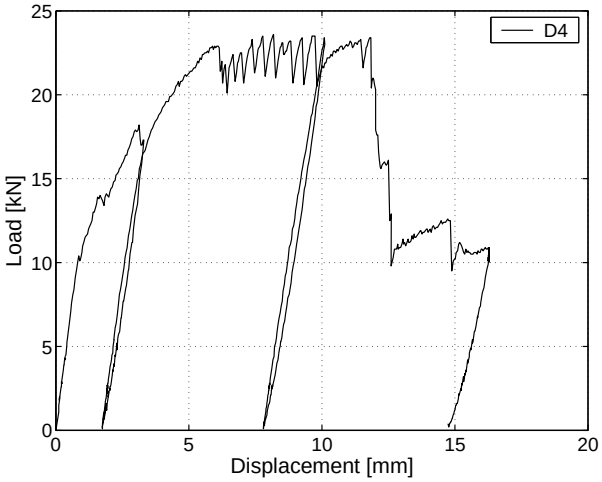

(a) Displacement - between axes B-C

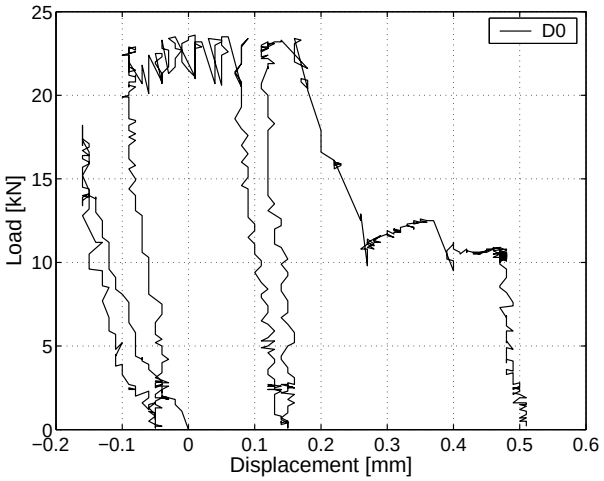

(b) Displacement at free support axis B

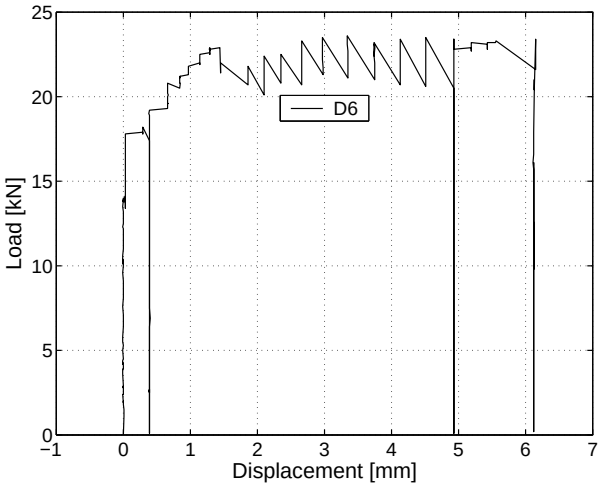

(c) Horizontal displacement of LC - axis A

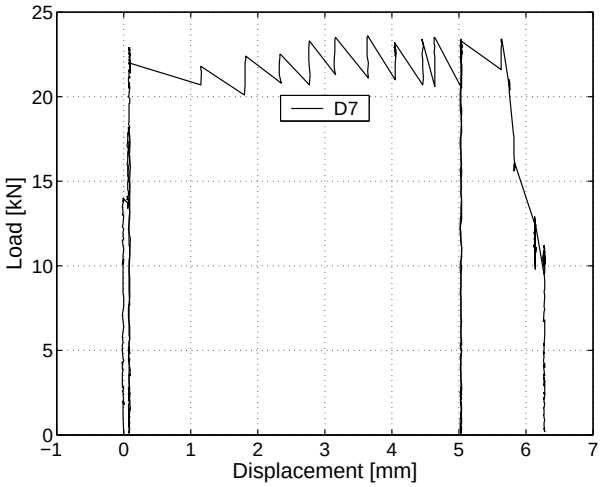

(d) Horizontal displacement of NC - axis A

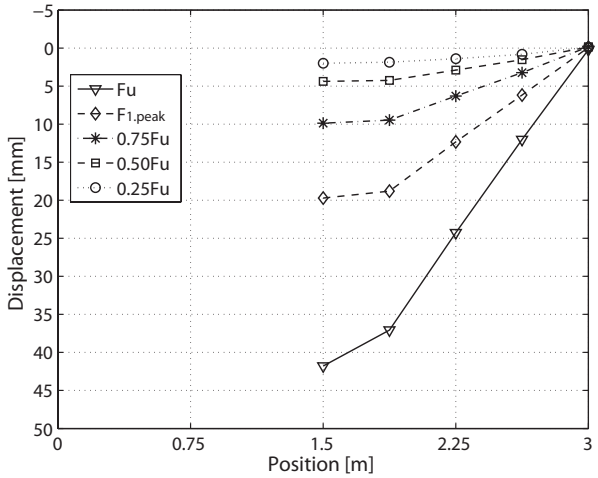

(e) Displacement along beam

Figure C.90: 1300-2: Displacements at different sections and along beam ($F_{1.peak} = 23.0\,\text{kN}$ with 18.8 mm and $F_u = 23.3\,\text{kN}$ with 40.4 mm corresponding deflections).

C.4.6.3 Omega-shaped extensometers

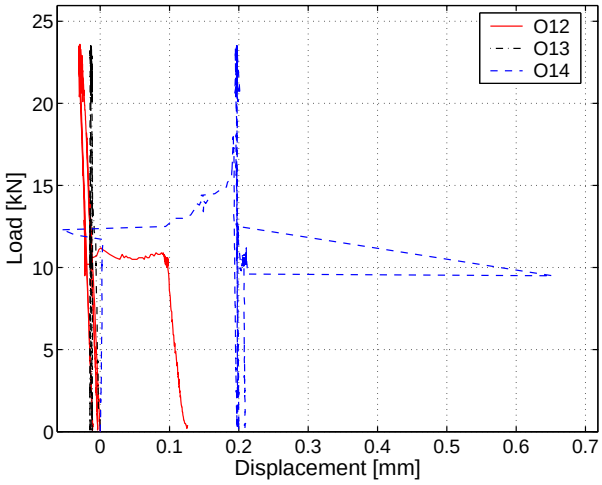

(a) Axis D (mid-span) - south

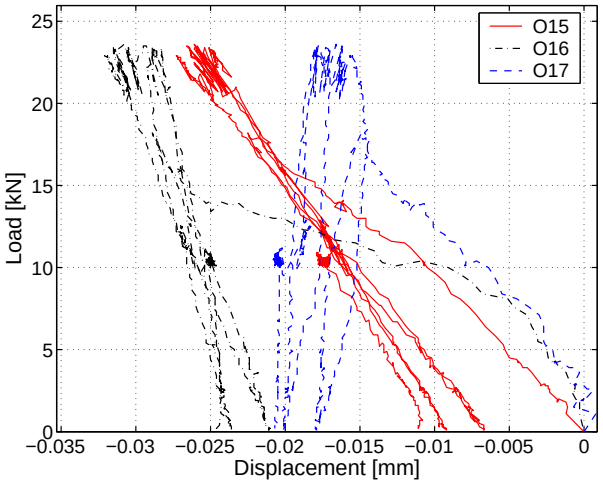

(b) Axis D (mid-span) - north

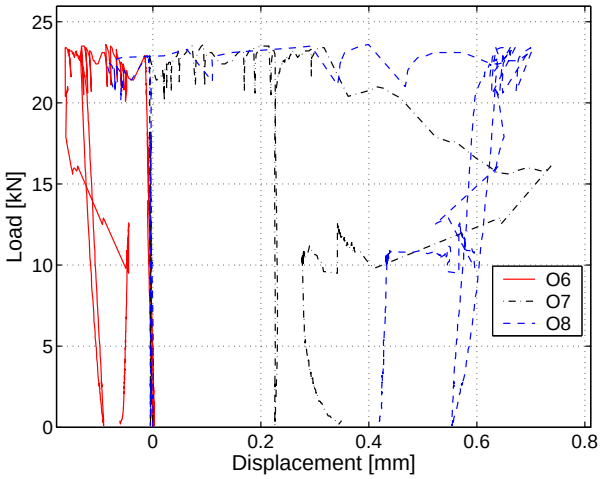

(c) Axis E - south

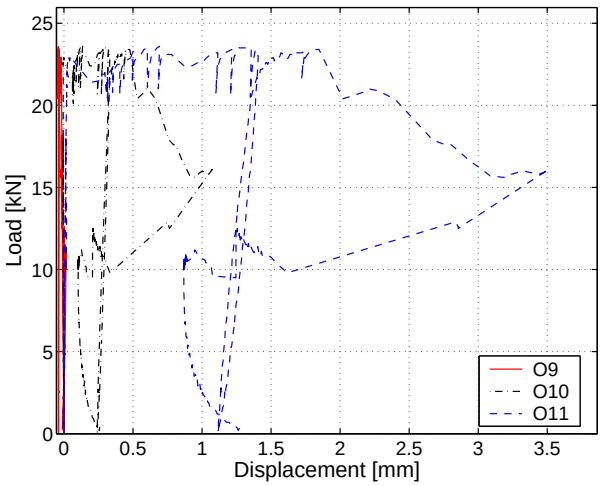

(d) Axis E - north

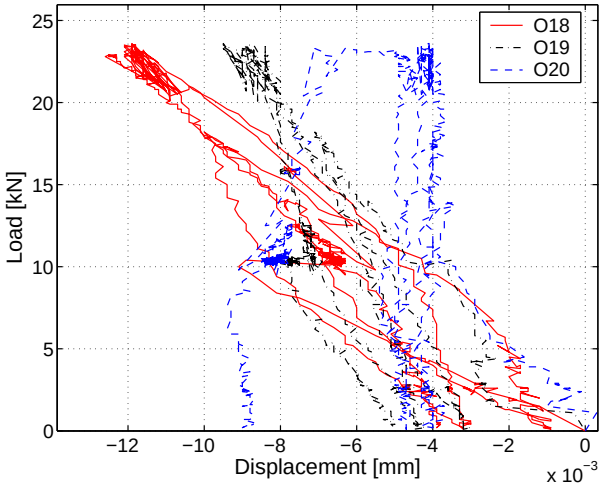

(e) Axis C - south

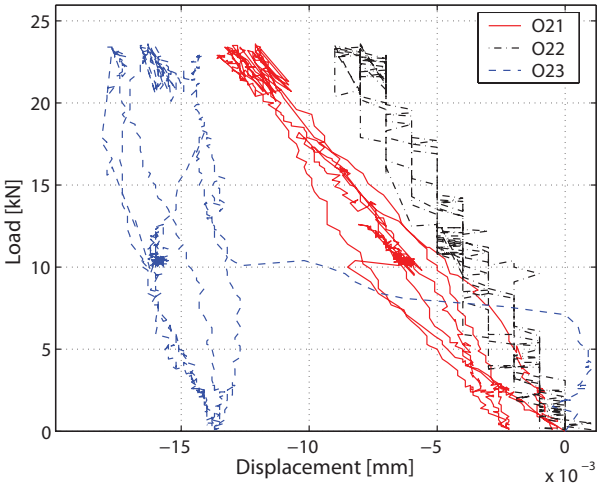

(f) Axis C - north

Figure C.91: 1300-2: Deformations in omega-shaped extensometers at axes C-E.

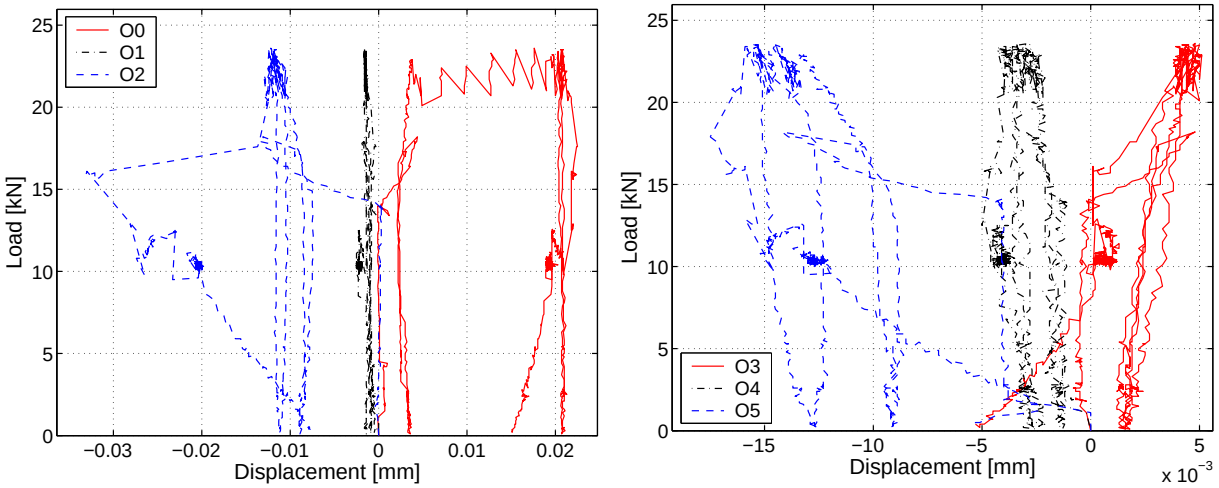

(a) Axis F - south

(b) Axis F - north

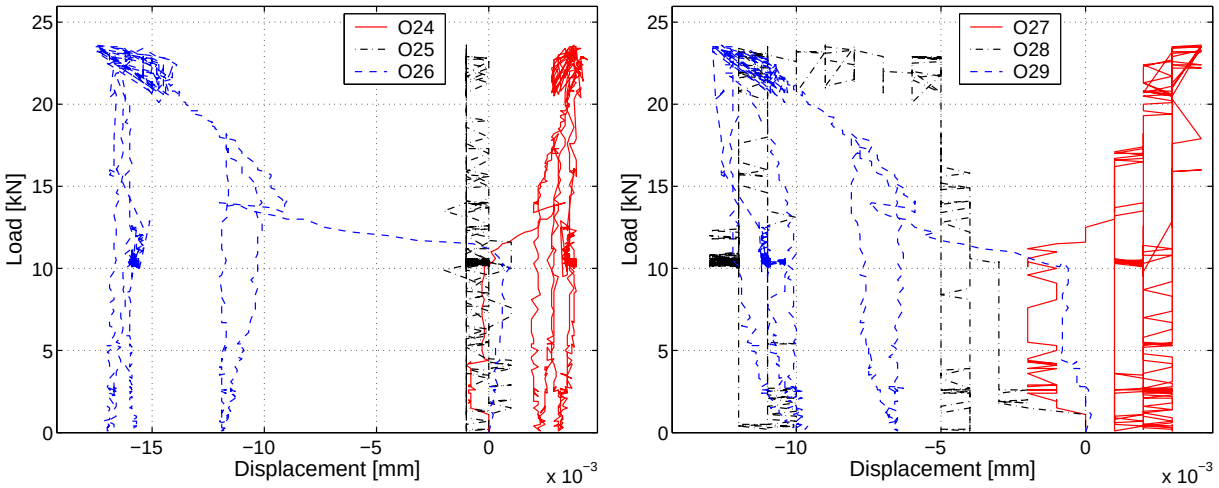

(c) Axis B - south

(d) Axis B - north

Figure C.92: 1300-2: Deformations in omega-shaped extensometers over supports.

C.4.6.4 Strain gages on GFRP profile

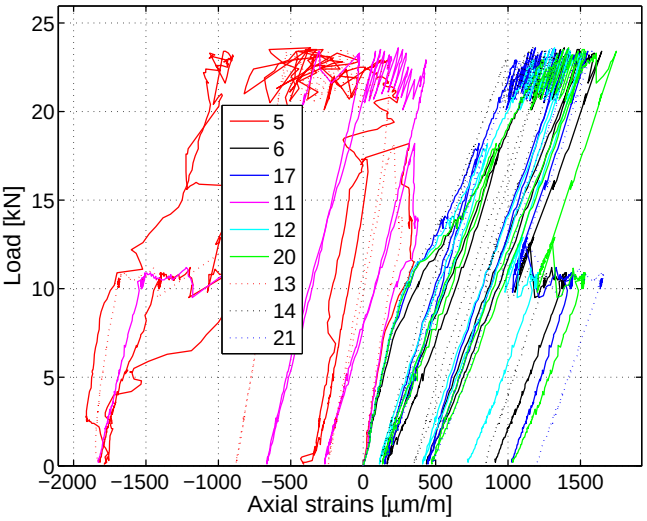

(a) Axial strains at axis D (mid-span)

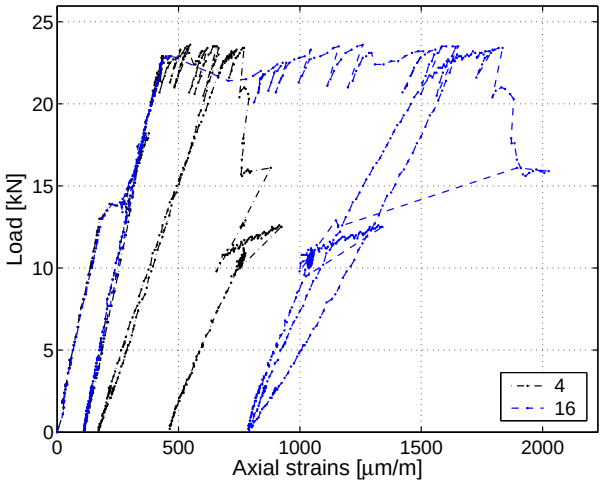

(b) Axial strains at axis E

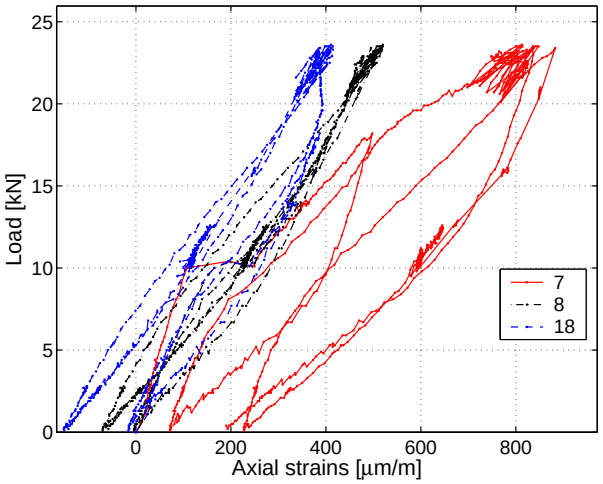

(c) Axial strains at axis C

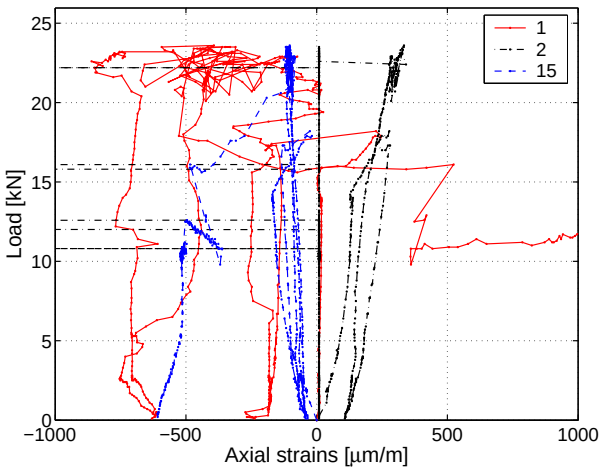

(d) Axial strains at axis F

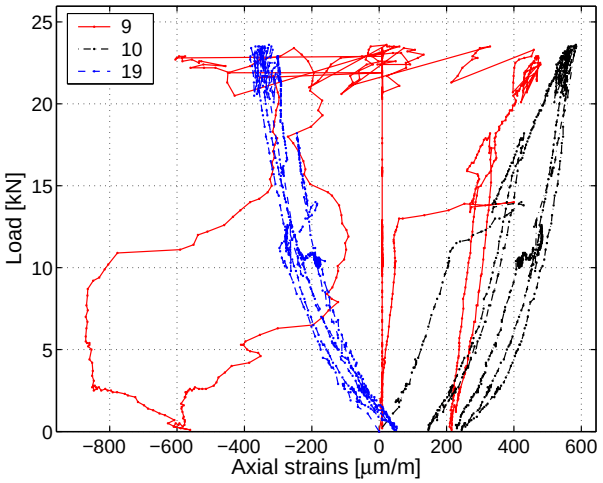

(e) Axial strains at axis B

Figure C.93: 1300-2: Axial strains in GFRP profile.

C.4.6.5 Axial strains through the cross section

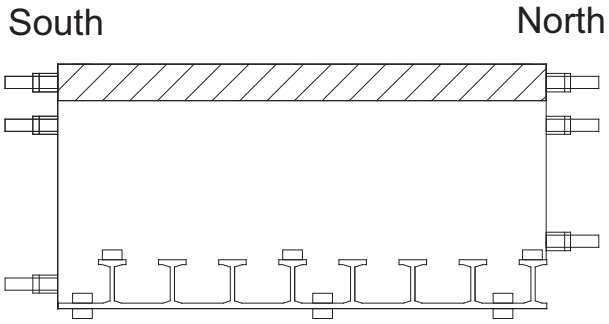

(a) Instrumentation location

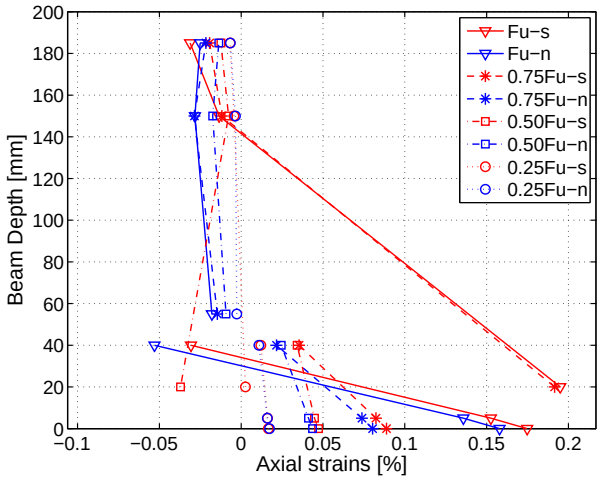

(b) Strain gages and omegas on north and south side

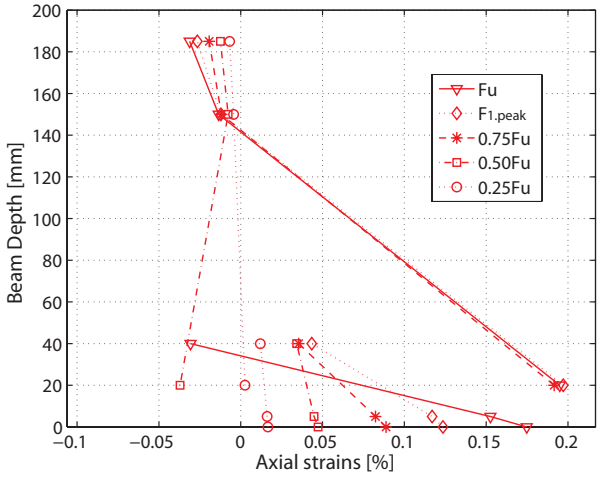

(c) South

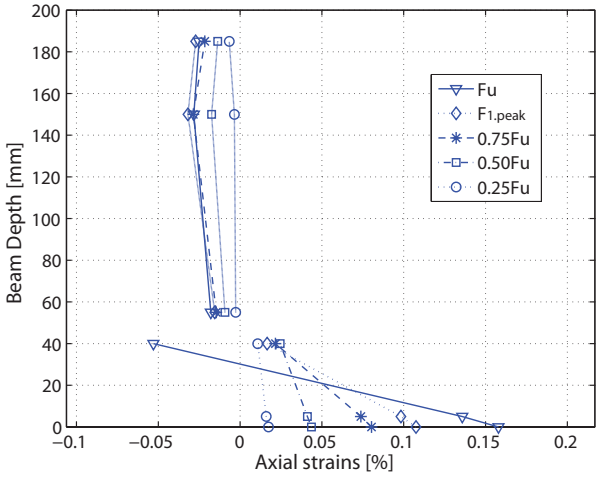

(d) North

Figure C.94: 1300-2: Axial strains through cross section at mid-span at different load steps at different load steps from strain gages and omega-shaped extensometers ($F_{1.peak} = 23.0\,\text{kN}$ with 18.8 mm and $F_u = 23.3\,\text{kN}$ with 40.4 mm corresponding deflections).

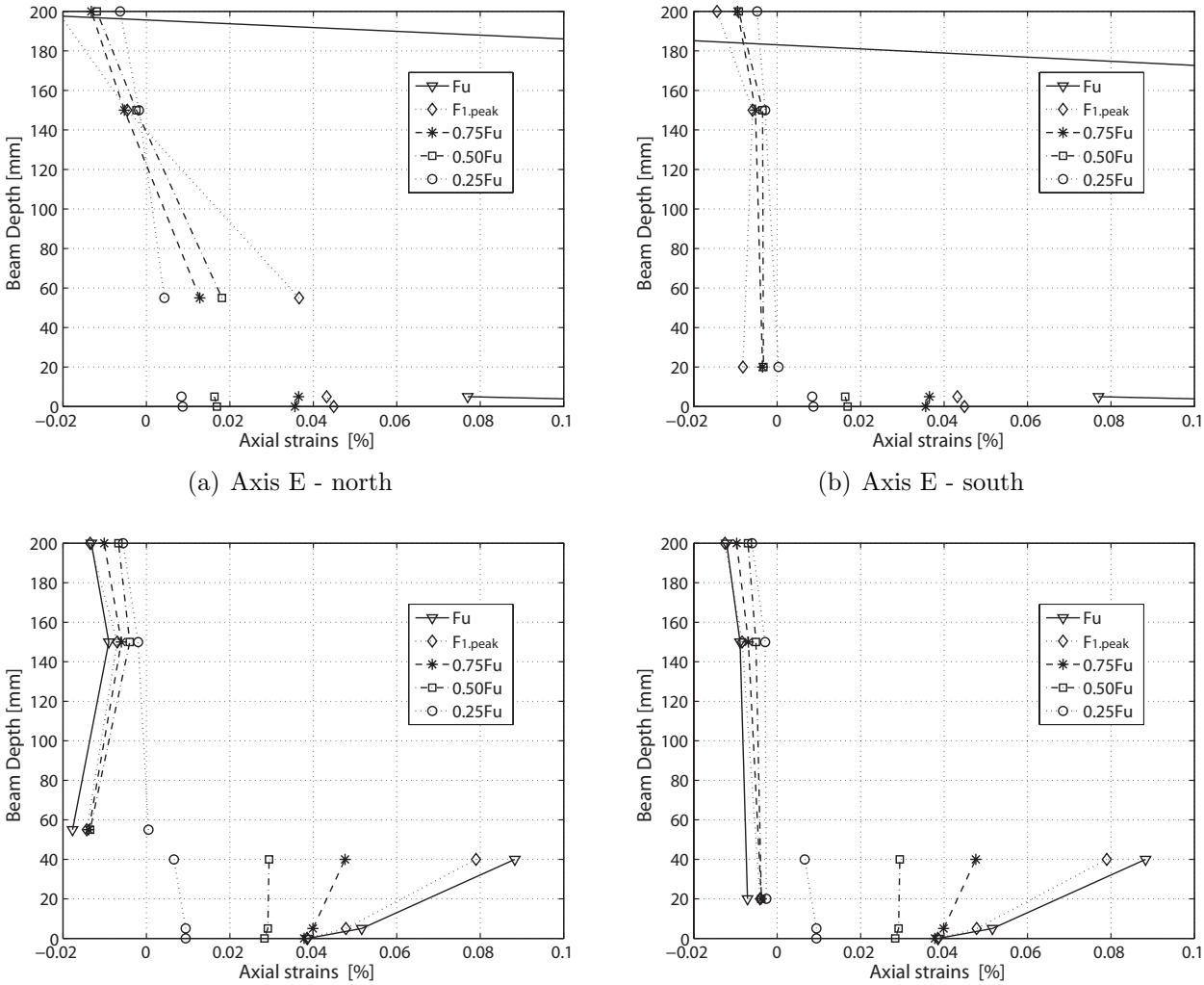

(a) Axis E - north

(b) Axis E - south

(c) Axis C - north

(d) Axis C - south

Figure C.95: 1300-2: Axial strains through cross section at 0.75 m and 2.25 m at different load steps from strain gages and omega-shaped extensometers ($F_{1.peak} = 23.0$ kN with 18.8 mm and $F_u = 23.3$ kN with 40.4 mm corresponding deflections).

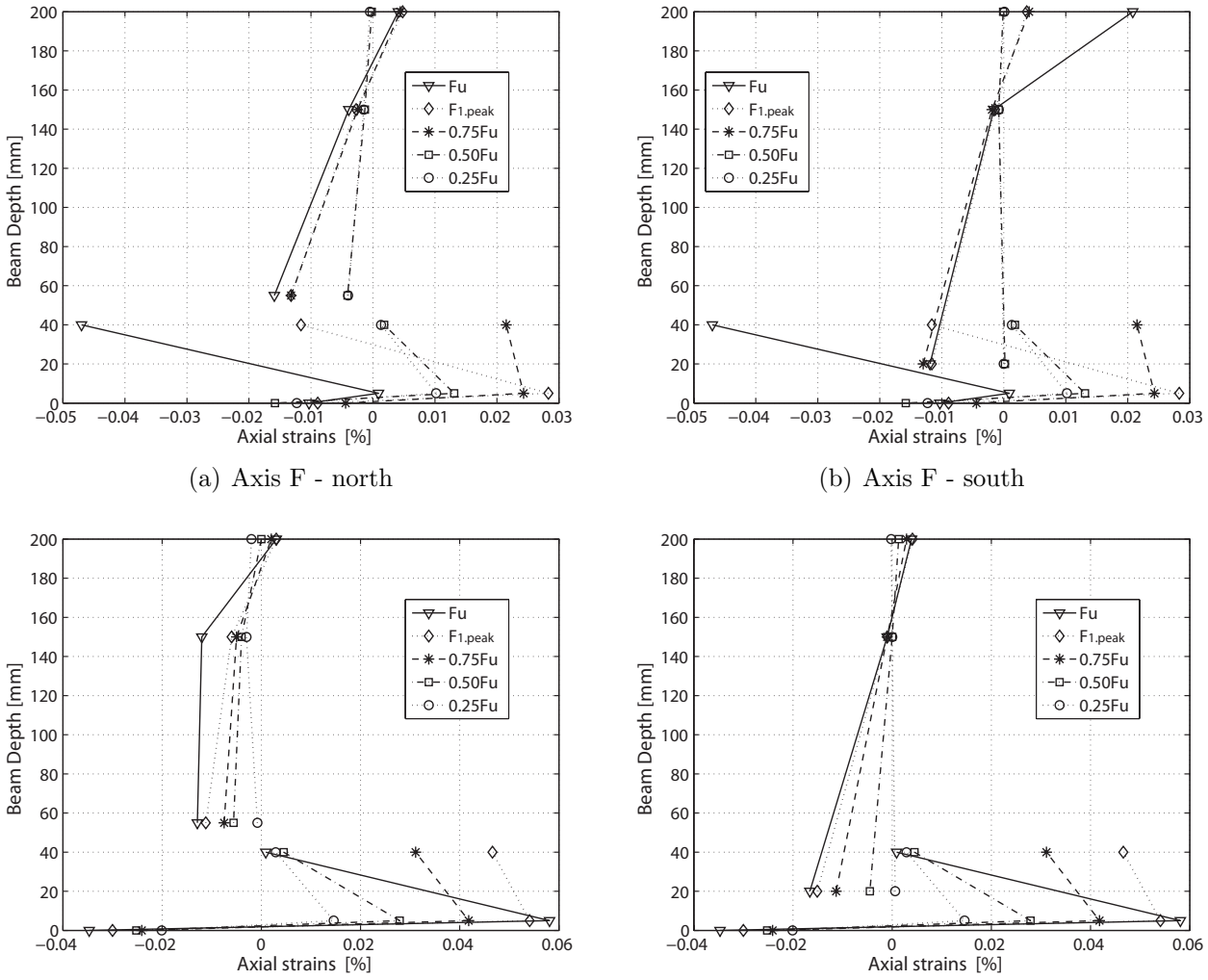

(a) Axis F - north

(b) Axis F - south

(c) Axis B - north

(d) Axial strains axis B - south

Figure C.96: 1300-2: Axial strains through cross section over supports at different load steps from strain gages and omega-shaped extensometers ($F_{1.peak} = 23.0\,\text{kN}$ with 18.8 mm and $F_u = 23.3\,\text{kN}$ with 40.4 mm corresponding deflection).

C.4.6.6 Axial strains along the beam

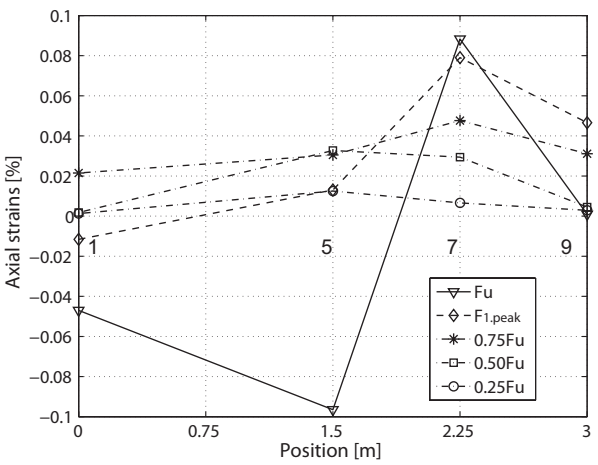

(a) Axial strains on top of T-upstands

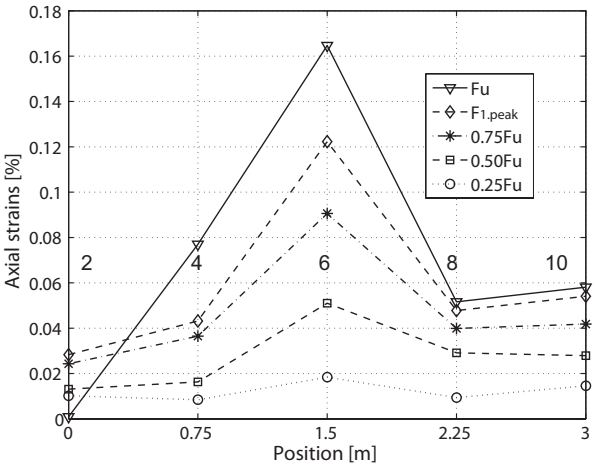

(b) Axial strains between T-upstands

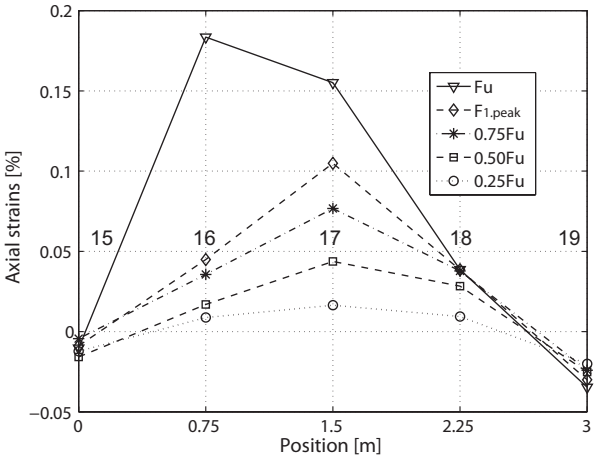

(c) Axial strains beneath GFRP sheet

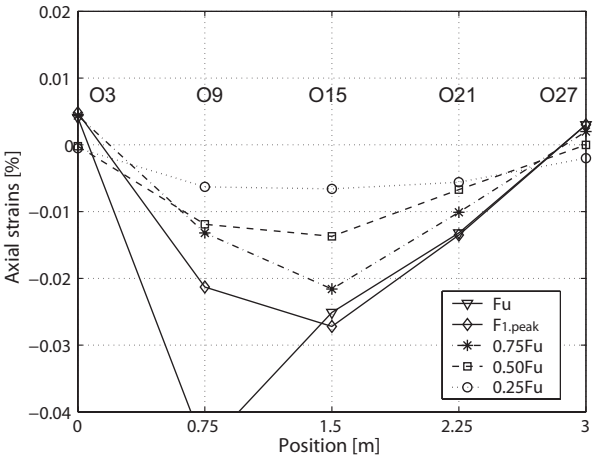

(d) Axial strains in NC layer - north

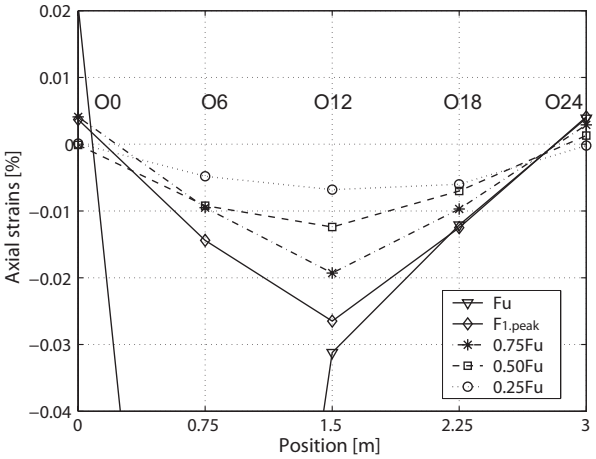

(e) Axial strains in NC layer - south

Figure C.97: 1300-2: Axial strains along beam at different load steps from strain gages and omega-shaped extensometers ($F_{1.peak} = 23.0\,\text{kN}$ with $18.8\,\text{mm}$ and $F_u = 23.3\,\text{kN}$ with $40.4\,\text{mm}$ corresponding deflections).

C.4.7 Beam 1300E-1: Failure description and measured results (low instrumentation)

C.4.7.1 Failure description

The failure process of beam 1300-1 is illustrated in Figures C.98, C.99 and C.100. The first small crack occurred next to the loading plate at a load of 20 kN (Figure C.99-a). Subsequently several small vertical and slightly inclined cracks in the tension zone of the LC developed and started to grow as from a load of 35 kN (Figure C.99-b-c). The ultimate load was reached at $F_u = 42.8$ kN with a corresponding deflection of 12.3 mm, where one of the cracks suddenly propagated through the beam depth and along the LC-NC interface to the loading plate and along the top of the GFRP T-upstands. As deflections increased, the load rapidly decreased to 36.7 kN and then to the final value of 3.4 kN. The crack simultaneously developed horizontally over the support to the beam end (Figure C.99-e-f). The experiment was then stopped. The epoxy-bonded interface remained undamaged and no debonding of the LC from the GFRP occurred. The failed specimen is shown in Figures C.101 and C.102.

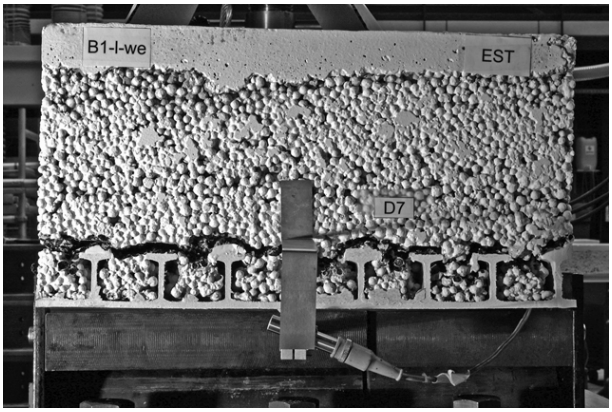

Figure C.98: 1300E-1: beam end after experiment.

(a) First crack under loading plate at 20 kN

(b) Several small cracks, at 32.3 kN and 8.12 mm deflection

(c) Longer cracks through LC core at loads above 35 kN

(d) Cracks at ultimate load at 42.8 kN and 12.3 mm deflection

(e) Cracks through beam at 26.7 kN and 13.7 mm deflection

(f) Failed beam at 3.4 kN and 16.4 mm deflection

Figure C.99: 1300E-1: Failure process.

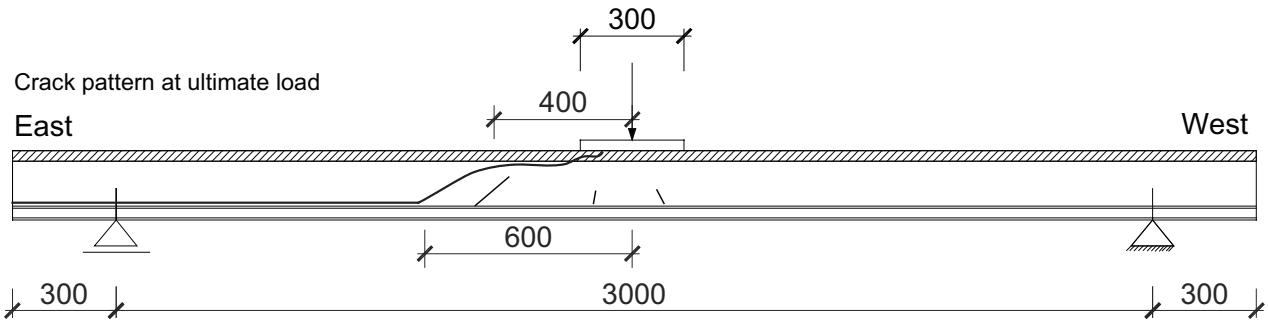

(a) View from north - cracked beam

(b) View from north

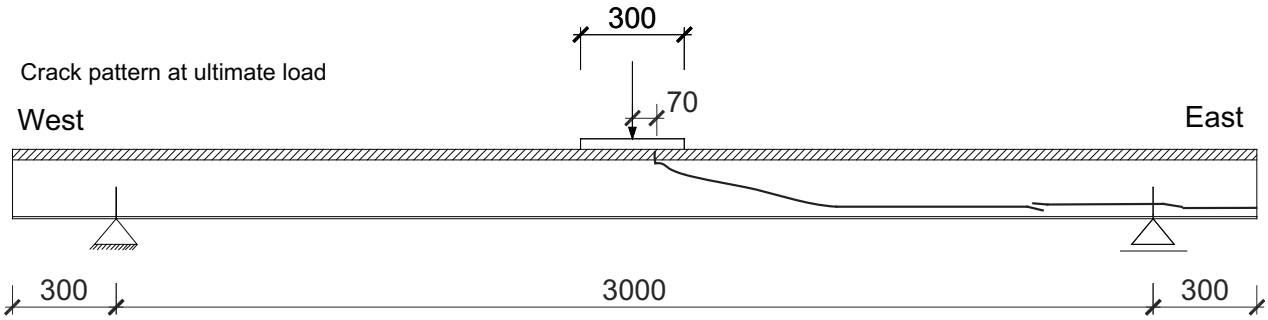

(c) View from south - cracked beam

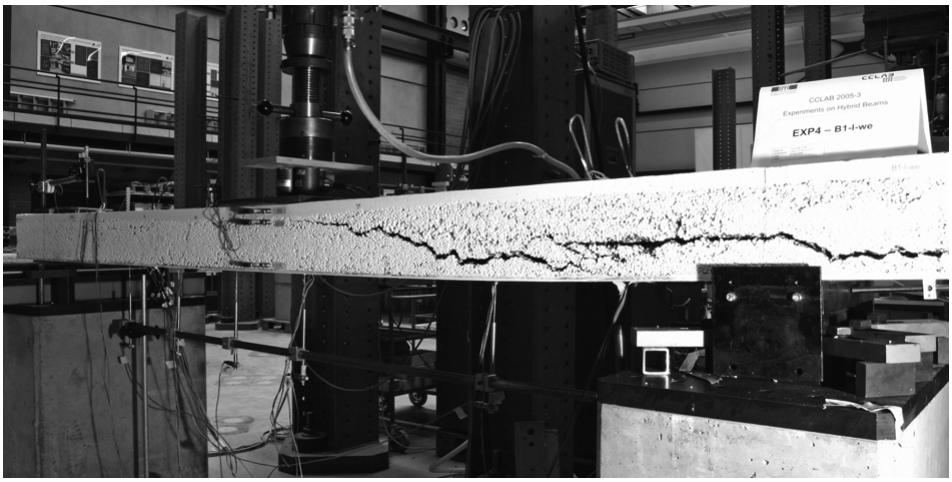

(d) View from south

Figure C.100: 1300E-1: Failed beam after experiment, still loaded.

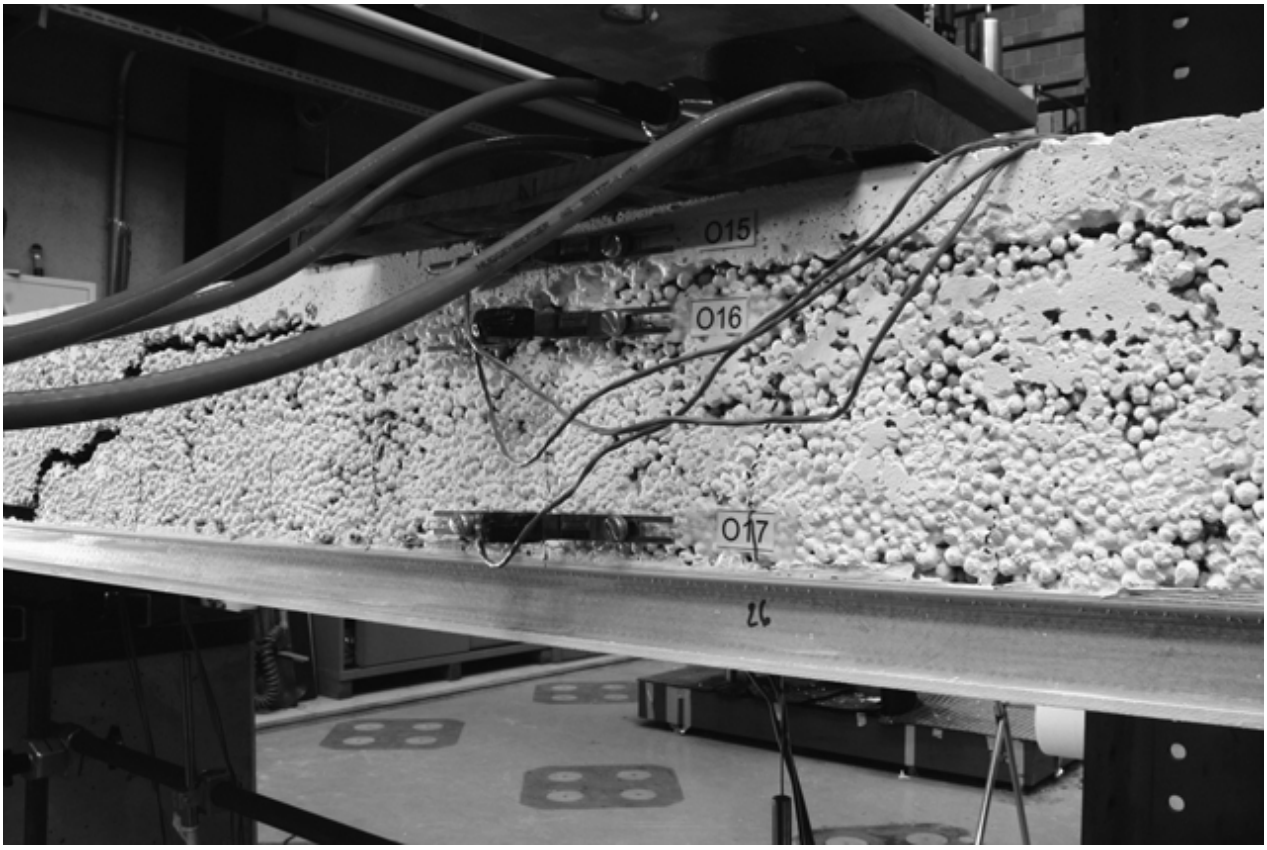

(a) View from north - mid-span - small cracks below loading plate

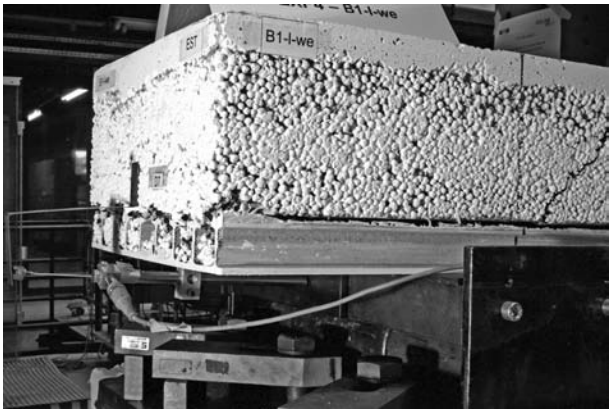

(b) View from north - axis B

(c) View from north - axis F

Figure C.101: 1300E-1: Failed beam after experiment, still loaded - north.

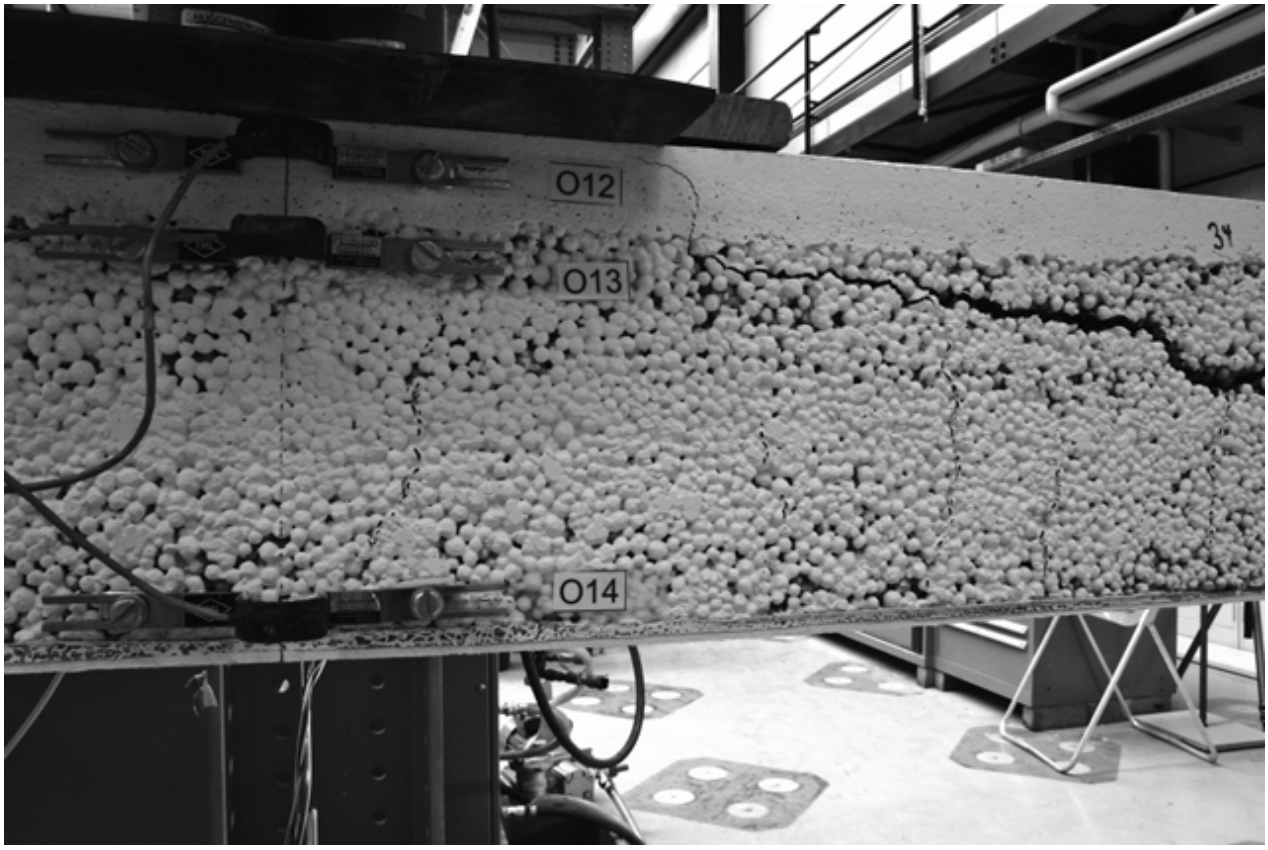

(a) View from south - mid-span

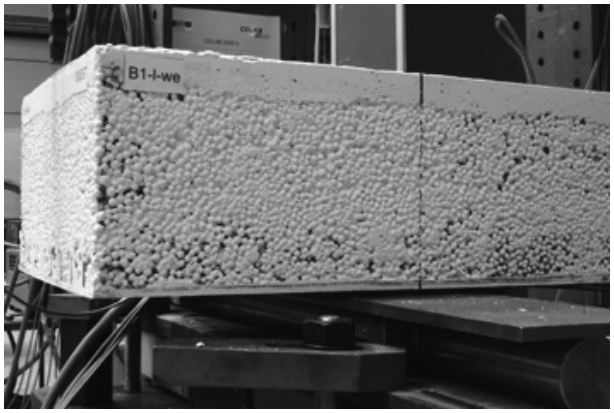

(b) View from south - axis F

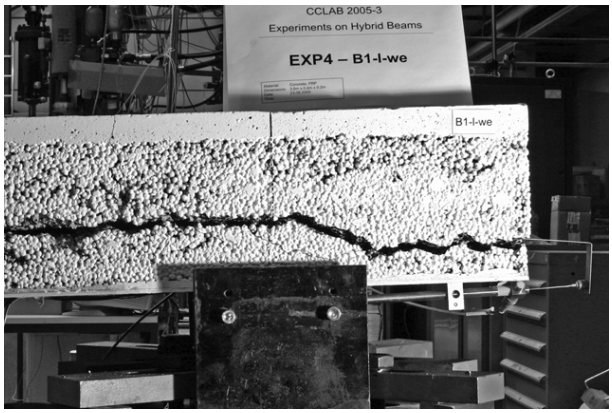

(c) View from south - axis B

Figure C.102: 1300E-1: Failed beam after experiment, still loaded - south.

C.4.7.2 Displacement transducers

Figure C.103 shows the load deflection response of the beam. Beam stiffness remained almost constant up to the cracking load of ∼13.0 kN and the beam then lost its stiffness slightly. At the ultimate load of 43.8 kN the final crack occurred with a corresponding deflection at mid-span of 12.3 mm. The load then dropped to 36.7 kN and remained stable up to a deflection of 14 mm. Subsequently the beam lost its stiffness and the load dropped to 3.4 kN. The experiment was then stopped. No debonding of the LC from the FRP occurred and no slippage at the beam end was measured, as shown in Figure C.104-d).

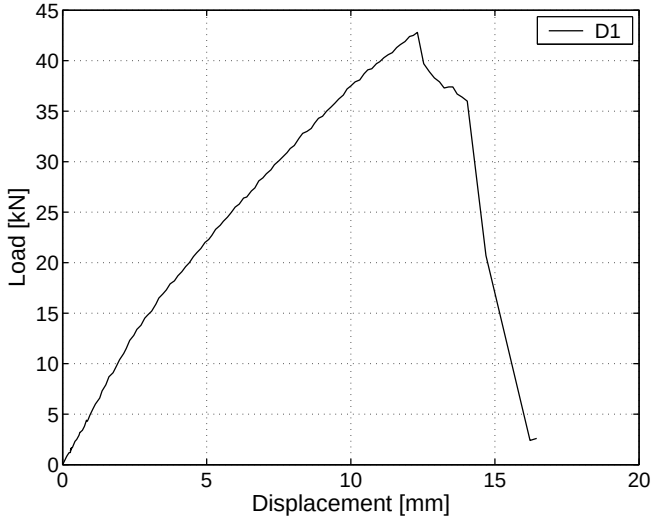

(a) Displacement at mid-span

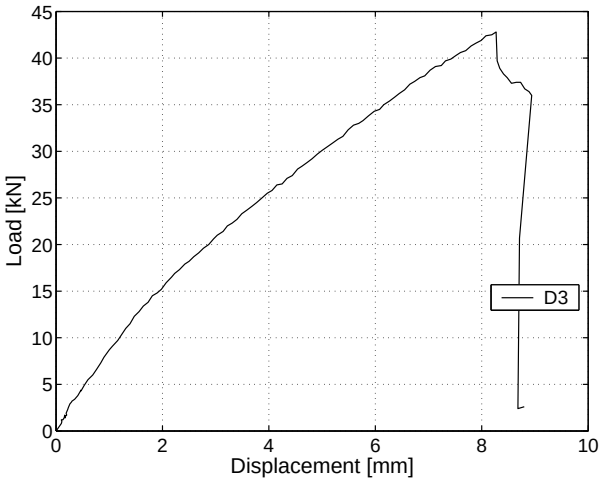

(b) Displacement - axis E

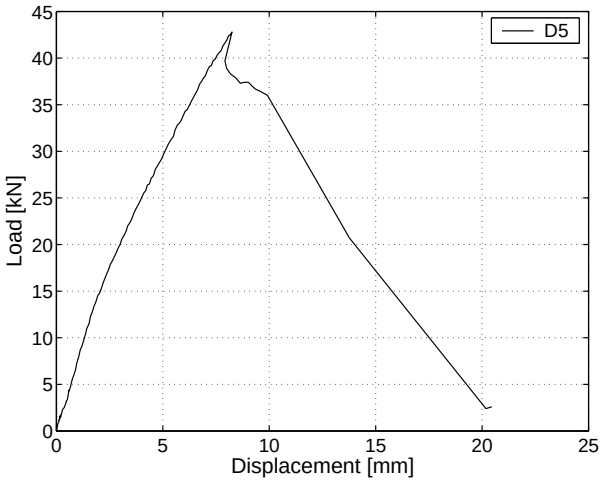

(c) Displacement - axis C

Figure C.103: 1300E-1: Displacement at mid-span, at 0.75 m and 2.25 m.

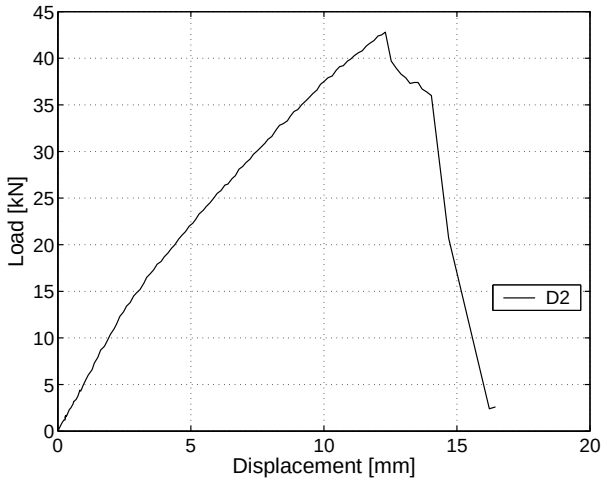

(a) Displacement - between axes D-E

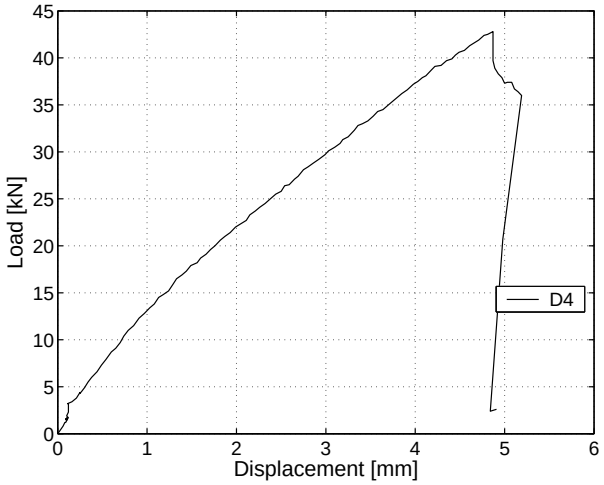

(b) Displacement - between axes E-F

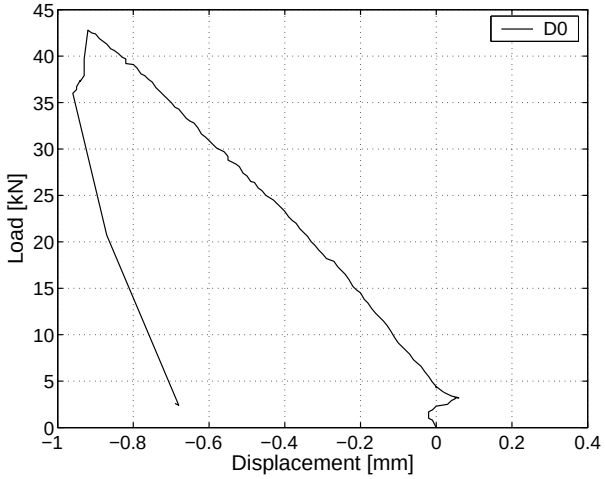

(c) Displacement at fixed support - axis F

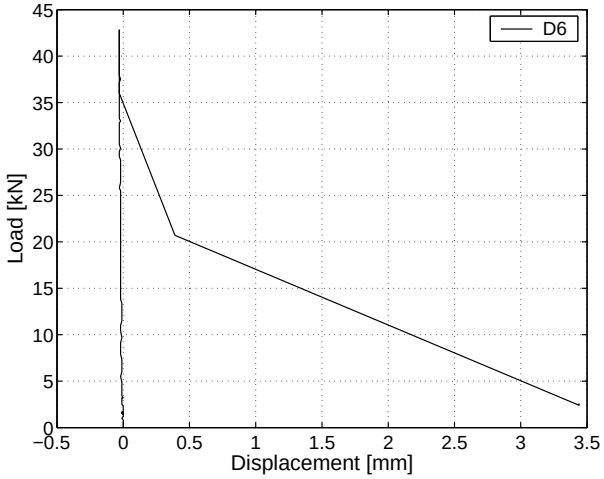

(d) Horizontal displacement of LC - axis A

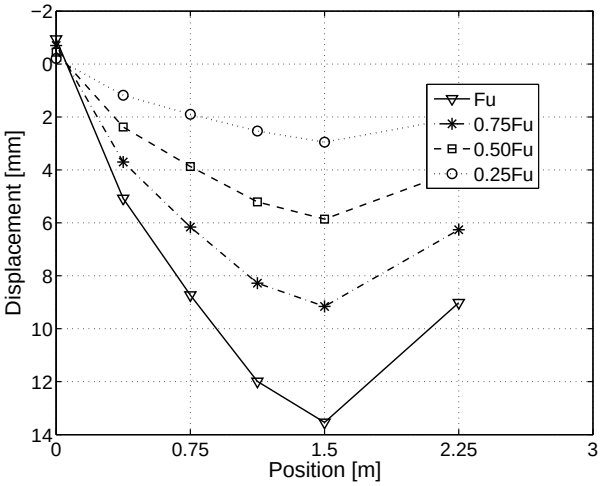

(e) Displacement along beam

Figure C.104: 1300E-1: Displacements at different sections and along beam.

C.4.7.3 Omega-shaped extensometers

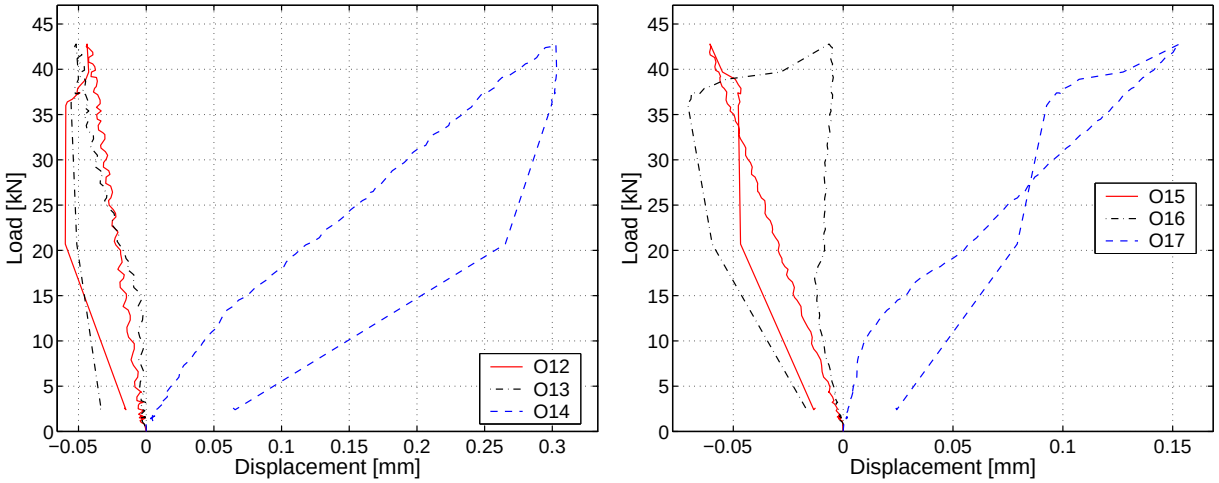

(a) Axis D (mid-span) - south

(b) Axis D (mid-span) - north

Figure C.105: 1300E-1: Deformations in omega-shaped extensometers at mid-span.

C.4.7.4 Strain gages on GFRP profile

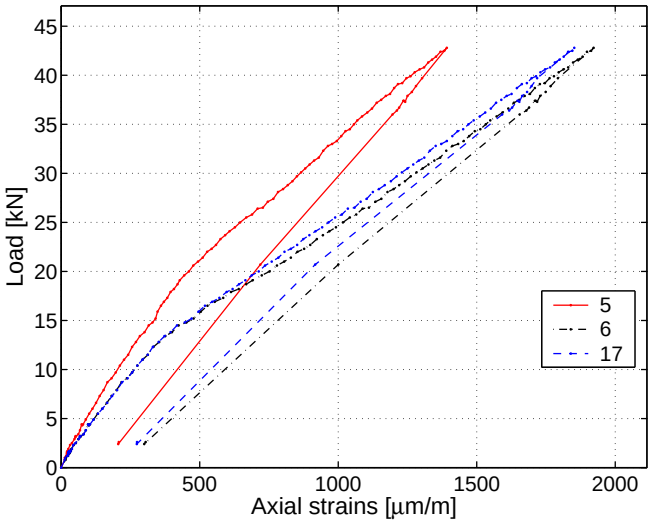

(a) Axial strains at axis D (mid-span)

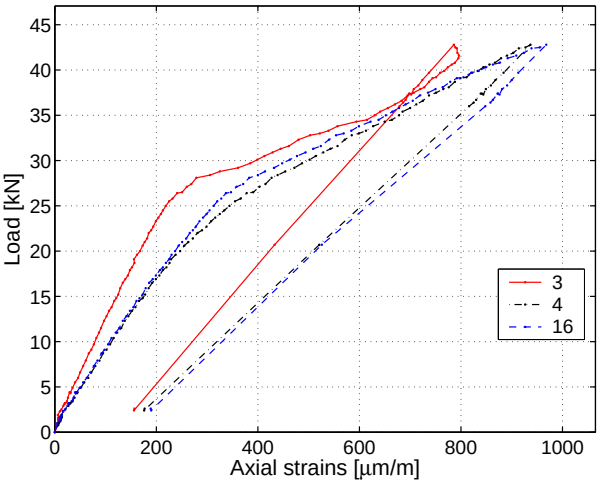

(b) Axial strains at axis E

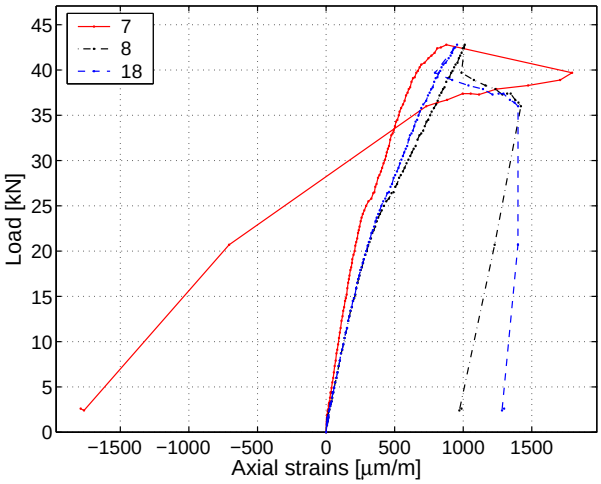

(c) Axial strains at axis C

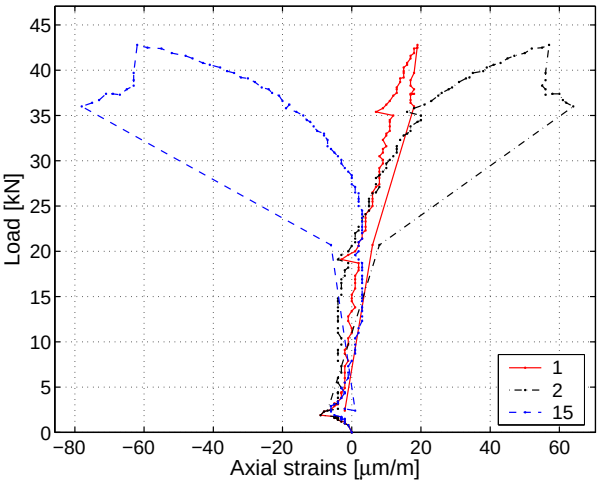

(d) Axial strains at axis F

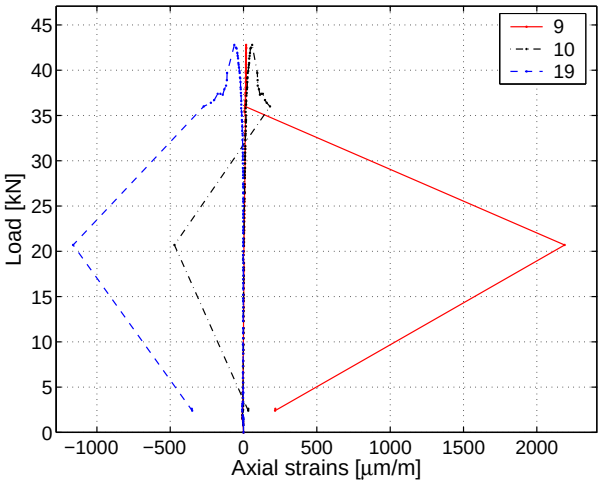

(e) Axial strains at axis B

Figure C.106: 1300E-1: Axial strains in GFRP profile

C.4.7.5 Axial strains through the cross section

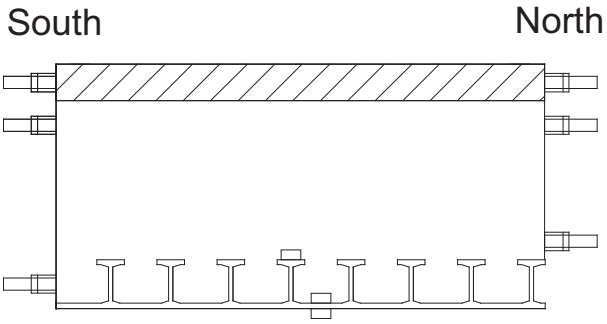

(a) Instrumentation location

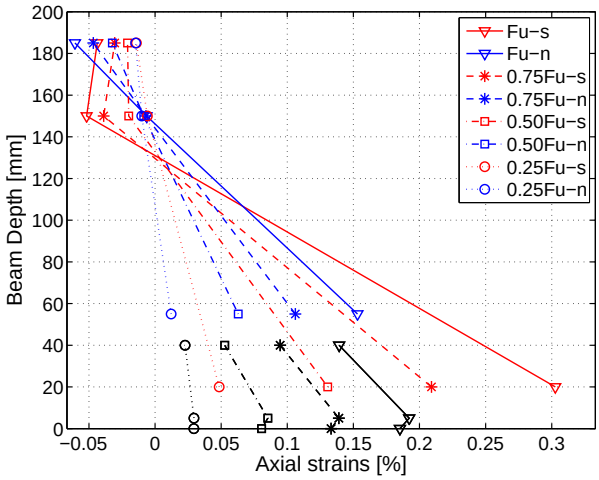

(b) Strain gages on centerline and omegas on north and south side

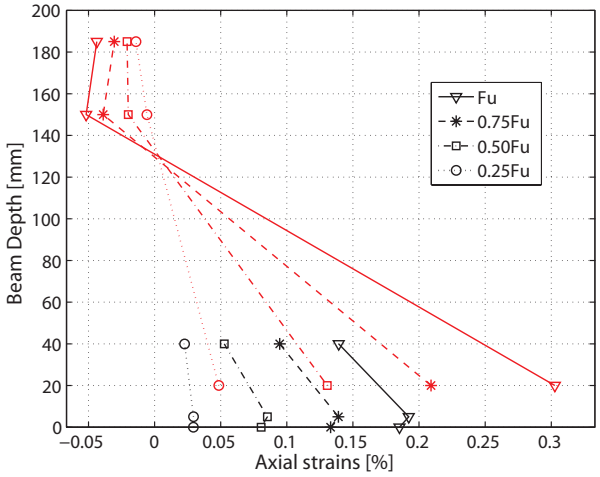

(c) South

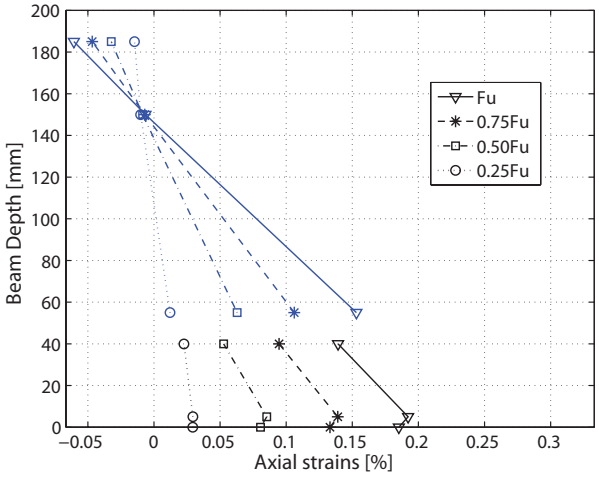

(d) North

Figure C.107: 1300E-1: Axial strains through cross section at mid-span at different load steps from strain gages and omega-shaped extensometers.

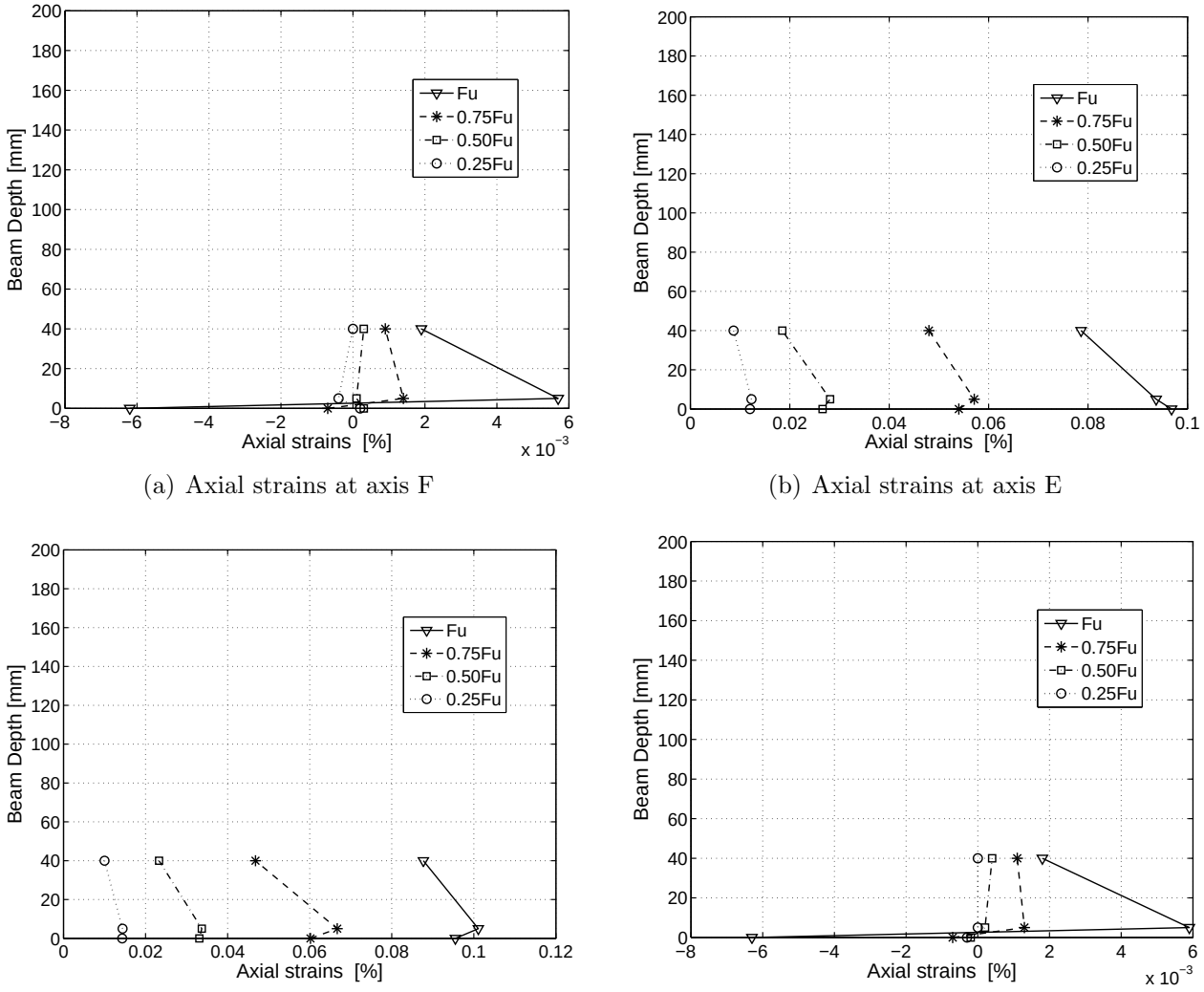

(a) Axial strains at axis F

(b) Axial strains at axis E

(c) Axial strains at axis C

(d) Axial strains at axis B

Figure C.108: 1300E-1: Axial strains through GFRP cross section at different load steps.

C.4.7.6 Axial strains along the beam

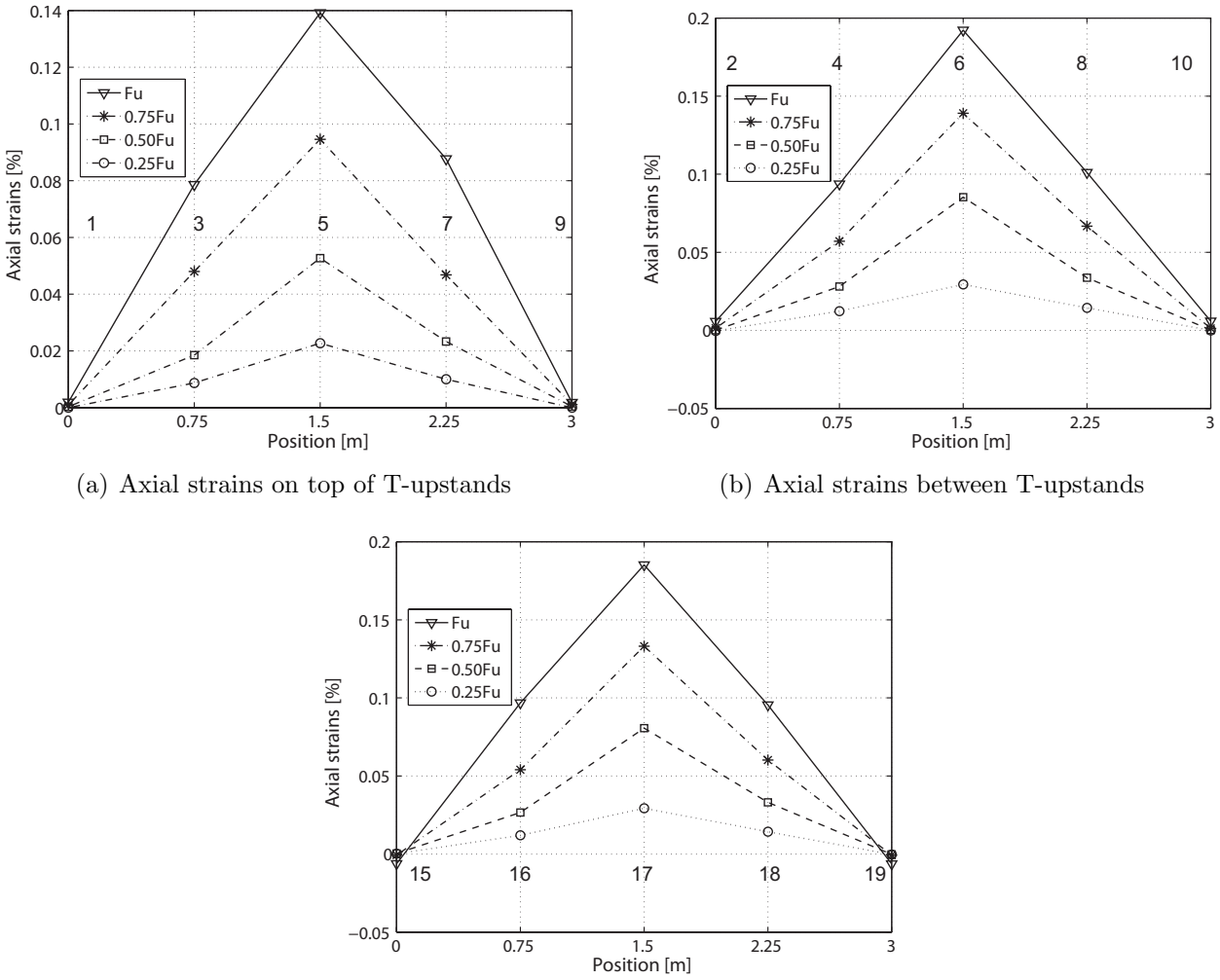

(a) Axial strains on top of T-upstands

(b) Axial strains between T-upstands

(c) Axial strains beneath GFRP sheet

Figure C.109: 1300E-1: Axial strains in GFRP profile along beam at different load steps.

C.4.8 Beam 1300E-2: Failure description and measured results (full instrumentation)

C.4.8.1 Failure description

The failure process of beam 1300E-2 is illustrated in Figures C.110, and C.111. Up to a load of 35.4 kN and mid-span deformation of 8 mm, where a second load cycle was performed, no cracks or noises occurred. During the reloading process the first small cracks in the tension zone of the lightweight concrete started to develop at 25 kN below the loading plate. All cracks were very small and vertically distributed with a spacing of approximately 10 cm. The first small noises were audible at a load of 36.3 kN. A loud noise at 43 kN next to omega-shaped extensometer O22 indicated the imminent failure. The beam failed in a brittle and immediate manner at the load $F_u = 50.5$ kN and a corresponding deflection of 14.1 mm. Since the epoxy-bonded interface remained undamaged, no debonding of the LC from the GFRP occurred. The failed specimen is shown in Figures C.112 and C.113.

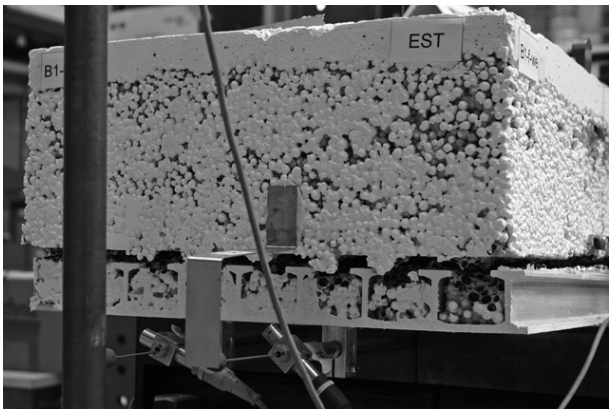

Figure C.110: 1300E-2: beam end after experiment.

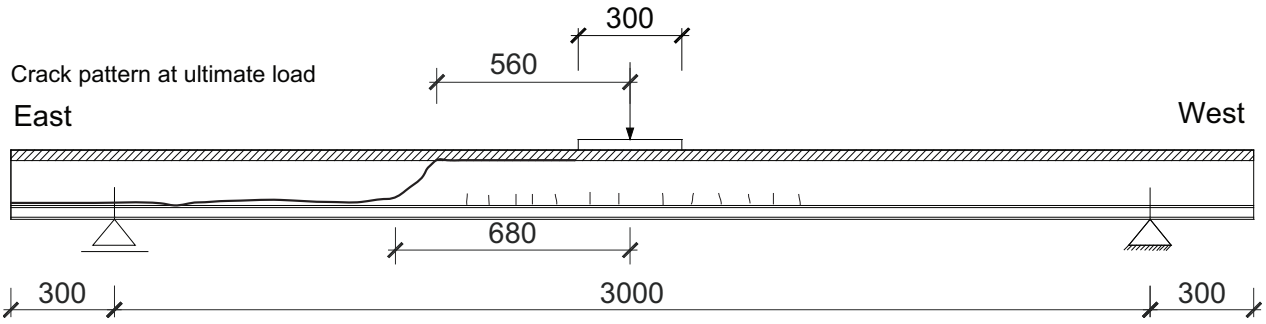

(a) View from north - Cracked beam

(b) View from north

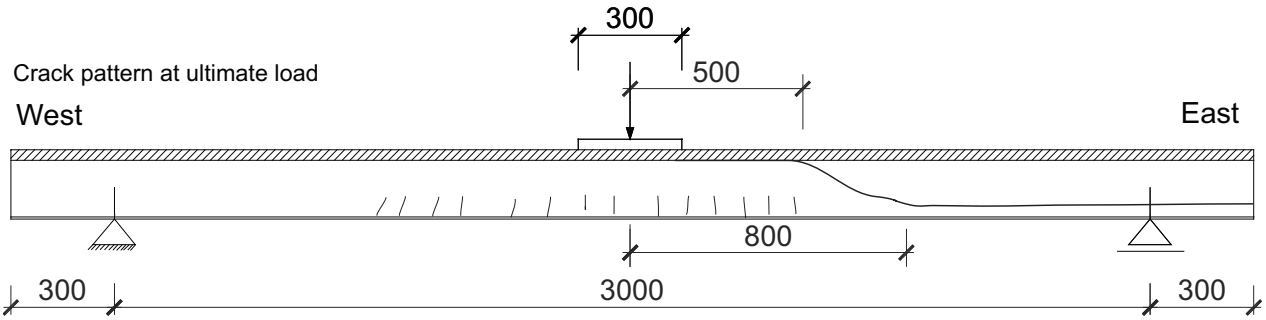

(c) View from south - Cracked beam

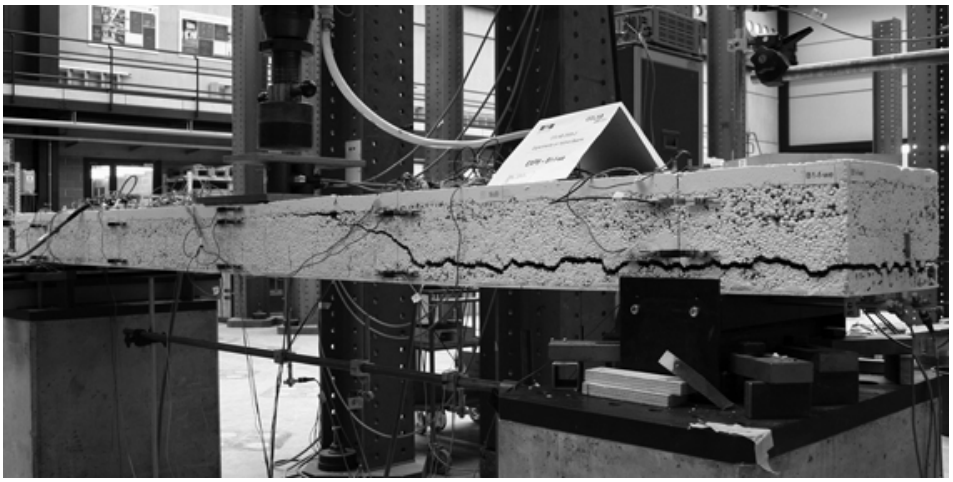

(d) View from south

Figure C.111: 1300E-2: Failed beam after experiment, still loaded.

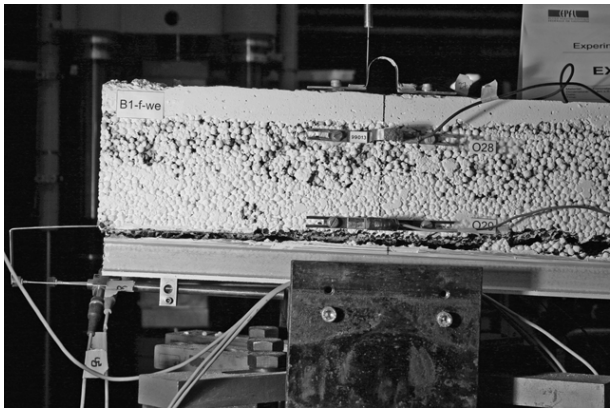

(a) View from north - axis B

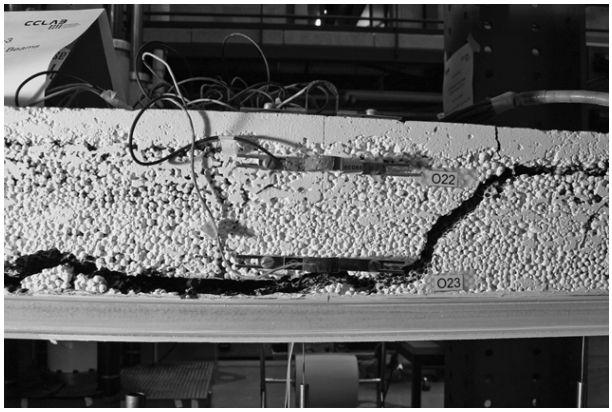

(b) View from north - axis C

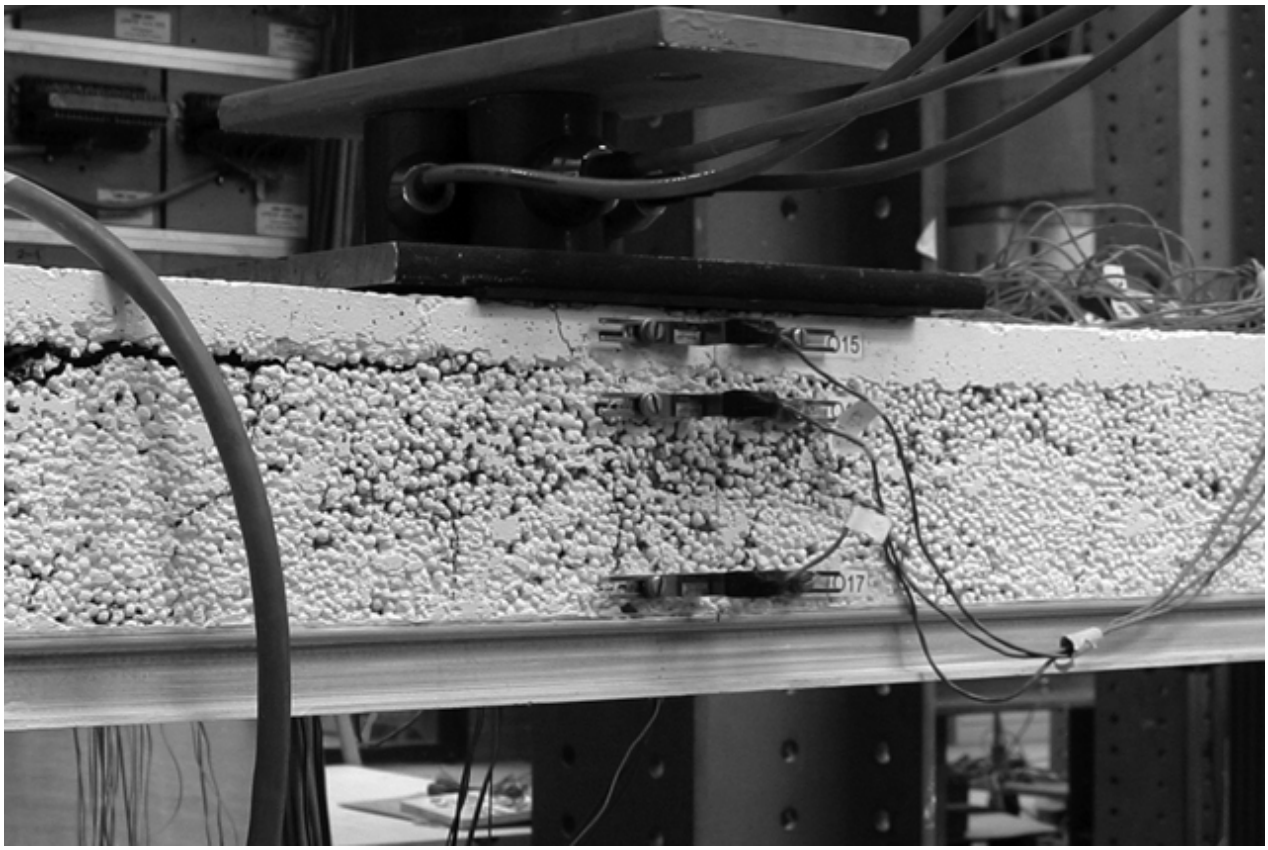

(c) View from north - mid-span

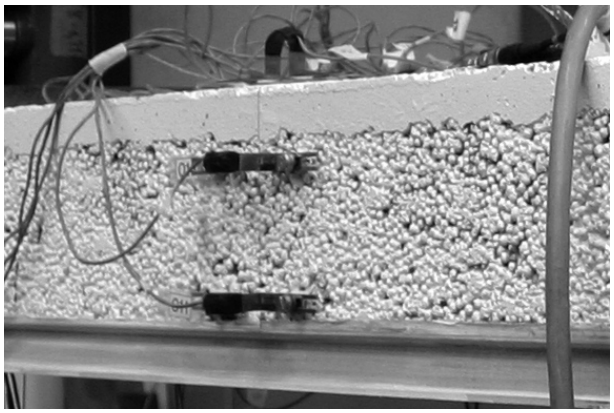

(d) View from north - axis E

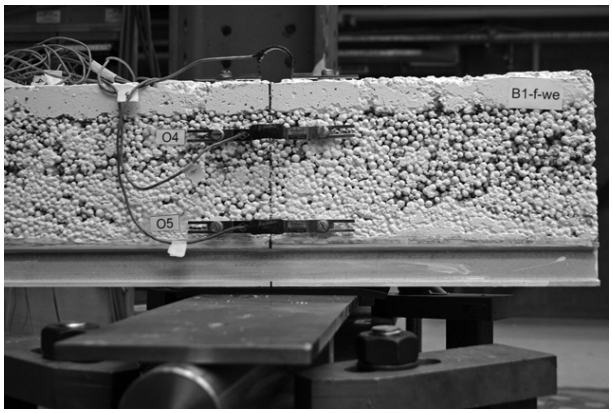

(e) View from north - axis F

Figure C.112: 1300E-2: Failed beam after experiment, still loaded - north.

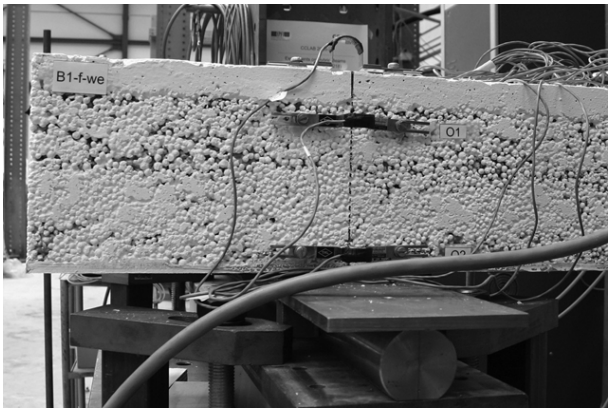

(a) View from south - axis F

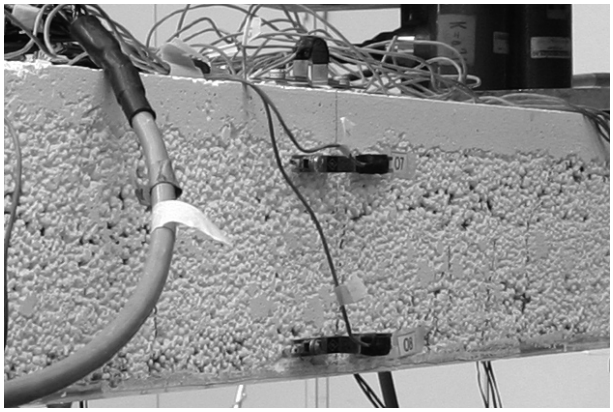

(b) View from south - axis E

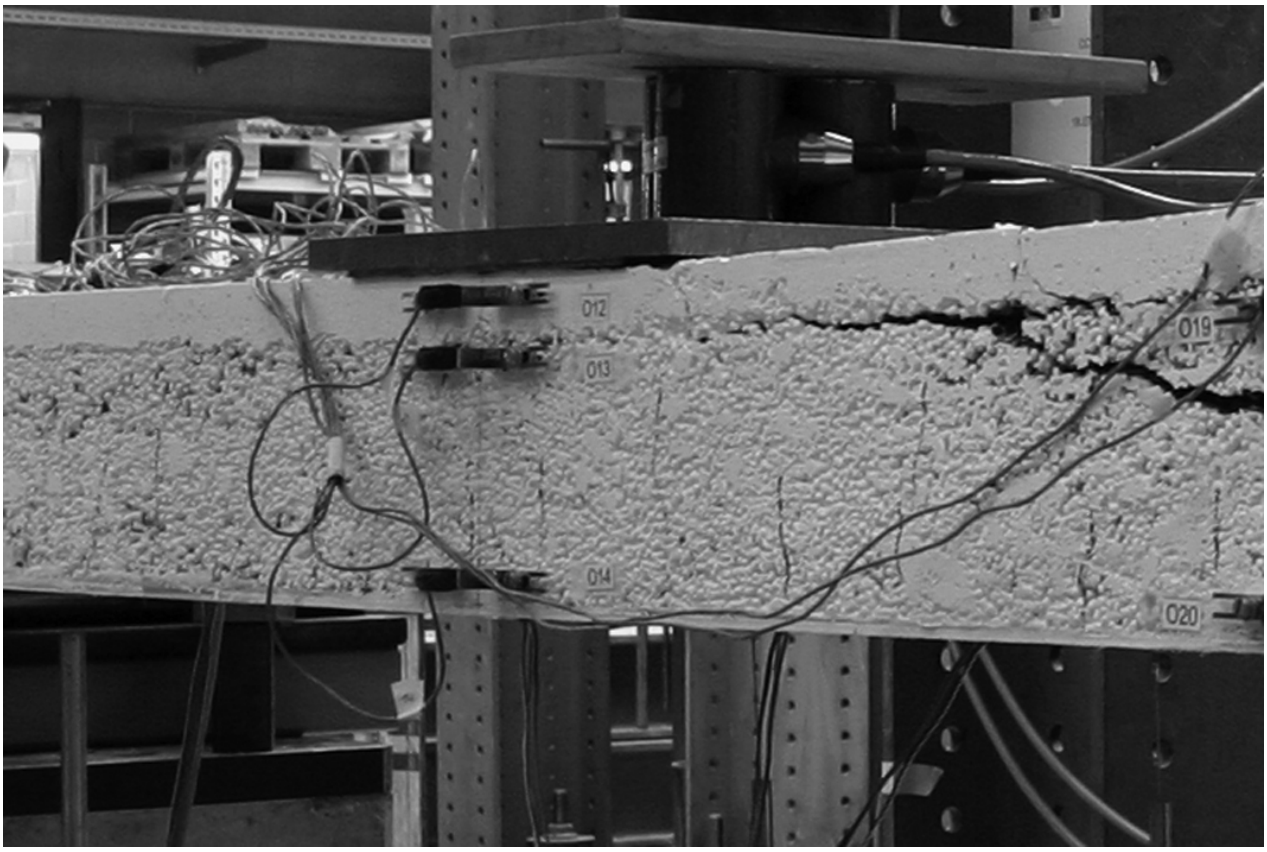

(c) View from south - mid-span

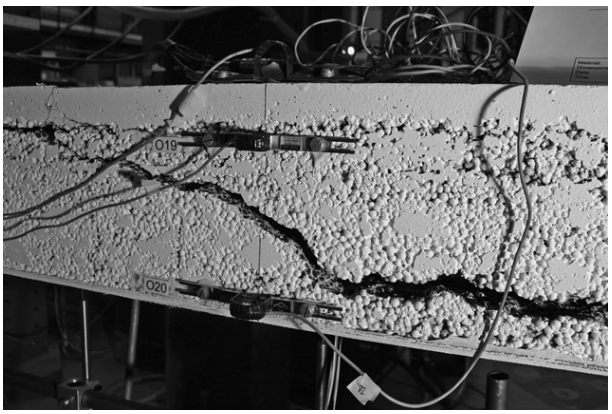

(d) View from south - axis C

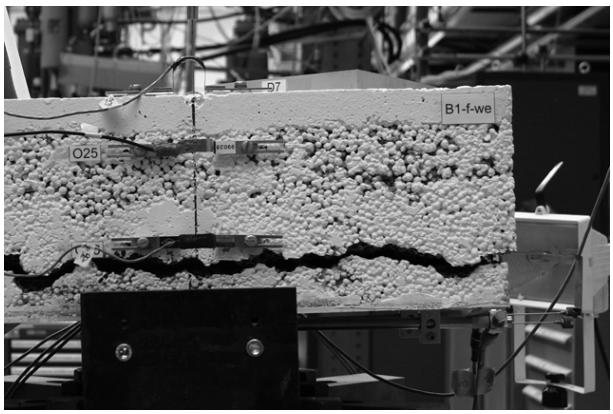

(e) View from south - axis B

Figure C.113: 1300E-2: Failed beam after experiment, still loaded - south.

C.4.8.2 Displacement transducers

Figure C.114 shows the load deflection response of the beam. Beam stiffness remained almost constant up to the cracking load of approximately 12.5 kN where the beam lost its stiffness slightly. The unloading was performed at a load of 35.4 kN and mid-span deformation of 8 mm. A small remaining deformation of 1.1 mm was measured and during reloading an identical stiffness to that observed at the beginning of the experiments. At 50.5 kN the beam failed with a corresponding mid-span deflection of 14.1 mm. The experiment was subsequently stopped. No slippage at the beam end was measured, as shown in Figure C.115-d).

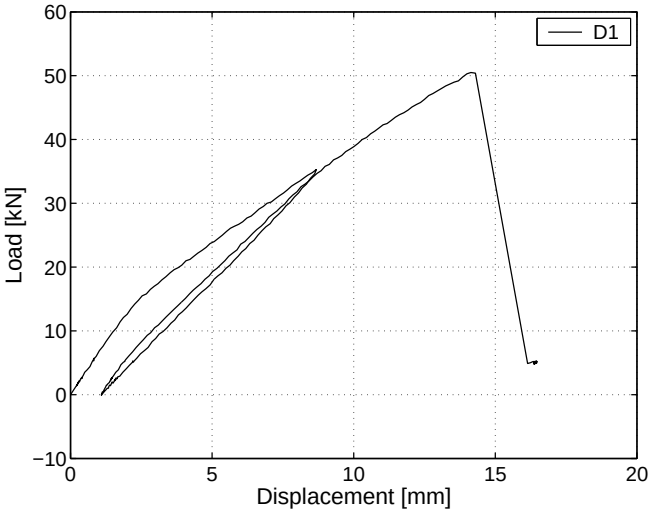

(a) Displacement at mid-span

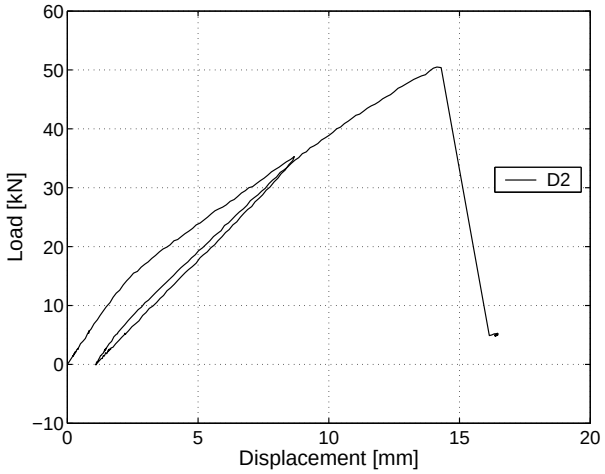

(b) Displacement - between axes C-D

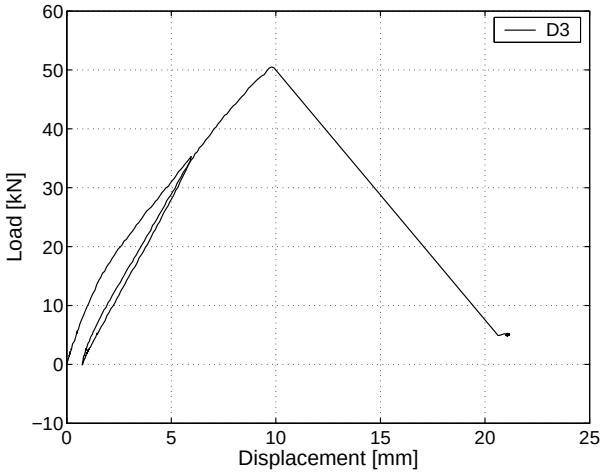

(c) Displacement - axis C

Figure C.114: 1300E-2: Displacement at mid-span, at 0.75 m and 2.25 m.

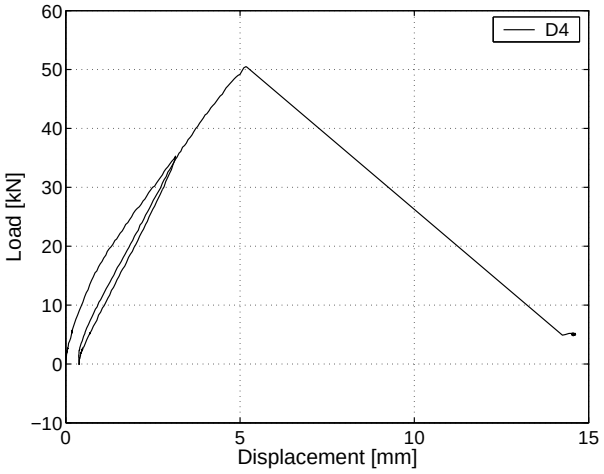

(a) Displacement - between axes B-C

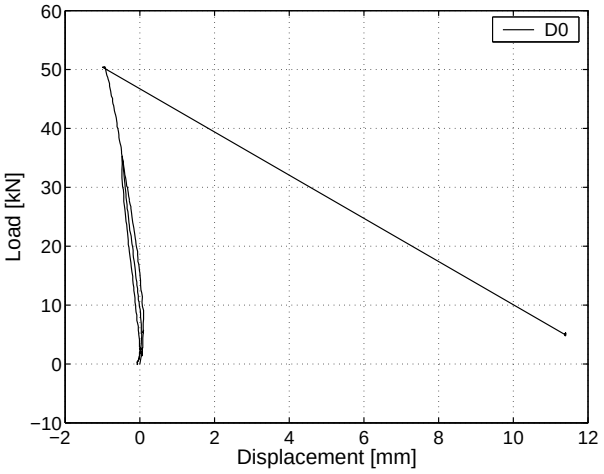

(b) Displacement at free support axis B

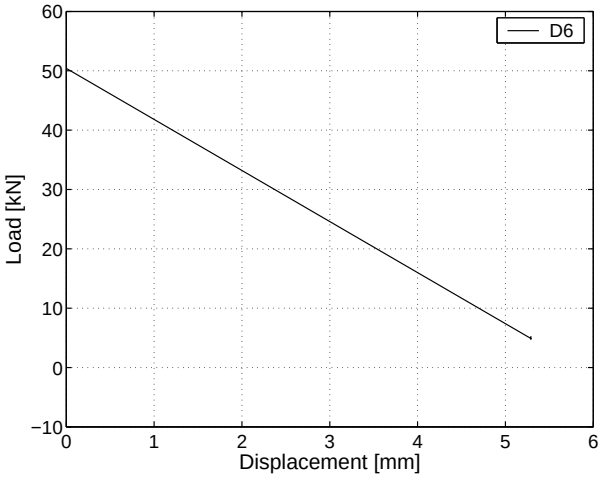

(c) Horizontal displacement of LC - axis A

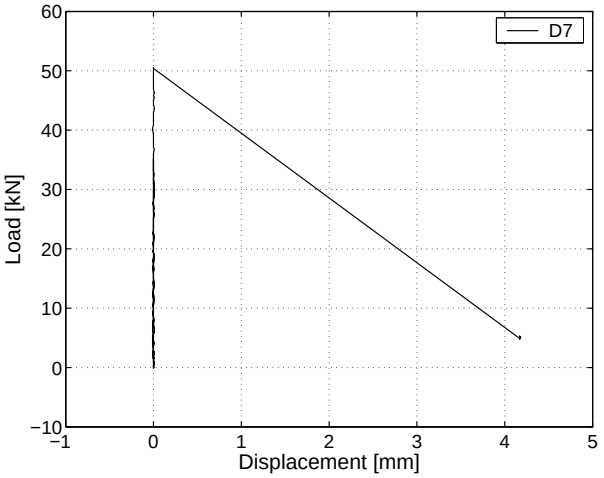

(d) Horizontal displacement of NC - axis A

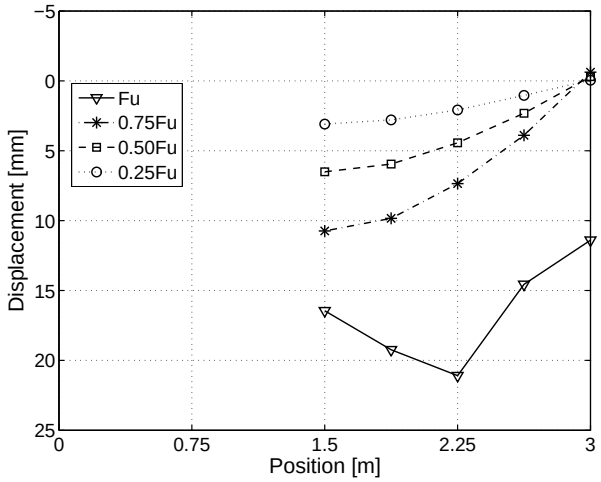

(e) Displacement along beam

Figure C.115: 1300E-2: Displacements at different sections and along beam.

C.4.8.3 Omega-shaped extensometers

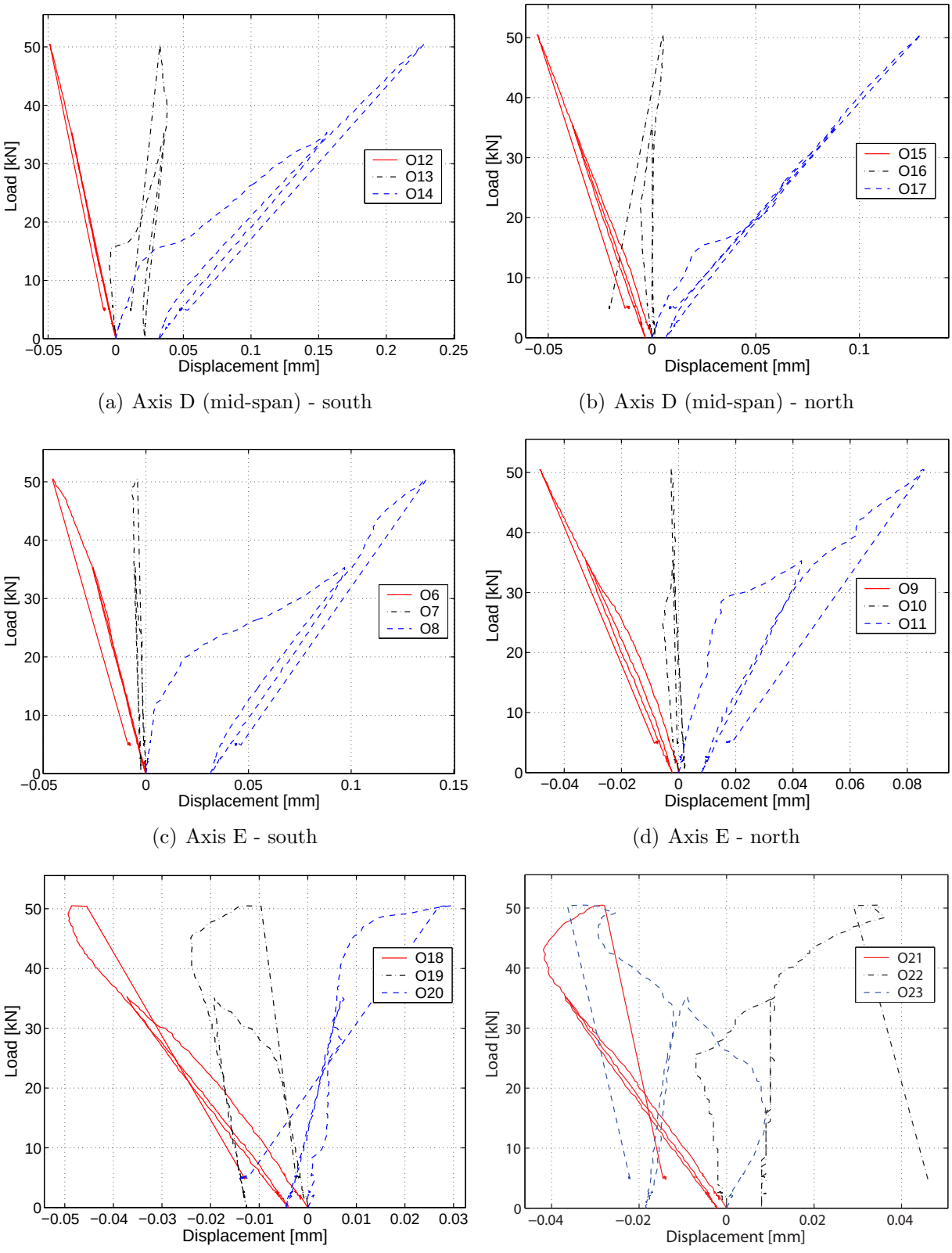

(a) Axis D (mid-span) - south

(b) Axis D (mid-span) - north

(c) Axis E - south

(d) Axis E - north

(e) Axis C - south

(f) Axis C - north

Figure C.116: 1300E-2: Deformations in omega-shaped extensometers at axes C-E.

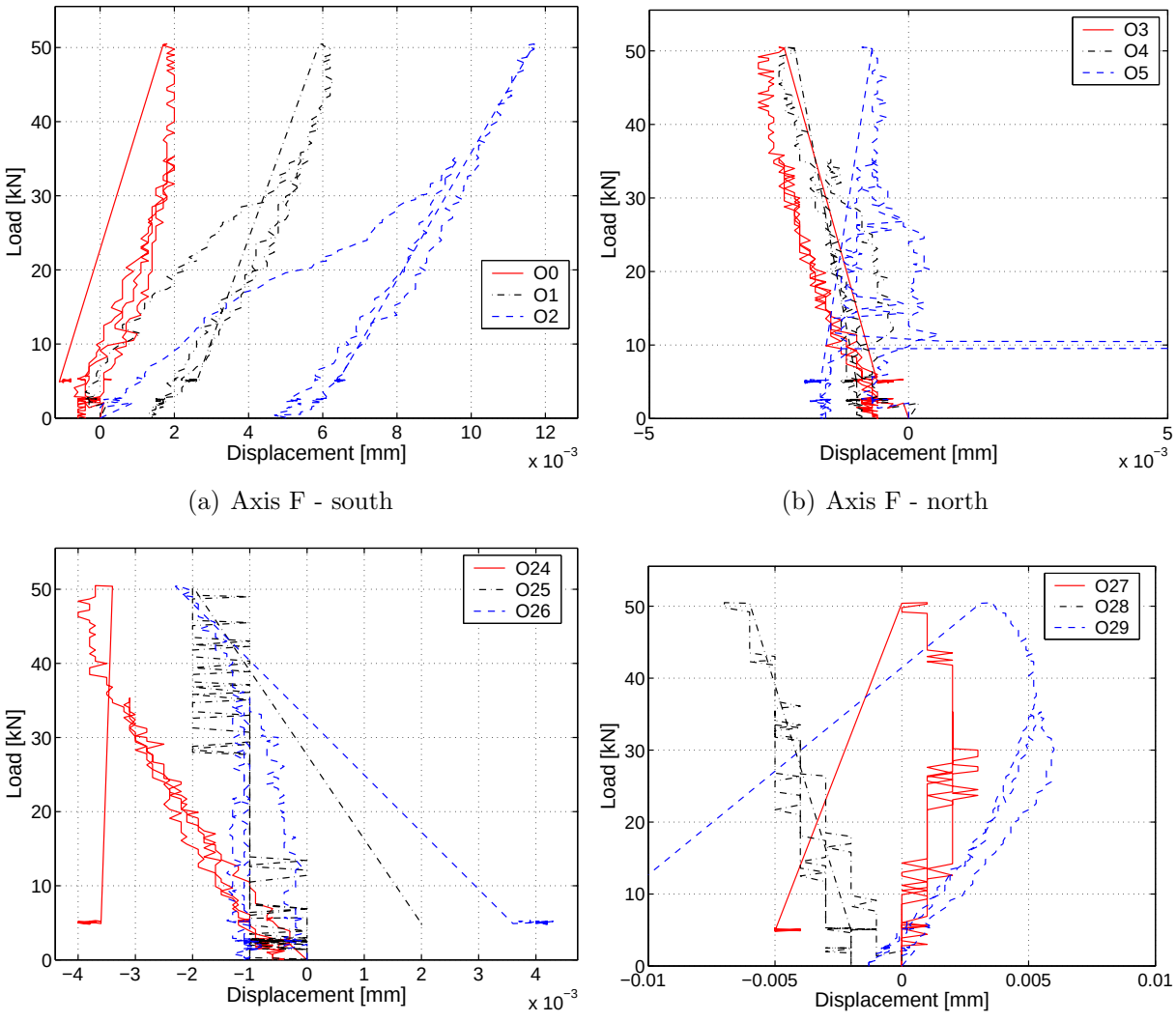

(a) Axis F - south

(b) Axis F - north

(c) Axis B - south

(d) Axis B - north

Figure C.117: 1300E-2: Deformations in omega-shaped extensometers over supports.

C.4.8.4 Strain gages on GFRP profile

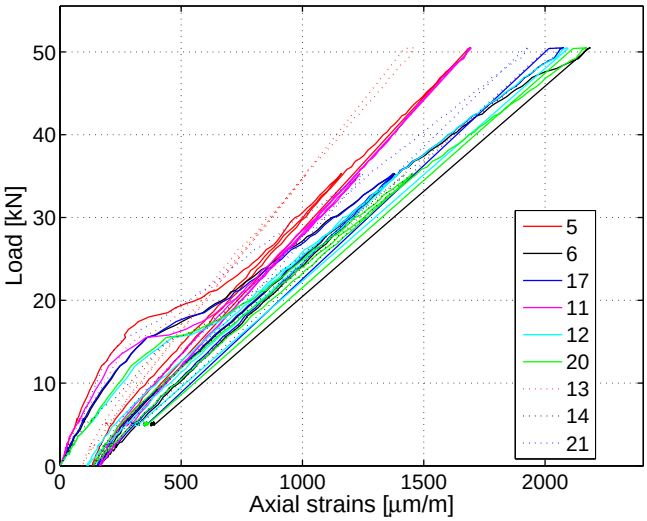

(a) Axial strains at axis D (mid-span)

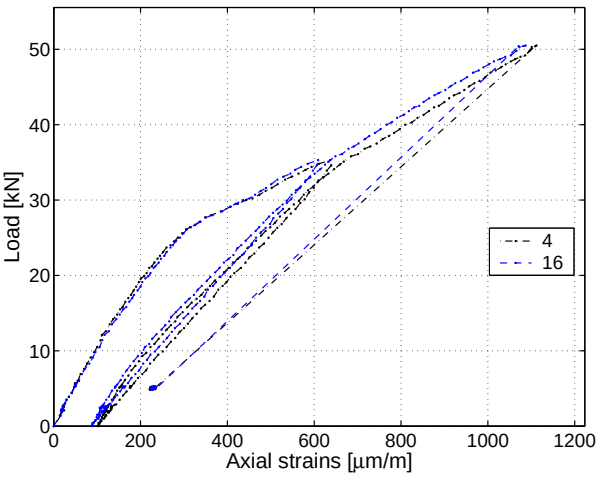

(b) Axial strains at axis E

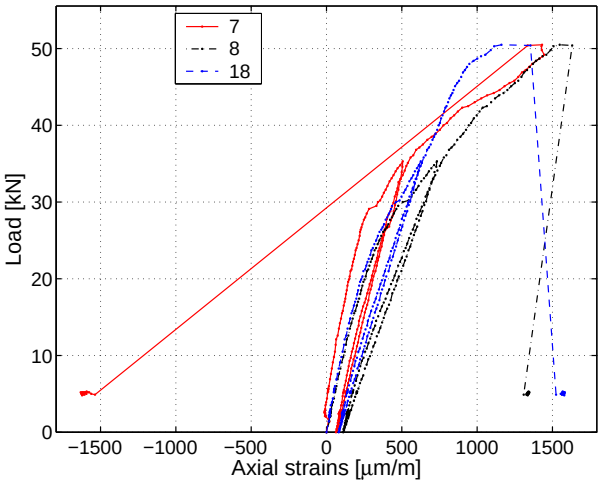

(c) Axial strains at axis C

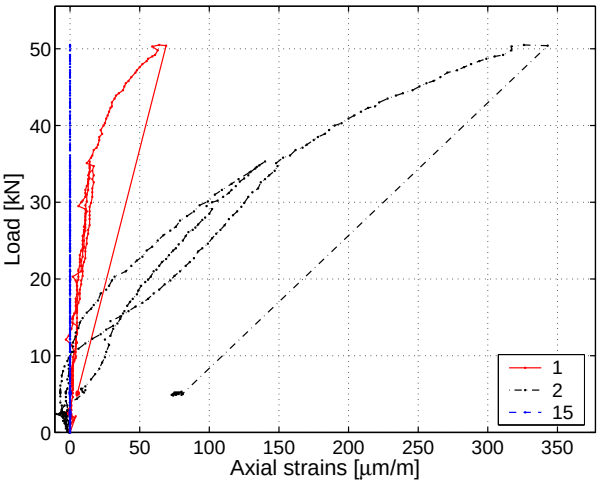

(d) Axial strains at axis F

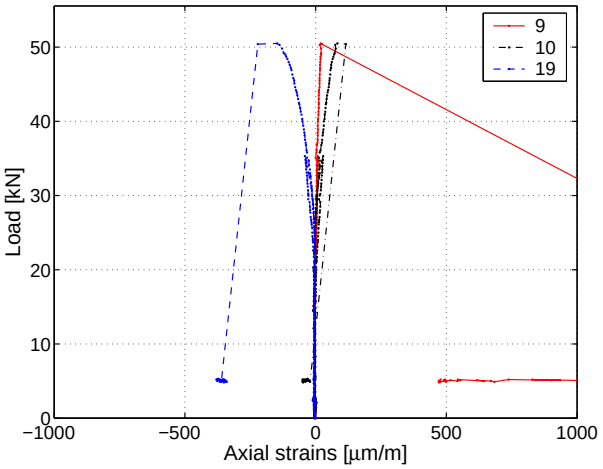

(e) Axial strains at axis B

Figure C.118: 1300E-2: Axial strains in GFRP profile.

C.4.8.5 Axial strains through the cross section

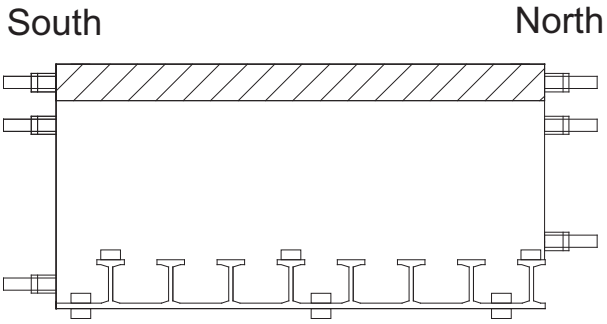

(a) Instrumentation location

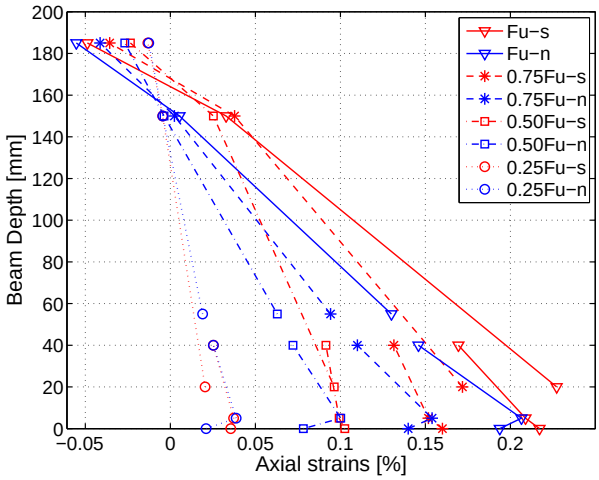

(b) Strain gages and omegas on north and south side

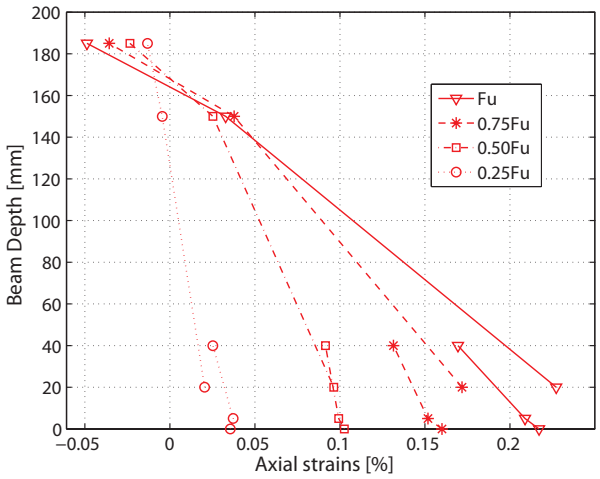

(c) South

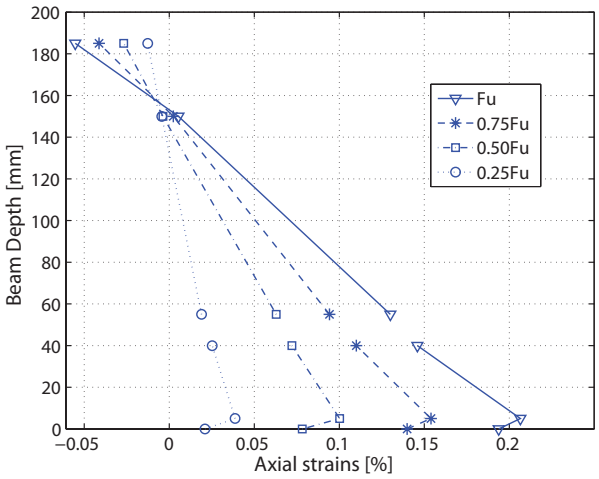

(d) North

Figure C.119: 1300E-2: Axial strains through cross section at mid-span at different load steps from strain gages and omega-shaped extensometers.

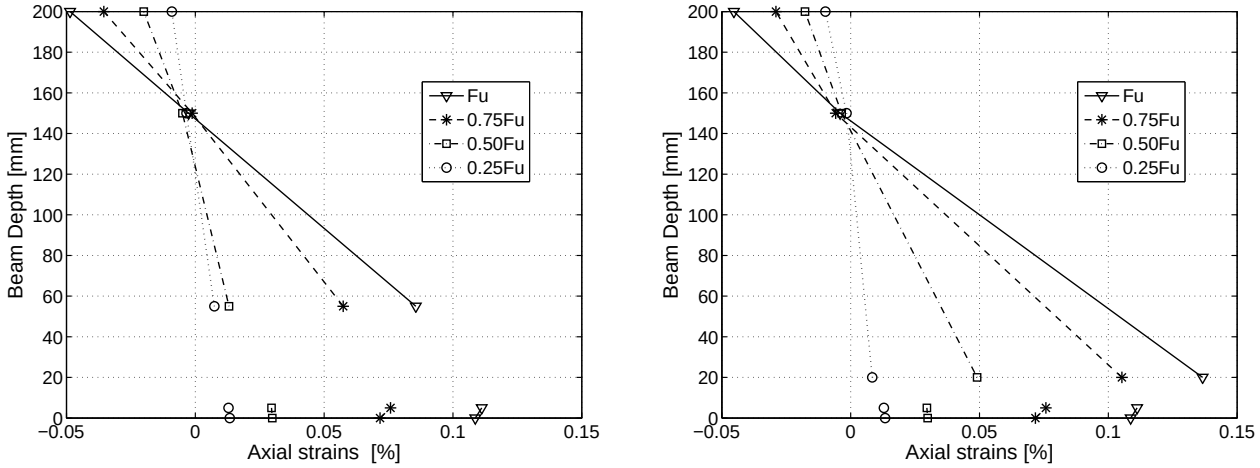

(a) Axis E - north

(b) Axis E - south

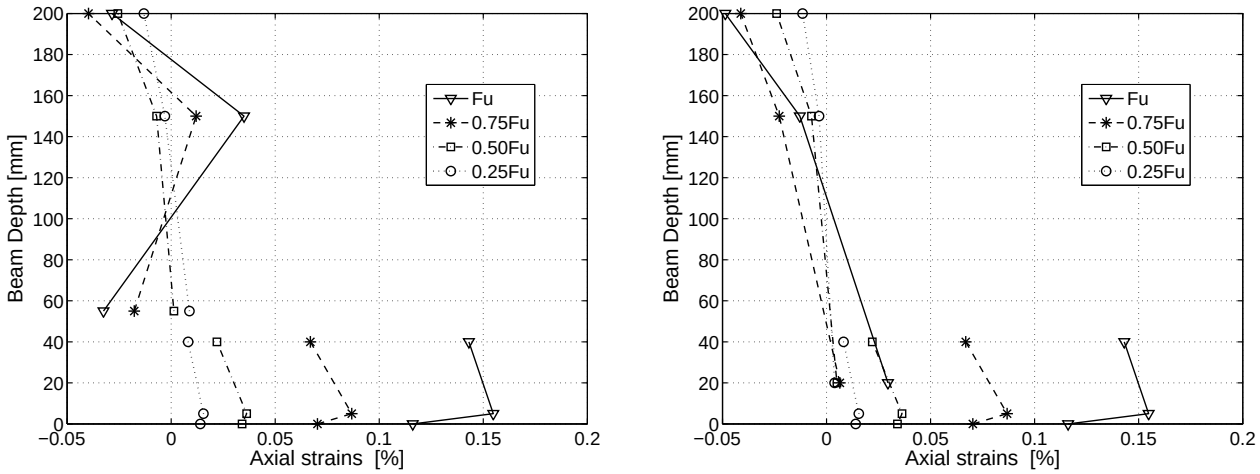

(c) Axis C - north

(d) Axis C - south

Figure C.120: 1300E-2: Axial strains through cross section at 0.75 m and 2.25 m at different load steps from strain gages and omega-shaped extensometers.

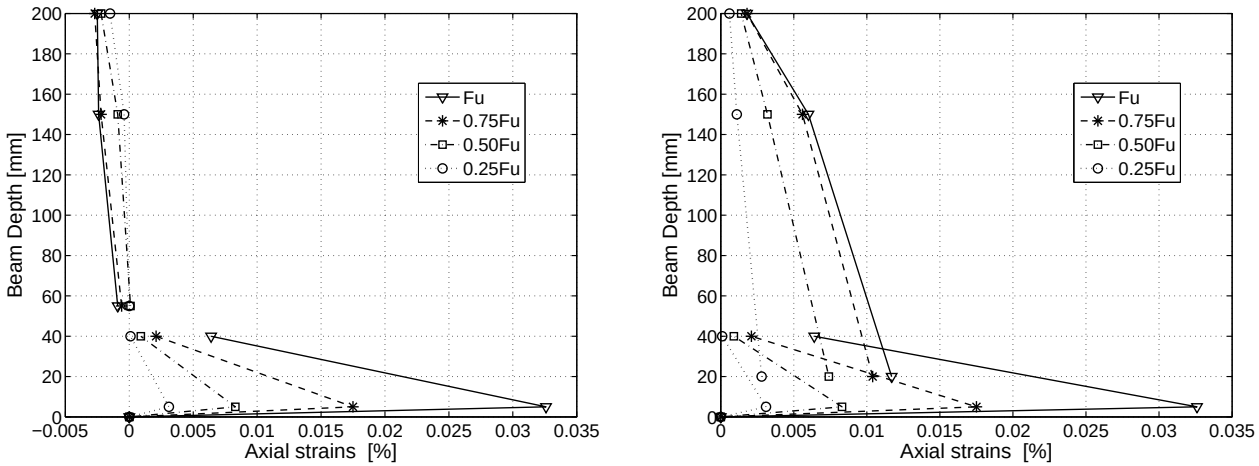

(a) Axis F - north

(b) Axis F - south

(c) Axis B - north

(d) Axis B - south

Figure C.121: 1300E-2: Axial strains through cross section over supports at different load steps from strain gages and omega-shaped extensometers.

C.4.8.6 Axial strains along the beam

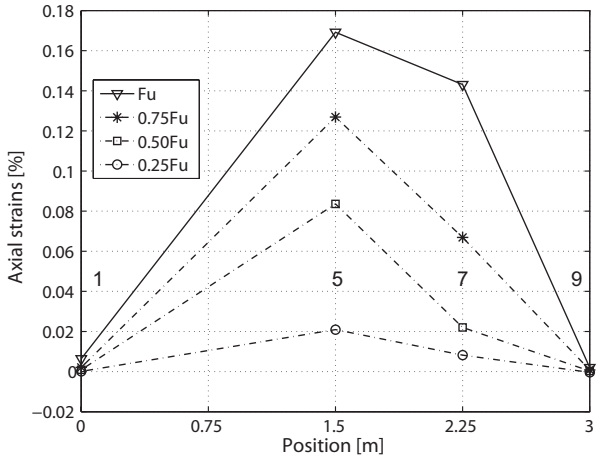

(a) Axial strains on top of T-upstands

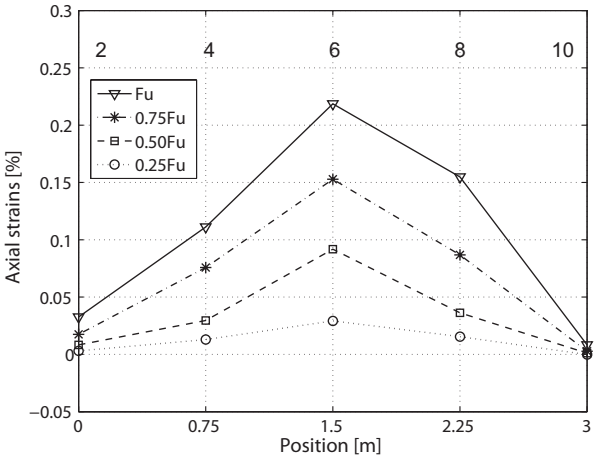

(b) Axial strains between T-upstands

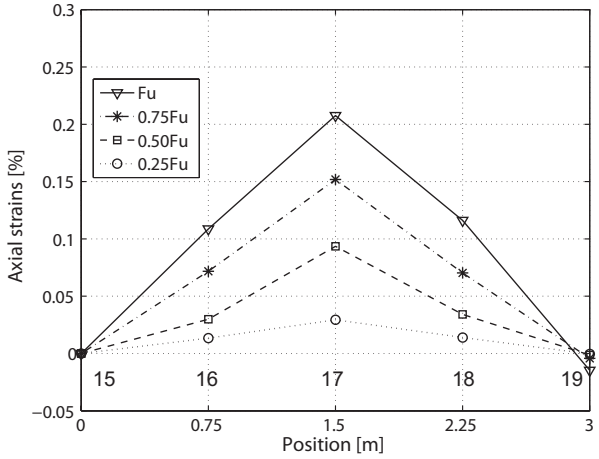

(c) Axial strains beneath GFRP sheet

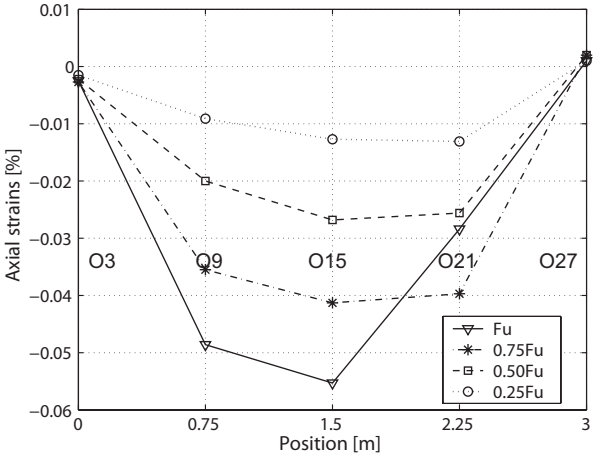

(d) Axial strains in NC layer - north

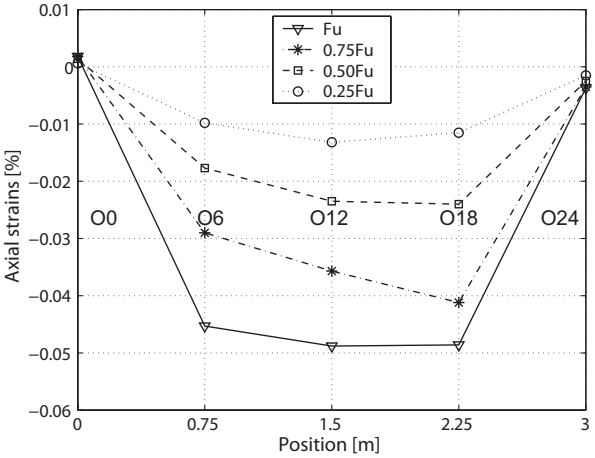

(e) Axial strains in NC layer - south

Figure C.122: 1300E-2: Axial strains along beam at different load steps from strain gages and omega-shaped extensometers.

C.5 Results of S2 series

C.5.1 Beam 1000: Failure description and measured results

C.5.1.1 Failure description

The failure process and crack pattern of the beam up to the end of the experiment are illustrated in Figures C.123, C.124, C.125 and C.126 and described in the following. Every 5 kN the displacement of the jack was stopped in order to document the cracking process and take pictures. A second load cycle was performed at a load of 25 kN. All the instrumental equipment worked well from the beginning of the experiment

The failure process of the beam started with inner cracking resulting in small noises at a load of 6.0 kN. The first obvious but small cracks appeared at a load of 9.0 kN under the loading plate in the west and east sides and four more short ones occurred in the east side with an average spacing of 32 cm. Further loading resulted in cracking and at a load of 15 kN the cracks got longer and additional new vertical cracks could be observed on average every 23 cm in the east side and 19 cm in the west side. The crack opening was approximately 0.01-0.05 mm. The cracks subsequently started to develop vertically up to the NC layer, although their opening remained approximately 0.05 mm. Some new vertical cracks developed, and the average crack spacing at 20 kN was thus reduced to 15 cm on the east side and 14,4 cm on the west side. At this load the first cracks reached the LC-NC interface. At 25 kN a load cycle was performed. The cracks closed during the unloading process.

During reloading several audible cracks could be noticed under loads of 5.8, 7, 8.8, 14, 18, and 20 kN. Reloading was performed constantly up to 30 kN, where the further cracking process was documented. At this load, horizontal cracks in the LC-NC interface were first observed. The crack opening was between 0.10 and 0.15 mm.

At a load of 35 kN the jack was stopped in order to observe the crack development properly, but immediately the beam failed and one vertical crack turned and propagated horizontally in the northern beam part, approximately 40 cm from the mid-span. The load dropped to 23 kN. The beam was however able to slightly regain its stiffness. At the same time the LC started to be pushed out of the GFRP profile. While the load increased to 27 kN the main crack propagated towards the support. Subsequently the load dropped again and the main crack developed along the top of the T-upstands to the end of the beam. Figure C.127 illustrates the pushing out and shear failure of the LC along the top of the T-upstands. The southern end of the beam remained almost undamaged.

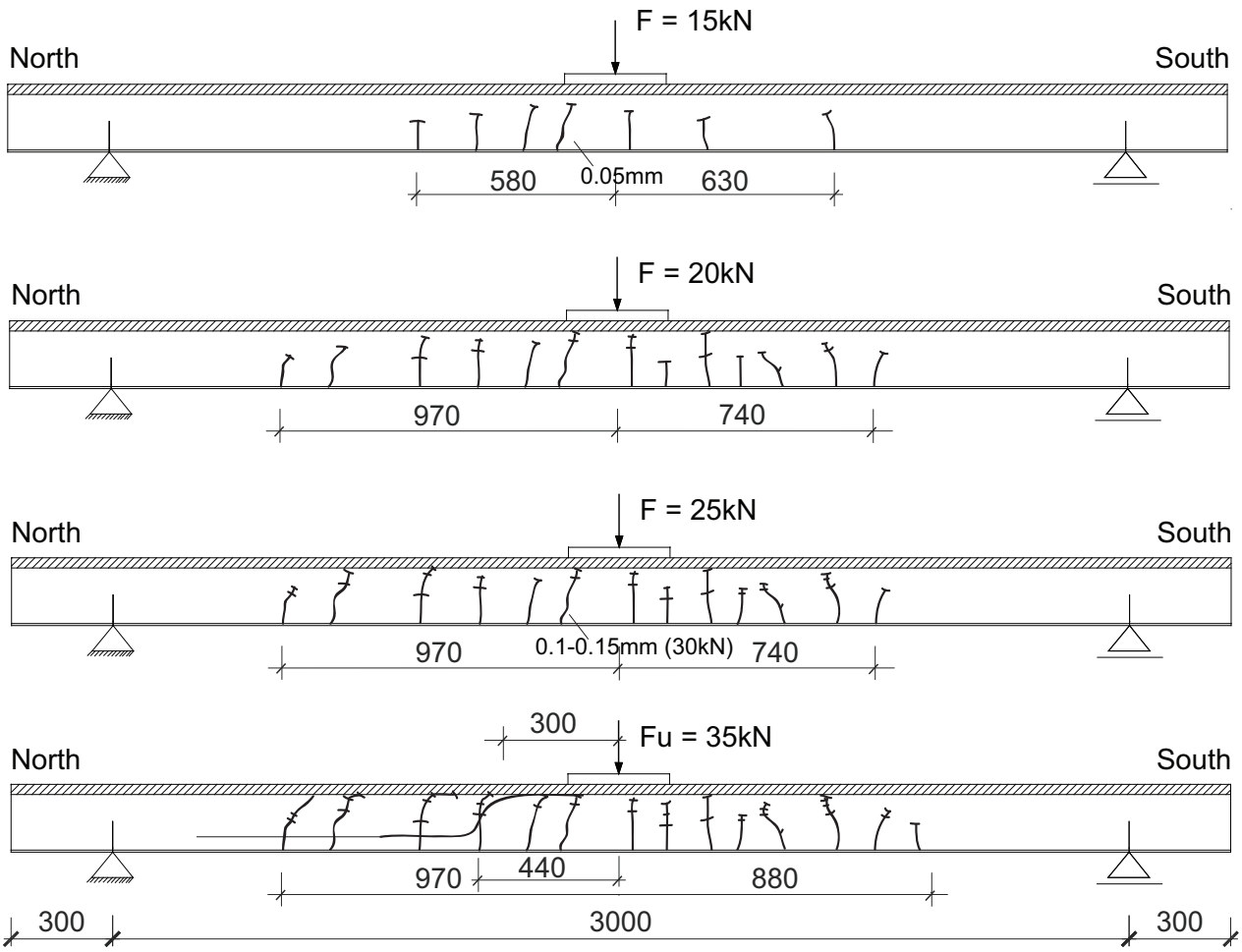

Figure C.123: 1000: Failure process.

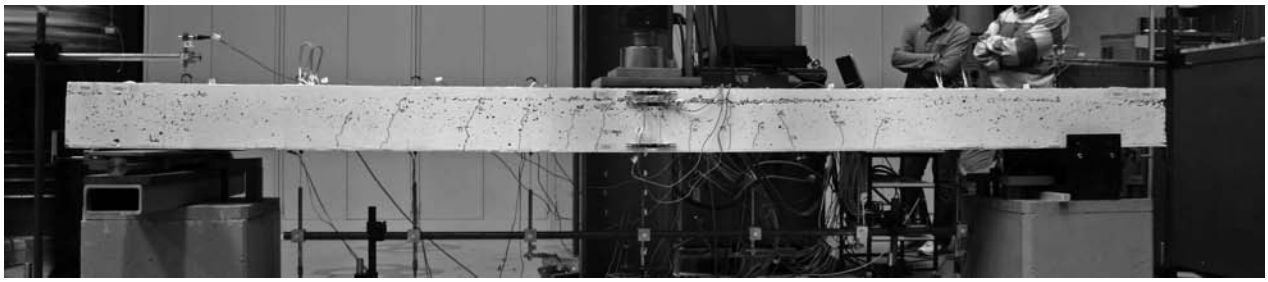

(a) Crack distribution at 25.0 kN - first load cycle

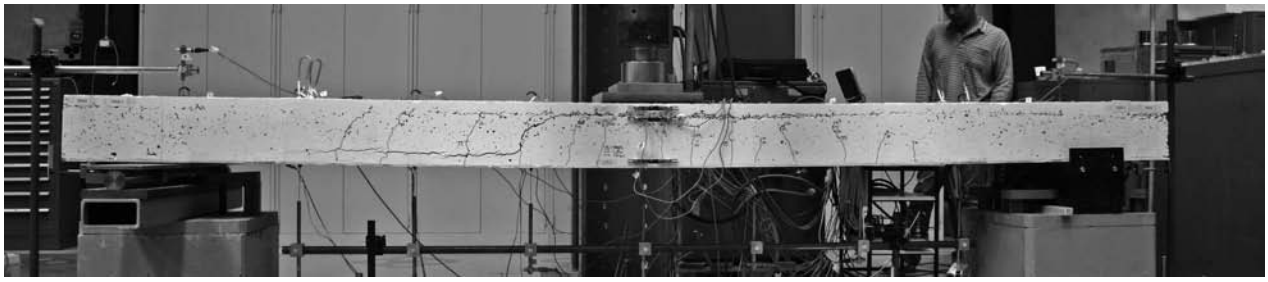

(b) Development of main crack at max load 35.0 kN

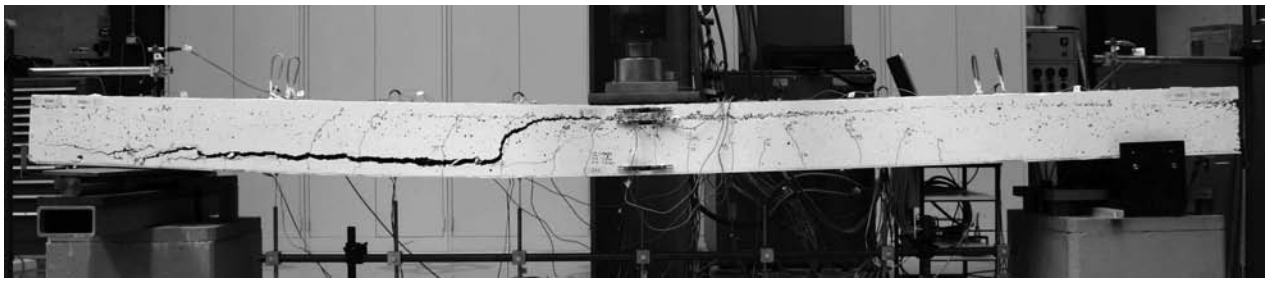

(c) Crack pattern after drop in load $\sim$ 25 kN

Figure C.124: 1000: Failure process.

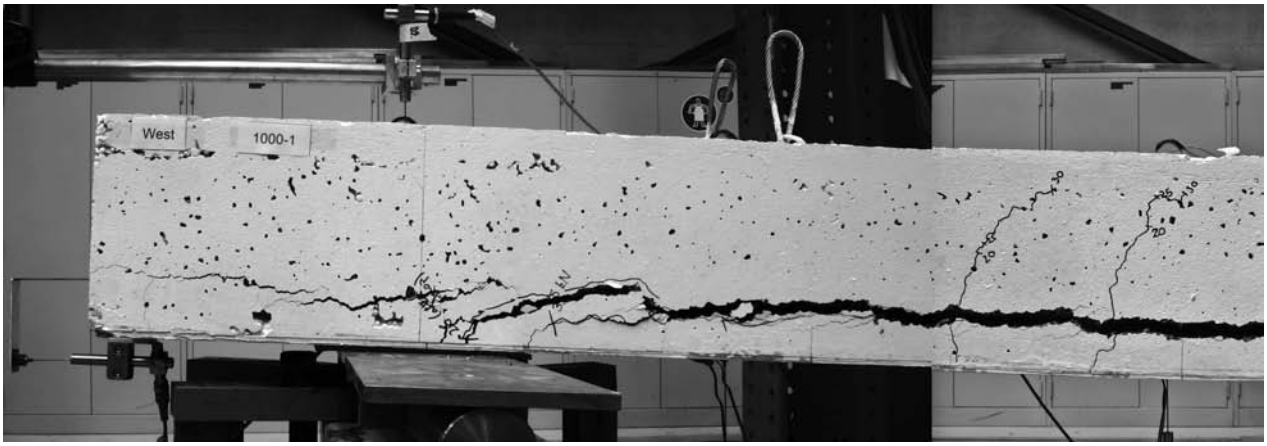

(a) North west

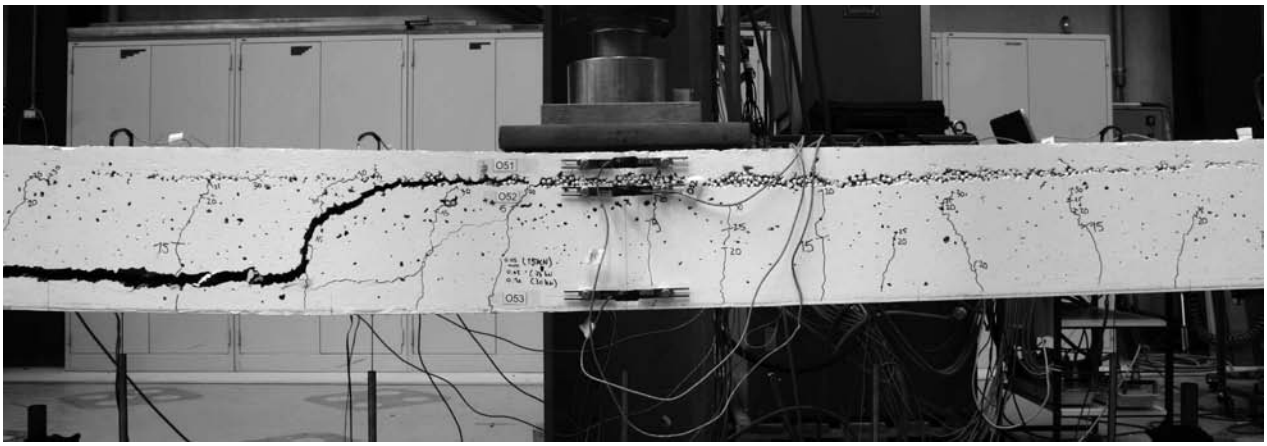

(b) Mid-span west

(c) South west

Figure C.125: 1000: West side of cracked beam after experiment, still loaded.

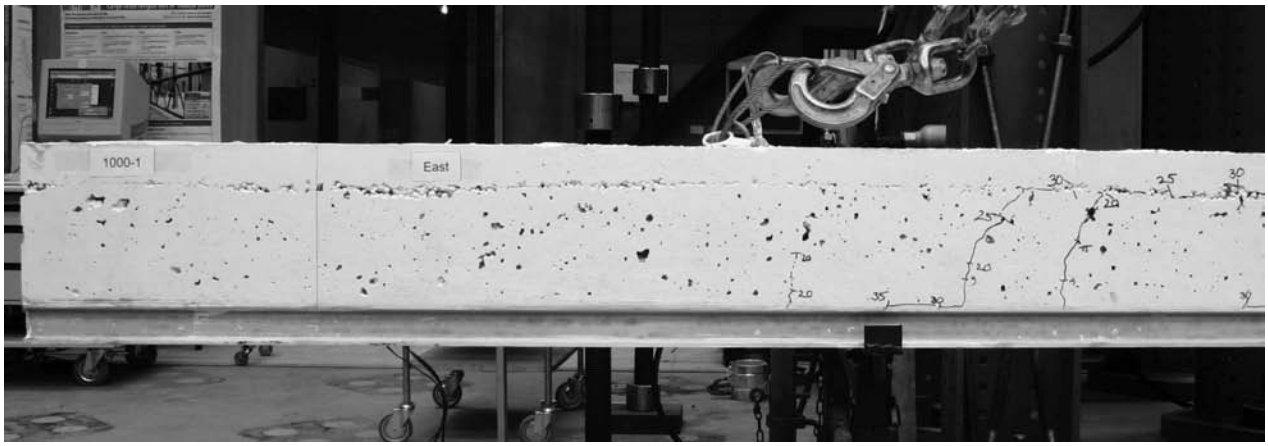

(a) North east

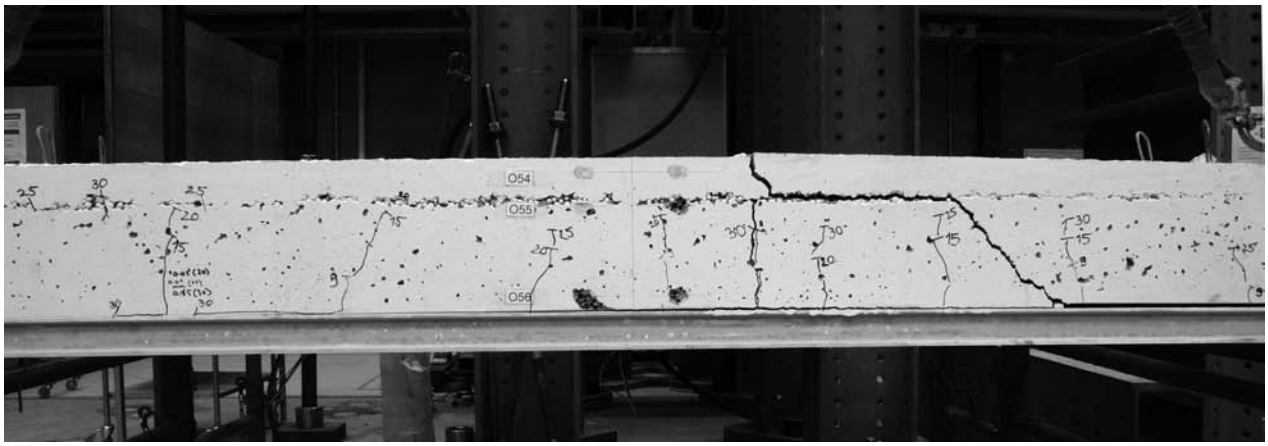

(b) Mid-span east

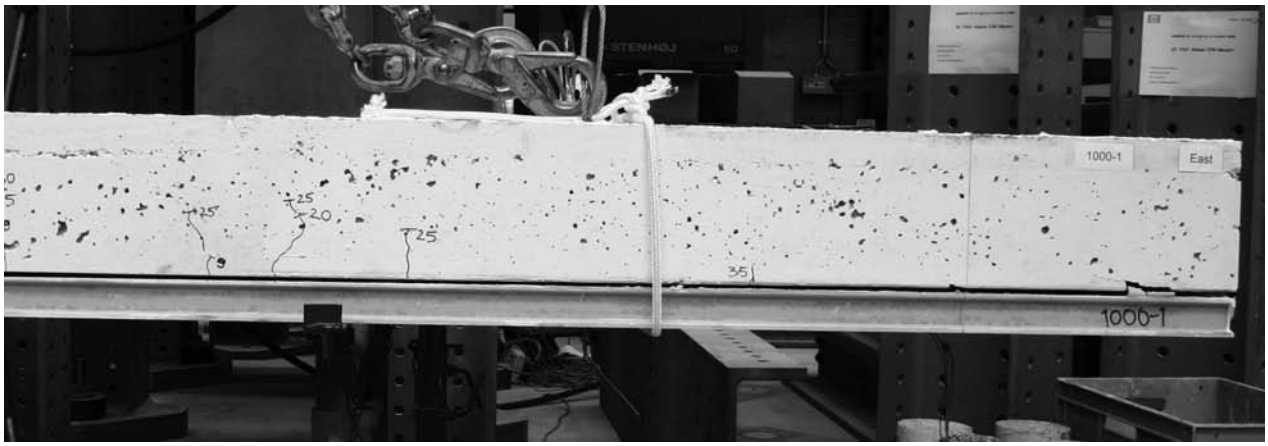

(c) South east

Figure C.126: 1000: East side of cracked beam after experiment, unloaded.

(a) Northern end

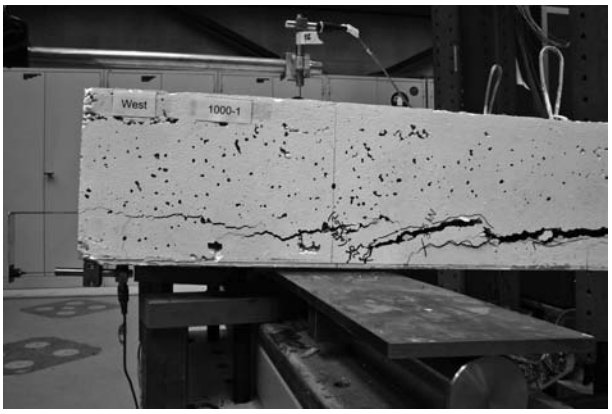

(b) North west

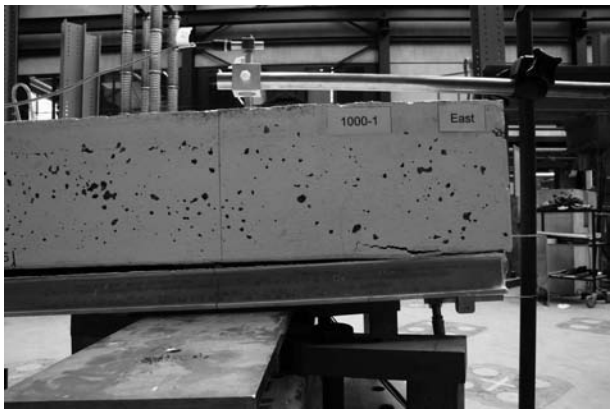

(c) North east

Figure C.127: 1000: LC being pushed out of GFRP profile at northern beam end.

C.5.1.2 Displacement transducers

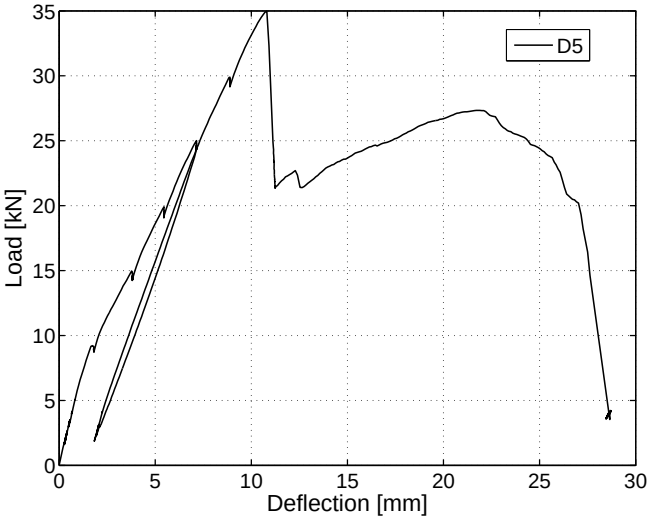

(a) At mid-span axis F

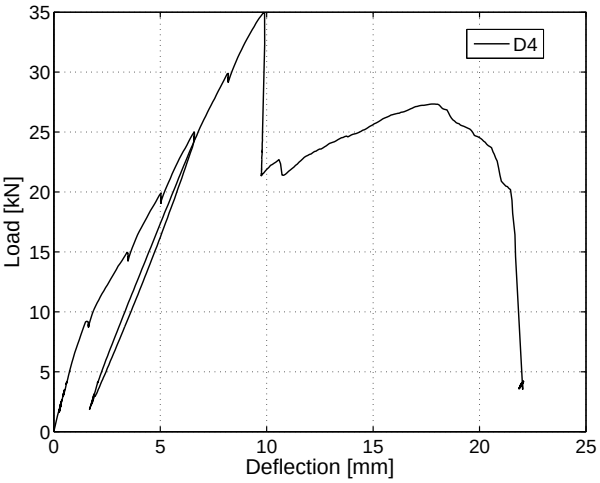

(b) Axis E

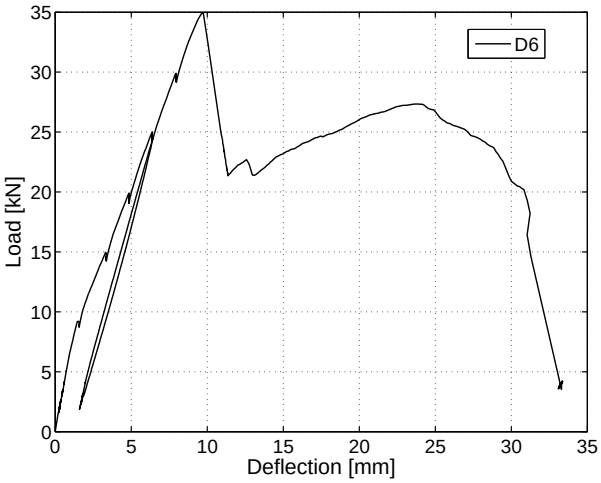

(c) Axis G

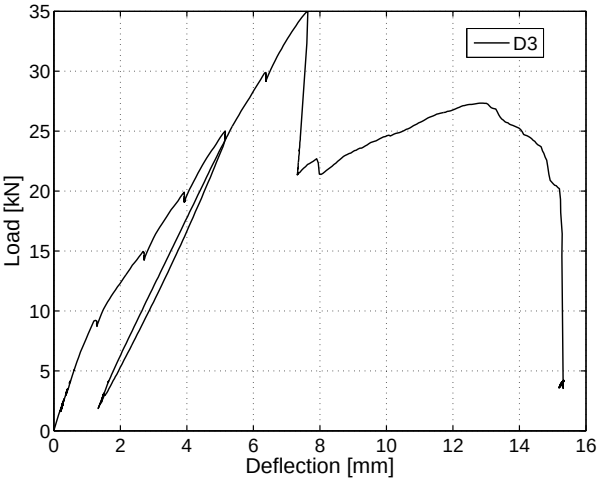

(d) Axis D

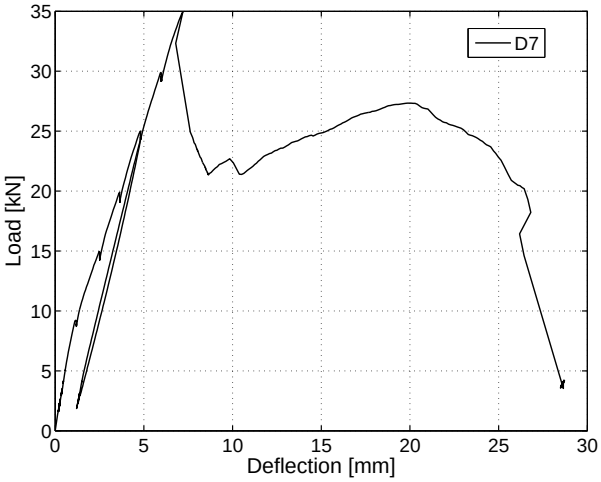

(e) Axis H

Figure C.128: 1000: Displacement at axes D,E,G,H.

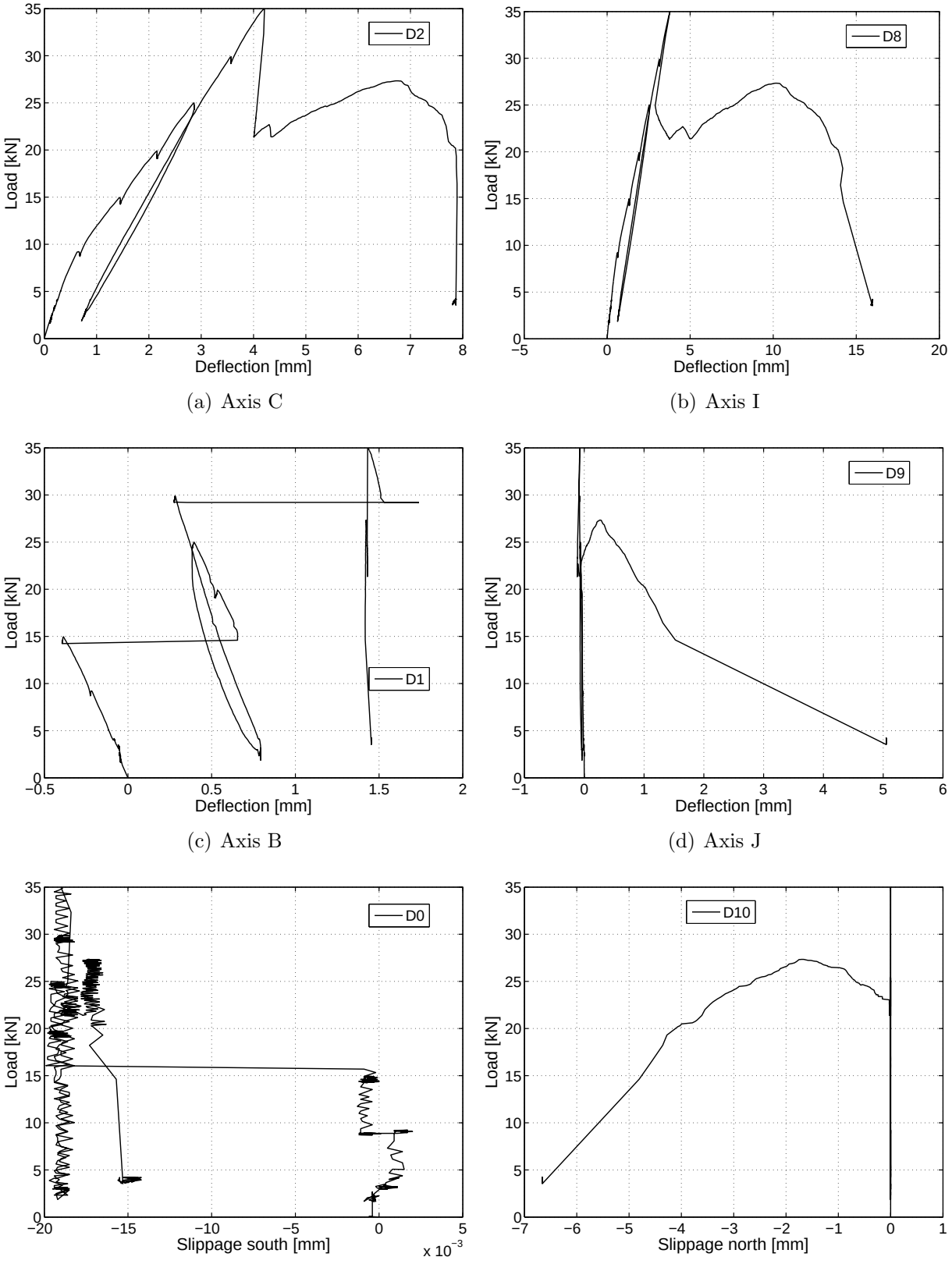

(a) Axis C

(b) Axis I

(c) Axis B

(d) Axis J

(e) Slippage axis A - south

(f) Slippage axis K - north

Figure C.129: 1000: Displacement at axes B,C,I,J and slippage at beam ends.

C.5.1.3 Omega-shaped extensometers

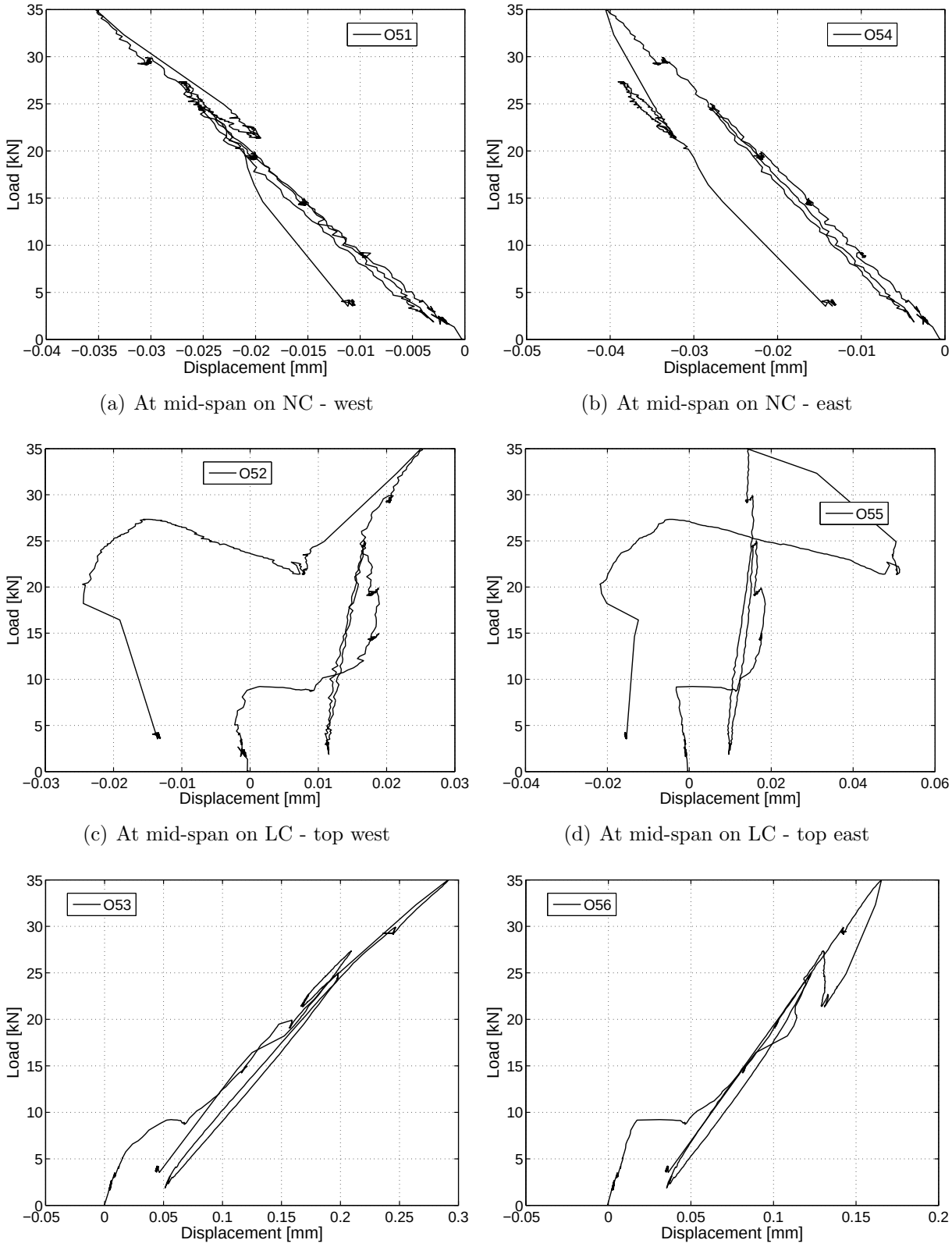

(a) At mid-span on NC - west

(b) At mid-span on NC - east

(c) At mid-span on LC - top west

(d) At mid-span on LC - top east

(e) At mid-span on LC - bottom west

(f) At mid-span on LC - bottom east

Figure C.130: 1000: Deformations in omega-shaped extensometers at mid-span.

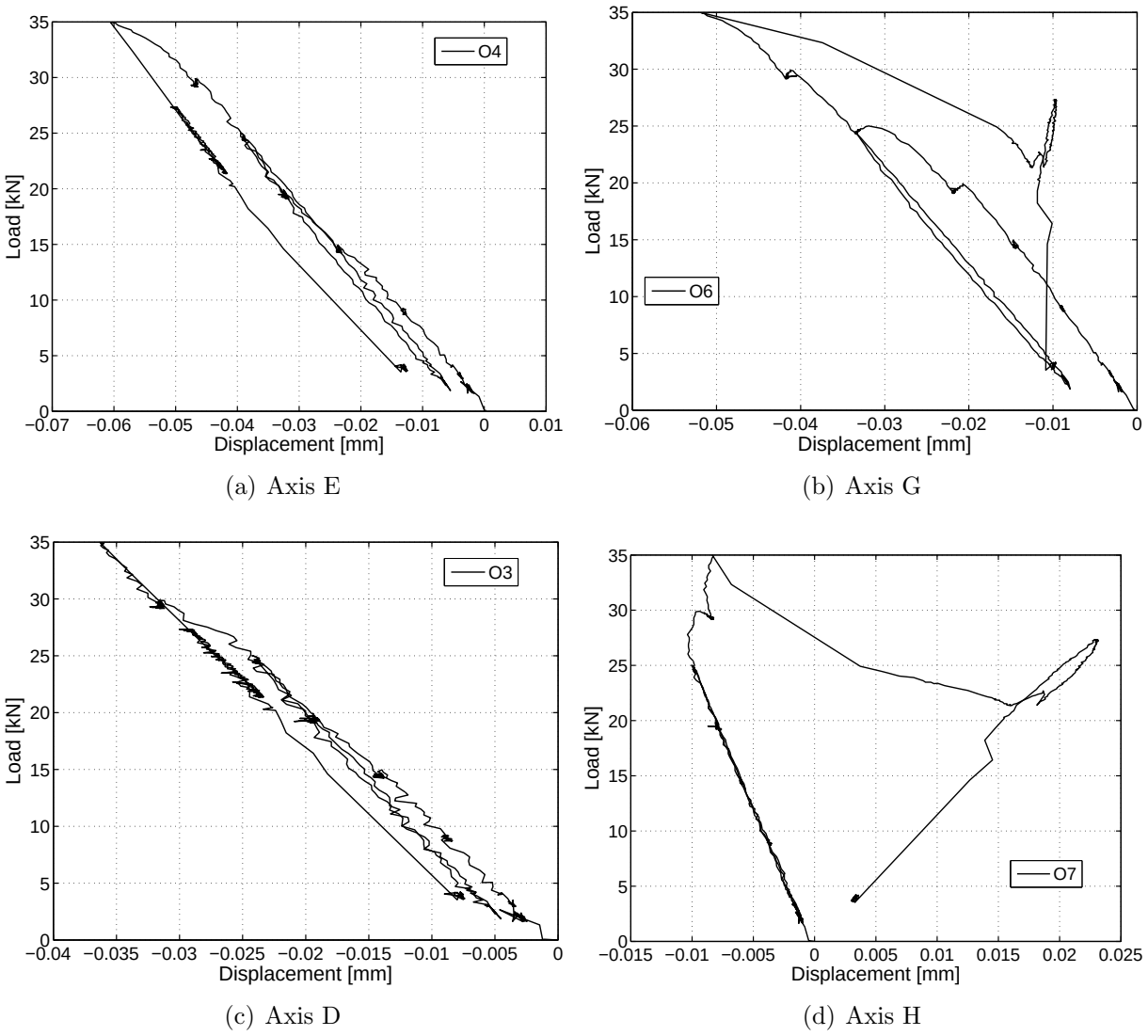

(a) Axis E

(b) Axis G

(c) Axis D

(d) Axis H

Figure C.131: 1000: Deformations in omega-shaped extensometers - axes D,E,G,H.

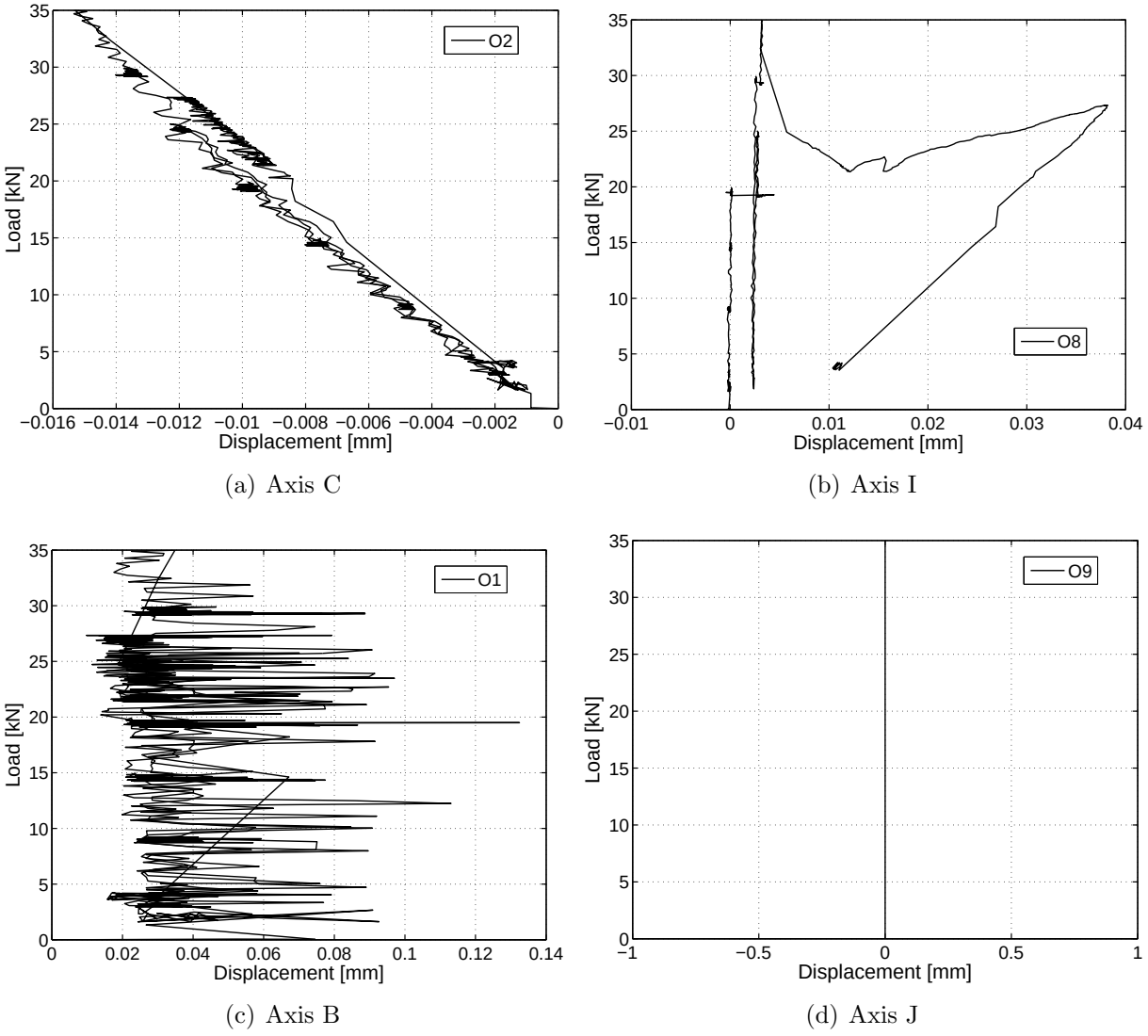

(a) Axis C

(b) Axis I

(c) Axis B

(d) Axis J

Figure C.132: 1000: Deformations in omega-shaped extensometers - axes B,C,I,J.

C.5.1.4 Strain gages on GFRP profile

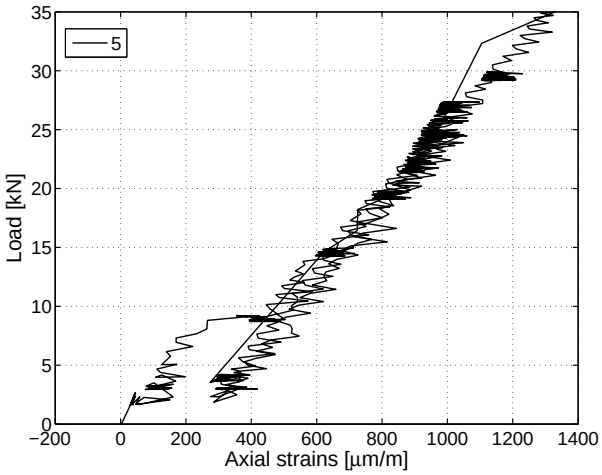

(a) At mid-span axis F on T-upstands

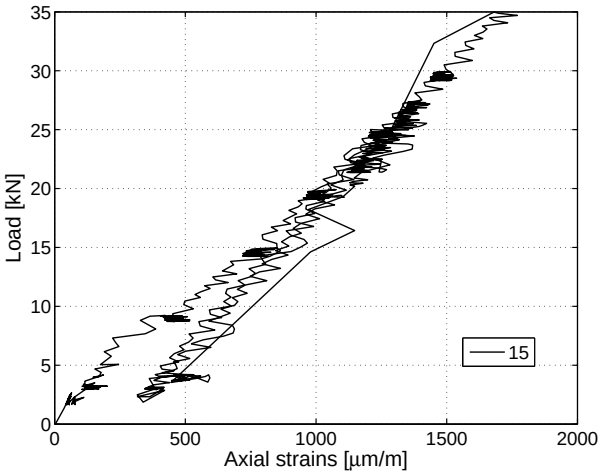

(b) At mid-span axis F beneath GFRP sheet

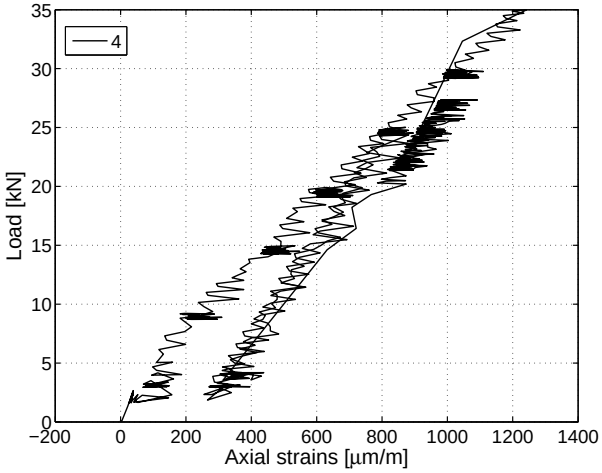

(c) Axis E on T-upstands

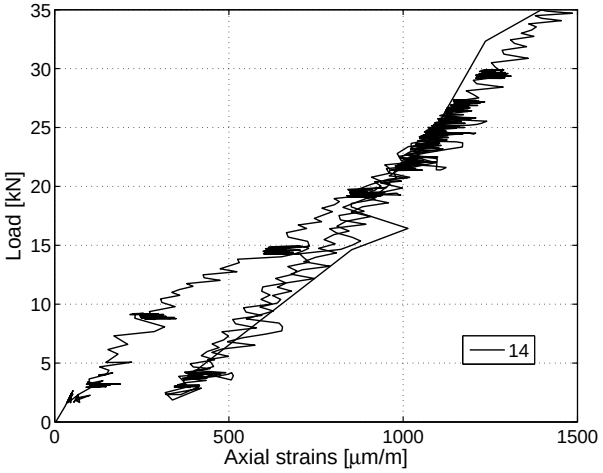

(d) Axis E beneath GFRP sheet

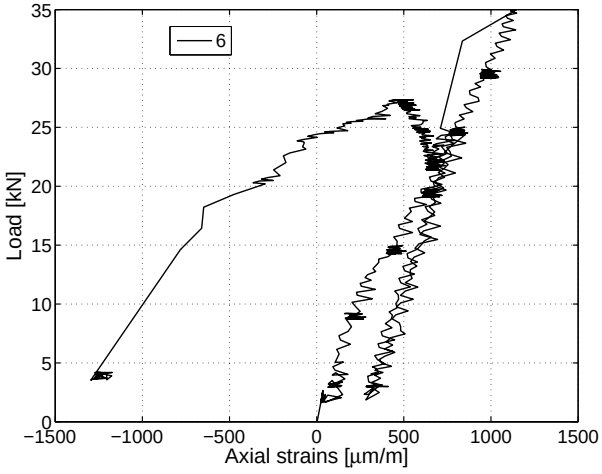

(e) Axis G on T-upstands

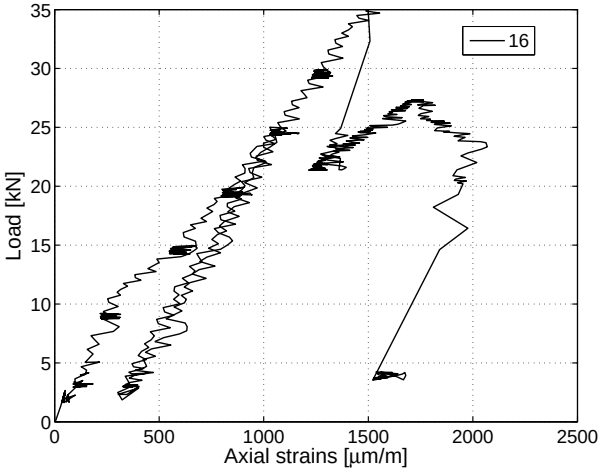

(f) Axis G beneath GFRP sheet

Figure C.133: 1000: Axial strains in GFRP profile - axis E,F,G.

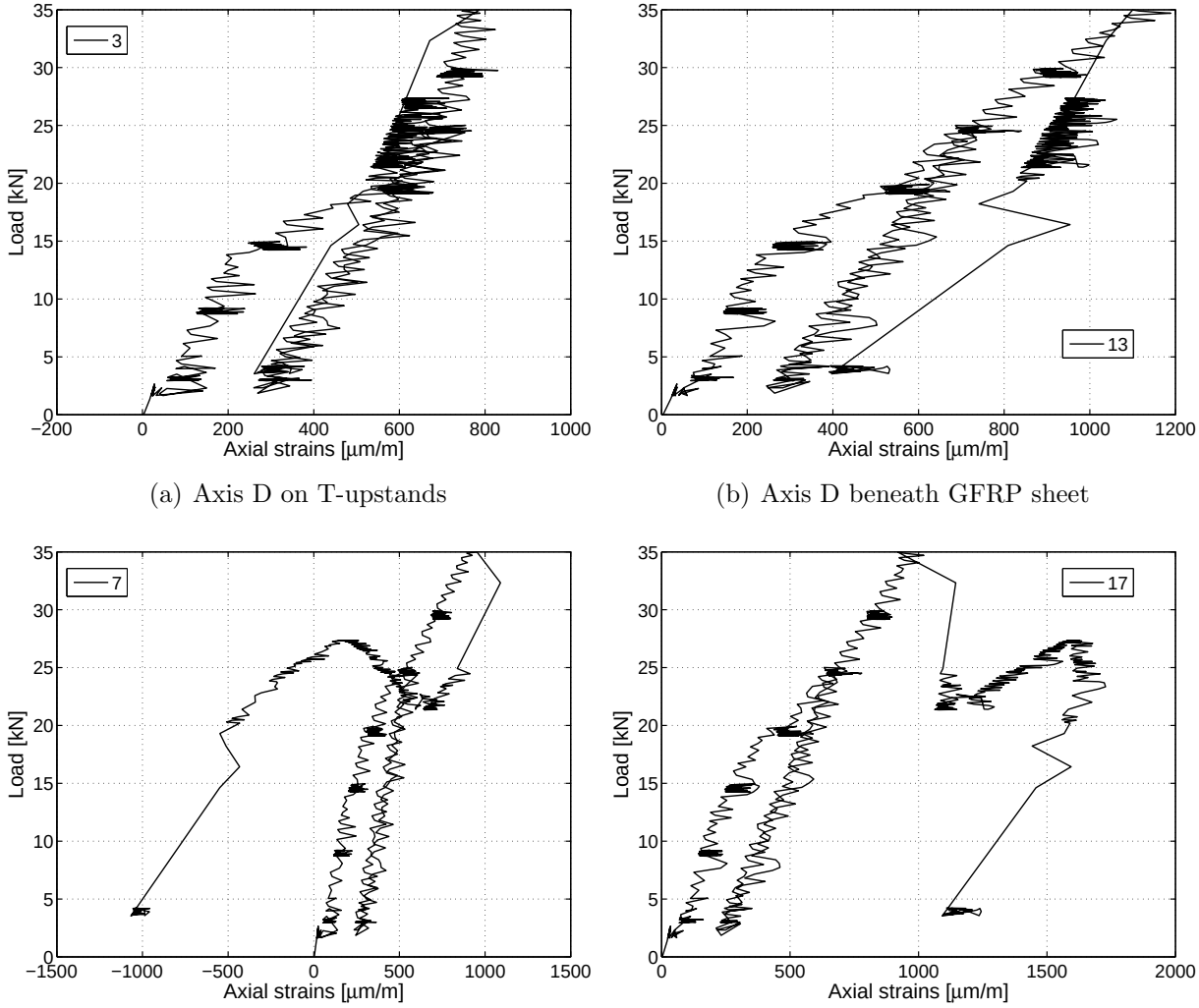

(a) Axis D on T-upstands

(b) Axis D beneath GFRP sheet

(c) Axis H on T-upstands

(d) Axis H beneath GFRP sheet

Figure C.134: 1000: Axial strains in GFRP profile - axis D,H.

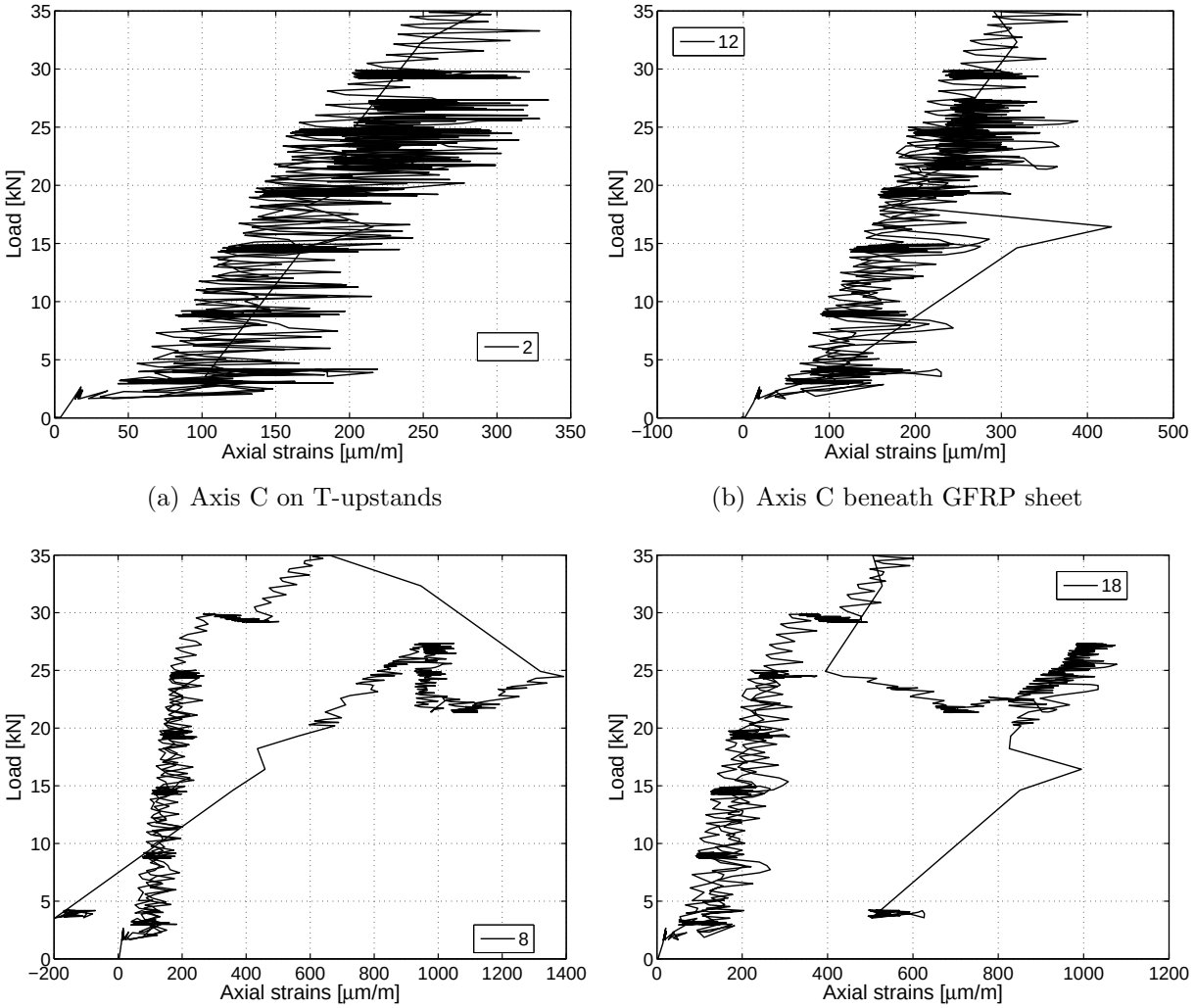

(a) Axis C on T-upstands

(b) Axis C beneath GFRP sheet

(c) Axis I on T-upstands

(d) Axis I beneath GFRP sheet

Figure C.135: 1000: Axial strains in GFRP profile - axis C,I.

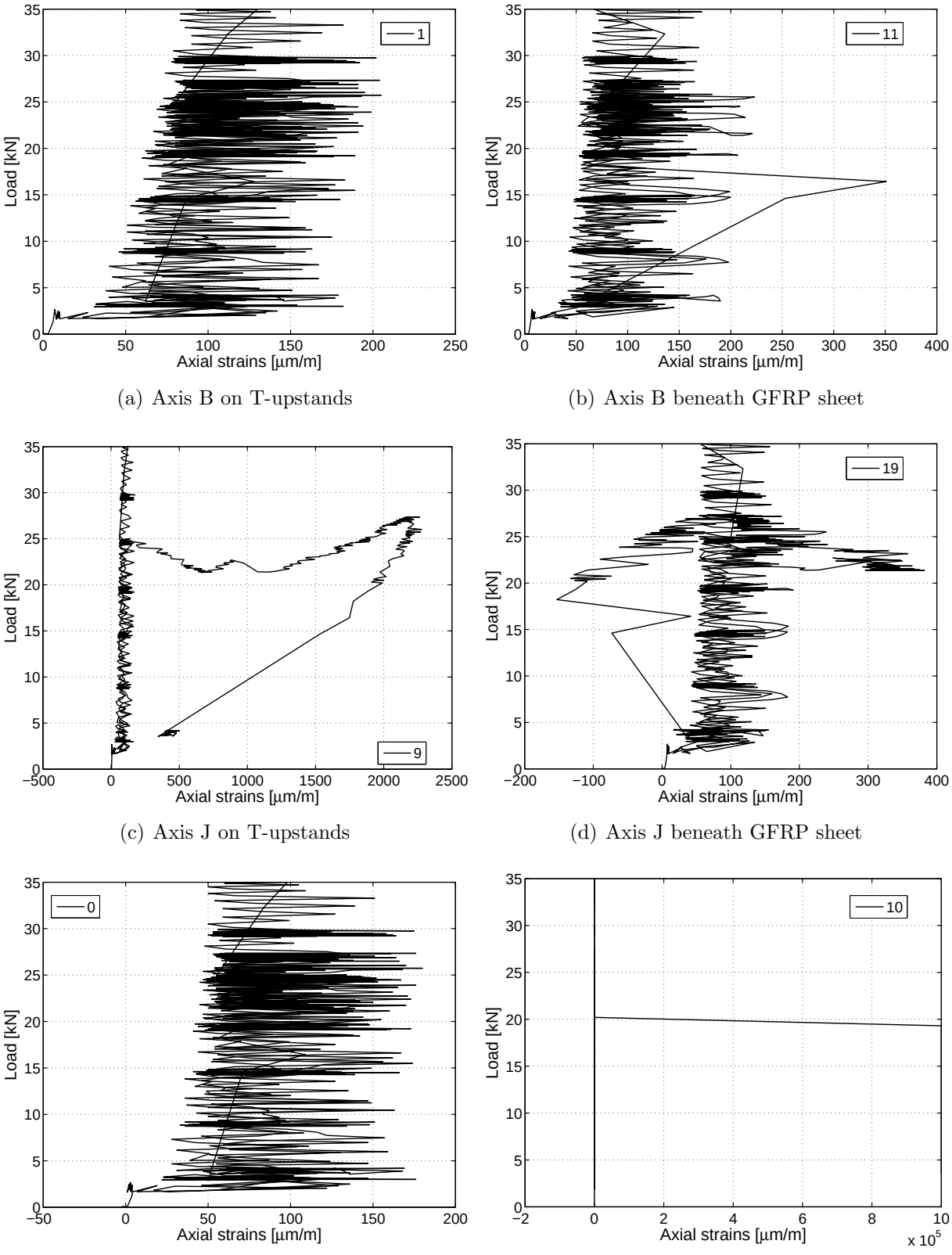

(a) Axis B on T-upstands

(b) Axis B beneath GFRP sheet

(c) Axis J on T-upstands

(d) Axis J beneath GFRP sheet

(e) Axis A on T-upstands

(f) Axis K on T-upstands

Figure C.136: 1000: Axial strains in GFRP profile - axis A,B,J,K.

C.5.1.5 Axial strains along the beam at 5-kN load steps

The strains along the beam at different load steps are indicated in the following graphs. The measurement points are connected with lines, while the dashed lines represent the $5, 15$ and 25-kN load steps and the continuous lines the $10, 20$ and 30-kN load steps. The thickest line illustrates the strains at ultimate load.

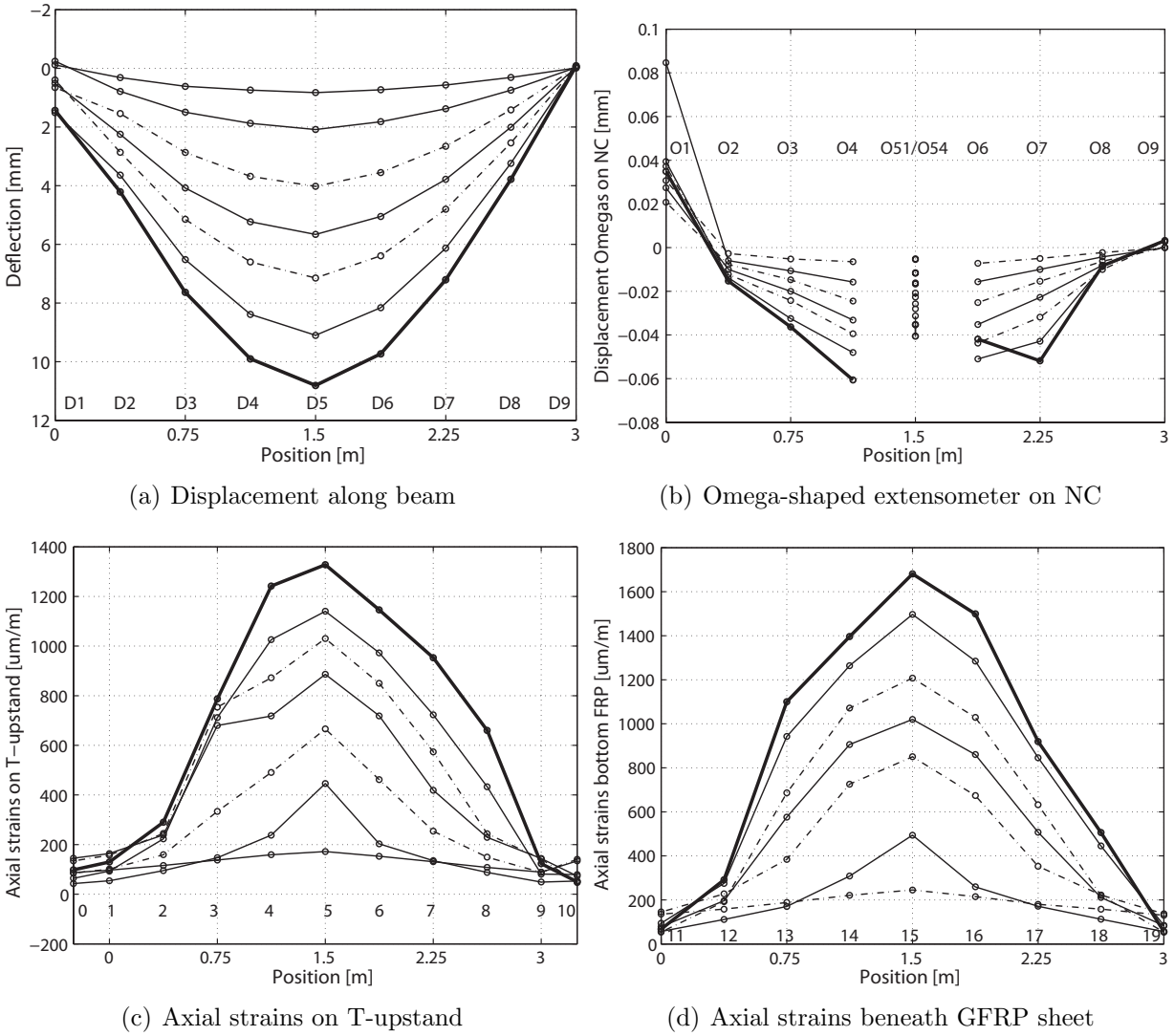

(a) Displacement along beam

(b) Omega-shaped extensometer on NC

(c) Axial strains on T-upstand

(d) Axial strains beneath GFRP sheet

Figure C.137: 1000: Displacement and strains along beam.

C.5.1.6 Axial strains through the cross section at 5-kN load steps

The strains through the cross section measured in the GFRP and on the concrete surface at different load steps are indicated in the following graphs. The measurement points are connected with lines, while the dashed lines represent the loads of 5 kN steps and the continuous lines the 10-kN steps. The thickest line illustrates the strains at ultimate load.

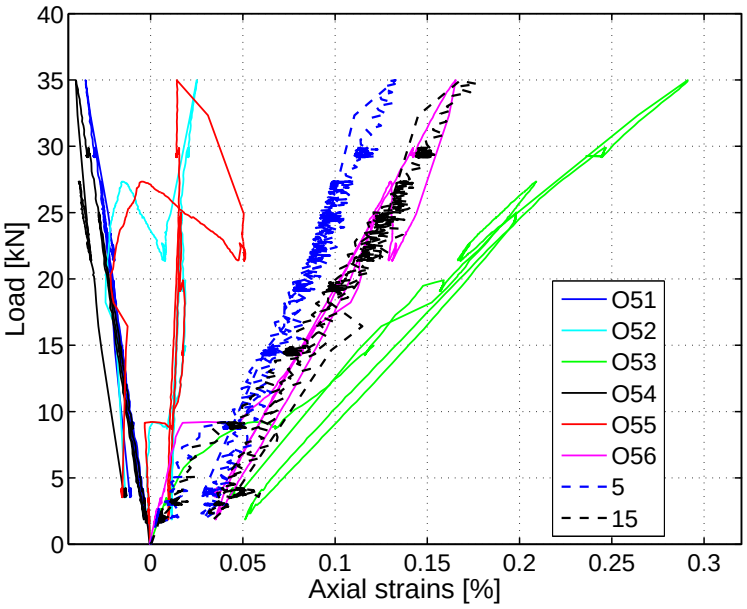

(a) Mid-span

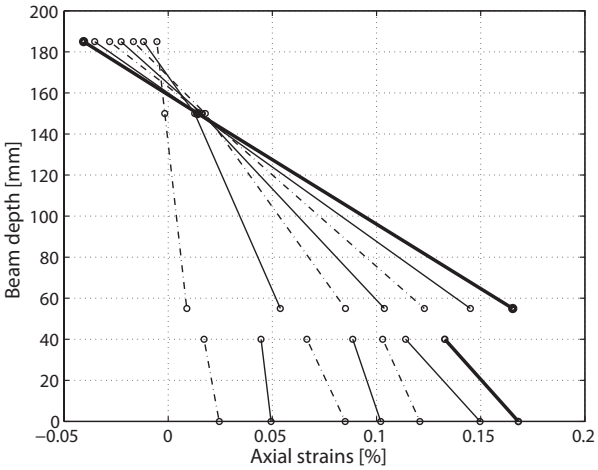

(b) Omegas at east side

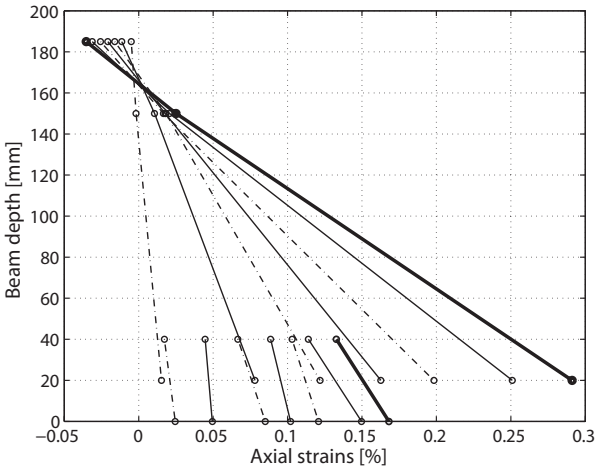

(c) Omegas at west side

Figure C.138: 1000: Strain development through cross section at mid-span at different load steps from strain gages and omega-shaped extensometers.

C.5.2 Beam 1000E: Failure description and measured results

C.5.2.1 Failure description

The failure process and crack pattern of the beam up to the end of the experiment are illustrated in Figures C.139 and C.140 and described in the following. Due to technical problems with the jack during the preparation of the experiment, the beam was loaded without any measurements being recorded. It is possible that the beam reached its cracking load, since audible cracking was noticed. Every 5 kN the displacement of the jack was stopped in order to document the cracking process and take pictures. Strain gage 7 on the bottom side of the GFRP profile was damaged while removing the formwork from the beams.

The first two visible cracks were noticed at a load of 8.0 kN. Subsequently, beam stiffness decreased slightly and cracks developed more or less vertically next to the loading plate. The crack length ranged between 4 and 15 cm. At a load of 15 kN the width of the crack next to the loading plate was approximately 0.01 mm. At this load a new inclined crack crossing the LC layer and developing at the LC-NC interface was observed. Subsequently further cracks developed with reduced crack spacings. At a load of 20 kN the width of the cracks next to the loading plate was 0.02 mm, while the opening of the inclined crack in the northern part reached 0.1 mm. At a load of 25 kN the cracked region was approximately 150 cm wide. On the southern side of the beam the cracks were vertically distributed with an average crack spacing of 8 cm. The cracks on the northern side were more and more inclined and the closer they were to the supports, the greater their spacing. Several cracks propagated through the LC-NC interface towards the mid-span.

At 30 kN a load cycle was performed. The cracks closed during the unloading process. Reloading was performed constantly up to 30 kN, where the further cracking process was documented. The crack pattern remained unchanged with the exception of a new crack in the southwest side of the beam.

At a load of 39.2 kN the most inclined crack on the northern side suddenly propagated through the depth of the beam, along the LC-NC interface to the loading plate in one direction and along the top of the FRP T-upstands, just above the FRP-LC interface, to the support and up to the beam end in the other direction.

Up to the end of the experiment, no debonding of the LC from the GFRP occurred and no slippage at the beam end was measured. After the brittle failure, the load dropped and the experiment was stopped.

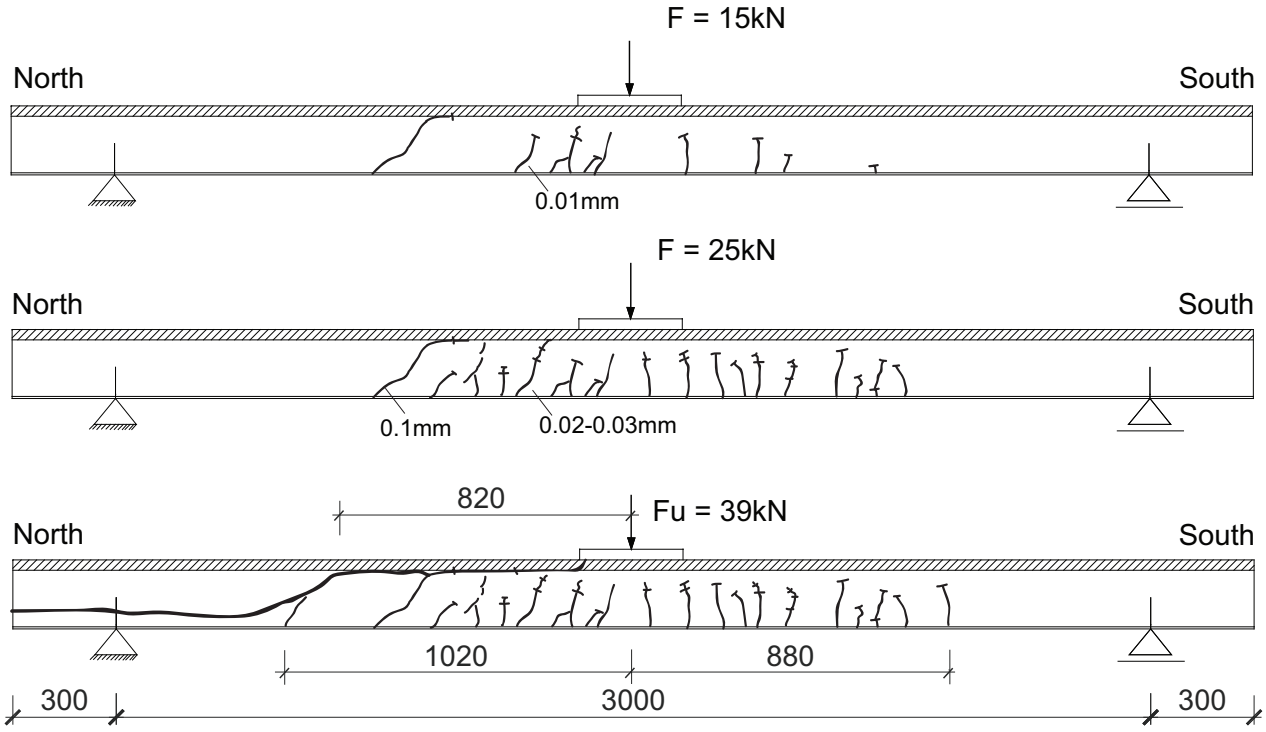

Figure C.139: 1000E: Failure process.

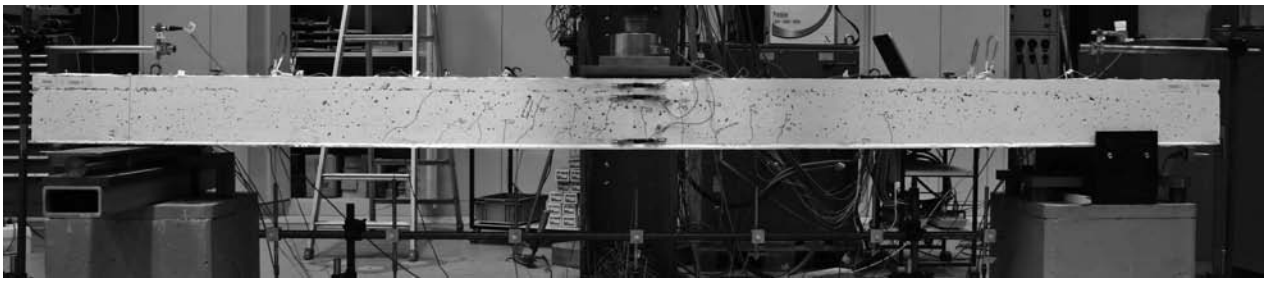

(a) Crack pattern at 20 kN - first load cycle

(b) Crack pattern at 30 kN - second load cycle

(c) Crack pattern at ultimate load

Figure C.140: 1000E: Failure process.

C.5.2.2 Displacement transducers

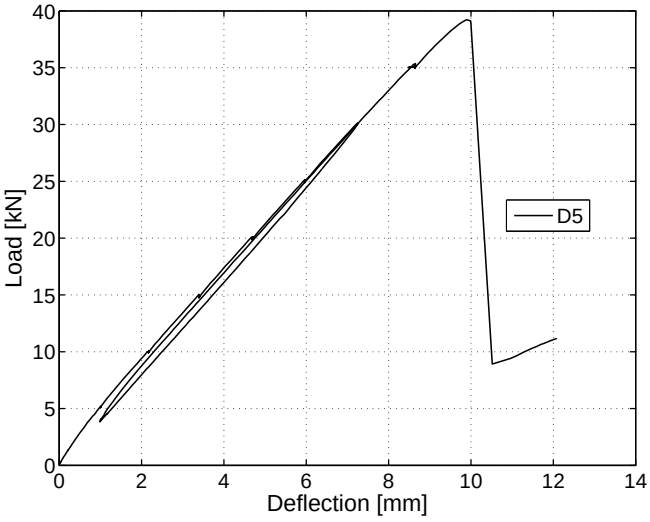

(a) At mid-span axis F

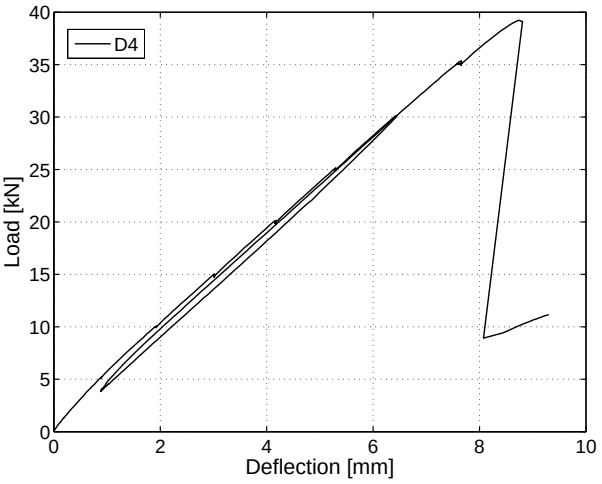

(b) Axis E

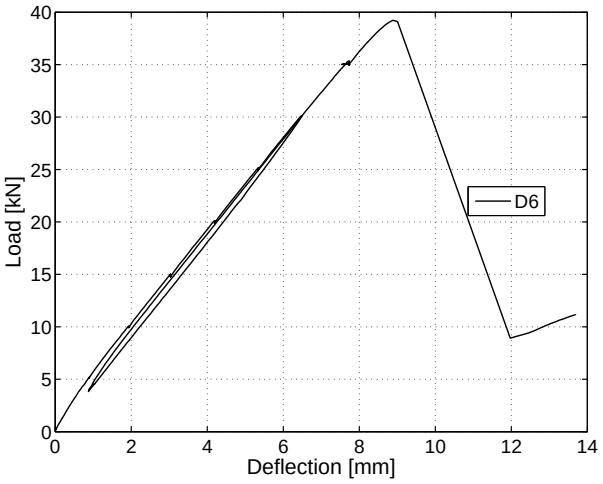

(c) Axis G

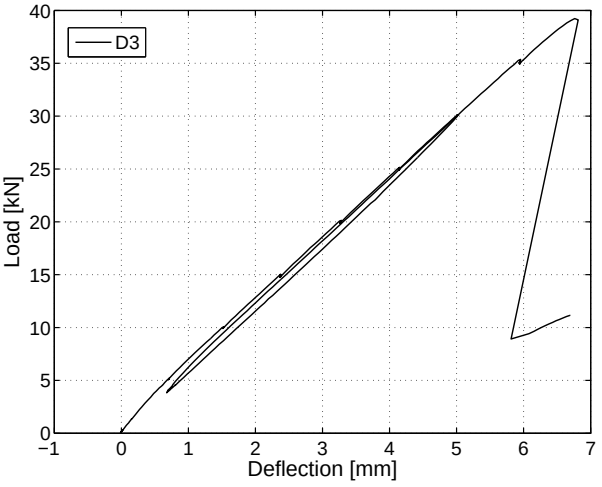

(d) Axis D

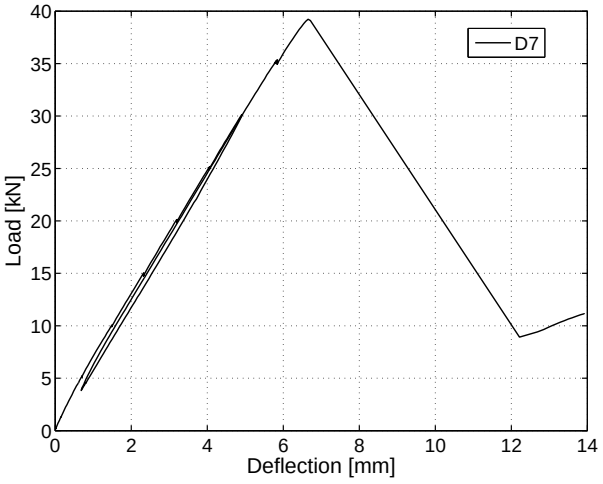

(e) Axis H

Figure C.141: 1000E: Displacement at axes D,E,G,H.

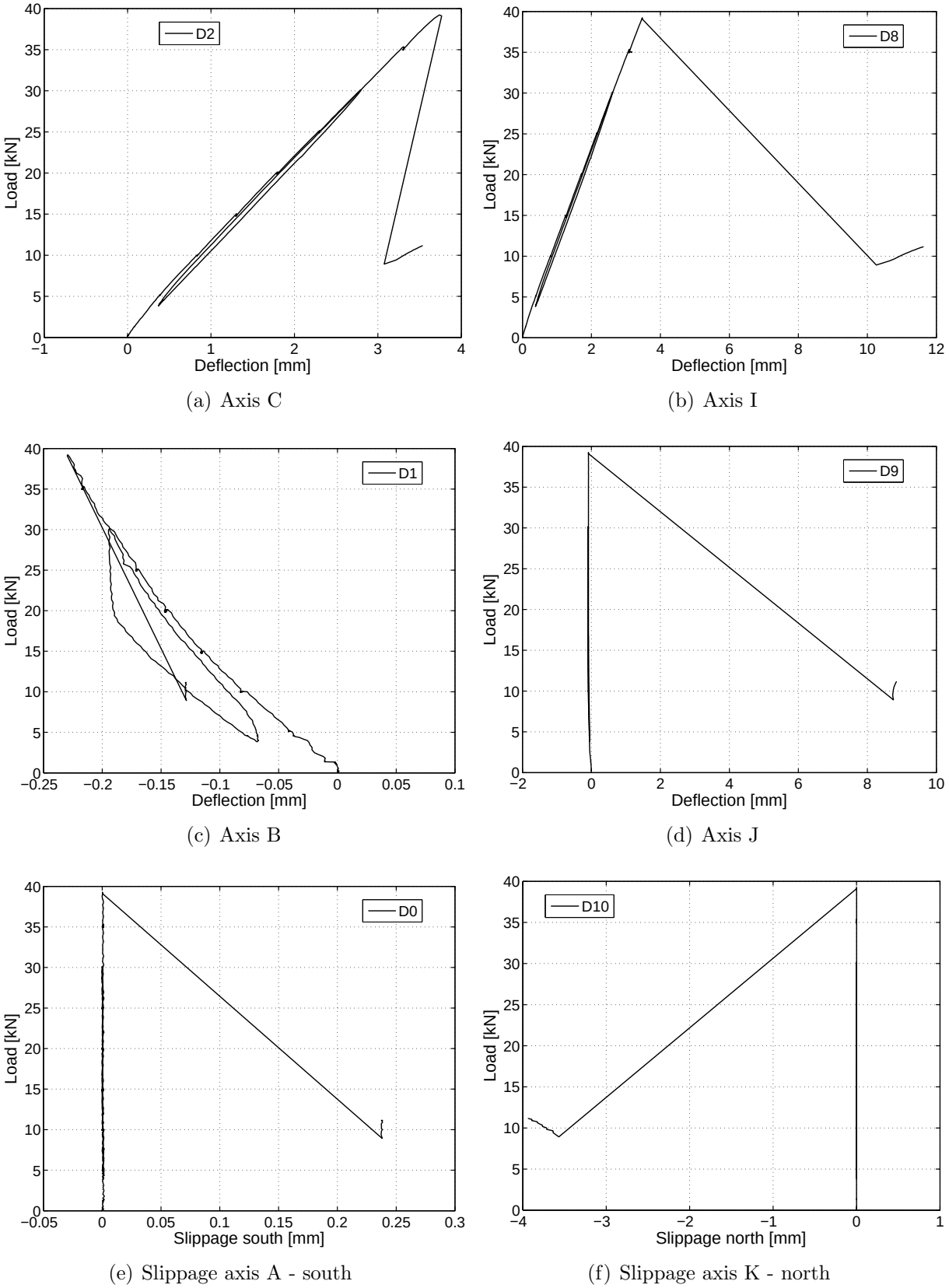

(a) Axis C

(b) Axis I

(c) Axis B

(d) Axis J

(e) Slippage axis A - south

(f) Slippage axis K - north

Figure C.142: 1000E: Displacement at axes B,C,I,J and slippage at beam ends.

C.5.2.3 Omega-shaped extensometers

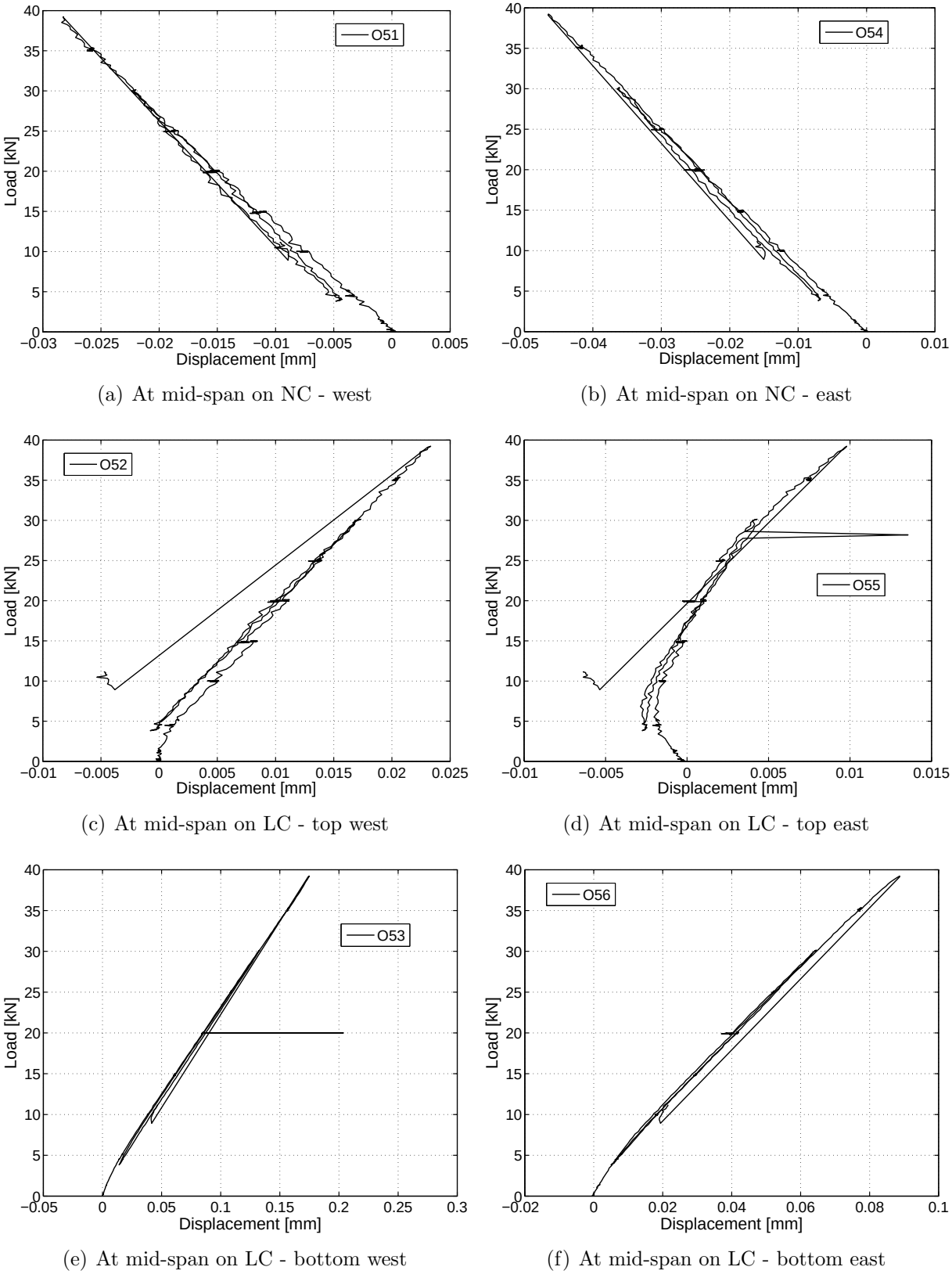

(a) At mid-span on NC - west

(b) At mid-span on NC - east

(c) At mid-span on LC - top west

(d) At mid-span on LC - top east

(e) At mid-span on LC - bottom west

(f) At mid-span on LC - bottom east

Figure C.143: 1000E: Deformations in omega-shaped extensometers at mid-span.

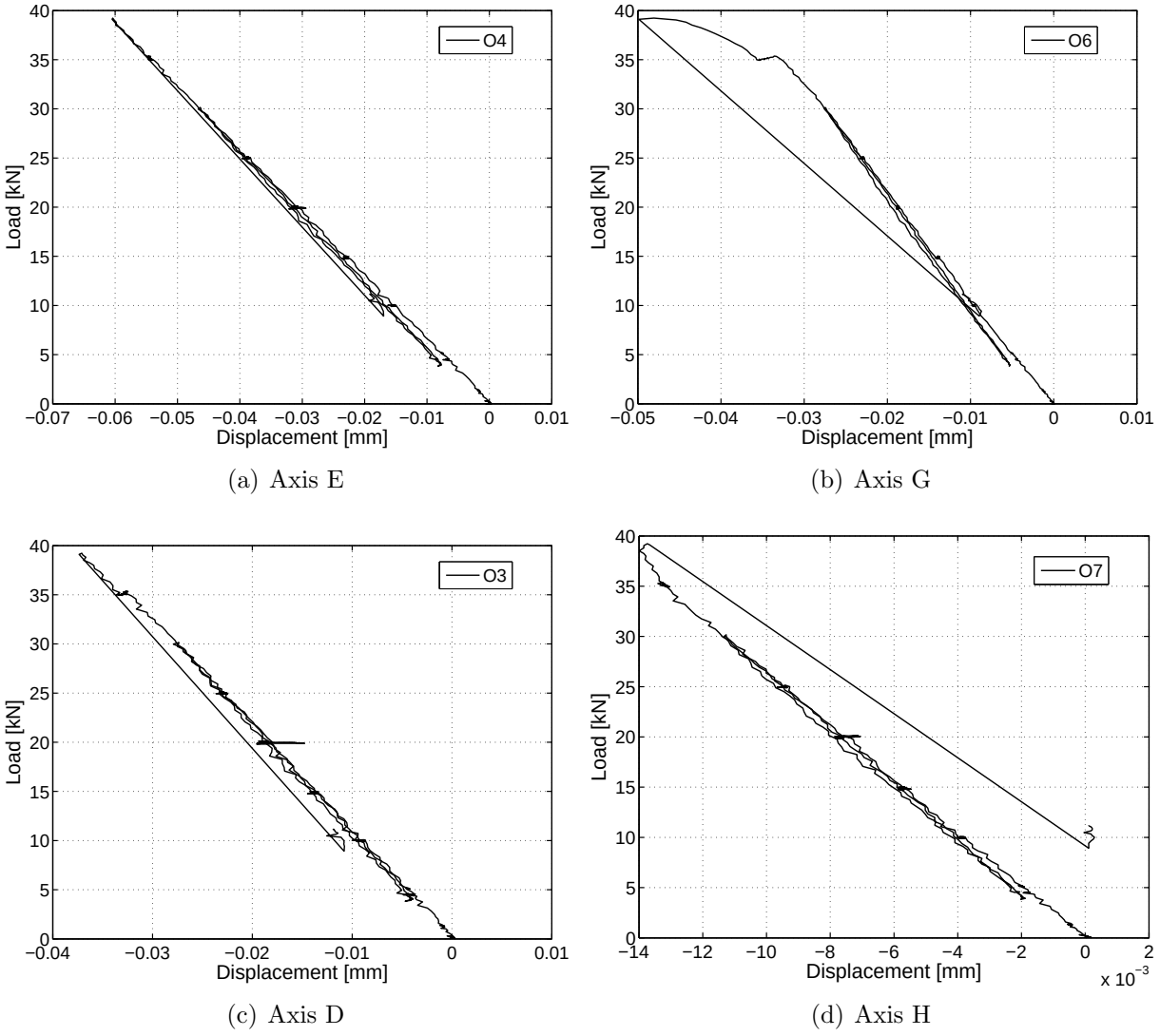

(a) Axis E

(b) Axis G

(c) Axis D

(d) Axis H

Figure C.144: 1000E: Deformations in omega-shaped extensometers - axes D,E,G,H.

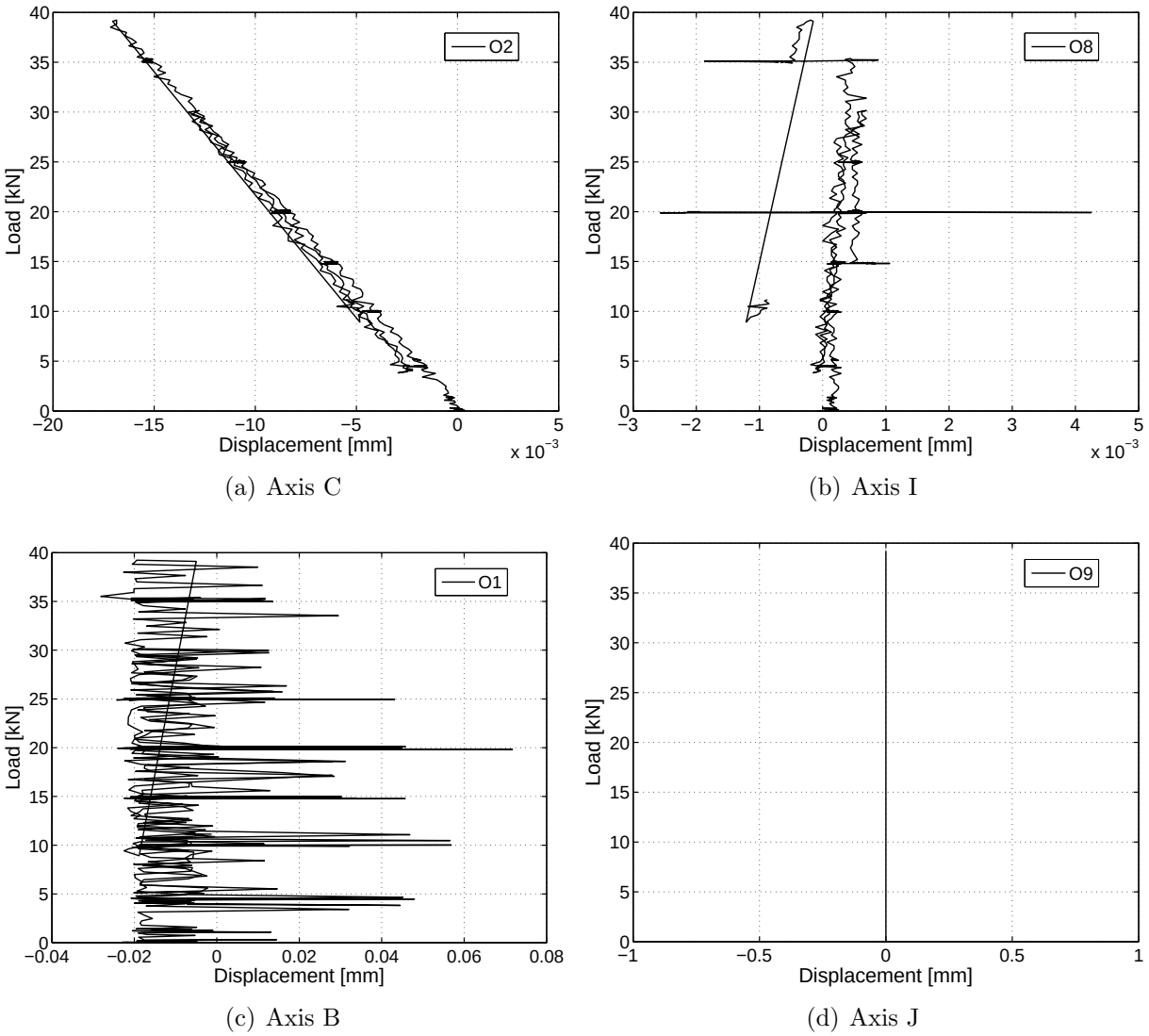

(a) Axis C

(b) Axis I

(c) Axis B

(d) Axis J

Figure C.145: 1000E: Deformations in omega-shaped extensometers - axes B,C,I,J.

C.5.2.4 Strain gages on GFRP profile

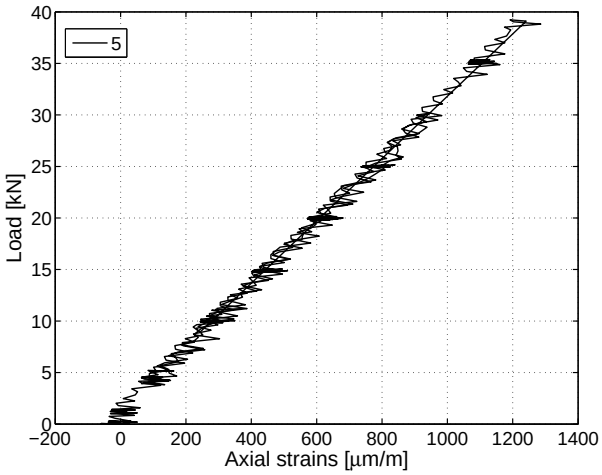

(a) At mid-span axis F on T-upstands

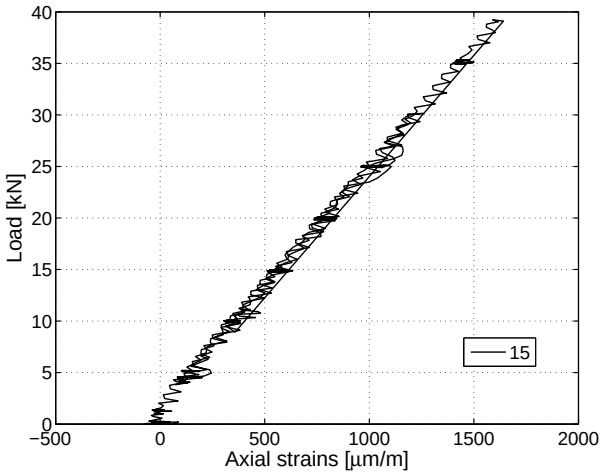

(b) At mid-span axis F beneath GFRP sheet

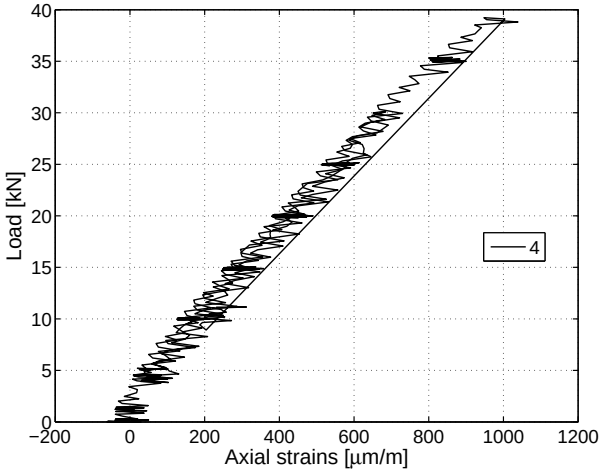

(c) Axis E on T-upstands

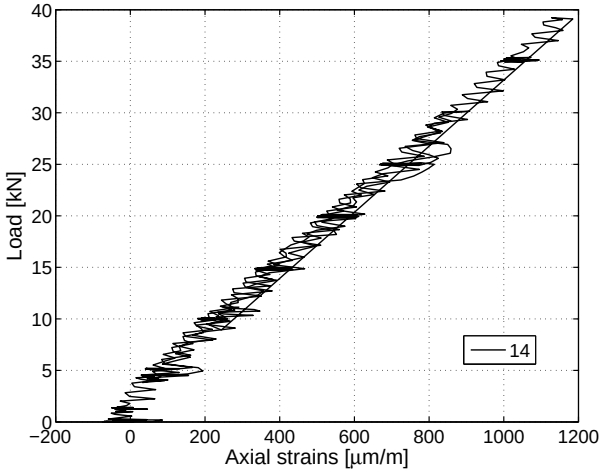

(d) Axis E beneath GFRP sheet

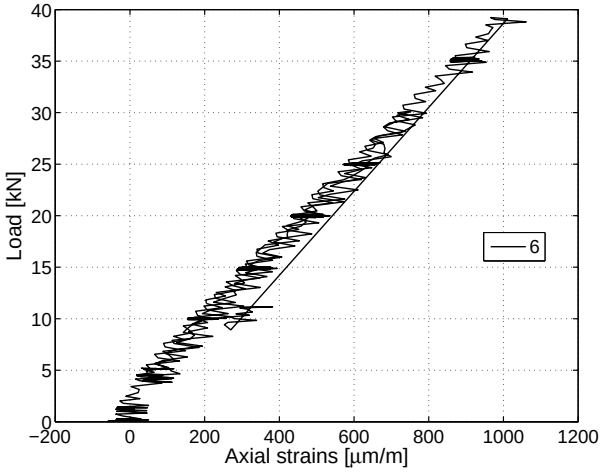

(e) Axis G on T-upstands

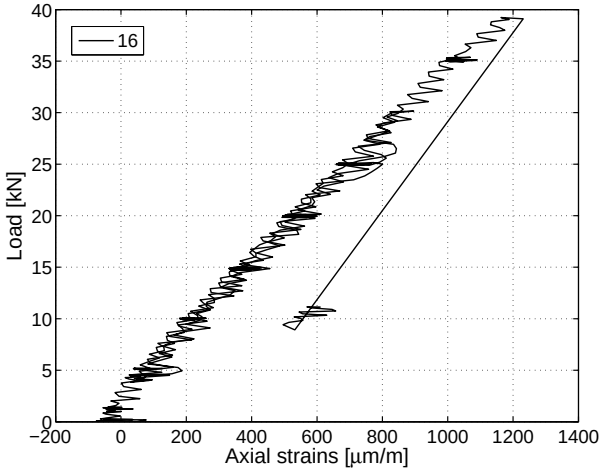

(f) Axis G beneath GFRP sheet

Figure C.146: 1000E: Axial strains in GFRP profile - axis E,F,G.

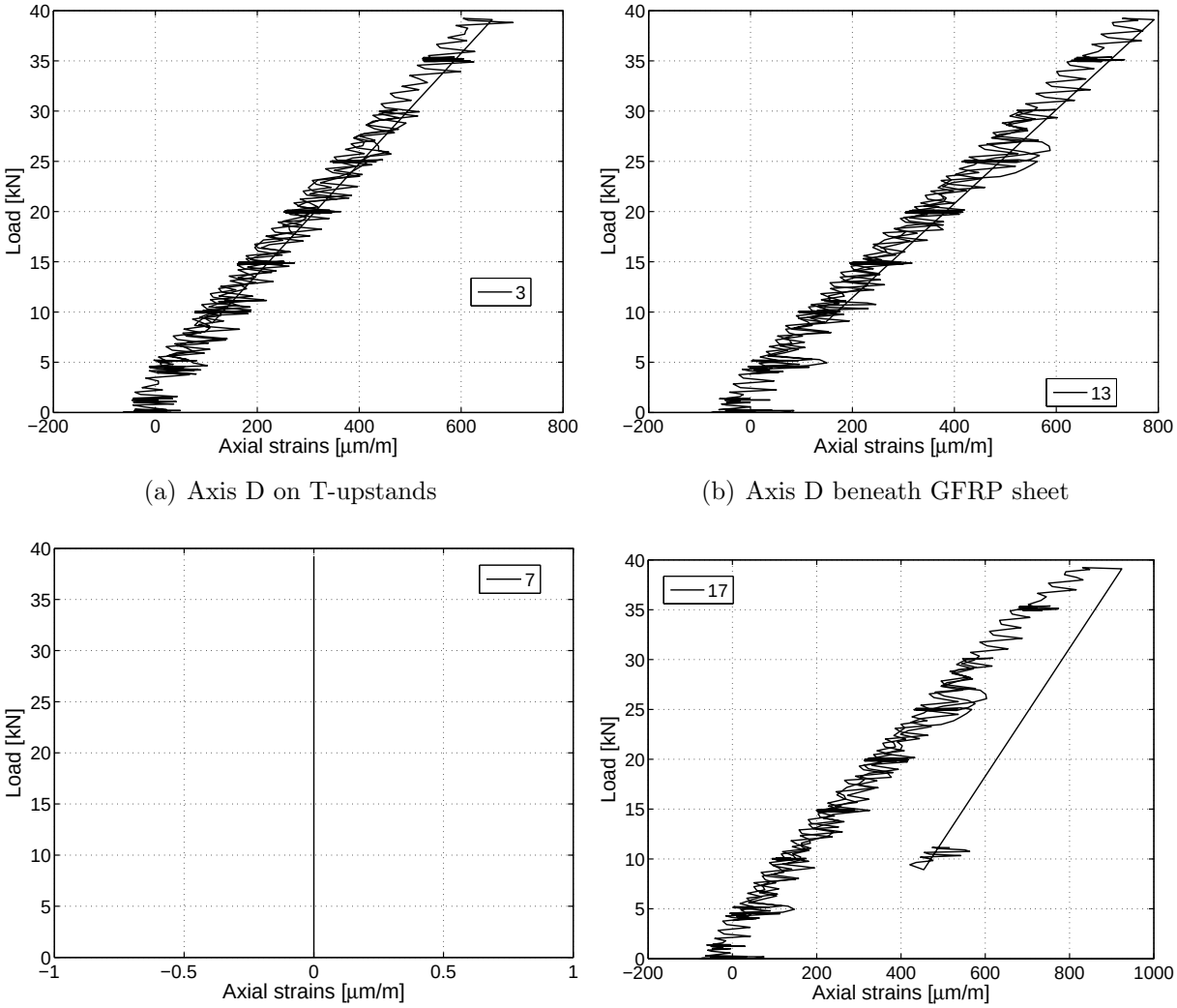

(a) Axis D on T-upstands

(b) Axis D beneath GFRP sheet

(c) Axis H on T-upstands

(d) Axis H beneath GFRP sheet

Figure C.147: 1000E: Axial strains in GFRP profile - axis D,H.

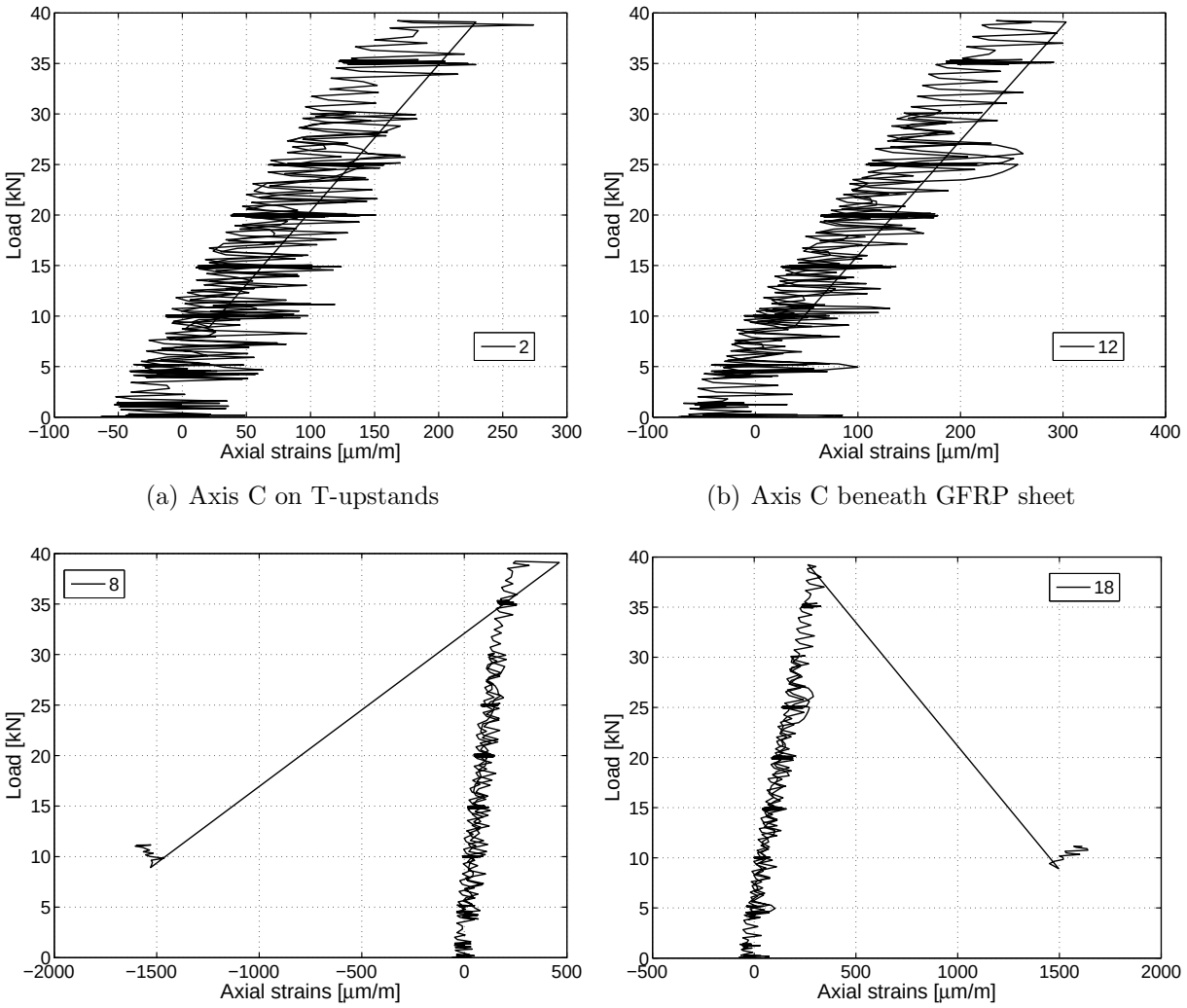

(a) Axis C on T-upstands

(b) Axis C beneath GFRP sheet

(c) Axis I on T-upstands

(d) Axis I beneath GFRP sheet

Figure C.148: 1000E: Axial strains in GFRP profile - axis C,I.

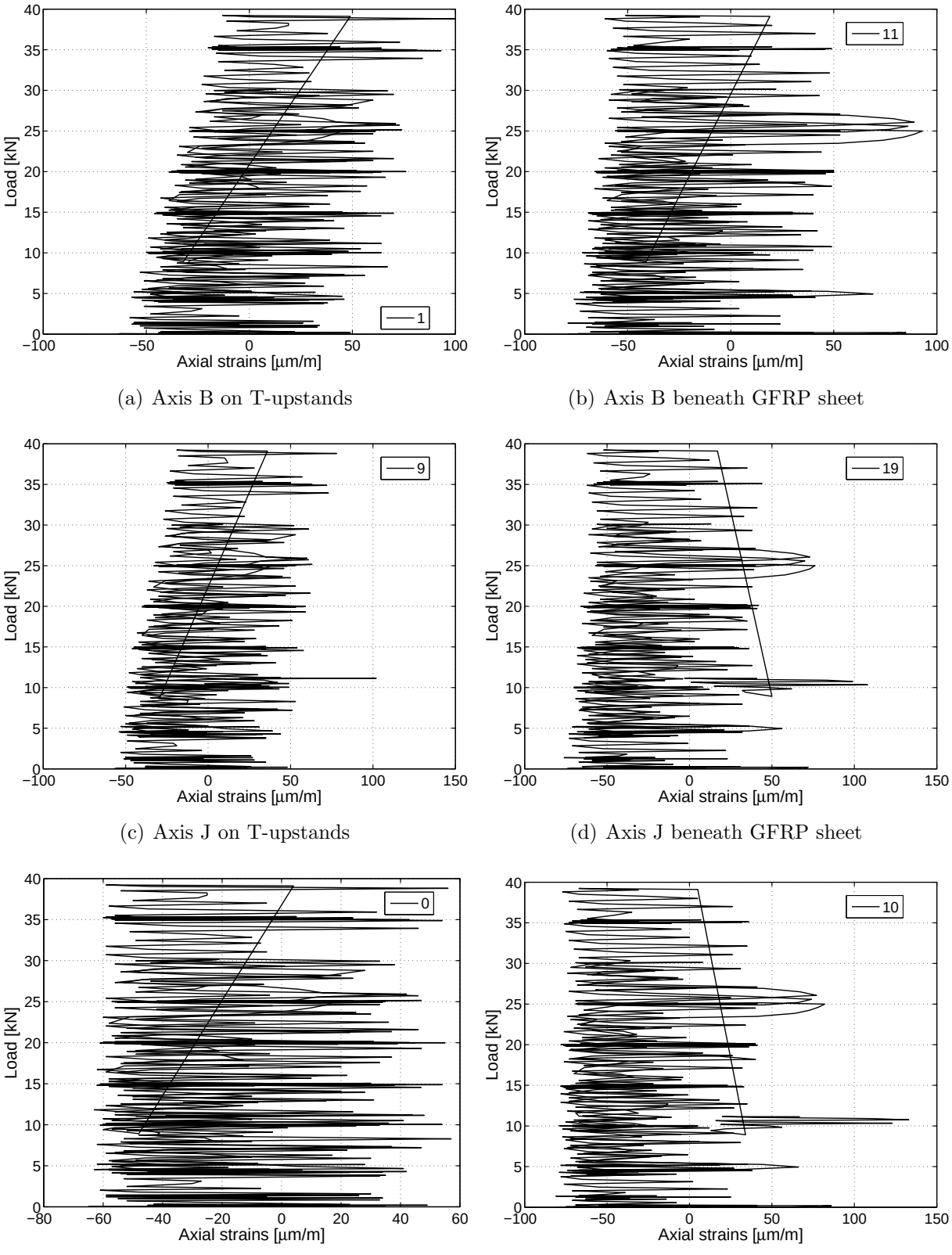

(a) Axis B on T-upstands

(b) Axis B beneath GFRP sheet

(c) Axis J on T-upstands

(d) Axis J beneath GFRP sheet

(e) Axis A on T-upstands

(f) Axis K on T-upstands

Figure C.149: 1000E: Axial strains in GFRP profile - axis A,B,J,K.

C.5.2.5 Axial strains along the beam at 5-kN load steps

The strains along the beam at different load steps are indicated in the following graphs. The measurement points are connected with lines, while the dashed lines represent the $5, 15$ and 25-kN load steps and the continuous lines the $10, 20$ and 30-kN load steps. The thickest line illustrates the strains at ultimate load.

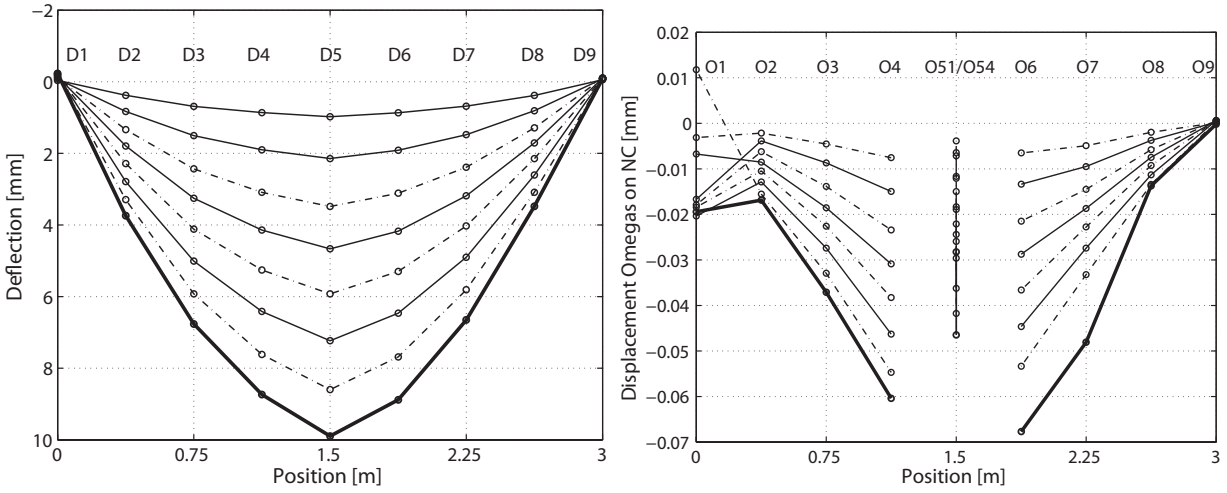

(a) Displacement along beam

(b) Omega-shaped extensometer on NC

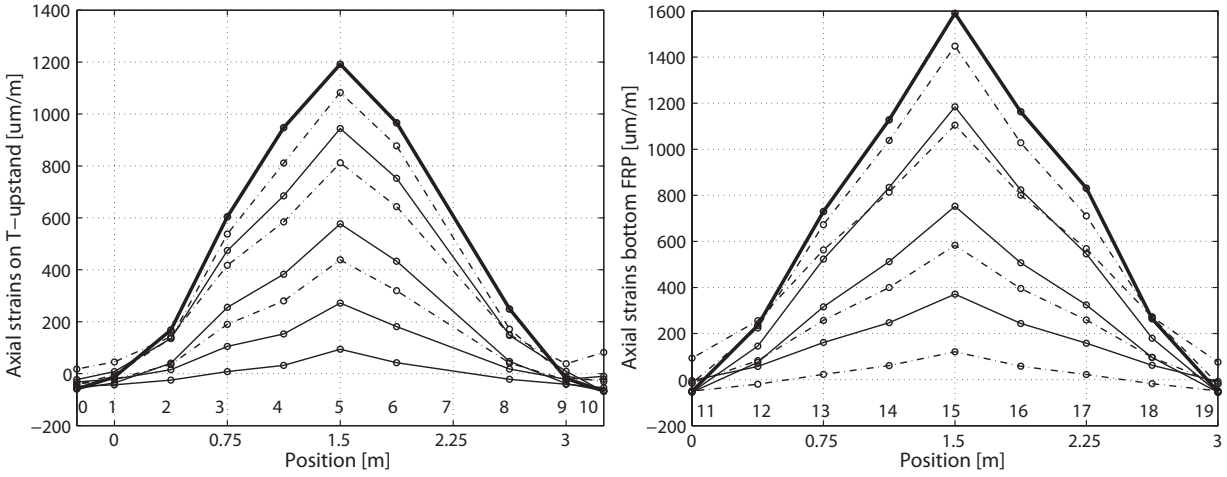

(c) Axial strains on T-upstand

(d) Axial strains beneath GFRP sheet

Figure C.150: 1000E: Displacement and strains along beam.

C.5.2.6 Axial strains through the cross section at 5-kN load steps

The strains through the cross section measured in the GFRP and on the concrete surface at different load steps are indicated in the following graphs. The measurement points are connected with lines, while the dashed lines represent the loads of 5 kN steps and the continuous lines the 10-kN steps. The thickest line illustrates the strains at ultimate load.

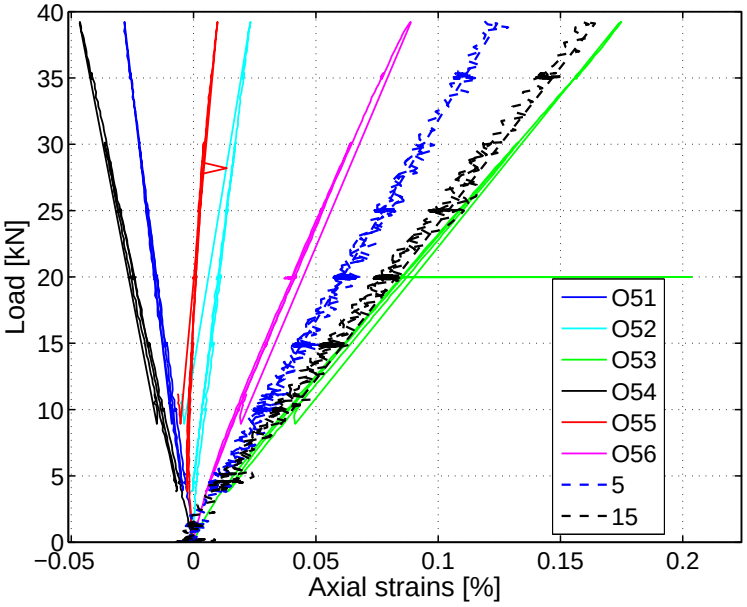

(a) Mid-span

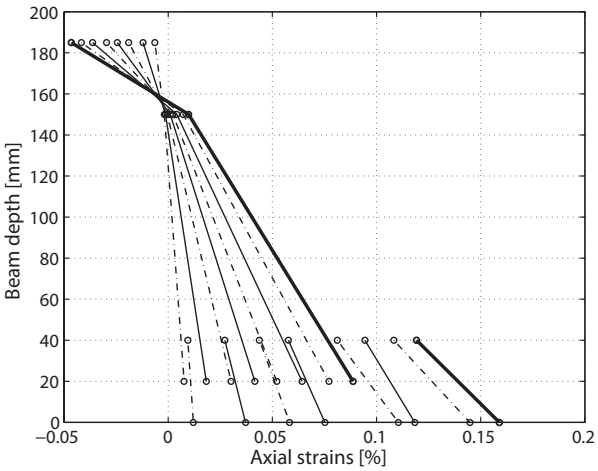

(b) Omegas at east side

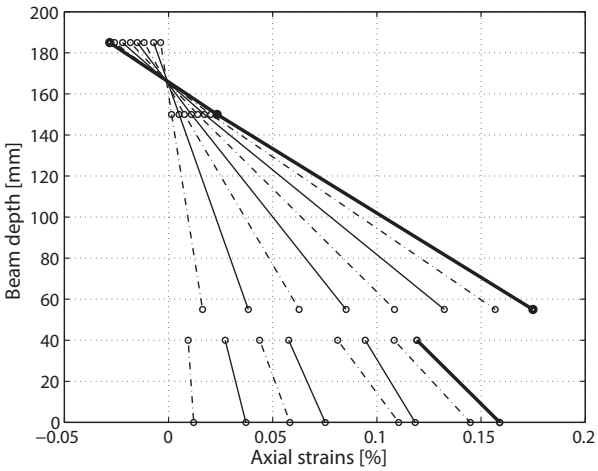

(c) Omegas at west side

Figure C.151: 1000E: Strain development through cross section at mid-span at different load steps from strain gages and omega-shaped extensometers.

C.5.3 Beam 1000A: Failure description and measured results

C.5.3.1 Failure description

The failure process and crack pattern of the beam up to the end of the experiment is illustrated in Figures C.152, C.153 and C.154 and described in the following. Every 5 kN the displacement of the jack was stopped in order to document the cracking process and take pictures.

The first cracks were noticed at a load of 5.0 kN in the tension zone of the LC along the whole beam length. The crack spacings did not show any regularity. The cracks were more or less vertically distributed with lengths of between 5 and10 cm. Subsequently further cracks developed and the existing cracks grew longer. At a load of 15 kN the crack spacings were between 10 and 20 cm. The width of the cracks next to the loading plate reached values of approximately 0.1 mm. The vertical cracks did not yet reach the NC layer. On the northern side a crack between the NC anchor block and the LC could be observed. Further loading resulted in new cracks that were regularly and still vertically distributed. At a load of 20 kN an inclined crack next to the anchor block and approximately 15-cm-long horizontal crack along the LC-NC interface were observed on the south-west side. The width of the crack next to the loading plate increased from 0.15 mm to 0.2 mm at a load of 25 kN, where a second load cycle was performed. The cracks closed during the unloading process. Measurements showed crack widths of between 0.02 and 0.05 mm at a load of 2 kN after unloading. Reloading was performed constantly up to a load of 30 kN, where the further cracking process was documented. The average crack spacing then reached 13 cm.

At a load of 32 kN three loud noises occurred. However, no obvious change could be noticed. At 37.8 kN the beam failed when a crack suddenly propagated through the depth of the LC on the northern side. This crack was slightly inclined and developed further along the LC-NC interface and along the top of the FRP T-upstands, just above the FRP-LC interface, up to the anchor block. The load dropped to a value of 19.9 kN, where a short stabilization could be noticed followed by a load cracking and second drop in the load. At the same time, omega-shaped extensometer O6 detached from the concrete surface. The experiment was then stopped. The anchor blocks remained undamaged, and no slippage at the beam ends was measured.

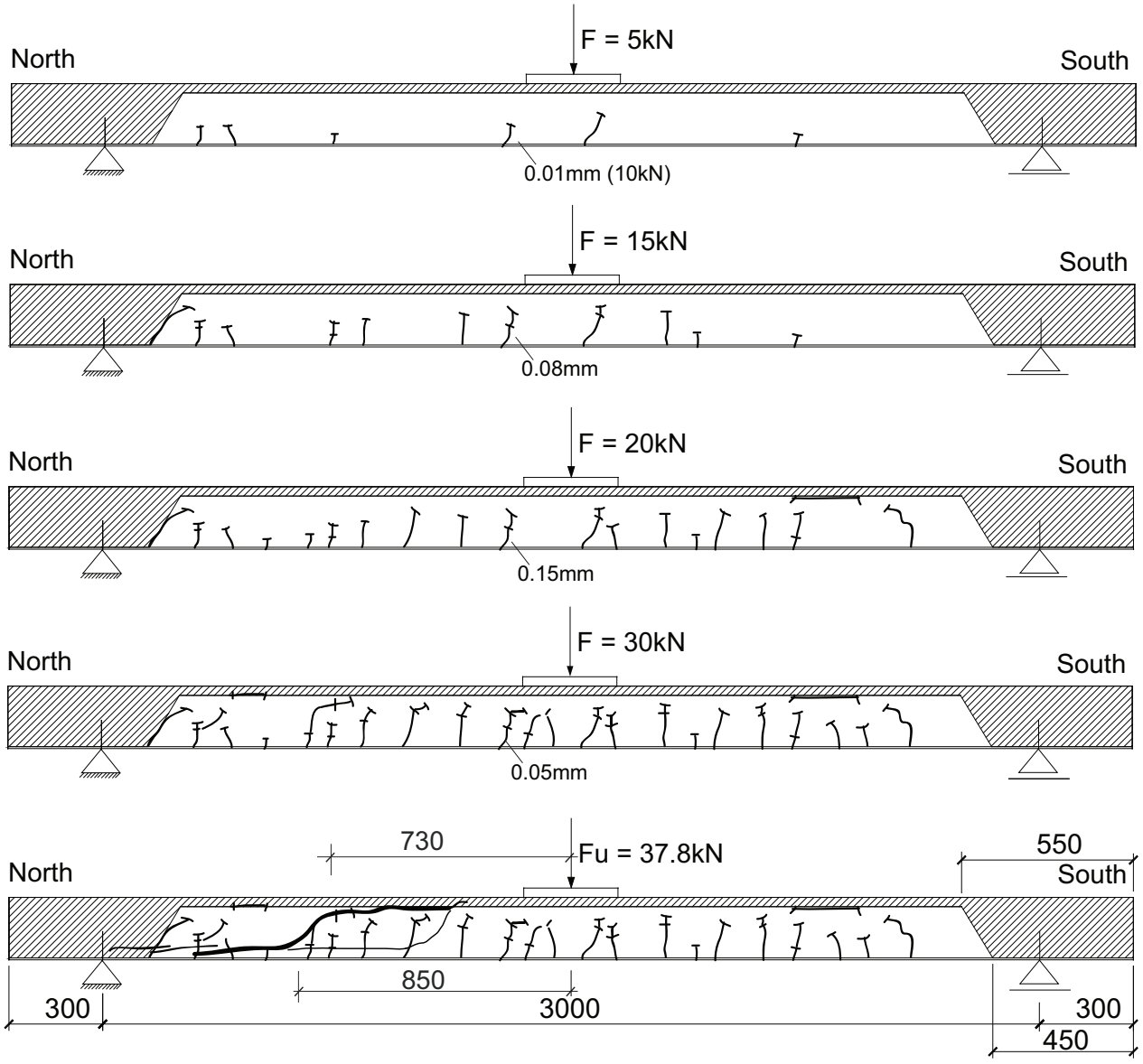

Figure C.152: 1000A: Failure process.

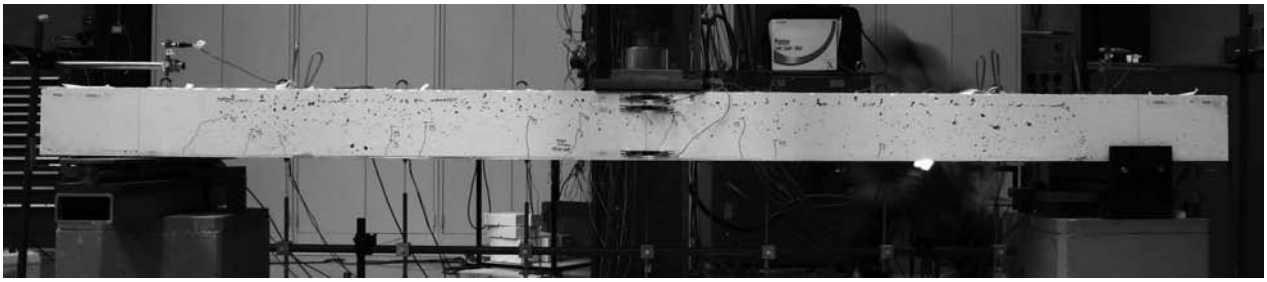

(a) Crack pattern at 15.0 kN - first load cycle

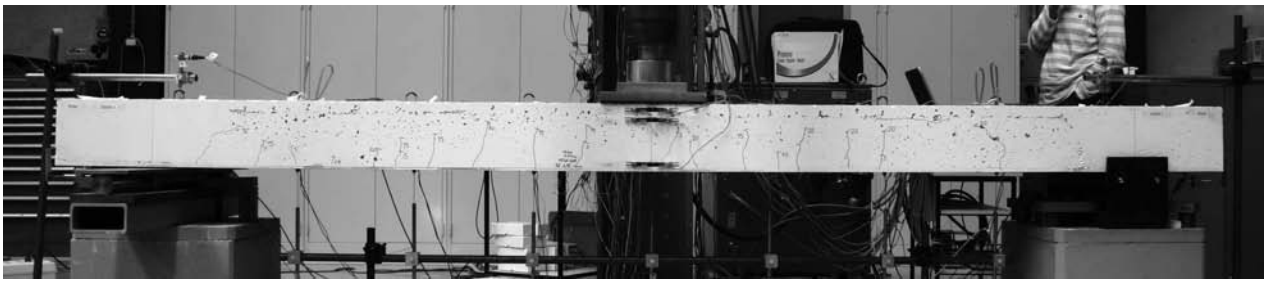

(b) Crack pattern at 20.0 kN - first load cycle

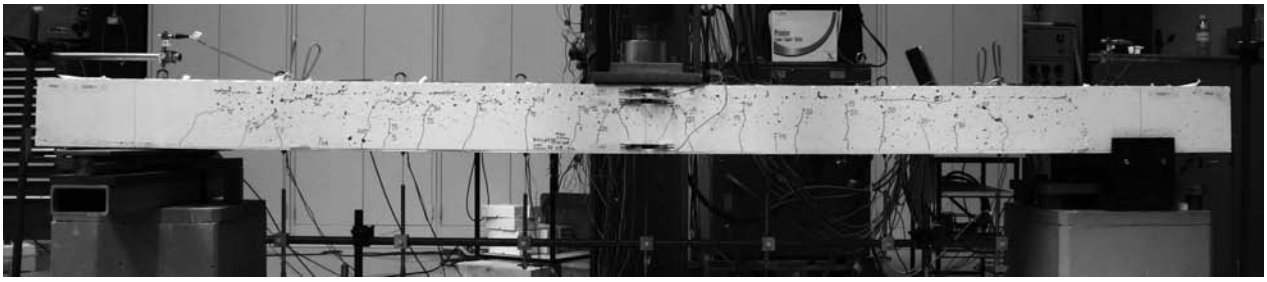

(c) Crack pattern at 30.0 kN - second load cycle

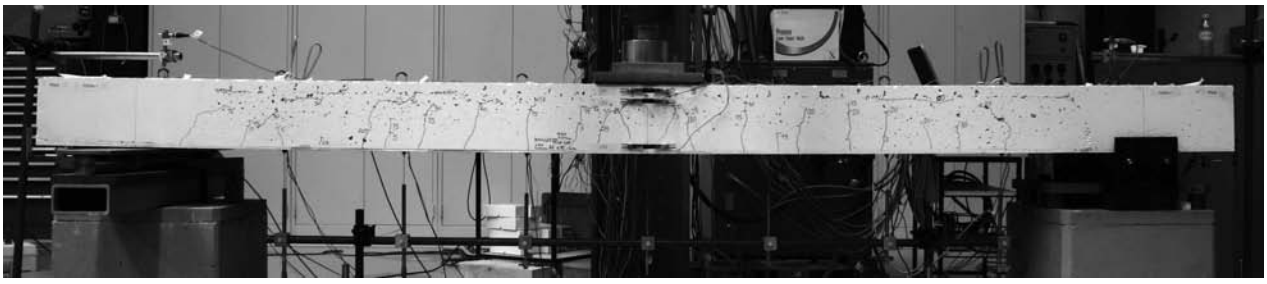

(d) Failure at ultimate load 37.8 kN

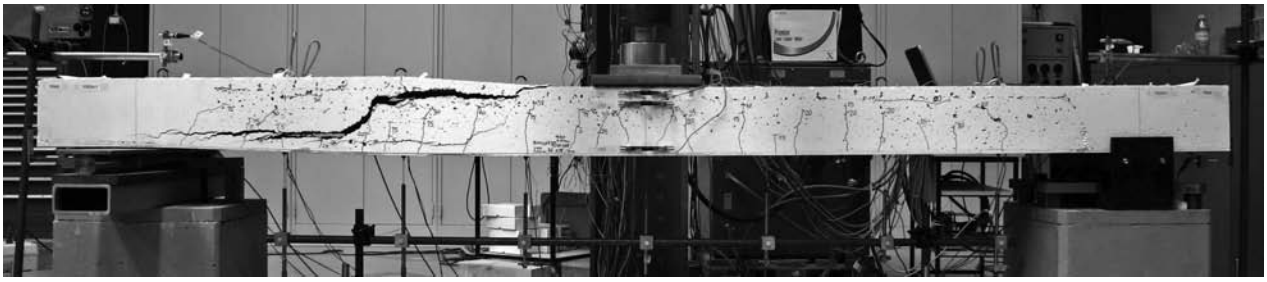

(e) Failed beam after experiment, still loaded

Figure C.153: 1000A: Failure process.

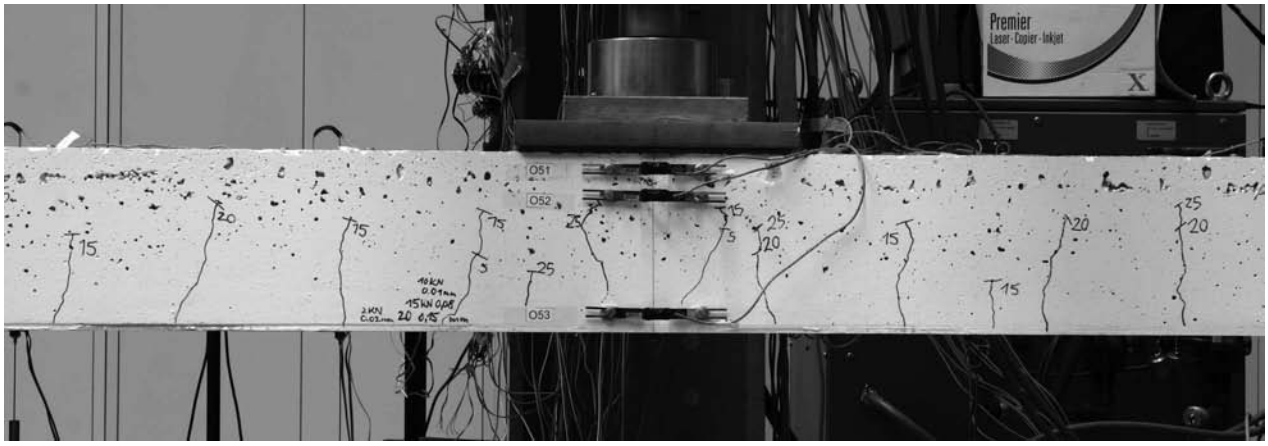

(a) Vertical cracks at 25.0 kN - first load cycle

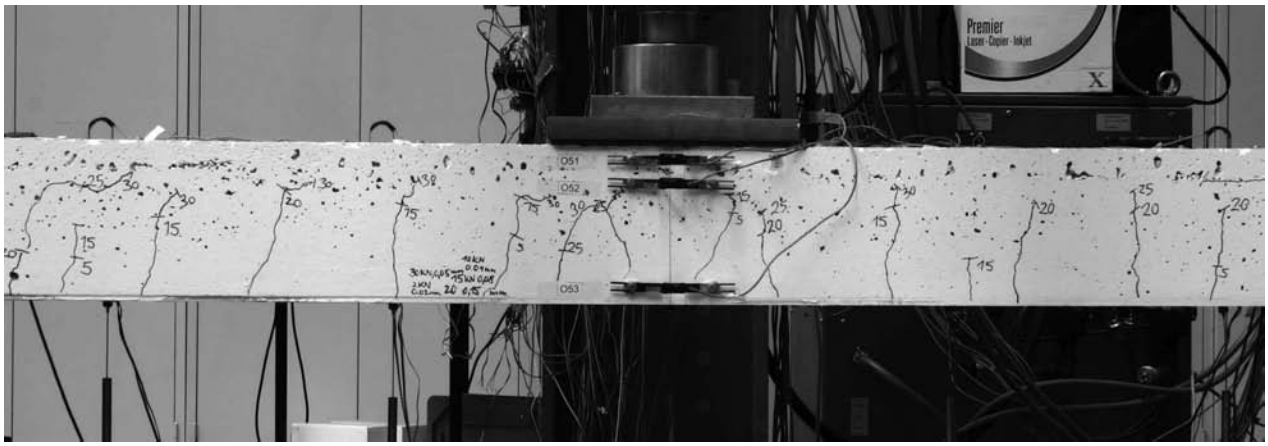

(b) At 30.0 kN - second load cycle

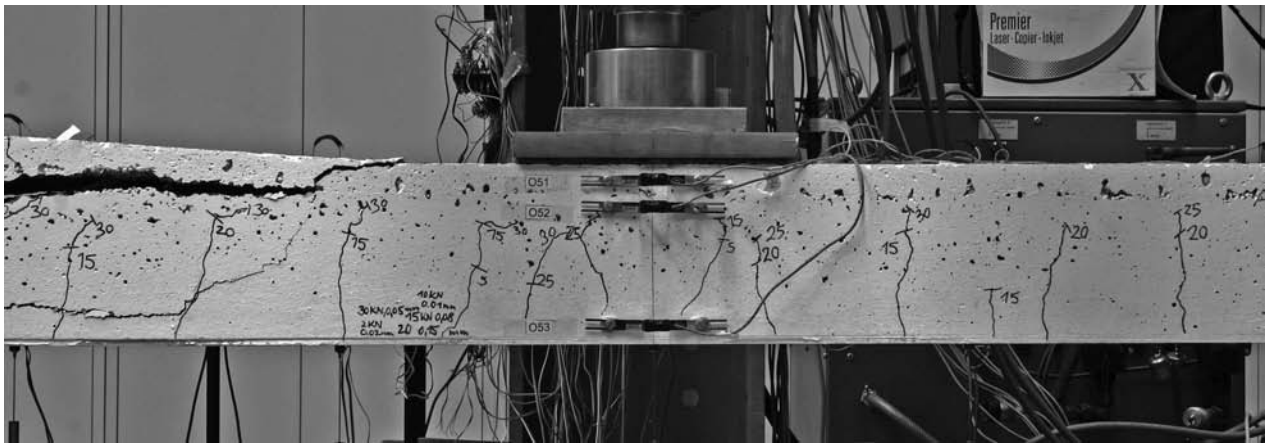

(c) Crack pattern of failed beam

Figure C.154: 1000A: Crack pattern next to loading plate.

C.5.3.2 Displacement transducers

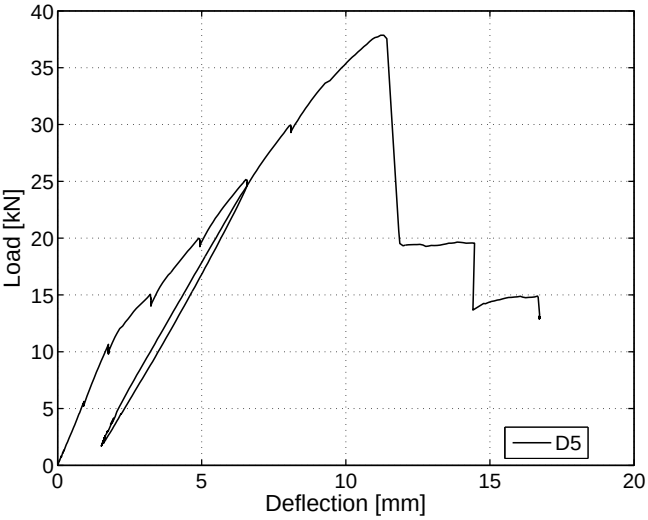

(a) At mid-span axis F

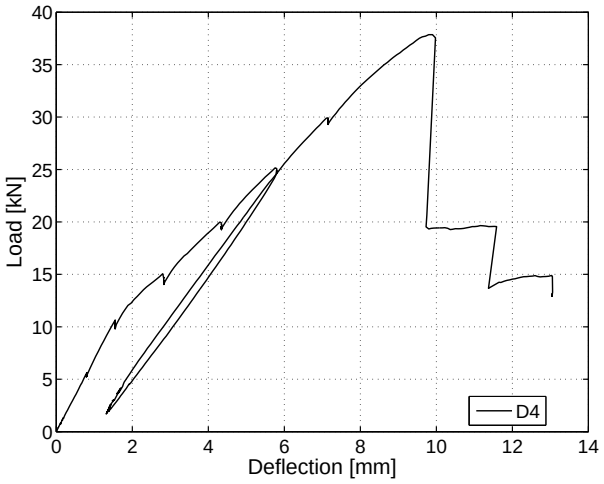

(b) Axis E

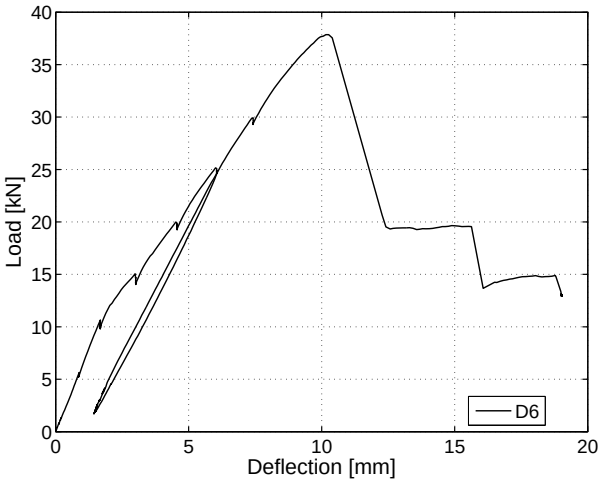

(c) Axis G

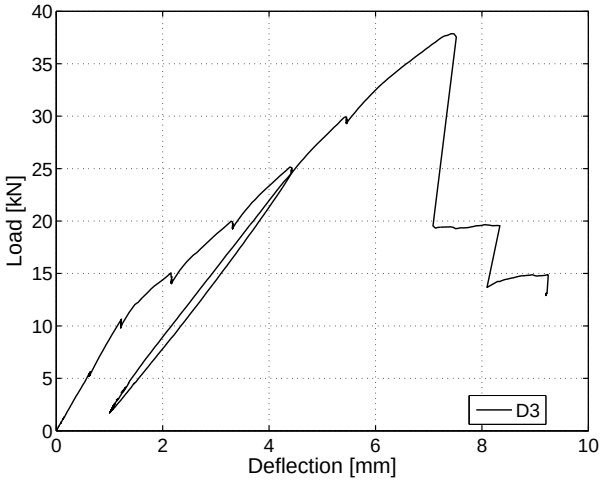

(d) Axis D

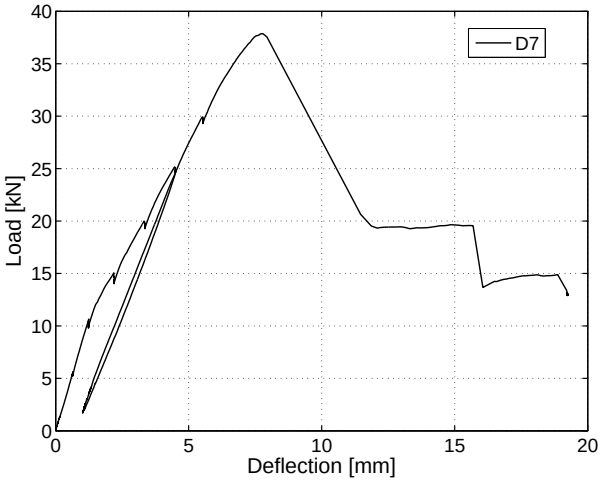

(e) Axis H

Figure C.155: 1000A: Displacement at axes D,E,G,H.

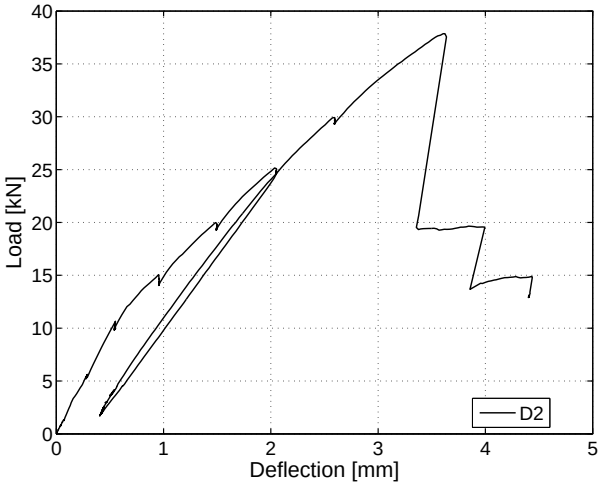

(a) Axis C

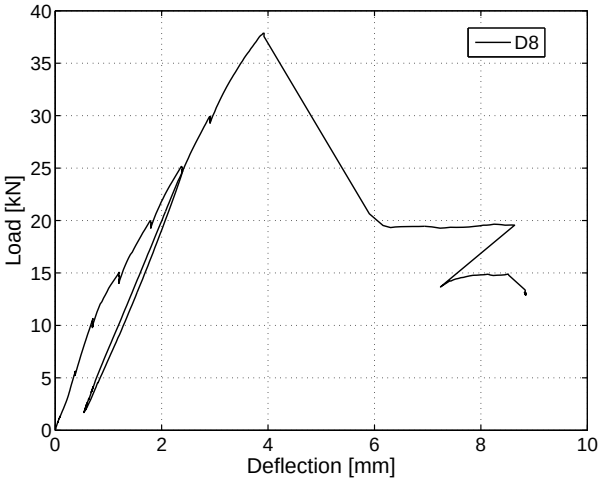

(b) Axis I

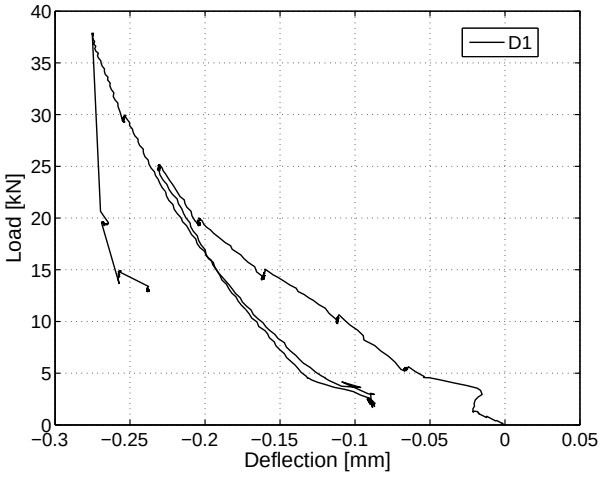

(c) Axis B

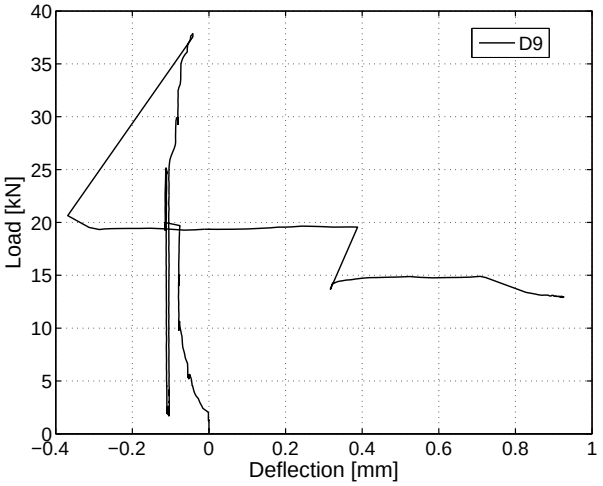

(d) Axis J

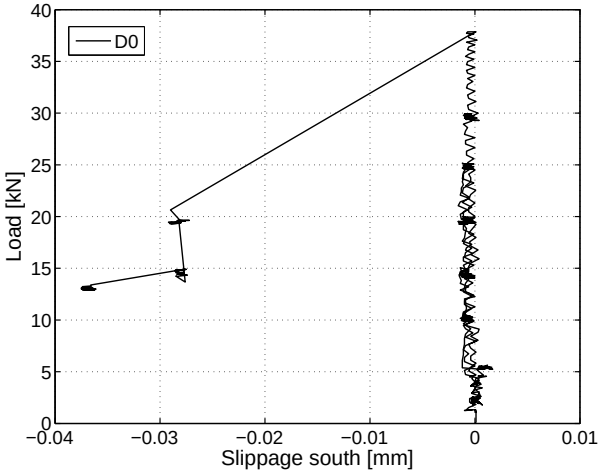

(e) Slippage axis A - south

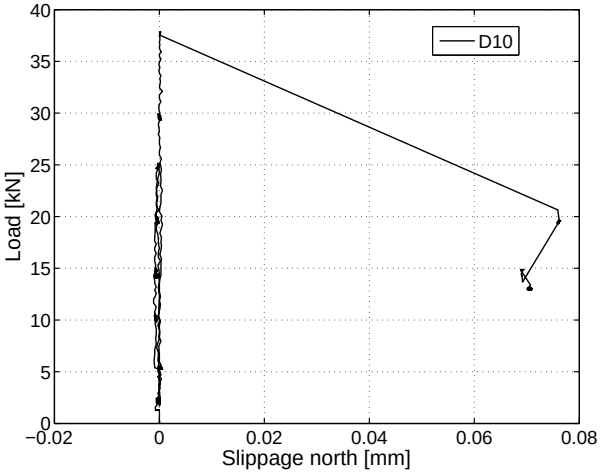

(f) Slippage axis K - north

Figure C.156: 1000A: Displacement at axes B,C,I,J and slippage at beam ends.

C.5.3.3 Omega-shaped extensometers

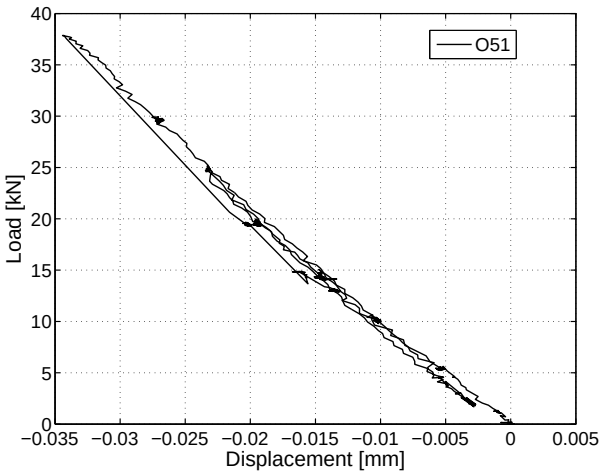

(a) At mid-span on NC - west

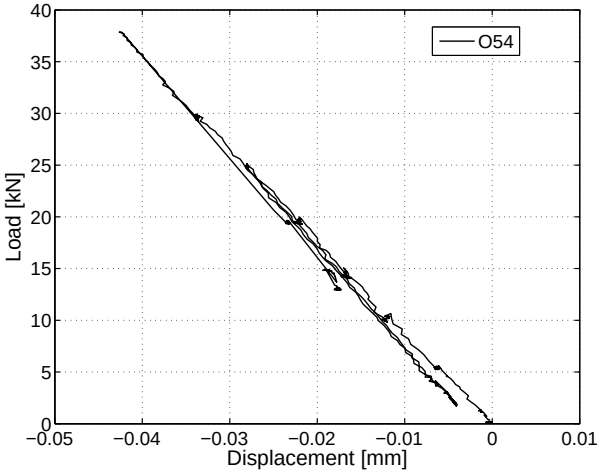

(b) At mid-span on NC - east

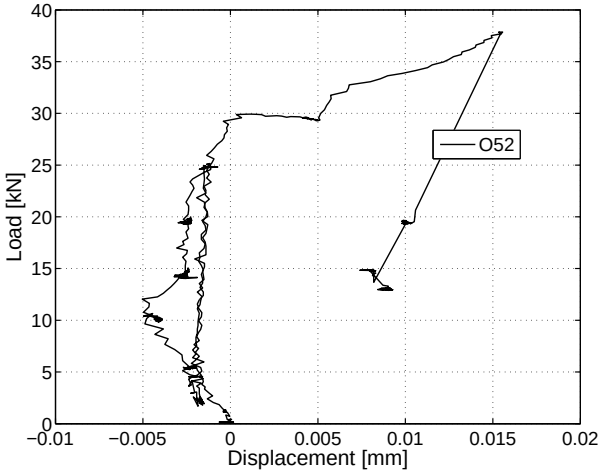

(c) At mid-span on LC - top west

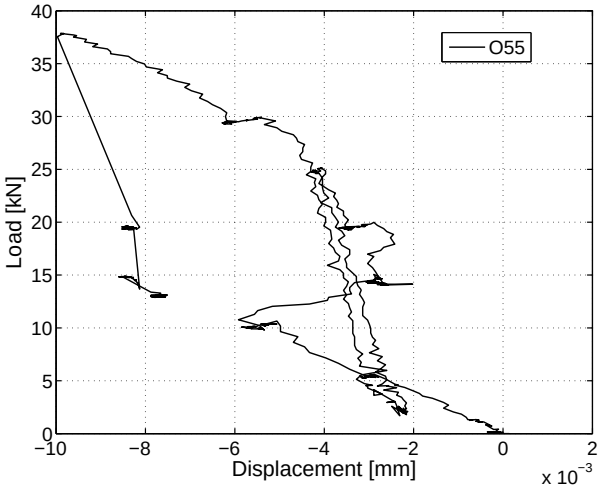

(d) At mid-span on LC - top east

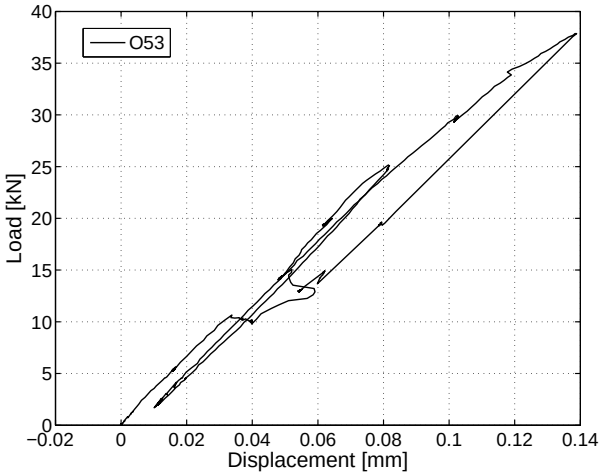

(e) At mid-span on LC - bottom west

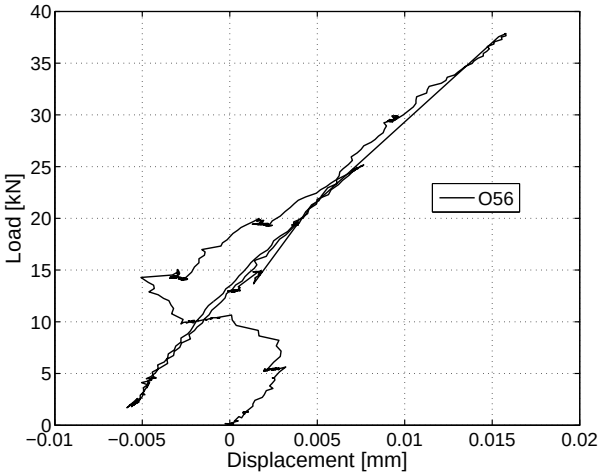

(f) At mid-span on LC - bottom east

Figure C.157: 1000A: Deformations in omega-shaped extensometers at mid-span.

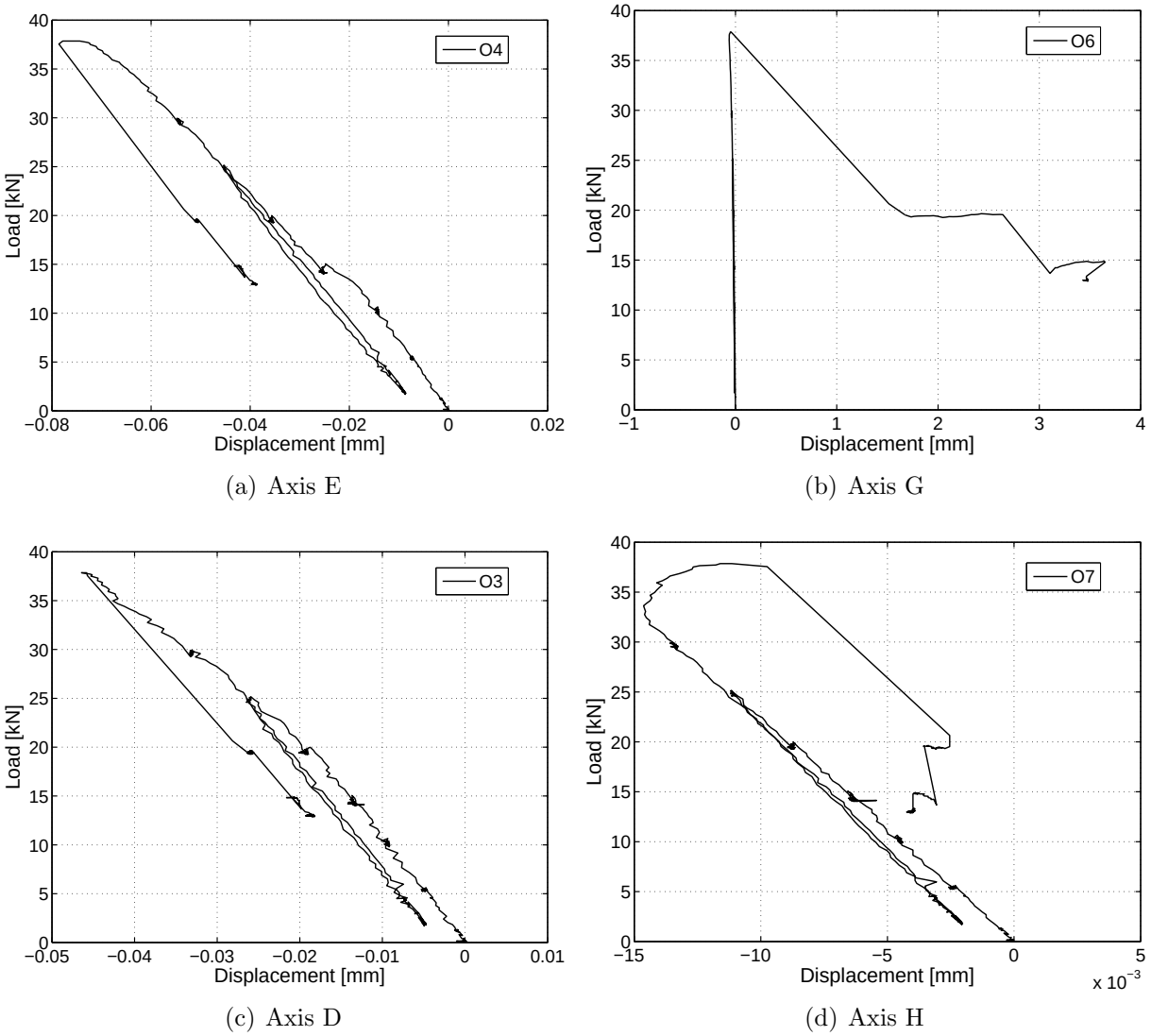

(a) Axis E

(b) Axis G

(c) Axis D

(d) Axis H

Figure C.158: 1000A: Deformations in omega-shaped extensometers - axes D,E,G,H.

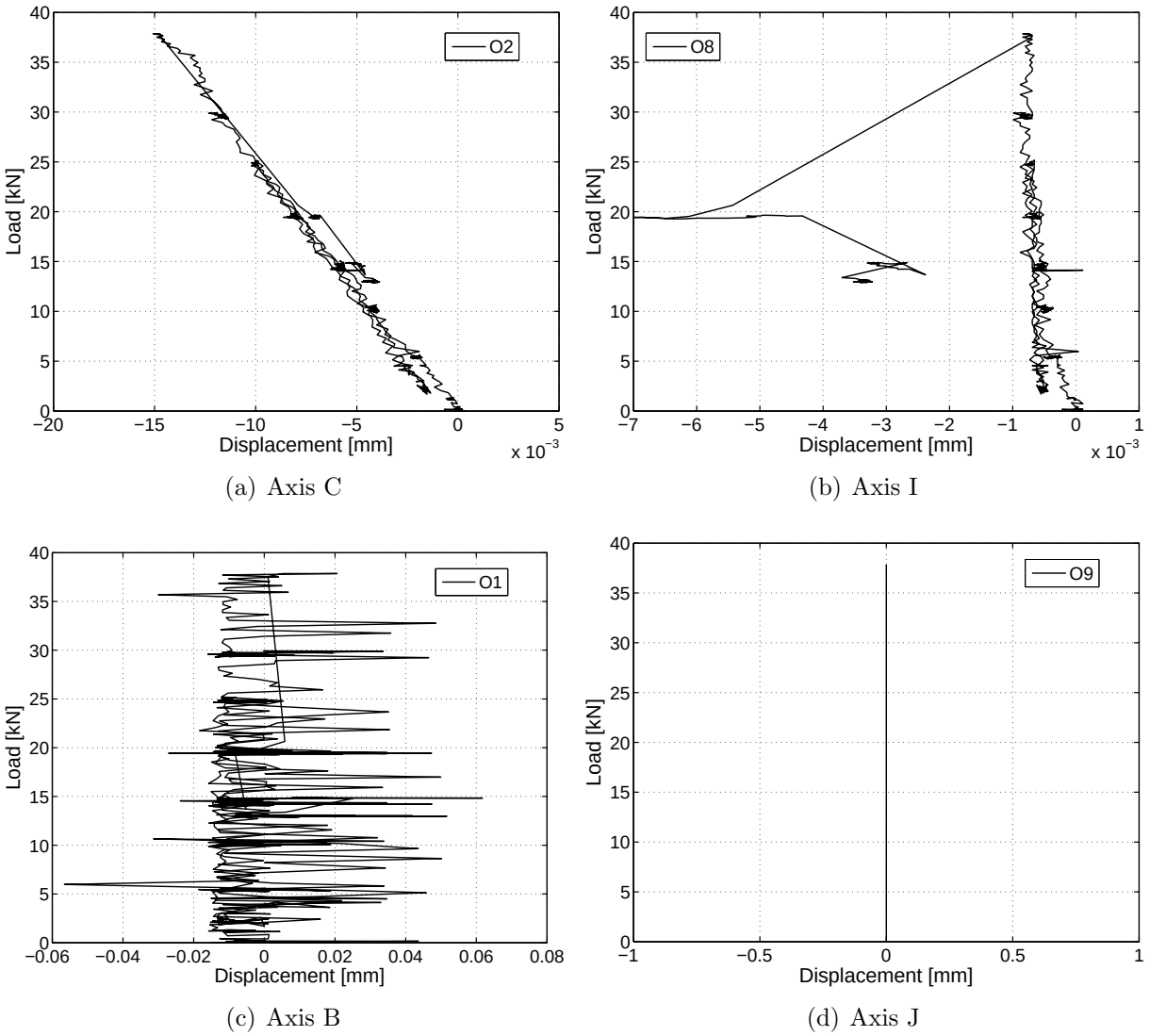

(a) Axis C

(b) Axis I

(c) Axis B

(d) Axis J

Figure C.159: 1000A: Deformations in omega-shaped extensometers - axes B,C,I,J.

C.5.3.4 Strain gages on GFRP profile

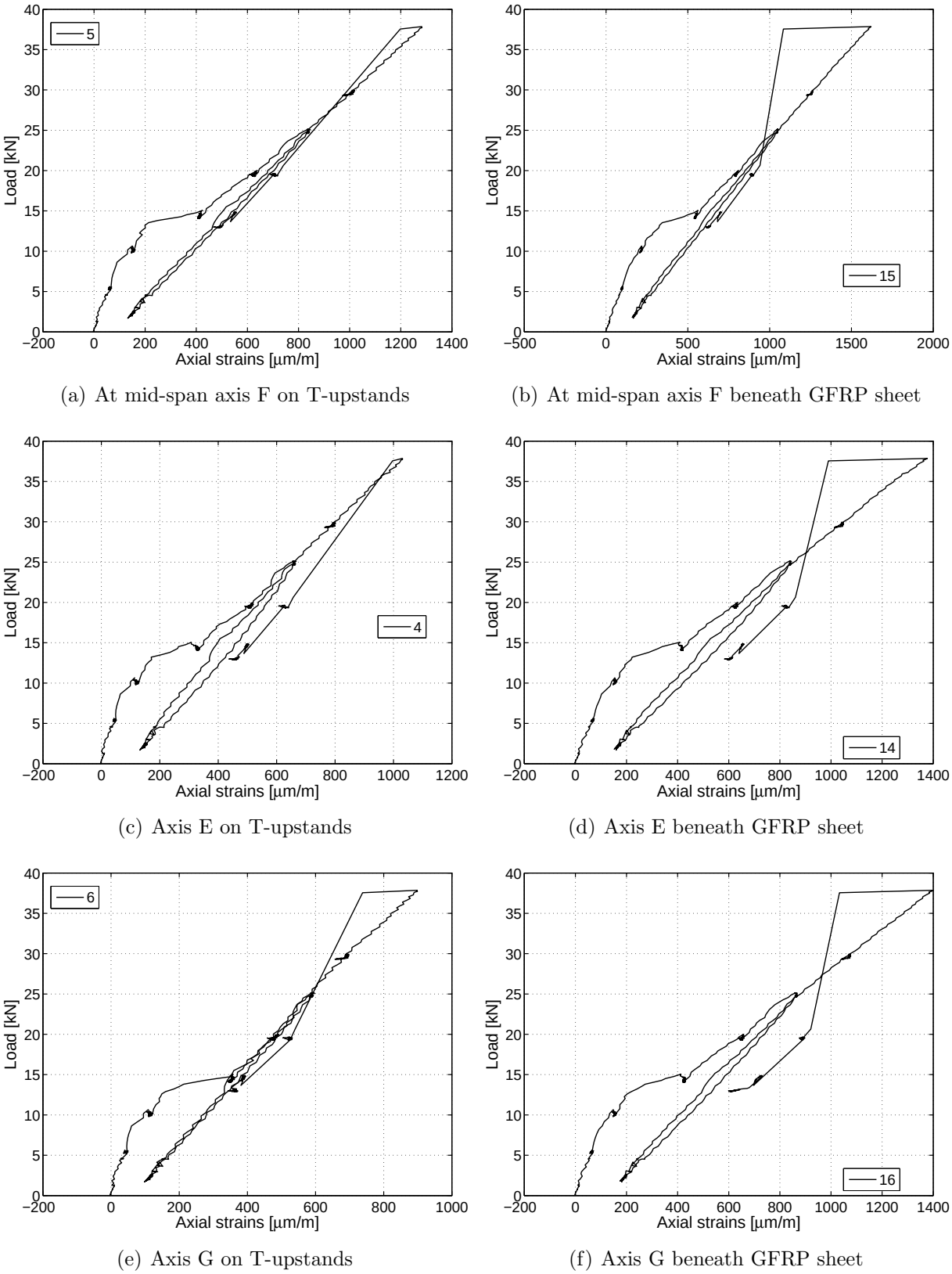

(a) At mid-span axis F on T-upstands

(b) At mid-span axis F beneath GFRP sheet

(c) Axis E on T-upstands

(d) Axis E beneath GFRP sheet

(e) Axis G on T-upstands

(f) Axis G beneath GFRP sheet

Figure C.160: 1000A: Axial strains in GFRP profile - axis E,F,G.

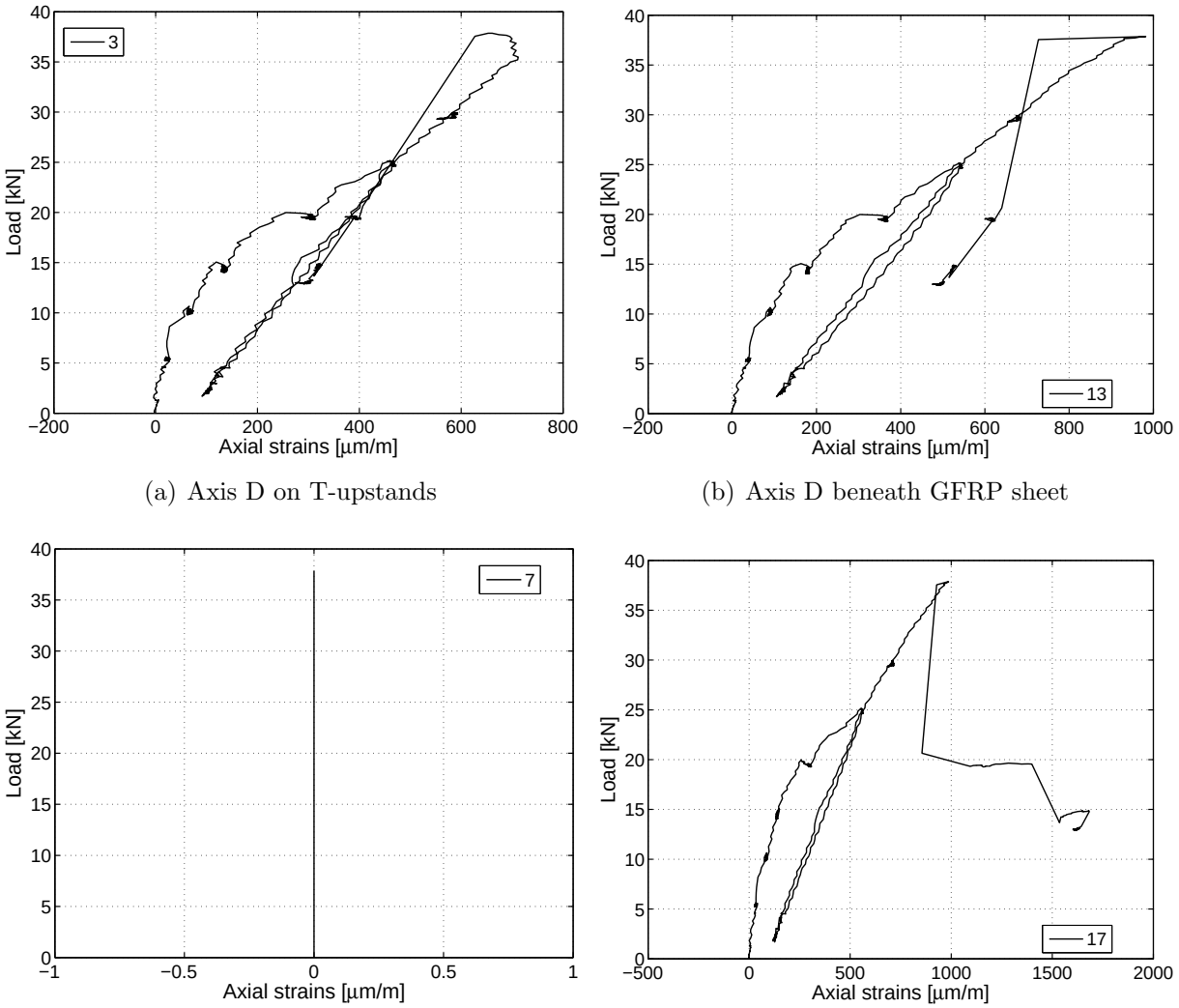

(a) Axis D on T-upstands

(b) Axis D beneath GFRP sheet

(c) Axis H on T-upstands

(d) Axis H beneath GFRP sheet

Figure C.161: 1000A: Axial strains in GFRP profile - axis D,H.

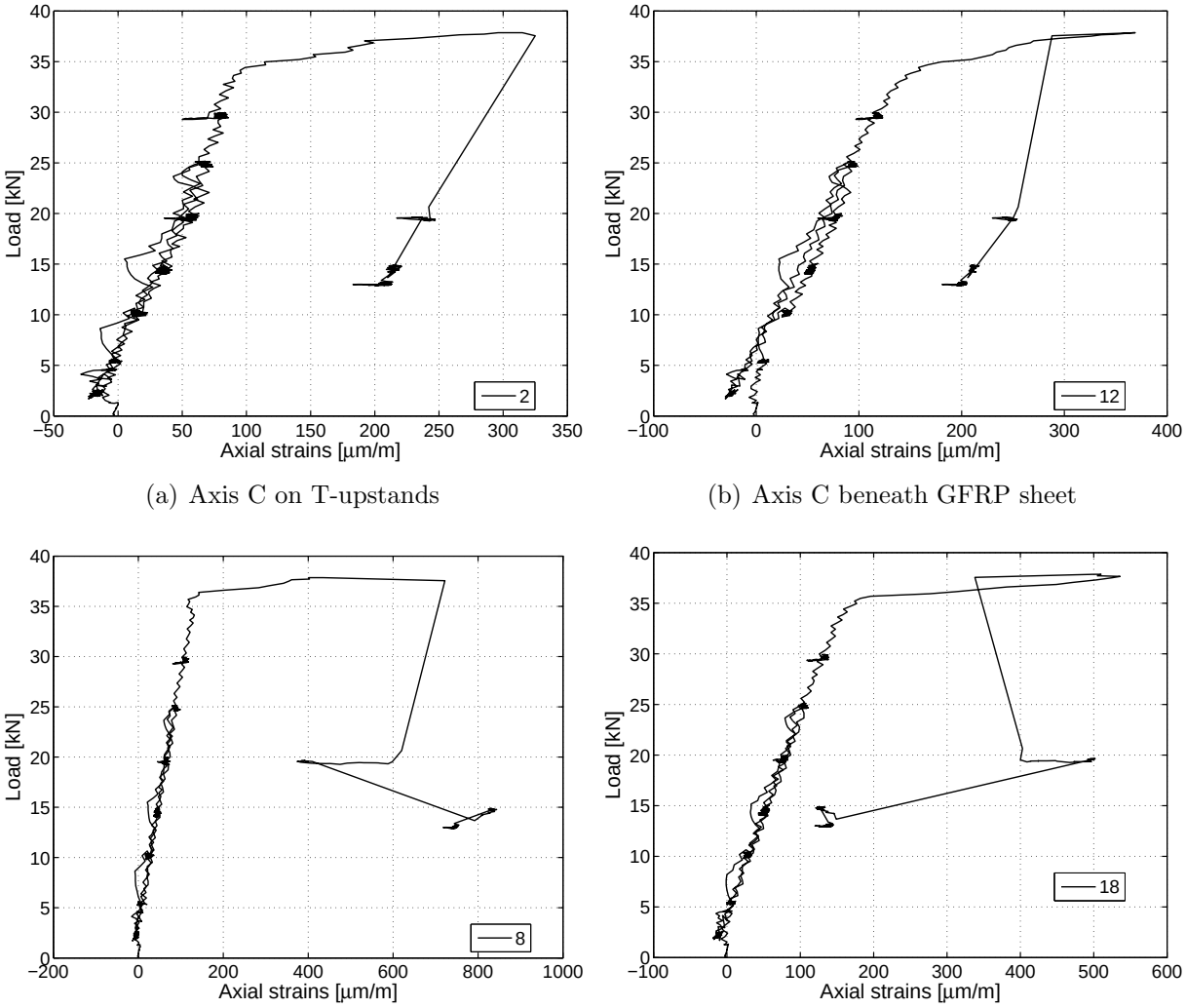

(a) Axis C on T-upstands

(b) Axis C beneath GFRP sheet

(c) Axis I on T-upstands

(d) Axis I beneath GFRP sheet

Figure C.162: 1000A: Axial strains in GFRP profile - axis C,I.

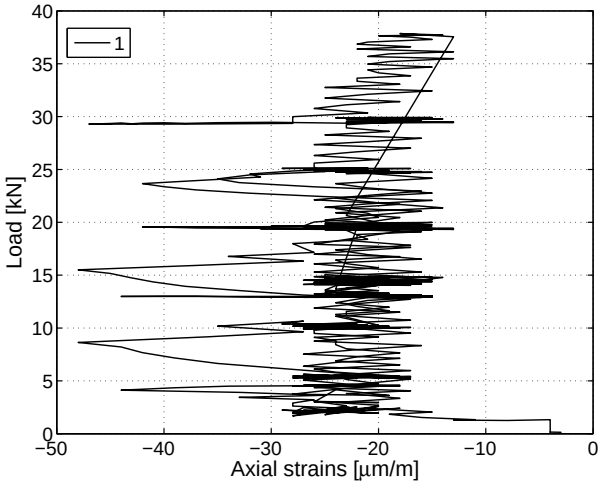

(a) Axis B on T-upstands

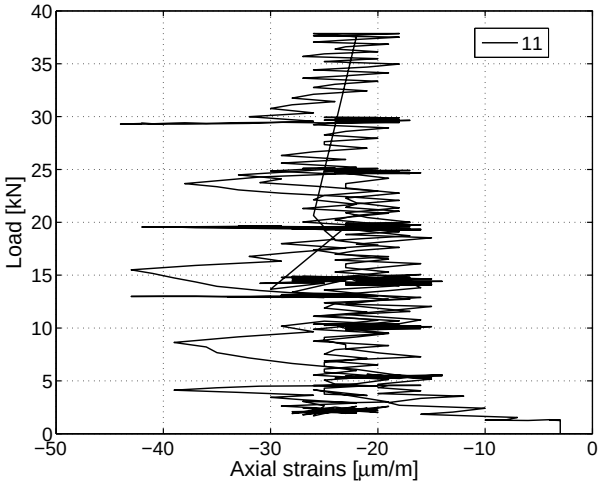

(b) Axis B beneath GFRP sheet

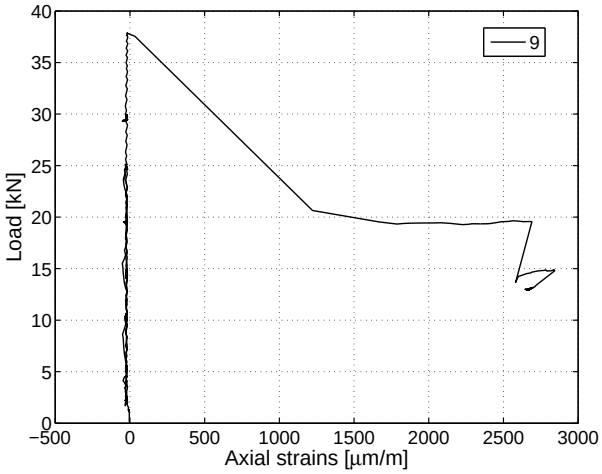

(c) Axis J on T-upstands

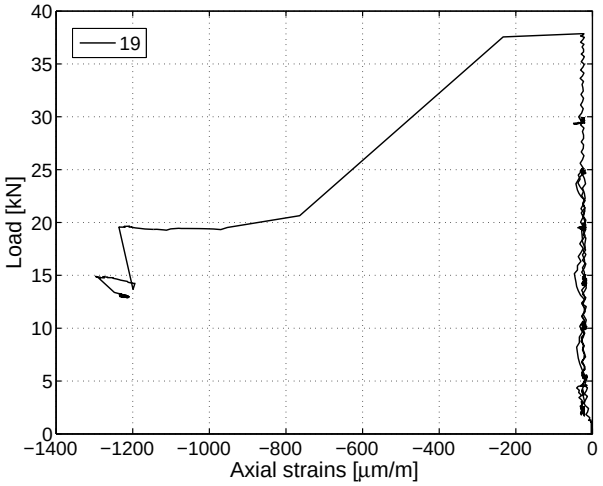

(d) Axis J beneath GFRP sheet

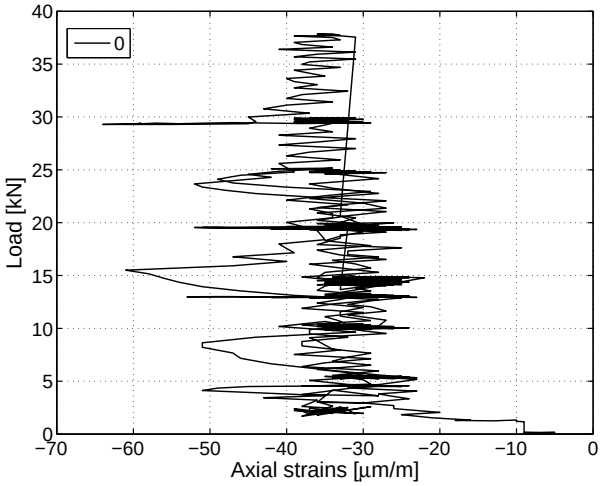

(e) Axis A on T-upstands

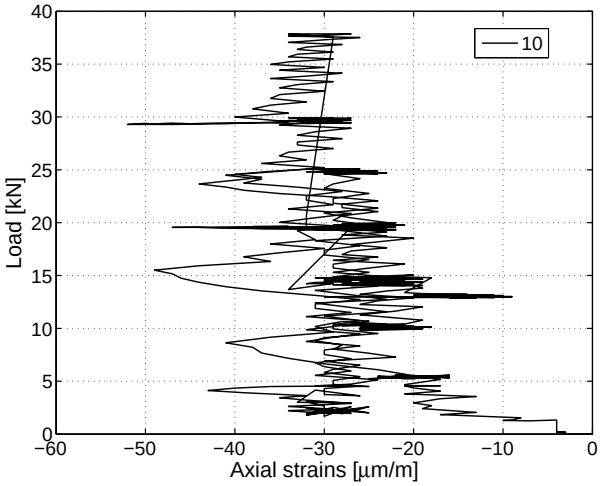

(f) Axis K on T-upstands

Figure C.163: 1000A: Axial strains in GFRP profile - axis A,B,J,K.

C.5.3.5 Axial strains along the beam at 5-kN load steps

The strains along the beam at different load steps are indicated in the following graphs. The measurement points are connected with lines, while the dashed lines represent the $5, 15$ and 25-kN load steps and the continuous lines the $10, 20$ and 30-kN load steps. The thickest line illustrates the strains at ultimate load.

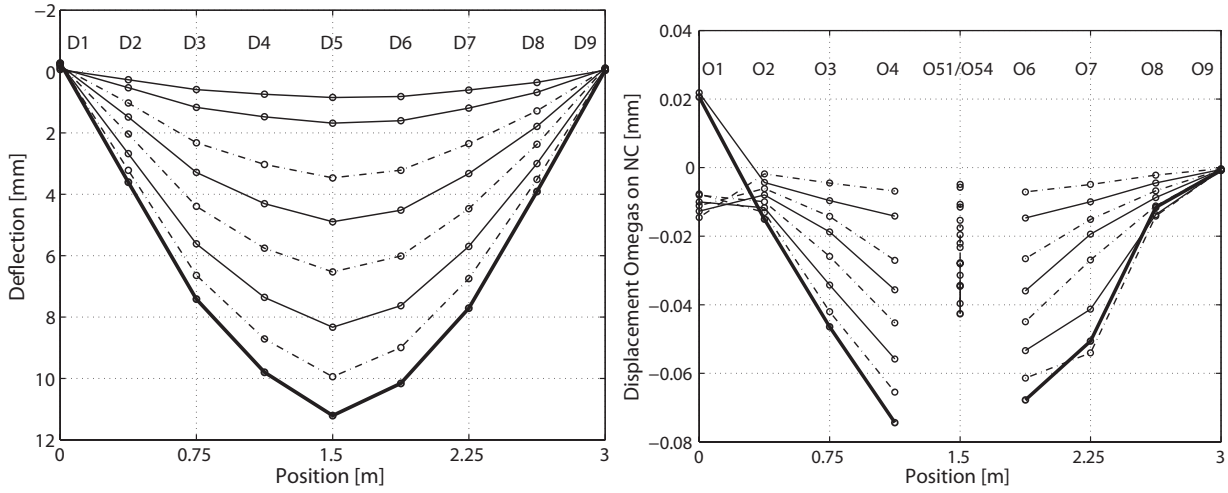

(a) Displacement along beam

(b) Omega-shaped extensometer on NC

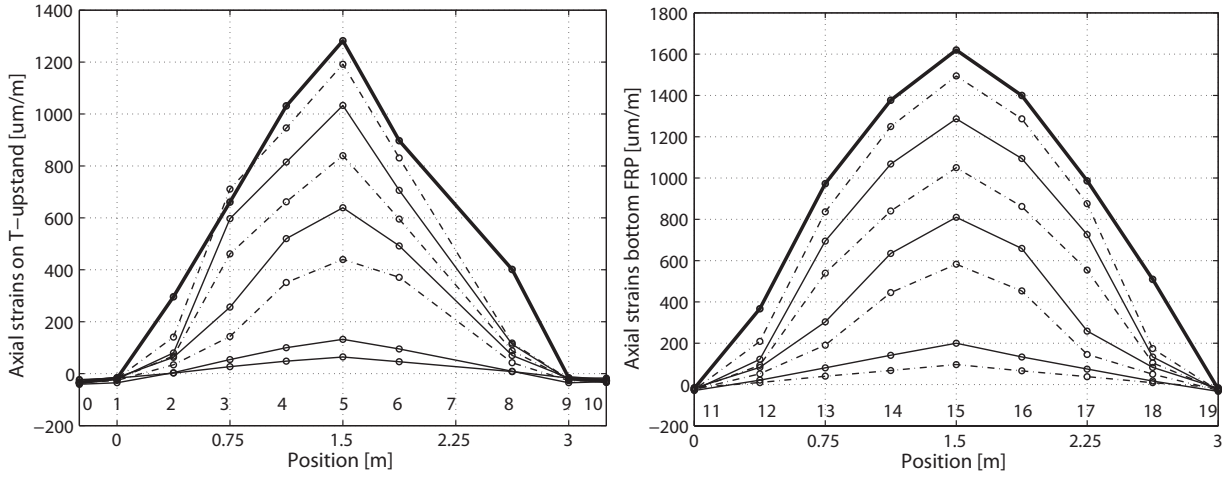

(c) Axial strains on T-upstand

(d) Axial strains beneath GFRP sheet

Figure C.164: 1000A: Displacement and strains along beam.

C.5.3.6 Axial strains through the cross section at 5-kN load steps

The strains through the cross section measured in the GFRP and on the concrete surface at different load steps are indicated in the following graphs. The measurement points are connected with lines, while the dashed lines represent the loads of 5 kN steps and the continuous lines the 10-kN steps. The thickest line illustrates the strains at ultimate load.

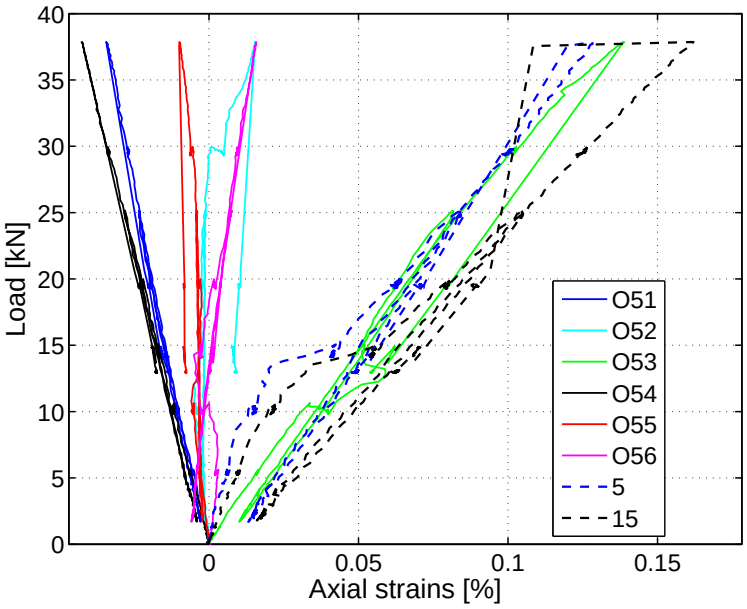

(a) Mid-span

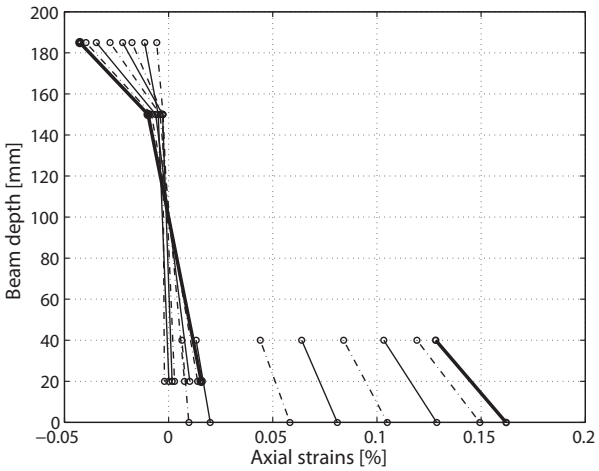

(b) Omegas at east side

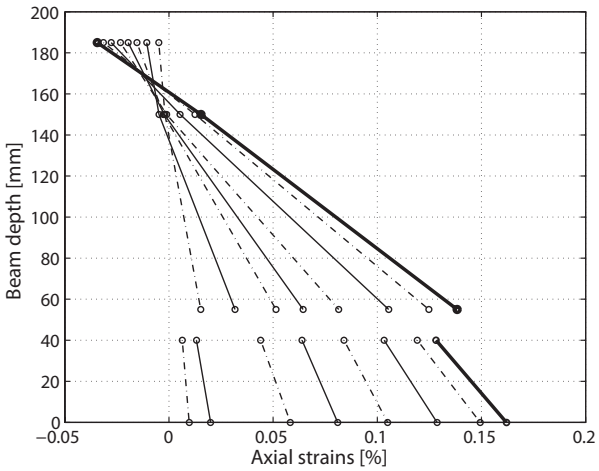

(c) Omegas at west side

Figure C.165: 1000A: Strain development through cross section at mid-span at different load steps from strain gages and omega-shaped extensometers.

C.5.4 Beam 1000EA: Failure description and measured results

C.5.4.1 Failure description

The failure process and crack pattern of the beam up to the end of the experiment are illustrated in Figures C.166, C.167 and C.168 and described in the following. As from 10 kN, the displacement of the jack was stopped every 5 kN in order to document the cracking process and take pictures. No second load cycle was performed.

It should be noted, that strain gage 11 was destroyed during the removal of the formwork.

The first four cracks were noticed at a load of 5.0 kN in the tension zone of the LC along the whole beam length. The cracks were vertically distributed with average lengths of 7 cm. Subsequently further cracks developed in between the existing cracks, one in the LC-NC interface at the northern anchor block. At a load of 15 kN the cracks had a spacing of between 10 and20 cm and openings of approximately 0.25-0.3 mm. The cracks were still predominately vertical with lengths of approximately 10 cm, with the exception of three cracks which were inclined in the southern direction. At a load of 20 kN the cracks in the northern part of the beam started to reach the NC layer. It could be noticed that these cracks were longer and more inclined than those in the southern part of the beam. The average crack spacing was approximately 13 cm. During further loading horizontal cracks could be observed in the southern part of the beam in the mid-depth of the LC layer and the LC-NC interface. The crack pattern at 30 kN was more dense with an average spacing of 8-9 cm. The crack width now reached 0.4 mm.

At a load of 34 kN loud cracks occurred in the southern part of the beam. At 37.2 kN the beam failed when a crack suddenly propagated through the depth of the LC on the southern side. This crack was inclined and developed further along the LC-NC interface on one side and along the top of the FRP T-upstands on the other side, just above the FRP-LC interface, up to the anchor block. The load dropped to a value of 17 kN and the experiment was stopped. The anchor blocks remained undamaged, and no slippage at the beam ends was measured.

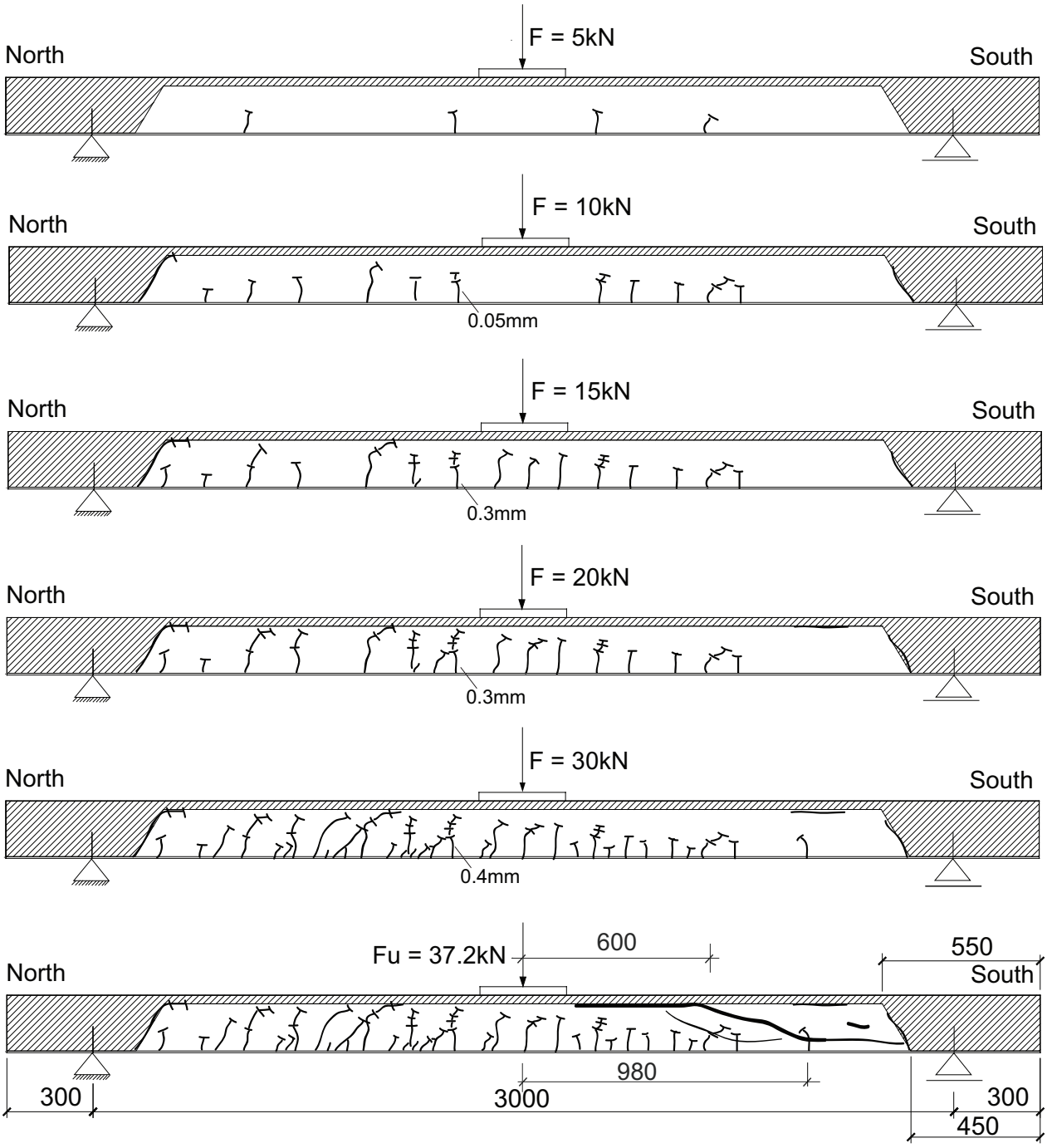

Figure C.166: 1000EA: Failure process.

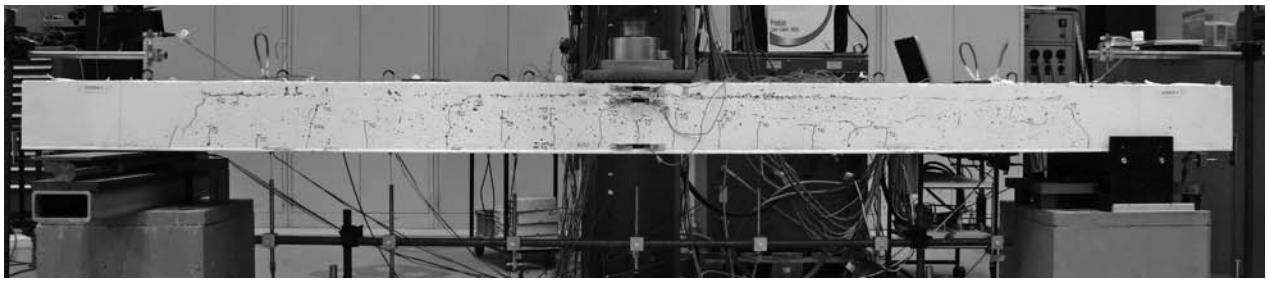

(a) Crack pattern at 15.0 kN

(b) Crack pattern at 30.0 kN

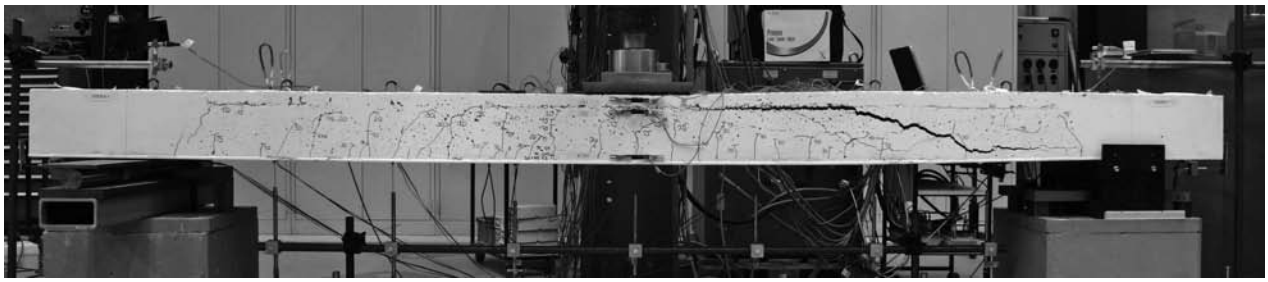

(c) Crack pattern at ultimate load

Figure C.167: 1000EA: Failure process.

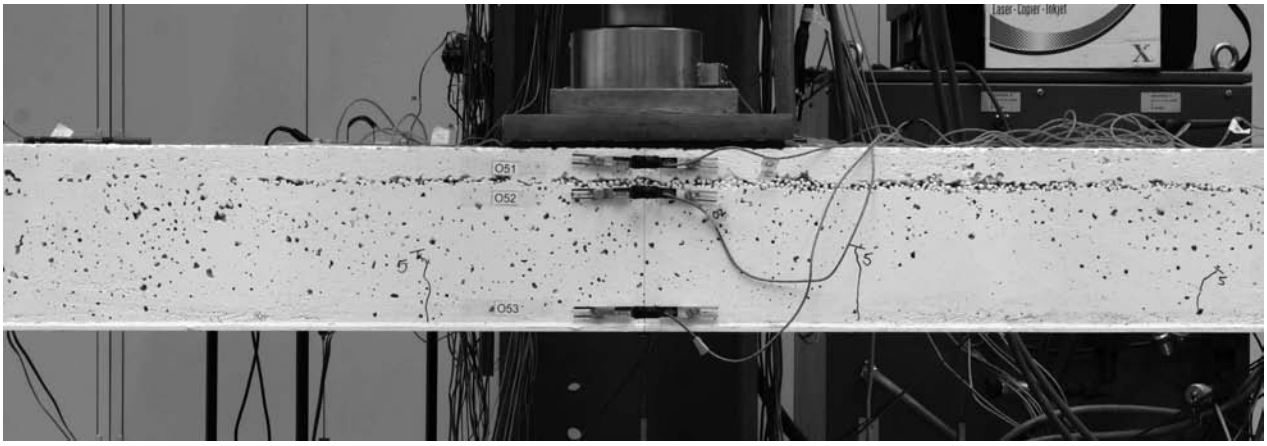

(a) Crack pattern at 5.0 kN

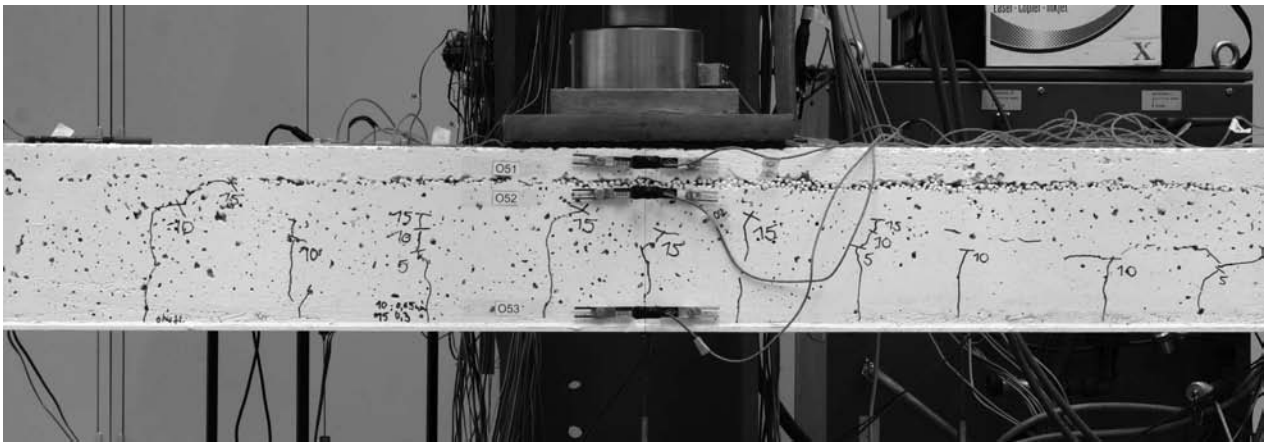

(b) Crack pattern at 15.0 kN

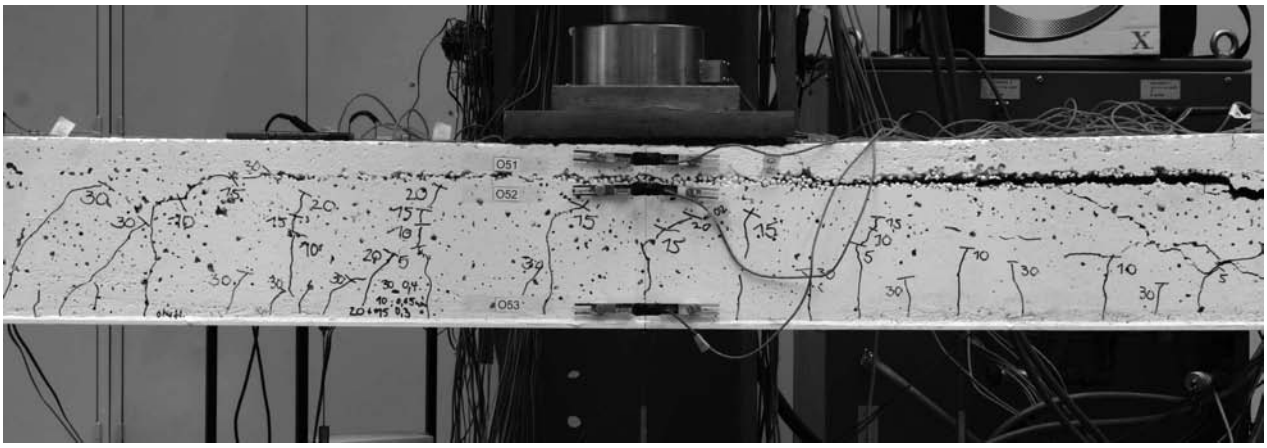

(c) Crack pattern at ultimate load

Figure C.168: 1000EA: Crack pattern next to loading plate.

C.5.4.2 Displacement transducers

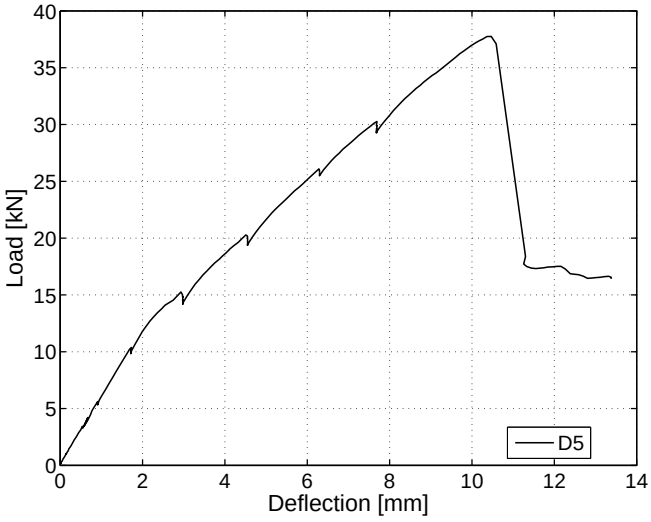

(a) At mid-span axis F

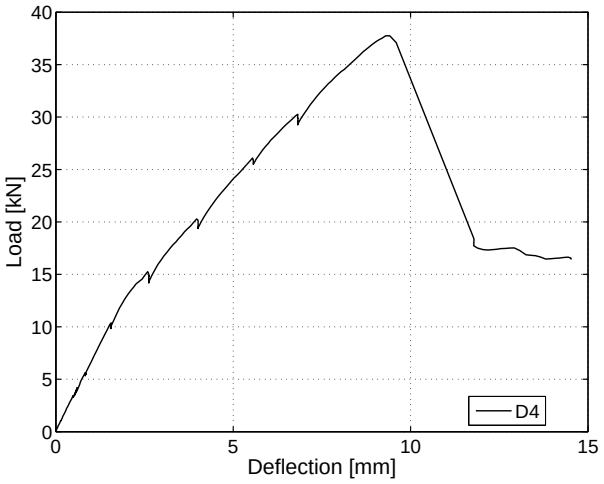

(b) Axis E

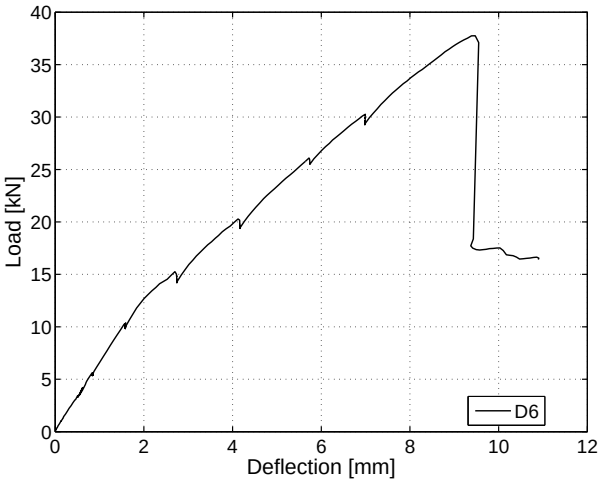

(c) Axis G

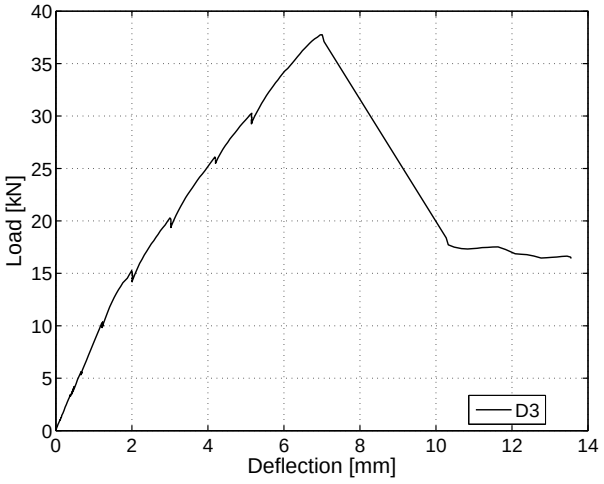

(d) Axis D

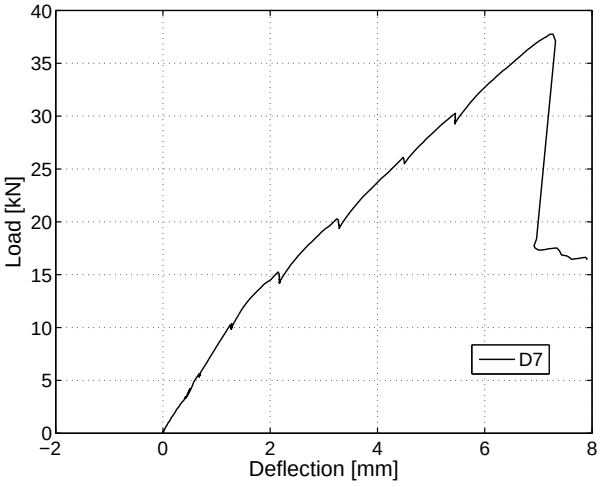

(e) Axis H

Figure C.169: 1000EA: Displacement at axes D,E,G,H.

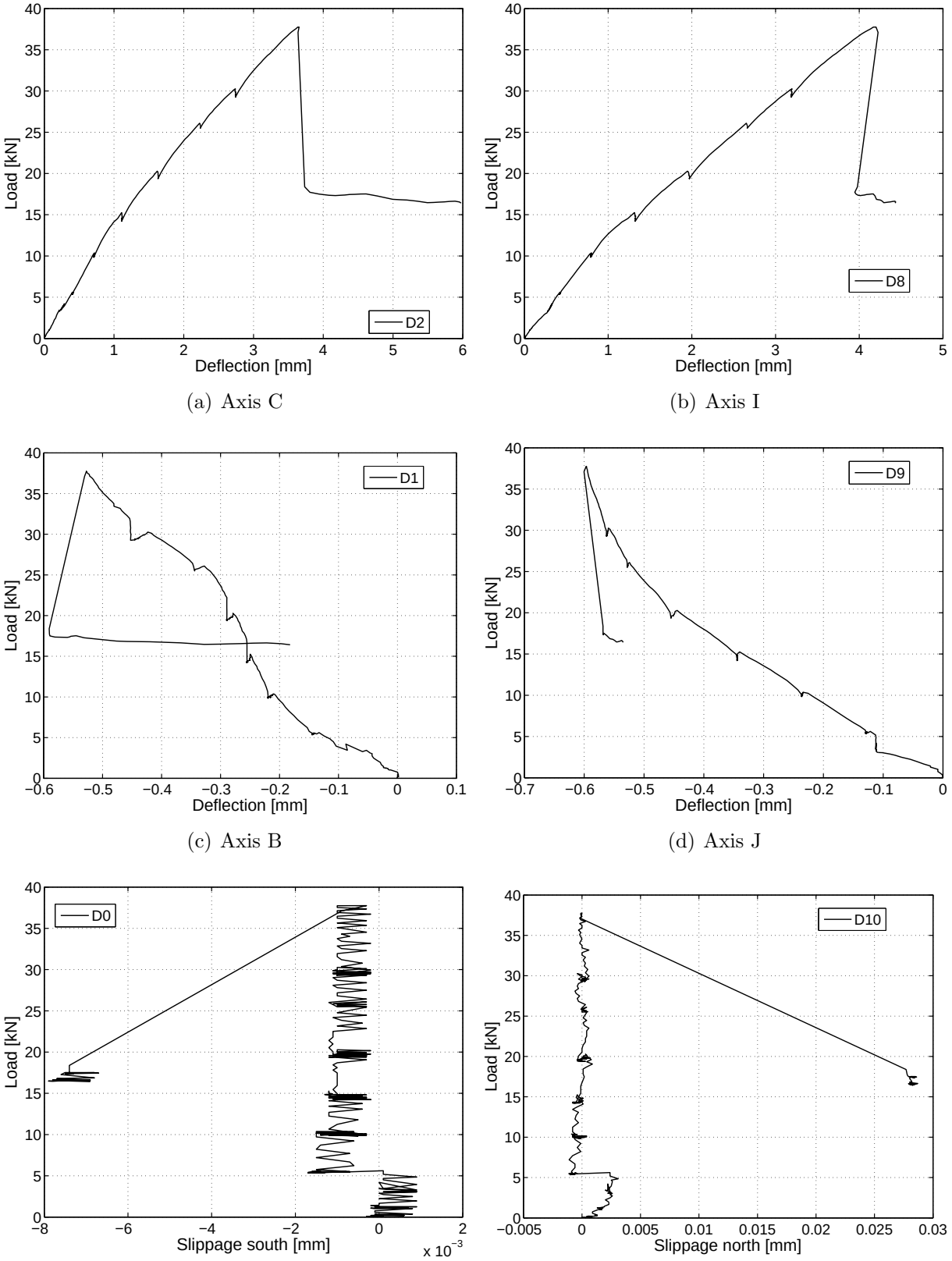

(a) Axis C

(b) Axis I

(c) Axis B

(d) Axis J

(e) Slippage axis A - south

(f) Slippage axis K - north

Figure C.170: 1000EA: Displacement at axes B,C,I,J and slippage at beam ends.

C.5.4.3 Omega-shaped extensometer

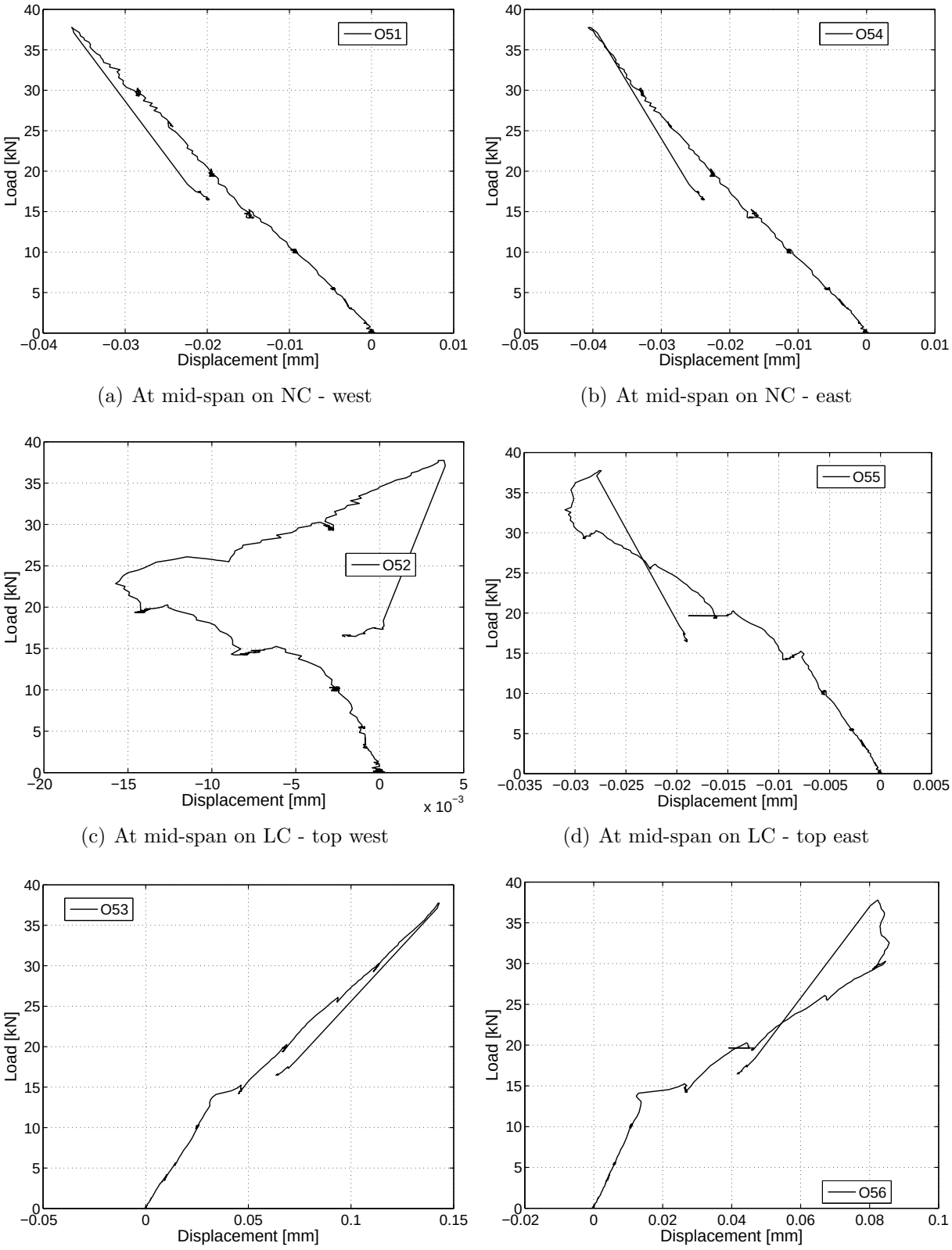

(a) At mid-span on NC - west

(b) At mid-span on NC - east

(c) At mid-span on LC - top west

(d) At mid-span on LC - top east

(e) At mid-span on LC - bottom west

(f) At mid-span on LC - bottom east

Figure C.171: 1000EA: Deformations in omega-shaped extensometers at mid-span.

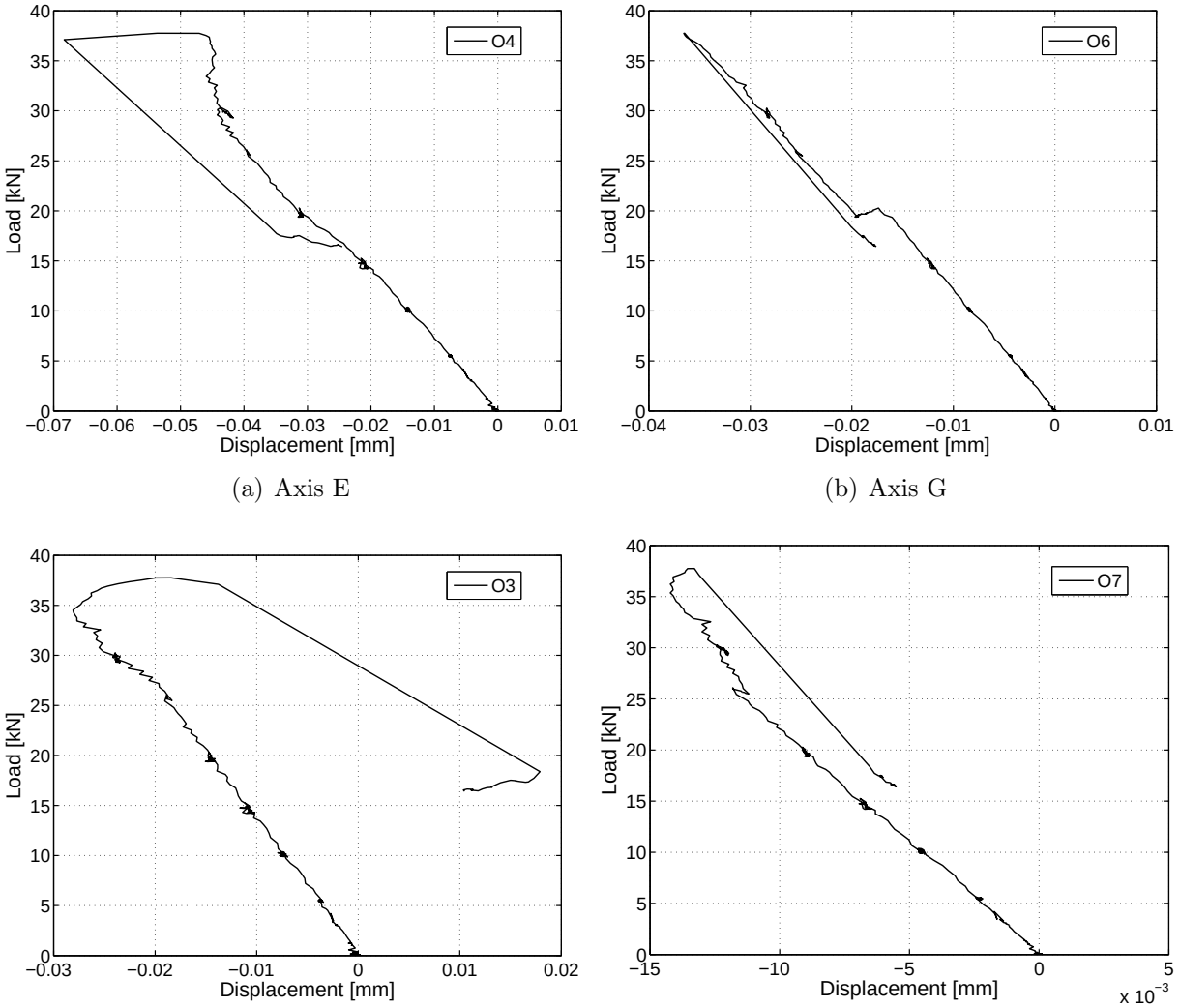

(a) Axis E

(b) Axis G

(c) Axis D

(d) Axis H

Figure C.172: 1000EA: Deformations in omega-shaped extensometers - axes D,E,G,H.

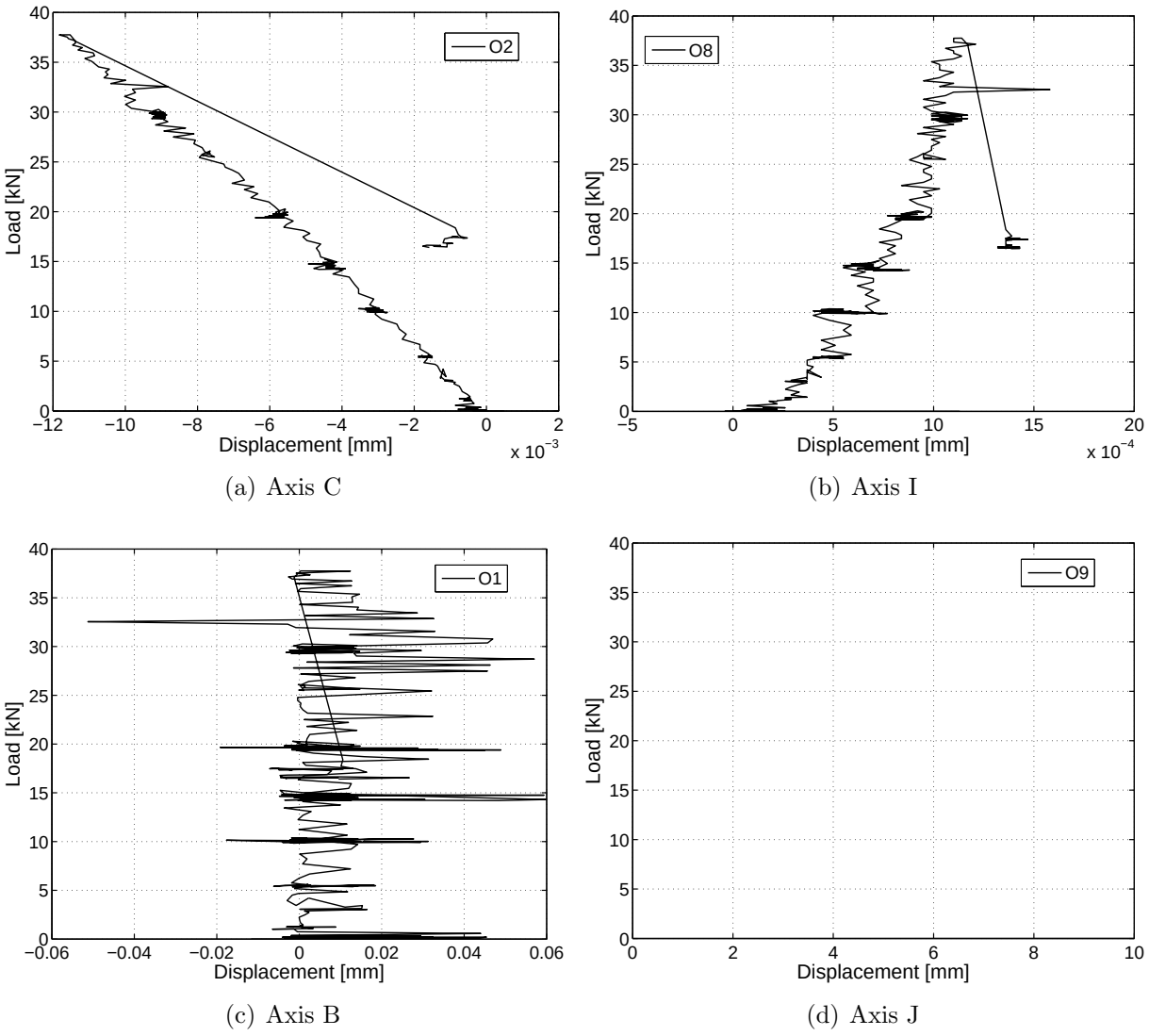

(a) Axis C

(b) Axis I

(c) Axis B

(d) Axis J

Figure C.173: 1000EA: Deformations in omega-shaped extensometers - axes B,C,I,J.

C.5.4.4 Strain gages on GFRP profile

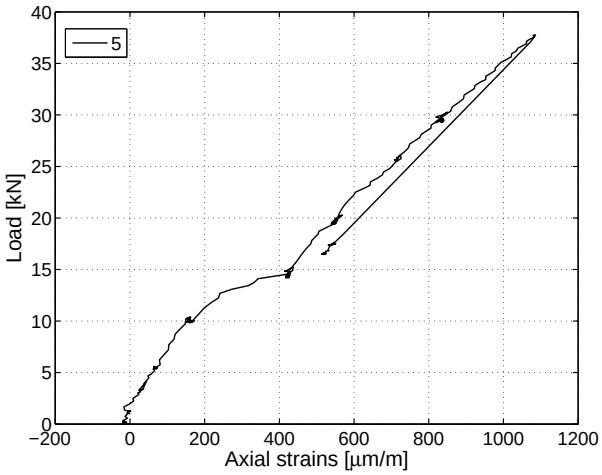

(a) At mid-span axis F on T-upstands

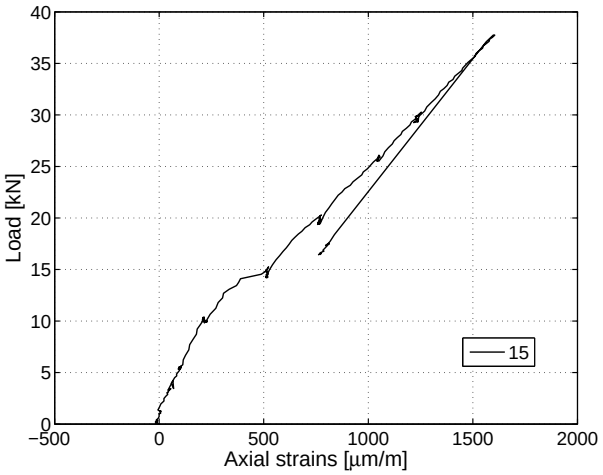

(b) At mid-span axis F beneath GFRP sheet

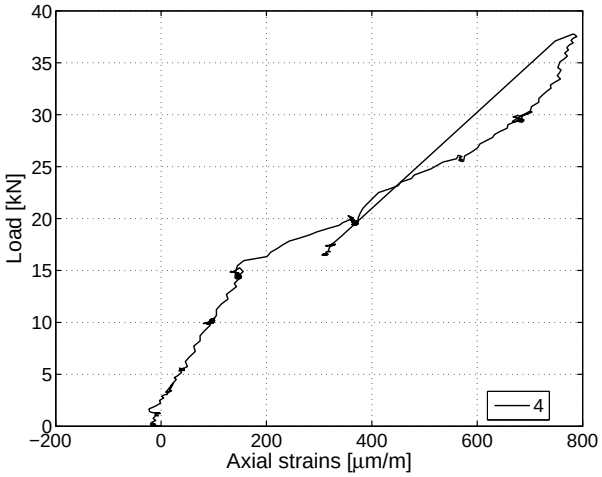

(c) Axis E on T-upstands

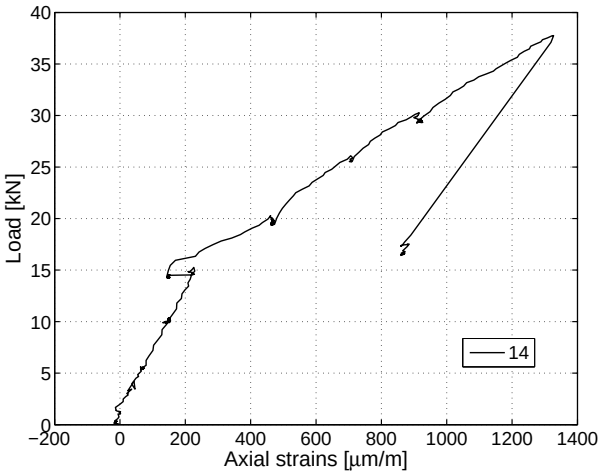

(d) Axis E beneath GFRP sheet

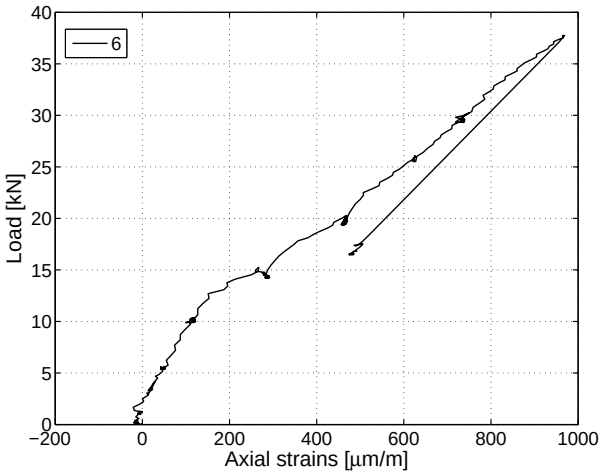

(e) Axis G on T-upstands

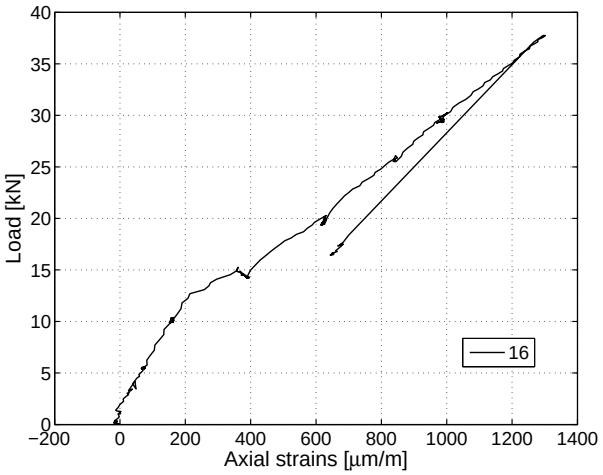

(f) Axis G beneath GFRP sheet

Figure C.174: 1000EA: Axial strains in GFRP profile - axis E,F,G.

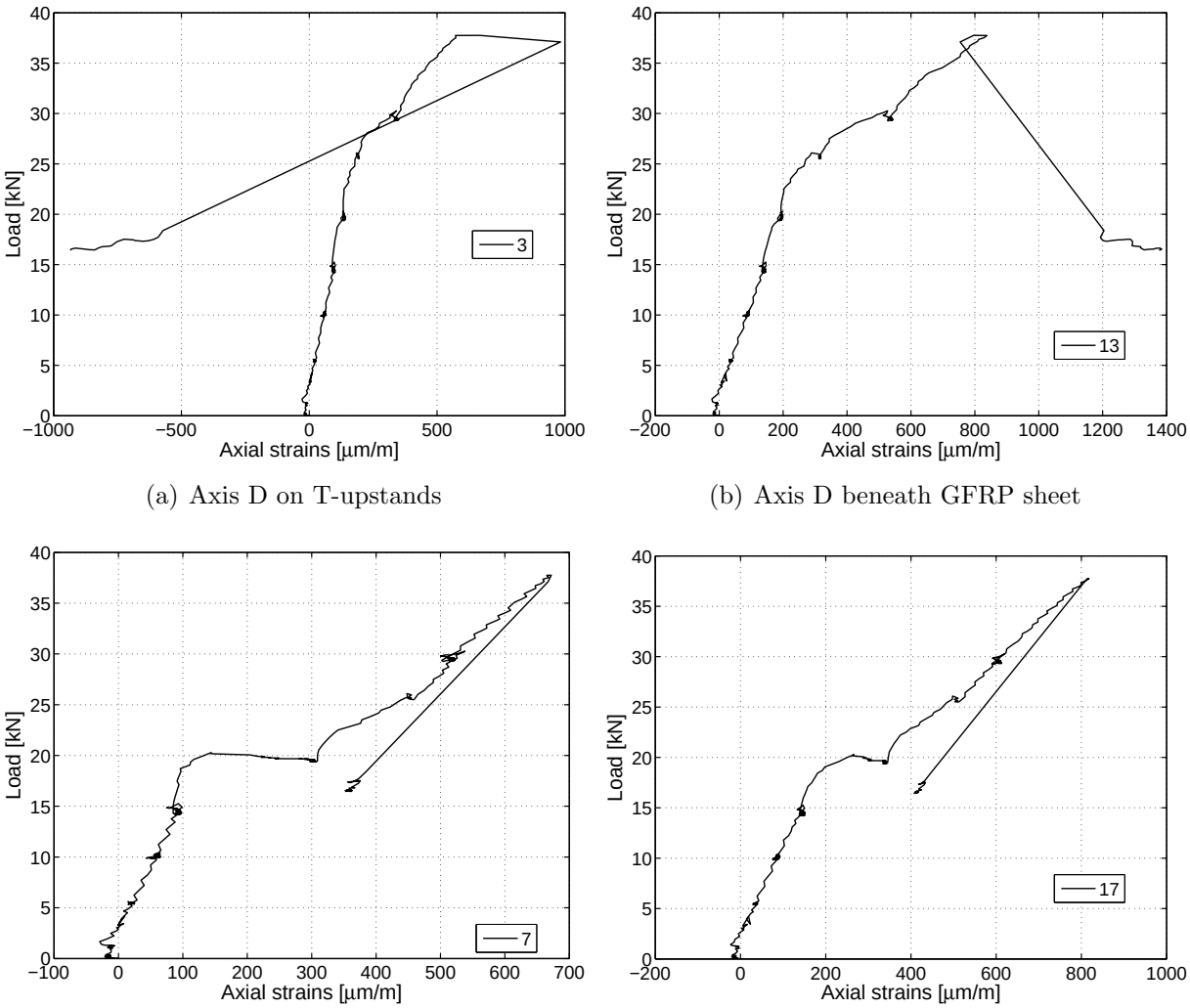

(a) Axis D on T-upstands

(b) Axis D beneath GFRP sheet

(c) Axis H on T-upstands

(d) Axis H beneath GFRP sheet

Figure C.175: 1000EA: Axial strains in GFRP profile - axis D,H.

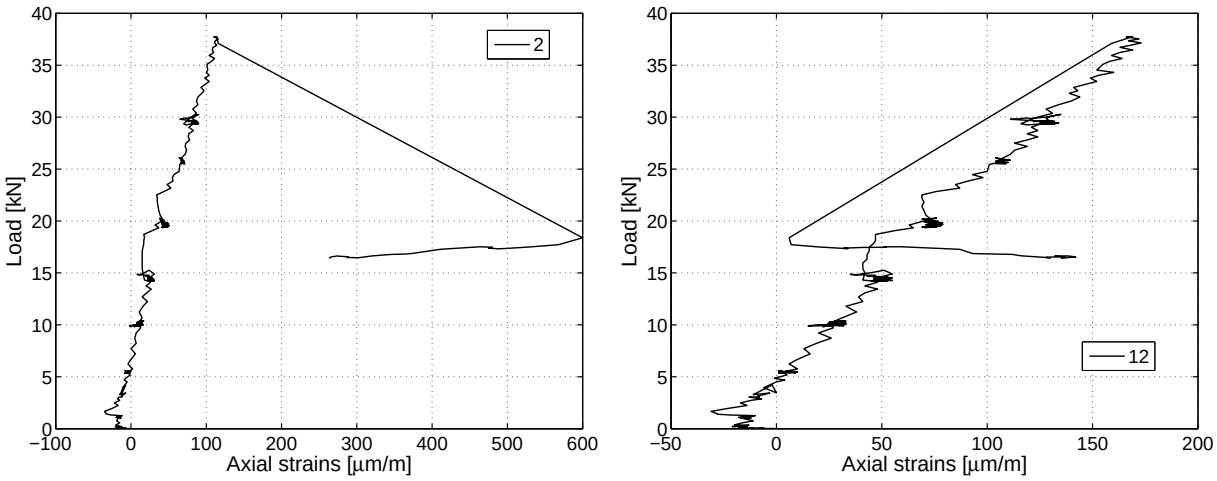

(a) Axis C on T-upstands

(b) Axis C beneath GFRP sheet

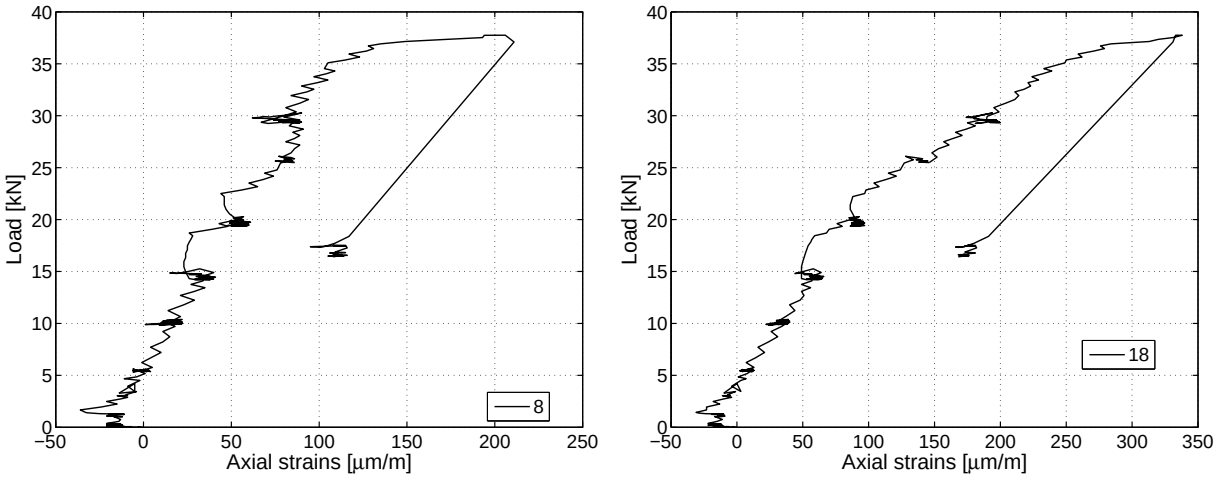

(c) Axis I on T-upstands

(d) Axis I beneath GFRP sheet

Figure C.176: 1000EA: Axial strains in GFRP profile - axis C,I.

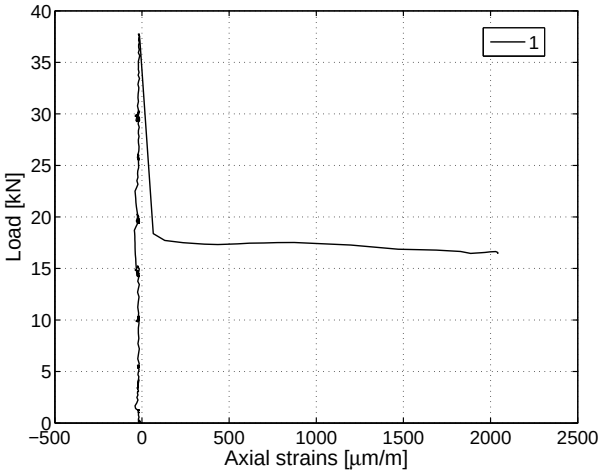

(a) Axis B on T-upstands

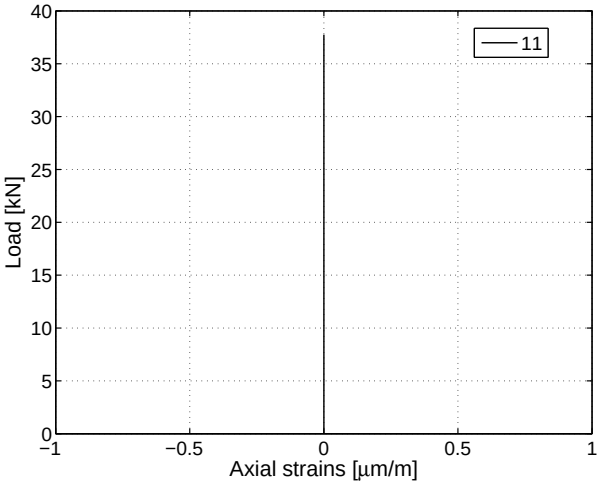

(b) Axis B beneath GFRP sheet

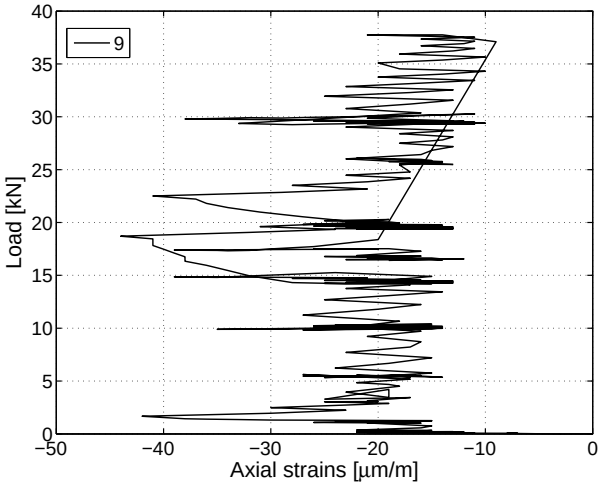

(c) Axis J on T-upstands

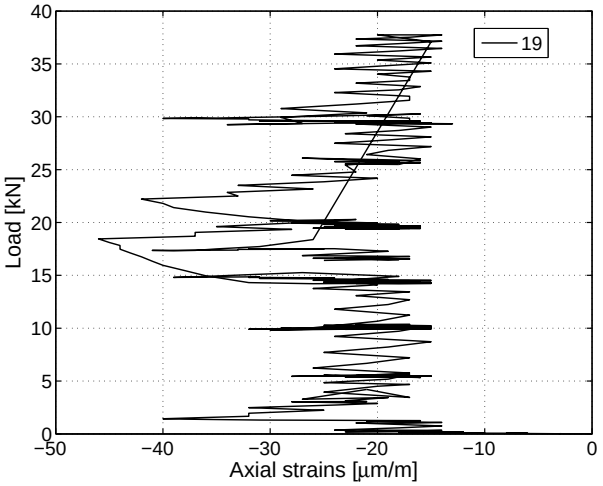

(d) Axis J beneath GFRP sheet

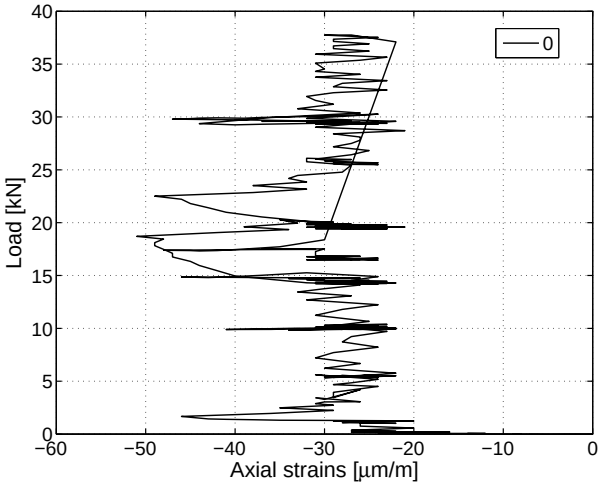

(e) Axis A on T-upstands

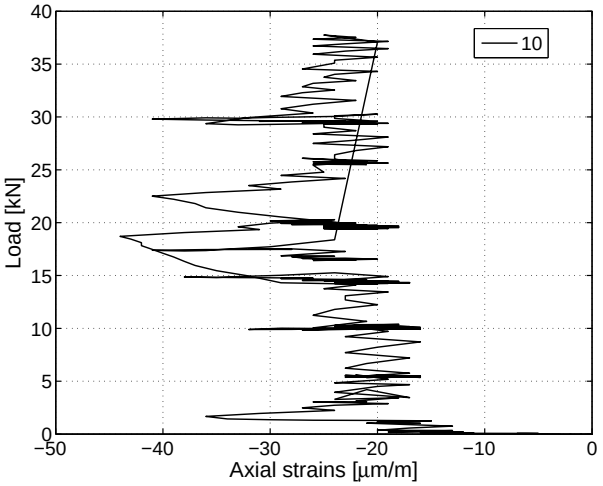

(f) Axis K on T-upstands

Figure C.177: 1000EA: Axial strains in GFRP profile - axis A,B,J,K.

C.5.4.5 Axial strains along the beam at 5-kN load steps

The strains along the beam at different load steps are indicated in the following graphs. The measurement points are connected with lines, while the dashed lines represent the $5, 15$ and 25-kN load steps and the continuous lines the $10, 20$ and 30-kN load steps. The thickest line illustrates the strains at ultimate load.

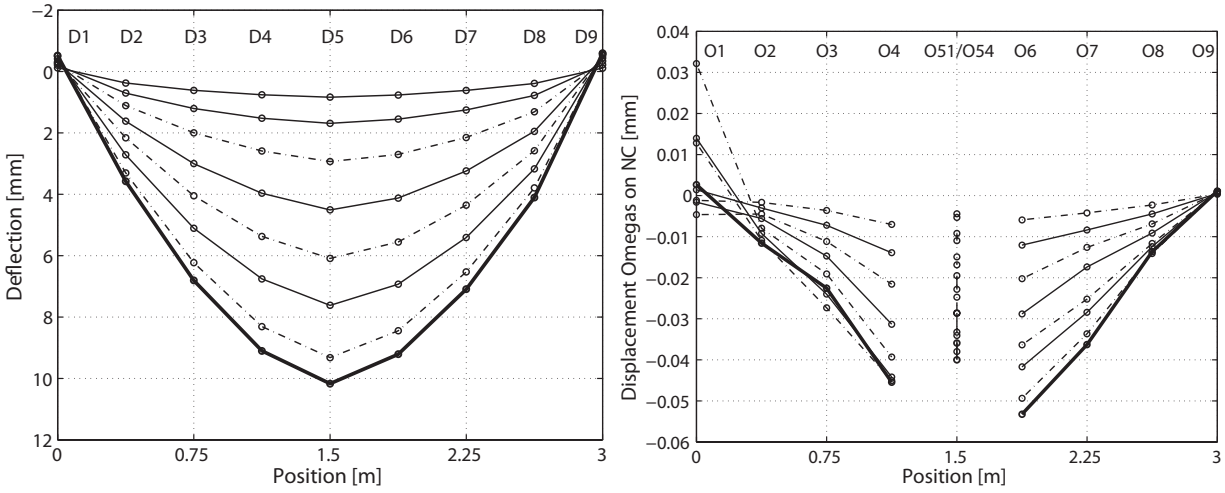

(a) Displacement along beam

(b) Omega-shaped extensometer on NC

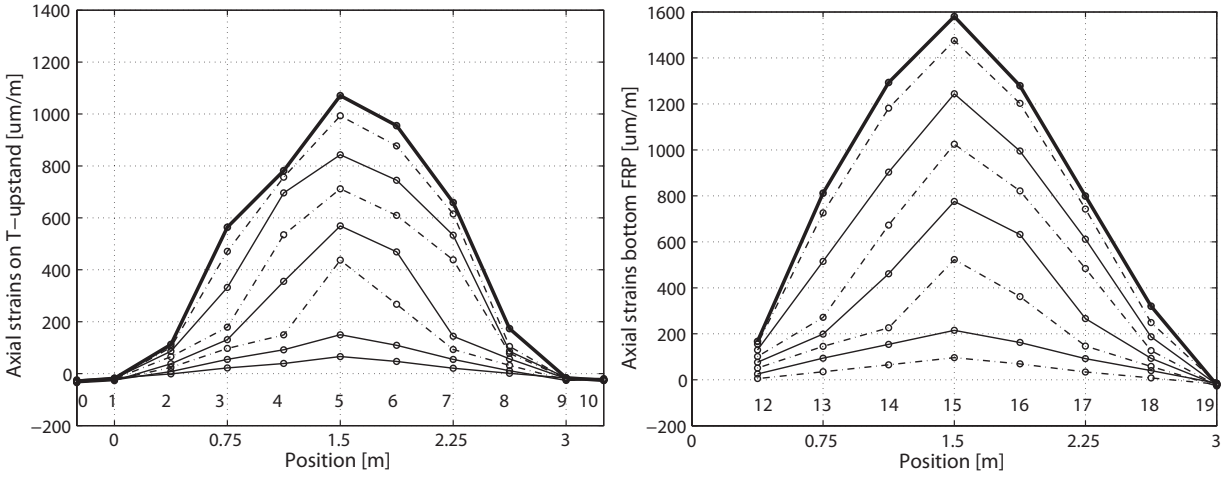

(c) Axial strains on T-upstand

(d) Axial strains beneath GFRP sheet

Figure C.178: 1000EA: Displacement and strains along beam.

C.5.4.6 Axial strains through the cross section at 5-kN load steps

The strains through the cross section measured in the GFRP and on the concrete surface at different load steps are indicated in the following graphs. The measurement points are connected with lines, while the dashed lines represent the loads of 5 kN steps and the continuous lines the 10-kN steps. The thickest line illustrates the strains at ultimate load.

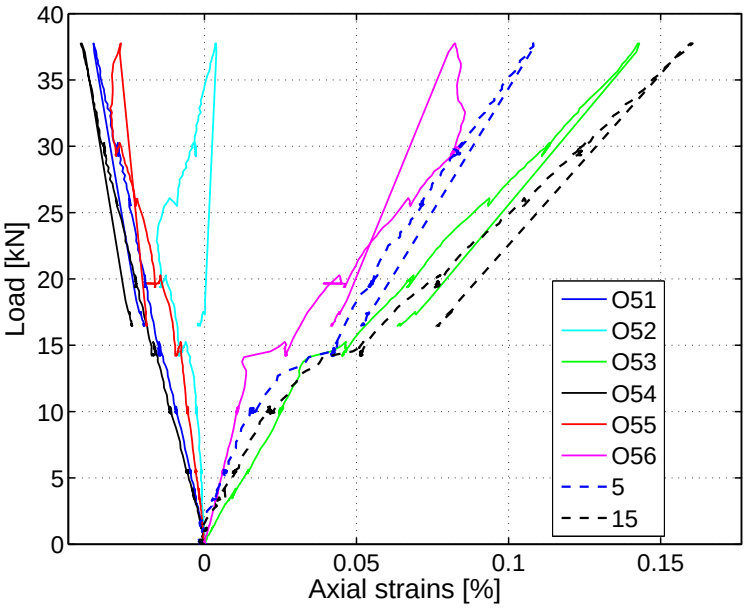

(a) Mid-span

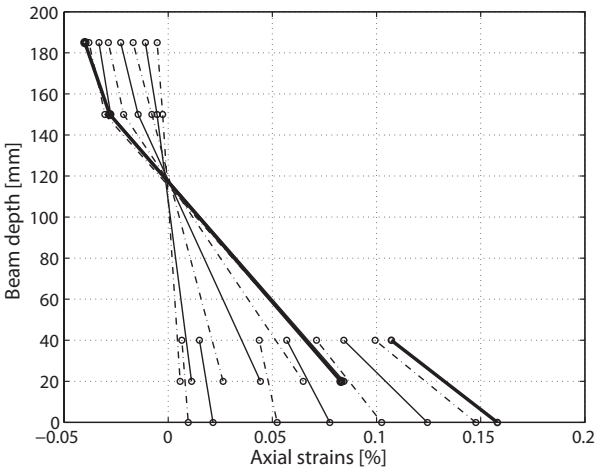

(b) Omegas at east side

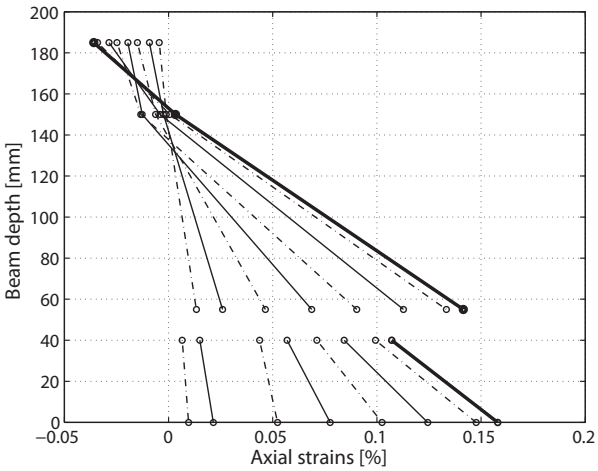

(c) Omegas at west side

Figure C.179: 1000EA: Strain development through cross section at mid-span at different load steps from strain gages and omega-shaped extensometers.

C.6 Summary of main results

The main results of the long-span beam series S1 and S2 are shown in the following tables.

Table C.2: Experimental results at ultimate load for SLWAC beams - S1 (negative signs = compression).

Beam	Ultimate load [kN]	Cracking load [kN]	Mid-span deflection [mm]	Axial stress NC [MPa]	LC [MPa]	FRP [MPa]
900-1	9.3	∼6.5	11.5-17.3	-3.3	-0.8	11.8
900-2	11.5	∼7.5	9.4	-3.7	0.0	12.6
1300-1	32.1	∼9.5	47.8	-10.0	0.3	30.5
1300-2	23.3	∼10.0	40.4	-9.0	0.2	30.2
900E-1	31.2	∼10.5	8.7	-9.9	-1.7	49.5
900E-2	30.4	∼11.5	8.1	-8.4	-1.8	35.7
1300E-1	42.8	∼13.0	12.3	-15.6	-2.5	42.6
1300E-2	50.5	∼12.5	14.1	-15.6	1.7	47.8

Table C.3: Experimental results at ultimate load for ALWAC beams - S2 (negative signs = compression).

Beam	Ultimate load [kN]	Cracking load [kN]	Mid-span deflection [mm]	Axial stress NC [MPa]	LC [MPa]	FRP [MPa]
1000	35.0	∼9.0	11.5	-11.7	1.3	38.7
1000E	39.2	∼8.0	9.9	-11.5	1.1	38.6
1000A	37.6	∼5.0	11.4	-10.4	0.2	37.3
1000EA	37.1	∼5.0	10.6	-10.2	-0.8	36.0

Appendix D

Experiments on short-span beams on DVD

D.1 Introduction

D.1.1 Objectives

The main purpose of this S3 experimental series was to investigate the structural behavior of the hybrid beam specimens described in Appendix C under direct load transmission behavior. The undamaged sides of the tested hybrid beams were cut to 1.2-m-long specimens and experimentally investigated under three point-bending with a span of 600 mm, representing a shear span-to-depth ratio of $a/d = 1.6$, where a is the distance from the load axis to the support axis, and d the effective depth of the slab. For details concerning the material properties see Appendix B.

D.1.2 Experimental Program

The experimental program consisted of eight specimens summarized in the following table:

Table D.1: Experimental configuration of short-span specimens.

Specimen	LC type	GFRP-LC Interface	Experiment date
900Es-1	LC900	epoxy-bonded	14.11.2006
900Es-2	LC900	epoxy-bonded	16.11.2006
1300Es-1	LC1300	epoxy-bonded	13.11.2006
1300Es-2	LC1300	epoxy-bonded	22.11.2006
1300s-1	LC1300	unbonded	23.11.2006
1300s-2	LC1300	unbonded	14.11.2006
1000s	LC1000	unbonded	26.10.2006
1000Es	LC1000	epoxy-bonded	09.11.2006

D.2 Experimental procedure

D.2.1 Test setup and loading equipment

All specimens were simply supported on rollers with a span length of 0.6 m and subjected to three-point bending via one hydraulic jack. Its capacity was 1000 kN in static loading with a possible Displacement range of up to ± 125 mm. The load was applied at mid-span through a 150 x 400 x 25 mm^3 loading plate. The width of the support plates was 100 mm. The experimental setup and specimen geometries are shown in Figure D.1. The experiments were conducted in a laboratory environment at room temperature (∼20°C) without any impact of temperature changes or moisture.

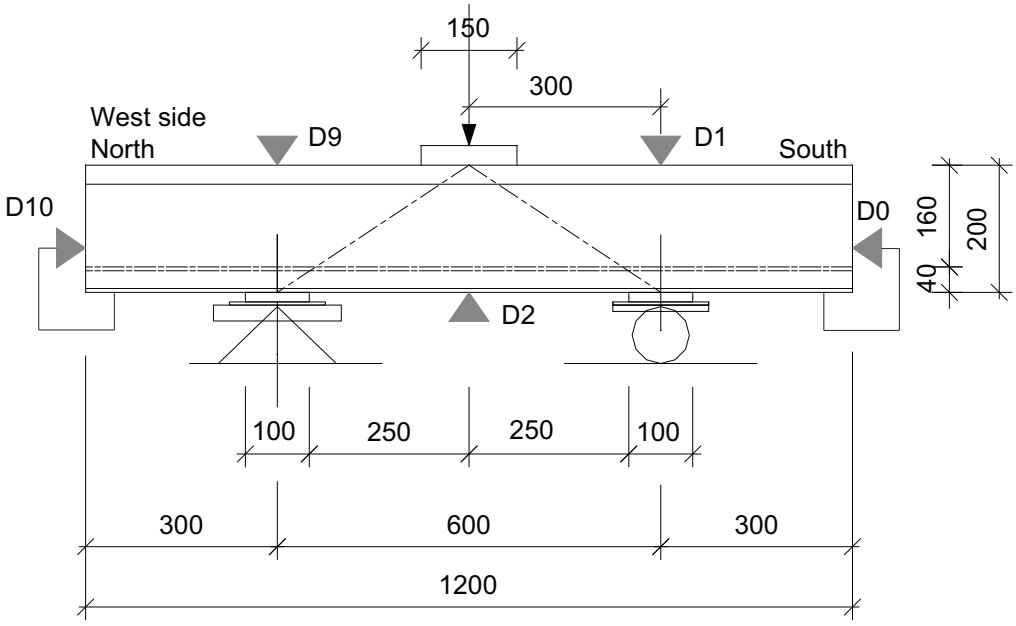

Figure D.1: Overview of setup and part of instrumentation (displacement transducer).

D.2.2 Instrumentation

All tests were performed with automated measurements every 9-10 s. The data acquisition unit was an HBM (Hottinger Baldwin Messtechnik GmbH, Germany) UPM 100 with 100 channels.

The recorded data were as follows: the load of the jack using three load cells, the displacement at several sections of the beam using displacement transducers, axial strains in the GFRP section measured with strain gages, deformation on the LC and NC surfaces using omega-shaped extensometers, and measurement of the displacement of points defined by a dense grid on half of the specimen using photogrammetry.

Figures D.1 and D.2 illustrate the positions and labeling of the instrumentation of the specimens.

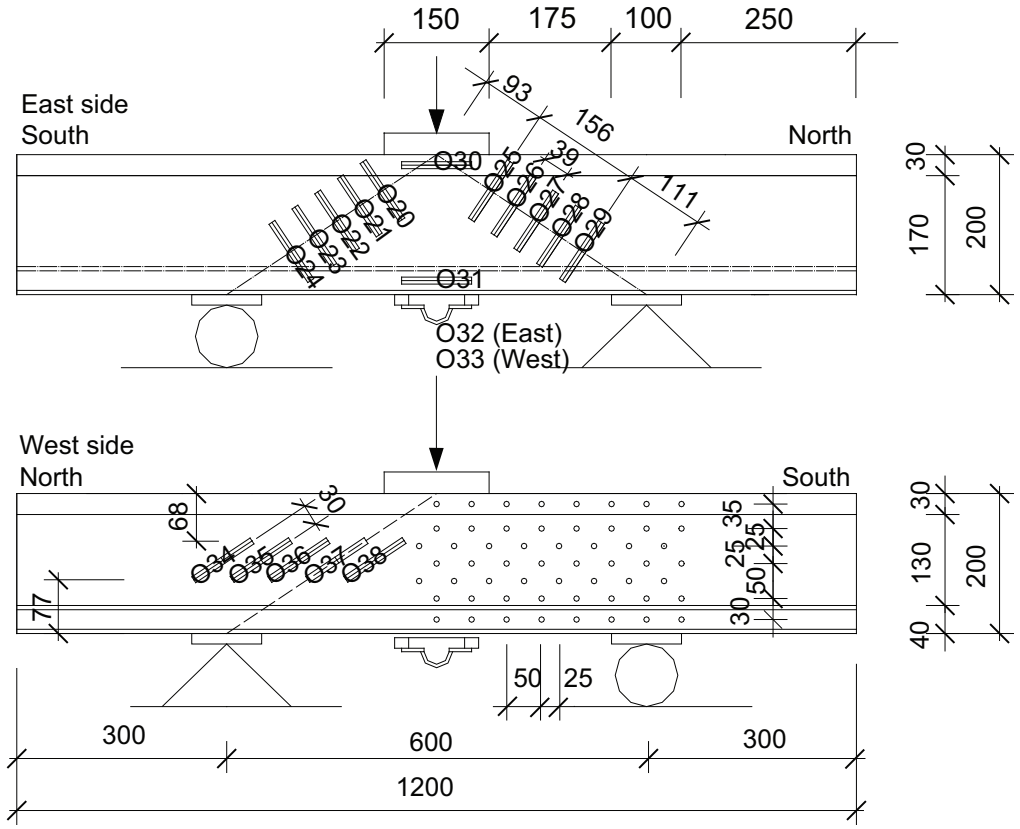

(a) At specimen side

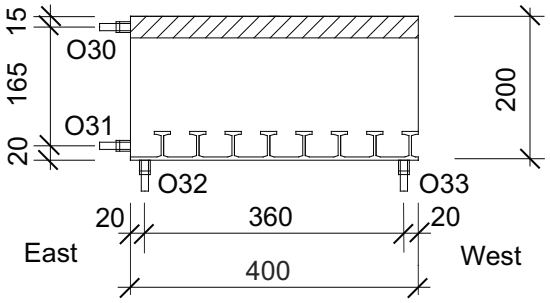

(b) At mid-span

Figure D.2: Position and labeling of omega-shaped extensometers.

Linear voltage displacement transducers

Five linear voltage displacement transducers (LVDTs) from HBM of type W50 (± 50 mm and with an accuracy of ± 0.10 mm) were used: D2 was placed on the bottom centerline of

the specimen to measure vertical displacements at the mid-span. D1 and D9 were placed over the supports on the top centerline of the specimen, i.e. on the normal concrete layer. All specimens were instrumented with the horizontal displacement transducers D0 and D10, which were placed at the beam ends to measure the slippage between the lightweight concrete and GFRP profile.

Omega-shaped extensometers

The same PI-2-100 omega-shaped extensometers were glued onto the concrete surface in order to measure deformations on the LC and NC as described in Appendix C (accuracy ± 0.01 mm and gage length of 100 mm). At the eastern side of the mid-span, O30 captured the strains on the NC, O31 on the lower part of the LC and O32 and O33 on the bottom side of the GFRP sheet. Additionally 2x5 extensometers (O20-O24 and O25-O29) measured deformation perpendicular to the diagonal compressive strut at a distance of 39 mm. For all specimens, O34-O38 were glued parallel to the theoretical diagonal at a distance of 30 mm on the western specimen side, with the exception of specimen 1000s, which was not equipped with these gages. The labeling and positions of the omega-shaped extensometers are shown in Figure D.2.

Photogrammetry

Using a Sony XCL-U1000 digital camera, the displacement of the specimen could be recorded. For this a dense grid of points was glued between the centerline and the support of the western specimen side, see Figure D.2. Only the first experimentally investigated specimen, 1000s, was equipped over the total span, but since the camera was too far away and the recorded deformation was thus unsatisfactory, the camera was placed in such a way that only half of the span was recorded for the following specimen. However, scatter remained considerable and thus the results are not reported here.

D.3 Results of S3 series

D.3.1 Specimen 900Es-1: Failure description and experimental results

D.3.1.1 Failure description

The failure process and crack development in the specimen up to the end of the experiment are illustrated in Figures D.3 and D.4. The first small noises were noticed at a load of 57 kN, although no cracks were observed. At 60 kN some noises were noticed next to gage O20, followed by the development of a diagonal crack at a load of 75 kN, crossing O22-O23. At 90 kN the diagonal crack on the south-east side propagated through the whole LC layer. At a load of 96 kN this crack developed horizontally through the LC-NC interface from the southern edge of the loading plate towards mid-span.

The ultimate load was reached at 98 kN with the propagation of an inclined crack in the north-east part of the specimen crossing half of the NC layer and a drop in the load to 81 kN. The specimen slightly regained stiffness and a second load peak was reached at a load of 83 kN when a horizontal crack propagated along the FRP-LC interface up to the north end of the specimen. This crack was also evident in the west part of the specimen, crossing O35. The load dropped significantly to 47 kN. Figure D.3-a shows the specimen (west side) before the two peak loads and D.3-b the specimen after the second peak load. Despite the loss in stiffness of the specimen, the load could be slowly increased. A second diagonal crack developed in the west part of the specimen between O37 and O38. Loud cracks were noticed, always concurring with an irregularity in the load-deflection curve. At 113 kN failure occurred in the web of the outer T-upstand above the northern support and the experiment was stopped. The failed specimen after the experiment is shown in Figure D.4.

Due to the risk of damaging the omega-shaped extensometer, O25-O29 and O35 were removed after the second load peak and the appearance of large cracks at a load of 56 kN. O38 was also removed at a load of 82 kN.

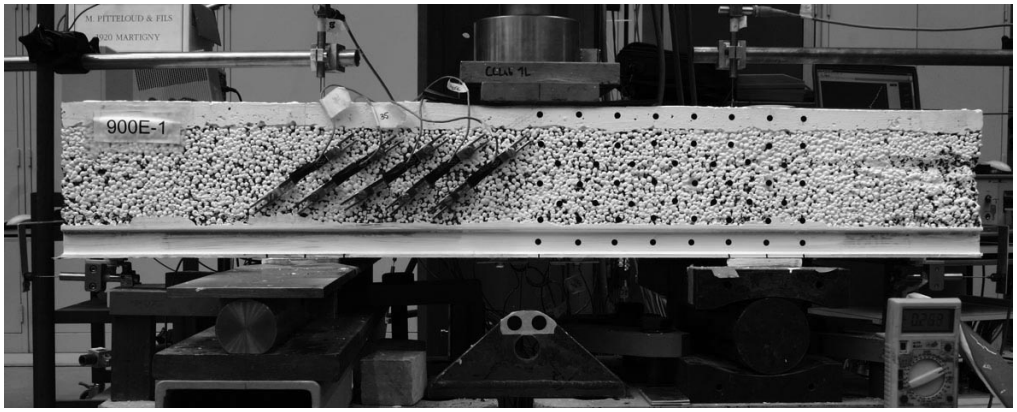

(a) At 34 kN - no cracks observed

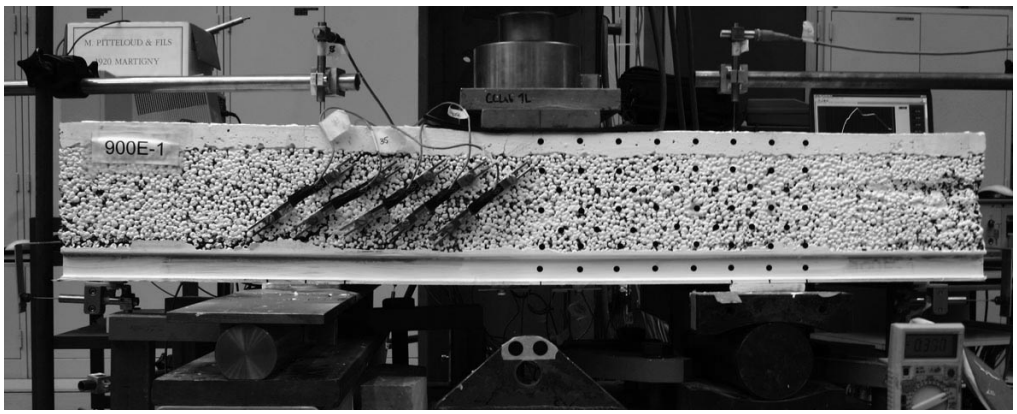

(b) After ultimate load at 48 kN (post-peak)

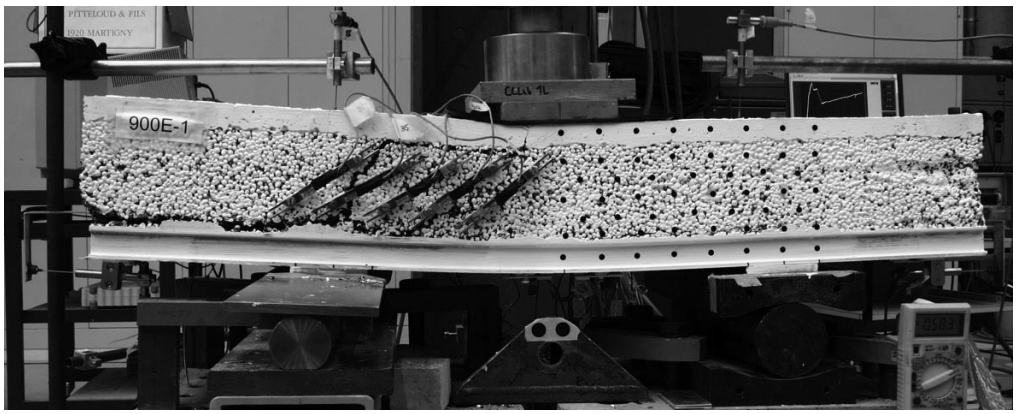

(c) At 75 kN (post-peak)

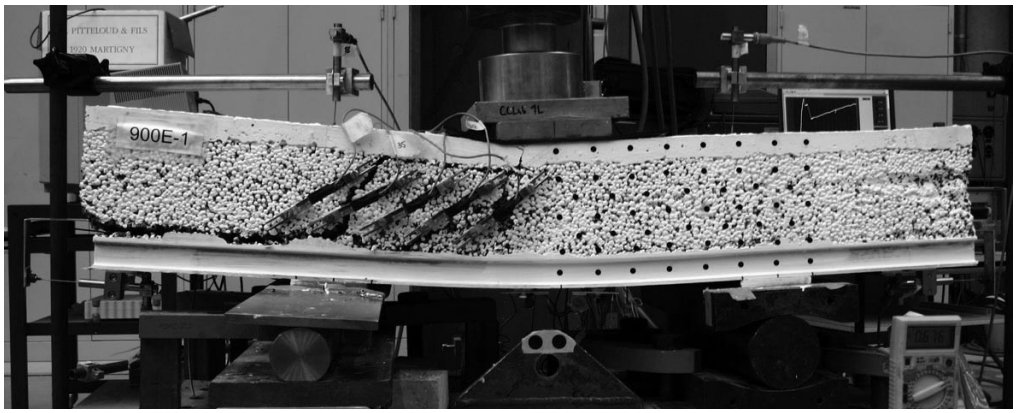

(d) At 88 kN (post-peak)

Figure D.3: 900Es-1: Failure process on west side (north left, south right).

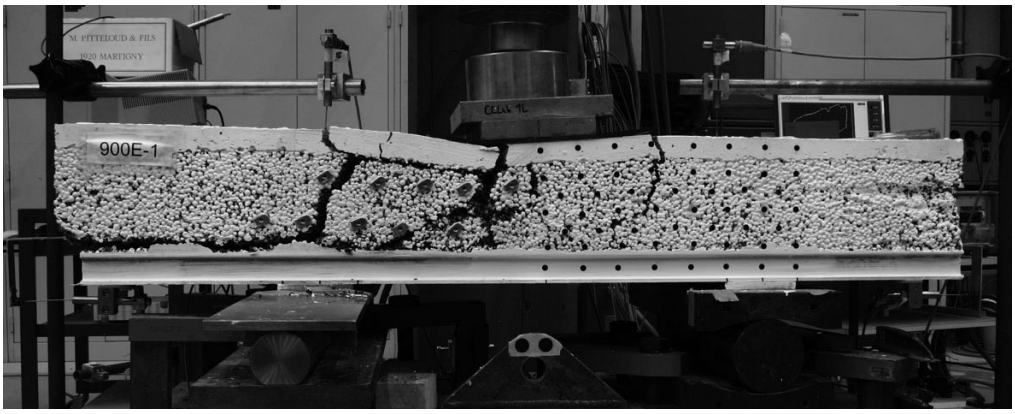

(a) At end of experiment

(b) Sheared LC-NC unity at north end, after experiment

Figure D.4: 900Es-1: Failed specimen on west side and north end.

D.3.1.2 Displacement transducers

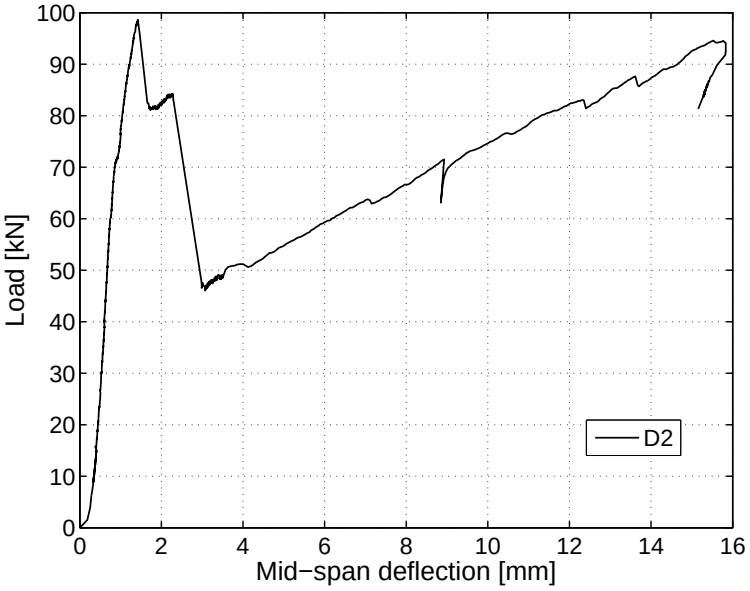

(a) At mid-span

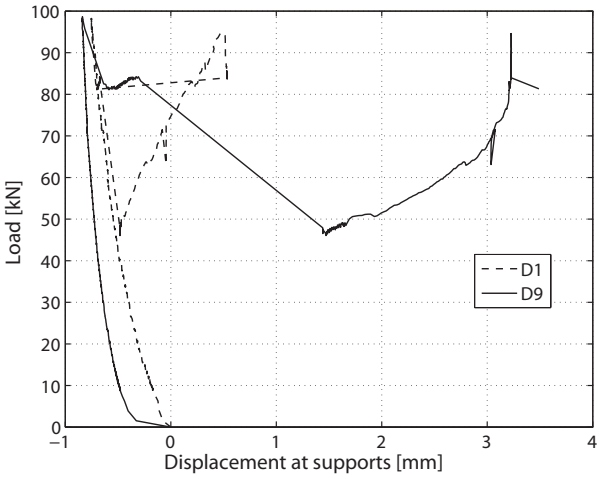

(b) At supports

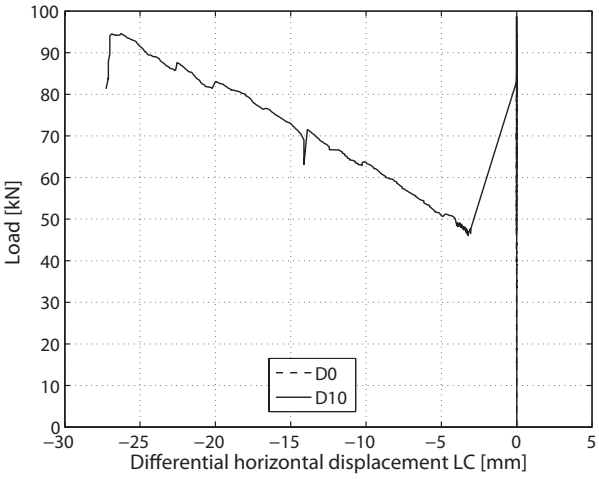

(c) Diff. horizontal displacement within failed LC

Figure D.5: 900Es-1: Displacement measurements.

D.3.1.3 Omega-shaped extensometers

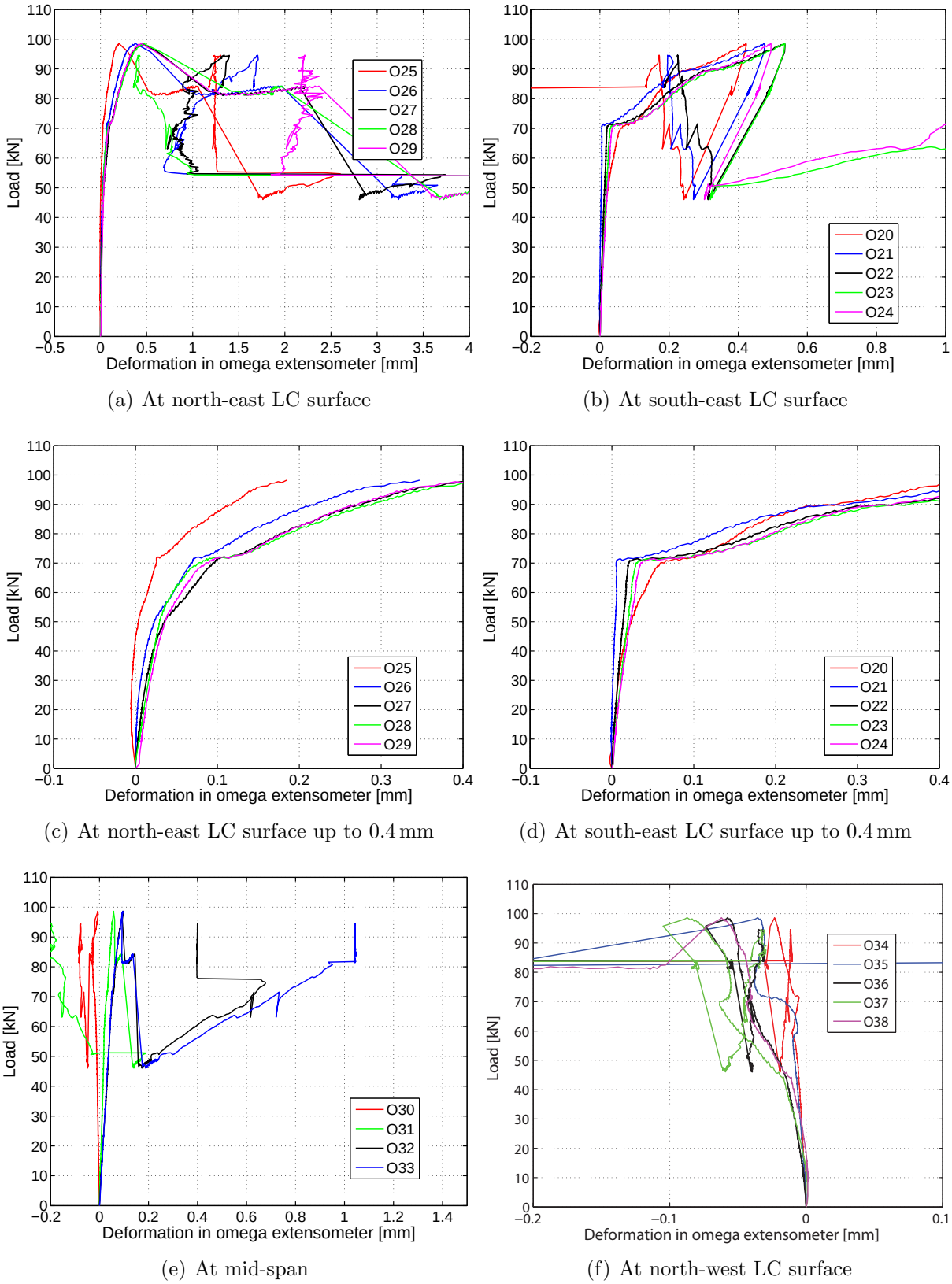

(a) At north-east LC surface

(b) At south-east LC surface

(c) At north-east LC surface up to 0.4 mm

(d) At south-east LC surface up to 0.4 mm

(e) At mid-span

(f) At north-west LC surface

Figure D.6: 900Es-1: Deformations in omega-shaped extensometers.

D.3.1.4 Deformations at different load steps perpendicular to the diagonal

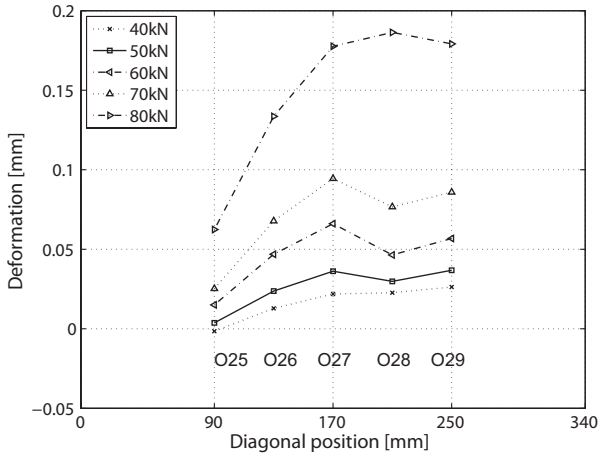

(a) O25-O29 along north-east diagonal

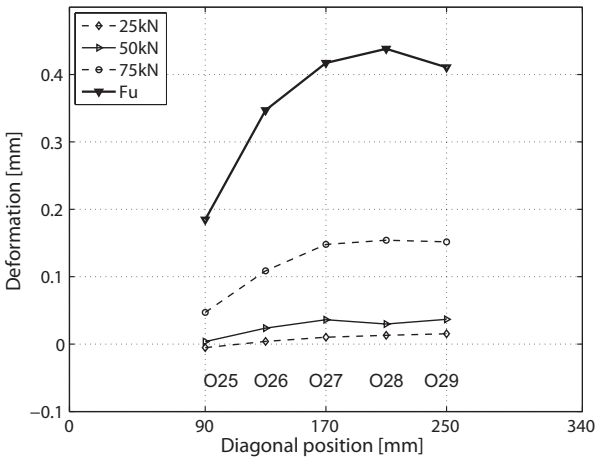

(b) O25-O29 up to F_u

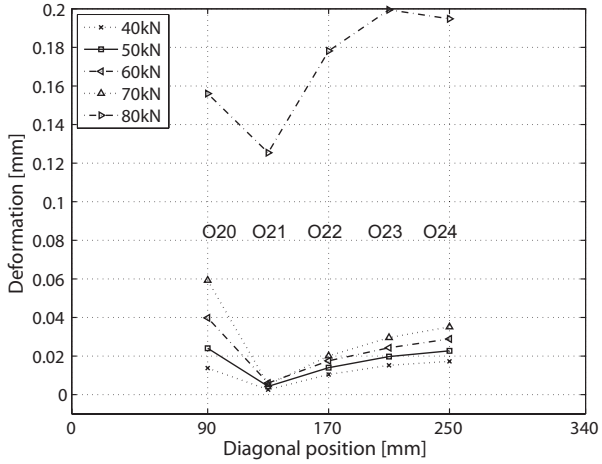

(c) O20-O24 along south-east diagonal

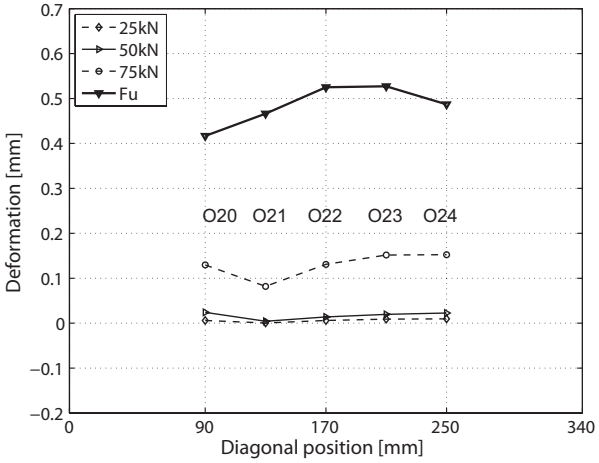

(d) O20-O24 up to F_u

Figure D.7: 900Es-1: Deformations at different load steps perpendicular to diagonal.

D.3.1.5 Deformations at different load steps through the cross section and along the diagonal

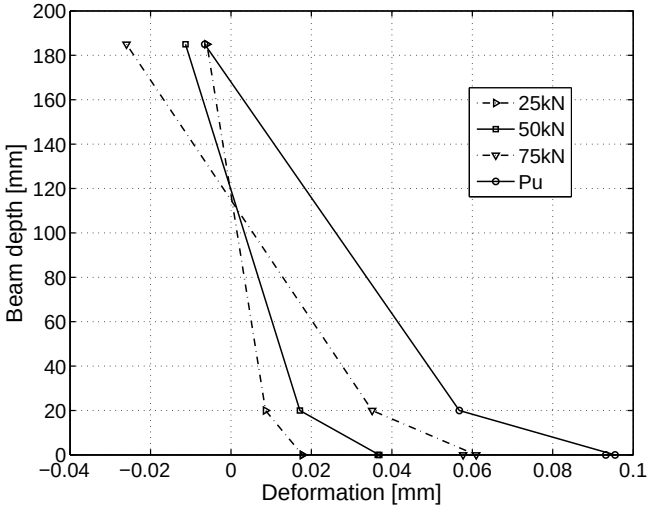

(a) Deformations through cross section on east side

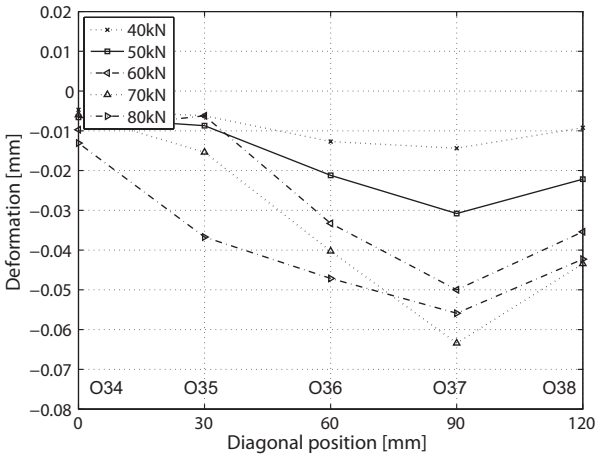

(b) O34-O38 along north-west diagonal

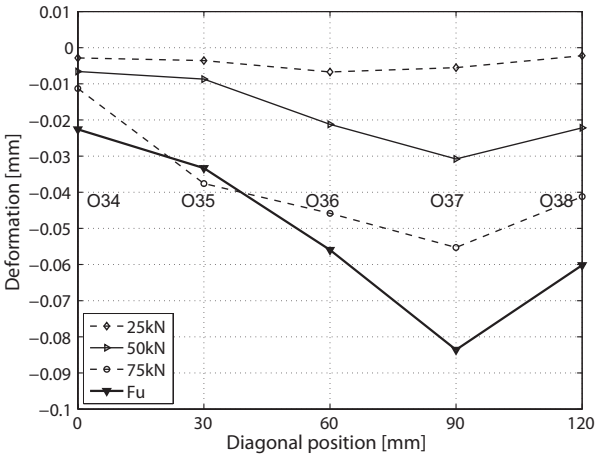

(c) O34-O38 up to F_u

Figure D.8: 900Es-1: Deformations at different load steps.

D.3.2 Specimen 900Es-2: Failure description and experimental results

D.3.2.1 Failure description

The failure process and crack development in the specimen up to the end of the experiment are shown in Figures D.9 and D.10. The first audible cracks were noticed at a load of 60 kN. Although no obvious cracks were observed, noises occurred at a load of 76 kN in the south-east part of the specimen. Only at a load of 80 kN could the first crack be observed on the north-west side, next to O37 and crossing O36. The ultimate load was reached at 83 kN and simultaneously the diagonal cracks in the north-east part of the specimen crossing the attachment points of O26-O27 became evident. A second drop in the load occurred when a diagonal crack opened in the southern part of the specimen, through O20-O24 on the east side. At the same time the FRP-LC interface on the north-west side of the specimen failed starting from the crack propagating towards the northern specimen end, (Figure D.9-c). Subsequently the northern crack opened continuously and developed along the LC-NC interface towards mid-span. The load remained more or less constant for some minutes with a slight load minimum when the NC layer broke above the loading plate. When a mid-span deflection of 6 mm was reached, the cracked specimen regained stiffness and the load could be increased up to 109 kN, where the jack reached its deformation limit. The crack development after the first load drops is shown in Figure D.10-a-c. The experiment was stopped here.

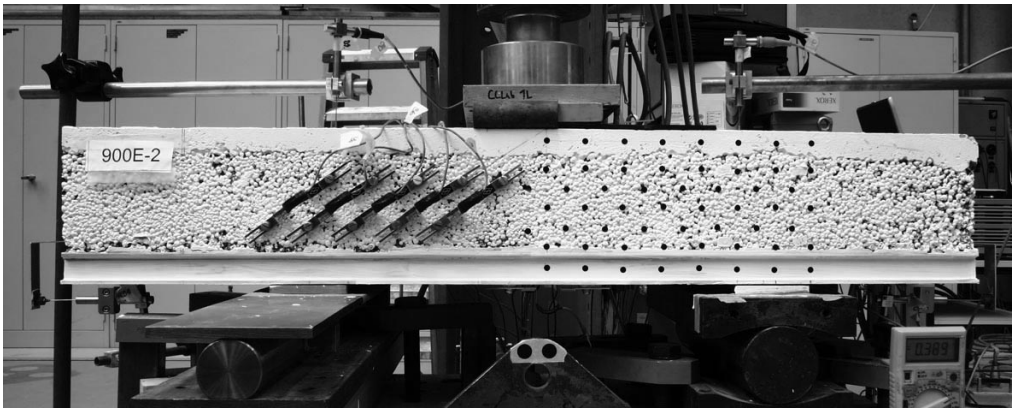

(a) At 50 kN - no cracks observed

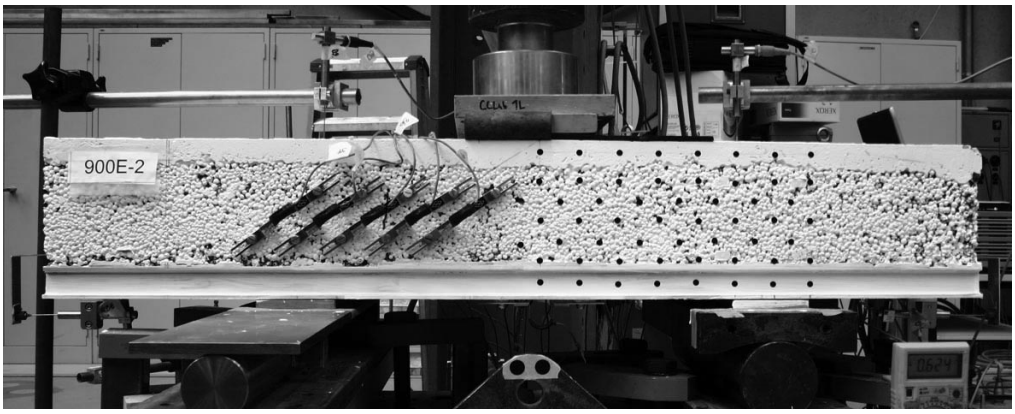

(b) At ultimate load 83 kN

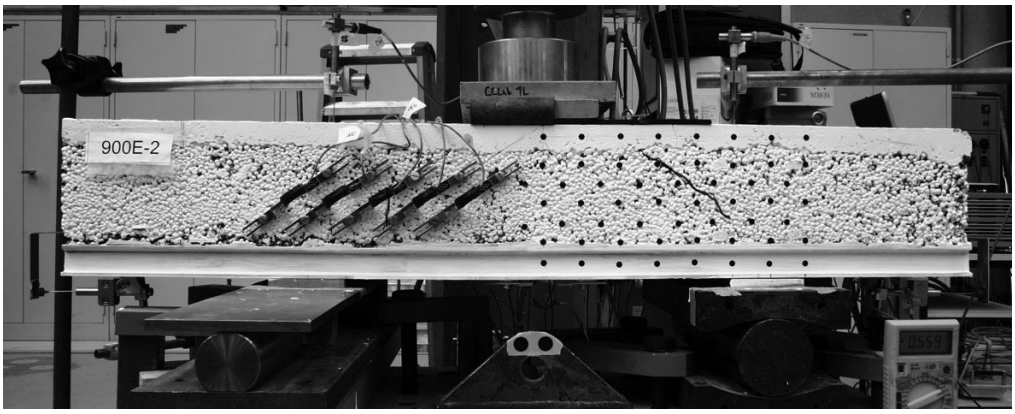

(c) At 73 kN (post-peak)

Figure D.9: 900Es-2: Failure process on west side (north left, south right).

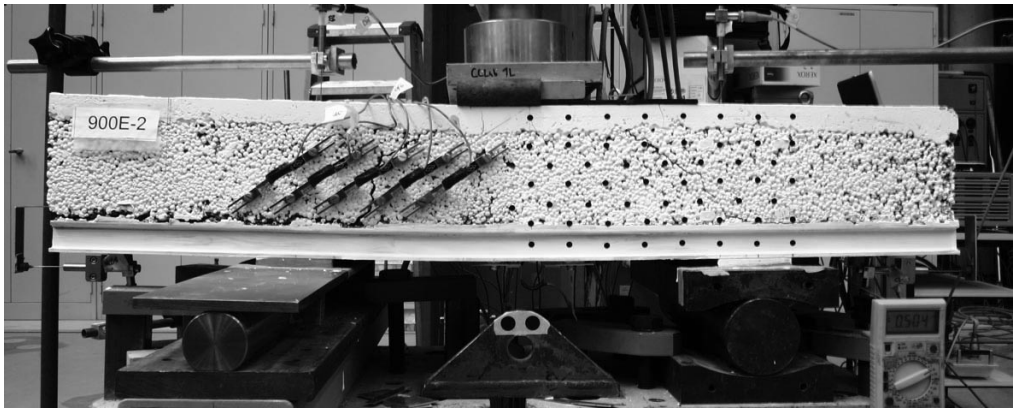

(a) At 69 kN (post-peak)

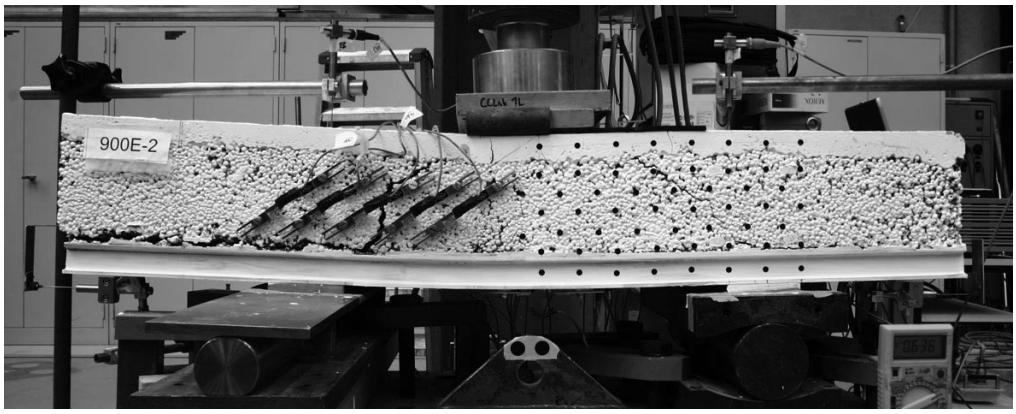

(b) At 83 kN (post-peak)

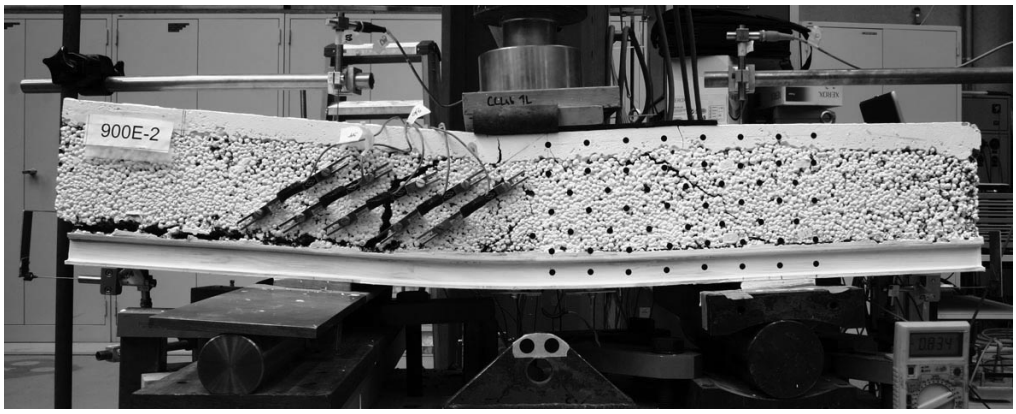

(c) At 109 kN (post-peak)

Figure D.10: 900Es-2: Post-peak failure process continuation on west side (north left, south right).

D.3.2.2 Displacement transducers

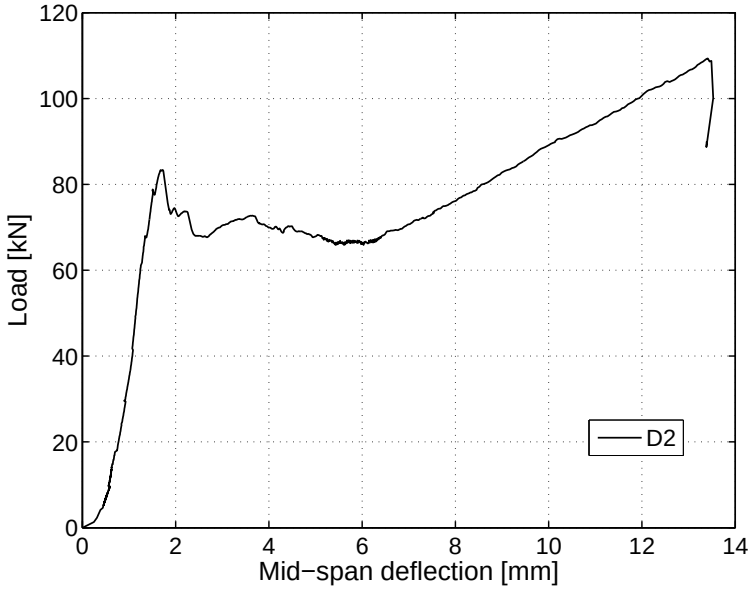

(a) At mid-span

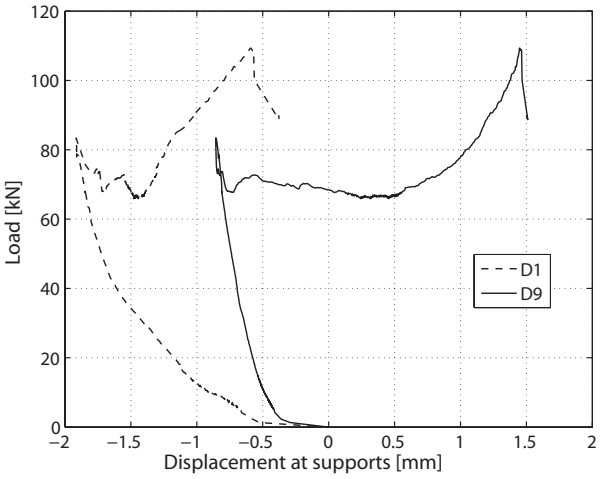

(b) At supports

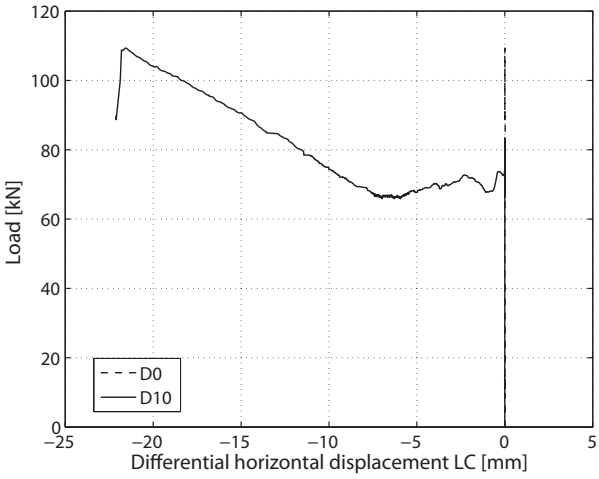

(c) Diff. horizontal displacement within failed LC

Figure D.11: 900Es-2: Displacement measurements.

D.3.2.3 Omega-shaped extensometers

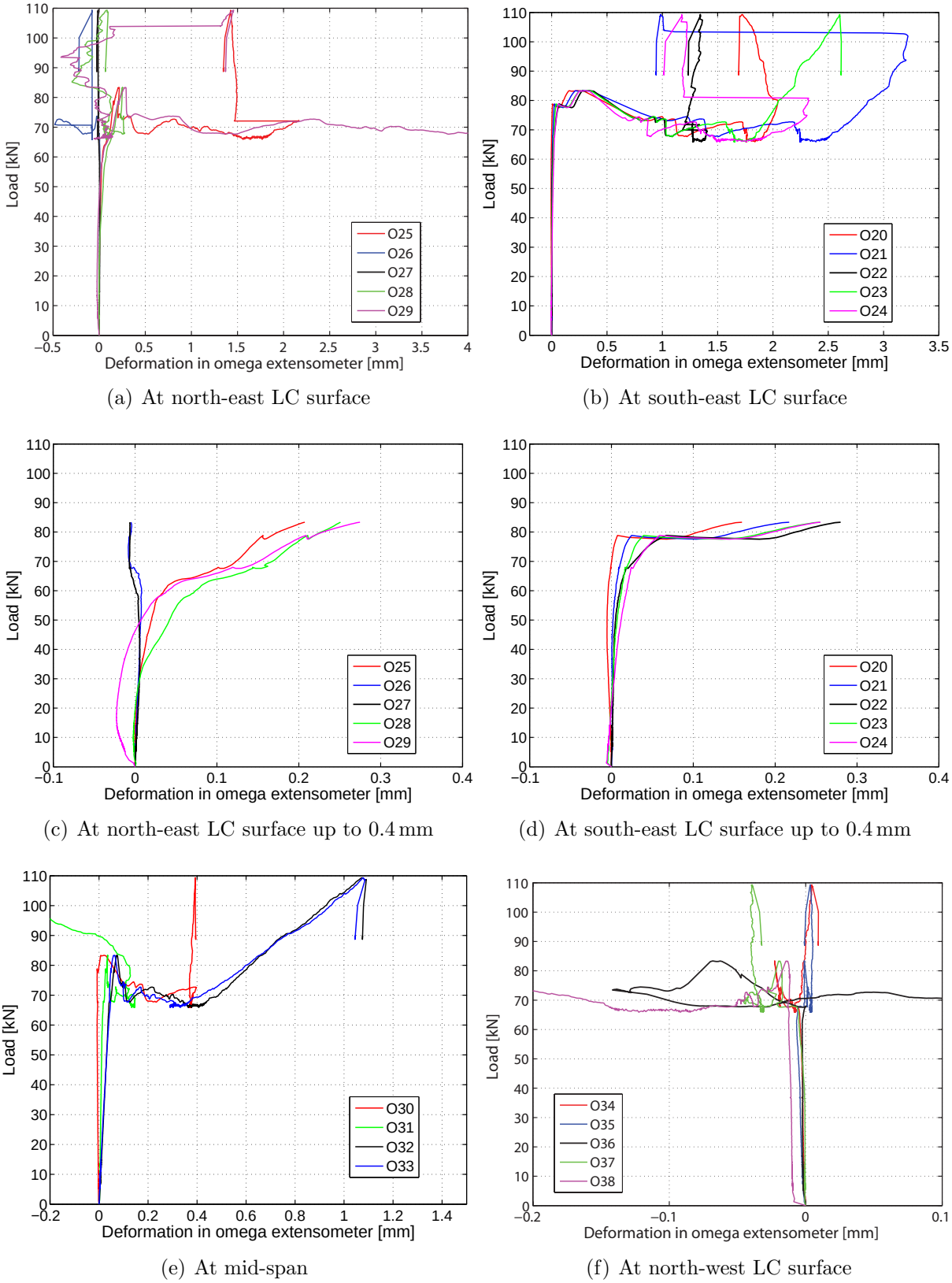

(a) At north-east LC surface

(b) At south-east LC surface

(c) At north-east LC surface up to 0.4 mm

(d) At south-east LC surface up to 0.4 mm

(e) At mid-span

(f) At north-west LC surface

Figure D.12: 900Es-2: Deformations in omega-shaped extensometers.

D.3.2.4 Deformations at different load steps perpendicular to the diagonal

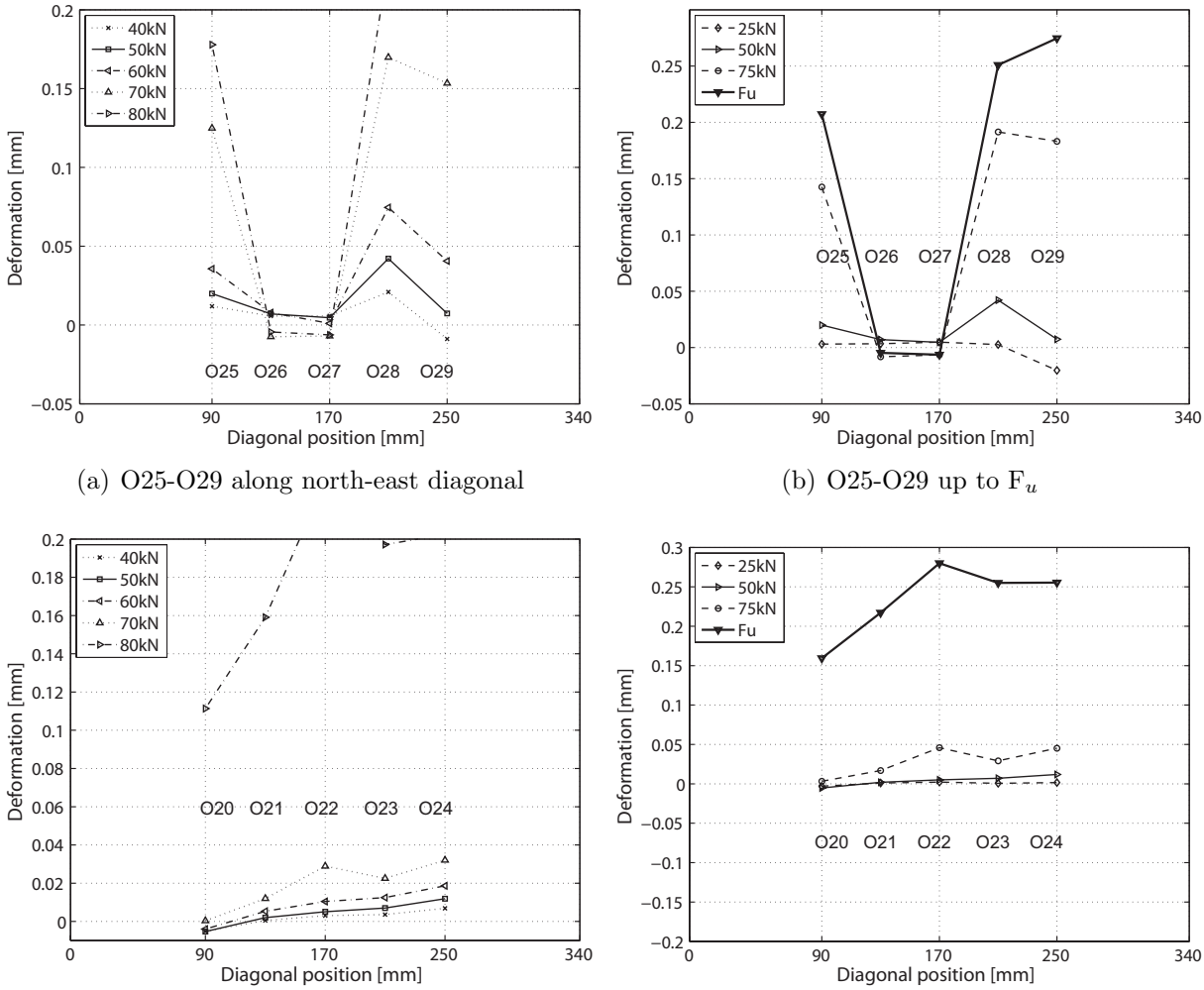

(a) O25-O29 along north-east diagonal

(b) O25-O29 up to F_u

(c) O20-O24 along south-east diagonal

(d) O20-O24 up to F_u

Figure D.13: 900Es-2: Deformations at different load steps perpendicular to diagonal.

D.3.2.5 Deformations at different load steps through the cross section and along the diagonal

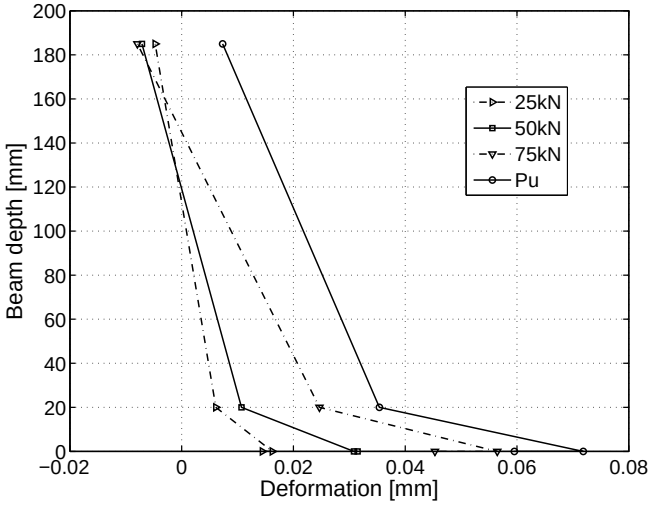

(a) Deformations through cross section on east side

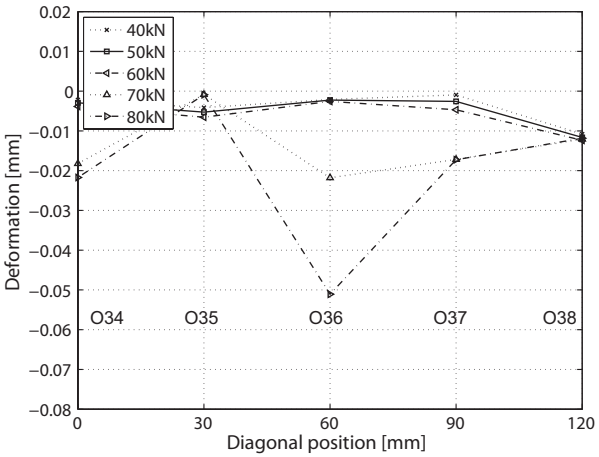

(b) O34-O38 along north-west diagonal

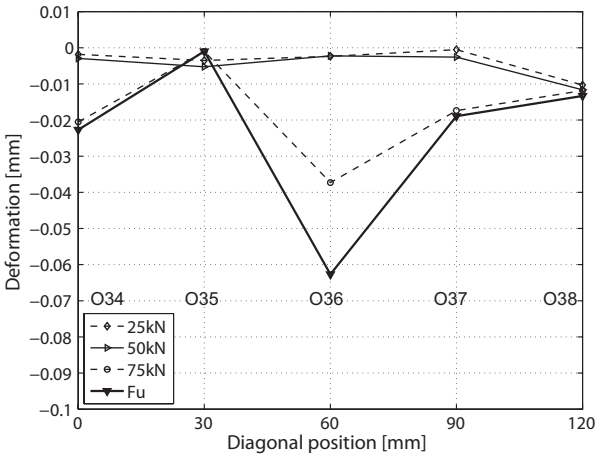

(c) O34-O38 up to F_u

Figure D.14: 900Es-2: Deformations at different load steps.

D.3.3 Specimen 1300s-1: Failure description and experimental results

D.3.3.1 Failure description

The failure process and crack development in the specimen up to the end of the experiment are illustrated in Figures D.15, D.16 and D.17.

The first crack and a kink in the load deflection response were noticed at a load of 40 kN crossing the LC layer on the east part of the specimen, just next to extensometer O31. Subsequently the specimen started to slip out of the GFRP profile on the northern side. The crack width was already 0.5 mm. At the west side of the specimen, next to the loading plate, a vertical crack started to develop, see Figure D.15-b, and as from a load of 55 kN, the crack started to cross the NC layer through the gage length of O30. The NC layer was half cracked at a load of 70 kN. The LC layer continuously slipped out of the GFRP Plank profile and both vertical cracks - on the east and west sides - continued to open. At a load of approximately 80 kN horizontal cracks could be observed in the eastern part of the specimen, just above the T-upstands, one on the northern and one in the southern part of the span, see Figure D.17-a. A loud noise occurred at a load of 80 kN, although no further cracks developed; only the vertical crack, separating the southern LC layer from the northern part of the specimen, got wider and the LC slipped out of the northern side of the specimen. Only as from a load of 90 kN, could slippage of over 0.04 mm be measured at the southern end of the specimen. At 132 kN loud noises were noticed, followed by a drop in the load. The crack width at mid-span was approximately 15 mm, indicating that the GFRP was the only load-bearing element. Despite several (3-4) loud noises and load drops, the load could be slightly increased up to the ultimate load of 143 kN. Then a drop in the load occurred and the outer T-webs of the GFRP Plank profile started to buckle, see Figure D.16-d. The experiment was then stopped.

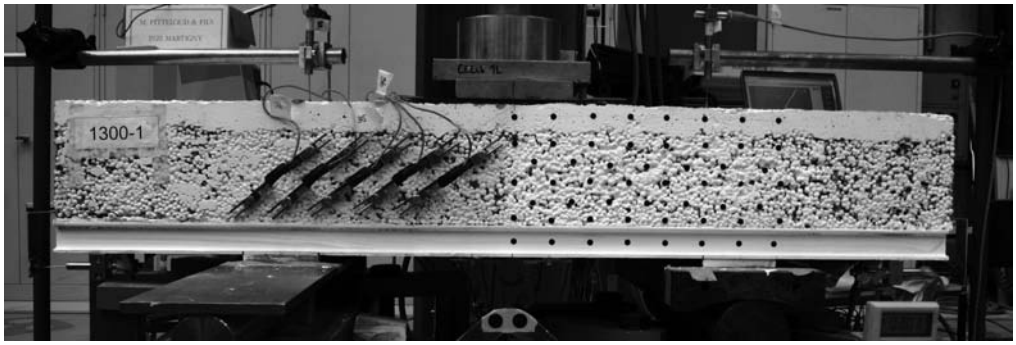

(a) At 40 kN - no cracks observed

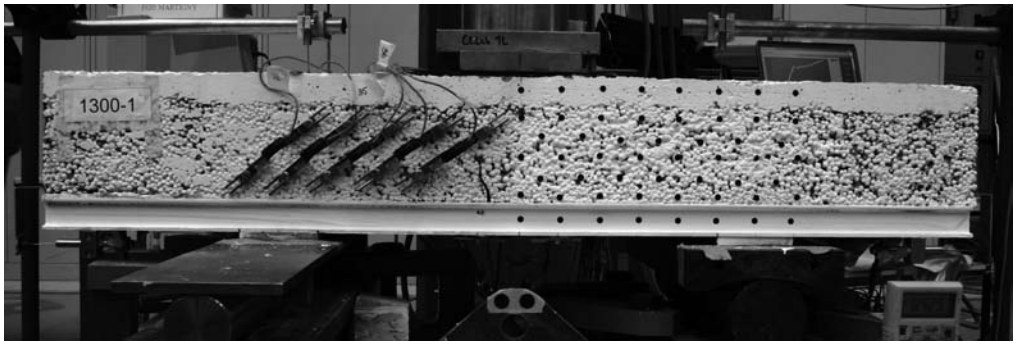

(b) At 55 kN

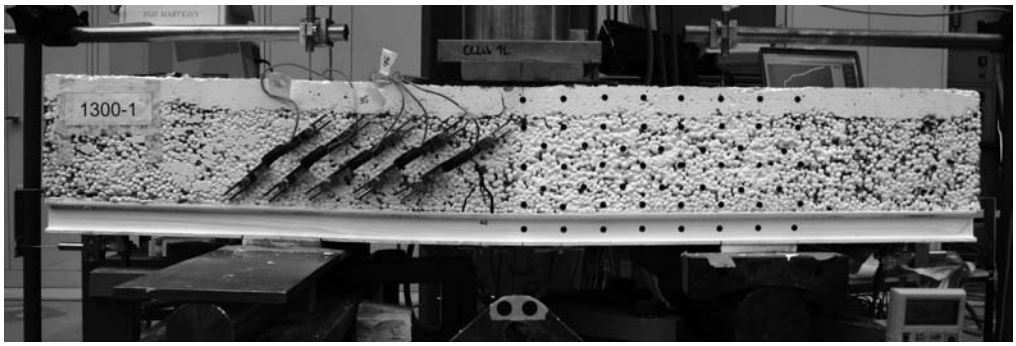

(c) At 80 kN

(d) Horizontal cracks on eastern part of specimen at 80 kN

Figure D.15: 1300s-1: Failure process on west side (north left, south right).

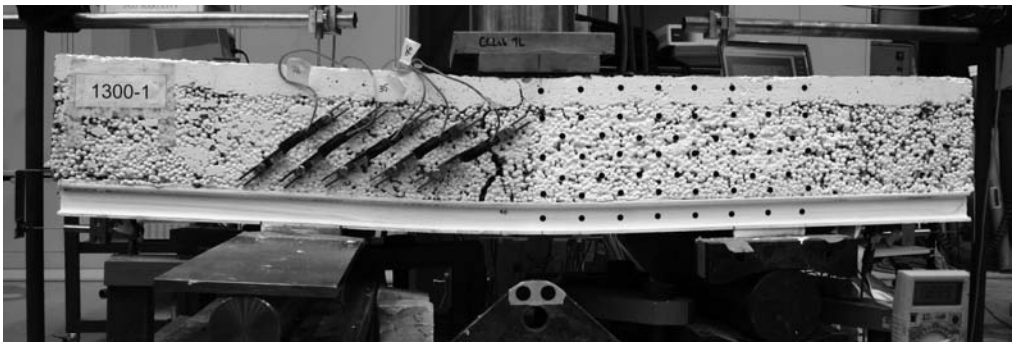

(a) At 115 kN

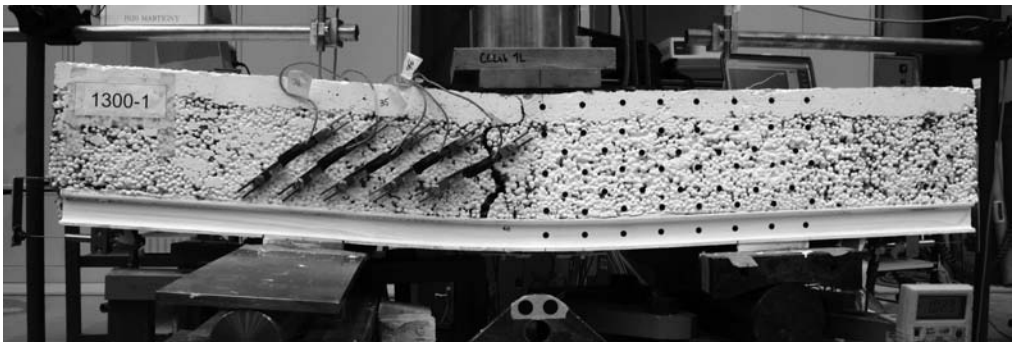

(b) At ultimate load approx. 140 kN

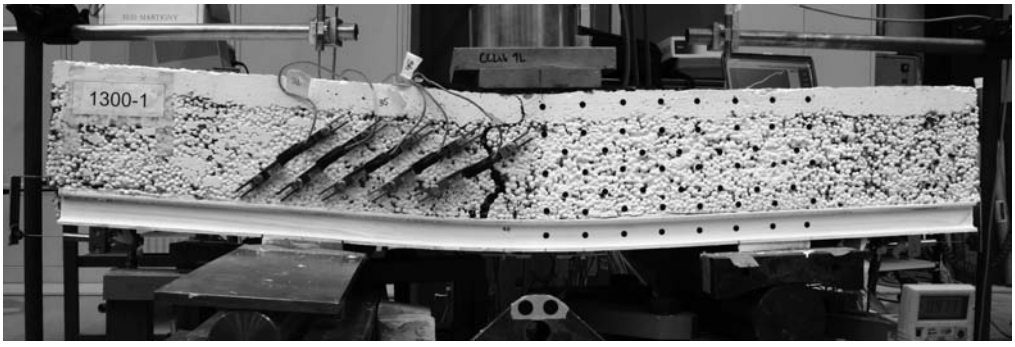

(c) At 130 kN (post-peak)

(d) FRP failure

Figure D.16: 1300s-1: Failure process on west side, continuation.

(a) Failed specimen east part

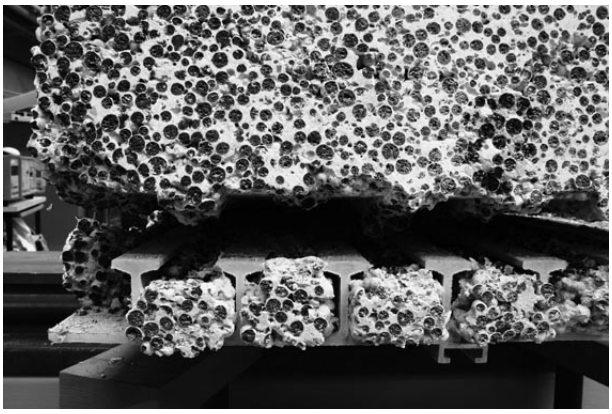

(b) Failed FRP-LC interface north-east

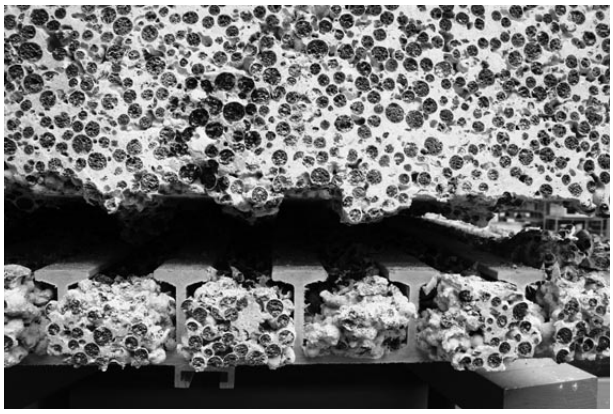

(c) Failed FRP-LC interface north-west

Figure D.17: 1300s-1: Failed specimen and slippage in interfaces.

D.3.3.2 Displacement transducers

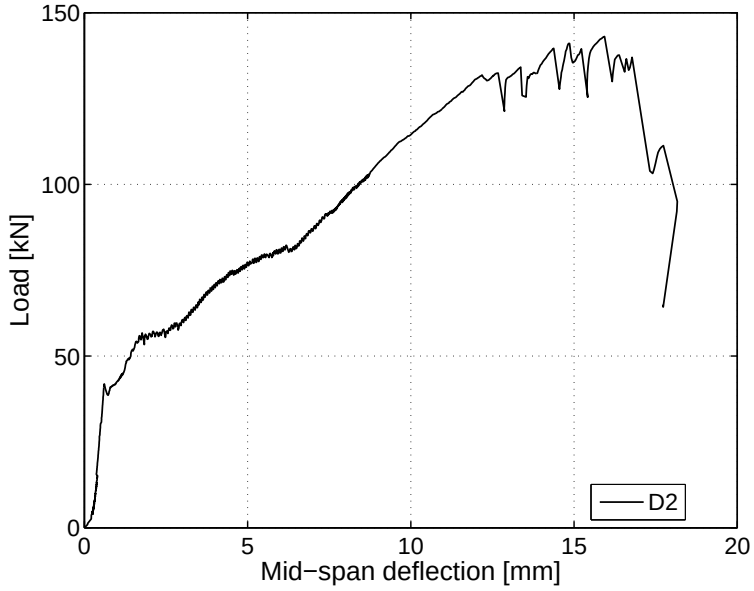

(a) At mid-span

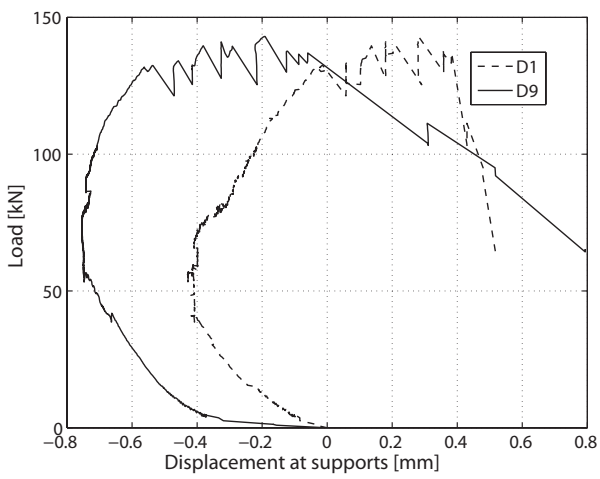

(b) At supports

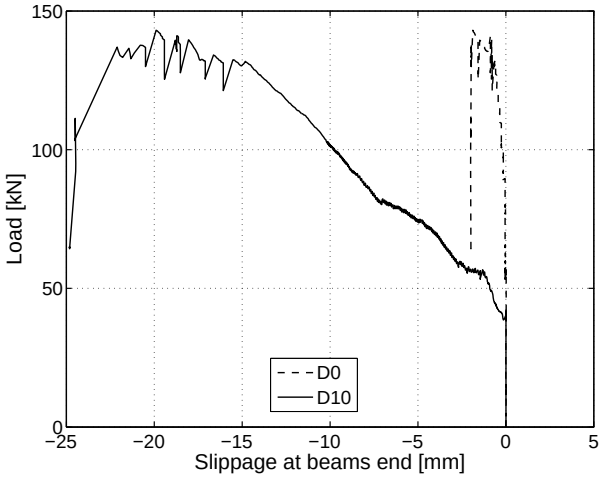

(c) FRP-LC slippage

Figure D.18: 1300s-1: Displacement measurements.

D.3.3.3 Omega-shaped extensometers

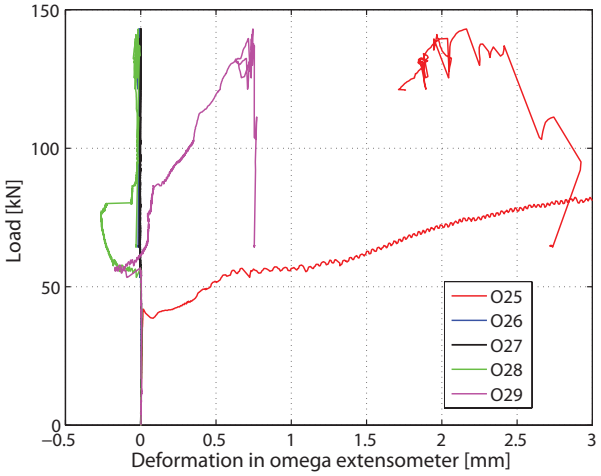

(a) At north-east LC surface

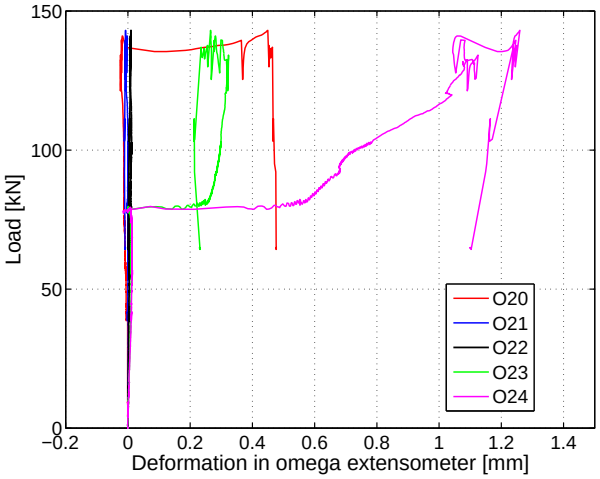

(b) At south-east LC surface

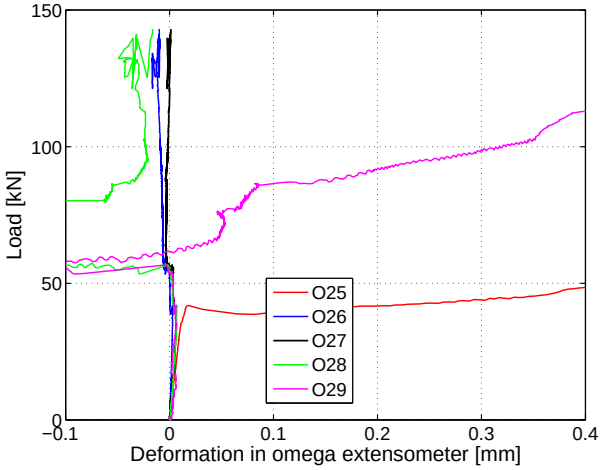

(c) At north-east LC surface up to 0.4 mm

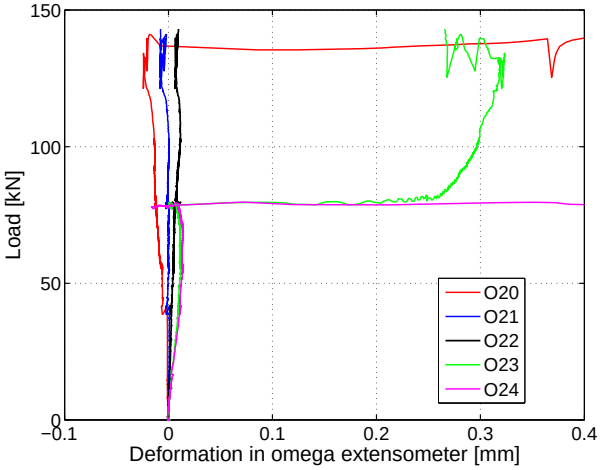

(d) At south-east LC surface up to 0.4 mm

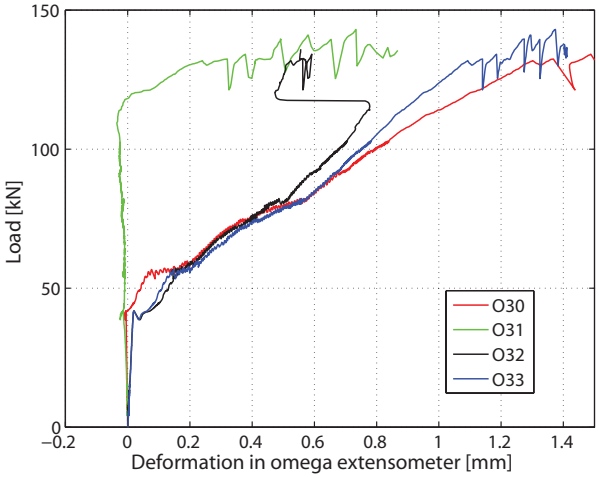

(e) At mid-span

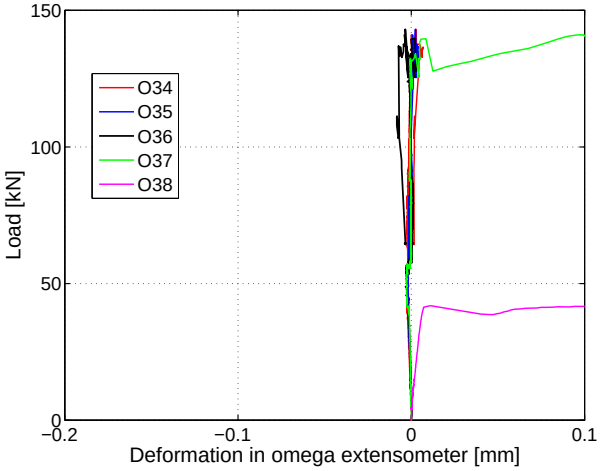

(f) At north-west LC surface

Figure D.19: 1300s-1: Deformations in omega-shaped extensometers.

D.3.3.4 Deformations at different load steps perpendicular to the diagonal

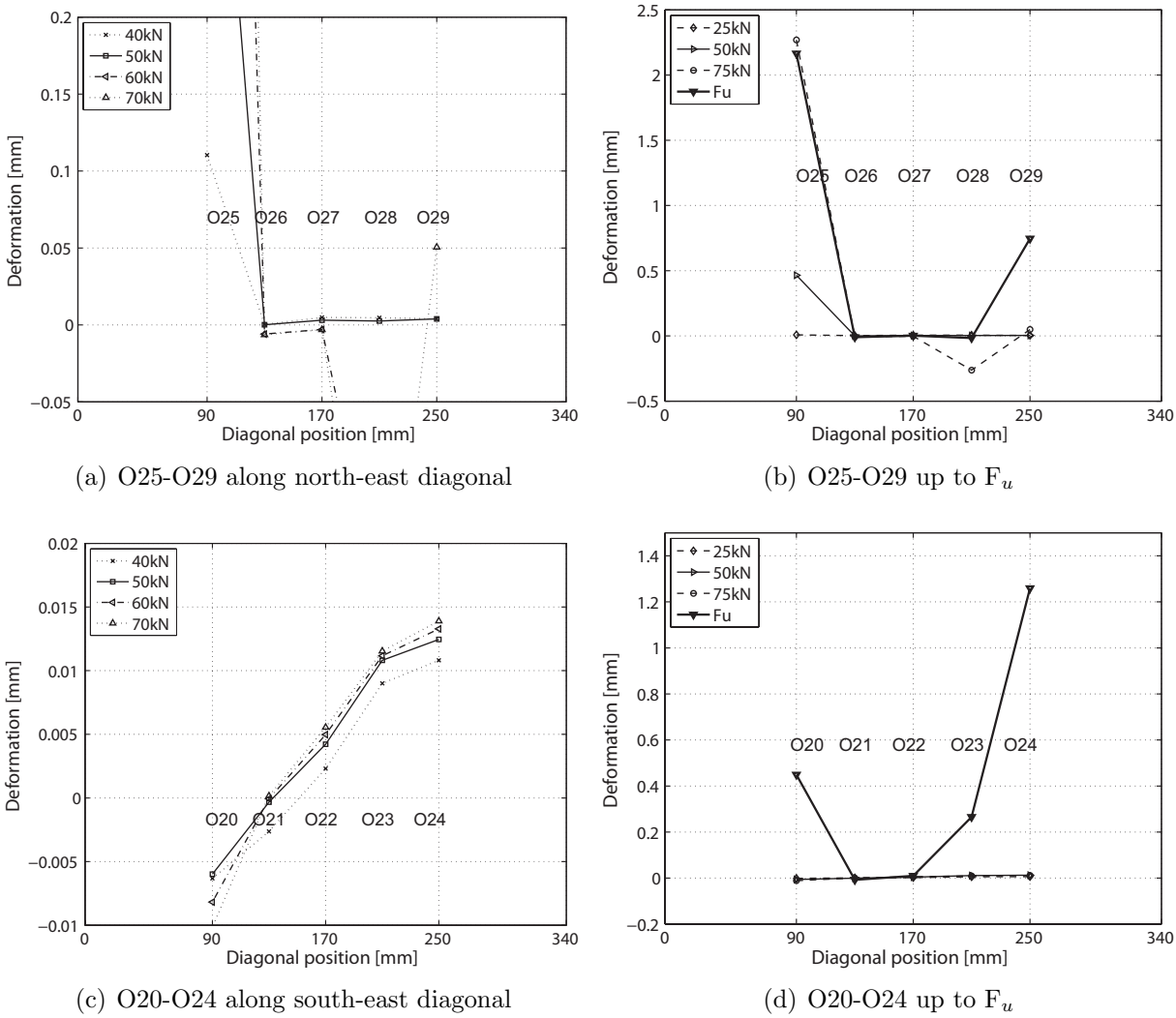

(a) O25-O29 along north-east diagonal

(b) O25-O29 up to F_u

(c) O20-O24 along south-east diagonal

(d) O20-O24 up to F_u

Figure D.20: 1300s-1: Deformations at different load steps perpendicular to diagonal.

D.3.3.5 Deformations at different load steps through the cross section and along the diagonal

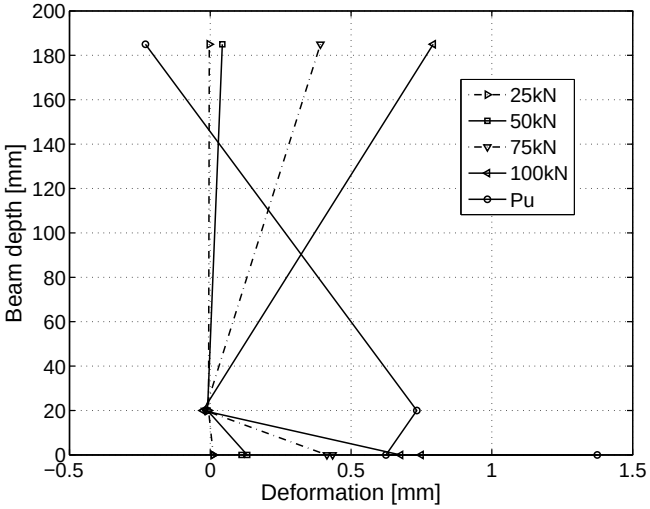

(a) Deformations through cross section on east side

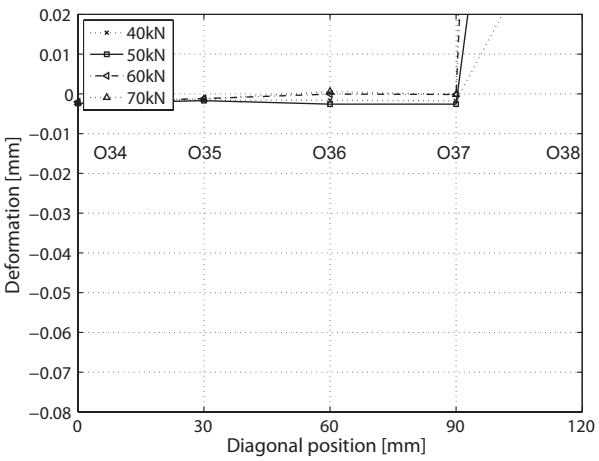

(b) O34-O38 along north-west diagonal

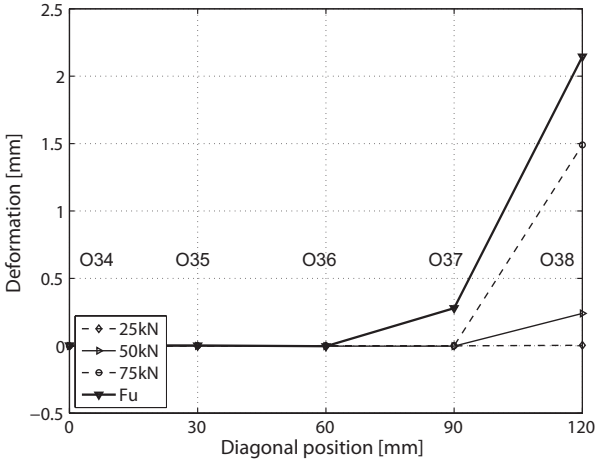

(c) O34-O38 up to F_u

Figure D.21: 1300s-1: Deformations at different load steps.

D.3.4 Specimen 1300s-2: Failure description and experimental results

D.3.4.1 Failure description

The failure process and crack development in the specimen up to the end of the experiment is illustrated in Figures D.22, D.23 and D.24.

The first noises were noticed at 40 kN, followed by a visible vertical crack, approximately 50 mm south from the centerline of the specimen and outside the gage length of O30 and O31. Subsequently, at a load of 46 kN, the LC started to slip out of the GFRP profile in a southern direction. Thus specimen stiffness decreased significantly and further load increasing became very slow. At a load of 60 kN a loud noise occurred and several - up to four - vertical cracks started to develop in the eastern part of the specimen, all next to the loading plate and rapidly crossing the whole LC layer. At a load of 66 kN the first crack in the western part of the specimen became visible approximately 25 mm from the centerline towards the south, see Figure D.22-a. With increasing deflection and loading, further vertical cracks became evident on the west side of the specimen. The crack at 50 mm from the center line was the most pronounced. Its opening is illustrated in Figure D.22-b-d. A new vertical crack just beyond the loading plate was observed on the eastern part of the specimen at 75 kN in the gage length of O31. As from the load of 89 kN, one crack on each side crossed half the NC layer, see Figure D.22-d. Simultaneously a horizontal crack above the T-upstands developed over the south-east support. Its length was approximately 240 mm and it developed towards the southern end of the specimen. Loud cracks were noticed at 102 kN and 114 kN, concurring with small changes in measurements. At approximately 130 kN two loud noises signaled two drops in the load. The ultimate load was reached at 146 kN, when a loud noise was audible followed by a pronounced load decrease to 103 kN. The crack pattern just after the ultimate load is shown in Figure D.23-a. A slight further load increase was possible however, and then the GFRP failure occurred in the web of the outer T-upstand above the southern support at a load of 112 kN, see Figure D.23-b. The experiment was stopped here. The crack pattern of the eastern part of the specimen after the experiment is illustrated in Figure D.24.

(a) At 66 kN

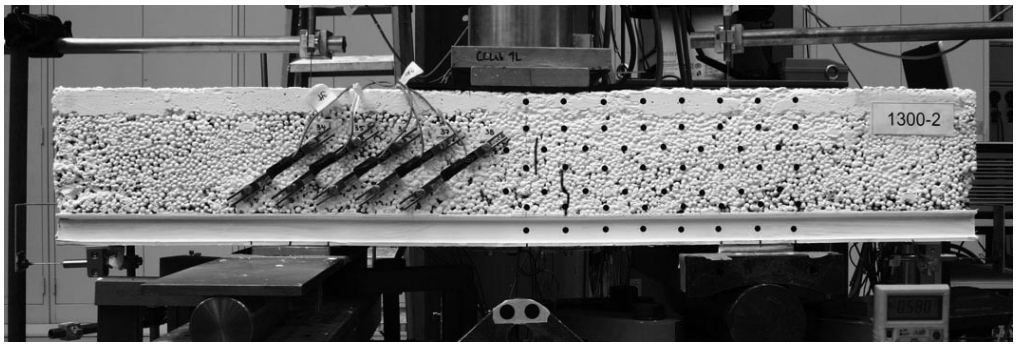

(b) At 75 kN

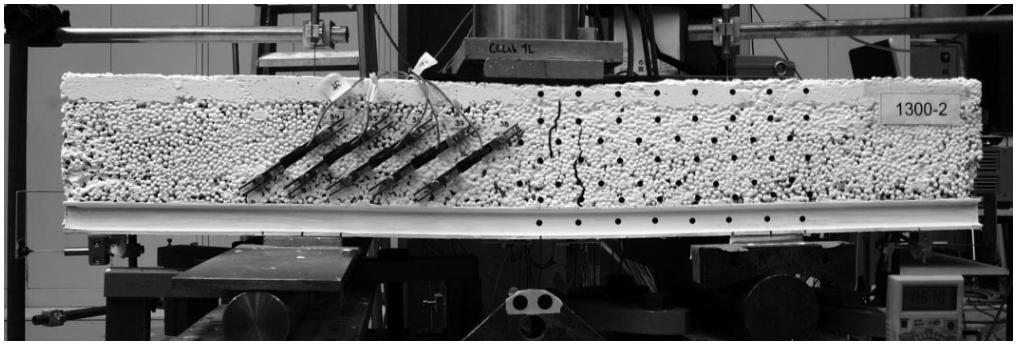

(c) At 87 kN

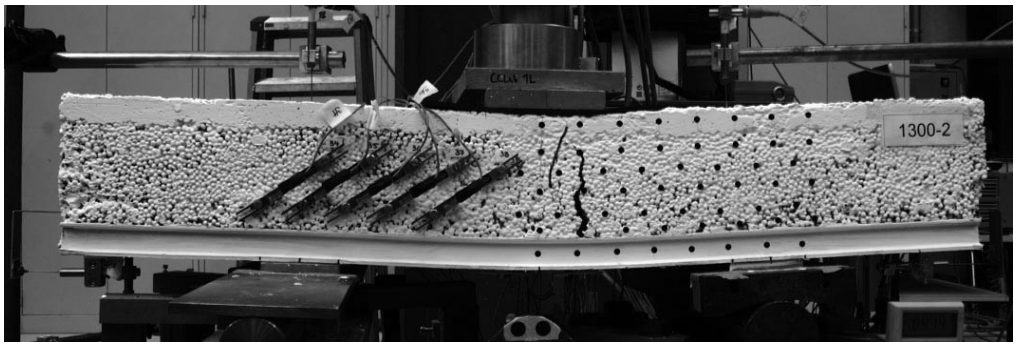

(d) At 119 kN

Figure D.22: 1300s-2: Failure process on west side (north left, south right).

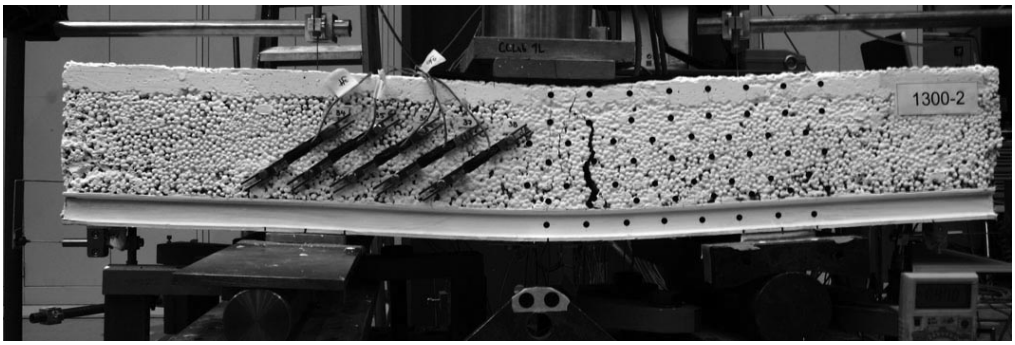

(a) After ultimate load - approx. 126 kN (post-peak)

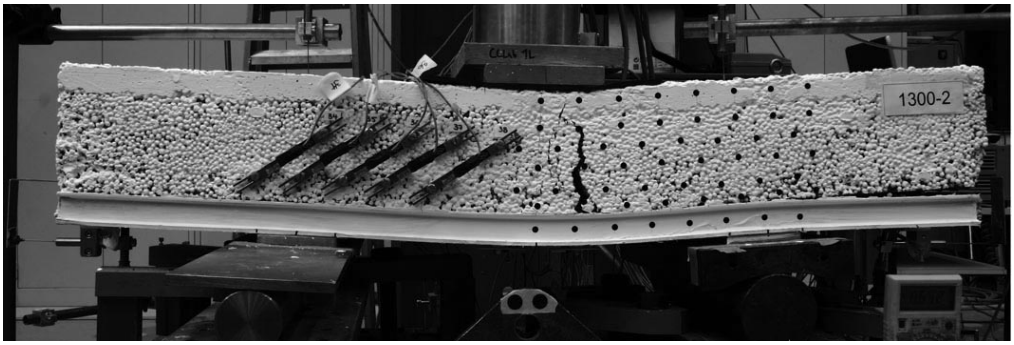

(b) After FRP failure - at 85 kN (post-peak)

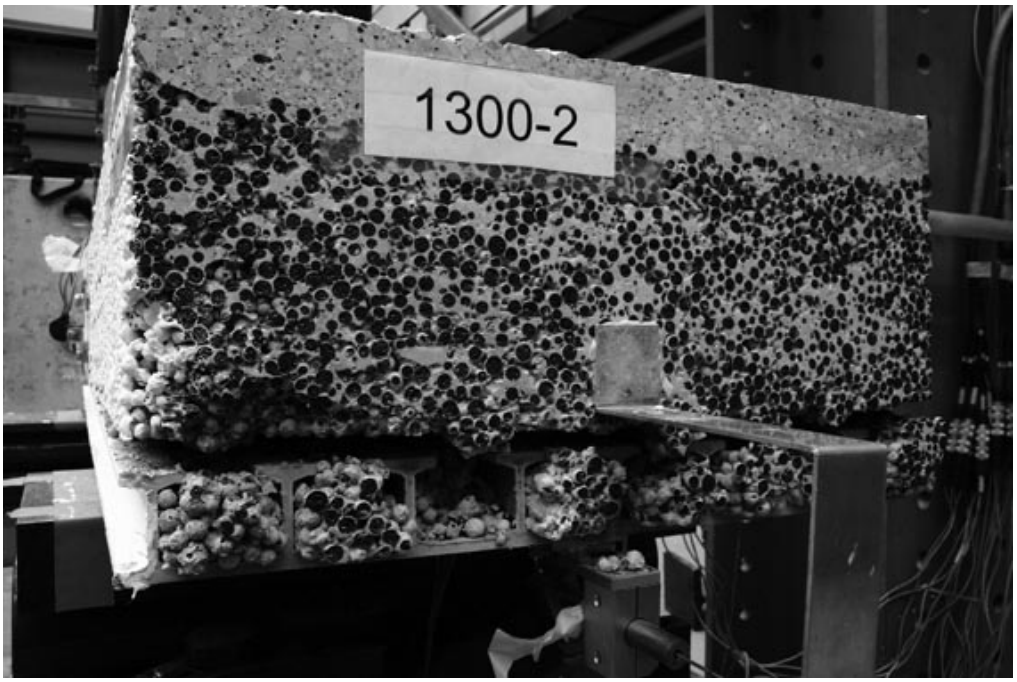

(c) At end of experiment - southern part of specimen

Figure D.23: 1300s-2: Failure process on west side, continuation.

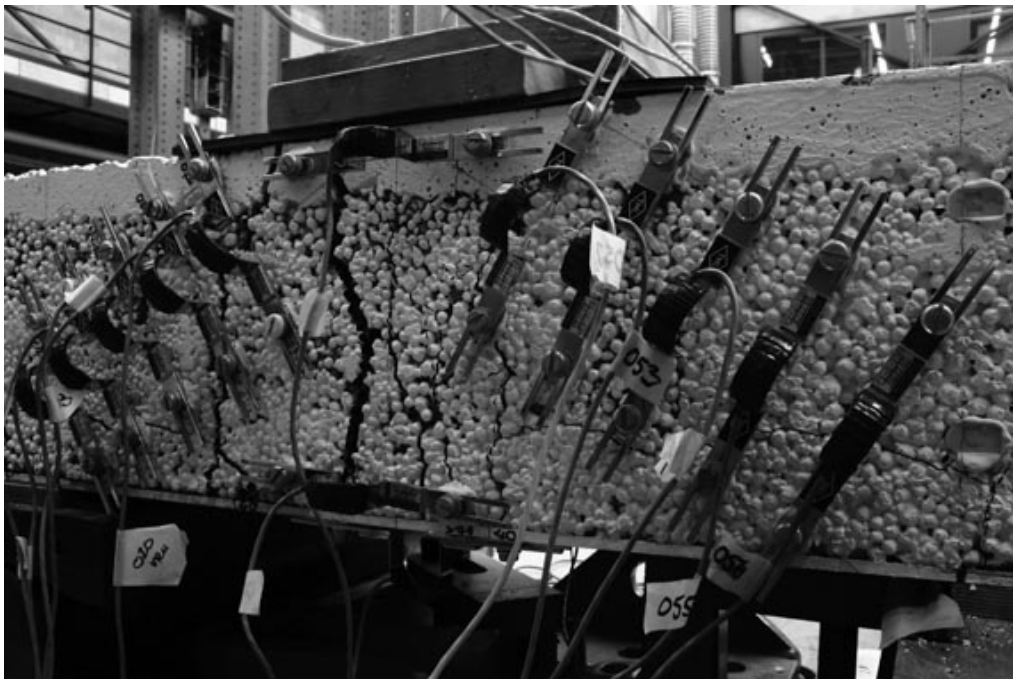

(a) Eastern part of specimen

(b) South-east

Figure D.24: 1300s-2: Crack pattern in east side at end of experiment.

D.3.4.2 Displacement transducers

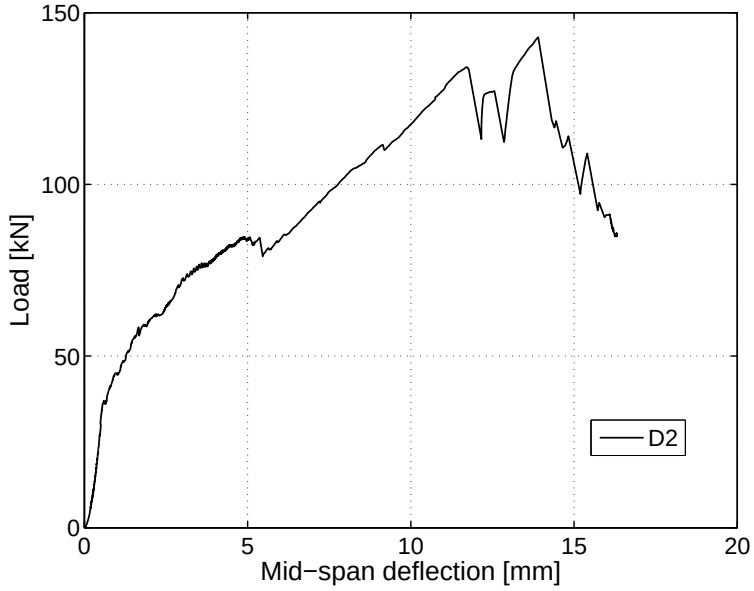

(a) At mid-span

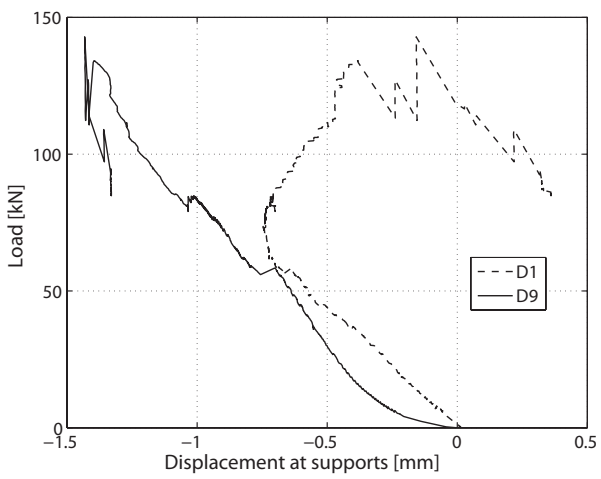

(b) At supports

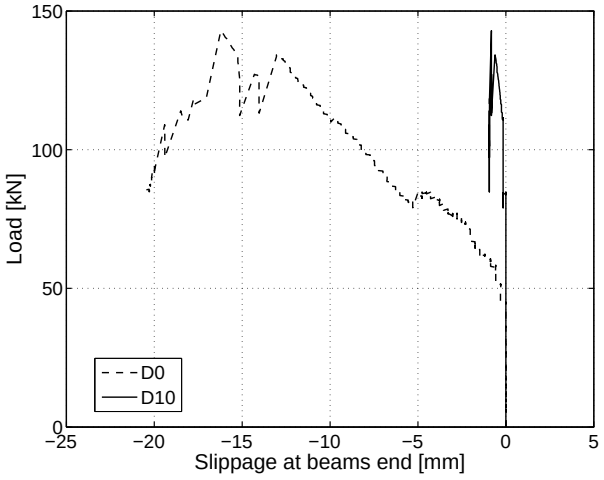

(c) FRP-LC slippage

Figure D.25: 1300s-2: Displacement measurements.

D.3.4.3 Omega-shaped extensometers

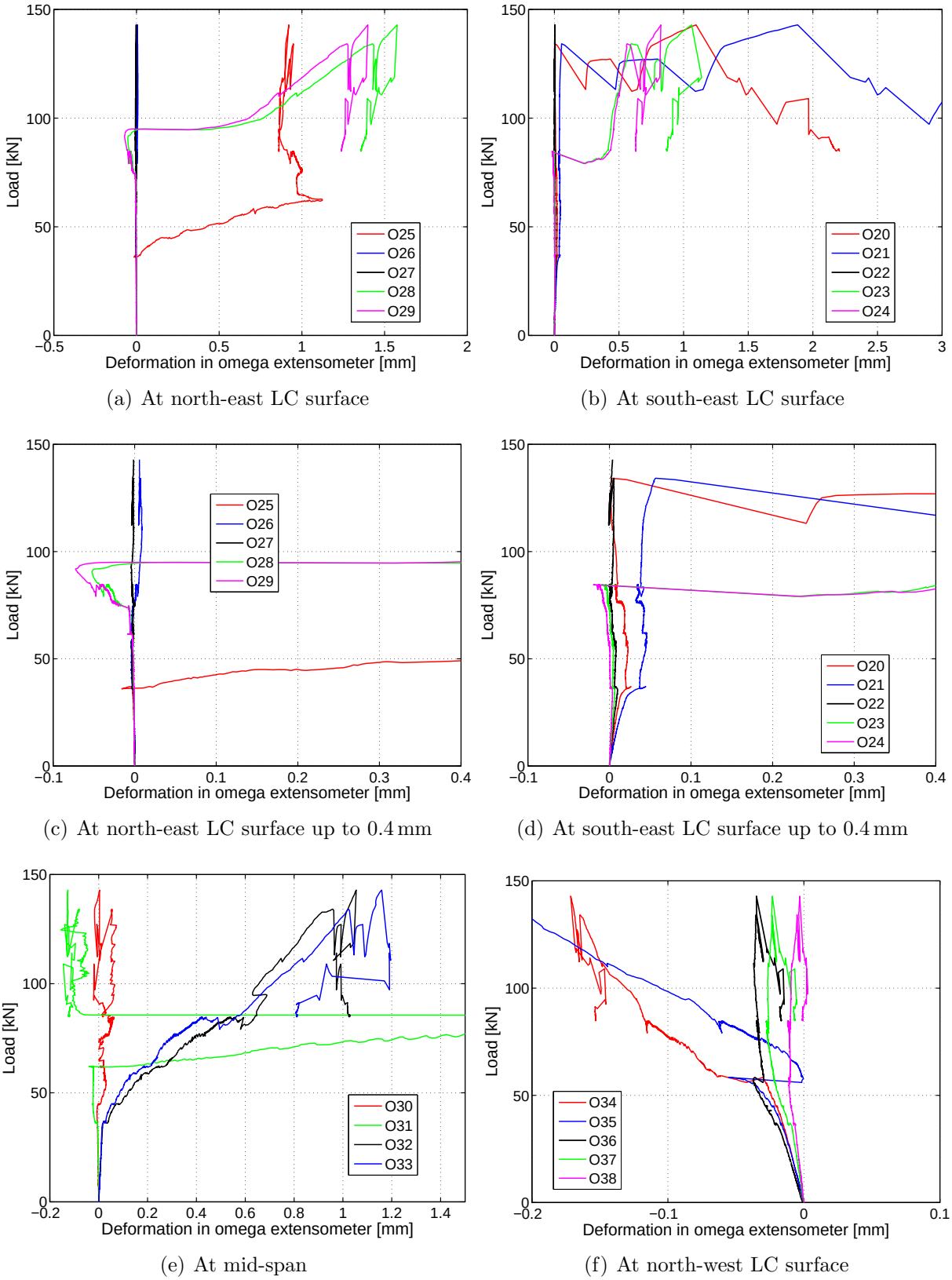

(a) At north-east LC surface

(b) At south-east LC surface

(c) At north-east LC surface up to 0.4 mm

(d) At south-east LC surface up to 0.4 mm

(e) At mid-span

(f) At north-west LC surface

Figure D.26: 1300s-2: Deformations in omega-shaped extensometers.

D.3.4.4 Deformations at different load steps perpendicular to the diagonal

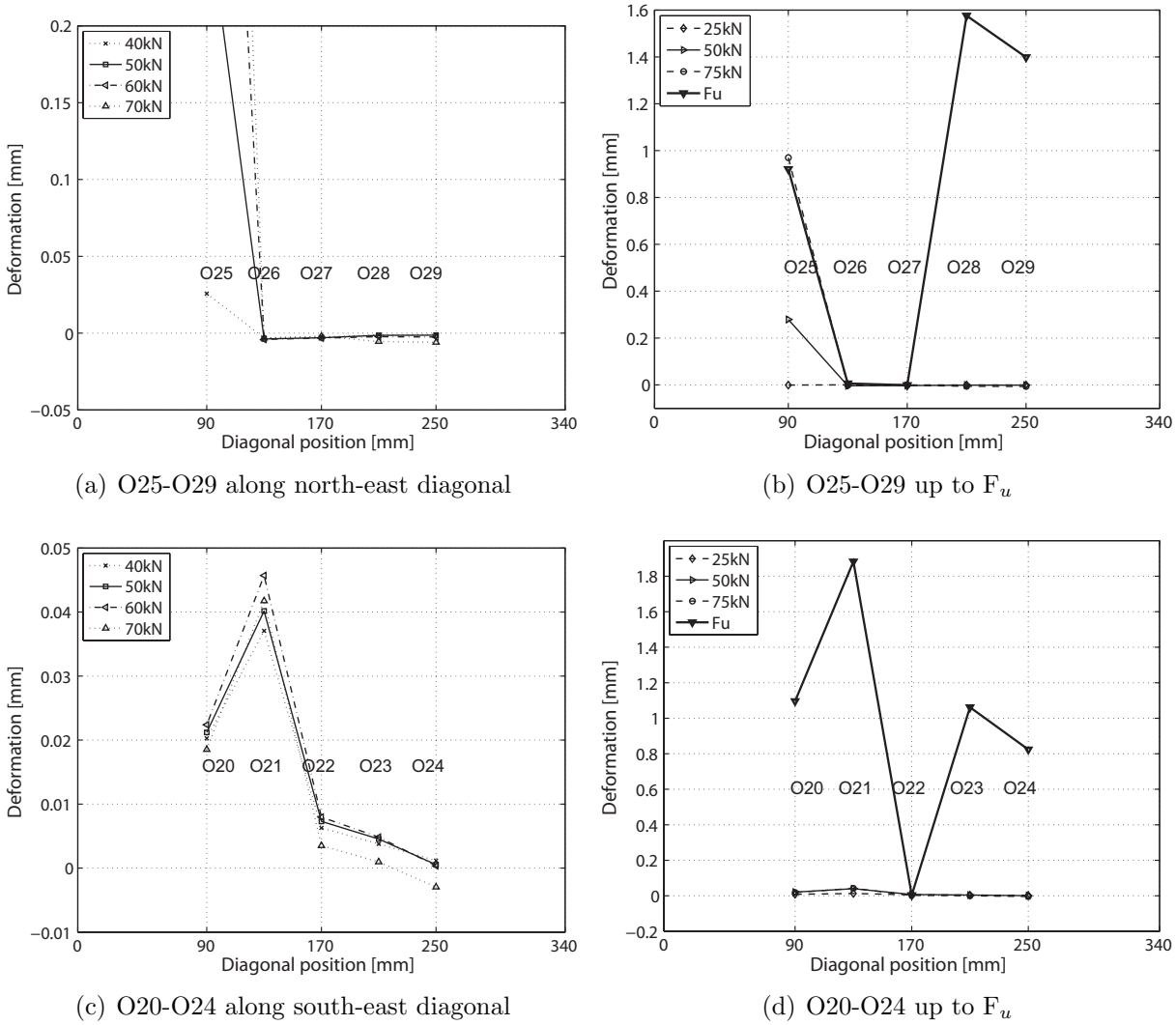

(a) O25-O29 along north-east diagonal

(b) O25-O29 up to F_u

(c) O20-O24 along south-east diagonal

(d) O20-O24 up to F_u

Figure D.27: 1300s-2: Deformations at different load steps perpendicular to diagonal.

D.3.4.5 Deformations at different load steps through the cross section and along the diagonal

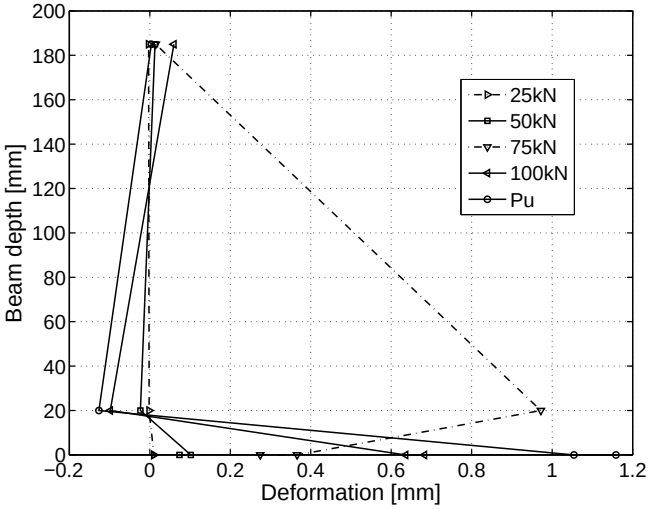

(a) Deformations through cross section on east side

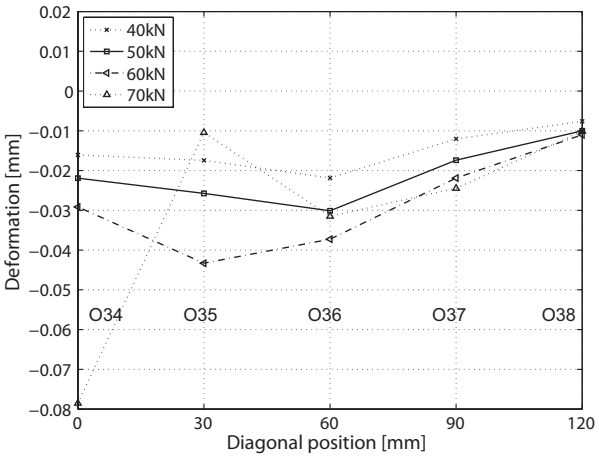

(b) O34-O38 along north-west diagonal

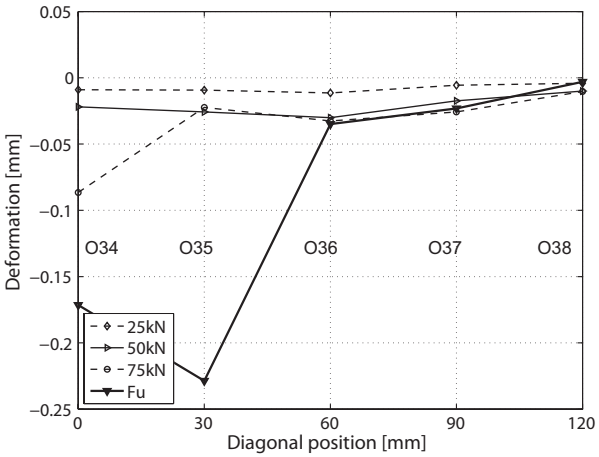

(c) O34-O38 up to F_u

Figure D.28: 1300s-2: Deformations at different load steps.

D.3.5 Specimen 1300Es-1: Failure description and experimental results

D.3.5.1 Failure description

The failure process is illustrated in Figure D.29 and D.30. Up to a load of 55 kN neither cracks nor noises were noticed. Subsequently some noises could be noticed and a crack started to develop vertically between the O35 omega-shaped extensometer in the north-west part of the specimen. It extended through the lower half of the LC layer, and its width was approximately 0.02 mm. Up to a load of 80 kN no further observations could be made, apart from an increase in the length and width of the north-west crack, described above.

At 85 kN noises could be noticed above the northern support, followed by an inclined crack on the north-east side. Consequently a slight disturbance in the almost linear elastic load deflection response could be measured. Subsequently, the north-east crack propagated diagonally at approximately 88 kN and crossed O27, O28 and O29. Up to a load of 102 kN the width of this crack grew to approximately 0.05 mm, while its visible length remained the same. At the same time, a diagonal crack could be observed through O20-O24 in the south-east part of the specimen, while the south-west part remained undamaged. At a load of 155 kN a diagonal crack at the south-west side opened significantly and consequently the load dropped to 145 kN and the specimen lost stiffness, (Figure D.29-a). However, a further load increase could be achieved, while all cracks grew longer and wider.

The ultimate load was reached at 204 kN, due to the opening of the crack in the northern part and simultaneous bond failure of the FRP-LC and the LC-NC interfaces, see Figure D.29-b-c. The load dropped slowly to 145 kN, when buckling of the T-webs of the GFRP was observed. Figure D.30-a shows the interface shear failure, indicating that the shearing surface crossed the LC, while the epoxy layer remained undamaged. The experiment was then stopped.

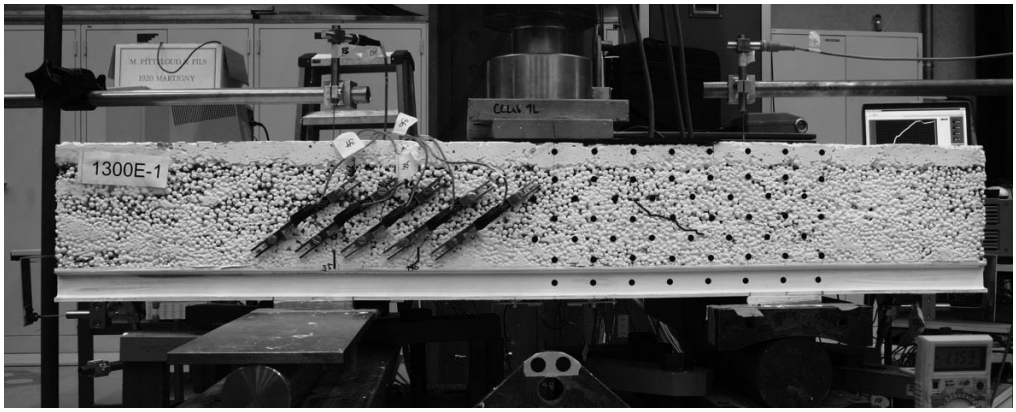

(a) At 170 kN

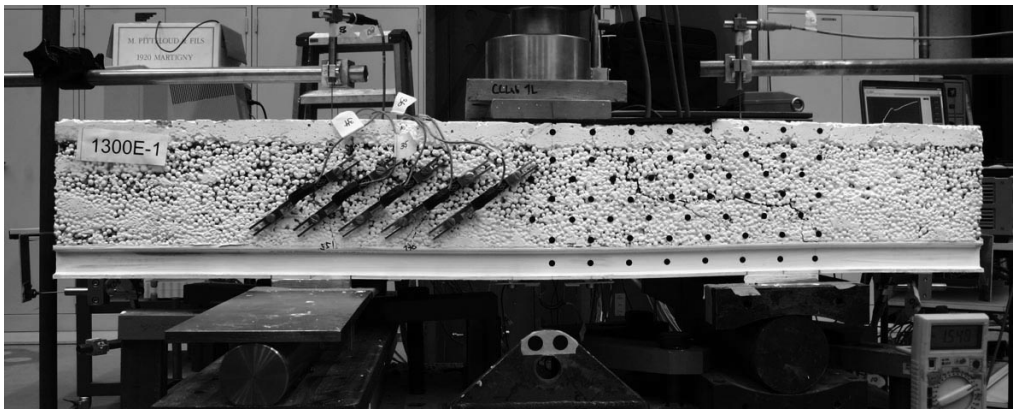

(b) At ultimate load 204 kN

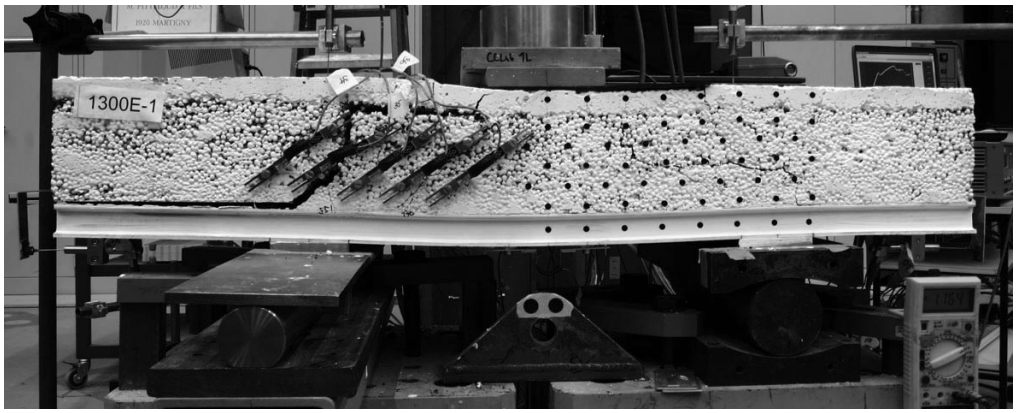

(c) At 150 kN (post-peak)

Figure D.29: 1300Es-1: Failure process on west side (north left, south right).

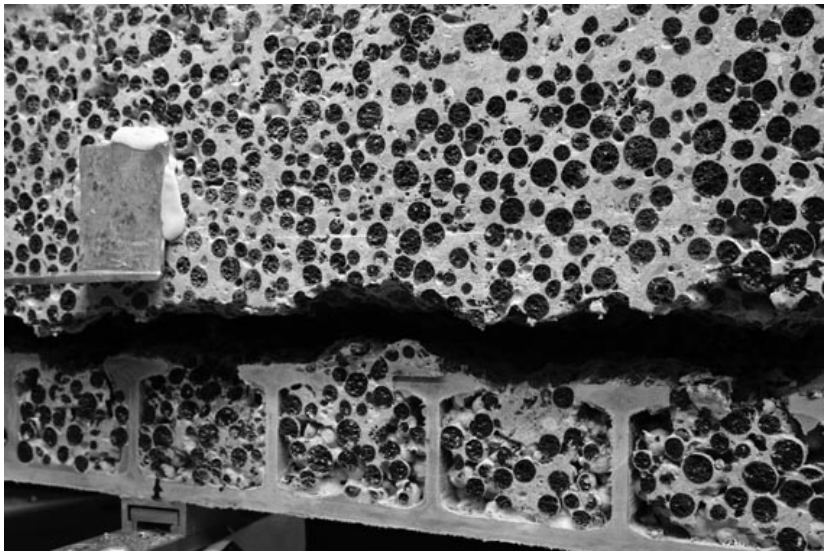

(a) Interface failure

(b) At approximately 140 kN (post-peak) - crack development above O23 and O24

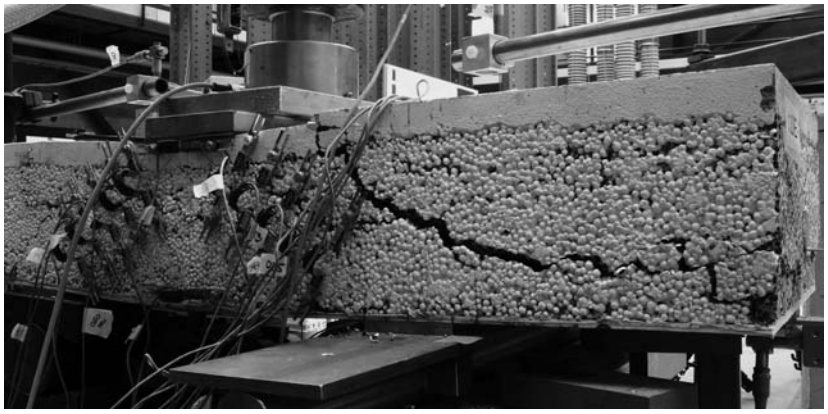

(c) Final crack development above all omega gages

Figure D.30: 1300Es-1: interface failure and crack development in east part of specimen.

D.3.5.2 Displacement transducers

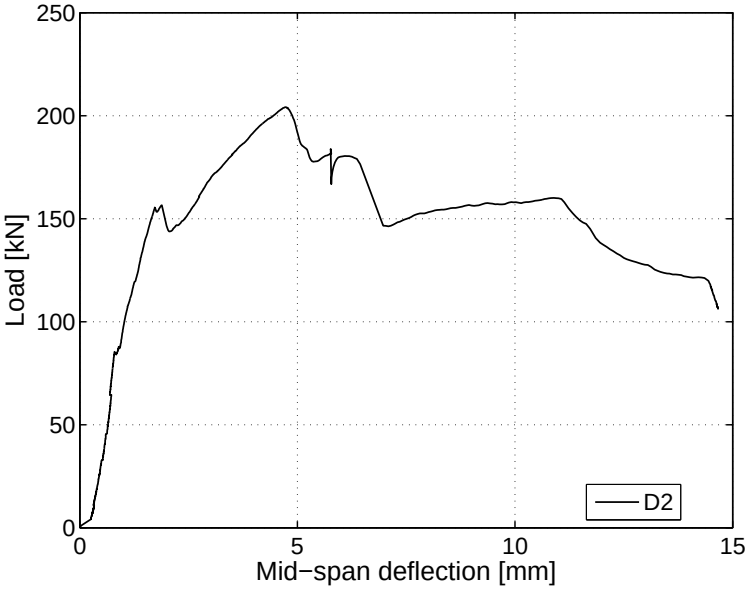

(a) At mid-span

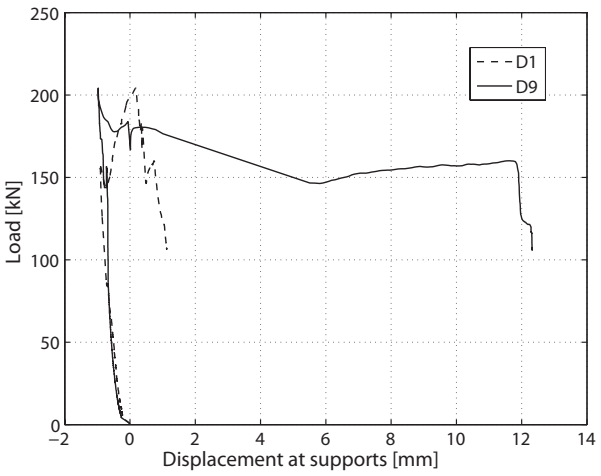

(b) At supports

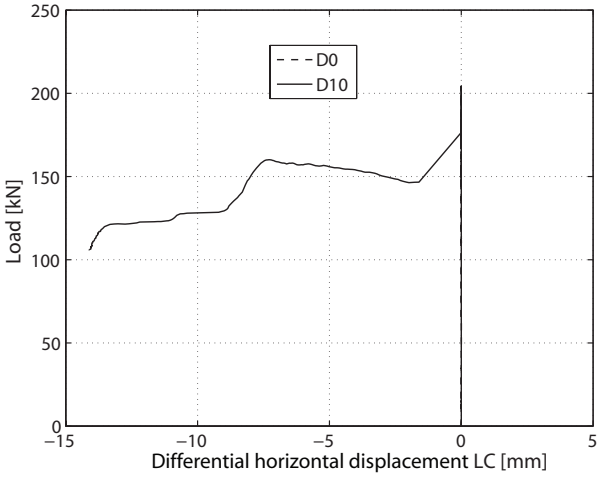

(c) Diff. horizontal displacement within failed LC

Figure D.31: 1300Es-1: Displacement measurements.

D.3.5.3 Omega-shaped extensometers

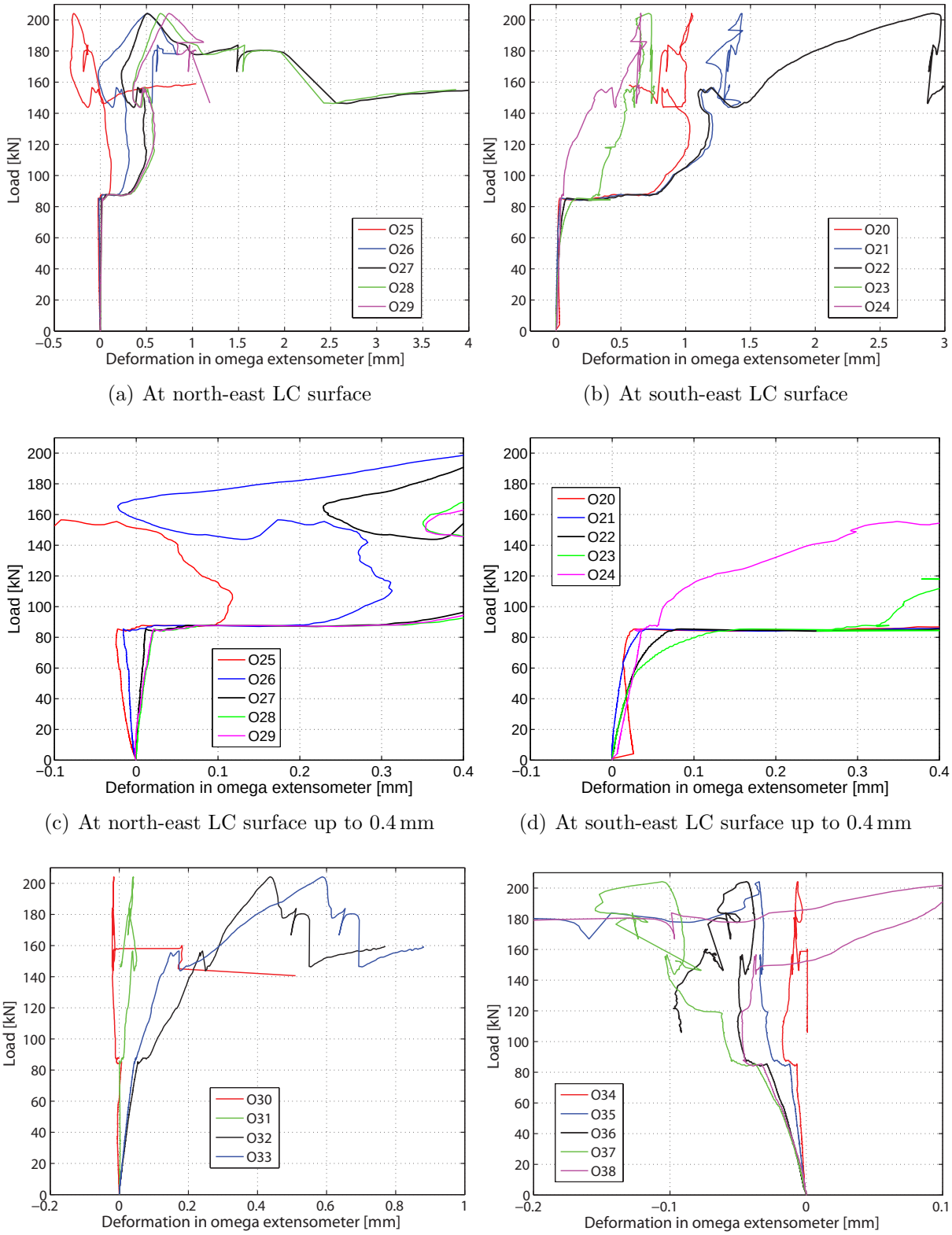

(a) At north-east LC surface

(b) At south-east LC surface

(c) At north-east LC surface up to 0.4 mm

(d) At south-east LC surface up to 0.4 mm

(e) At mid-span

(f) At north-west LC surface

Figure D.32: 1300Es-1: Deformations in omega-shaped extensometers.

D.3.5.4 Deformations at different load steps perpendicular to the diagonal

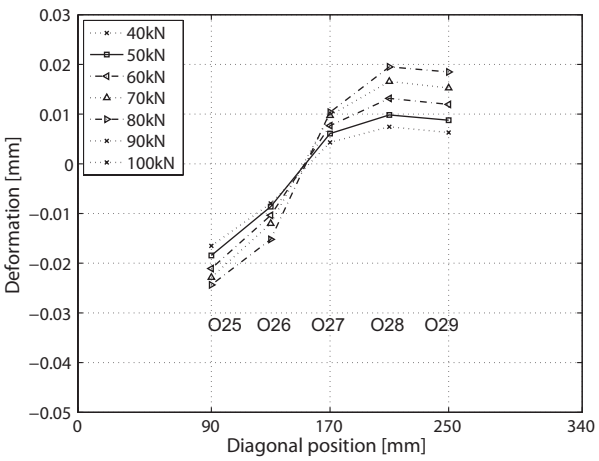

(a) O25-O29 along north-east diagonal

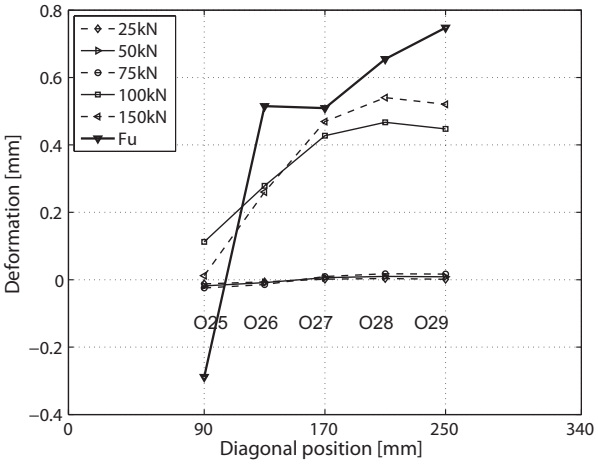

(b) O25-O29 up to F_u

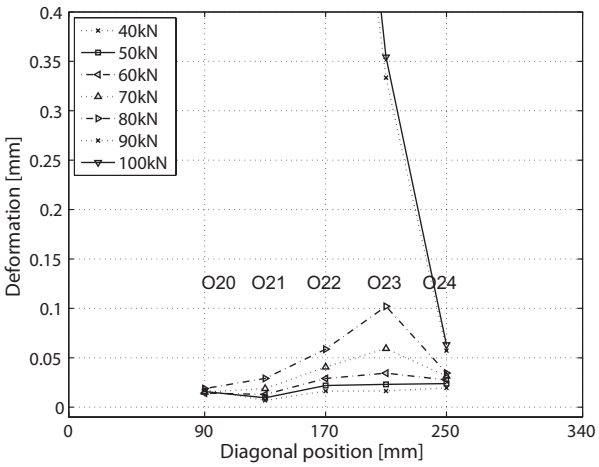

(c) O20-O24 along south-east diagonal

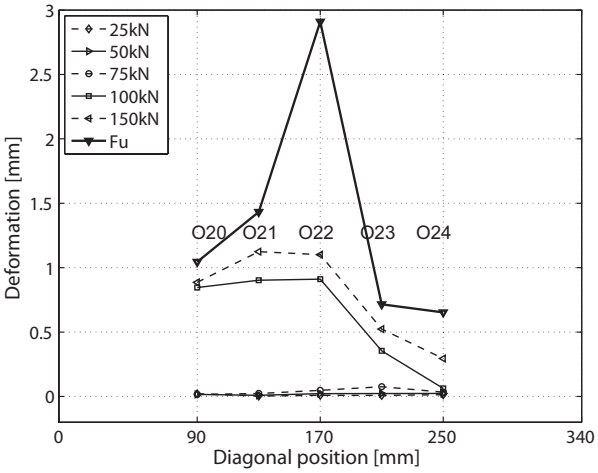

(d) O20-O24 up to F_u

Figure D.33: 1300Es-1: Deformations at different load steps perpendicular to diagonal.

D.3.5.5 Deformations at different load steps through the cross section and along the diagonal

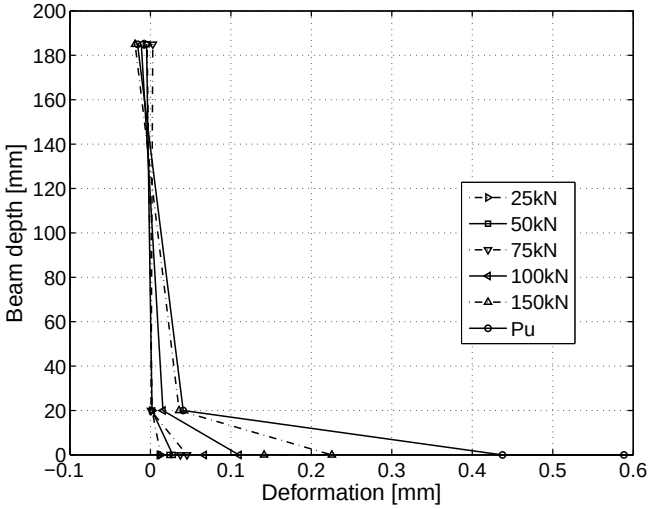

(a) Deformations through cross section on east side

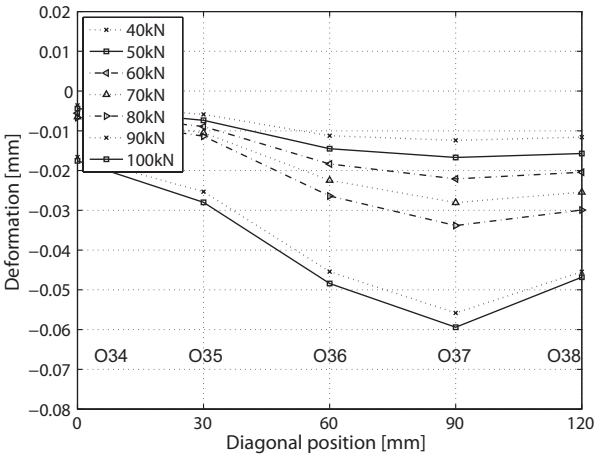

(b) O34-O38 along north-west diagonal

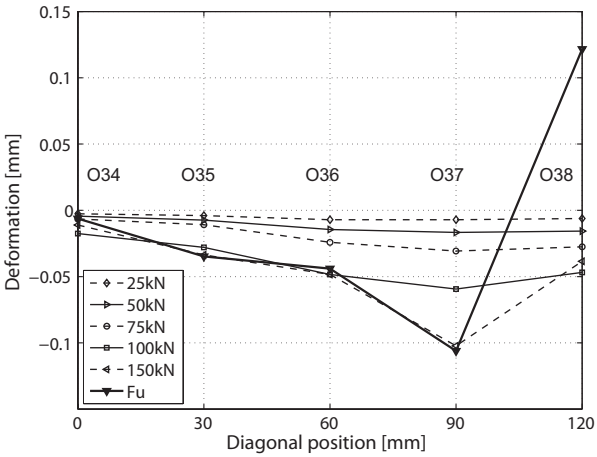

(c) O34-O38 up to F_u

Figure D.34: 1300Es-1: Deformations at different load steps.

D.3.6 Specimen 1300Es-2: Failure description and experimental results

D.3.6.1 Failure description

The failure process is illustrated in Figures D.35, D.36 and D.37. The first audible cracks were noticed at a load of 85 kN. Although no obvious cracks were observed, crack noises were audible on the southern support at 90 kN. Subsequently a diagonal crack was observed between O20 and O21, which developed slowly through O22,O21 and O20. At a load of 106 kN a loud noise was followed by the propagation of the crack through the NC surface. At 153 kN the NC layer was broken across the total width on the south-east side. Besides the crack on the top of the specimen and the diagonal crack on the north-eastern part, as illustrated in Figure D.37, no other cracks could be observed in the LC layer. However, it was noticed that O24 detached from the LC surface. The first peak load was observed at 179 kN, when a diagonal crack propagated diagonally on the north-west side, between O36 and O37. The specimen regained stiffness and a plateau could be maintained around the ultimate load of 185.2 kN. O21 and O22 detached and further cracks on the NC surface could be observed. As a consequence, a short jump in the load deflection was measured. When a mid-span deflection of 6.5 mm was reached, the load dropped to 146 kN due to the opening of the diagonal crack through the LC on the north side (Figure D.36-a-c). The experiment was stopped at a mid-span deflection of 11.8 mm as no further load increase could be expected.

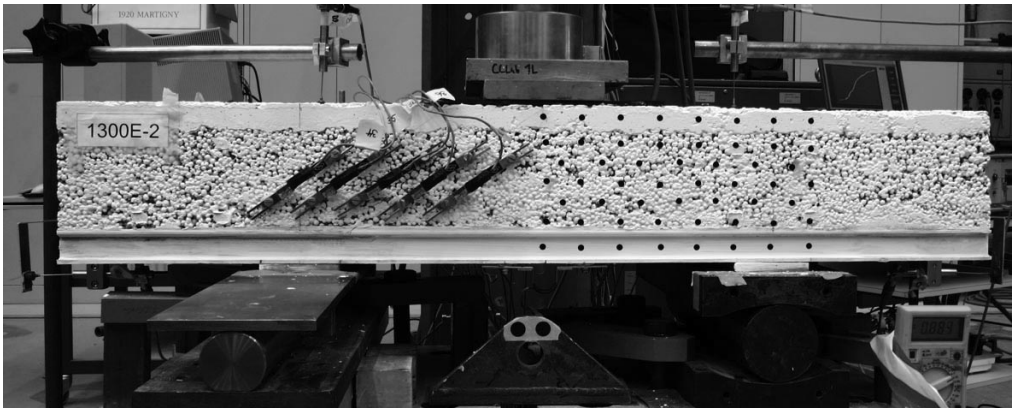

(a) At 114 kN - no cracks observed on west side

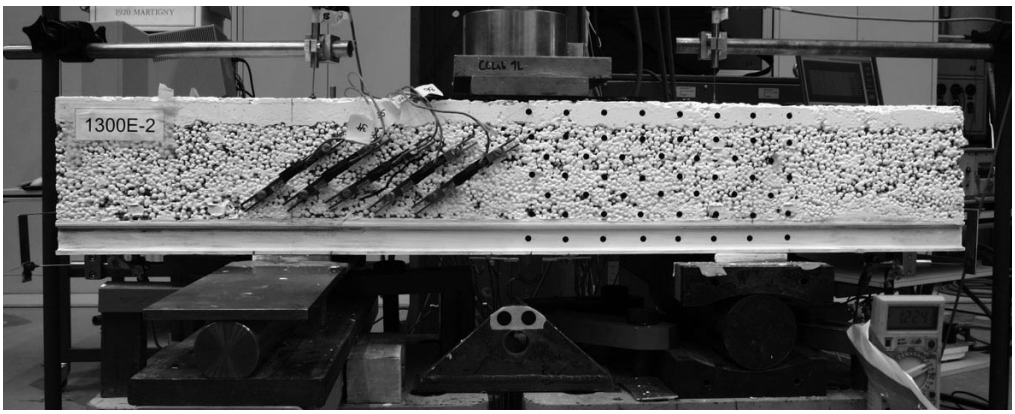

(b) At 159 kN - diagonal crack between O36 and O37

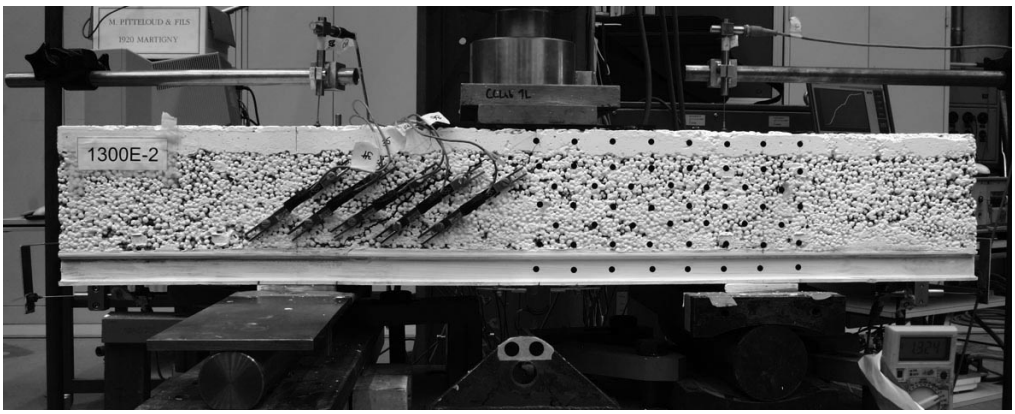

(c) At 173 kN

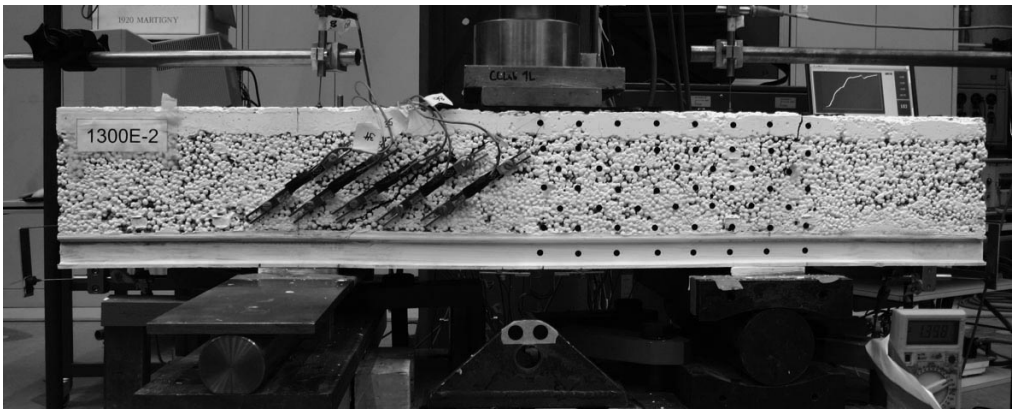

(d) At 180 kN

Figure D.35: 1300Es-2: Failure process on west side (north left, south right).

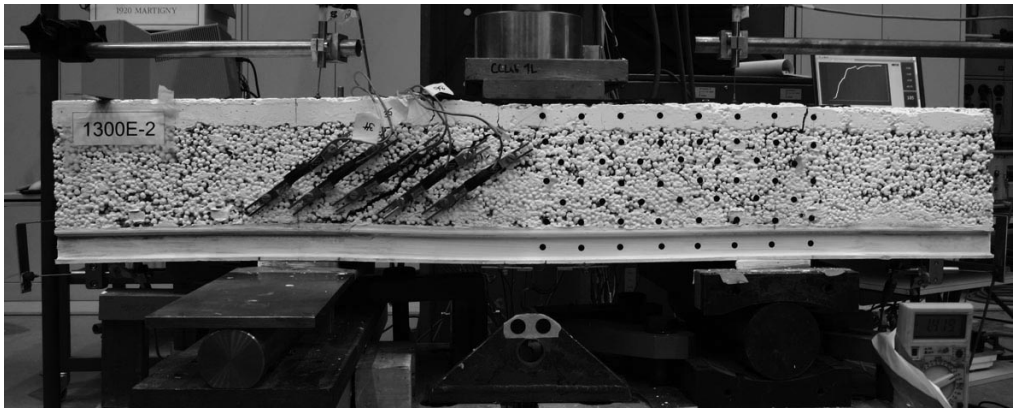

(a) At 185 kN (post-peak)

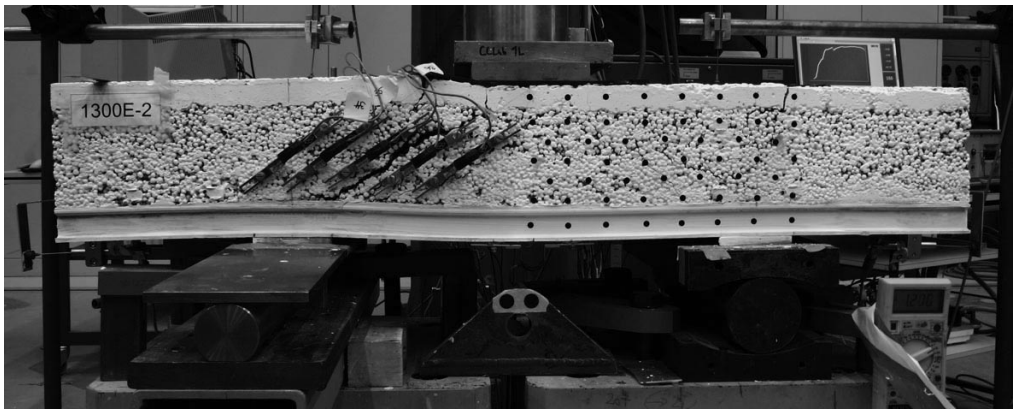

(b) At 166 kN (post-peak)

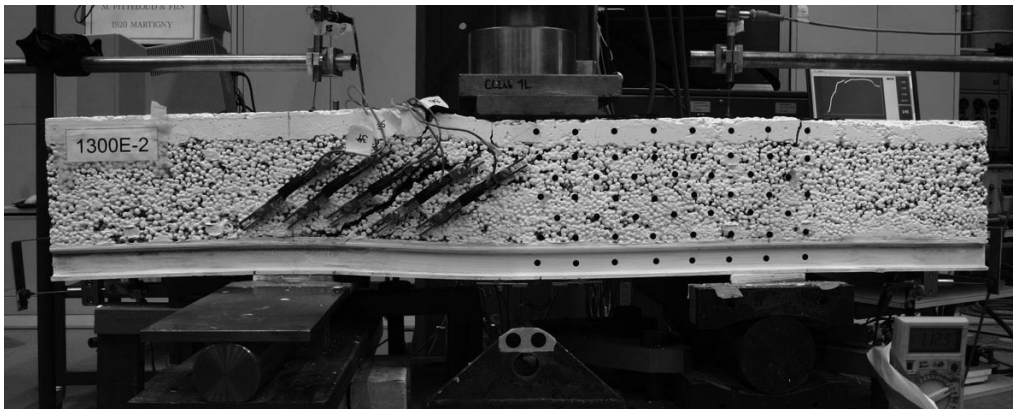

(c) At 146 kN (post-peak)

Figure D.36: 1300Es-2: Failure process on west side, continuation.

(a) At approximately 165 kN - crack development above O20, O21 and O23

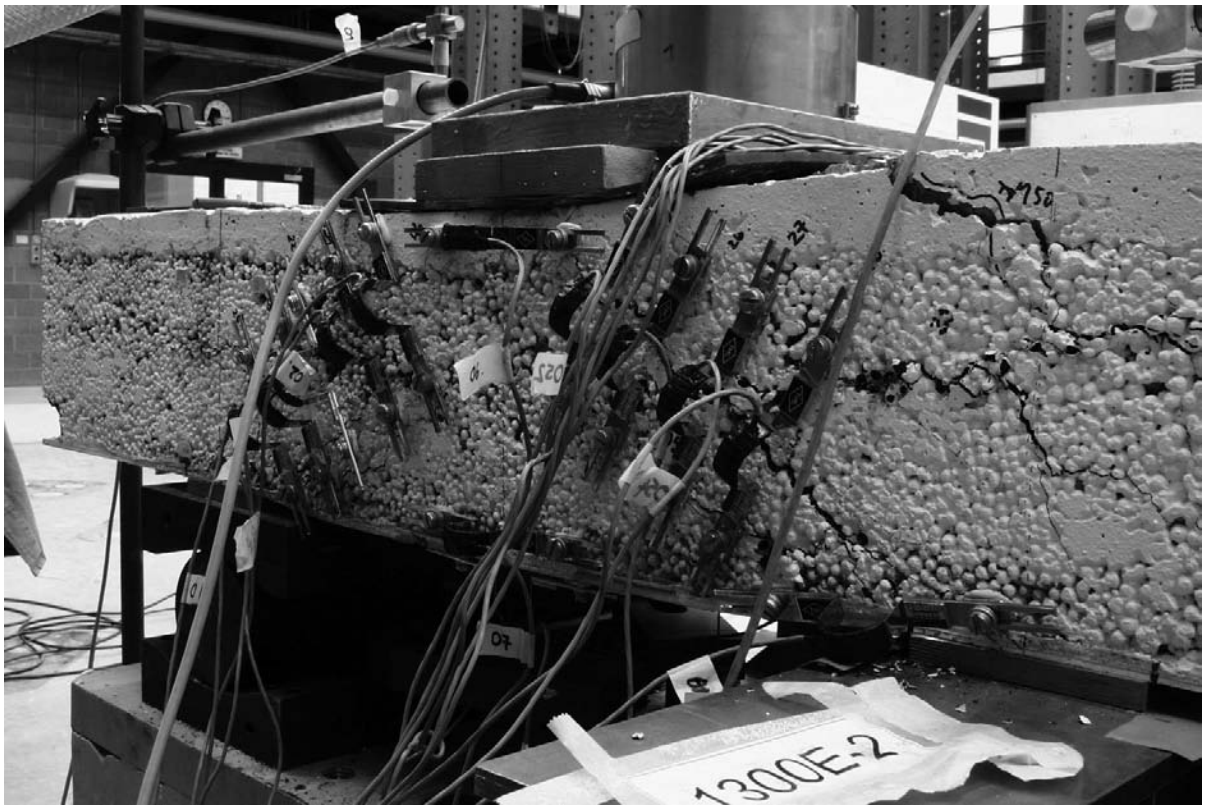

(b) After ultimate load F_u

Figure D.37: 1300Es-2: Crack development in eastern part of specimen.

D.3.6.2 Displacement transducers

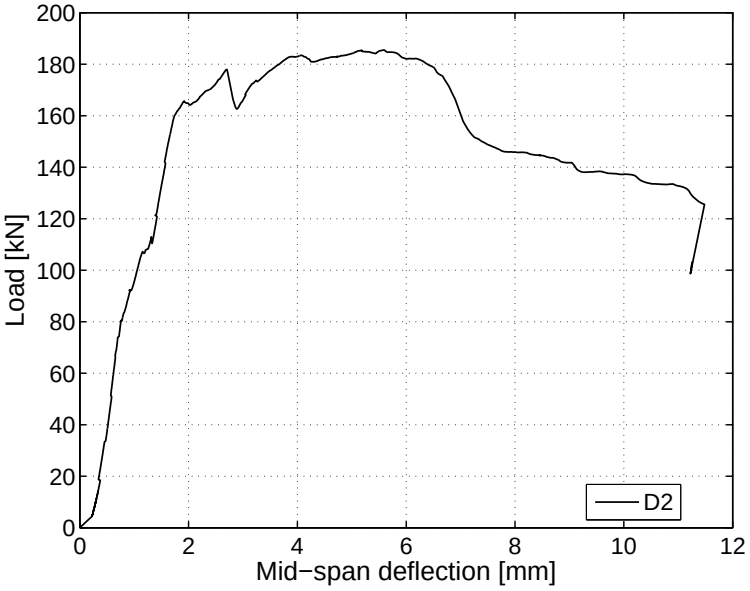

(a) At mid-span

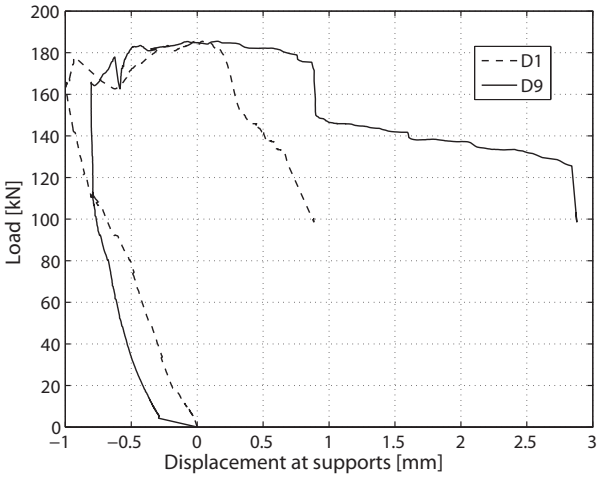

(b) At supports

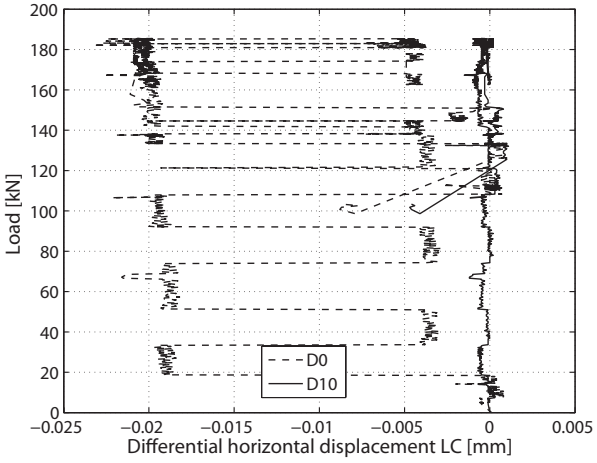

(c) Diff. horizontal displacement within failed LC

Figure D.38: 1300Es-2: Displacement measurements.

D.3.6.3 Omega-shaped extensometers

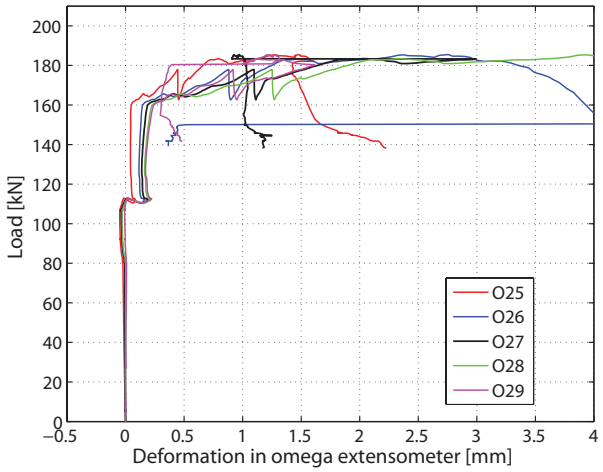

(a) At north-east LC surface

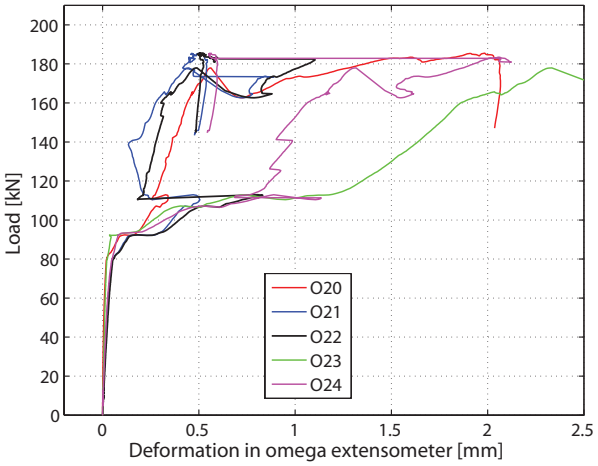

(b) At south-east LC surface

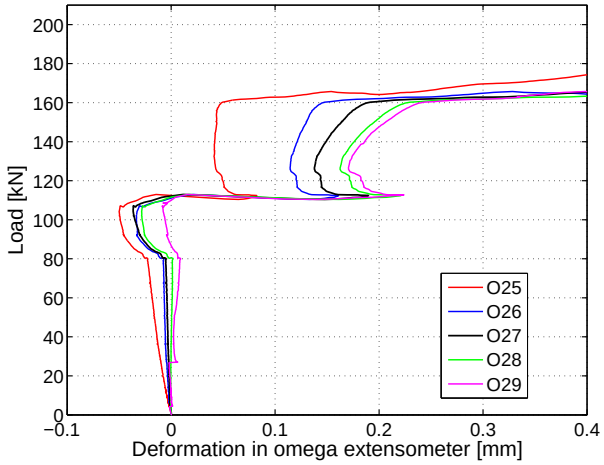

(c) At north-east LC surface up to 0.4 mm

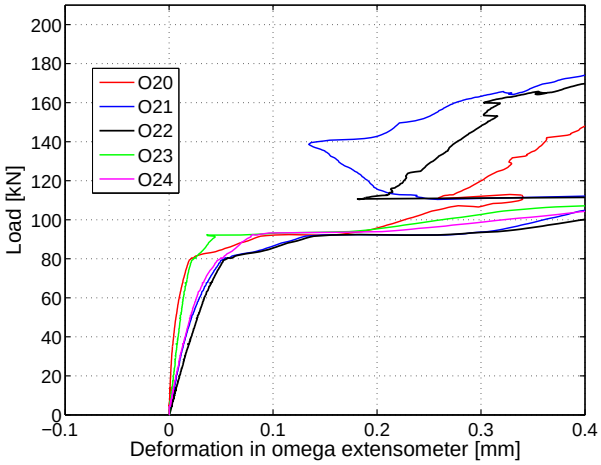

(d) At south-east LC surface up to 0.4 mm

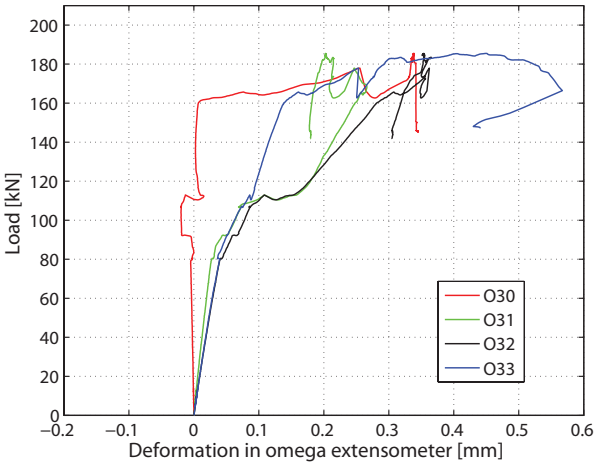

(e) At mid-span

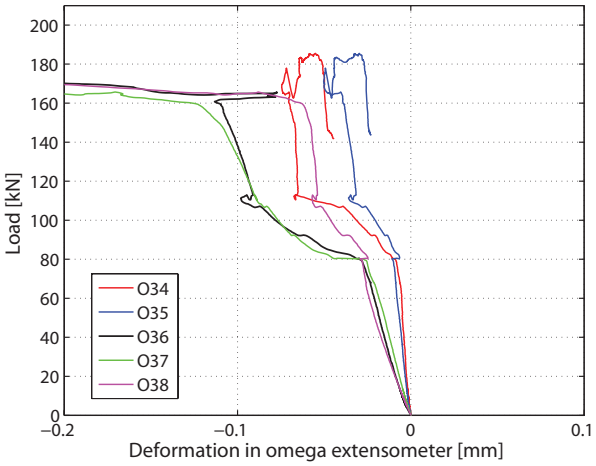

(f) At north-west LC surface

Figure D.39: 1300Es-2: Deformations in omega-shaped extensometers.

D.3.6.4 Deformations at different load steps perpendicular to the diagonal

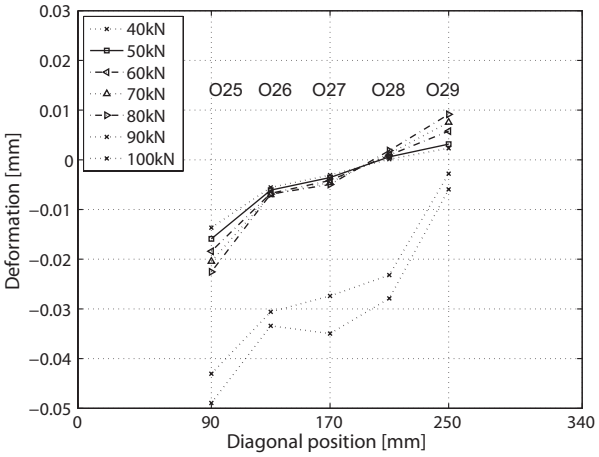

(a) O25-O29 along north-east diagonal

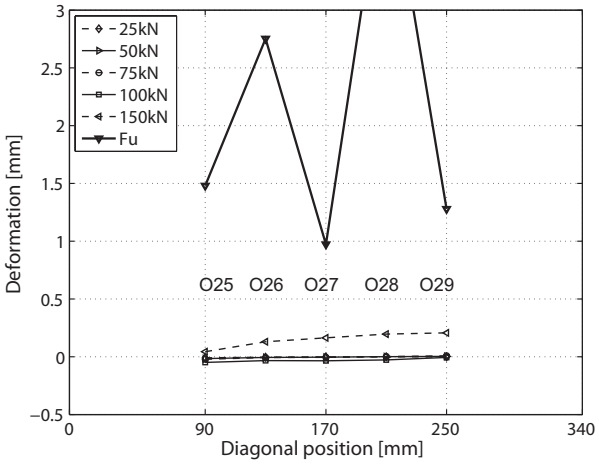

(b) O25-O29 up to F_u

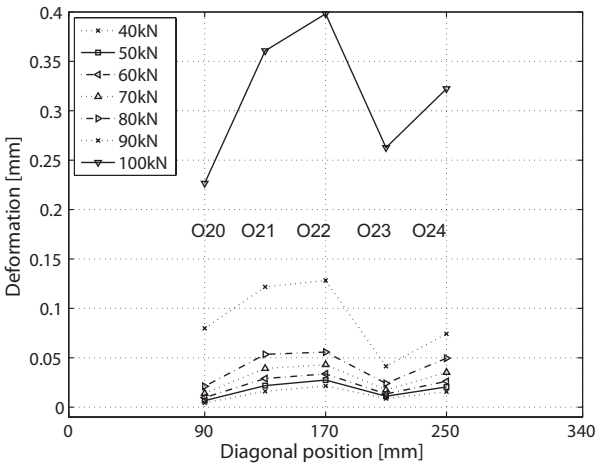

(c) O20-O24 along south-east diagonal

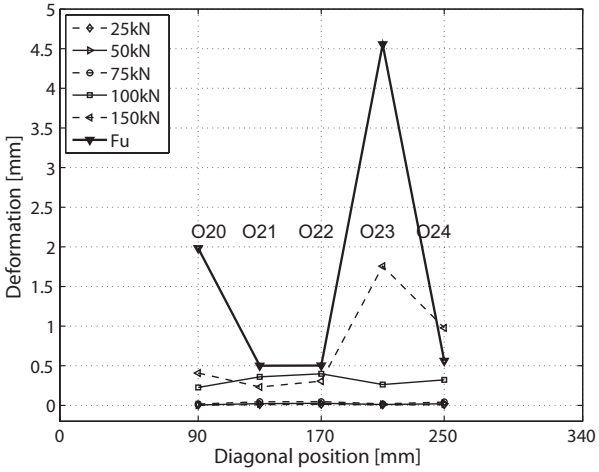

(d) O20-O24 up to F_u

Figure D.40: 1300Es-2: Deformations at different load steps perpendicular to diagonal.

D.3.6.5 Deformations at different load steps through the cross section and along the diagonal

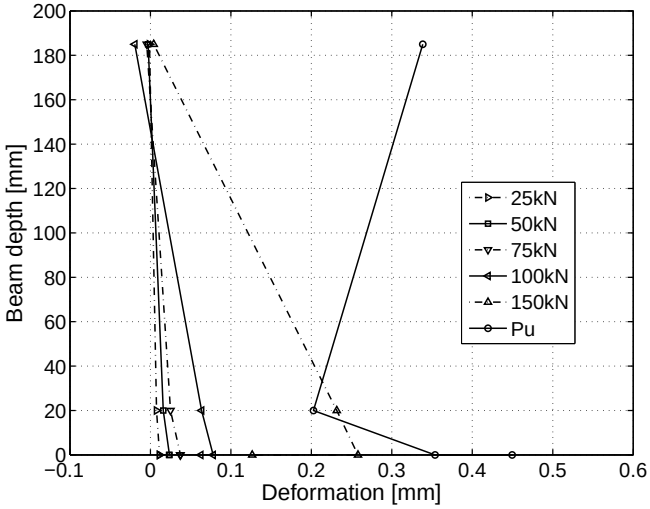

(a) Deformations through cross section on east side

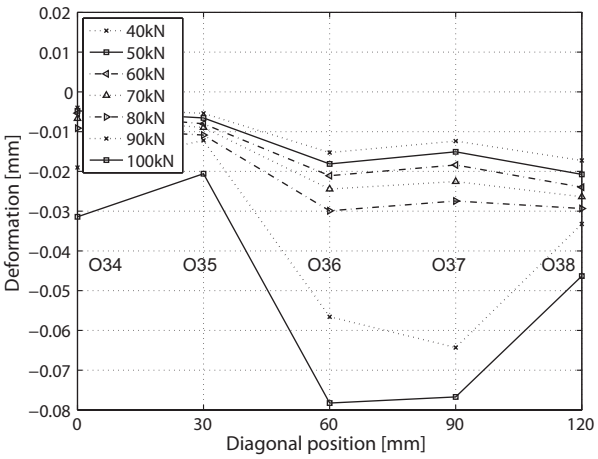

(b) O34-O38 along north-west diagonal

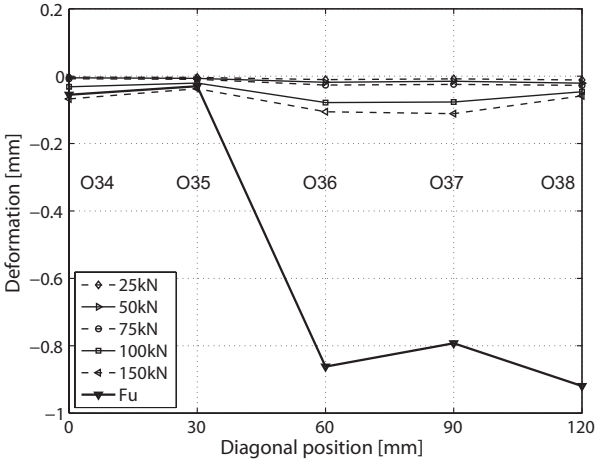

(c) O34-O38 up to F_u

Figure D.41: 1300Es-2: Deformations at different load steps.

D.3.7 Specimen 1000s: Failure description and experimental results

D.3.7.1 Failure description

The failure process is illustrated in Figures D.42 and D.43. The first audible cracks were noticed at a load of 42 kN. The first visible diagonal cracks were observed at a load of 44 kN in the eastern part of the specimen between O21 and O22 and next to O23 and O24. Short vertical cracks in the lower part of the LC were also observed. At 44 kN the jack stopped for several seconds due to insufficient pressure, and therefore the measurements differed slightly and a short deloading had to be carried out. Subsequently, a loud noise was noticed at a load of 45 kN, followed by a pronounced crack between omega gages O20,O21 and O22, and next to O23 and O24. At 65 kN the crack width was 0.2 mm on the western side. On the eastern part of the specimen, where only one crack at mid-span was observed, the crack width amounted to 0.12 mm. Starting at a load of 70 kN, several almost parallel cracks propagated on the south-east side. At 80 kN a diagonal crack on the north-east was observed, propagating between O27, O28 and O29, see Figure D.43-a. At this point, all the cracks on the south-east side developed up to the NC layer. The crack width increased, reaching values of between 0.3 and 0.4 mm at 95 kN. At the loading of 130 kN, the diagonal cracks were very well pronounced through the whole LC depth on the north-east and south-east sides. At 150 kN, a crack width of 0.5 up to 1.5 mm could be observed in the south-eastern part and the LC started to push out of the GFRP on the southern side while the crack in the northern part did not exceed 0.8 mm. At 130 kN the crack propagated through omega gage O30. At 163.9 kN the ultimate load was reached. Subsequently a load of 160 kN was maintained until a new crack started to grow above the omega gages, parallel to the theoretical diagonal in the south-east part of the specimen. The load then dropped slightly down to 130 kN while the southern cracks grew significantly. The final drop in load was reached when the whole southern LC-NC unit broke open, as illustrated in Figure D.43. The experiment was then stopped.

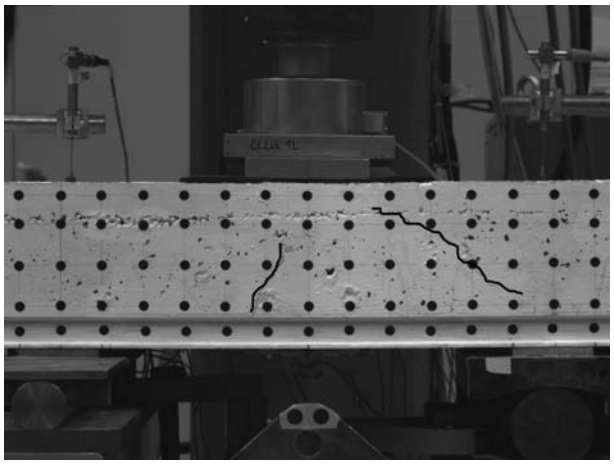

(a) At ultimate load

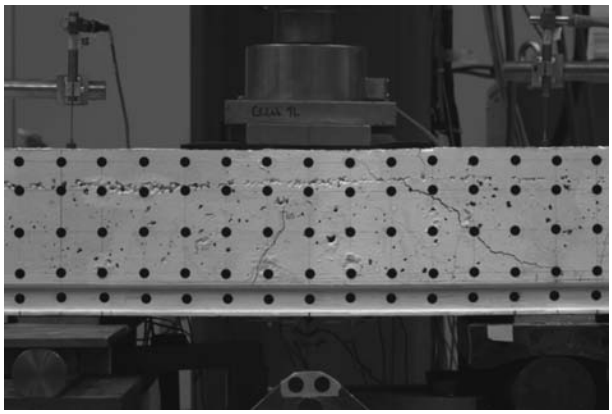

(b) At 160 kN (post-peak)

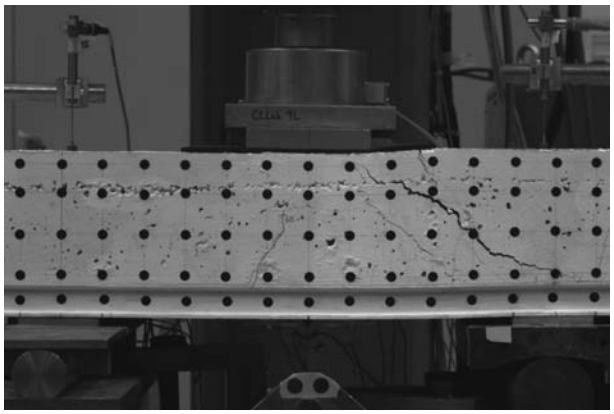

(c) At 150 kN (post-peak)

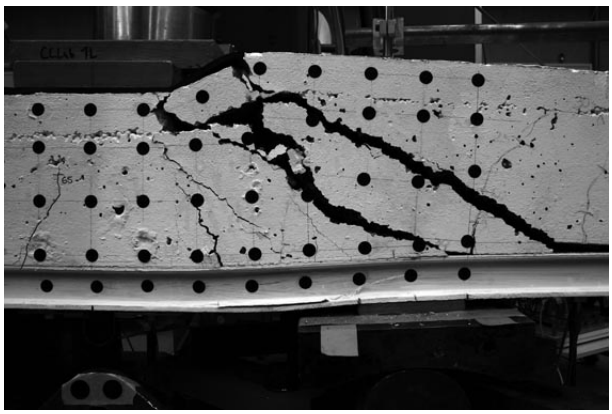

(d) Detail of crack (see (e))

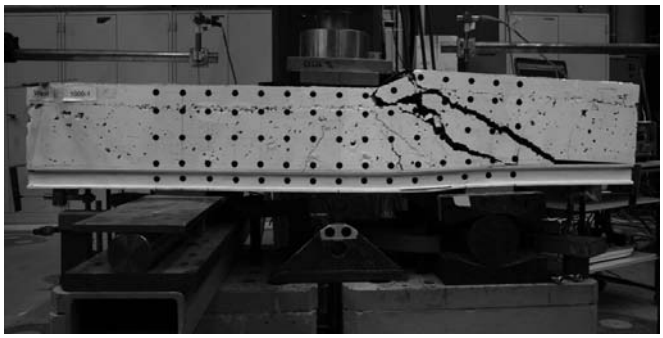

(e) At end of experiment

Figure D.42: 1000s: Failure process on west side (north left, south right).

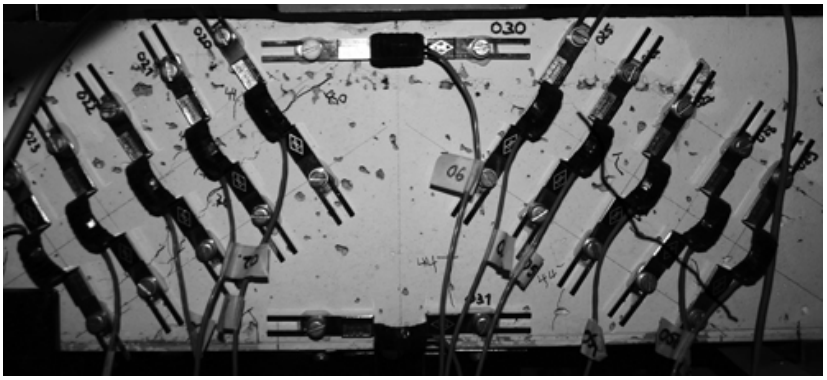

(a) Crack development on east part of specimen at approximately 80 kN

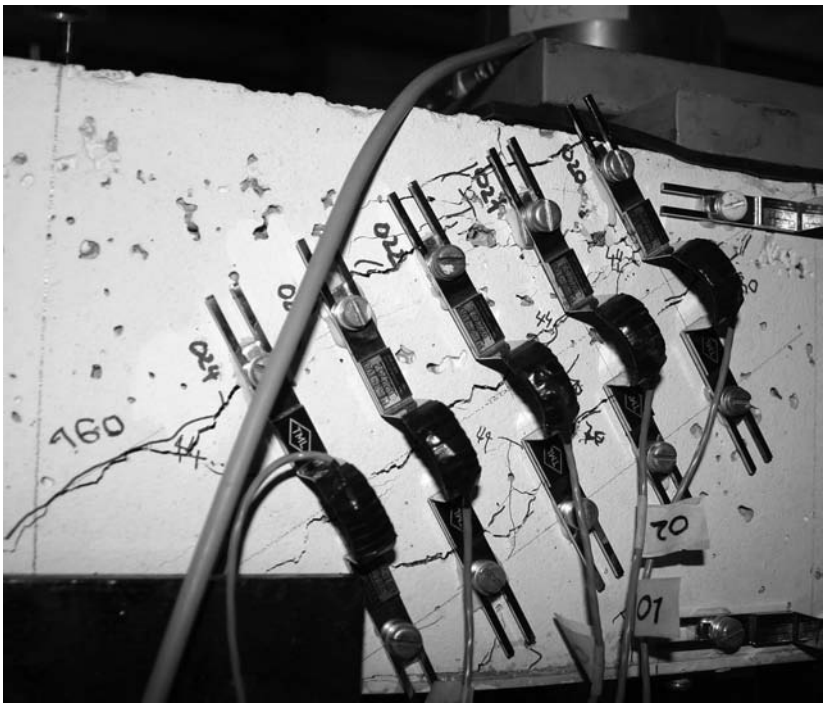

(b) Crack development in east part of specimen after ultimate load (post-peak)

(c) Pushing out of LC block at end of experiment

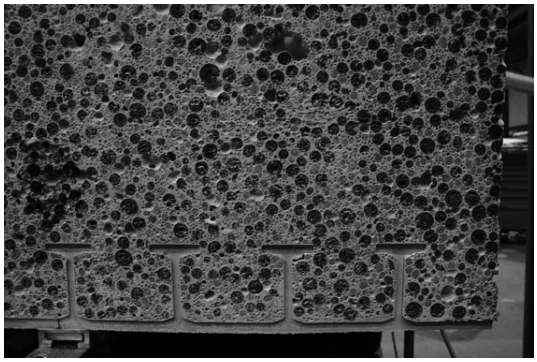

(d) Pushing out of LC between T-upstands at end of experiment

Figure D.43: 1000s: Crack development in east part of specimen and pushing out of LC.

D.3.7.2 Displacement transducers

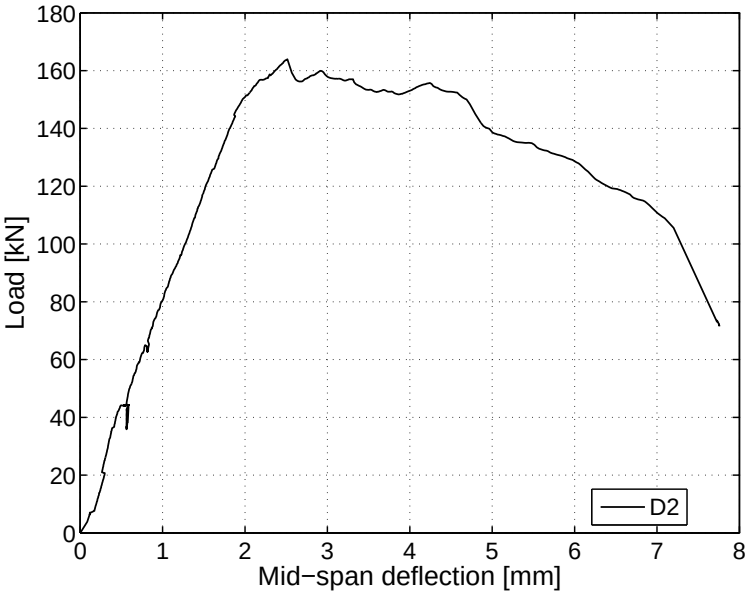

(a) At mid-span

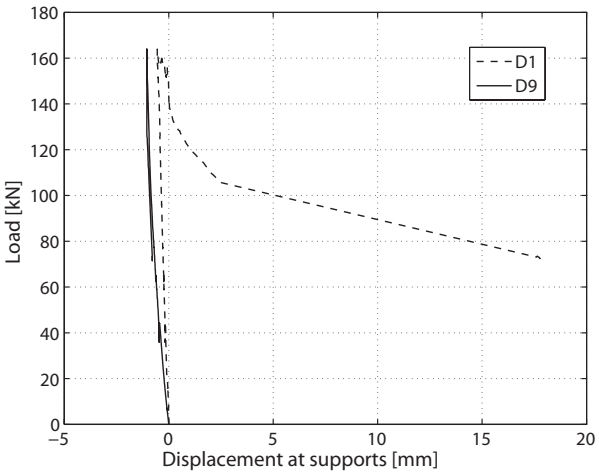

(b) At supports

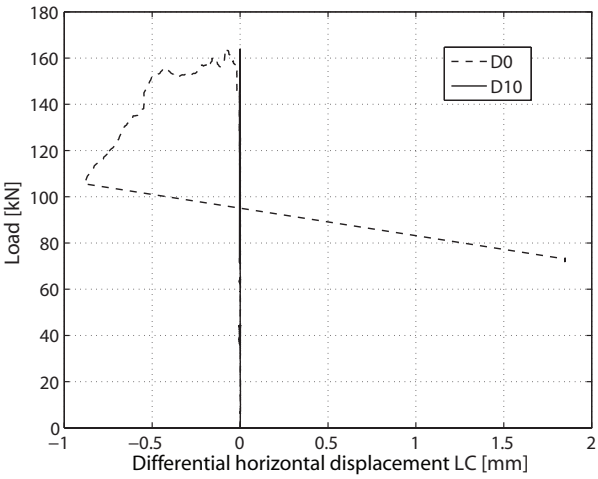

(c) Diff. horizontal displacement within failed LC

Figure D.44: 1000s: Displacement measurements.

D.3.7.3 Omega-shaped extensometers

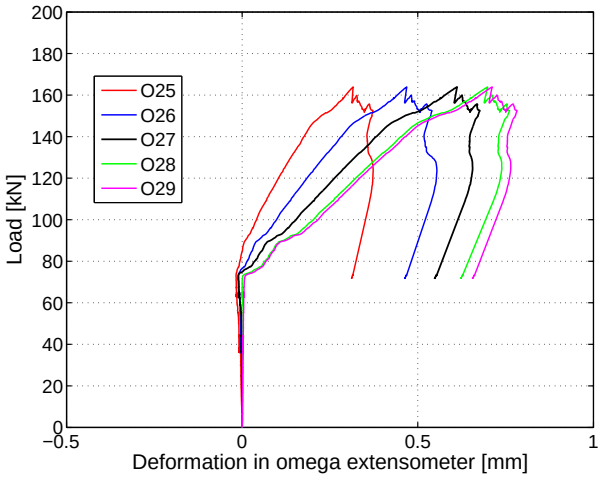

(a) At north-east LC surface

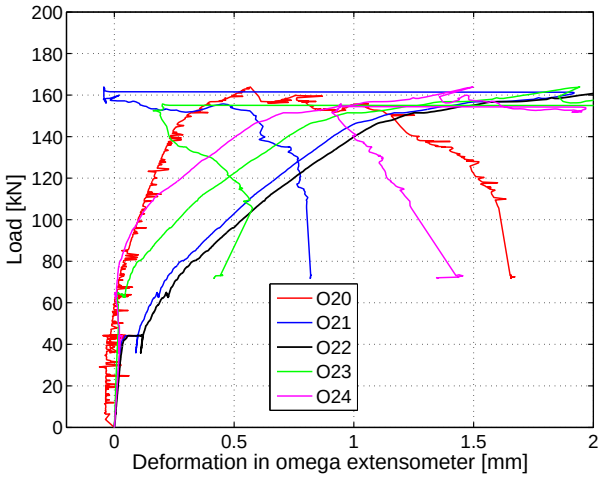

(b) At south-east LC surface

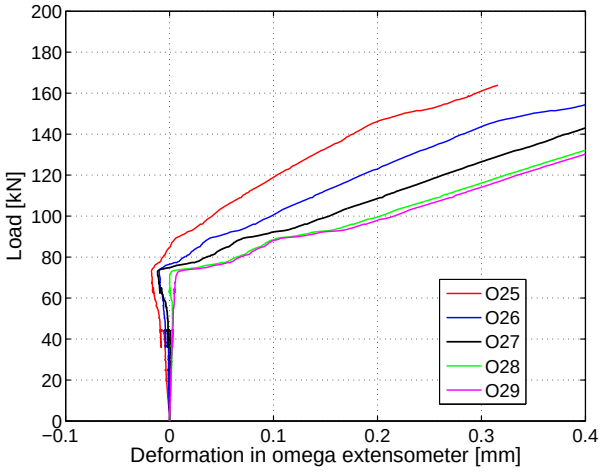

(c) At north-east LC surface up to 0.4 mm

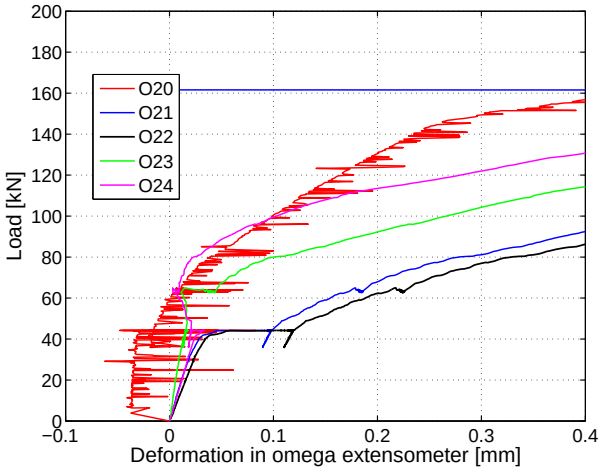

(d) At south-east LC surface up to 0.4 mm

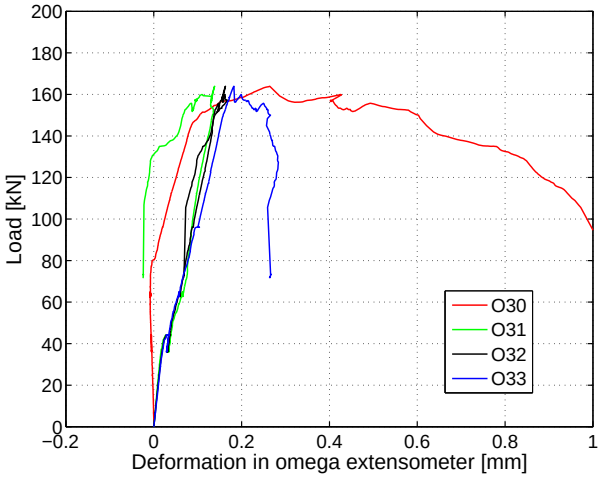

(e) At mid-span

Figure D.45: 1000s: Deformations in omega-shaped extensometers.

D.3.7.4 Deformations at different load steps

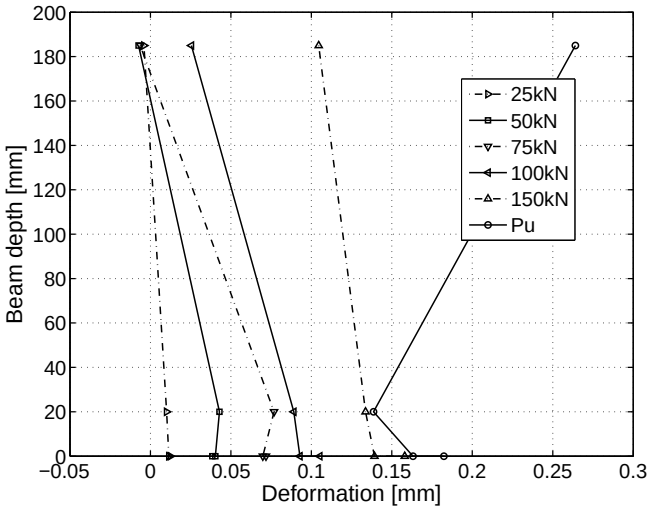

(a) Deformations through cross section on east side

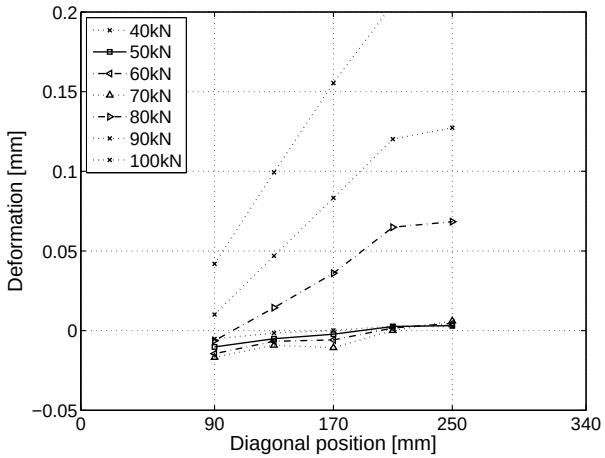

(b) O25-O29 along north-east diagonal

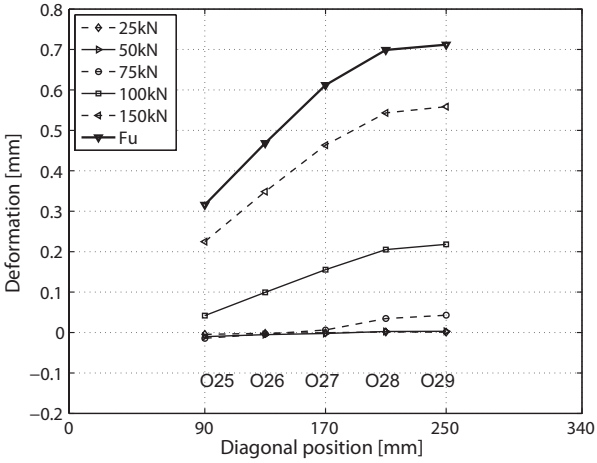

(c) O25-O29 up to F_u

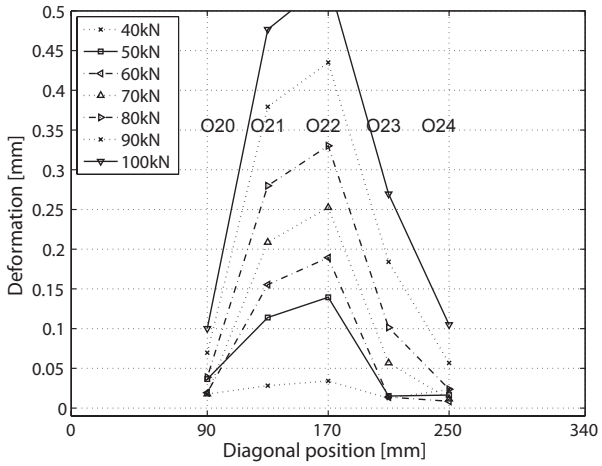

(d) O20-O24 along south-east diagonal

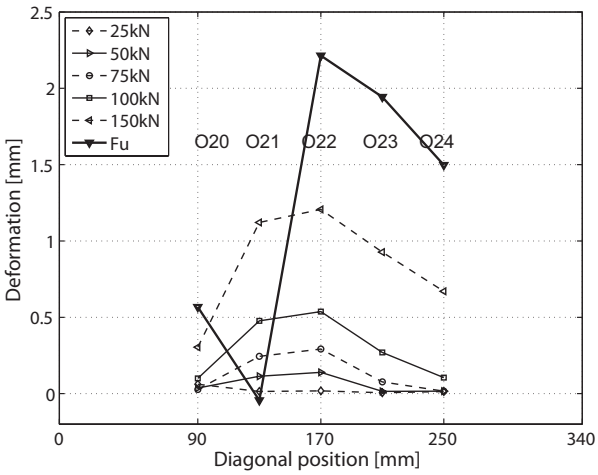

(e) O20-O24 up to F_u

Figure D.46: 1000s: Deformations at different load steps.

D.3.8 Specimen 1000Es: Failure description and experimental results

D.3.8.1 Failure description

The failure process is illustrated in Figures D.47, D.48 and D.49. The first very small crack was observed at a load of 35 kN between omega gages O21 and O22, followed by a small noise next to the support at approximately 43 kN. At 50 kN a diagonal crack developed through the midline of O20 to O24 on the south-east side of the specimen. Later, small noises were noticed at a load of 65 kN. At 70 kN a further crack started to develop on the south-east side of the specimen, at the lower fixation of gage O22. Simultaneously, a diagonal crack developed in the north-east part of the specimen, starting next to gage O27. At a load of 80 kN the cracks exhibited an average width of 0.05 mm. All cracks propagated increasingly with increased loading, always from the mid-depth of the specimen towards the upper and lower parts. At approximately 100 kN the diagonal south-east crack reached the LC-NC interface next to the loading plate and developed towards the mid-span, see Figure D.49-a. The first crack in the northern west side of the specimen was observed at approximately 130 kN. Like the other cracks, it developed diagonally between the compression omegas O36 and O37. The diagonal crack in the south-east part of the specimen reached a width of 0.2 mm at a load of 190 kN. The ultimate load of the specimen was reached at 200.8 kN (Figure D.47-a). Subsequently the northern diagonal crack opened more and more. In addition, a second and more vertical crack developed approximately 50 mm from the centerline (Figure D.47-d) and subsequently the principal diagonal crack developed horizontally along the FRP-LC and LC-NC interfaces. The failure process and horizontal crack development up to the end of the experiment are illustrated in Figure D.48. The final drop in load to 95 kN occurred when the FRP-LC interface was totally damaged throughout the whole length, and thus the experiment was stopped here.

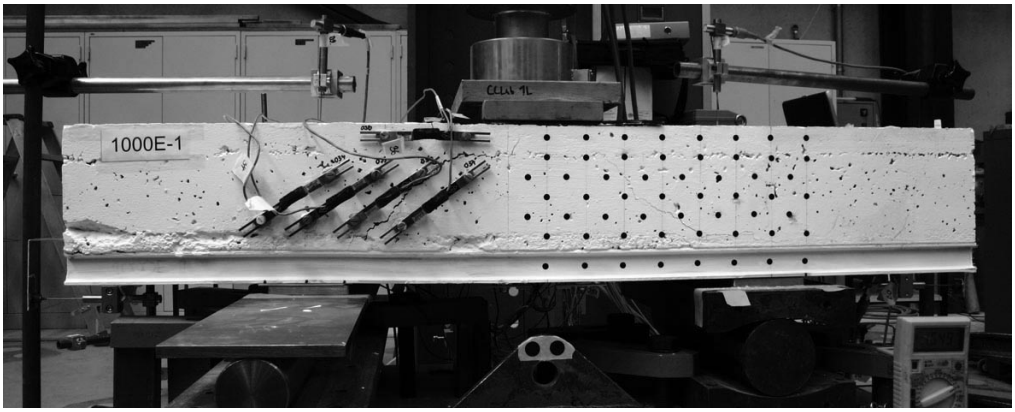

(a) At ultimate load

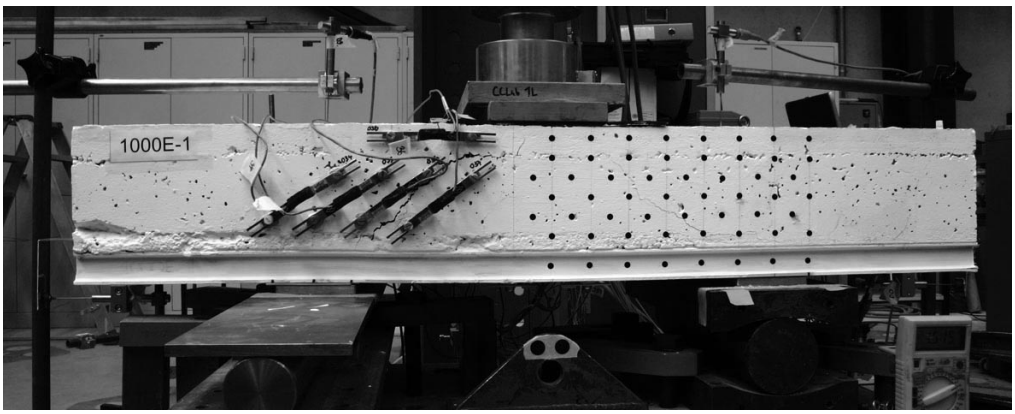

(b) At 196 kN

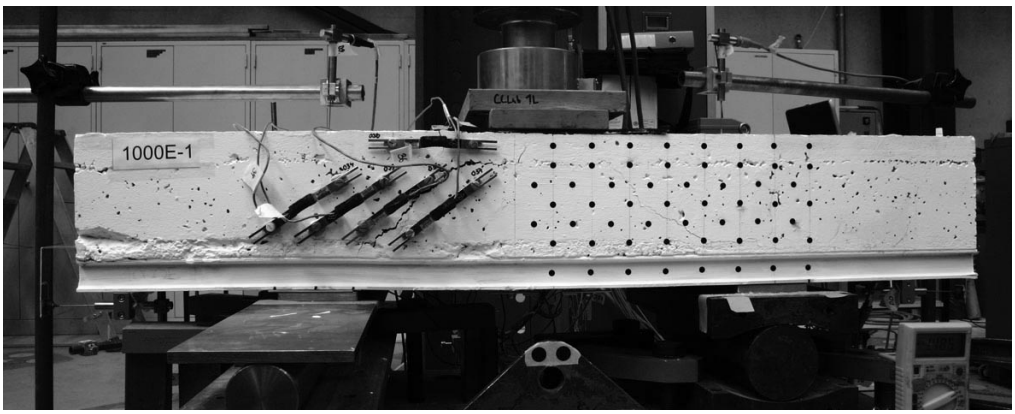

(c) At 193 kN (post-peak)

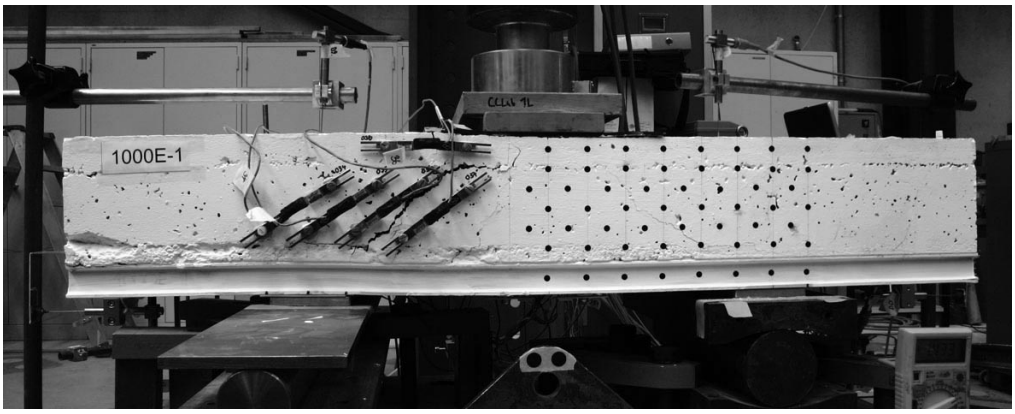

(d) At 187 kN (post-peak)

Figure D.47: 1000Es: Failure process on west side (north left, south right).

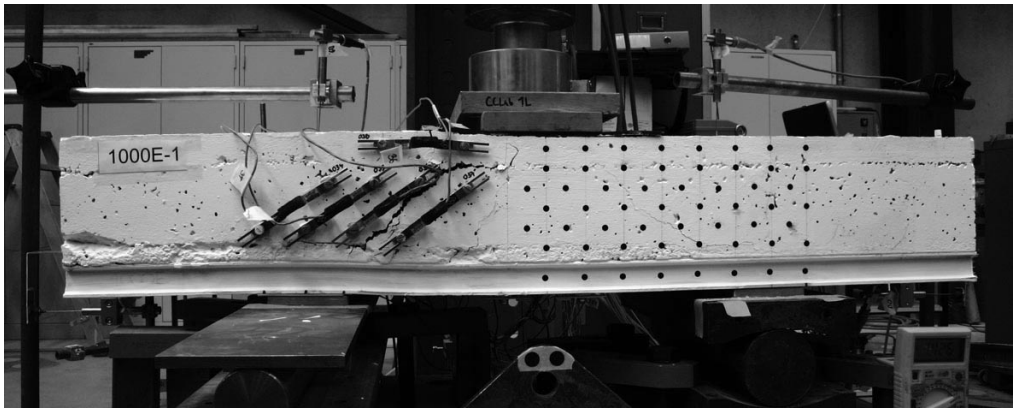

(a) At 186 kN (post-peak)

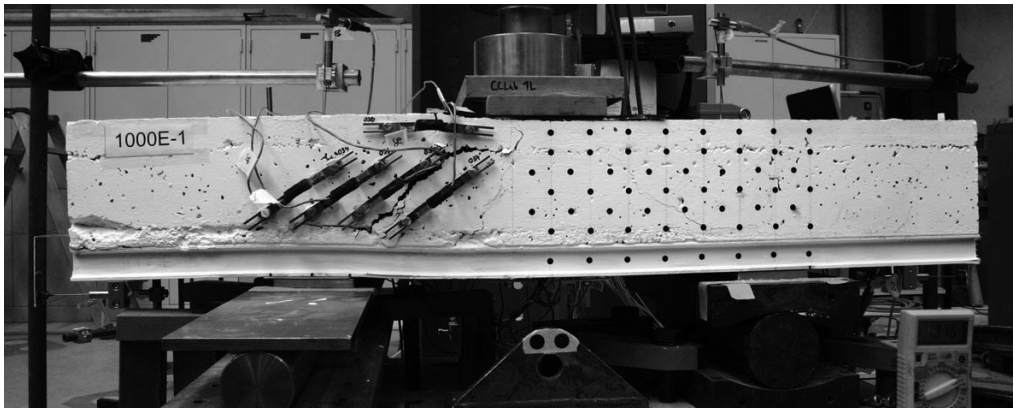

(b) At 180 kN (post-peak)

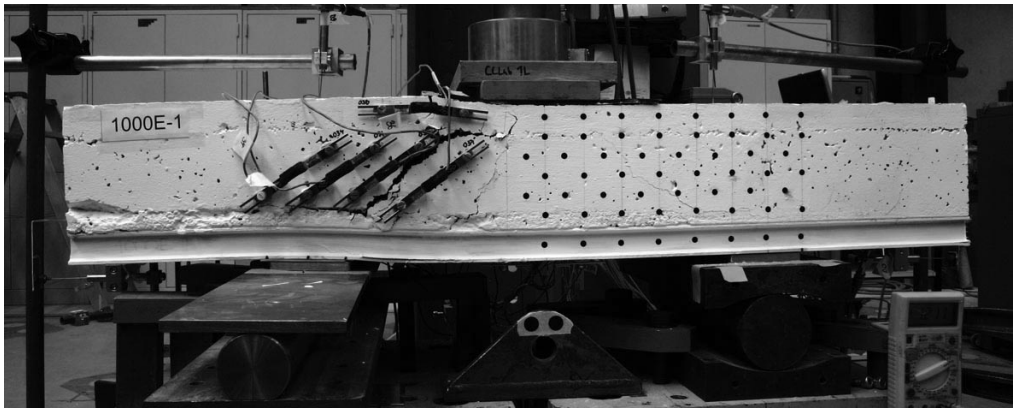

(c) At 157 kN (post-peak)

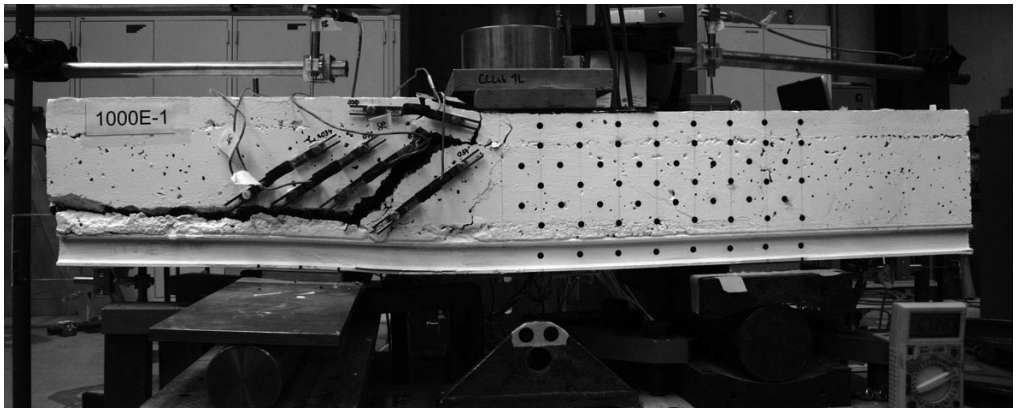

(d) At 95 kN (post-peak)

Figure D.48: 1000Es: Failure process on west side, continuation.

(a) At approximately 100 kN south-east

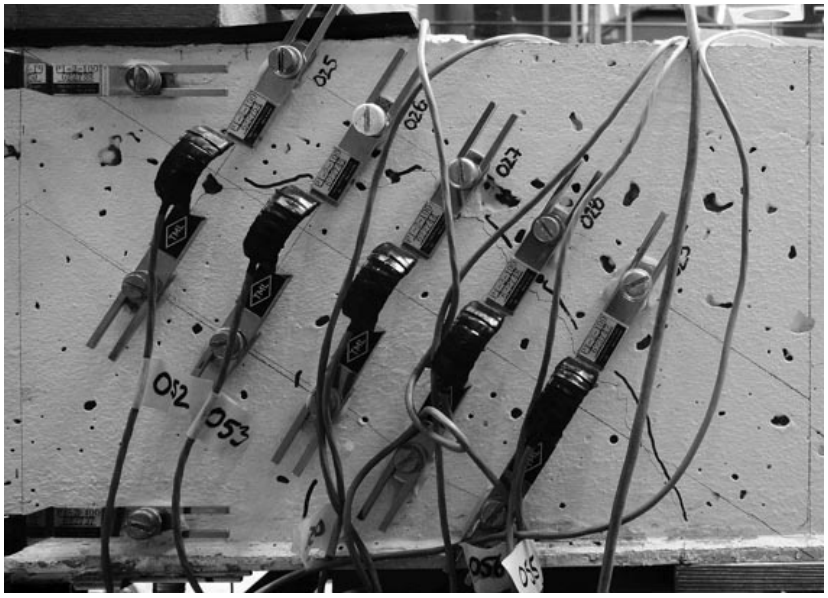

(b) At approximately 100 kN north-east

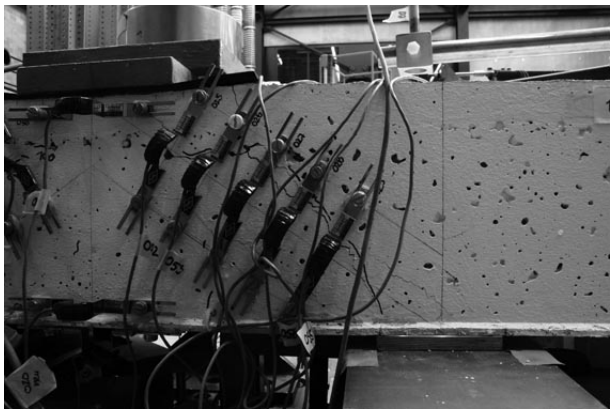

(c) After ultimate load

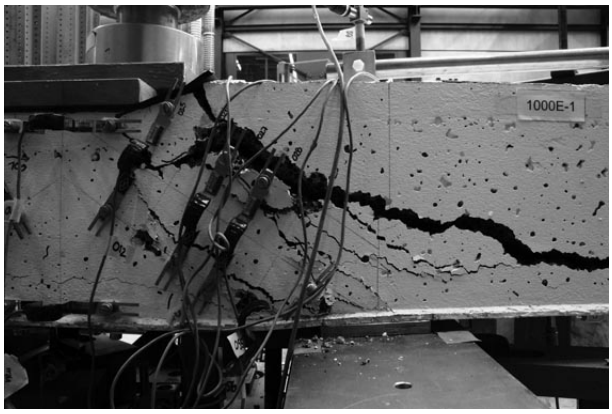

(d) Final crack

Figure D.49: 1000Es: Crack development in east part of specimen.

D.3.8.2 Displacement transducers

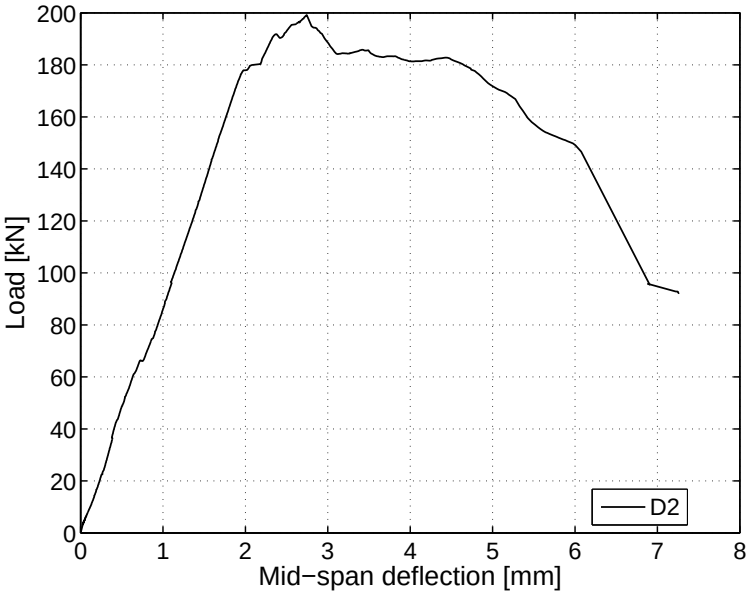

(a) At mid-span

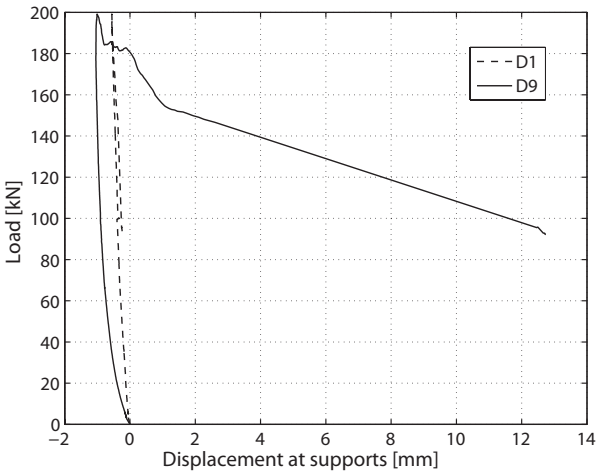

(b) At supports

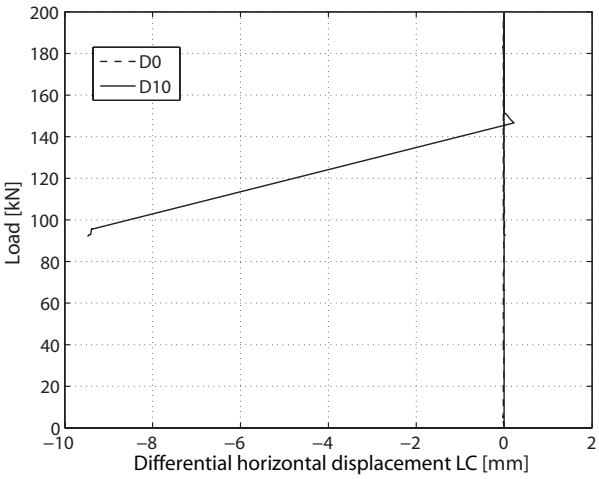

(c) Diff. horizontal displacement within failed LC

Figure D.50: 1000Es: Displacement measurements.

D.3.8.3 Omega-shaped extensometers

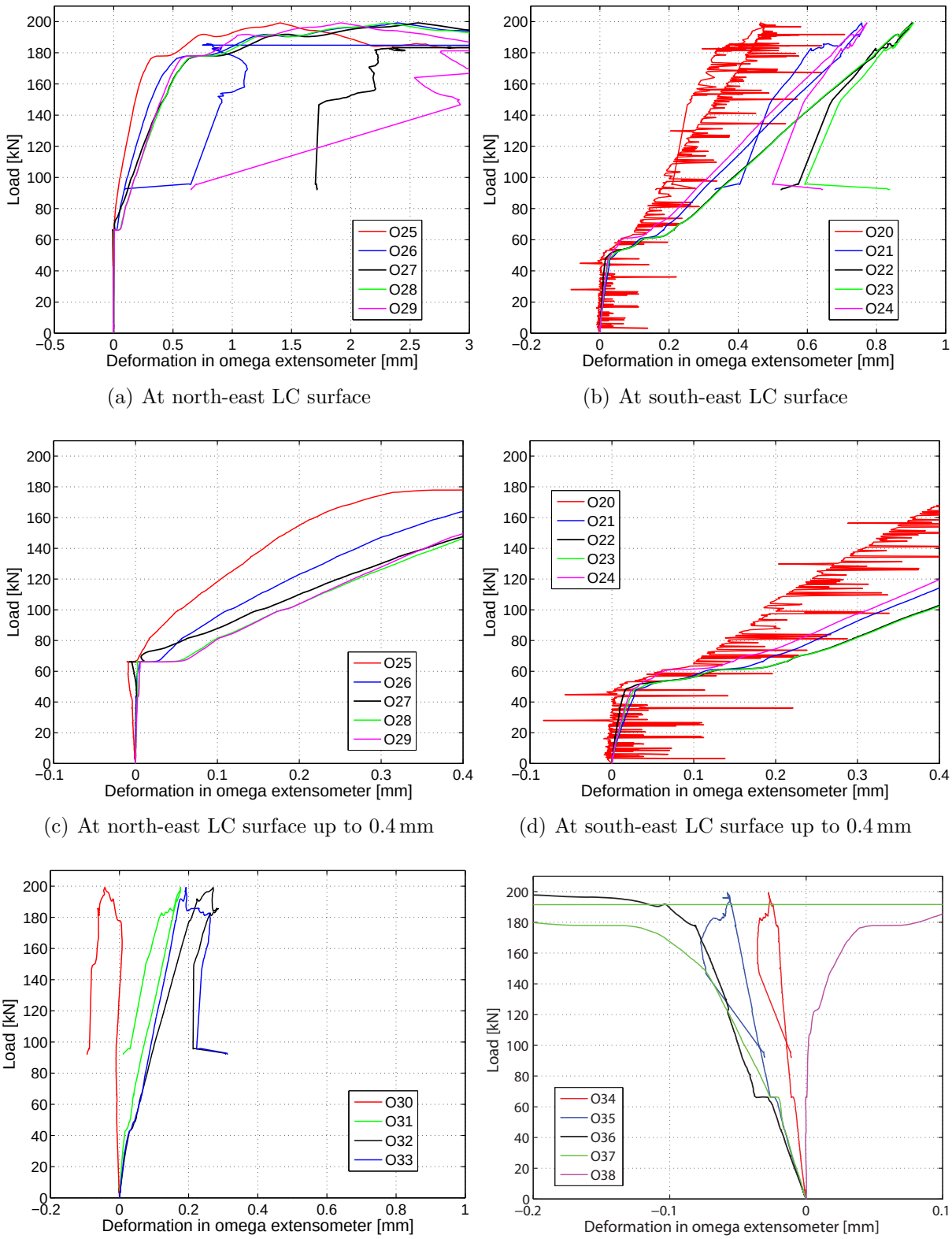

(a) At north-east LC surface

(b) At south-east LC surface

(c) At north-east LC surface up to 0.4 mm

(d) At south-east LC surface up to 0.4 mm

(e) At mid-span

(f) At north-west LC surface

Figure D.51: 1000Es: Deformations in omega-shaped extensometers.

D.3.8.4 Deformations at different load steps perpendicular to the diagonal

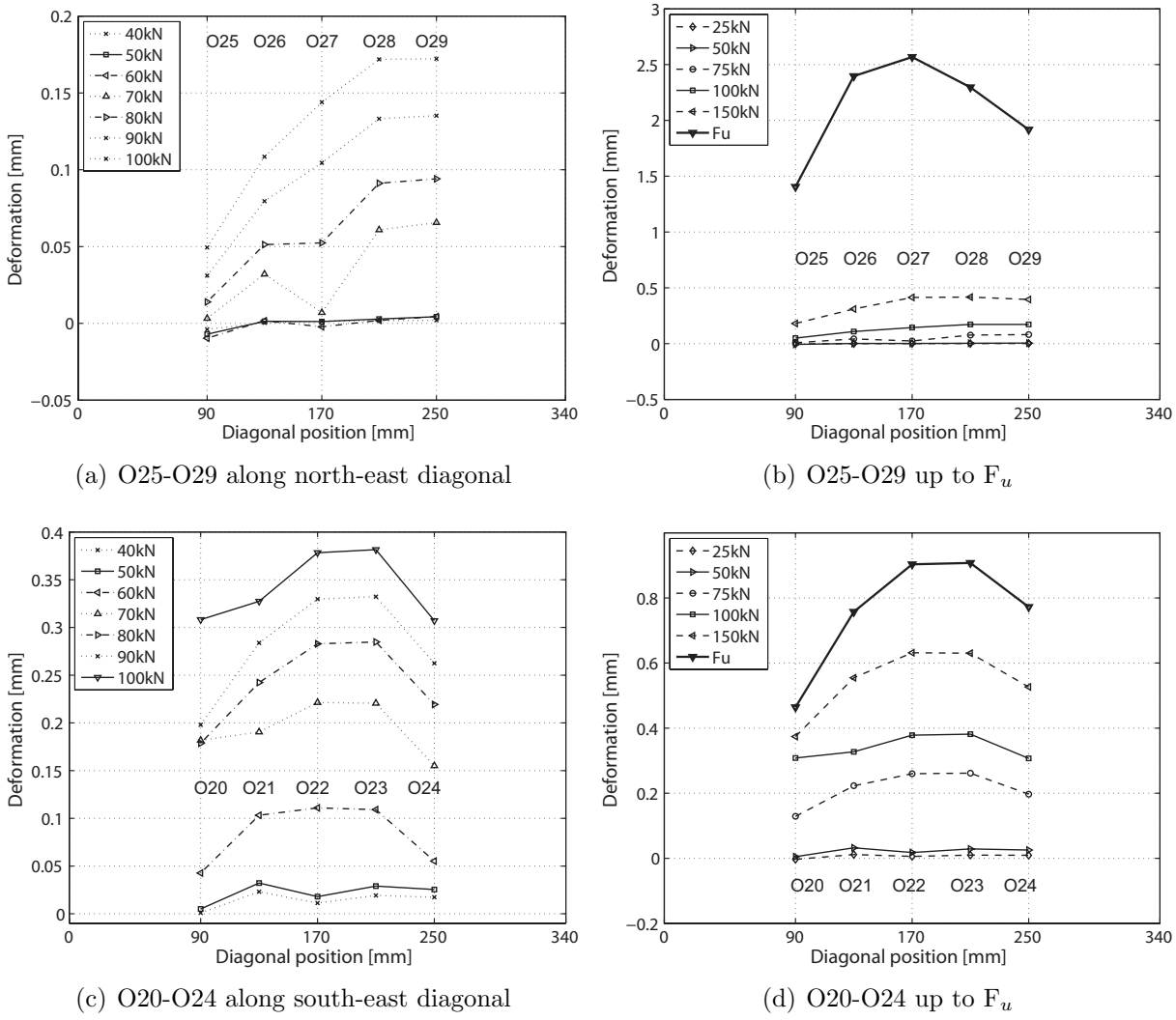

(a) O25-O29 along north-east diagonal

(b) O25-O29 up to F_u

(c) O20-O24 along south-east diagonal

(d) O20-O24 up to F_u

Figure D.52: 1000Es: Deformations at different load steps perpendicular to diagonal.

D.3.8.5 Deformations at different load steps through the cross section and along the diagonal

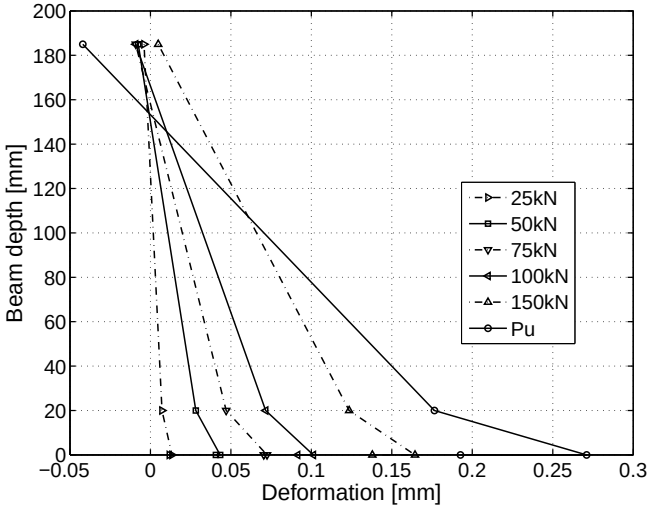

(a) Deformations through cross section on east side

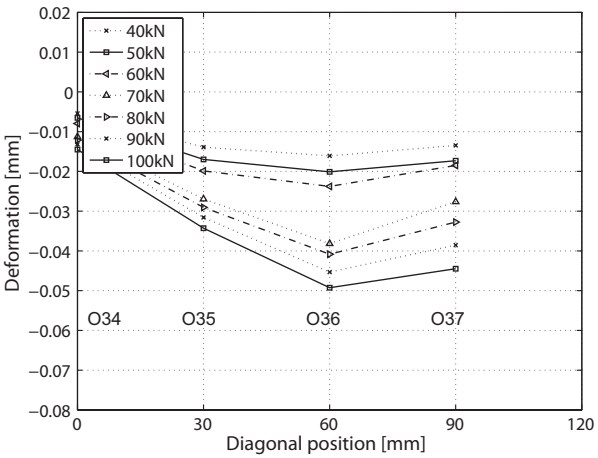

(b) O34-O37 along north-west diagonal

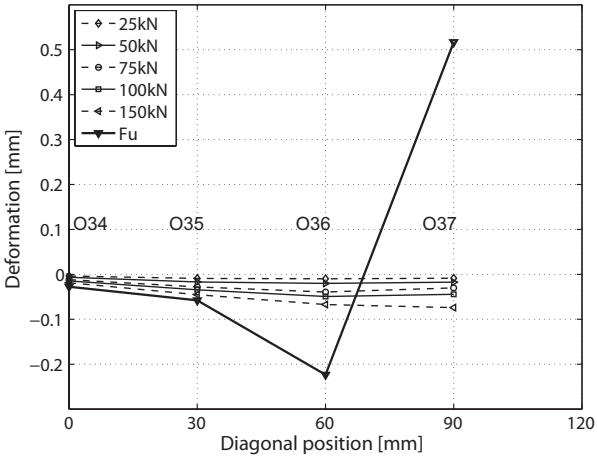

(c) O34-O37 along north-west diagonal up to F_u

Figure D.53: 1000Es: Deformations at different load steps.

D.4 Summary of main results

The main results of the short-span beam experiments are shown in the following tables.

Table D.2: Ultimate loads, LC cracking loads from visual observation and measurements.

Beam	Ultimate load [kN]	Cracking load at first visual crack [kN]	Cracking load from omega gages	
		* diagonal crack ** vertical at mid-span	Southern diagonal from O22 [kN]	Northern diagonal from O27 [kN]
1300s-1	143	40**	-	-
1300s-2	146	40**	-	-
900Es-1	98	75*	(72)	70
900Es-2	83	80*	(70-80)	65
1300Es-1	204	85*	87	87
1300Es-2	185	85*	80	80
1000s	164	44*	45	(75)
1000Es	201	35*	50	(68)

Table D.3: Deformations of NC, LC and FRP at mid-span (* crack in gage length of extensometer, negative signs = compression).

Beam	Ultimate load [kN]	Deformation [mm]		
		O30, NC	O31, LC	av. O32/O33, FRP
900Es-1	98	-0.007	0.057	0.095
900Es-2	83	0.007	0.035	0.066
1300s-1	143	1.195*	0.734*	0.999
1300s-2	146	0.003	-0.126	1.108
1300Es-1	204	-0.016	0.041	0.519
1300Es-2	185	0.358*	0.202	0.402
1000s	164	0.264*	0.140	0.172
1000Es	201	-0.042	0.177	0.233